UNIVERSITY OF KWA-ZULU NATAL

AN INVESTIGATION INTO THE VISCOSITY OF HEAVY MEDIUM SUSPENSIONS

N.T MABUZA

AN INVESTIGATION INTO THE VISCOSITY OF HEAVY MEDIUM SUSPENSIONS

Nhlanganiso Talent Mabuza

BScEng (University of Natal)

Submitted in fulfilment of the academic
requirements for the degree of

MScEng

In the

Department of Chemical Engineering
University of Kwa-Zulu Natal, Howard College Campus, Durban.

January 2005

ABSTRACT

This project investigated the viscosity of heavy medium suspensions. Heavy medium suspensions are used extensively in the minerals processing industry for separation of valuable materials from gangue on the basis of density. Rheological profiles for ferrosilicon and magnetite suspensions were determined using a laboratory-scale viscometer developed in the School of Chemical Engineering, University of KwaZulu-Natal, Howard College Campus, Durban. Ferrosilicon suspensions with specific gravities ranging from 2.0-3.2 were investigated in the presence of clay, to simulate higher density separations such as those used in the diamond industry, where slime build up can be a problem. Magnetite suspensions were prepared at specific gravities ranging from 1.6 - 2.6 to simulate separation densities used in the coal cleaning industry. Mixtures of suspensions of fine magnetite, and coarse magnetite, were also prepared to see what the effect of a coarser medium would have on the viscosity of the suspensions. The effect of viscosity on the separation efficiency of heavy medium separations was also investigated, using a laboratory-scale Dense Medium Separator designed and developed in the department. Suspensions with specific gravities between 1.6 and 1.8 were used to separate coal samples in the following size ranges: -4mm + 1mm; -1mm + 500μm; and -4mm + 500μm.

The rheograms for ferrosilicon suspensions showed that at low shear rates the suspensions behaved as pseudo-plastic liquids, while at high shear rates the behaviour resembled that of dilatant fluids. At low specific gravities the behaviour of magnetite suspensions was pseudo-Newtonian. For specific gravities greater than 2.0, the suspensions became pseudo-plastic. The effect of a locally available dispersant (DP001), on the viscosity of the heavy medium suspensions, was also investigated. For ferrosilicon / clay mixtures, a reduction in viscosity of up to 20 percent was achievable for some specific gravities and slimes level. It was also observed that the dispersant had little effect or none at all, on the viscosity of uncontaminated ferrosilicon suspensions. Addition of the dispersant to fine magnetite suspensions achieved viscosity reductions between 8 and 10 percent. It was observed that the presence of coarse magnetite reduced the viscosity of fine magnetite suspensions by as much as 40 % at certain coarser solid ratios. Adsorption tests using a UV spectrometer showed that there was little or no DP001 adsorbed onto the surfaces of uncontaminated ferrosilicon particles. The results showed that DP001 was adsorbed onto the surfaces of magnetite #1 particles, with almost half the amount of l

g DP001 / kg Mag #1 added to a test suspension of specific gravity 2.2 being adsorbed. This explained why magnetite #1suspensions were more susceptible to DP001 addition compared to ferrosilicon suspensions.

For some of the coal size ranges separated, it was observed that there was a reduction of approximately 22% in the separation efficiency of the process as the specific gravity was increased. For some of the coal samples, an improvement in separation efficiency between 11% and 17% was achievable with DP001 additions of 1g DP001/kg solids, and 2g DP001/kg solids. The presence of coarse magnetite media initially improved the separation efficiency by up to 50% for some coal samples. However, as DP001 was added, there was a decline in the separation efficiency.

In conclusion, the measured rheological profiles of the suspensions were comparable with those found in literature. It was shown that media particle size distribution affects the viscosity of heavy medium suspensions. It was also shown that surface active agents can be used to reduce the viscosity of heavy medium suspensions.

PREFACE

The work in this thesis was performed at the University of Kwa-Zulu Natal, Howard College Campus, Durban, from January 2003 to January 2005. The project was supervised by Dr Jon Pocock.

I hereby declare that this entire dissertation is my own work, unless stated otherwise in the text, and that it has not been submitted, in whole or in part, for a degree to any other University or Institution.

_____

Nhlanganiso Talent Mabuza

As supervisor of the above mentioned student, I am satisfied with his work, and hereby approve this dissertation for submission:

_____

Dr Jon Pocock

ACKNOWLEDGEMENTS

I wish to express my sincere gratitude and appreciation to the following persons who have contributed towards the completion of this investigation:

- First and foremost, I would like to thank God for giving me the gift of life.
- Lignotech SA for sponsoring the project
- My supervisor, Dr Jon Pocock, for his assistance and guidance during the duration of the project. And my co-supervisor Professor Brian Loveday.
- The Department of Chemical Engineering workshop staff, particularly Mr K. Jack and Mr L Henwood, for the construction of the rheometer and heavy medium cyclone.
- The entire staff at the Department of Chemical Engineering for making my stay within the department pleasurable.
- The late Dr Fiona Graham for the SEM pictures. And Dr Gregg Whitmore for the Malvern analyzer tests.
- My fellow postgraduate students for their friendship and encouragement over the past two years. Particularly Retselisitsoe Taole, Allen Hemphill, Lakesh Maharaj, Alex Hwengwere, Mohamed Abdul-Kader, Etienne Wilson, Jason Knock, Ildephonse Habyalimana, and Denny Mwasiswebe.
- My family and friends for always being there whenever I needed their support. Particularly my mother for her constant love and support. I love you all.
- To my girlfriend for her patience and renewed love for me.
- And lastly, to the memory of my father. Whose words of wisdom still guide and protect me. Mshengu Mshabalala.

TABLE OF CONTENTS

LIST OF TABLES

LIST OF FIGURES

NOMENCLATURE

Symbol	Description	Units
□	bob-cone angle	^{o}
D	shear rate	s^{-1}
C_1-C_6	model parameters	
P_{20}	20% passing size solids	mm
P_{80}	80% passing size solids	mm
n	power law index	-
T	temperature	^{o}C
□	V_s/V_{Tot} ratio of the volume occupied by the solid phase to the total volume of the medium	-
ϕ	Bobbin speed	rpm
$□_1$	value of □ for non-magnetic component	-
$□_2$	value of □ for magnetic component	-
$□_{m/max}$	value of □ in the condition of maximum packing	-
□	1/□	-
□	bobbin angular speed	rad/s

□	density	kgm^{-3}
□	torque	Nm
□	shear stress	Nm^{-2}
□$_0$	yield stress	Nm^{-2}
μ_a	apparent viscosity	Pa.s
μ_f	viscosity of dispersing fluid	Pa.s
□$_1$	□$_1$/□ volume fraction of the non-magnetic component in the total solid	-
□$_2$	(1- □$_1$)	-
$\dot{\gamma}$	Shear rate	s^{-1}
V_s	volume occupied by solid	m^{-3}
V_{Tot}	Total volume of suspension	m^{-3}
□	bobbin angular velocity	s^{-1}

LIST OF ABBREVIATIONS

Abbreviation	Description
DMS	Dense Medium Separation
DP001	Development product 001
HMS	Heavy Medium Separation
H-B	Herschel-Bulkley
FeSi	Ferrosilicon
Mag #1	Magnetite #1
Mag #2	Magnetite #2
RBM	Richards Bay Minerals

Chapter 1

Introduction

1.1 What is Heavy Medium Separation?

Heavy medium separation (HMS) is an important industrial separation process used for separating minerals according to their densities. It can be applied in mineral dressing, where it is used to remove light-weight rock at an early stage after a crushing process. Here it is used as a sorting treatment, used to remove ores of a grade too low to warrant treatment in concentrators. Essentially, it is used to reduce the unnecessary energy costs which would otherwise be incurred from the treatment of a non-economic ore i.e. one that is high in gangue material. Secondly, heavy medium separation can also be applied in ore concentration. Heavy medium separation is also used in coal preparation. Here HMS is used to produce a commercially graded end-product by separating cleaner coal from the heavier high-ash and associated shales and discard [Wills (1997)]. Coal is a heterogeneous material comprised of combustible and non-combustible material. The non-combustible material is called ash, such that a coal with high non-combustible material is said to have high-ash content

Heavy medium separation is one of the simplest industrial gravity separation processes. Its principle method of separation is based on the specific gravity of the heavy medium and the feed material being separated [Pryor (1960), Wills (1997)]. Minerals are fed into the heavy medium such that minerals with densities less than the medium float and those with densities heavier than the medium sink. Theoretically, heavy medium separation can be used for any density separation. In practice, however, the range of densities due to incomplete liberation and natural density profiles means that heavy medium separation is applicable to any ore provided there is a high enough difference in density between the particles. Figure 1.1 illustrates the main principle of operation in heavy medium separations.

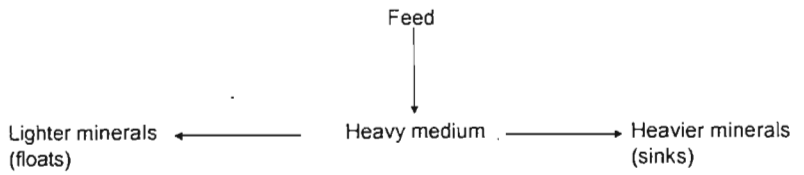

Figure 1.1 Principle of heavy medium separation [Wills (1997)]

1.2 Stages in heavy media separation

The heavy media used can be a solution of a salt in water, a heavy organic liquid, or a suspension of solids in water. Solutions of salts in water have been abandoned because of the high capital costs needed to run the plant. The high costs of salt regeneration and the corrosive nature of these solutions led to the abandonment of the use of these solutions [Pryor (1960)]. Heavy liquids have been confined to laboratory use, to determine the feasibility of heavy medium separation on an ore. Most heavy liquids release harmful vapours and must be handled in well ventilated areas. For this reason, the use of heavy liquids as a medium in industrial separations has been found to be impractical. Nowadays heavy medium suspensions are prepared by adding fine solid particles in water. A typical dense medium separation circuit is shown in Figure 1.2 and Figure 1.3 [Horsfall (1993)].

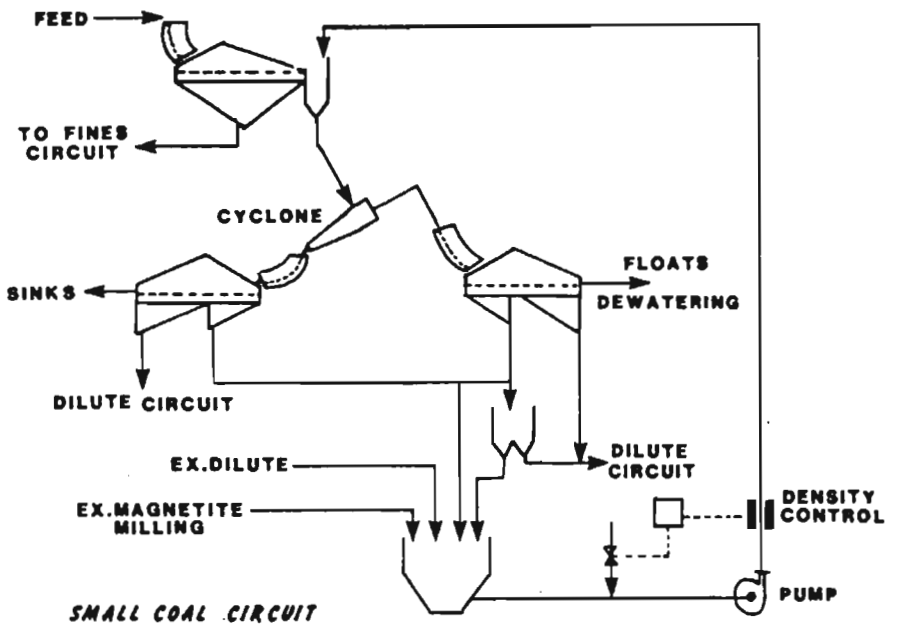

Figure 1.2 Stages in heavy media separation for small coal circuit [Horsfall (1993)]

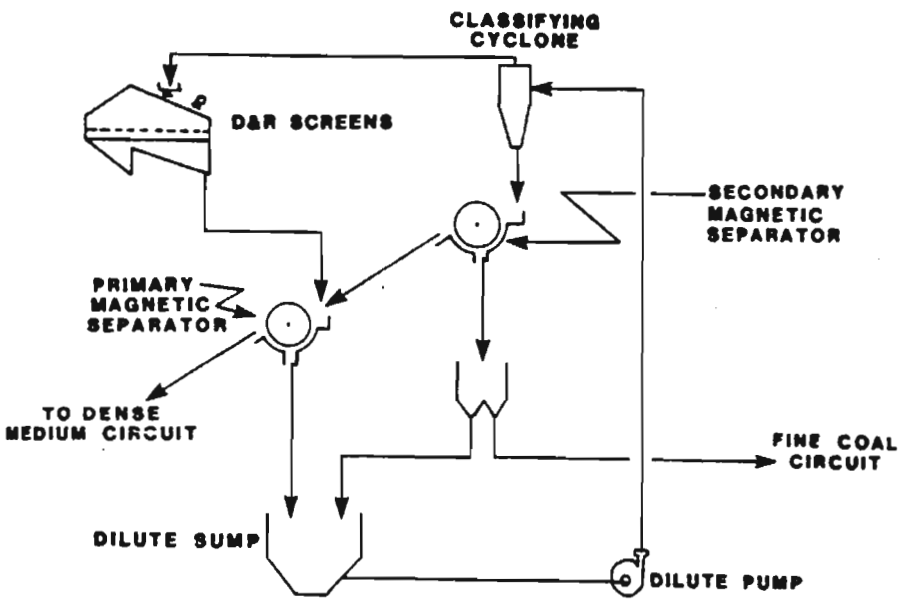

Figure 1.3 Stages in heavy media separation for dilute medium circuit [Horsfall (1993)]

The main stages in heavy medium separation are divided into the sections given below:

a) Presentation of a suitably prepared feed.

b) Separation into floats and sinks in a vessel containing the dense medium.

c) Withdrawal of products, and removal from them of adherent dense media.

d) Cleaning and reconstitution of the medium followed by a return to the separator of clean dense medium.

The feed to the cyclone is suitably prepared by screening in order to remove some of the fine material, which has a tendency of increasing the suspension viscosity. The de-slimed feed is then fed into the separating vessel (cyclone in this case) to obtain an overflow and underflow product (Figure 1.2). The floats and sinks are then sent to screens where they are washed to remove any adhered media particles. After dewatering, the products are removed, and the underflow from the screens is sent to the dilute medium circuit (Figure 1.3). Here the media is reconstituted by passing it through magnetic separators.

There are a number of solids which have been used to prepare dense medium suspensions. The most common solids used are galena, magnetite, and ferrosilicon. Minor types include pyrites, chalcopyrite, hematite, barites, and clay. The criteria used to determine which solids are suitable are based on the physical properties of the particles. The solid particles must have a reasonably high density; must be hard spheres, and must be easily recoverable from the suspension. Galena is mostly used in lead-zinc concentrators, at suspension specific gravities as high as 4.0 [Wills (1997)]. Magnetite is used predominantly in the coal industry to separate clean coal from high-ash coal. Magnetite is used to prepare suspensions with specific gravities ranging between 1.6 and 2.5. Ferrosilicon is the most widely used medium for preparation of suspensions with specific gravities greater than 2.5. Ferrosilicon is an alloy of iron and silicon. The ratio of iron and silicon is such that the corrodibility of the alloy is small, without compromising the recovery of the particles. Both magnetite and ferrosilicon are magnetically recoverable. This method of recovery is more cost effective compared to the method of recovery of galena and the minor type solids. The latter solids are recovered through flotation, which is an expensive process [Wills (1997)].

1.3 Parameters involved in heavy medium separations

The separating vessels used in heavy medium suspensions can be classified under two groups: static (gravitational) separators, and dynamic separators. For an ore particle being separated using heavy medium separation, there are three main forces acting on the particle [Napier-Munn (1990)]. The first force is a downward or penetrating force. In static baths this force is the gravitational force on the particle, and in dynamic separators (e.g. centrifugal separators) the force is often a centrifugal force. The second force is a buoyant force, equal to the weight of the fluid displaced by the particle. This type of force is common among static separators and is one of the forces accounted for by Stoke's Law. This force always acts in the direction opposite to gravitational / centrifugal forces. The third type of force is the drag force. This type of force also acts in a direction opposite to gravitational / centrifugal forces. The drag force on a particle can either be due to viscous resistance or turbulent resistance, depending on the type of flow regime prevailing in the separating vessel. The most significant difference between the two types of drag force is that viscosity is one of the parameters in viscous resistance, while it is absent in turbulent resistance.

Particle size and density difference are important parameters common to both types of resistances. Density difference refers to the difference in density between the particles and the separating fluid. If the modulus of the density difference is high, separation of particles occurs quite easily even at small particle size ranges. However, if the modulus of density difference is small, the separation of the particles becomes difficult at small particle sizes. The efficiency of separation decreases at small particle sizes because of the slower settling-rates of the particles. For separations to be effective on a difference in specific gravity of 0.1 or less, the particles should be larger than 3 mm in diameter. For small particle sizes (□300 μm) centrifugal forces can be used to increase the settling-rate of the particles [Wills (1997)].

The two most important rheological parameters in heavy medium separation are the viscosity and stability of the suspensions [Collins et al. (1983)]. The viscosity is defined in terms of the resistance to flow of the fluid. In the context of heavy medium separations, this refers to the resistance of the fluid towards particle penetration. A high viscosity has been shown to reduce the efficiency of heavy medium separations [Collins et al. (1983) and Napier-Munn (1990)]. A high viscosity results in fine particles, and those with specific gravities close to that of the suspension being unable to penetrate the suspension. This results in the misplacement of high density

material to the floats product. The stability is defined in terms of the settling rate of the suspension. Heavy medium suspensions often stratify and become non-homogenous. This is caused by the high density of the solid particles making up the suspensions. These solid particles settle out of the suspension, often leading to difficulties in achieving the correct specific gravity. A suspension with a low settling rate is said to have a high stability i.e. stability is the reciprocal of settling rate. The stability and viscosity of heavy medium suspensions depend on the specific gravity of the suspension, the media particle size distribution, media particle shape, and presence of slimes / clays.

The viscosity and stability of heavy medium suspensions are mutually dependant on each other. This means that altering one of them has a direct effect on the other. A high viscosity results in a higher stability, whilst a lower viscosity results in a much lower stability. This often causes problems for plant operators since most suspensions are inherently viscous because of the presence of clay and slimes in the suspensions. Thus a trade-off exists between having a suspension with a high viscosity and stability, or having a suspension with a lower viscosity and stability. Most plant operators would rather work with suspensions which are less viscous, with a much lower stability, than having to work with suspensions which have a high viscosity [Valentyik (1972)].

1.4 Objectives of the Investigation

The main objective of this project was to investigate the viscosity of heavy medium suspensions. The media particles used were ferrosilicon and magnetite. The effect of a surface active agent on the viscosity of heavy medium suspensions was also to be investigated.

To achieve the above, the project was divided into the following investigations to:

- Survey the available literature on the viscosity of heavy media suspensions, and also the methods of reducing the viscosity of heavy media suspensions through the use of dispersants.

- Perform rheological measurements using a viscometer in order to determine the rheological profiles of the suspensions. The behaviour of the liquids was then used to infer what is likely to happen in separating vessels.

- Perform rheological measurements using a surface active agent (DP001). The results of the experiments can be used to predict whether or not a dispersant affects the viscosity of the suspensions.

- Perform rheological measurements to determine the effect of media particle size distribution and shape on the viscosity of the suspensions.

- Perform experiments to determine the effect of viscosity and the dispersant have on the separation efficiency in a dynamic separator. The dynamic separator chosen for the project being a dense medium cyclone.

Chapter 2

Literature Review

This chapter contains the findings of a review into the literature relating to the rheology of Heavy Medium Suspensions. The two rheological parameters which are discussed are the viscosity and stability of heavy medium suspensions. The first part of this section is mainly concerned with how media particles and solids volume concentration affect the rheology of suspensions, including the effect of media particle size distribution and particle shape. The second part deals with the effect of surface active chemicals, and their chemistry, on the rheology of heavy medium suspensions.

2.1 Heavy Media

Heavy medium separations are based on the density differential between the heavy medium and the material being separated. Thus, heavy media of suitable density need to be available in industry to enable the separation of ores from unwanted material.

Over the past years there have been a number of mediums used to separate materials in heavy medium separations. These are presented by Pryor (1960) and Wills (1997):

1. Solutions of salts in water

2. Organic liquids

3. Suspensions of solids in water

2.1.1 Solutions of salts in water

Solutions of salt in water have been used in coal preparation. They were used for the separation of clean coal from high-ash coal. An example of a salt in water is calcium chloride ($CaCl_2$) solution, with a typical separation specific gravity of 1.35.

Salts were chosen on the basis that they should not react with the ore being treated in such a way as to reduce the selling value of the final product [Pryor (1960)]. The main difficulty associated with the use of salts in water is the high operating cost incurred from the regeneration of the salts through evaporation. This high energy input demand is what ultimately led to the use of such solutions becoming obsolete. Another factor that also led to the discontinued use of solutions of salt in water is the high corrosive nature of the solutions. Problems occur due to the corrosion of separating vessels and other unit operations in the circuit.

2.1.2 Organic Liquids

Organic liquids are chiefly used in laboratory experiments to determine the feasibility of heavy medium separation on a particular ore [Wills (1997)]. They are also used to verify the most economical separating density. Sink-float tests are performed on the ore by preparing liquids covering a range of densities in incremental steps. A more detailed description of sink-float analysis is contained in Appendix A2

Typical organic liquids used are tetrabromoethane ($C_2H_2Br_4$), ethylene dibromide ($C_2H_4Br_2$), pentachloromethane (C_2HCl_5), and trichloroethylene (C_2HCl_3) [Pryor (1960)]. These liquids have low viscosity, good stability, and are non-corrosive. The most commonly used organic liquid is tetrabromoethane (TBE), which has a specific gravity of about 2.96. To give a range of specific gravities below 2.96, TBE is diluted with white spirit, carbon tetrachloride, or acetone.

The use of organic liquids has never been successfully extended to industrial use because of the toxic nature of these liquids. Even for laboratory use certain safety measures have to taken during their use. These include: handling the liquids in well ventilated areas; use of safety equipment outlined in their safety data sheets; and use of water-sealed equipment to prevent their evaporation. A safety data sheet for tetrabromoethane is contained in Appendix A2.

2.1.3 Suspensions of solids in water

The heavy medium commonly used in industrial separations is a thick pulp of some heavy mineral in water, which essentially behaves as a heavy liquid. These suspensions are prepared by adding an aggregation of solid spheres to a liquid. Heavy medium suspensions can be classified as a heterogeneous system comprised of a disperse phase, and a continuous phase. The solid particles represent the disperse phase, while the liquid represents the continuous phase [Jinescu (1974)]. The disperse phase may itself also be a heterogeneous system comprised of solid particles of different nature and form. In some industrial processes solid particles of different form and nature have been used at different concentrations to facilitate the separation of certain mineral ores. Collins et al. (1983) used a mixture of atomised ferrosilicon and magnetite mixtures in the separation of a tin ore in a Vorsyl and cyclone separator.

The liquid can either be a Newtonian liquid or a non-Newtonian liquid. In almost all, if not all, industrial processes the liquid used is water, which is a Newtonian fluid. Generally, if the suspension continuous phase is a Newtonian liquid (e.g. water), the behaviour of the suspension is Newtonian for relatively small solid volume concentrations, usually below 30% by volume [Wills (1997), Pryor (1960)]. Above this value the suspension becomes non-Newtonian due to particle-particle interactions of a hydrodynamic nature. The suspension usually acquires minimum shear stress needed before movement of the suspension can occur. Feed material comprised of small particles, or particles with densities close to the suspension density, have difficulty in overcoming the surface force offered by the suspension, requiring the use of centrifugal forces in place of gravity forces, or the reduction of the suspension viscosity through agitation. If the suspension continuous phase is a non-Newtonian liquid the suspension exhibits non-Newtonian behaviour at both high and low solid volume concentrations. At low solid volume concentrations the non-Newtonian behaviour is due the non-Newtonian nature of the continuous phase. At high solid volume concentrations the non-Newtonian behaviour is due to both particle-particle interactions and the non-Newtonian nature of the continuous phase [Jinescu (1974)].

The media particles used to prepare heavy media suspension are chosen according to the following qualities [Pryor (1960)]:

a. Hardness: The chosen medium particles must not easily breakdown under working conditions. Particle breakdown introduces fines into the system, resulting in an increase in the apparent viscosity of the suspension.

b. Chemical stability: The medium particles must not be chemically corrosive, or liable to react with the ore minerals undergoing treatment. The products of corrosion also introduce fine material into the system. As will be shown later, ferrosilicon particles are manufactured such that the silicon content is enough to delay the onset of particle corrosion.

c. Low settling rate at moderate viscosity: The settling rate of the solid particles is one of the important rheological properties of heavy medium suspension. Suspensions are said to be stable when the settling rate of the medium particles is low. The stability of the suspension can be improved by using very fine medium particles. However, this increases the suspension viscosity, reducing the separation efficiency of the process. Thus, the medium particles must form a fairly stable suspension without having to be below 10 μm, on average.

d. Density: At a constant suspension density, higher particle densities reduce the viscosity of the suspension by reducing the solid volume concentration. Hence, the density of the medium particles must be high enough to give the required suspension density under reasonably non-viscous conditions.

e. Regeneration: Because of the fouling nature of heavy medium processes, the media has to be cleaned after each cycle before further use. The medium chosen must be easily recoverable from the mineral surfaces through washing and reconstitution.

f. Non-fouling: After the ore has been cleaned and washed, a certain amount of medium lodges in cracks in the lumps of the cleaned ore. The chosen medium must not be of a nature or form deleterious to subsequent treatment of the ore.

Table 2.1 lists some the heavy media able to meet some of the above specifications. The table also lists the method of regeneration for the heavy media.

Table 2.1 Heavy media and their methods of regeneration [Pryor (1960)]

Material	Method of Regeneration
Galena	Froth-Flotation
Magnetite	Magnetic Separation
Ferrosilicon	Magnetic Separation
Pyrites	No regeneration
Copper Pyrites	Obsolescent
Hematite	Obsolescent

Galena is a soft mineral with a specific gravity of 7.4 - 7.6. Galena is used to maintain suspensions with a specific gravity of 3.3. At densities higher than these the viscosity of the suspensions become unmanageable, making the separation of small particles or those with densities close to the suspension density very difficult. The regeneration process of galena by froth-floatation is more expensive and more difficult than the recovery of magnetic materials. Galena is also fairly soft and tends to slime easily, and it also has a tendency to oxidize, which has a negative effect on flotation efficiency [Wills (1997)]. Because of this, and the fact that the material itself is expensive, the use of galena as heavy media has been abandoned in almost all industrial heavy medium separations.

Magnetite is a common, relatively cheap mineral existing in many localities. Some famous localities are Binnental, Switzerland; Pfitschal, Tyrol, Austria; and the Phalaborwa mine, Limpompo, South Africa. The largest magnetite deposits are in northern Sweden. Other large deposits are in Norway, Romania, and Russia. Magnetite is the only mineral that exhibits ferromagnetism, although other minerals like ilmenite and hematite have weakly magnetic behaviour [http:// geology.about.com (22/02/04)]. Most magnetite occurs in small grains and has a specific gravity between 5.0 and 5.2. It is extensively used in coal preparation, and is used to maintain suspension densities of up to 2500 kgm^{-3} [Pryor (1960), Wills (1997)]. Because of its relatively low specific gravity compared to ferrosilicon, magnetite is rarely used at specific gravities above 2.5 because of the associated high viscosity of suspensions above this specific

gravities. Aplan et al. (1960) also showed that, due to processing, magnetite media contained much higher fines content than ferrosilicon media. The presence of these fines is also a contributing factor towards the non-Newtonian behaviour of magnetite suspensions at high suspension densities. Magnetite is easily recoverable from the heavy medium circuit through magnetic separation.

Ferrosilicon (FeSi) is now the most widely used media for heavy medium suspensions of ores with a specific gravity in the range of approximately 2.5 to 4.0 [Collins .et.al. (1974)]. Ferrosilicon is an alloy of iron (Fe) and silicon (Si) which usually contains not less than 82 % iron, and 14-16 % silicon. To reduce the corrodibility of the medium, the silicon content should not fall below 14 %. Also, the silica content should not exceed 16 % as this has the tendency to decrease both the magnetic susceptibility of the medium, and its specific gravity [Collins et al. (1974), Rodis et al. (1960), and Wills (1997)].

There are two types of ferrosilicon media available in South Africa: milled ferrosilicon and atomised ferrosilicon. The difference between the two types of ferrosilicon arises from the different methods of their production.

The standard method for the manufacture of milled ferrosilicon is to melt steel scrap, quartz, and a reductant in a submerged arc-furnace [Collins et al. (1974)]. The molten alloy is tapped into a sand bed, allowed to cool, after which it is broken into lumps, and finally crushed in two stages and milled to the required size range. The furnace is charged on a semi-continuous basis, and is usually tapped into a ladle every two hours. The temperature of the melt on tapping is approximately 1600 °C.

Atomised ferrosilicon is manufactured using two methods. The first method, developed by Knapsack-Grieshein AG in Germany, atomises the molten liquid after it is tapped from an induction furnace [Collins et al. (1974), Rodis et al. (1960)]. Ferrosilicon of 75 percent silicon is diluted with high-grade steel scrap in an induction furnace. The furnace is tapped every three hours at a charge temperature of approximately 1550 °C. The molten alloy stream enters an atomising stream cone where it comes into contact with a cone of steam, and the melt is immediately broken into fine particles, which are quenched in water. The resultant ferrosilicon pulp is filtered, dried, and classified to remove oversize material.

The second method of manufacturing atomised ferrosilicon was developed by ISCOR in South Africa [Collins et al. (1974)]. The atomised ferrosilicon is also produced in an induction furnace. In this case, however, the stream of molten alloy is broken up in a series of concentric cones of high pressure water. The granulated product is dried and screened, and the oversize is milled to the required size in a ball mill in closed circuit with an air classifier. The milled powder is then atomised by allowing it to fall through a flame which has an oxidising centre and a reducing outer zone. This permits each individual particle to be melted without being oxidised. After atomisation the powder is quenched in waste gas to prevent oxidation.

As mentioned above, the difference in physical properties between the two types of ferrosilicon arises from their different methods of production. The milled grade tends to be rough and angular in shape, whereas atomised ferrosilicon is smooth and largely spherical or rounded in shape [Williams et al. (1986)]. As will be shown in a later section, this difference in shape has marked effects on the rheological properties of aqueous suspensions of the two types of ferrosilicon. It is thus important to properly select the most suitable type of ferrosilicon for a given separation. Selection is usually based on the viscosity and stability requirements of the medium. Collins et al. (1974) and Ferrara et al. (1986) give the general criteria used in the selection of which type of ferrosilicon medium to use:

- Operating Density: Generally, for separations above 3.0 for static baths, and 3.2 for cyclones, the use of atomised ferrosilicon is preferred because above these values the viscosity of milled ferrosilicon suspensions rises to unmanageable proportions.

- Ore size: The type of separating vessel used is usually determined by the size of the ore being treated. For very large ore particle sizes (above 100 mm) static separators are used, whereas dynamic separators are used for the separation of fine ore particles. Because of the higher centrifugal forces encountered in dynamic separators, a finer medium, with a moderate viscosity, and high stability is necessary. Hence, at a particular specific gravity, atomised ferrosilicon would be chosen above the milled grade.

- Sharpness of Separation: At low specific gravities either the milled or atomised grade can be used. However, depending on the accuracy of separation required, milled ferrosilicon is preferred because it is cheaper.

- Corrosion Resistance: The occurrence of corrosion is deleterious because corrosion leads to loss of ferrosilicon; The finely divided products of corrosion impair the separation efficiency of the process by increasing the viscosity of the medium; In situ corrosion often leads to the cementing of ferrosilicon particles when they stand in water, caused by the electrochemical oxidation of the ferrosilicon surface to produce non-magnetic iron oxides. Making the start-up of heavy medium processes very difficult after a long shut-down. Rodis .et.al. (1960) have shown that milled ferrosilicon is more susceptible to corrosion than the atomised grade because of its rough, angular shape. For plants operating under abnormal conditions such as high density, high temperature, and acidic or saline water, atomised ferrosilicon is the preferred choice.

- Costs: The cost of manufacturing atomised ferrosilicon is more than double that of milled ferrosilicon. However, when a choice between the two grades is being made, careful consideration into the overall advantage of each grade must be taken into cognizance. These include lower consumption due to corrosion; adhesion, and magnetic separator losses; greater efficiency of separation; and a smaller bulk concentrate, reducing subsequent treatment costs.

2.2 The Rheology of Heavy Medium Suspensions

The two most important rheological variables in the operation of heavy medium separation plants are the viscosity and the settling rate of the medium. As mentioned earlier, if the medium viscosity is too high the separation of near-gravity and fine ore particles becomes too difficult. Conversely, if the viscosity is reduced by either dilution, the use of coarse graded medium, or by the rigorous cleaning of slimes from the circuitry, then the problem of a rapidly settling media arises. This results in an excessive density differential, with a lot of near gravity material exiting with clean ore or coal overflow.

Medium viscosity is important in DMS processes because it determines the rate at which ore particles sink or float in the medium. It also influences the partitioning of the medium itself in the separation vessel under gravitational or centrifugal forces, thus affecting the ore separation, the pumping characteristics of the medium, and the incidence of medium loss through adhesion on drain and rinse screens. Rheology is therefore an important factor to consider when selecting the appropriate medium for a given application, and an important property to control in the process.

The particle size distribution and the shape of the particles are the main physical properties in defining rheology, and ferrosilicon media are therefore manufactured in a range of grades (or size distributions) and shapes (milled or atomised) [Dunglison et al. (1999)].

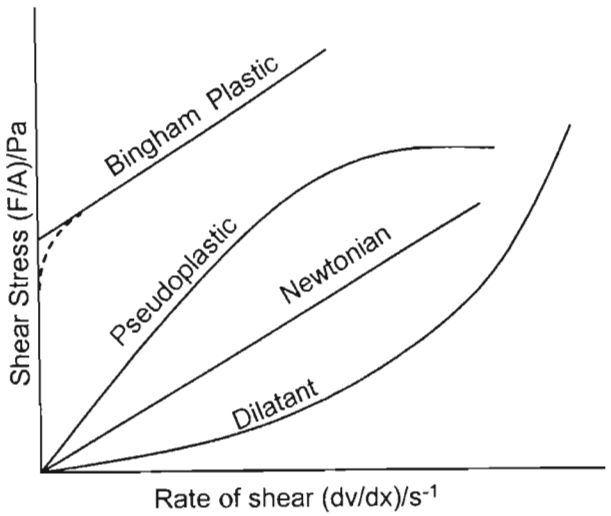

Figure 2.1 Rheograms for various types of suspensions [Aplan et al. (1964)]

The rheological behaviour of heavy media suspensions can either be Newtonian or non-Newtonian. Viscosity may be defined as the resistance to flow of a liquid. Expressed mathematically:

$$\frac{F}{A} = \tau = \mu \frac{dv}{dx} = \mu \dot{\gamma} \tag{2.1}$$

where □is the shear stress, μ the fluid viscosity, and $\dot{\gamma}$ the shear rate.

Fluids which follow Equation 2.1 are called Newtonian fluids, and the slope of the shear curve is the Newtonian viscosity. The rheological behaviour of Newtonian fluids is completely described by their viscosity. From Equation 2.1 it can be seen that a plot of shear-stress versus shear-rate is a straight line through the origin, the slope is constant and the viscosity is independent of the rate of shear. This is illustrated in Figure 2.1

However, dense medium suspensions are rarely that simple, and they fall into three general types of fluids; Bingham plastics, pseudo-plastics, and dilatants. The rheograms of these fluids are shown in Figure 2.1. A brief description of the different types of non-Newtonian behaviour, and the equations governing them is given below [Perry et al. (1997), Eirich (1967)]:

Bingham fluids include those for which a finite stress is required before continuous deformation occurs; these are called yield-stress materials. The Bingham plastic fluid is the simplest yield-stress material, represented by the following equation:

$$\tau = \tau_y + \mu \frac{dv}{dx} \tag{2.2}$$

where τ_y is the fluid yield stress.

Laskowski et al. (1999) define yield stress as the minimum value of shear stress which must be exceeded before a fluid can be made to flow. The occurrence of a yield stress in heavy medium suspensions is caused by inter-particle attractive forces. These forces lead to the formation of structural aggregates in the suspension. They also restrict the positional change of volume elements, and the suspension acquires a solid character [Whitmore et al. (1960)]. If external forces lower than the inter-particle forces are applied to the suspension, the suspension will not flow. The aggregate network can only be broken when the externally applied forces become large enough such that they overcome the yield point. This property of Bingham plastic fluids affects the pumping characteristics of the suspension the separation efficiency of dense medium separators.

In practice the curve is noted to bend downward as it nears the stress axis, due to plug flow. Relatively few materials have been found to exhibit true Bingham plastic behaviour, and this rheological type is important in that it serves as a limiting case for the pseudo-plastic (shear-thinning) type. Typical examples of suspensions of this type are clay slurries, oil-well drilling muds, and cement plant slurries [Perry et al. (1997), Eirich (1967)].

Shear thinning fluids are those for which the ratio of the stress to the rate of shear decreases with the rate of shear. These fluids have been called pseudo-plastic, but this terminology is outdated and discouraged. They are similar to Bingham Plastic suspensions, but show no yield value. The

line relating the shear stress to the shear rate passes through the origin and is curved convex to the shear-stress axis up to a certain shearing stress, but is approximately linear with shear rate beyond that point [Govier et al. (1957)]. At high shear rates shear-thinning fluids behave like Bingham plastic fluids in that there is a near linear relationship between the shear stress and the shear rate. They typically obey the following power law model over a range of shear rates:

$$\tau = k\dot{\gamma}^{n} \quad (n < 1) \tag{2.3}$$

The apparent viscosity is,

$$\mu = k\dot{\gamma}^{n-1} \tag{2.4}$$

The factor 'k' is the consistency index or the power law coefficient, and 'n' is the power law exponent. The exponent 'n' is dimensionless, while 'k' is in units of kg/ms^{2-n}. This type of flow behaviour is typically exhibited by colloidal solutions such as carboxymethyl cellulose [Perry et al. (1997), Eirich (1967)].

Dilatant, or shear thickening fluids are the opposite situation of pseudo-plastic fluids. They show increasing viscosity with increasing shear rate. Over a limited range of shear rate they may be described by Equations 2.3 and 2.4, with the value of 'n' being greater than one [Perry et al. (1997)]. Examples of dilatant suspensions are quick-sand, barium sulphate suspensions, aqueous suspensions of starch granules, and mica in water.

The type of non-Newtonian behaviour mentioned thus far have all been time independent. However, some suspensions have shown a change in rheological properties over a specific period of time whilst operation conditions remained constant. Such rheological time dependency could have an influence on the design of dense media plant circuitry, particularly the residence time of the slurries in each of the process units. The two types of time-dependant flow are thixotropy and rheopexy [Slatter at al (2000)]. Thixotropic behaviour occurs because of the degradation of the structure strength during the shear loading interval, and structure recovery during the unloading interval. Alternatively, thixotropy can be defined as the decrease in yield value of a suspension subjected to mild vibrations. This type of behaviour is a character of certain types of clay [Eirich (1960)]. Rheopexy is the opposite of thixotropy, with a build up of strength during the load phase,

and the decomposition of the structure strength during the discharge phase. Although rheopectic behaviour occurs very rarely compared to thixotropy, it is important because to a small degree high concentrated solutions of surfactants sometimes exhibit this type of behaviour

The use of the term viscosity as a measure of the consistency of non-Newtonian fluids is highly misleading and incorrect. As mentioned above, the viscosity of Newtonian fluids is proportional to the ratio between the unit shear-stress and shear-rate. The term viscosity has been applied to this same ratio in the case of non-Newtonian fluids. However, as illustrated in Figure 2.1, the ratio of unit shear-stress and shear-rate for Bingham plastics, pseudo-plastics and dilatants varies, depending upon the shear-rate [Govier et al. (1957)]. Thus, while Newtonian fluids can be characterized by the viscosity, which is independent of the shear-rate, non-Newtonian fluids are described by a series of 'apparent viscosities' spanning the range of shear-rate of interest.

For a constant suspension specific gravity, a higher density solid will reduce the viscosity and stability of the suspension by reducing the percentage volume of particles. A spherical medium reduces the viscosity and stability of the suspension by providing more slippage between adjacent solids in the suspension. A coarser medium reduces the viscosity and stability of the suspension by reducing the solid particle surface area, which in turn reduces the apparent solids volume concentration [Collins et al. (1983)].

Although most suspensions show non-Newtonian behaviour, it is usually difficult to predict the type of non-Newtonian behaviour occurring in different systems [Lapsin et al. (1988)]. The type of non-Newtonian behaviour can vary within a single class of systems, especially when the concentration is varied. Some concentrated suspensions can show shear-thinning behaviour at low shear rates, and shear-thickening at higher shear rates. Collins et al. (1974) found that for ferrosilicon suspensions at low shear rates showed shear-thinning behaviour, and shear-thickening behaviour at higher shear rates. The above authors also found that by increasing the degree of contamination of the suspensions, or increasing the suspension specific gravity, the suspensions acquired a yield stress. The figure below shows the effect of suspension density on the viscosity of some common heavy medium suspensions. It can be seen from the figure that the critical density for magnetite suspensions is much lower than that of ferrosilicon suspensions.

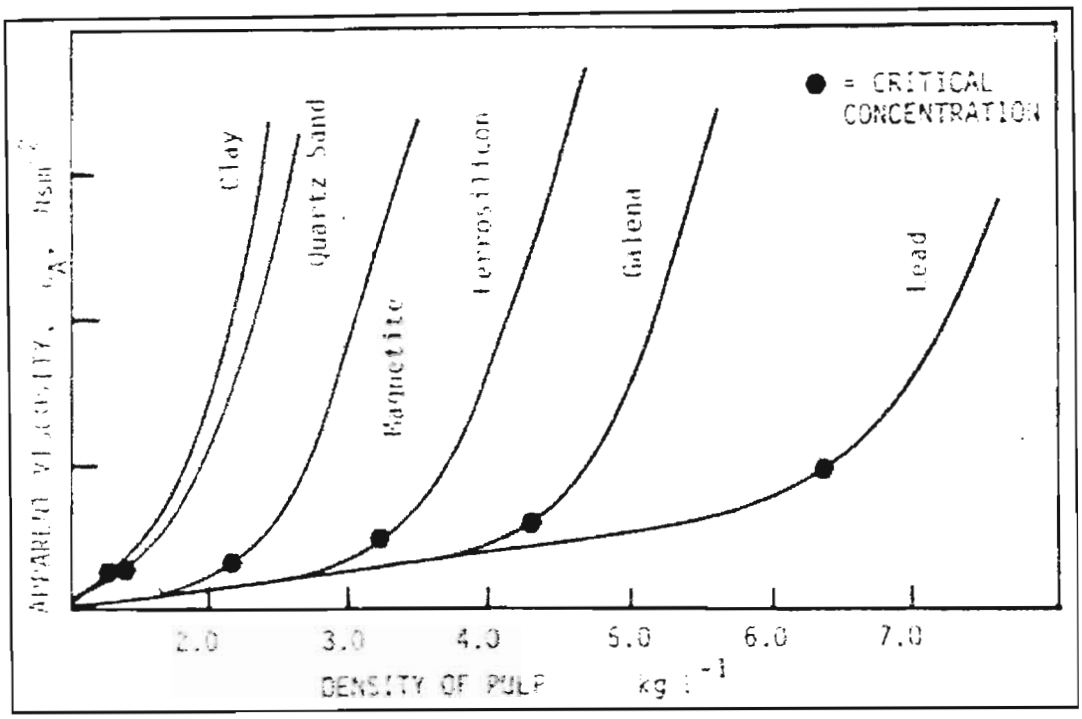

Figure 2. 2 Effect of pulp density upon apparent viscosity for various suspended medium [Burt (1984)]

Despite the fact that ferrosilicon media are more costly compared to magnetite media, they are still used to maintain suspensions at high specific gravities because of the much higher viscosity and stability problems associated with magnetite suspensions at the same specific gravities. These much higher viscosities reduce the separation efficiency of fine ores and near specific gravity material. The reduction of magnetite suspension viscosities at these high specific gravities can be achieved through the use of coarser magnetite media compared to ferrosilicon media at the same specific gravities [Collins et al. (1983)]. The main problem associated with the use of a coarser medium is the increase in the settling rate of the medium. To alleviate this problem fine media or slimes would have to be used together with the coarse media to reduce the settling rates of the media. Alternatively, the viscosity can be reduced by using dispersants. There are a great variety of dispersants which may be used, such as: alkali phosphates; sodium silicate; ethylenediaminetetracetic acid; surface active agents, such as lignosulphonates and petroleum sulphonates [Aplan et al. (1964)]. The chemistry and nature of surface active agents will be detailed in a later section.

Viscosity may be defined as the resistance to flow of a liquid. In the previous section the different types of flow behaviour of fluids were defined. Fluids can either show Newtonian behaviour or non-Newtonian behaviour. Heavy medium suspensions usually show non-Newtonian behaviour; being either Bingham plastic, shear-thickening, or shear-thickening.

Bevilacqua et al. (1999) did a study on the rheology of low density suspensions in dense medium separation of post-consumer plastics. Although the paper dealt with the separation of plastics, the rheological and performance data obtained were found to be very similar to the dense medium separation of coal. The dense medium solutions were prepared using clays at different size distributions. They found that between a shear rate 0–300 s^{-1} the rheological behaviour was pseudo-plastic with yield stress (Bingham plastic). As the size distribution varied, suspensions containing a higher percentage of fine material showed higher yield stress values.

As mentioned previously, there are two types of commercial ferrosilicon solids available in industry; milled and atomised ferrosilicon. Ferrara et al. (1986) found that ferrosilicon suspensions behaved like Newtonian fluids at low densities (pseudo-Newtonian behaviour). They also found that by increasing the density and the degree of contamination of the suspensions (e.g. with clay) the yield stress value increased. Collins et al. (1974) found that ferrosilicon suspensions show pseudo-plastic characteristics at low shear rates, and dilatant characteristics at higher shear rates. An increase in the density of the media resulted in an increase in the dilatant behaviour of the suspensions. This critical value of pulp density for the atomised grades was shown to be much higher than for the milled grades.

Shi et al. (1996) simulated slurry rheology as a function of slurry properties to illustrate the nature of the effects of solids concentration and particle size on rheology. The simulated rheological behaviour tallied well with many observations from industrial grinding slurries. The results showed that at low solids concentration (15 % solids by volume), slurries behave as dilatant fluids. Increasing the fines content leads to an increase in the dilatant trend, and also the development of a yield stress. At intermediate solids concentration (30 % solids by volume), and relatively coarse size, the flow exhibits the characteristics of a classic Bingham plastic. However, at an intermediate density with a high content of fines, the dilatant trend is still present. As the slurry density increases to 45 % solids by volume and the fines content increases, all slurries behave as pseudo-plastic with a yield stress. The higher the fines content of the slurry, the more apparent is the pseudo-plastic trend. The following conclusions were drawn from their study:

- When slurries contain relatively low solids concentration and high contents of fines (typically less than 42 % solids by volume and more than 25-35 % -38μm e.g. tertiary mill or regrind mill discharge slurries), their rheological character is likely to be dilatant.

- When slurry densities are increased and the amount of fines content is reduced (e.g. 44-58 % solids by volume and less than 20 % -38μm), the slurries are likely to exhibit pseudo-plastic characteristics.

- Increasing either fines content or slurry density leads to increased yield stress for both dilatant and pseudo-plastic flows.

Klimpel (1982) also found that many coals and mineral slurries exhibit dilatant character at relatively low slurry densities (less than 40-45 % solids volume for typical size distributions). He also found that increasing the slurry density increases the trend towards pseudo-plastic behaviour.

In some industrial processes ferrosilicon and magnetite are not used separately to make up the medium, but different combinations of the solids are used. The ratio of ferrosilicon to magnetite is largely governed by the medium specific gravity required. For specific gravities greater than 3.0 Ferrosilicon is largely employed on its own. Dilution with magnetite largely takes place at specific gravities below 3.0. Combinations of ferrosilicon and magnetite result in changes in the flow behaviour of the resultant medium compared to that of the individual solid media. Collins et al. (1983) performed experiments on different ratios of ferrosilicon and magnetite solutions. They found that pure ferrosilicon solutions showed Newtonian behaviour at low densities and low shear rates, and pseudo-plastic behaviour at high shear rates for either high or low densities. Mixtures of ferrosilicon and magnetite were found to be essentially pseudo-plastic at low magnetite levels (□25 % magnetite), but showed Bingham plastic conditions at higher levels (□50 % magnetite). The yield stress of the medium was observed to increase with an increase in the magnetite content. Aplan et al. (1964) attributed this yield stress to the increase in finer material due to the addition of magnetite. They showed through size distribution curves that magnetite media contain about 20 – 30 % more finer material than ferrosilicon media.

Laskowski et al. (1999) stated that the rheological properties of magnetite suspensions are mainly controlled by solid content (medium density), particle size distribution, particle shape, clay

contamination and demagnetization. Magnetite suspensions, even when fine, have been observed to be very unstable. As will be shown later in this section, this poses severe problems for rheological measurements and requires the use of specially designed viscometers. It has been observed that magnetite suspensions display non-Newtonian behaviour. The rheological behaviour of these suspensions is a function of shear rate and exhibits pseudo-plastic characteristics at low shear rates (up to about 300 s^{-1}) and dilatancy at high shear rates [Laskowski et al. (1999)].

Increasing the medium density has a drastic influence on the medium rheology. An increase in medium density results in an increase in the solid content of the medium i.e. an increase in solid volume percentage. This results in an increase in particle-particle interactions (friction and collision), thereby increasing the viscosity of the suspensions. Collins et al. (1983) indicated that on a semi-log plot the relationship between apparent viscosity and magnetite content is linear.

Stability is a property of the suspension considered as a non-homogeneous two-phase system and is related to the rheology of the solid phase in an environment constituted by the liquid phase. The relative movement of the solids in the liquid phase under mass and surface forces determines the suspensions degree of homogeneity, an important medium property in heavy medium separations. Medium stability determines the density gradient of the medium in the separation zone and thus influences separation efficiency [Bozzato et al. (2000)]. Therefore, it is one of the most important parameters to keep under control.

2.2.1 Effect of particle size / size distribution

Table 2.2 shows the different size distributions of milled and atomised ferrosilicon media used in heavy medium separations.

Table 2.2 Size range consistency of some typical ferrosilicon media [Burt (1984)]

Name Size μm	65D milled wt%	100D milled wt%	150D milled wt%	270D milled wt%	Normal fine atomized wt%	Cyclone 60 atomized wt%	cyclone 40 atomized wt%
+210	1	-	-	-	1	-	-
-210 +150	2	-	-	-	7	-	-
-150 +105	5	1	1	-	10	2	-
-105 +74	12	4	1	-	15	5	2
-74 +44	35	30	23	10	10	22	20
-44	45	65	75	90	45	73	90

Ferrosilicon and magnetite media used in the preparation of heavy medium suspensions are available in different size distributions. Sizing for quality control is carried out by conventional screening down to 38 μm and by sub-sieve methods, thereafter by cycloning methods to about 5 μm [Collins et al. (1974)]. The size distributions of the media taken from heavy medium circuits have been found to be well represented by the Rosin-Rammler distribution:

$$W_R = 100e^{(x/a)^b} \tag{2.5}$$

Equation 2.5 can be linearized as follows;

$$\ln\ln\frac{W_R}{100} = b(\ln x - \ln a) \tag{2.6}$$

Where W_R = % mass retained,

x = size (determined by nominal aperture), and

a, b = constants.

By plotting ln ln (W_R/100) versus ln x a straight line is obtained with a gradient equal to 'b'. The characteristic size distribution is generally defined as the size at which x = a. This results in $W_R = 100e^{-1} = 36.8$ % [Wills (1997)]. It is also important to note that for Equation 2.6 to have real roots, the value of x should be greater than that of the constant a.

It has been found that for ferrosilicon size distributions, the linear correlation for straight lines fitted in this way is normally close to ideal. The ability of FeSi size distributions to be represented in this way is extremely useful both for specification purposes, and in the evaluation of research and plant tests [Collins et al. (1974)].

The size distribution of any media chosen for application in heavy medium separations has a direct influence on the viscosity and stability of the media. For a constant dense medium specific gravity, a coarser media type reduces the stability and viscosity of the media. Conversely, using a finer media type increases both the stability and the viscosity of the media. Aplan et al. (1964), using size distribution curves, showed that samples of commercial ferrosilicon contained less fine material than magnetite. The finer media is known to be more viscous at higher suspension gravities, giving ferrosilicon suspensions an inherent advantage over magnetite suspensions at higher densities. Collins et al. (1983) also found that the viscosity of pure ferrosilicon suspensions is much lower than that of pure magnetite suspensions, or ferrosilicon - magnetite suspensions at constant volume concentrations. They attributed this to the effect of particle shape and size range of the magnetite relative to ferrosilicon. Grobler et al. (2002), using ferrosilicon media, also showed that increasing the amount of fines content in the media resulted in an increase in the viscosity of the ferrosilicon suspensions.

He et al. (1994) performed some experiments to determine the effect of dense medium properties on the separation performance of a dense medium cyclone. They used four magnetite samples, which covered a broad range of particle size distributions. They showed that the separation efficiency was highly dependant on media particle size. They found that viscosity and stability of the suspensions increased as the media size distribution became finer. With coarser magnetite, they found that the stability of the suspensions was too low at low specific gravities, resulting in low separation efficiencies. The stability improved as the specific gravity of the suspensions increased.

However, the presence of fine material in heavy medium suspensions results in a more stable suspension. Collins et al. (1983) define the stability of as the reciprocal of the settling rate. That is, a low settling rate corresponds to a high stability. The fine material can be used to improve the stability of the medium by reducing the settling rate of the medium particles. Grobler et al. (2002) also showed that particle size distribution affected both the viscosity and stability of heavy medium suspensions. They did tests using ferrosilicon suspensions with different size distribution: 41 % less than 45 μm; 35 % less than 45 μm; 29 % less than 45 μm; and 23 % less than 45 μm. They found that as the particle size distribution decreased, there was an increase in the stability of the suspensions. The stability of suspensions containing particles with 23 % less than 45 μm was found to be more than double that of particles with 41 % less than 45 μm.

As will be shown in Chapter 4, the two types of heavy medium separators can be classified under Static Separators, or Centrifugal Separators. The type of separator used gives an indication of the size distribution of the medium to be used. Static separators use gravity to separate the ore particles, and are generally governed by Stoke's Law. This means that the media used should be of low viscosity and moderate stability. Hence, for gravity separators a coarser media range should be used. However, high g-forces prevail in centrifugal separators, demanding higher medium stability and low viscosity. The high stability is obtained by using a fine media range. This results in high viscosities as well, and as will be shown later, the viscosity can be reduced by the use of surface active chemical agents which reduce the viscosity without compromising the high stability of the media.

2.2.2 Effect of particle shape

The effect of particle shape is best illustrated by comparing the difference in rheological properties of milled ferrosilicon and atomised ferrosilicon. Milled ferrosilicon are rough and angular in shape, whereas atomised are largely spherical or rounded in shape. The inter-particle slippage of the particles affects the viscosity of the media. Aplan et al. (1964) and Collins et al. (1974) have shown that the viscosities of suspensions comprised of atomised ferrosilicon are significantly lower than those of milled ferrosilicon, owing to the greater friction of collision of the irregularly shaped milled particles, which requires a larger energy input to achieve a given deformation of the suspension. The spherical or atomised ferrosilicon solids present the best chance for inter-particle slippage, and are thus less viscous. On the other hand, grades of milled ferrosilicon show greater stability than grades of atomised ferrosilicon of equivalent size analysis.

It has been reported by Ferrara et al. (1986) that while the size distribution of the spherical particles is similar to that of the milled or ground form, the suspensions formed tend to be less viscous at higher specific gravities. This superior property of atomised ferrosilicon allows very high pulp specific gravities to be obtained (up to 3.8), which has made possible the separation of ores that were not previously amenable to be treated. In general, it is not usual to use milled ferrosilicon at a medium specific gravity in excess of 3.0. Collins et al. (1974) show that, for ferrosilicon manufactured in South Africa, viscosity and stability increase with both the fineness of the ferrosilicon and pulp specific gravity. However, the viscosity of atomised ferrosilicon was found not to be significantly dependant on the fineness of the media. Hence, if a more stable suspension is required at a particular viscosity, it is necessary to use a grade of atomised ferrosilicon that is finer than that of the milled ferrosilicon that might be used under the same conditions.

Corrosion resistance of the solid particles plays an important role in the manufacture of ferrosilicon powders. The inclusion of 14-16 % Si in the alloy results in a relatively high resistance to corrosion, or rusting. The finely divided products of corrosion tend to increase the viscosity of the medium, impairing the separating efficiency of the process. Corrosion is a surface phenomenon which results from the electrochemical oxidation of the ferrosilicon surface to produce non-magnetic iron oxides [Collins et al. (1974)]. Under static conditions a passive layer is rapidly built up on the surface, preventing the progress of further corrosion. Under plant conditions this passive layer is continually being removed by abrasion, accelerating the corrosion process. The irregularly shaped milled ferrosilicon particles have a greater surface area than the rounded atomised ferrosilicon particles, and are therefore more susceptible to rusting. In addition, the sharp points and crevices of the milled particles make ideal nucleation points for the corrosion process. The resistance to corrosion of the atomized ferrosilicon solids is extremely high owing to a passivity imported to them during the quenching process during their manufacture.

2.3 Rheology modification of heavy medium suspensions

Once a particular material has been chosen for the heavy medium separation process, the rheology of the media can be modified through the following ways:

1) Addition of slimes or clays.

2) Addition of polymeric compounds or other reagents.

3) Demagnetisation of the circulating medium.

Before discussing the different ways of modifying the rheology of the medium, some properties of clays / talc's and water will be briefly discussed.

The dispersing liquid in almost all industrial applications of DMS is water. Thus, the properties of water in relation to its solid – liquid interaction are of considerable importance. The unique properties of water include its ability to form hydrogen bonds, and its ionizing solvent power. It can dissolve and ionize more salts than any other solvent. Liquid water has a three dimensional structure of infinitely extending networks of anions and cations. Each cation is screened by two anions (the coordination number is 2), and each anion is tetrahedrally surrounded by four equidistant cations. In order to understand the fluidity of water one has to realize that the above picture of its structure is a description of the location of the protons over a time average. The protons can change their positions without losing screening, which means that they temporarily submerge in the electron cloud of the two O^{2-} ions so that only over a time average do the protons assume positions which are equidistant from both O^{2-} [Eirich (1960)].

The viscosity of water is determined to a large extent by the mobility of the protons in its three-dimensional structure. It is also one of the anomalous properties of water. The structural picture which describes water as a three-dimensional network of ions suggests that water should be rigid. However, the fluidity of water is abnormally high due to the mobility of the protons. Conditions which increase the tendency of the electrons to remain within the electron clouds of O^{2-} ions, and change water from a three-dimensional network of ions towards an aggregate of molecules lower its viscosity e.g. applying pressure to water decreases its volume and increases the electron cloud density of the O^{2-} ions, favouring the interpenetration of the protons into the electron cloud. Thus,

water, unlike other fluids, becomes more fluid under pressure. For charged particles in water, the field strength of the particles determines the mobility of the protons in the water molecule. Particles with a high surface charge density (e.g. clays and talc powders) immobilize the protons, favouring the three-dimensional structure such that the viscosity of the water is increased.

The structure of all clay minerals consists essentially of mica-like layer lattices in which the ultimate building units are silica, alumina and water, frequently with appreciable quantities of iron, alkalis, and alkaline earths. In general the term clay implies a natural, earthly, fine-grained material which develops plasticity when mixed with a limited amount of water. What all clays have in common is that they are 'infinitely extending' networks only in two dimensions. Thus, the minerals consist of stacks of sheets. On account of this structural characteristic, clay minerals occur as anisodimensional, either thin plates most less than 2 microns in diameter, or as elongated tubes and lathes [Eirich (1960)].

When minerals are comminuted or liberated from their ores, suspensions of fine (1μm) or colloidal particles generally result. Such small particles are generally small enough to be unaffected by gravity and as a result; their interactions with each other and other larger particles are controlled by a range of attractive and repulsive inter-particle forces [Johnson et al. (2000)]. There are a number of forces influencing the interaction of colloidal particles. The magnitude and nature of these interactions can be controlled by manipulation of a range of experimental parameters. These include (but are not restricted to) the particle size, the solution pH, the nature and concentration of simple electrolyte ions, and the addition of other soluble and/or surface-active species including surfactants, polymers and electrolytes.

The addition of small quantities of ore slimes or clays has been found to increase significantly the viscosity and stability of DMS suspensions. In some cases the slimes represent an undesirable constituent of the ore being treated, and a proportion of the circulating medium has to be continuously removed and cleaned through magnetic separators. Laskowski et al. (1999) states that the nature of the clay contaminant has a profound effect on the viscosity increase of magnetite suspensions. They found the viscosity rise was greater with montmorillonites than with kaolinite and also that sodium montmorillonites caused a higher rise in the viscosity than did calcium variety. Aplan et al. (1964) performed experiments to find the effect of manganese ore slimes, bentonite (sodium montmorillonites), and kaolinite on the viscosity of ferrosilicon media. They found that the addition of 10 % manganese ore slimes changed the viscosity profile of

atomised ferrosilicon to one nearly identical to an uncontaminated, milled ferrosilicon suspension. They also showed that bentonite is about five times as effective as kaolinite in increasing the apparent viscosity of atomised ferrosilicon suspensions.

Grobler et al. (2002) did tests to investigate the stability of ferrosilicon suspensions. They showed that particles smaller than 45 μm, and especially the ore fines, played an important role in the settling behaviour of the solids. The ore slimes they used for their tests contained mainly hematite (78%), silica (12%), and alumina (9%), and had a size distribution of 70 per cent smaller than 10 μm, with 34 per cent smaller than 1 μm. Tests were performed by adding 2 % and 5 % slimes. The stability of the suspensions increased with the amount of slimes added. At 5 % slimes content, the stability of the suspensions was more than double that at 0 % slimes content. They also observed an increase in viscosity with slimes content. They attributed this to the fact that slimes or contaminants have a lower density than ferrosilicon particles; a contaminated medium will thus need to contain a higher solids concentration to achieve the same density. A higher solids concentration will result in a much higher resistance to flow. High amounts of certain types of clays, particularly bentonites, exhibit thixotropic behaviour. This means that at certain clay contamination levels, the behaviour of the suspensions could vary. This could have a significant effect on the rheological properties of the contaminated suspensions, and on the separation efficiency.

2.3.1 Surface forces acting between colloids/clays in aqueous media

The effect of the different slime contaminants is dependant on the type of inter-particle forces occurring within the medium. There are a number of forces acting between colloidal particles, and these are discussed below. Only the forces considered relevant to the project will be briefly discussed in this section. Further details on these and other forces can be found in Johnson et al. (2000).

2.3.1.1 Van der Waals forces

Van der Waals forces occur almost everywhere within colloidal systems, and are caused by the interaction between instantaneous dipoles generated within the atoms comprising each particle. On a microscopic scale, atoms are non-polar in nature, but dipoles are formed through the

displacement of the centre of the electron cloud relative to that of the positive nucleus. Each dipole formed then induces instantaneous dipoles within atoms in neighbouring particles. Van der Waals forces are independent of conditions such as the system pH and the presence of surfactant and polymeric species. These forces have, however, been shown to be strongly dependent on the particle size, as shown by the following equation:

$$F_{VAW} = -\frac{aA_H}{12H^2} \qquad (a >> H) \tag{2.7}$$

F_{VDW} = Van der Waals force, a = particle radius, H = distance between adjacent particles, and A_H = a materials property termed the Hamaker constant.

2.3.1.2 Electrical double layer forces

When mineral particles are brought into contact with an aqueous environment they often acquire a substantial surface charge. This can occur through either through specific ion adsorption, isomorphous ion substitution, or differential ion dissolution and ionisation of surface sites. This process is of particular relevance to oxide minerals (e.g. Fe_3O_4), and involves the protonation / deprotonation of surface hydroxyl sites (M-OH) via the following process:

$$H_2O + M - O^- \underset{OH^-}{\overset{H^+}{\Leftrightarrow}} M - OH \underset{OH^-}{\overset{H^+}{\Leftrightarrow}} M - OH_2^+ \tag{2.8}$$

where H^+ and OH^- are referred to as the potential determining ions.

The experimental parameters which can be used to modify electrical double layer forces are changing the suspension pH, addition of charged surface –associating species to the suspension, controlling and regulating the type and quantity of electrolytes present n the suspension, and changing the particle size.

2.3.1.3 Structural ('hydration') forces

When two particles interacting across an aqueous medium are brought into close proximity, a short range repulsive force is often observed. This interaction is believed to be related to the presence of a strongly surface-associated layer of water on each of the particle, and is enhanced when the surface posses a strong hydrogen bonding ability. The strength and range of repulsion of these forces can be manipulated through the control and type of electrolytes in solution. In addition, however, the nature of the particles (and their affinity for solution electrolyte ions) can also be controlled through both pH-induced changes to the surface charge and adsorption of other ions, polymers or surfactants from solution.

2.3.1.4 Steric and electrosteric forces

As mentioned, the rheology of mineral suspensions can be altered by the use of surface active agents to either reduce or increase the viscosity and stability of the suspension. These surface active agents are usually polymers of varying lengths. The interaction behaviour observed when two surfaces bearing layers of adsorbed polymers are brought together is often substantially different to that noted for rigid, smooth surfaces. In particular, a steric repulsion is generally measured when surfaces coated with a stable polymer approach to a separation less than twice the thickness of the polymer layer. This force is believed to result from two separate effects; a rise in osmotic pressure caused by the increased concentration of the polymer layers between the surfaces, and an elastic force due to compression of the polymer layers. Practically, Steric and electrosteric forces in mineral suspensions can most readily be manipulated by controlling the type, size and concentration of the adsorbed species used to effect dispersion.

2.3.2 Surface active agents

There are two important mineral process used for the separation of solid particles from a suspension; gravity concentration and floatation. The preparation of slurries for each of the above processes occasionally requires the use of surface active agents to improve the separation efficiency. As previously mentioned, gravity concentration uses gravity or centrifugal forces to separate dense particles from less dense particles. The slurry used in this application, particularly in heavy medium separations, should have a low viscosity and moderate - high stability. This type

of separation suits a dispersed suspension where the particles in the medium do not show a tendency towards agglomeration. Floatation on the other hand requires the solution to show a tendency towards sedimentation through the agglomeration of the particles in the medium.

The process by which particles in solution either become dispersed or agglomerate is believed to be due to the zeta potential of the medium particles and fine contamination particles. For example, Jones et al. (1999) showed the effect of zeta potential on the type of agglomeration in aqueous silica – iron oxide slurries. The presence of small quantities of iron oxide, particularly if the particles are small, causes co-agglomeration with silica particles into flocs. The interaction occurs because the zeta potential of iron oxide is positive and that of silica is negative at neutral pH. Thus there exists a net attractive force between their respective particles. These flocs also retain a portion of the continuous phase, which effectively increases the apparent solids volume fraction, and the viscosity of the suspension becomes very high. As the flocs are sheared they break into smaller aggregates, releasing some of the retained fluid, which decreases the apparent volume fraction. The viscosity consequently decreases until a point is reached when no more floc structure exists and the particles move freely in the slurry. The formation of this structure on resting gives rise to an apparent yield stress, and the breaking down of this structure leads to shear thinning behaviour, both these effects being caused by particle – particle interaction. These conditions are depicted in Figure 2.2.

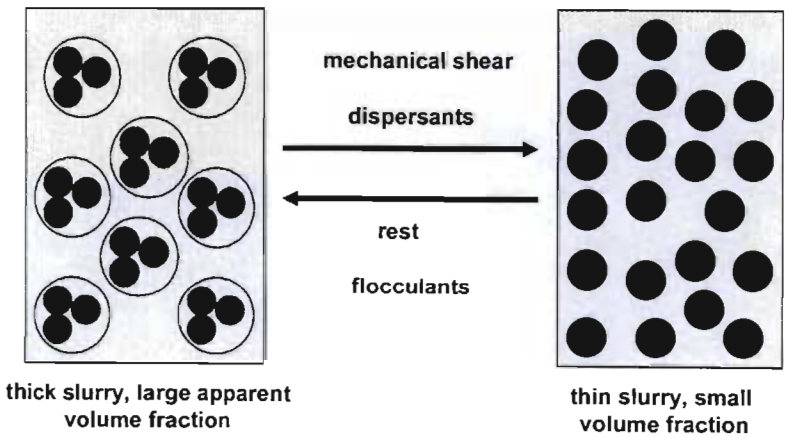

Figure 2.3 Mechanism of shear thinning behaviour [Jones et al. (1999)]

For heavy medium suspensions a well dispersed suspension, either contaminated or uncontaminated, is required. As mentioned before, the increase in viscosity of a contaminated suspension is caused by the interaction of the contaminants with the solid particles of the suspension. The increase in apparent volume caused by the particle – particle interaction results in an increase in the suspension viscosity. There are two ways in which the viscosity of the suspension can be reduced:

1) Dilution with water in order to retain moderate solids volume concentration.

2) Use of surface chemical agents which reduce the particle – particle interaction of the suspension.

Dilution commonly occurs through addition of make-up water to the suspension, and since water is an expensive commodity and because it also alters the suspensions density, the latter method of reducing viscosity with the aid of surface active agents has become the most widely used, and has been a main focus of research. For the silica – iron oxide slurries reported by Jones et al. (1999), sodium tripolyphosphate was used as the chemical dispersant. Sodium tripolyphosphate selectively binds to the iron oxide particles and because the polyphosphate is a multi - charged anion, the surface charge of the iron oxide becomes negative and the interaction with silica particles is destroyed. In general, viscosity modifiers which act as drag reducing agents are polyionic negatively charged species. The viscosity modifiers alter the particle – particle interaction and hence the yield stress rather than the actual high shear viscosity, although there is a decrease in apparent viscosity. While stable, well dispersed systems may display Newtonian behaviour, aggregated suspensions exhibit pseudo – plastic behaviour with a Bingham yield stress.

Using coal suspensions, Laskowski et al. (1992) provided an instructive example illustrating dispersion in industrial applications. They showed that hydrophobic coal particles become completely hydrophilic in the presence of clays which form a 'slime coating' on coal surfaces. Coal hydrophobicity could be restored by simply adding a dispersant, sodium hydrogen phosphate. Both the coal and clay particles were found to acquire more negative zeta potential values in the 50 – 100 gm^{-3} sodium hydrogen phosphate solutions. This is an example of electrostatic stabilization; the specific adsorption of phosphate anions increases the negative charge of the coal particles, bringing about strong coulombic repulsion which keeps the clay

particles apart from the coal surface, thereby restoring the natural floatability of coal [Laskowski et al. (1992)]. This example illustrates very well the slime coating phenomenon which is usually observed in the presence of colloidal particles (e.g. clays and talc powders).

While dispersants definitely lower the apparent viscosity of a suspension, according to Aplan et al. (1964) their use leads to a substantial increase in the settling rate, or a decrease in the stability of the suspension. They studied the rheological properties of ferrosilicon suspensions purposely contaminated with slime constituents and found that under proper conditions it is possible to have both a very stable suspension and a low viscosity. For atomised ferrosilicon suspensions with a specific gravity of 3.3, purposely contaminated with manganese ore slimes, sodium hexametaphosphate (calgon) was used as the dispersing agent. They found that between 0.01 and 0.03% (w/w) calgon additions a very stable media is obtained, and the apparent viscosity is essentially at its lowest value. However, if the dispersant concentration is increased above 0.03% in this instance the ferrosilicon suspension suddenly is no longer stabilized, and very high settling rates are observed. Typical viscosity reducing agents used for ferrosilicon suspension are given in Table 2.3.

Surface active agents can either be ionic or non-ionic polymers. The ideal structure of a polymer is one that combines the advantages of anionics and nonionics. This enables the polymer to perform satisfactorily over wide variations in temperature, salinity, and pH [Valentyik (1976)]. Such polymers show very little adsorption on the common minerals and hence polymer consumption is minimized. Most of the chemical dispersants shown in Table 2.3 are anionic polymers. Anionic polymers generally show superior performance compared to nonionic polymers. The main disadvantage associated with using anionic polymers is that they are usually adversely affected by salt, elevated temperatures, and high or low pH.

Table 2.3 Viscosity reduction of slime contaminated heavy media suspension with various chemical dispersants [Aplan et al. (1964)].

Suspension	sp.gr	Apparent viscosity of uncontaminated Suspensions of this specific gravity	Reagent	Apparent viscosity, Pa.s, at various addition levels (% by w solids) 0	0.01	0.016	0.025	0.05	0.1	0.18	0.5
Spherical FeSi with 1% bentonite	3.6	0.11	Calgon	1.70	1.42			1.24		0.85-0.90	
Spherical FeSi with 10 % manganese ore slimes	3.3	0.07	Calgon	0.38	0.26	0.19		0.18			
Spherical FeSi with 10 % manganese ore slimes	3.3	0.07	Daxad*	0.35				0.28	0.25		0.18
Spherical FeSi with 10 % manganese ore slimes	2.9	0.04	Calgon	0.24	0.17		0.12	0.06		0.06	
Spherical FeSi with 10 % manganese ore slimes	2.9	0.04	Trisodium phosphate	0.24	0.24		0.24	0.19		0.08	
Spherical FeSi with 10 % manganese ore slimes	2.9	0.04	Sodium silicate	0.24	0.21		0.18	0.15		0.07	
Ground FeSi with 10% Kaolinite clay	2.8	0.10	Daxad*	0.54	0.30			0.18			
Ground FeSi with % Talc	2.8	0.10	Daxad*	0.65	0.34			0.28			

*Daxad 11 KLS is a sulphonated naphthalene formaldehyde condensate

Laskowski et al. (1999) also discusses the effect of chemical additives (organic and inorganic) on the rheology of heavy medium suspensions as observed by others. The general effect of these modifiers (polyethyleneoxides, polyvinylalcohol, carboxymethyl cellulose, guar gum, dextrin, sodium alginate, lignin, hydrolysed ployacrylamide and sulphonated polystyrene), as claimed by others, is to reduce the yield stress rather than the plastic viscosity. However, some results seemed to indicate that the addition of polymer modifiers resulted in an increase in both yield stress and plastic viscosity. The increased stability of the media was attributed to the increased yield stress, which resulted in an infinite viscosity in the case of settling small particles (medium particles), and relatively low viscosity for large pieces of rock, allowing them to move freely in the fluid. An opposite conclusion was reached by other workers, after conducting a series of experiments to investigate the effect of polymer modifiers and found that both viscosity and yield stress decreased initially with increasing polymer dosage, until a plateau was reached.

Tests conducted by Valentyik (1976) on the rheological properties of heavy media suspensions stabilized by polymers showed that the viscosity of heavy medium suspensions could be controlled through the use of low cost additives which lower viscosity while retaining a favourable low settling rate. The rheological properties of polymers are such that they present an infinite viscosity to small particles and relatively low viscosity to large particles, allowing them to move freely in the fluid. Polymer solutions have been shown to exhibit shear thinning properties. It is this shear thinning characteristic that contributes so greatly to the suspending properties of polymers. The solution structure is sufficient to prevent fine particles from settling, yet these solutions show little resistance to flow. The viscosity of certain polymer solutions is also significantly increased through a mechanism of crosslinking, which further increases their power to suspend media solids without affecting the movement of large particles. This improves the operation of heavy medium separations by reducing media losses and cheaper grinding costs because coarser media solids can be used. The control of heavy media plants is also improved through easier start-up and good pumping characteristics. The aim of the investigation was to see whether the using of clays as a stabilizing agent could be replaced by using polymers instead. The chosen polymer for their investigations was Xanthamona Carbohydrate (Kelzan XC). The heavy media constituents used were magnetite, magnetite-ferrosilicon in 50/50 ratio, and ferrosilicon alone. For all the three types of media tested, there was a considerable improvement in the viscosity of the suspensions with very small amounts (less than 0.1%) of polymer addition. They found that there was a maximum attainable stability for given medium specific gravity beyond which flocculation took place, and this was characterized by a faster settling rate. This result showed that there was no practical advantage gained by adding polymers in quantities larger than 0.1%, except for medium specific gravities less than 2.0.

Valentyik et al. (1976) performed experiments to compare the rheological properties of heavy media suspensions stabilized by polymers and bentonite clays. Their work was a continuation of the work presented by Valentyik (1972). The heavy media constituents used were magnetite and ferrosilicon in four size ranges: 65 to 100, 100 to 150, 150 to 270, and 270 to 500 mesh. The polymer used in this investigation was also Xanthamona. Their results showed that there is clearly an advantage in using polymers compared to conventional clays. For instance, for a given settling rate, any addition of an amount equal to 0.01 - 1.00%, the plastic viscosity or yield stress values are always lower for polymer-supported media. They also found that the plastic viscosity increased slowly for polymer-supported media than for clays. This is due to the lower polymer concentrations required, since polymers dissolve and are not suspended in the solution. The

advantage of using polymers over conventional clays means that more accurate and efficient separations are possible as apparent viscosities encountered by particles are much lower.

2.3.3 Effect of demagnetisation

Commercial heavy media are generally magnetic (e.g. ferrosilicon and magnetite) to allow simple recovery and regeneration processes. In heavy medium separation plants passage through magnetic separators in the medium recovery circuit induces a residual magnetisation which causes flocculation or aggregation of the magnetised particles. This agglomeration results in an increase in the apparent solids volume concentration. Agglomeration also retains part of the suspension in the formed flocs, reducing the amount of free suspension or the continuous phase in the medium. This effect generally increases the medium viscosity. The effect can be minimised by demagnetising or depolarising the medium after magnetic recovery.

In practise, the control of medium viscosity in heavy medium separation plants is seldom carried out. Instead it is more usual to manage viscosity by selecting the operating conditions which will limit it to an acceptable range based on previous experience. These operating conditions include selection of the correct medium grade (size distribution and shape); control of medium density; minimisation of contamination through efficient feed preparation (sometimes the presence of slimes is tolerated because of their stabilization effect); and installation of demagnetisation coils in the plant.

Napier-Munn et al. (1990) studied the effect of demagnetisation on medium viscosity in a dense medium cyclone plant. The plant utilised 400 mm cyclones at a medium-to-ore ratio of 9:1, gravity fed with an 8 m head. Two separate measurements were made: firstly, the effect of demagnetisation was demonstrated by monitoring the medium viscosity in one circuit for an 8 hour period in which the demagnetizing coil was switched on then off again; secondly, the effects of contamination were studied by monitoring viscosity as a function of density. The results showed that the apparent viscosity decreased when the coil was switched on, and increased to its normal values after the coils were switched back off again.

The design of the coil with regard to attenuation characteristics and field strength is of considerable importance. It is believed that there is an inverse relationship between the coil strength and the viscosity of the circulating medium in heavy medium circuits. In general,

atomized ferrosilicon is believed to require a field strength for demagnetization that is four times higher than that for milled ferrosilicon. In the above mentioned case, Rodis et al. (1960) found, through laboratory tests, that atomized ferrosilicon can be more intensely magnetized than the milled grade. Hence, the capacity of the magnetizing coil can be decreased in order to achieve the same effect.

2.4 Modelling Slurry Rheology

It is industrially important to understand how alterations in slurry properties lead to changes in the rheology of a suspension. A quantitative correlation for rheology in terms of slurry properties is thus important because it can be used to predict process performance from simple slurry properties. Rheology modelling also becomes important in cases where certain rheological measurements cannot be made. For example, in hydrocyclones it is difficult to know the rheological properties of the suspension within the cyclone. The properties of the suspension are simulated from equations derived from independent experimental measurements.

Rheology modelling begins with the establishment of rheological equations of state corresponding to the behaviour of fluids. There are basically two stages in the development of fluid dynamics theory. The first stage is represented by the classical approximation of the "ideal" or "perfect" fluid. This is an imaginary fluid, considered to be incompressible and devoid of viscosity. Since the fluid is frictionless, shear stresses within the fluid are zero. These relationships have the disadvantage that they cannot be applied to real fluids, whether compressible or incompressible (within the limits of the experiment) but viscous. The introduction of the boundary layer concept made it possible to apply relationships derived for ideal fluids to real fluids, but only outside the boundary layer. It is assumed that the friction effect is generated within a relatively thin fluid layer adjacent to the solid surface and defined as the boundary layer. Flow outside the boundary layer is assumed to occur without friction, so that this portion of the fluid can be approximated in terms of an "ideal" fluid [Jinescu (1974)].

The second stage in the development of fluid dynamics theory consisted in establishing the principles of fluid dynamics for the simplest category of viscous fluids i.e. Newtonian fluids, whose flow behaviour can be expressed by a linear relationship between the shear stress and the shear rate of the suspension. However, industrially utilized fluids are not all characterized by a linear relationship between the shear stress and the shear rate. These types of fluids are called

non-Newtonian fluids, and it has become necessary to also establish rheological equations of state corresponding to the behaviour of these fluids.

A suspension is a representation of a heterogeneous material i.e. a disperse system of elastic or rigid particles in a liquid. The liquid represents the continuous phase of the suspension, and the solid particles the disperse phase. Calculation of physical properties involving suspensions is only possible if their physical properties are known. The study of suspensions dynamics imposes the determination of the rheological equations of state and the dependence of the coefficients of the equation on the concentration of the solid phase. The most widely used way to determine the behaviour of a suspension consists in establishing (based on experimental observation of its rheological behaviour) a mathematical model (a known rheological equation of state), following which the parameters of the equation are determined by measurements using an appropriate viscometer. In other instances the rheological behaviour of suspension is expressed in terms of empirical relationships which are valid only for the conditions of the experiment.

Generally, if the suspension continuous phase is a Newtonian liquid (e.g. water), the behaviour of the suspension is Newtonian for relatively small concentrations of solid particles. If a certain value of the solid-particle concentration is exceeded, the behaviour of the suspension becomes non-Newtonian. It follows that the value of the solid-particle concentration up to which the behaviour of the suspension is Newtonian depends on the nature, form, and dimensions of the solid particles. Industrially this value can differ for magnetite, milled ferrosilicon, and atomised ferrosilicon. For suspensions whose dispersion medium is a non-Newtonian liquid the suspensions exhibit a non-Newtonian behaviour at small concentrations of the solid phase, as well as at large concentrations. At small solid-phase concentrations, the non-Newtonian behaviour is due to the continuous phase. At relatively large concentrations of the solid phase, the non-Newtonian behaviour is accentuated by the effect of particle interaction. The rheological equations of state, as well as the viscosity expression of such a suspension, depend on the nature, shape, dimensions and concentration of the solid phase, the rheological nature of the liquid phase, and sometimes also on time. Table 2.4 summarizes various derived rheological equations of state.

Table 2.4 Rheological Models for heavy medium suspensions [Laskowski et al. (1999)]

Name	Model
Newton	$\tau = \mu.D$
Bingham	$\tau = \tau_{pl} + \mu_{pl}.D$
Ostwald	$\tau = K.D^n$
Herschel-Bulkley	$\tau = \tau_0 + K.D^n$
Casson	$\tau = [\tau^{1/2} + (\mu_c.D)^{1/2}]^2$

Where τ is the shear stress, τ_{pl} and τ_0 is the yield stress, μ is the suspensions viscosity, K is a constant, n is the flow behaviour index, and D is the shear rate.

2.4.1 The viscosity of spherical-particle suspensions

2.4.1.1 Suspensions with a small concentration of the solid phase

In this discussion suspensions having a small solid-phase concentration are those in which the solid phase occupies less than 10% of the total volume of the suspension. Einstein was the first person to publish an investigation in this area; based on the equations of hydrodynamics, the coefficient of shear viscosity was calculated for very dilute solutions. He hypothesised the following conditions:

1) The solid particles are hard and spherical in shape.

2) The mean distance is very large compared to the mean solid-particle size; the movement is slow, so that the kinetic energy of the solid particles is negligible.

3) There is no liquid slip relative to the particle surface.

4) The particle density is equal to that of the continuous medium so that there are no settling-out effects.

Based on these hypotheses, Einstein derived the following equation for the relative viscosity of a suspension:

$$\mu_r = \frac{\mu_s}{\mu} = 1 + 2.5\Phi \tag{2.9}$$

Where μ_s is the suspension viscosity; μ is the liquid phase viscosity; □ is the volumetric concentration of the solid phase:

$$\Phi = \frac{V_s}{V}, \text{ where } V = V_l + V_s \tag{2.10}$$

V_s is the volume of uniformly distributed solid particles, V_l is the volume of the liquid phase, and V is the total volume occupied by the suspension.

Equation 2.9 can be put in the following general form:

$$\mu_r = 1 + k_E\Phi \tag{2.11}$$

Coefficient k_E depends on a series of parameters which can be neglected in the case of real suspensions.

2.4.1.2 Suspensions with a high solid-phase concentration

Suspensions with a high solid-phase concentration are considered to be those in which the solid phase exceeds 10% by volume i.e. 0.1 < □ □ □$_{max}$. □$_{max}$ is the maximum attainable concentration and depends on the void fraction corresponding to a more or less compact arrangement of the spheres [Jinescu (1974)]:

$$\Phi_{max} = \frac{V_{s,max}}{V} = 1 - \varepsilon \tag{2.12}$$

Where □= V_o/V is the porosity, and V_o the void volume. The porosity depends on the particle-size distribution and uniformity.

For suspensions used in DMS the spheres are not equal in size, and □ can be determined experimentally from the following equation:

$$\varepsilon = 1 - \frac{\rho_v}{\rho} = 1 - \Phi_{max} \tag{2.14}$$

Where □$_v$ is the bulk density of the spheres, and □is the skeletal density.

The relative viscosity can be found from the Arrhenius relationship:

$$\mu_r = \exp(k\Phi) \tag{2.15}$$

Mooney (1951) also extended Einstein's equation for an infinitely dilute suspension of spheres to apply to a suspension of finite spheres. For a monodisperse system (i.e. a system having only one disperse phase) he obtained the following equation:

$$\mu_r = \exp\left(\frac{2.5\Phi}{1 - k\Phi}\right) \tag{2.16}$$

Mooney's analysis was limited to rigid, spherical particles. Also, his approach was partly empirical in that the interaction parameters were left for experimental determination, no effort being made to obtain their values from hydrodynamic theory. Mooney introduces the space-crowding effect of suspended spheres on each other. That is, in a two component system, for example, spheres of size r_1 and partial volume concentration □$_1$ crowd spheres of size r_2 into the remaining free volume 1-□$_{12}$□$_1$, where □$_{12}$ is the crowding factor. The Einstein viscosity equation postulates a suspension so dilute that there is no appreciable interaction between spheres. Mooney postulates that in extending the equations to higher concentrations, first order interactions must be taken into account. This interaction is described as essentially a crowding effect.

The modelling of slurry rheology can also be extended to include different types and size range of contaminants. Ferrara et al. (1990, 1992) considered the solid phase of the medium as made up of

by a binary blend of a magnetic component and a non-magnetic component. Two series of experiments were carried out using FeSi as the magnetic component, and two types of limestone as the non-magnetic contaminant. Under steady-state conditions, they supposed that the characteristics of the medium (chemical composition, size and particle shape) were constant. These assumptions lead to a two component model.

Using a semi-empirical model (Quemada model) as their basic model, the following expression was written for a two component system, comprised of a non-magnetic component (1) and magnetic component (2):

$$\mu = \mu_f(1-\square\square)^{-2} \tag{2.17}$$

Where:

$$\square = \square_1\square_1 + 2(\square_1\square_2)^{0.5}\square_1(1-\square_1) + \square_2(1-\square_2)^{0.5} \tag{2.18}$$

where $\square = 1/\square$; $\square_1 = 1/\square_1$; $\square = 1/\square_2$; $\square_1 = \square_1/\square$, the volume fraction of the non-magnetic component in the total solid; and $\square_2 = (1-\square_1)$, the volume fraction of the magnetic component in the total solid.

The above two equations are concerned with the rheological properties made up of a non-magnetic component (1) and a non-magnetic component (2). A major constraint for the above equations is the maintenance of a constant medium density. To maintain a constant medium density, $\square$ a variation in the content of one component should be compensated by an appropriate variation in the total solid phase composition. This is expressed by the following constraint relation:

$$\square = \square_f(1-\square) + (\square_1\square_1 + \square_2\square_2)\square \tag{2.19}$$

where $\square_f$, $\square_1$, and $\square_2$ are the fluid density, density of the non-magnetic solid, and density of the magnetic component, respectively.

The conclusions drawn from the experimental work, using ferrosilicon and two types of limestone as the non-magnetic contaminant (fine limestone 0.2 mm and coarse limestone in the size class -0.5mm+0.2mm) were:

- The results showed that the apparent viscosity of the tested suspensions depended mainly on the ratio of the volume occupied by the solid phase to the total volume of the medium and to a lower extent on the volume fraction of the non-magnetic component in the solid. The apparent viscosity decreased slowly as the shear rate was increased, indicating a pseudo-plastic behaviour of the tested samples.

- The results of the correlation were better for the fine limestone, compared with the coarser limestone. This was attributed to experimental errors which would have arisen from the lower stability of the coarser limestone.

- It was noted that the prediction capability of the model did not vary appreciably when using less experimental values for calculating the model parameters. This fact is very important for the practical use of the model in plant control.

Napier-Munn et al. (1996) modelled the rheology of slurries based on the output reading of a Debex on-line viscometer [Reeves (1985); Napier-Munn et al (1996)]

The Debex on-line slurry viscometer is rotated at a constant speed by a DC micrometer or stepper motor in a baffled cup. The retarding torque on the bobbin caused by the viscous resistance of the slurry in the cup is reflected in an increase in the current draw of the motor which is measured and displayed in units of milli-volt (mV). The mV reading and associated bobbin rotational speed are then converted to a turbulence-corrected shear stress flow curve using a special calibration algorithm [Napier-Munn et al. (1996)].

To predict the viscometer raw readings a polynomial equation describing the Debex readings (mV) as a function of bobbin angular velocity ( ) was employed. The equation is of the general form:

$$mV = a_o + a_1 \square + a_2 \square^2 + a_3 \square^3 \qquad (2.20)$$

The following phenomenological assumptions were made in developing the model:

- Coefficient a_0 is only determined by a variable which is related to the yield stress of the slurry, and therefore reflects the effect of particle hydrodynamics.
- Coefficient a_1 is also a factor of the hydrodynamic interaction of the particles. Solids volume fraction, particle size, chemical conditions and slurry temperature may affect the intensity of these interactions.
- Coefficient a_2 may also be affected by particle interactions. However, the effect of these interactions will become weaker with the bobbin action becoming stronger.
- With the bobbin rotation a strong function in the cubic term, particle interactions may be ignored and coefficient a_3 mainly reflects the mechanical action of the bobbin.

This lead to the following expression:

$$mV = C_1(HD-1) + C_4 HD\Omega + C_5 \frac{\Phi}{P_{80}}\Omega^2 + C_6\Omega^3 \tag{2.21}$$

Where:

$$HD = \exp\left(\frac{\Phi}{1-\Phi(P_{20})^{C_2}\exp(C_3 T)}\right) \tag{2.22}$$

and,

□ = volume solids concentration (proportion)

T = temperature (°C)

□ = bobbin angular velocity (rad/s)

P_{20} = 20% passing size solids (mm)

P_{80} = 80% passing size solids (mm)

C_1-C_6 = model parameters to be determined experimentally for particular slurries or slurry types

The flow curve for the slurry, and local viscosity, can be obtained by applying the calibration algorithm discussed by Napier-Munn et al. (1996). The model is a semi-empirical model, and does not account explicitly for other variables such as particle shapes, extreme values of particle size (particularly fine), electrochemical conditions or complex interaction of these variables.

It was observed that the set of parameters obtained from the model are not universal, but differ for different slurries. This is due to the complexity of the mineralogy, chemistry and particle shape of the slurries. Under such circumstances part, or all, of the parameters may need to be re-fitted to measurement data from particular slurry.

From their model, Napier-Munn et al. (1996) showed that a simple type of slurry can exhibit a wide range of rheological behaviour, from pseudo-plastic to dilatant, and with varying yield stress, depending on the prevailing particle size and solids concentration:

- When a suspension contains relatively low solids concentration and a high content of fines, its rheological character is likely to be dilatant.

- When the suspension density increases and fines content reduce, the suspension is likely to exhibit a pseudo-plastic character.

- Increasing either fines content or suspension density leads to increased yield stress for both dilatant and pseudo-plastic flows.

2.4.1.3 Effect of pressure and temperature

Pressure and temperature affect the viscosity of the suspension by acting on the viscosity of the liquid phase as well as by their effect on the characteristics of the solid phase [Jinescu (1974)].

a) Effect of pressure

The viscosity of the liquid phase increases with pressure (excluding H_2O), in accordance with a general expression of the form:

$$\mu(p) = \mu(p_o)\exp[C_1(p - p_0)] \quad (2.23)$$

Where μ(p) is the viscosity at the pressure p, $\mu(p_o)$ the viscosity under normal pressure p_o, and C_1 is a constant.

The solid phase is affected by pressure through a reduction in porosity or void fraction, as the pressure increases, which obey a relationship similar to:

$$\varepsilon(p) = \varepsilon(p_o)\exp[-C_2(p - p_o)] \quad (2.24)$$

Where □(p), and □(p_o) are the porosities at pressure p and atmospheric pressure p_o, respectively. C_2 is a constant. However, for the work in this project there was no pressure effect.

b) Effect of temperature

The viscosity of the liquid phase decreases with an increase the temperature. This dependence is expressed by the Arrhenius equation:

$$\mu = A\exp(\frac{E}{RT}) \quad (2.25)$$

Where A is a coefficient depending on the nature of the liquid, E the flow energy of activation, R the gas constant, and T the absolute temperature.

Another relationship which is often used for the relationship of liquid viscosity with temperature is:

$$\mu = a\exp(-bT) \quad (2.26)$$

Where a and b are constants.

The effect of temperature on the solid phase of the suspension is only common in suspensions containing compressible particles (e.g. latex, asphalts). The temperature effect is evidenced by

variations in the void fraction. Thus, for the hard, incompressible solids used in dense medium separations, the effect of temperature on the solid phase is zero.

2.5 Conclusion

The literature survey undertaken above gives a clear insight into the viscosity of heavy medium suspensions. The literature review has outlined the media properties affecting the viscosity and stability of heavy medium suspensions. The increase in apparent viscosity may be due to either inherent or acquired causes. The causes of inherent viscosity are the density, shape and size distribution of the solid used for the media and of the media suspensions specific gravity. Acquired viscosity may be due to things such as overly magnetized media, but is usually due to slimes or media particle attrition. The literature review has also shown that the rheology of heavy medium suspensions can be manipulated through the use of surface active chemicals. These chemicals can be either used as stabilizing agents or as viscosity reducers. In either case, they are used to improve the separation efficiency of a particular ore.

The findings in this section will help as a guide to the development of the next sections. The next sections deal with viscosity measurement and separating vessels. The results of other researchers were used to determine what type of rheometer and separating vessel best suit our application. From their results we were also able to ascertain what the limiting factors in our investigation were.

Chapter 3

Rheology Measurement

As mentioned in Chapter 2, the most important rheological properties of heavy medium suspensions are their viscosity and stability. This chapter is devoted to the measurement of suspension viscosity. Viscosity plays an important role in the separation efficiency of ore particles. It is thus imperative to develop instruments capable of measuring the viscosity of the suspensions. The devices used to measure suspension viscosity are called rheometers or viscometers. There are different types of viscometers used for different types of fluids. The type of viscometer used to measure the viscosity of any suspension is highly dependent on the properties of the suspension. For instance, viscometers used to measure the viscosity of Newtonian fluids may be different to those used to measure the viscosity of settling suspensions. Even within a class of viscometers, the different dimensions of the viscometers, depending on the manufacture standard, can be made different in order to accommodate this difference in suspension properties. In general the types of viscometers used in the mineral industry can be classified under two different groups: Tube viscometers, and Rotational viscometers.

3.1 Tube viscometers

The simplest type of viscometer for the study of fluids of low viscosity is the full capillary apparatus. Most capillary viscometers are modifications of the Ostwald viscometer shown in Figure 3.1.

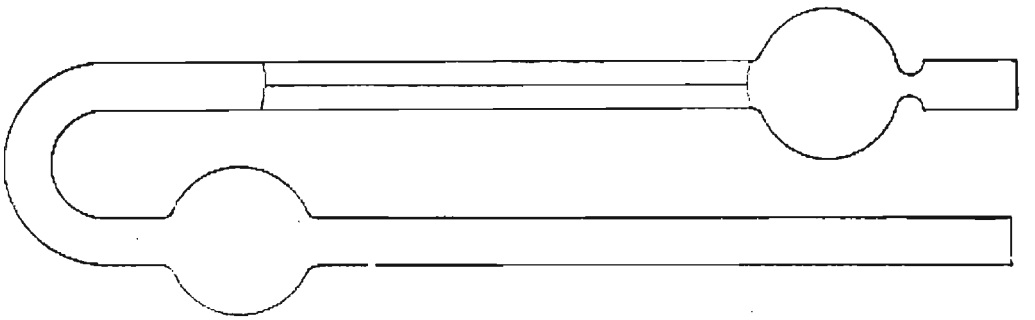

Figure 3.1 Ostwald viscometer [Blair (1969)]

The Ostwald viscometer (mounted vertically) depends on the measurement of the time taken for a given volume of liquid to fall through a capillary [Blair (1969) and Whorlow (1980)]. The rate of fall of the liquid depends on the density (□) and the viscosity (μ) of the liquid, so that the time of fall is in fact, proportional to $\mu/$□ i.e. the kinematic viscosity of the liquid. Although Ostwald viscometers are very accurate at measuring the viscosity of Newtonian fluids, they are not suitable for the measurement of non-Newtonian fluids. The main difficulty in using capillary viscometers is the fact that the "head" or pressure is falling continuously in the capillary tube. As such, in many modified capillary viscometers the tested material flows under an applied pressure [Blair (1969)].

To demonstrate how the equations governing the forces acting in capillary viscometers are developed, consider the streamline flow of a Newtonian fluid through a capillary tube of length □L, radius 'R' under a pressure difference □P [Blair (1969) and Whorlow (1980)]. The flow through the capillary is illustrated in Figure 3.2.

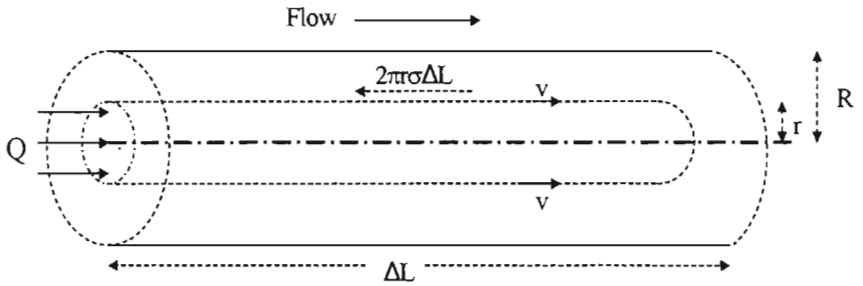

Figure 3.2 Forces on a short cylinder in capillary [Whorlow (1980)]

If we consider a short section of the pipe sufficiently far from the ends of the tube, the following assumptions can be made [Whorlow (1980)]:

1. The flow of the fluid is parallel to the axis.

2. The velocity 'u' of any fluid element is a function of radius 'r' only, giving axial symmetry.

3. The fluid flowing through the capillary is incompressible.

4. The fluid velocity at the wall of the capillary is zero.

5. The normal stress is isotropic.

The velocity gradient, which is the velocity rate of change in the radial direction, diminishes as the r increases. When r = 0, the velocity gradient is at its maximum. When r = R (radius of capillary), the velocity gradient is zero since it is assumed that there is no slip at the wall [Blair (1969)]. The pressure difference □P acts over an area of □a^2, so that the force F will be:

$$F = \square P \ \square R^2 \tag{3.1}$$

Since the area of the wall is 2□R□L, the stresses at the wall and at a distance r respectively are:

$$\tau_{wall} = \frac{R\Delta P}{2\Delta L} \tag{3.2}$$

Following from Newton's law, which states that the shear stress is proportional to the shear rate, the following equation for velocity gradient is obtained:

$$\frac{du}{dr} = -\frac{1}{\mu} \cdot \frac{\Delta \Pr}{2\Delta L} \tag{3.3}$$

where μ is the viscosity of the fluid. To get the radial velocity variation Equation 3.3 is integrated with respect to r:

$$u = -\frac{\Delta P}{2\Delta L\mu} \int r.dr \tag{3.4}$$

The boundary condition of Equation 3.4 is that the velocity of the fluid is equal to zero at the wall of the capillary .i.e. when r = a. After integration the following equation for radial velocity is obtained:

$$u = \frac{\Delta P(R^2 - r^2)}{4\Delta L\mu} \tag{3.5}$$

To obtain the volumetric flowrate (Q) of the fluid in the capillary the velocity in the concentric area is integrated between 0 and R:

$$Q = \int_0^R u.2\pi r dr \tag{3.6}$$

Substituting Equation 3.5 into Equation 3.6 and integrating, the following equation is obtained:

$$Q = \frac{\pi R^4 \Delta P}{8 \mu \Delta L} \tag{3.7}$$

Equation 3.6 is the Hagen-Poiseuille equation.

For Newtonian fluids the shear rate varies from a maximum near the vicinity of the wall, to zero at the centre of the capillary. Hence, to calculate the viscosity of fluids using capillary viscometers, the conditions at the shear stress and shear rate at the wall are used. For Newtonian fluids the viscosity is given calculated from Equation 3.7:

$$\mu_w = \frac{\pi R^4 (\Delta P / \Delta L)}{8Q} \tag{3.8}$$

However, for non-Newtonian fluids the situation is more complex. Correction factors need to be added to account for the deviation of the fluid from Newtonian behaviour. One such correction factor is the Rabinowitsch correction, shown in the equation below:

$$\mu_w(\dot{\gamma}) = \frac{\pi R^4 (\Delta P / \Delta L)}{8Q\left(\frac{3}{4} + \frac{1}{4}\frac{d \ln Q}{d \ln \sigma_w}\right)} \tag{3.9}$$

The term in the brackets is called the Rabinowitsch correction [Barnes et al. (1989)]. When shear-thinning fluids are being tested, the derivative d(lnQ)/d(ln□w) is greater than 1and for power-law liquids is equal to 1/n. Figure 3.3 shows the different velocity profiles for the laminar flow of power-law liquids in a capillary tube as 'n' varies. For Newtonian fluids the value of *n* is equal to one. Note the increase in the wall shear rate and the increasingly plug-like nature of the flow as 'n' decreases.

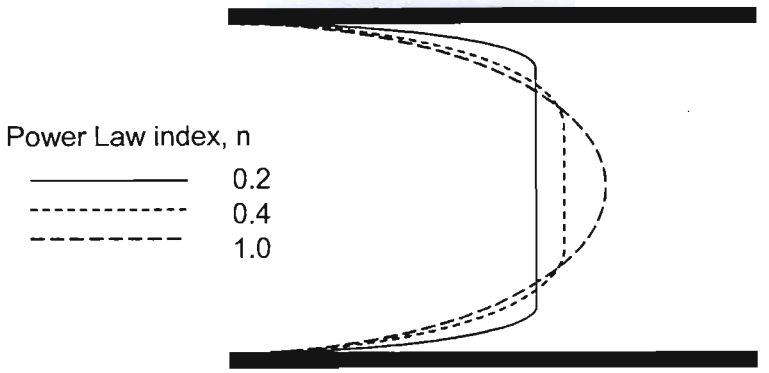

Figure 3.3 The velocity profile for the laminar flow of power-law liquids, calculated for the same volumetric throughput [Barnes et al. (1989)]

Equation 3.9 shows how the viscosity can be calculated in a capillary viscometer if the flowrate Q, the pressure difference across the capillary, and the dimensions of the capillary are known. The pressure gradient can be measured using various devices. The most common method is by connecting holes in wall of the capillary to pressure transducers. To avoid end effects the holes on the capillary wall must be far away from the ends [Barnes et al. (1989)]. Usually, end effects (entrance effects and exit effects) are avoided by ensuring that the aspect ratio of the capillary is greater than one hundred.

3.2Rotational viscometers

Rotational viscometers have two main advantages over capillary viscometers: Firstly, a particular fluid can be sheared for as long as desired so that permanent or temporal changes can be monitored; Secondly, with appropriate design, an approximately uniform shear rate can exist throughout the fluid in contrast to the variation of the shear rate in capillary viscometer from zero at the axis to a maximum at the wall [Whorlow (1980)].

Rotational viscometers consist of a stationary part and a rotating part. The fluid is placed between the stationary and rotating parts of the viscometer such that either the shear stress or the shear rate can be obtained. In a rotational test with controlled shear rate, the torque to which the measuring bob is exposed to by the internal resistance of the fluid is measured. The torque is measured by either a force sensor (e.g. load cell) or a measuring drive system. The torque is then converted to the shear stress at the bob such that shear stress vs. shear rate profiles can be obtained. In a

controlled shear stress test, a torque is applied to the measuring system and a result the deflection angle or speed which the measuring system carries out towards the fluid is measured [Barnes et al. (1989) and Slatter et al. (2000)].

The pseudo-fluids used in dense medium separations are seldom Newtonian in behaviour. They can either be dilatant or plastic depending on the shear rate and the solids volume concentration. The biggest difficulty in choosing the right type of viscometer to use in measuring the viscosity of dense medium suspensions is the rapid settling rate of the solids in the suspension. The suspension needs to be continuously agitated in order to minimise this settling effect. As a result many viscometers have been modified to test suspensions of different solids concentration and composition.

For rotational viscometers there are two types of measuring principles, as shown in Figure 3.4 [Slatter et al (2000), Harris (1977)]:

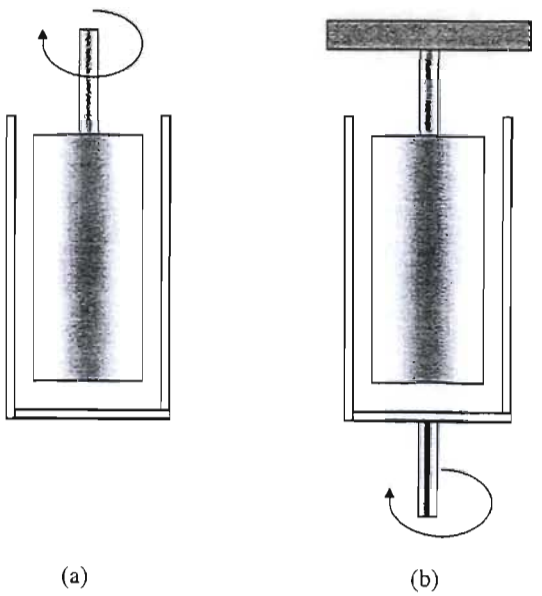

Figure 3.4 Cylinder measuring system according to (a) Searle's principle (b) Couette's principle [Slatter et al. (2000)]

a) *Searle's principle*: Rotating measuring bob, stationary measuring cup (or still standing lower plate respectively). Most rheometers work according to this method. The rheometer used in this project was also based on this principle.

b) *Couette's principle*: Rotating measuring cup (or rotating lower plate respectively), still standing measuring bob. Only a few rheometers work according to this method. Measuring systems according to Couette's principle cause a problem concerning temperature control with liquids because of the friction of the sealings, since a rotating surface has to be sealed against the temperating medium (e.g. water). For this reason they are seldom used unless in a temperated room.

Most of the work presented in this section will be based on rheometers working according to Searle's principle.

3.2.1 Concentric-cylinder viscometer

A typical concentric-cylinder viscometer operating under Searle's principle is shown in Figure 3.4 (a). The accuracy of the results from a concentric-cylinder viscometer depends to great extent on the measuring gap between the concentric cylinders. Ideally, the shear rate and shear stress should be linearly distributed between the measuring gap.

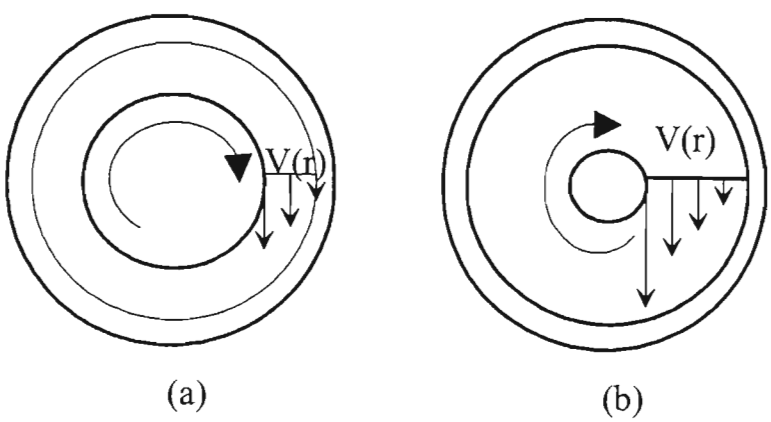

Figure 3.5 Cross sections of measuring systems with different gap sizes. The function of the circumferential speed v(r) is presented [Slatter et al. (2000)]

A narrow measuring gap (Figure 3.5 (a)) gives the desired linear course of speed function quite accurately. When using a wide measuring gap (Figure 3.5 (b)) the speed function has a curve-like course which is difficult to calculate and which is rheologically undesired, particularly for pseudoplastic fluids and those with an apparent yield. This leads to poor results which are often irreproducible when measuring data are analyzed.

For solid-liquid suspensions great care must be taken in selecting the right type of measuring gap. The gap should be big enough to accommodate the solid particles in suspension, and the same time the gap should be able to give reproducible results when measured data are analyzed.

3.2.2 Double gap concentric-cylinder viscometer

The double gap viscometer is primarily used to measure the viscosity of fluids with low viscosity. The viscometer has a large shearing area which is used to detect sufficiently high torque values to enable meaningful evaluation of the results. A diagram of a double gap viscometer is shown in Figure 3.6.

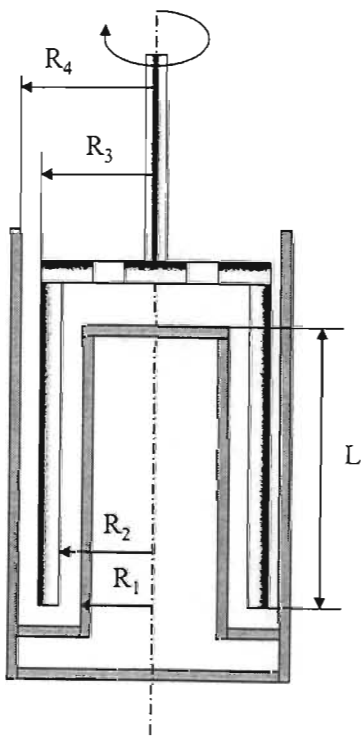

Figure 3.6 Double gap viscometer [Slatter et al. (2000)]

The viscometer also works under Searle's principle, with a rotating bob and stationary cup. The measuring bob is shaped like a tube. The measuring cup has a cylindrical core part and therefore shows a ring gap [Slatter et al. (2000)]. This type of viscometer is unlikely to be used to measure the viscosity of dense medium suspensions since the viscosity of these suspensions are moderately high. However, because of the high shearing area, this type of viscometer can be used to measure the flow curves at low shear rates. This can be used to estimate the relative yield stresses of dense medium suspensions, which is often difficult to obtain with other viscometers.

According to DIN 54453 standards, the radii and immersion length of the viscometer (figure 3.5) should be constrained under the following relation [Slatter et al. (2000)]:

$$\delta = \frac{R_4}{R_3} = \frac{R_2}{R_1} \leq 1.15 \tag{3.10}$$

$$L \geq 3R_3 \tag{3.11}$$

The relatively large shearing area, which detects the torque or shear stress of the fluid, is composed of the inner and outer surface of the measuring bob. This makes the viscometer more sensitive to torque measurement than concentric-cylinder viscometers.

3.2.3 High-shear viscometer

This type of viscometer is used to obtain high shear rates. Sometimes, high shear rates are required to measure the viscosity of samples with high viscosities. The high shear rates are obtained by using a very small relation of radii between the cylinders. The radii are shown in Figure 3.7 [Slatter et al. (2000)].

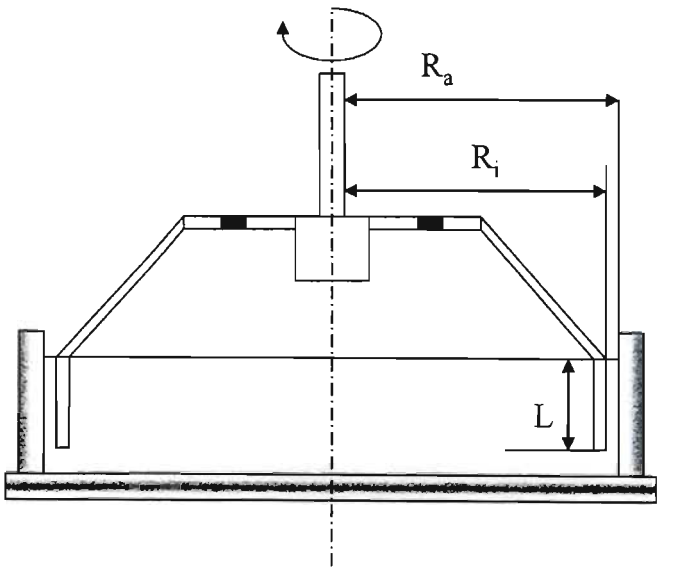

Figure 3.7 High-shear viscometer [Slatter et al. (2000)]

The shear rate is calculated from the following equation:

$$\dot{\gamma} = \frac{v}{h} \text{ (Where } h = R_a - R_i) \tag{3.12}$$

From Equation 3.12, the shear rate increases as the cylinder gap width is reduced if the viscometer is running at the same speed. High-shear viscometers are run at shear rates not in excess of 10 000 s^{-1} because of the thermal energy encountered as the fluid is sampled at these rates, which would influence the apparent viscosity by heating up the fluid. For the measurement of suspensions the value of the measuring gap 'h' should be large enough to accommodate the solid particles.

3.2.4 Cone-plate viscometer

In the cone-plate viscometer the shear rate can be considered to be the same everywhere in the fluid provided the gap angle β is small. The value of β is usually less than 4°. Above this value, the requirements for the calculation of the viscosity of the fluid are no longer given [Barnes et al. (1989) and Slatter et al. (2000)]. Figure 3.8 shows a diagram of a cone-plate viscometer with a truncated cone tip.

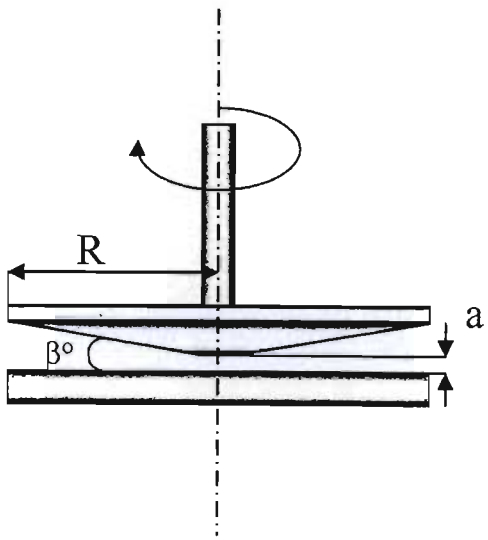

Figure 3.8 Cone-plate viscometer [Barnes et al. (1989) and Slatter et al. (2000)]

The shear rate in the fluid is given by the following equation:

$$\dot{\gamma} = \frac{\omega}{\beta} \tag{3.13}$$

The shear stress, measured from the torque at the surface of the cone, is given by the following equation:

$$\sigma = \frac{3M}{2\pi R^3} \tag{3.14}$$

The viscosity of the fluid is calculated by dividing Equation 3.14 by Equation 3.13:

$$\mu = \frac{3M\beta}{2\pi R^3 \omega} \tag{3.15}$$

Cone-plate viscometers are usually truncated because this reduces the abrasion of the cone and the bottom plate since there is no friction between them. Friction between the cone and plate would also result in an additional torque being required to drive the viscometer. This would result in falsified high viscosities. However, because of the small values of β, cone-plate viscometers cannot be used to measure the viscosity of solid suspensions whose particle sizes are greater than 10 microns.

3.2.5 Plate-plate viscometer

In the plate-plate viscometer shown in Figure 3.9, the fluid is placed between the plates. In order to get meaningful results, the value of the plate distance 'h' should be small compared to the plate radius 'R'.

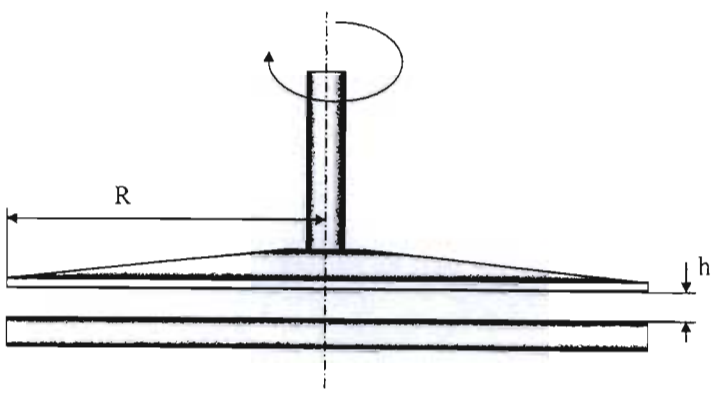

Figure 3.9 Plate-plate viscometer [Barnes et al. (1989) and Slatter (2000)]

The shearing area is equal to the area of the top plate. Unlike cone-plate viscometers, the shear rate in plate-plate viscometers is a function of the radius of the plate [Slatter et al. (2000)]. The shear rate increases linearly from zero at the axis to its maximum at the rim of the plate. The shear rate at the rim of the plate is given by the following equation:

$$\dot{\gamma} = \frac{\omega R}{h} \tag{3.16}$$

The shear stress at the rim of the plate is equal to Equation 3.14. Thus, the viscosity at the rim of the plate is given by the following equation:

$$\mu = \frac{3Mh}{2\pi R^4 \omega} \tag{3.17}$$

When testing suspensions, in order to get meaningful results, the value of the measuring gap 'h' should be at least ten times greater than the size of the aggregate particles.

3.3 Effect of stability on rheological measurement

The instability of heavy medium suspensions makes rheology measurement very difficult. This has led to different modifications in rheometer designs to try and solve the problems caused by the settling tendency of heavy media. The two most common types of rheological measuring devices are tube viscometers and rotational viscometers. Neither can provide accurate measurements for rapidly settling suspensions. In particular, measurements made with tube viscometers are influenced by the wall effect and the tubular pinch effect [Klein et al. (1990)]. These effects cause non-homogeneous conditions in the suspension that are difficult to model and result in inaccurate results.

In rotational viscometers the settling out of media particles also results in non-homogeneous conditions in the measuring zone. In a conventional bob and cup arrangement, particles settle out leaving a solid depleted zone near the top of the annular gap between the cup and bob. This reduces the resistance to rotation experienced by the bob [Klein et al. (1990)]. If the depth of the sludge exceeds the distance between the bottom of the cup and the bottom of the bob, it will impede the rotation of the bob, resulting in results suggesting high viscous resistance of the media.

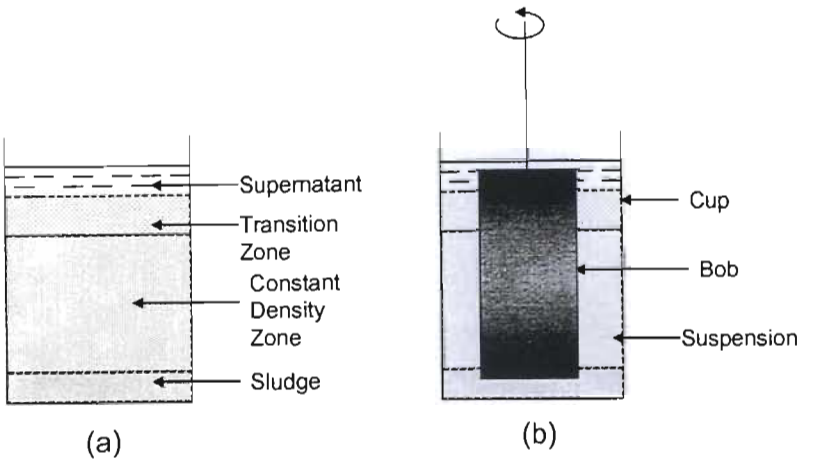

Figure 3.10 Sedimentation of particles: (a) a settling column, (b) a single gap concentric cylinder cup and bob arrangement [Klein et al. (1990)].

Figure 3.10 shows the solids concentration profile at a given time for a typical sedimenting suspension. Figure 3.10 (b) shows the solids concentration profile for a typical cup and bob arrangement containing sample with the same concentration profile as that shown in Figure 3.10 (a). Clearly, any measurements made on unstable suspensions use these devices are very questionable.

3.4 On-line viscosity measurement

As mentioned in this section, the main problem with measuring the viscosity of dense medium suspensions is the high settling rate of these suspensions, particularly at low specific gravities. To measure the viscosity of these suspensions, industrial suspensions need to be able to overcome this settling nature. Over the years, the most commonly used on-line viscometer has been the bob and cup viscometer. This type of viscometer is a modification of the concentric-cylinder viscometer described in section 3.2.1. Almost all industrial bob and cup viscometers work under Searle's principle. Recently there has also been a tendency to use capillary on-line viscometers. This section will give an example of both capillary and rotational on-line viscometers.

3.4.1 An industrial capillary on-line viscometer

Goosen et al. (2004) have developed a tube viscometer which was specifically designed for use with fine segregating slurries such as dense medium suspensions. This viscometer has been termed the FeSi viscometer. A schematic diagram of the viscometer configuration is shown in Figure 3.11.

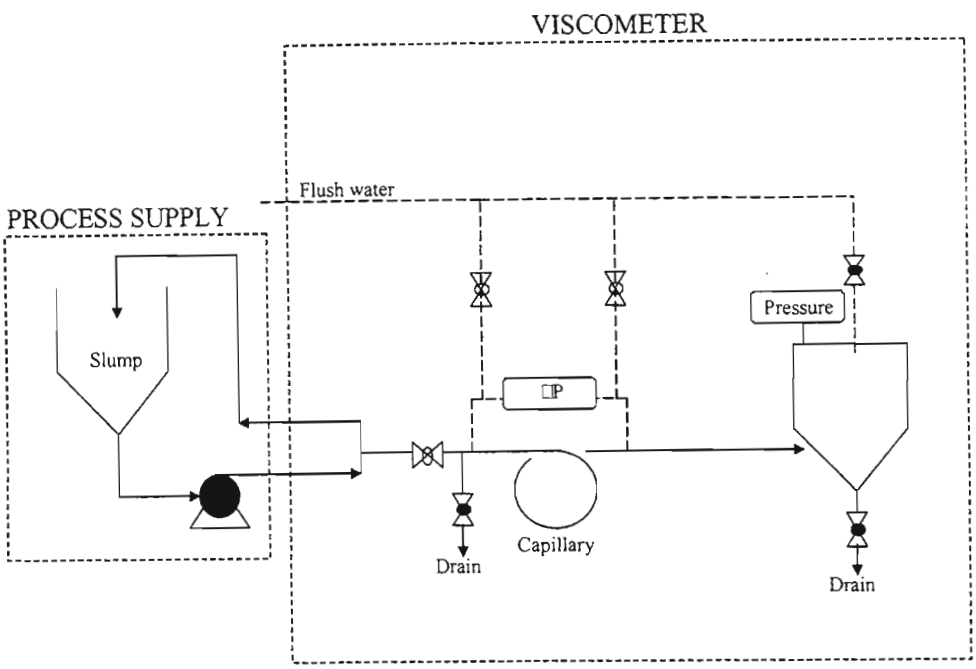

Figure 3.11 Schematic of the FeSi viscometer Apparatus [Goosen et al. (2004)]

Feed to the viscometer is supplied through a pressurised slurry source, which could be a tapping close to a pump discharge in the dense media circuit [Goosen et al. (2004)]. The valve configuration is important for the proper pressure measurement across the capillary. To reduce the settling rate of the slurry common under laminar flow conditions, the measurement tube is coiled in vertical loops. The differential pressure across the measurement tube is measured using a differential pressure transmitter and appropriate tapping points. The differential pressure is used to calculate the shear stress at the capillary wall using methods similar to those described in Section 3.1. The flowrate of the slurry through the measurement tube and into the receiving vessel

is determined from the rate of change of vessel pressure. These results are used to calculate the bulk shear rate in the measurement tube.

3.4.2 An industrial on-line rotational viscometer

Reeves (1985) describes an industrial viscometer used to measure the viscosity of dense media and other mineral suspensions. The viscometer can be used on-line to monitor the viscosity continually on a plant or off-line to investigate the rheological behaviour of suspensions. The viscometer (Debex viscometer) is of rotational design and employs a specially designed bobbin that is rotated in a sample of the suspension under investigation. The bobbin is submerged in the fluid and is rotated at a fixed rate by a DC micromotor and ancillary electronic equipment. The rate of rotation may be selected manually and, once chosen, is maintained by the electronics. If a retarding force is applied to the motor by the viscous resistance of the fluid, additional voltage is required to maintain a constant rate of rotation. The voltage is measured and displayed continually electronically. The motor has been found to be sensitive to changes in temperature, which causes the rotation rate of the bobbin to drift. To overcome this, the motor is surrounded by a heating jacket that maintains a constant, higher than ambient temperature.

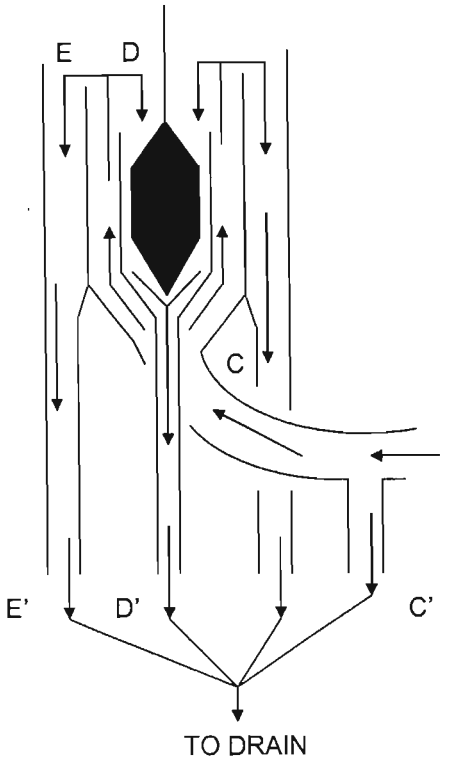

Figure 3.12 Debex on-line viscometer [Reeves (1986), Napier-Munn et al. (1996)]

A schematic section of the viscometer is shown in Figure 3.12. Feed to the viscometer is degritted by a cyclone or a screen, the undersize passing to a constant head tank B. the sample then flows by gravity into the 'U-shaped' section, where a proportion is drained through the pipe C' to reduce the flow rate. This pipe also allows the constant-head tank to drain when the viscometer is switched off (an important for rapidly settling solids). The remainder of the sample flows upward through the annulus, C, before overflowing both inwards into the measuring chamber, D, and outwards to drain E. For rapidly settling suspensions the upward velocity of the suspension is greater than the settling velocity of the solid particles. The annulus, C, and the measuring chamber are both fitted with baffles to eliminate rotational movement of the fluid.

For the measurement of Newtonian fluids the viscometer is calibrated with aqueous glycerine solutions of known viscosity. The measuring chamber, D, is plugged and filled with solution. The solution viscosity is measured by means of another suitable viscometer and compared with the on-line viscometer reading. The procedure is repeated to produce a calibration graph that correlates the viscometer reading with viscosity. For non-Newtonian fluids the calibration becomes more difficult and tedious because of the settling out of solids from suspensions [Napier-Munn (1996), Reeves (1985)].

Napier-Munn et al (1996) extensively covers the calibration of both Newtonian and non-Newtonian fluids. The derivation of the shear stress equations assumes that the flow past the bobbin is laminar. However, the flow in the Debex viscometer is turbulent in even for a static fluid. In turbulent flow the internal motion of the fluid is not smooth but includes many whorls and vortices. Since irregular flow leads to greater dissipation of energy than occurs in laminar flow, the apparent shear rate is diminished by turbulence to a value below that expected for laminar flow at a given applied shearing stress, resulting in a higher apparent viscosity. If this is not corrected the resulting flow curves take on the appearance of dilatancy, even though the fluid may be Newtonian.

These problems were believed to be associated with the wide gap between the measuring cup and the rotating bobbin, and the existence of baffles, both of them causing Taylor vortices and turbulence. When the inner cylinder is rotating and the outer cylinder is at rest, the fluid near the inner wall experiences a higher centrifugal force and shows a tendency to be propelled outwards. When a certain Reynolds number is exceeded, vortices appear in the flows whose axes are located along the circumference and which rotate in alternately opposite directions.

3.5 Rotational measuring system according to DIN 53 019 and ISO 3219

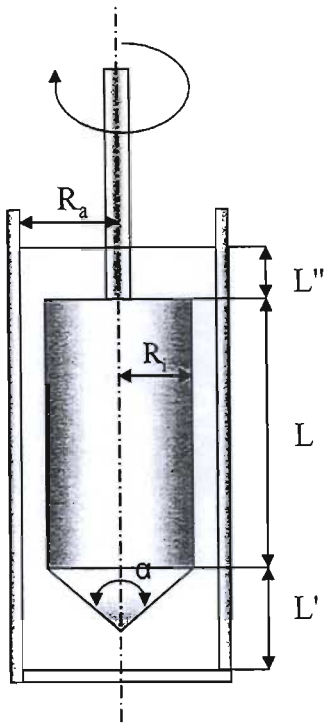

Figure 3.13 Cylinder measuring system according to DIN 53019 / ISO 3210 [Slatter et al. (2000)]

Most rotating measuring systems are specified according to DIN 53019 and ISO 3219 standards (Figure 3.13). These standards are used to specify the dimensions of the bob and measuring cup, and apply to systems using Searle's principle. The following rules apply [Slatter et al (2000), www.RheoNet.de/standards/iso_cp.htm (18/10/2004)]:

$$\delta = \frac{R_a}{R_i} \leq 1{,}2 \tag{3.18}$$

Equation 3.18 gives the maximum value for the relation between the radii of the bob and cup of the measuring system.

$$\frac{L}{R_i} \geq 3 \qquad \text{(Preferably = 3)} \tag{3.19}$$

$$\frac{L'}{R_i} \geq 1 \quad \text{(Preferably = 1)} \tag{3.20}$$

$$\frac{L''}{R_i} \leq 1 \quad \text{(Preferably = 1)} \tag{3.21}$$

$$\frac{R_s}{R_i} \leq 0.3 \tag{3.22}$$

$90^\circ \square\square\square 150^\circ$ (preferably $\square = 120^\circ$) (3.23)

Representative shear stress

The equations derived below are valid for narrow measuring gap systems.

$$\tau_{rep} = \frac{\tau_i + \tau_a}{2} \tag{3.24}$$

$$\tau = \tau_{rep} = \frac{M}{2\pi L R_i^{\,2} c_L} = G_Z M \tag{3.25}$$

Where c_L is the correction factor and G_Z is a constant depending only on the geometry of the measuring system.

If the measuring systems according to DIN 53 019 / ISO 3219 are used, the following always applies:

$$\tau = 0.0446 \frac{M}{R_i^{\,3}} \tag{3.26}$$

Representative shear rate

The following applies:

$$\dot{\gamma}_{rep} = \frac{\dot{\gamma}_i + \dot{\gamma}_a}{2} \tag{3.28}$$

Thus the shear rate is:

$$\dot{\gamma} = \dot{\gamma}_{rep} = \omega \frac{(1+\delta^2)}{(\delta^2 - 1)} = \frac{(1+\delta^2)}{(\delta^2 - 1)} \frac{2\pi}{60} n \tag{3.29}$$

$$\omega = 2\pi \frac{n}{60} \tag{3.30}$$

If the measuring systems according to DIN 53 019 / ISO 319 are used, the following applies:

$$\dot{\gamma} = 1.291n \tag{3.31}$$

Note that in this measuring system the shear rate in the measuring gap is not constant at any place.

Representative shear viscosity

The following applies:

$$\mu_{rep} = \frac{\tau_{rep}}{\dot{\gamma}_{rep}} = \frac{0.0446M}{R_i^3 .1.291.n} = 0.0345.\frac{M}{R_i^2 .n} \tag{3.32}$$

The representative shear viscosity is calculated from the measured raw data, i.e. speed n (rpm) and torque M (Nm), radius of the measuring bob R_i and the mentioned conversion number.

Chapter 4

Separating Vessels

Separating vessels can be classified as either static (baths) or dynamic separators. The choice of separating vessel used is highly dependant on the ore particle size. For particle sizes larger than 10 mm, static separators are used. Below this size, and down to about 500 μm, dynamic separators are used. As will be shown later in this section, the separation efficiency for different sized particles differs according to the type of separation vessel used. Generally, above 10 mm particle size, the efficiency in static separators is greater than that of dynamic separators [Wills (1997)].

4.1 Static bath separators

Static separators are also called gravitational separators because the downward force acting on the particle is its own weight. These units are comprised of some sort of vessel into which the feed and medium are introduced, and the floats product is removed via paddles, or merely by overflow [Pryor (1960), Wills (1997)]. The biggest challenge in gravitational separator design is in ensuring that the sinks removal doesn't affect the downward currents in the vessel. The removal of the sinks product can be done through pumps, external / internal air lift, or sink lifters.

The different types of gravitational separators currently used in industrial dense medium separations are listed below:

- Wemco cone separator
- Drum separators
- Drewboy bath
- Norwalt washer

4.1.1 Wemco cone separator

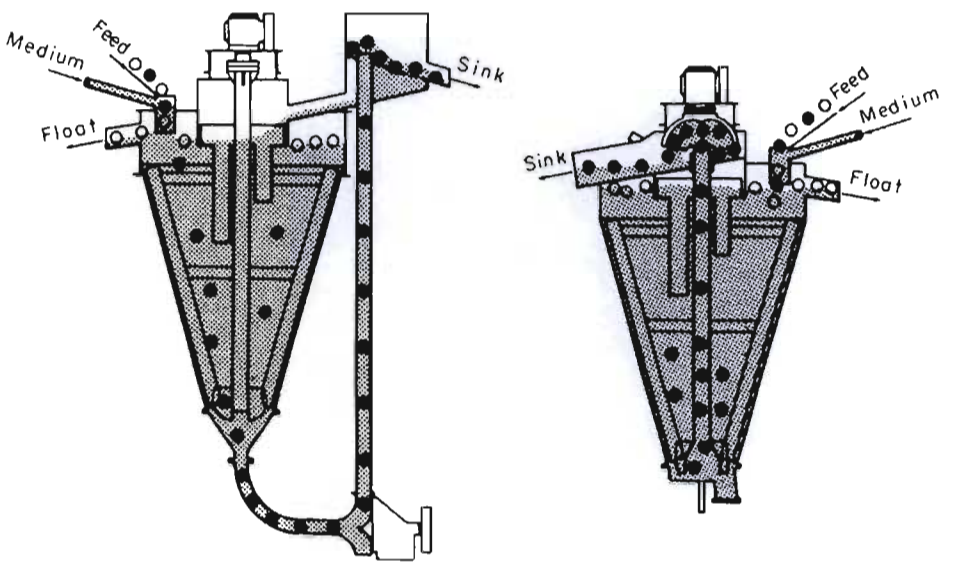

Figure 4.1 Wemco cone separator [Wills (1997)]

The Wemco cone separator is illustrated in Figure 4.1. This separator is one of the most widely used for ore treatment since it has a relatively high sinks capacity [Burt (1984), Wills (1997)]. The cone has a maximum diameter of about 6 metres, and can accommodate ore particles as large as 10 centimetres in diameter. The feed is fed onto the surface of the medium by free-fall, allowing it to plunge several centimetres into the medium. The medium is kept in suspension through gentle agitation via rakes mounted on the central shaft. The float product overflows a weir, whereas the sinks product is removed using a pump or by an external or internal air lift [Wills (1997)].

4.1.2 Drum separators

In drum separators separation is achieved by the continual removal of the sink product by lifters fixed to the inside of a rotating drum [Pryor (1960), Wills (1997)]. Like the Wemco cone separator, the floats product overflows a weir. However, in drum separators the weir is at the opposite end of the drum from the feed chute. To avoid the floats product from mixing with the sink-discharge action, longitudinal partitions are used to separate them. Compared to cone

separators, the pool depth in drum separators is much shallower. This reduces or minimises the settling out of the medium particles, resulting in a more uniform specific gravity throughout the drum.

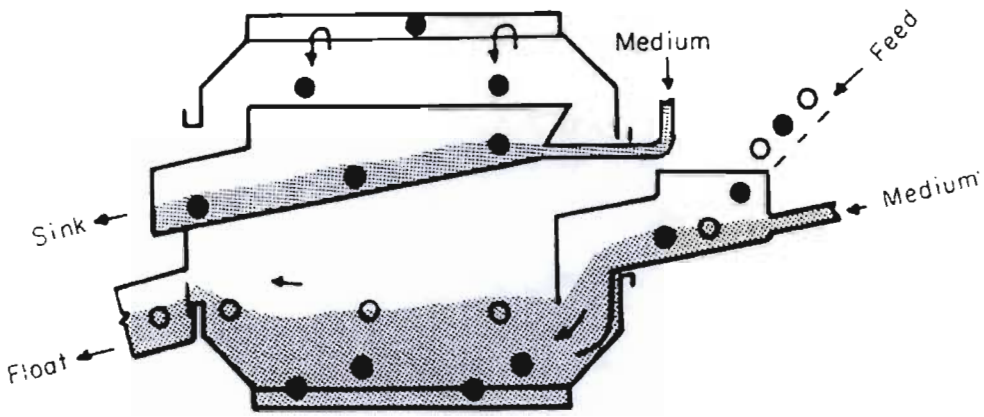

Figure 4.2 Single-compartment drum separator - side view [Wills (1997)]

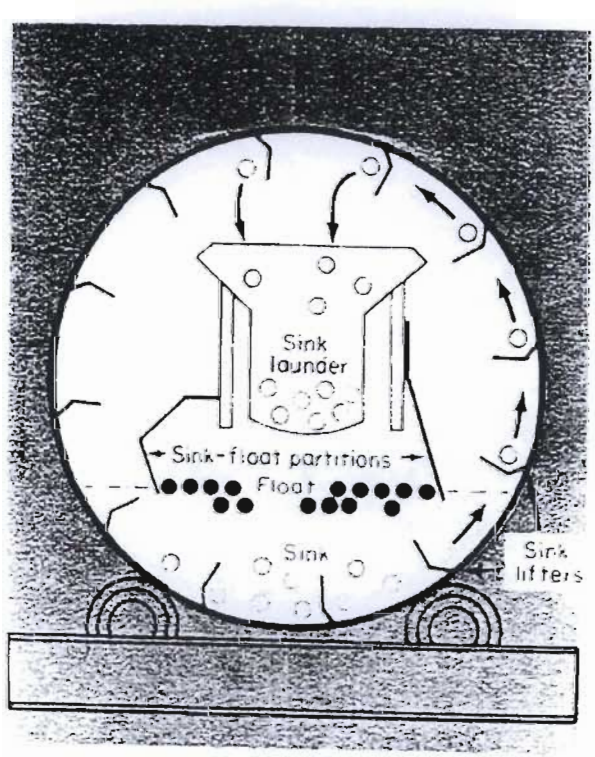

Figure 4.3 Single-compartment drum separator - end view [Wills (1997)]

Drum separators can either be single-stage or two-stage, depending on the specified recovery. The two-stage drum separator is essentially two drum separators mounted integrally and rotating together, with one drum feeding the other [Wills (1997)]. The lighter medium in the first compartment separates a pure float product, and its sinks product is used as feed into the second compartment, where the middlings and true sinks are separated. Figure 4.2 to Figure 4.4 are diagrams of typical drum separators. Because of their simplicity, reliability, and relatively small maintenance needs, drum separators have found wide applications in the coal industry.

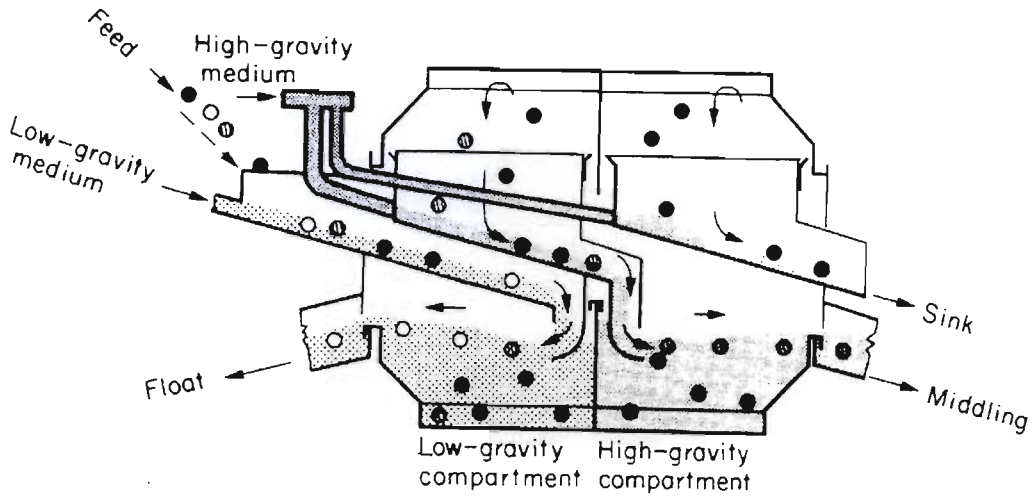

Figure 4.4 Two-compartment drum separator [Wills (1997)]

4.1.3 Drewboy Bath

Figure 4.5 shows a picture of the Drewboy bath separator. This type of separator has found wide use in the coal industry because of its high floats capacity [Wills (1997)]. Raw coal is fed into the separator at one end, and the float product is discharged from at the opposite end. Floats discharge is achieved through a star wheel with suspended rubber, or chain straps, while sinks are lifted out of the bottom of the bath by a radial-vaned wheel mounted on an inclined shaft [Pryor (1960), Wills (1997)]. The medium into the bath is fed at two points: at the bottom of the vessel, and together with the raw coal, the amount of feed through each point being controlled by valves.

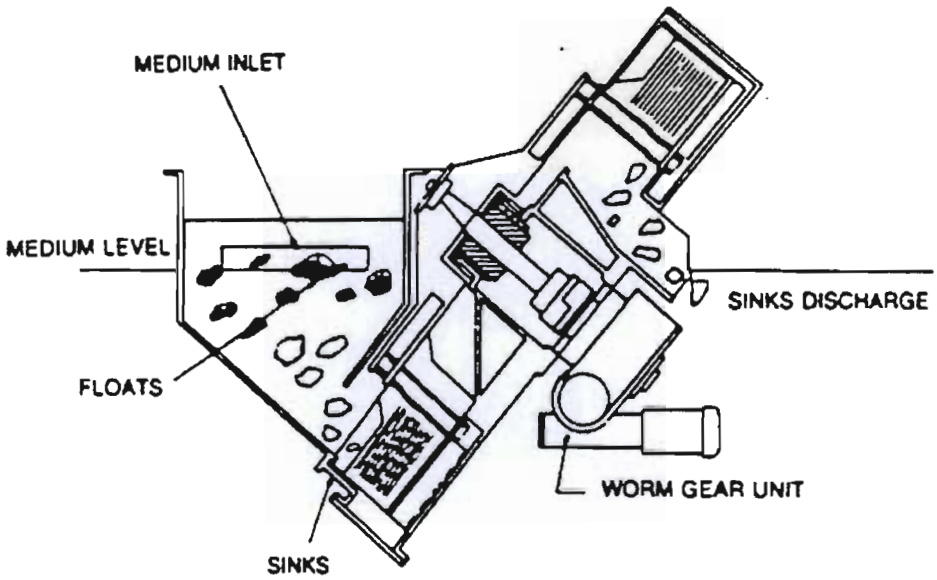

Figure 4.5 Drewboy bath [Horsfall (1993), Wills (1997)]

4.1.4 Nowalt washer

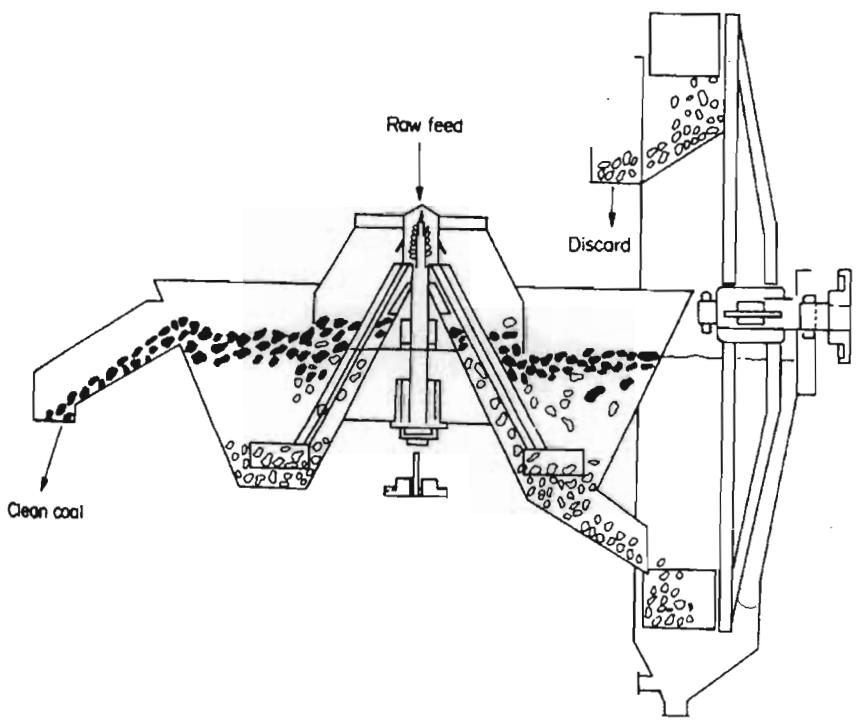

Figure 4.6 Nowalt washer [Horsfall (1993), Wills (1997)]

This type of separator was developed in South Africa, and most installations are found here [Wills (1997)]. Raw coal is fed into the centre of the annular separating vessel, which is mounted with stirring arms. The stirrers carry the float product and discharge it over a weir on the opposite end of the vessel, being carried out of the vessel by the medium flow. The sinks are discharged via a hole at the bottom of the bath into a sealed elevator, either of the wheel or the bucket type. Figure 4.6 shows a diagram of the Nowalt bath separator.

Table 4.1 classifies some of the different baths mentioned above, together with their performance characteristics. Classification is according to the method of floats removal [Horsfall (1993)].

Table 4.1 Performance characteristics of some bath separators [Horsfall (1993)]

Type	Name	General description
Low-flow, paddle-assisted floats removal	Drum separators	Cylindrical with annular baffles at each end; the feed end baffle has smaller aperture than the discharge end. Floats kept to centre by curtain: sinks lifted as drum rotates by internal lifters which drop discards onto internal chute
Low flow	Drewboy	Coal floats along medium surface being removed & discharged by rotating paddles or scrapers; sinks lifted by wheel elevator from bath bottom
Low/medium flow, no paddle	Norwalt	Coal enters bath centre, moves outwards in spiral path to peripheral discharge. Sinks scraped to discharge then lifted by wheel elevator from bath bottom.

4.2 Dynamic separators

Dynamic separators are sometimes referred to as centrifugal-type separators. As ore particle size decreases, particle movement under the influence of gravity becomes ever slower [Horsfall (1993)]. In order to increase the particle movement in the medium, centrifugal forces are employed. As mentioned in Chapter 1, the settling velocity of particles in a bath is directly proportional to the force of gravity. If particles are introduced with a stream of medium into a separating vessel in which they are subjected to a centrifugal force, exactly the same considerations will apply. Larger particles, and those with a higher density than the fluid, will move through it under the influence of the force; lighter particles will move with the bulk of the fluid [Horsfall (1993)]. There are a variety of centrifugal-type (dynamic) separators in use today. These include the following:

- The Dutch State Mines (DSM) cyclone
- The Vorsyl separator
- The Dyna Whirlpool separator
- Tri-Flo separator
- The Larcodems (LARge Coal DEnse Medium separator)

A brief description of the dynamic separators listed above is given in the following sections.

4.2.1 The Dutch State Mines (DSM) Cyclone

The DSM cyclone was introduced by the Dutch State Mines for the efficient cleaning of small coal particles [Horsfall (1993), Wills (1997)]. Its principle of separation is similar to that of the conventional cyclone. Properly designed, the cyclone can treat ores and coal in the size range 50-0.5 mm. Figure 4.7 shows the general construction of the cyclone. It should be noted that figure 4.7 shows the operating principle of the DSM cyclone. DSM cyclones are normally operated at angle to the horizontal of between 10° and 30°.

The ore is suspended in a very fine medium of either ferrosilicon or magnetite, and is introduced tangentially to the cyclone. The tangential inlet of the medium causes the medium to rotate rapidly, resulting in the formation of an air column, or vortex, in the centre of the column [Horsfall (1993)]. Most of the medium flows towards the centre of the vessel, and then out through the vortex finder. The vortex finder is a tube extended into the body of the cyclone, and prevents short-circuiting of feed directly into the overflow. To create the vortex and cause particle separation, the DSM cyclone requires a certain pressure. The pressure is usually calculated as being equivalent to a certain static head [Horsfall (1993), Wills (1997)]. The minimum static head is usually taken as 9 x D, where D is the diameter of the cyclone at the inlet.

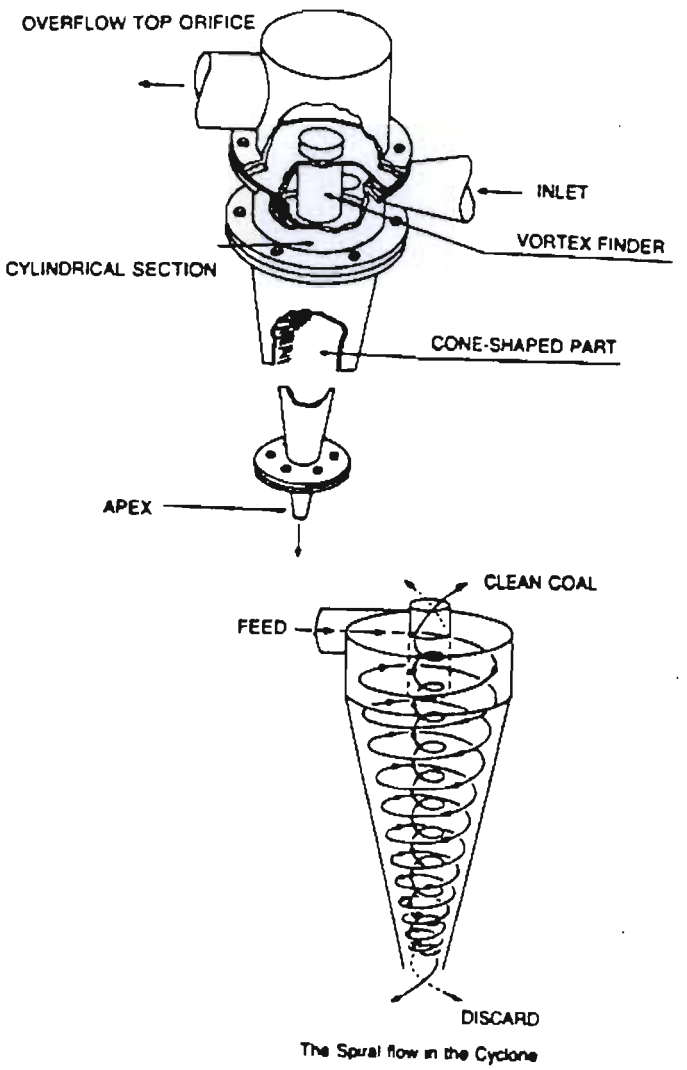

Figure 4.7 Dense medium Cyclone [Horsfall (1993)]

Particles within the cyclone are subjected to two opposing forces: an outward centrifugal force and an inward acting drag force [Wills (1997)]. When particles of mixed density enter a the DSM cyclone, those with a density lower than the medium density do not pass through the medium, but are caught in the flow towards the vortex finder. Hence, they exit the cyclone through the vortex finder as overflow. On the other hand, particles with densities greater than the medium density are able to penetrate the medium. These particles are thrown to the wall of the cyclone, and emerge at the apex of the cyclone, exiting as underflow.

One of the biggest challenges experienced in DSM cyclones is that the particles making up the medium are themselves affected by the centrifugal force. Segregation creates a density differential between the cyclone overflow and underflow. Factors that determine the extent of this differential are the cyclone diameter, pressure head, and medium grind [Horsfall (1993), Pryor (1960), and Wills (1997)]. As explained in Chapter 2, the media size distribution, particle shape, and slimes content determine the viscosity and stability of a suspension. To reduce the extent of particle segregation at low medium specific gravities, a medium with a finer size distribution, rougher particle shape, and moderate slimes content is usually the preferred choice.

4.2.2 The Vorsyl Separator

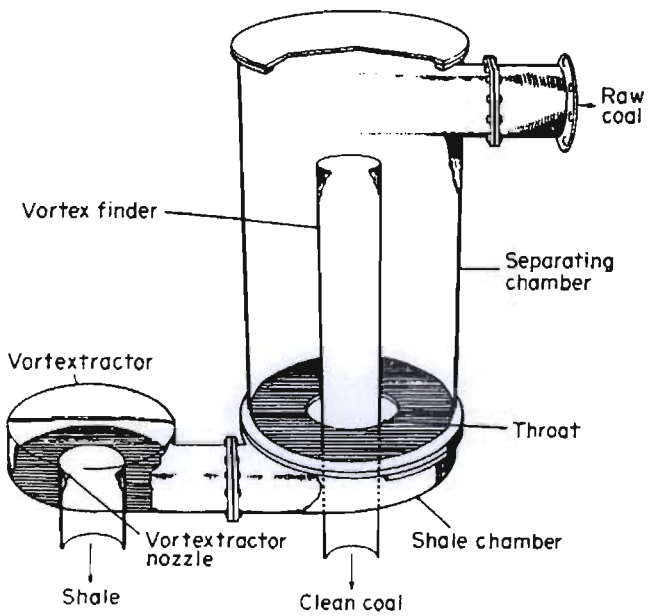

Figure 4.8 Vorsyl separator [Wills (1997)]

The Vorsyl separator is shown in Figure 4.8. This separator is mainly used in the coal industry to clean coal of small sizes up to about 30 mm [Wills (1997)]. Raw coal, together with a magnetite medium, is fed tangentially at the top of the column of the separating chamber under pressure. Lighter material passes into the clean coal outlet through the vortex finder, while middlings and heavy material move to the wall of the vessel due to the centrifugal acceleration induced. The particles spiral downwards towards the base of the vessel where the drag caused by the proximity of the orifice plate reduces the tangential velocity of the medium, and creates a strong inward flow towards the throat. This inward flow results in regions of high centrifugal forces within the vessel, resulting in further separation of the middlings and heavier particles (shale). The shale, together with a small amount of the medium, are discharged through the throat into the shale chamber, which is connected to a second shallow chamber known as the vortextractor by a short duct. The function of the Vortextractor is to dissipate the inlet pressure energy, such that a large diameter outlet nozzle can be used without the passing of an excessive amount of the medium [Wills (1997)].

4.2.3 The Dyna whirlpool (DWP) Separator

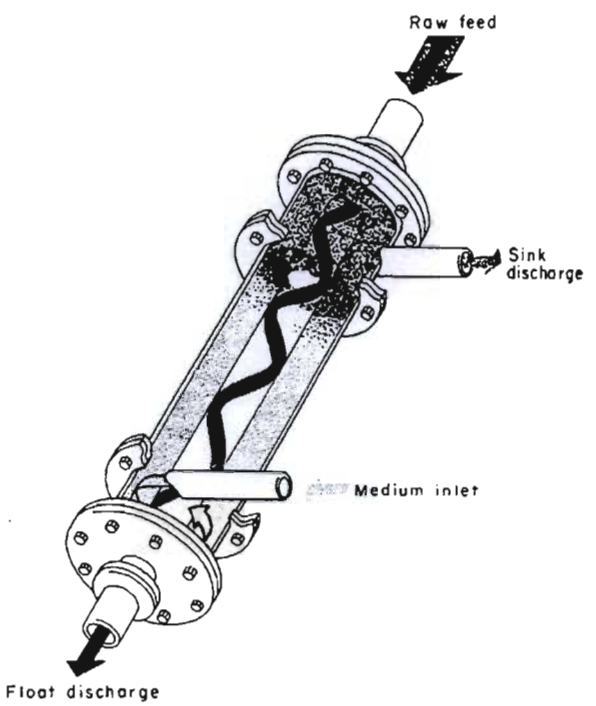

Figure 4.9 Dyna whirlpool [Horsfall (1993), Wills (1997)]

The Dyna whirlpool (Figure 4.9) has become the most used separator for the cleaning of coal with a size range between 30-0.5 mm [Wills (1997)]. It differs from the cyclone in having a completely cylindrical barrel, with the medium inlet being separated from the feed coal. The floats product discharges from the bottom end, the sinks product from the upper end, which is also completely different to the cyclone [Horsfall (1993)]. The separator is operated at an inclined position, and medium of the required specific gravity is pumped under pressure into the lower inlet. The main advantage of this is that the feed does not have to be introduced under pressure since the vortex is created by the medium pumped in at the lower end of the barrel. The medium entering with the feed must only have enough pressure to wash the feed into the separator. Particles with a specific gravity less than that of the medium pass through the vortex generated by the rotating medium. Particles with a much higher specific gravity are pushed to the outer wall of the barrel, and are discharged with the medium through the sink discharge pipe. Due to the proximity of the sinks discharge pipe and the feed inlet, the sinks are removed from the separator almost immediately, reducing wear on the outer walls of the unit. The reduction in wear, and since only the medium is pumped, decreases the maintenance costs, and also maintains performance of the unit. However, the Dyna whirlpool does not have the same sharpness of separation as the cyclone [Horsfall (1993)].

4.2.4 The Tri-Flo Separator

The Tri-Flo (Figure 4.10) separator can be regarded as two Dyna whirlpool separators bolted together [Horsfall (1993), Wills (1997)]. Floats from the first stage become the feed into the second stage. In this way a single unit gives three products.

The device can be operated with two media of differing specific gravities in order to produce sink products of individual controllable densities. Treatment using a single medium specific gravity produces a float and two sinks products which have slightly different separation densities [Wills (1997)]. Although the two-stage separation of the Tri-Flo separator increases the sharpness of separation, its main disadvantage is that only first stage floats can be re-treated. In most two-stage separations it is technically better to re-treat sinks [Horsfall (1993)].

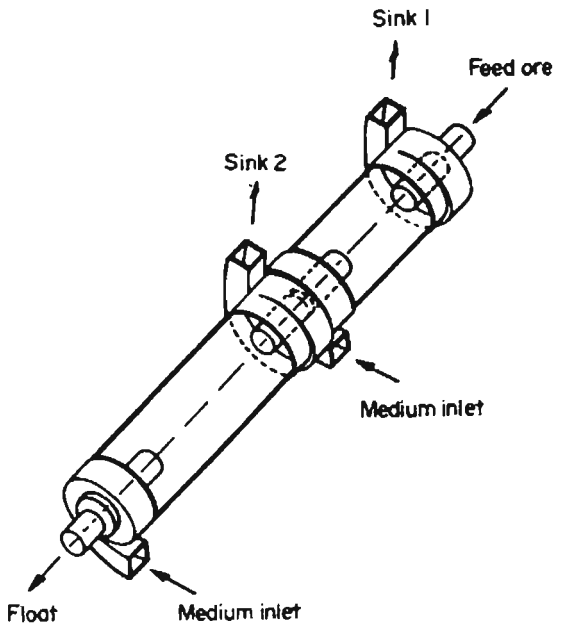

Figure 4.10 Tri-Flo separator [Wills (1997)]

4.2.5 The Larcodems (LARge Coal Dense medium separators)

The Larcodems (Figure 4.11) is virtually a scaled-up Dyna whirlpool (section 4.2.3). The difference being that it can treat a wider range of particles, particularly large particles that cannot be treated in the Dyna whirlpool. Larcodems can treat particles with sizes as large as 100 mm [Horsfall (1993)]. The unit also has at its reject end, a Vortextractor. The function of the Vortextractor is to impose back pressure in the reject stream, in order to restrain the rate at which the sinks product flows.

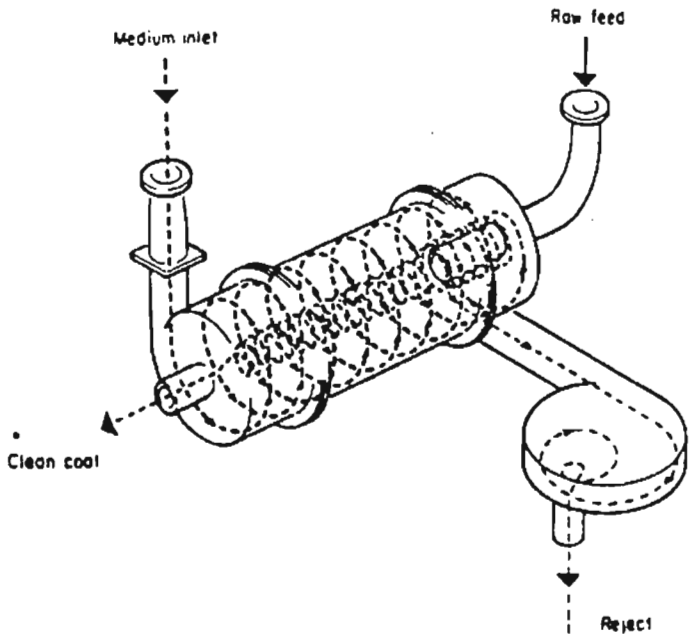

Figure 4.11 Larcodems washer [Horsfall (1993)]

4.3 Efficiency of Heavy Medium Separations

The efficiency of a heavy medium separation can loosely be defined in terms of the ease of separation of a particular ore by a separating vessel. As mentioned in Chapter 2, there are a lot factors which contribute to this ease of separation. These include: specific gravity of the medium; particle size distribution and shape; and slimes / clay content. The factors mentioned above are all properties of the media. Once the appropriate media properties have been chosen, other factors such as ore-particle size, ore-particle density, and type of separation vessel determine the separation efficiency.

Let us first consider the separation of particles in a static bath. When an ore sample is immersed in the fluid, particles which have a high specific gravity relative to the fluid sink, whilst those with a relatively low specific gravity rise to the surface of the fluid. The extent of this happening depends on the amount of time the particles have in the fluid i.e. the residence time of the ore particles in the fluid. The residence time allowed for the particles is highly dependant on the amount of feed with a specific gravity close to that of the separating fluid. Particles with specific gravities close to that of the fluid may not have time to reach the sink, or float product, and will be misplaced into the other product [Wills (1997)]. Particles with a specific gravity similar to the

fluid specific gravity have an equal chance of reporting to the sink or float product. Therefore, separation efficiency varies depending on the density of the particle, ranging from 100 %, where all particles report to the correct product, to 50 % where the particles have the same density as the medium. Thus, the ease, or difficulty of separation is dependant on the amount of material present which has a density close to that of the medium. On the other hand, the efficiency of a particular separating vessel depends on its ability of to separate material with densities close to that of the medium.

4.3.1 The Partition Curve

The partition curve, or the Tromp curve, was first introduced by K.F. Tromp in 1937 [Horsfall (1993)]. This is simply a curve which shows the percentage of the feed material of a certain density which reports to either the sinks or the floats product. If the separating vessel operates with perfect efficiency, the curve is a straight line. All particles with a density less than the separating density will report to the float product, and those with a density greater than the separating density will report to the sinks product. Particles with a density close to the separating density have an equal probability of reporting to either the sinks or the floats.

An example of a partition curve is shown in Figure 4.12. The curve is established by sampling floats and sinks products from a separator using float sink analysis (Appendix A1 and A2). Once the yields of the two products have been determined, the amount of material reporting to each density fraction is calculated. Figure 4.12 is a plot of the amount of feed material of a particular specific gravity reporting to the sinks. This type of plot is common in European collieries. In South Africa and the United States of America, the tendency is to plot the percentage passing to the floats product [Horsfall (1993)].

As shown in Figure 4.12, for an ideal separation all particles with a density higher than the separating density report to the sinks, while those with a smaller density report to the sinks. The curve for real separations approaches the ideal curve at densities far away from the separating density, meaning that efficiency is highest at these densities. The efficiency decreases for particles approaching the operating density.

Most partition curves give a reasonably straight-line relationship between the partition coefficient of 25 % and 75 %, and the gradient of this line is used as an indication of the efficiency of the process.

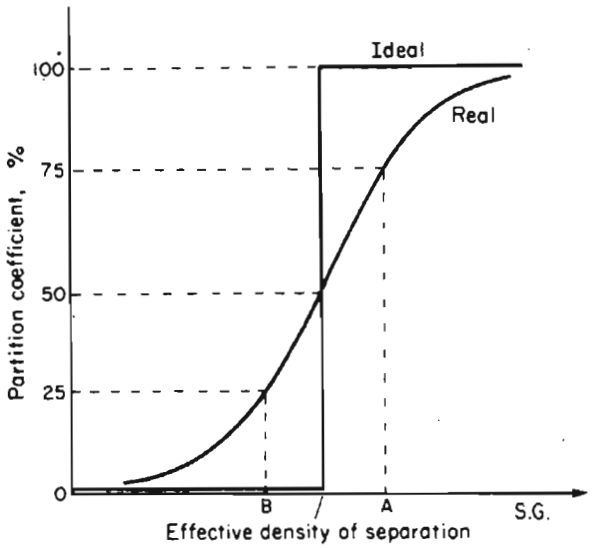

Figure 4.12 Partition or Tromp curve [Wills (1997)]

The parameter used to define the efficiency of a process is the 'probable error of separation' or the 'Ecart probable' (Ep). This is defined as half the difference between the density where 75 % reports to the sinks and that at which 25 % reports to the sinks [Horsfall (1993), Wills (1997)]:

$$Ep = \frac{d_{75} - d_{25}}{2} \tag{4.1}$$

The density at which 50 % of the feed material report to the sinks is known as the 'effective density of separation' (d_{50}), and this value is not necessarily equal to operating density. From Equation 4.1 it can be seen that as the line between 25 % and 75 % becomes vertical, the value of Ep becomes zero. Hence, the lower the Ep value, the more efficient the process. Details of the methods used in the construction of partition curves are given in Appendix A2.

4.3.2 Factors Affecting the Separation efficiency

In the previous section the Ep of separation process was defined. In this section we will take a look at the different factors which play a role in determining the separation efficiency of a process i.e. those affecting the Ep values. Before looking into these factors, a brief theory of the fluid-particle interactions occurring in heavy medium suspensions will be discussed.

4.3.2.1 Hydrodynamics of heavy medium separations

Heavy medium processes are hydrodynamic in nature because they involve the differential motion of particles of different properties through a fluid medium, under the influence of an external force, either gravity (static baths) or centrifugal (dynamic separators) force [Napier-Munn (1990)]. The behaviour of most heavy medium suspensions is non-Newtonian. This non-Newtonian behaviour, and the fact that Heavy medium suspensions are a two-phase system of a dense solid phase in water, makes the development of hydrodynamic equations governing these fluids extremely difficult. Furthermore, such suspensions are unstable, and also segregate under the influence of the same forces as those acting on the particles being separated. This results in a non-uniform distribution of the medium within the separating vessel.

For a spherical particle falling freely in a fluid, three forces act on the particle: a gravitational force acting downwards; an upward buoyant force equal to the weight of fluid displaced by the particle; and an upward acting drag force [Napier-Munn (1990), Wills (1997)]. The net force acting on the particle is then given by:

$$m\frac{dv}{dt} = \left(m - m^*\right)g - F_D \tag{4.2}$$

where m = mass of particle, m* = mass of fluid displaced by the particle, g = gravitational acceleration (9.81 ms^{-2}), and F_D = the drag force acting on the particle.

At the terminal velocity, the acceleration of the particle is zero i.e. dv/dt = 0. Hence, the drag force is:

$$F_D = (m - m^*)g \tag{4.3}$$

For a sphere, of diameter, d, and volume $\pi d^3/6$:

$$F_D = \frac{\pi}{6} g d^3 (\rho_s - \rho_f) \tag{4.4}$$

where ρ_s and ρ_f are the solid and fluid density, respectively.

The drag force is highly dependant on the flow regime. The flow regime is expressed in terms of Reynolds number, which is the dimensionless ratio of inertial to viscous forces on the particle by virtue of its motion in the fluid [Napier-Munn (1990)]:

$$\mathrm{Re}_p = \frac{\rho v d}{\mu} \tag{4.5}$$

where ρ is the fluid density, v is the particle velocity, d is the diameter of the particle, and μ is the fluid viscosity.

The inertial and viscous forces are important because they determine the relative influence of viscosity on the particle motion. At low velocities no separation of the boundary layer from the particle surface occurs, and the drag force on the particle is due only to skin friction, which is directly dependent upon the viscosity of the fluid. Under these conditions the drag force is called viscous drag. At high velocities the boundary layer thickens and separates from the surface of the particle. Eddies form in the wake of the particle, and the resultant energy loss gives rise to form drag. Under these conditions viscosity plays no role in determining the magnitude of the drag force on the particle [Napier-Munn (1990)].

For smooth solid spheres settling in a Newtonian fluid, the viscous drag acting on the particle is:

$$F_D = 3\pi d \mu v \tag{4.6}$$

Substituting Equation (4.6) into Equation (4.4), the particle terminal velocity under laminar flow is known as Stoke's law, and is given by the following expression:

$$v_t = \frac{g(\rho_s - \rho_f)d^2}{18\mu} \tag{4.7}$$

Newton assumed that the drag force was entirely due to turbulent resistance, and deduced the following expression:

$$F_D = 0.055\pi d^2 v^2 \rho_f \tag{4.8}$$

Substituting Equation (4.8) into Equation (4.4), the following expression for the terminal velocity under turbulent conditions is obtained:

$$v_t = \left(\frac{3gd(\rho_s - \rho_f)}{\rho_f}\right)^{1/2} \tag{4.9}$$

For particles settling in a quiescent Newtonian fluid of infinite extent, Stoke's law is valid for particles below about 50 μm, and Newton's law is valid for particle's larger than about 0.5 cm in diameter [Wills (1997)].

Although the expressions developed above are for particles settling in static baths, these can be extended to dynamic separators by generalizing the terminal velocity of a particle moving in a fluid. Generally, the terminal velocity of a particle moving in a fluid is given by [Napier-Munn (1990)]:

$$v_t = K\mu^{-a} d^b \tag{4.10}$$

where a =1 for laminar, a = 0 for turbulent flow; and b = 2 for laminar flow, b = ½ for turbulent flow.

By assuming that the main parameters of the separation are dependant upon the terminal velocity of the particle, the flow regime can be inferred by fitting values of a and b in an equation similar to Equation (4.10), with separating parameters such as ρ_{50} and Ep replacing v_t [Napier-Munn (1990)]. Most calculations, and direct estimates of terminal velocities, show that most particles separated in either static baths or dynamic separators move in the intermediate flow regime. Larger particles in both types of separators will experience fully turbulent flow, in which viscosity plays no role, whereas the finest near-gravity particles separated in dynamic separators like cyclones will approach laminar flow, in which the influence of medium viscosity is very high.

The problem with heavy medium suspensions is that at high medium specific gravities and high solid volume concentrations, their behaviour becomes non-Newtonian. In static baths another problem is that hindered settling sometimes prevails over free settling conditions. In dynamic separators, due to the high centrifugal forces, the particles comprising the heavy medium also undergo some classification. These factors compromise the separation efficiency of heavy medium separators, and make the prediction of partition curves and separation efficiency difficult.

4.3.2.2 Effect of Viscosity and stability on Separation Efficiency

The viscosity and stability have a direct impact on the separation efficiency of heavy medium separations. The viscosity determines the rate at which particles fall through the medium, particularly small particles and those with densities close to the medium density. Stability, on the other hand, determines the rate at which the particles making up the dense fluid segregate out of the suspension. The factors affecting both the viscosity and stability of heavy medium suspensions were also discussed in previous sections. High medium specific gravities, corresponding to a high solids volume concentration, result in relatively high medium viscosities and stability. A trade-off thus exists between choosing a medium with a high viscosity and stability, to choosing one with a low viscosity and stability. As mentioned earlier, the trend in industry is to work with a medium which has a moderately high viscosity and stability.

The efficiency in heavy medium separations is represented by the Ecart probable (Ep). In order for viscosity to have an impact on the Ep values of a particular separation, there must be a certain amount of viscous drag acting on the particle as it flows through the medium, for both static and

dynamic separators. Most heavy medium separations take place in the intermediate flow regime, in which the influence of viscosity on terminal velocity, and thus on ρ_{50} and Ep, is variable.

Napier-Munn (1990) discusses the results of other workers on the separation of coal in bath separators. The coal separated had a top size of 50 mm, and the lower size varied from 3 to 6 mm. in each case, the efficiency of separation declined as viscosity increased. This corresponds to an increase in Ep values with an increase in viscosity. It was also observed that the viscosity effects were strongest for coals with a high proportion of near-gravity material. In a separate investigation, efficiency data were correlated as follows:

$$Ep = 0.0085\left(\frac{\mu_p}{d}\right)^{1/2} \tag{4.11}$$

where μ_p = plastic viscosity (cP), and d = feed size (inches).

By comparing the exponents in Equation (4.11) to those in Equation (4.10), it was concluded that the particles moved mainly in the turbulent or upper intermediate regime. As shown in Section 4.3.2.1, this means that viscosity has only a little effect, if any, on the separations occurring in static baths. Experiments on Drewboy separators confirmed that turbulence prevailed in these separators, and that the main problem faced in bath separators is that coarse settling particles have a tendency to drag small particles with them.

In the early development of dynamic separators, it was generally believed that viscosity had little influence on their separation efficiency, because of the high rates of shear prevailing [Napier-Munn (1990)]. However, numerous experimental works have proven that viscosity does play a role, although the effects may be small at low medium densities and low contamination levels. Collins et al. (1983) showed that both suspension viscosity and stability have an effect on the separation efficiency of dynamic separators. They showed that a suspensions with a high viscosity resulted in lower separation efficiencies. They also showed that although lower viscosities resulted in higher efficiencies, there was a critical value beyond which the low stability of the suspension also resulted in inefficient separations. They showed that the separation efficiency of fine particles was much higher at lower suspension viscosities.

In the analysis of heavy medium separations using dynamic separators, particularly cyclones, other parameters apart from Ep values have been used to infer separation efficiency. One such parameter is the density of separation in the cyclone, which represents the density at which 50 % of the feed has an equal chance of reporting to either the overflow or under flow. The separation density is directly dependant on the amount of material reporting to the floats and sinks product. A lower separation density results in higher proportions of ore to the underflow, whereas a higher separating density results in a higher proportion of ore to the overflow. The separation density is not necessarily equal to the medium density, and this is confirmed by the following expression [Napier-Munn (1990)]:

$$\delta_{50} = \rho_f + K\left[\frac{D_c^3 \mu}{Qd^2}\right] \tag{4.12}$$

where Dc = cyclone diameter; Q = flowrate; K = geometry constant; □f = feed medium density, and μ = apparent viscosity.

Using dimensional analysis and carrying out experiments to confirm the analysis, Napier-Munn (1990) concluded that for stable media, both the separation density and the Ep increase with viscosity. This can easily be deduced from Equations (4.11) and (4.12).

Collins et al. (1983) showed that the separation density and Ep are a quantitative function of the medium density, normally the underflow density. They performed experiments on a Vorsyl separator and DSM cyclone using ferrosilicon and ferrosilicon / magnetite suspensions. They found that the viscosity and stability had a direct impact on the separating density and Ep of the separators. To infer the amount of particle segregation occurring in the separators, due to the unstable nature of heavy medium suspension, the density differential was used (□u – □o), where □u and □o are the underflow and overflow densities, respectively. The segregation of the medium also has an effect on the relationship between the underflow density and the separation density. For relatively low values of density differential, the separation density is usually higher than the underflow density. However, as these values increase, the separating density begins to drop below the underflow density. Under conditions of medium stability the separation density is equated to the underflow density for all types of media for the Vorsyl separator DSM cyclone used in the latter's work.

Analysis of the product streams from a Vorsyl separator indicated that little segregation of the medium occurred by particle size or density with cyclone differentials ($\square_a - \square_b$) up to 500 kgm^{-3}. Generally, segregation only became a serious problem when the differential exceeded 700 kgm^{-3} for a 1 / 1 cyclone 60 (and coarse FeSi) – magnetite mixture. It was then established that for this type of medium the cyclone underflow density increased linearly with cyclone feed density up to a differential of 500 – 600 kgm^{-3} and then stabilized at a constant density, which indicates that classification of the medium was occurring at this point.

Testwork conducted on the DSM cyclone also showed the same results as those for the Vorsyl separator. In this case, however, the transition point occurred at 800 kgm^{-3}. It was also found that although the separation density equated to the cyclone underflow density below this differential, it dropped rapidly above this level.

In order to maximise the efficiency of separations in both the DSM cyclone and the Vorsyl separator, an optimum density differential has to be reached. This value is also highly dependent on the ore particle size. Generally, the best working range for both separators is with a density differential of 200 – 500 kgm^{-3}, the optimum being at about 400 kgm^{-3} [Collins et al. (1983)].

4.3.2.3 Effect of Cyclone design and operating conditions on Separation Efficiency

The design of any separation vessel is critical to the degree of efficiency which can ultimately be achieved by the separator. The choice between the type of separating vessel to use, static bath or dynamic separator, depends to a large extent on the particle size range of the ore being treated. As the ore particle size decreases, the efficiency of static baths decreases below that of dynamic separators due to insufficient downward force on the particles. As the particle size increases, the efficiency of static baths exceeds that of dynamic separators. This is illustrated in Figure 4.13, which shows a plot of Ep versus particle size for both dynamic and static separators.

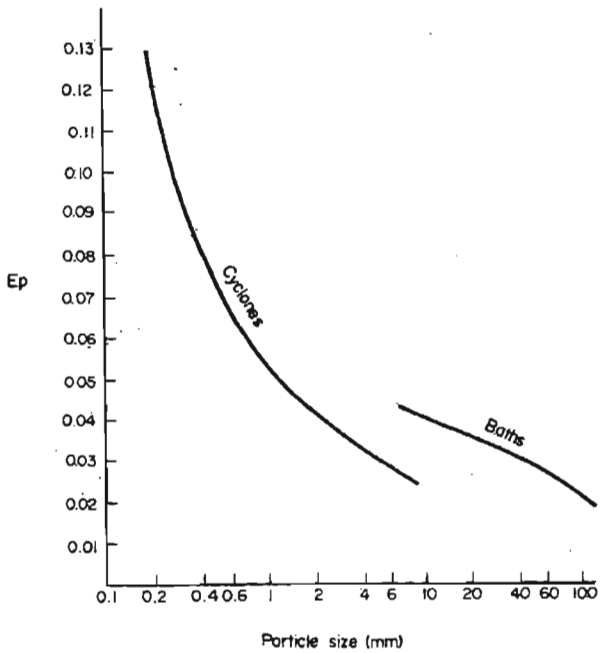

Figure 4.13 Effect of particle size on efficiency of heavy media suspensions [Wills (1997)]

This section will discuss the operating variables of dynamic separators, particularly cyclones, because a dynamic separator was used for this project. As mentioned in Section 4.2, dense medium cyclones are operated at an angle to the horizontal. The magnitude of the angle depends on the properties of the suspending medium and the operating variables of the cyclone, but ranges between 10° and 30°. The conventional operating angle is 20°. The main principle of separation in cyclones has already been explained in Section 4.2.1. However, the principal separating zone of the cyclone is normally accepted as being in the annular region between the periphery and the vortex finder [Collins et al. (1983), Wills (1997)]. The rates of shear decrease radially within the cyclone, with maximum shear rates achieved at the centre of the cone. Depending on the ore particle properties, this determines the choice of separating medium used. A pseudo-plastic medium will give low viscosities at the centre of the cone, whereas a dilatant medium will give high viscosities.

Lilge et al. (1958) did some experiments using magnetite, ferrosilicon, galena, and pyrite heavy media. The separating vessel used I their investigation was a Driessen cone. The operating principles of the cone are similar to those of a DSM cyclone, and as such, their observations can be extended to that of the DSM cyclone. The pilot-plant work done was on uranium ores in feed size ranges from (-5.6 mm + 325 μm) to (-2mm + 325 μm). The general conclusion drawn from

their results was that when a cone is operated at a particular medium specific gravity, a change of any of the other operating variables which cause an increase of apparent viscosity of medium will increase the amount of ore reporting to the underflow, thus decreasing the mineral separation efficiency. A summary of the operating variables they investigated, and their effect on particle separation efficiency, are given below.

4.3.2.3.1 Cone Inlet Area

The throughput capacity of the cone is a function of the overflow orifice diameter. Therefore, if the overflow orifice diameter and all other conditions in the cone, except inlet area, are kept constant, velocities, rates of shear and apparent viscosities in the cone will remain the same. The amount of feed material to the underflow and particle separation efficiency will also be the same for all inlet areas. For inlet areas smaller than the overflow orifice area, the inlet velocity increases, and this may induce turbulence at the intake of the cone which could lower the separation efficiency. It is thus considered advisable to have the inlet area approximately equal to the overflow orifice area.

4.3.2.3.2 Cone Inlet Pressure

Any increase in the cone inlet pressures increases the velocities. The rates of shear will be higher and, therefore, depending on the behaviour of the medium, apparent viscosities are either lower or higher. If the apparent viscosities are lower, the amount of material reporting to the underflow decreases, and there is an increase in mineral separation efficiency.

4.3.2.3.3 Cone ratio

The cone ratio is defined as the ratio of the underflow orifice diameter to the overflow diameter. An increase in the cone ratio increases the throughput capacity of the cone to some extent, provided the overflow diameter remains constant. If the inlet pressure is kept constant, velocities in the cone are higher for high cone ratios than for low ratios. Therefore, apparent viscosities in the cone will be somewhat lower for the high cone ratios than for low cone ratios, provided the medium is pseudoplastic.

4.3.2.3.4 Medium Split Ratio

The medium split ratio is defined as the cyclone overflow to underflow ratio. The underflow medium density and density differential are affected by the medium split ratio. At any given feed medium density, they both increase with the medium split ratio. The overflow medium density is almost unaffected by the medium split ratio [He et al. (1995)]. At a medium split ratio below 1.0, short-circuiting of light feed particles to the cyclone underflow occurs, resulting in low separation efficiency. The separation efficiency increases continuously with increasing split ratio, levelling off at a split ratio above 4.0. At a particular split ratio, a combination of smaller vortex finder and underflow orifice (spigot) diameters improves particle separation efficiency, at the expense of lower cyclone throughput.

4.3.2.3.4 Ore-to-Medium Ratio

The ore-to-medium ratio is defined as mass of ore to mass of medium. The ore particles being separated are usually much coarser than those of the media, resulting in a reduction in the average apparent viscosity with addition of ore to the medium. Therefore, the higher the ore-to-medium ratio, the better is the separation efficiency. This also has the effect of increasing the ore throughput in the cone. However, an increase in the ore-to-medium ratio increases the density differential of the cone. Care should be taken to ensure that this ratio does not exceed density differential values which result in the classification of the medium in the cone.

4.3.2.3.5 Shape of Cone

The slope of the conical section of the cone has no effect on the viscosity distribution in the cone, provided the cone diameter remains the same. Rates of shear and, therefore, apparent viscosities are the same for all cones whether tapered or truncated. This means that particle separation efficiency remains the same.

Chapter 5

Experimental Equipment

This Chapter describes the equipment used in the experimental work performed during this project. The main pieces of equipment used in the project were a rotational viscometer, Brookfield viscometer, and a DSM cyclone. Also described are analytical instruments used to determine the properties of the media used in these investigations. These are a Scanned Electron Micrograph, Malvern Sample analyzer, and UV Spectrometer.

5.1 Rheology Measurement

5.1.1 The Rotational Viscometer

The rheometer used in this project was designed and built within the School of Chemical Engineering, Howard College Campus, University of Kwa-Zulu Natal. The rheometer operates under Searle's principle; with a rotating bob and standing still cup. The principle operations of rotational viscometers were given in Chapter 3, Section 3.2.

The rheometers used in this project were designed using the DIN 53019 / ISO 3219 standards given in Section 3.5. It is important to note that these standards do not give the absolute sizes of the cylinder radii but their relation. The basic design of the rheometers was essentially similar to that shown in Figure 5.1, and the dimensions are shown in Table 5.1. A hole was drilled at the base of the cup. The base of the cup had a thickness of 8 mm. A pipe was then connected to the base (0.5 cm diameter), and this was the passed through a peristaltic pump, and the medium in cup was recycled back to the top of the cup.

Initial rheological measurements were carried out using a polyvinylchloride (PVC) bob and cup, and this rheoemter was designated as Rheometer 1. However, the results obtained using this rheometer were irreproducible due to the settling out of media particles. A second rheometer was designed to reduce the settling of the media particles. This rheometer was constructed out of

stainless steel for improved damping, and a chamfer was added at the base of the cup for improved circulation.

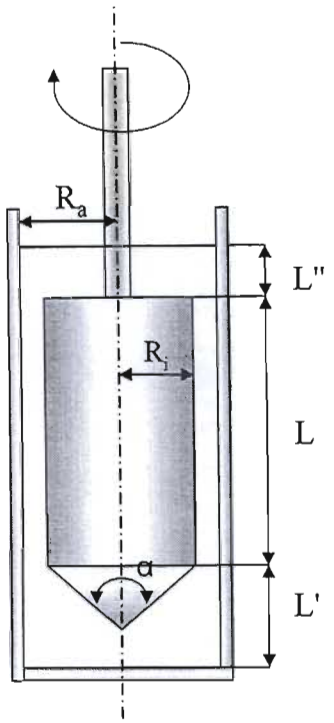

Figure 5.1 Cross-section of DIN 53019 / ISO3219 viscometer

Table 5.1 Rheometer dimensions of Rheometer 1 and Rheometer 2

Symbol	Description	Rheometer 1	Rheometer 2
R_a	Cup radius	24 mm	25 mm
R_i	Bob radius	20 mm	23 mm
L	Length of cylindrical section of the bob	60 mm	69 mm
L'	Distance between the lower edge of cylindrical part of the bob and the bottom of the measuring cup	20 mm	31 mm
L"	Immersed shaft length	50 mm	50 mm
Rs	Shaft radius	4 mm	4 mm
α	Cone-tip angle	120°	120°

5.1.2 Rheometer Modifications

The rheometer had to be modified because of the settling nature of the suspensions. A chamfer was put at the base of the cup in order to reduce the accumulation of solids. The bob was driven by a variable speed electric motor which could attain speeds up to 2000 rpm. The torque on the bob surface was measured using a load cell. The rheometer cup was mounted on a turntable on bearings. Fluid resistance experienced on the bob surface caused the turntable to move. This movement was measured by the load cell, and the value of the torque was displayed on a digital read out. A cross-section of the modified rheometer, together with the set-up, is shown in Figure 5.2. Figure 5.3 is a picture of the experimental set-up.

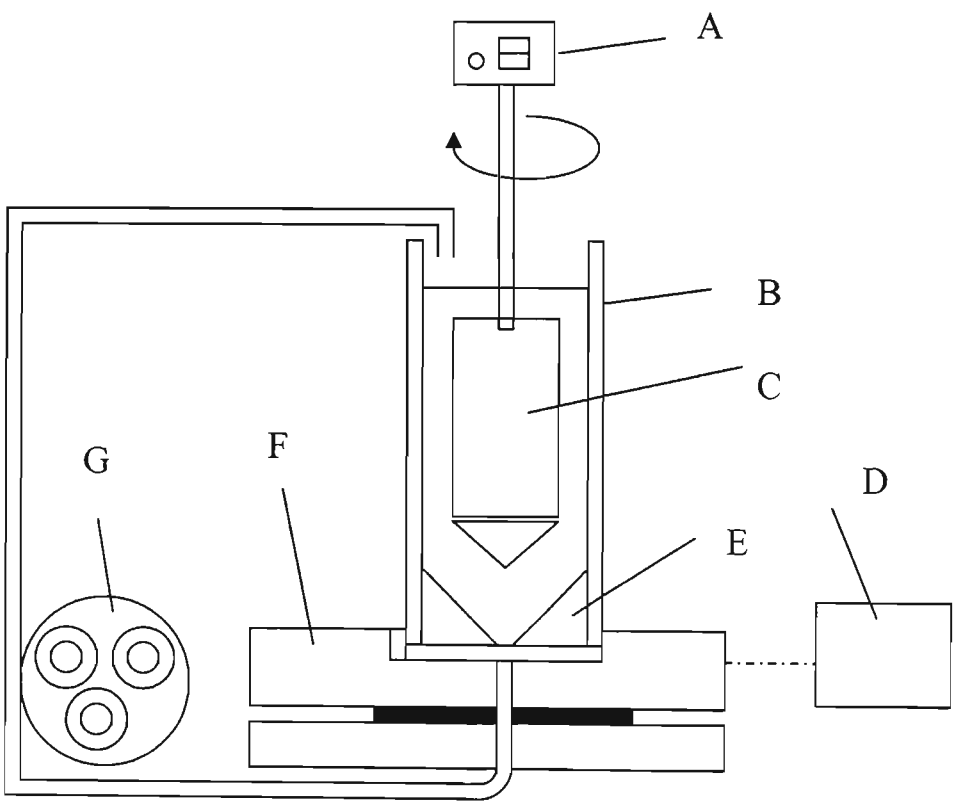

Figure 5.2 Schematic diagram of a modified rotational viscometer: A, variable speed motor; B, cup; C, bob; D, Load cell with digital readout; E, chamfer; F, turntable on Bearings; G, peristaltic pump

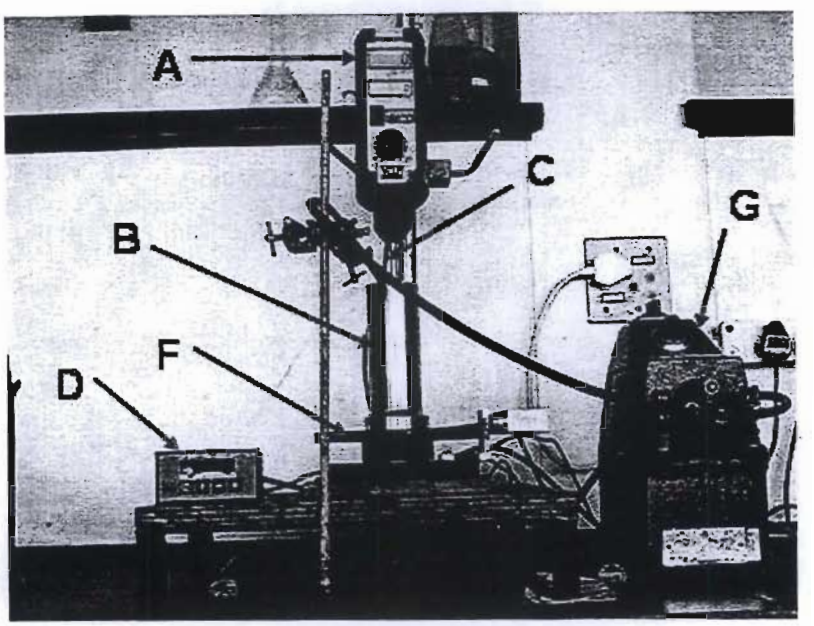

Figure 5.3 Experimental rheometer set-up: A, variable speed motor; B, cup; C, bob; D, Load cell with digital readout; E, chamfer; F, turntable on Bearings; G, peristaltic pump

The dimensions of the modified rheometer (Rheometer 2) are shown in Table 5.1. Apart from the inclusion of a chamfer in the modified rheometer, the measuring gap was also reduced. The material of construction was also changed to stainless steel in order to reduce wear of the bob and cup due to particle abrasion.

Table 5.2 shows how the dimensions of the rheometers compared to those specified by DIN 53019 / ISO 3219 standards. The definitions of these symbols were given in Table 5.1. Table 5.3 shows that only Rheometer 2 fully meets the criteria set out by the standards i.e. a much narrower gap size.

Table 5.2 Comparison of rheometer dimensions to those given by DIN 53019/ISO 3219

	DIN 53019/ISO 3219	Rheometer 1	Rheometer 2
□	□1.1 (preferably 1.0847)	1.20	1.09
L/R_i	□3.0 (preferably 3.0)	3.00	3.00
L'/R_i	□1.0 (preferably 1.0)	1.00	1.34
L''/R_i	□1.0 (preferably 1.0)	2.50	2.17
□	90° □□□150° (preferably 120°)	120°	120°
R_s/R_i	□0.30	0.02	0.02

5.2 The Dense Medium Cyclone

The separation tests were conducted on a pilot scale dense medium cyclone loop, illustrated in Figure 5.4. The loop is similar to that described by He et al. (1994). The cyclone was constructed using polyvinylchloride, and was operated at a cone angle of 20°.

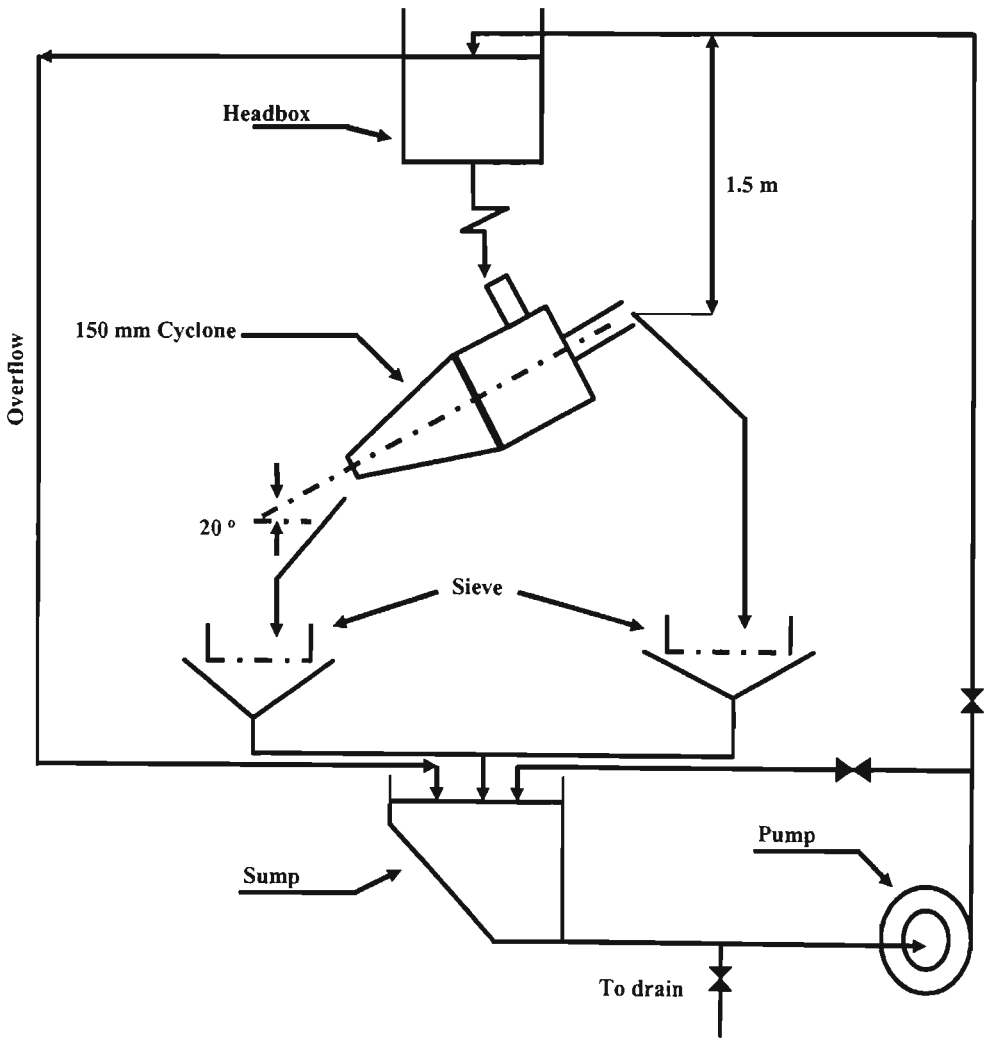

Figure 5.4 A schematic diagram of the 150 mm dense medium cyclone loop [He et al. (1994)]

The cyclone was gravity fed at a pressure head of 1.5 m ($10xD_c$). The cyclone vortex finder and spigot diameters were 65 mm and 50 mm, respectively. Coal samples were introduced in the Headbox and allowed to pass through the system for at least 2 minutes, before being collected on

hand-held screens of appropriate sizes. The density of the feed, overflow, and underflow were measured using a method similar to the density can method described by Wills (1997). Figure 5.5 shows a picture of the DMS cyclone loop.

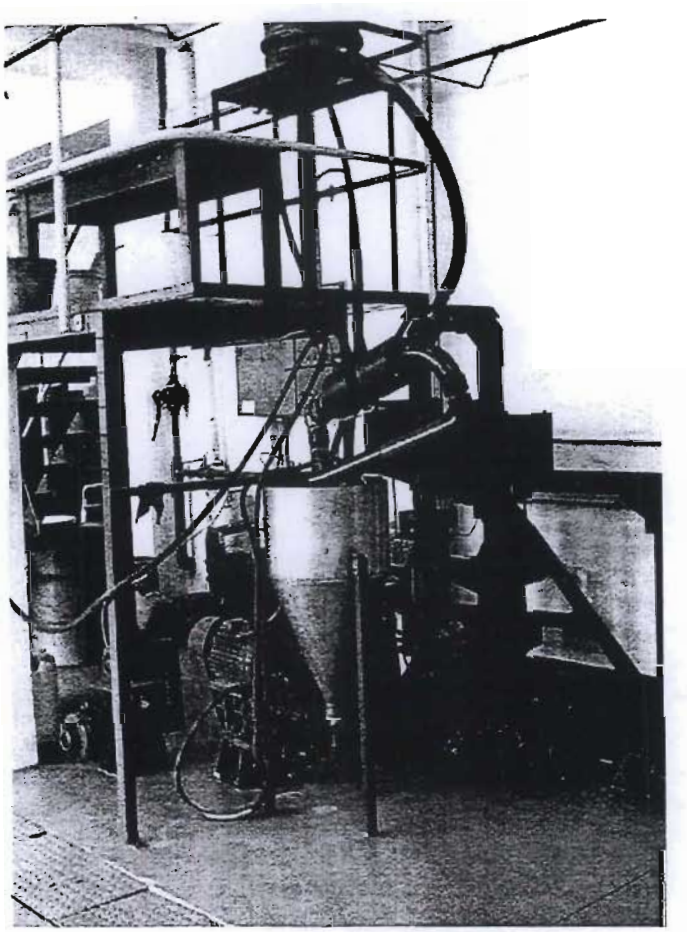

Figure 5.5 Picture of DSM cyclone loop

The loop also included an overflow pipe which returned the overflow back to the sump and a recycle loop between the pump and the sump. Before the loading of the magnetite solid particles, the required amount of water was first run through the system in order to prevent pipe blockages within the system. A more detailed description of the cyclone is included in Appendix A3.

5.3 Sundry Analytical Equipment

5.3.1 Brookfield Viscometer

The Brookfield viscometer was used in the calibration of the rheometers. The calibration procedure is presented in Appendix A1.

Manufacturer : Brookfield Engineering Laboratories, Inc.

Model : RVT

Serial number : 112168

5.3.2 Malvern Sample Analyzer

The Malvern Sample Analyzer was used to get the size distributions of the media used in the investigations. A picture of this apparatus is presented in Appendix A3. The analyzer used was the Metsizer 2000.

5.3.3 Scanned Electron Micrograph (SEM)

Two types of SEM units were used to view the media particle shape, and also to determine the mineral composition of the media. Pictures of the SEM units are given in Appendix A3.

A LEO 1450-Standard SEM was used to view the media particle shape. It consisted of a tungsten filament, an oxford energy disperser for spectrum analysis, and a backstator detector. Its serial number was 1450 0440.

To determine the mineral composition of the media, a Hitachi S-520 SEM unit was used. The unit also had a tungsten filament. During analyses the media particles become highly charged, which hinders their analyses. To prevent this, the particles are either gold, or carbon coated.

5.3.4 Spectrophotometer

The spectrophotometer was used to measure the absorbance of DP001 onto the media particles. The procedure for the measurement of DP001 absorbance is given in Appendix A2. A picture of the unit is given in Appendix A3.

Manufacturer : Laboratory and Science Equipment Co.

Make : UV-9100 Spectrophotometer

Serial number : 021329

Chapter 6

Experimental

Chapter 6 describes and discusses the experimental work performed in the investigation into the viscosity of heavy medium suspensions. The heavy media used in these investigations were 270D milled ferrosilicon, magnetite #1 (fine), and magnetite #2 (coarse). Smectite clay was used with the ferrosilicon suspensions to simulate slimes build-up which usually occurs in industrial separations.

Apart from the measurement of the viscosity of plain suspensions, the effects of a surface active agent called DP001 (Experimental series A), and particle size distribution (Experimental series B) on the viscosity of the suspensions were also investigated. The effect of both DP001 and media particle size distribution on the separation efficiency of a dense medium cyclone were also investigated (Experimental Series C).

The experimental result sections contained in this chapter are as follows:

6.1 Heavy Media Suspension Properties

6.2 Experimental Series A
The effect of DP001 on the viscosity of heavy medium suspensions

6.3 Experimental Series B
The effect of media particle size distribution and shape on the viscosity of heavy medium suspensions

6.4 Experimental Series C
The effect of DP001 and media particle size and shape on the separation efficiency in a dense medium cyclone

Each section discusses the aim of the particular experimental procedure, the equipment used, and the results obtained. The results in this section are presented such that they compliment only the specific aims of that experiment. Details of experimental results and raw data are presented in Appendix A1, while experimental procedures are contained in Appendix A2. Descriptions of experimental equipment are contained in Chapter 5 and Appendix A3.

6.1 Heavy Media Suspension Properties

6.1.1 Determination of the Media particle size distribution

6.1.1.1 Aim of the Experiment

The viscosity of heavy medium suspensions is largely dependant on the media particle size distribution. It is thus pertinent to know the particle size distribution of the media used in this investigation.

6.1.1.2 Experimental Method and Equipment

The media used in this investigation were: Ferrosilicon media; Magnetite #1 media; Magnetite #2 media; and Smectite clay. The densities of the media particles were determined using the density bottle technique described by Wills (1997), contained in Appendix A3. Table 6.1 gives the densities of the media particles.

Table 6.1Media particle density

Sample	Density (kgm^{-3})
Ferrosilicon	6800
Magnetite #1	4600
Magnetite #2	4600

The media particle size distributions were determined using a Malvern Sample Analyzer (Metsizer 2000). All tests were carried out at a temperature of 25 °C. Half a spatula of each sample was added to a 1000 ml beaker of water. The sample was then placed in the analyzer to obtain the size distribution. To minimise the agglomeration of some of the solid particles in the water, sodium hexametaphosphate was added to the water in order to disperse the solid particles. Four measurements were made for each sample, and the average sizes were plotted to obtain the size distribution.

6.1.1.3 Experimental results and Discussion.

Figure 6.1 shows the size distribution of the media particles.

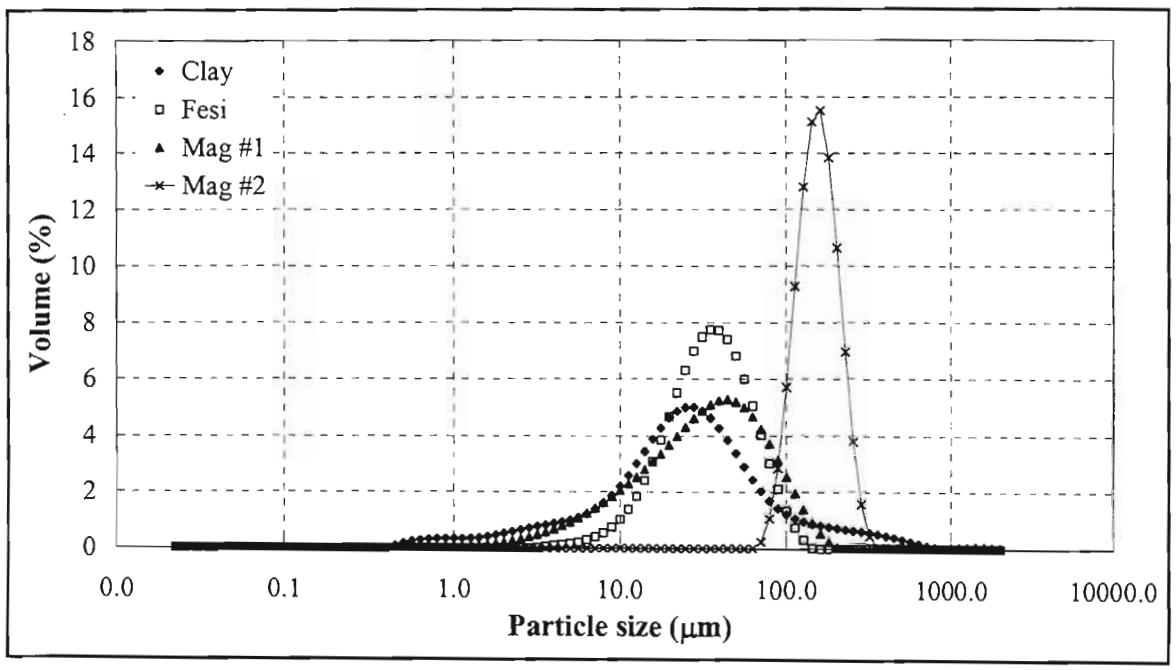

Figure 6.1 Media particle size distribution

Table 6.2 summarises the results obtained from Figure 6.1.

Table 6.2 Summary of media particle sizes

Sample	d_{mean} (µm)	d_{mode} (µm)	d_{50} (µm)
Ferrosilicon	38	35	33
Magnetite #1	45	42	32
Magnetite #2	150	144	145
Smectite clay / slime	48	25	45

The results show that magnetite # 2 is the coarsest of all the media tested, followed by magnetite #1, ferrosilicon, and lastly smectite clay / slime. Figure 6.1 also shows that magnetite #2 has the

narrowest range compared to the other particles. Magnetite #2 has a particle size range between 63-356 μm. The slime particles have the largest particle range, ranging from below 1 μm to 893.37 μm. However, the slime also has the smallest particle sizes, with 4.52 % of the particles less than 2.0 μm.

The results show that ferrosilicon particles have a smaller particle size range (3 to 142 μm) than magnetite #1 particles (0.8-224 μm). The average particle size of the ferrosilicon particles is also much less than those of the magnetite particles. However, the magnetite #1 media particles have a much higher percentage of fine particles. Magnetite #1 has 0.94 % particles less than 5.0 μm, whereas ferrosilicon has 0.17 %. The percentage particles below 2 μm are 0.87 % for magnetite #1, and zero for ferrosilicon. This is a feature of the size distributions of commercial ferrosilicon and ground magnetite [Aplan et al. (1964)]. These differences in the size distribution of the media have an appreciable effect on their rheological properties.

The results from the Malvern analyzer were then plotted to determine whether these particles follow the Rosin-Rammler distribution, which is given by:

$$\log\left[\ln\frac{100}{100-P}\right] = \log b + n\log d \qquad (6.1)$$

where P is the cumulative undersize in per cent, b is a constant, d is the particle size (μm), and n is a constant.

Of the media tested, only ferrosilicon and magnetite #1 were well represented by the Rosin-Rammler distribution. Their straight line plots are shown in Figure 6.2

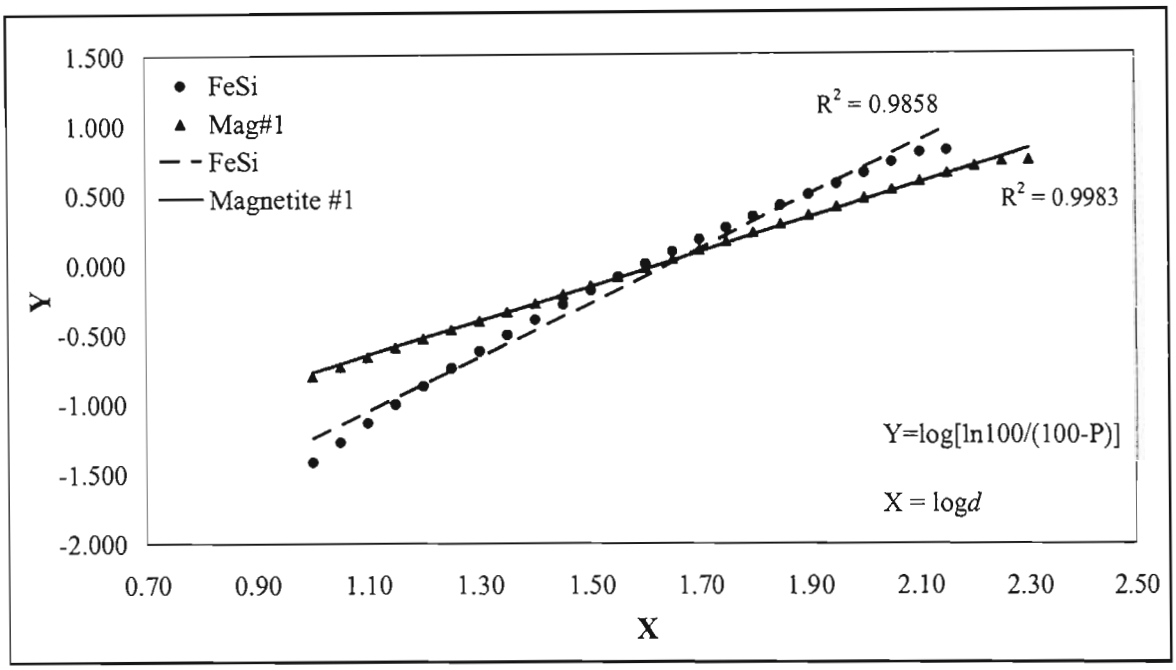

Figure 6.2 Rosin-Rammler plots for ferrosilicon and magnetite #1 media

The liner correlation coefficient is 0.9858 for ferrosilicon, and 0.9983 for magnetite #1. These are both in excess of 0.95, which is normally expected for ferrosilicon distributions [Collins et al. (1974)].

6.1.2 Media Particle Chemical and Physical Specifications

6.1.2.1 Aim of the Experiment

The aim of these experiments was to determine the physical and chemical properties of the media particles by evaluating their surface shape and elemental composition.

6.1.2.2 Experimental Method and Equipment

Both the media particle surface shape and elemental composition were determined using a Scanned Electron Micrograph (SEM). The SEM used was from the Physics department at the University of Kwa-Zulu Natal, Howard College campus. A more detailed description of the SEM is contained in Appendix A3.

6.1.2.3 Experimental Results and Discussion

6.1.2.3.1 Particle Shape

The media particle shape is important in heavy medium suspensions because it determines the extent to which particles interact with one another. For a particular medium, at a constant density, spherical particles will result in medium with a much lower viscosity and stability, whereas coarser media particles result in higher viscosities and stability [Collins et al. (1983)].This is mainly due to the inter-particle slippage, which is much greater for spherical particles, than for milled particles [Aplan et al. (1964)].

Particle shape is also important because, in some cases, it determines the media particle strength. Particles with sharp corners and edges are more likely to breakdown in the separation process than smoother particles. This has been observed in separation processes using atomised and milled ferrosilicon [Rodis et al. (1960)].

Figure 6.3 through Figure 6.6 shows the surface shape of the media particles obtained from the SEM, at a magnification equal to 560 times.

From Figure 6.3, it can be seen that the particle shape for the ferrosilicon particles is rough and angular. This is to be expected since it was mentioned at the beginning of this section that the ferrosilicon particle specification was 270D. Milled ferrosilicon particles always have a rough angular particle shape [Ferrara et al. (1986)].

There is a marked difference in the particle shapes of the magnetite media, as illustrated in Figure 6.4 and Figure 6.5. Magnetite #1 is rough and angular in shape, whereas magnetite #2 is smooth and almost spherical in shape. This is mainly due to fact that magnetite #2 was obtained from sands dunes at Richards Bay Minerals (RBM). The weathering of the particles on the sand dunes resulted in their more spherical shape.

Figure 6.6 also shows that the smectite clay / slim is rough and angular in shape. This will have a great influence on the rheological properties of ferrosilicon / clay suspensions. The much smaller

size distribution and angular shape of these particles will result in higher viscosities and improved stability when they are added to the ferrosilicon suspensions.

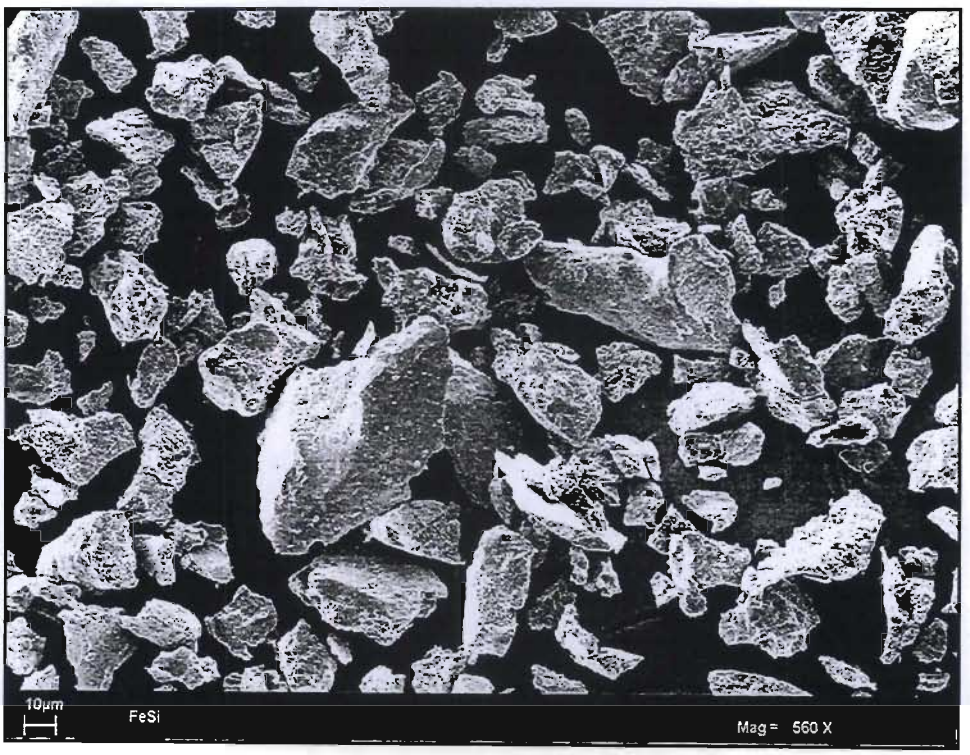

Figure 6.3 Ferrosilicon SEM particle shape

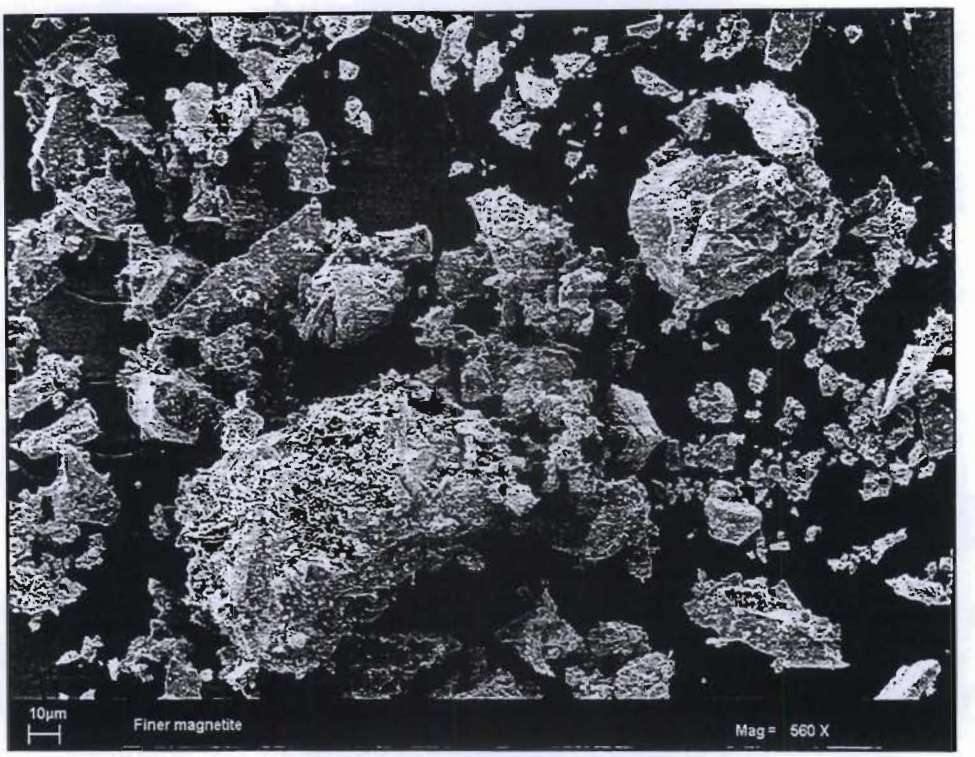

Figure 6.4 Magnetite #1 SEM particle shape

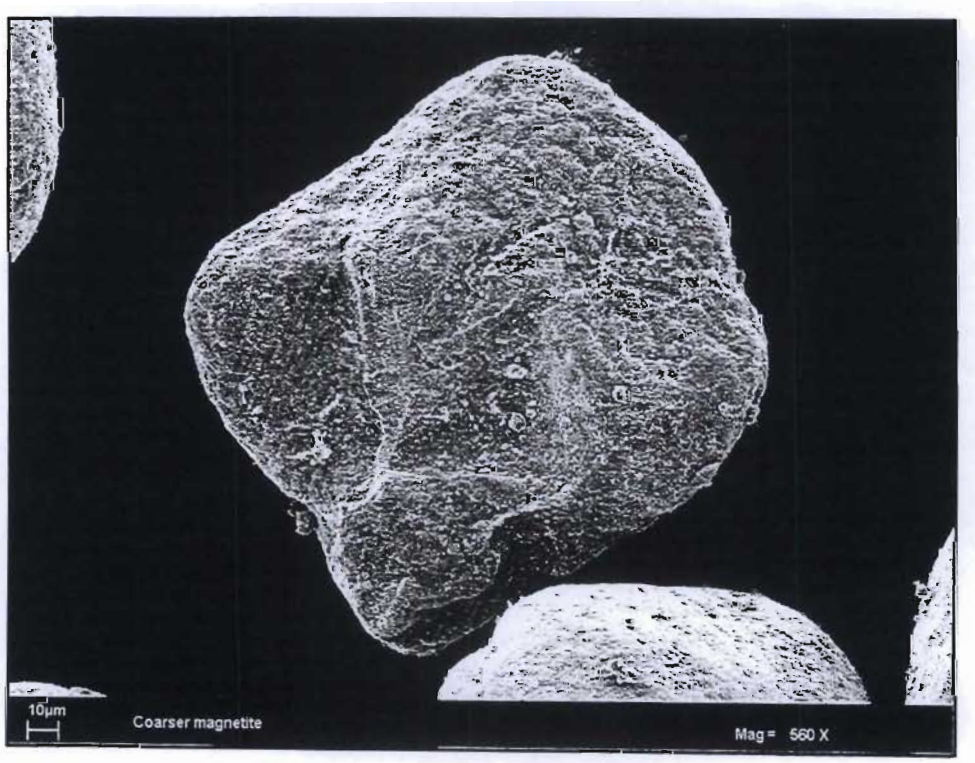

Figure 6.5 Magnetite #2 SEM particle shape

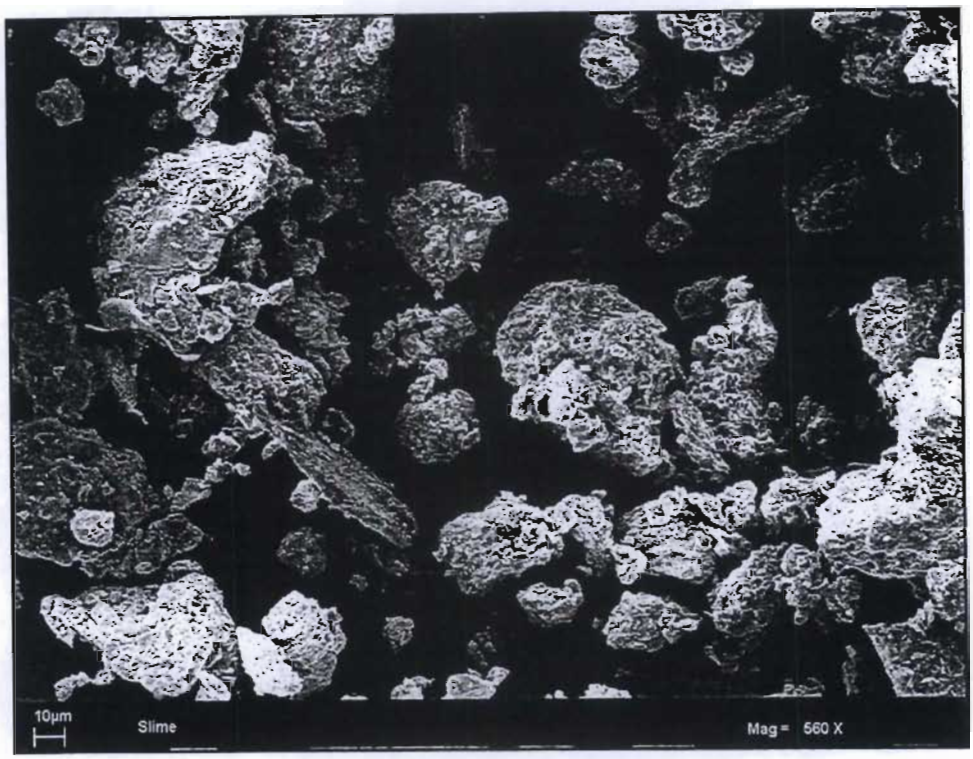

Figure 6.6 Slime (smectite clay) SEM particle shape

6.1.2.3.2Chemical / Elemental Specifications

Although the chemical / elemental specifications of the media particles have no relation to the context of the current investigations, they are presented here in consistency with the current section.

The elemental composition of the media particles determines the physiochemical properties of the media particles. This includes their interaction with the dispersing phase, and their magnetic susceptibility. For ferrosilicon particles, the amount of silicon should range between 14 to 16 % in order for them to be easily recoverable via magnetic capture, and also to reduce the corrodibility of the particles [Collins et al. (1974), and Wills (1997)]. Figure 6.7 shows the elemental composition of the ferrosilicon media used in these investigations. It is important to note that this is not a plot of the mass percentage, but only the elemental percentage

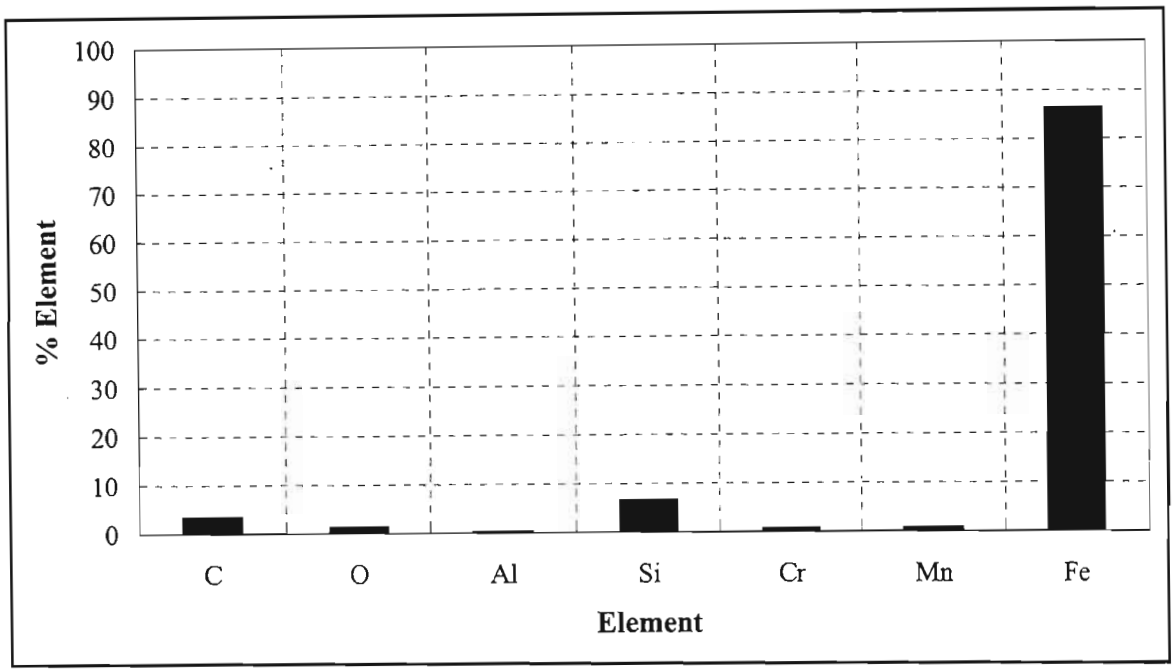

Figure 6.7 Elemental analysis of ferrosilicon media

The results show that the two highest elements in the ferrosilicon media are Iron (Fe) and Silicon (Si). The presence of carbon is probably due to calcium carbonate ($CaCO_3$), and the aluminium is probably due to the presence of aluminium oxide (Al_2O_3). The silicon comes from the quartz used in the manufacture of milled ferrosilicon. However, the percentage silicon appears to be much lower than that need for industrial heavy medium separations. This may be due to experimental error as the SEM could have only scanned one bit.

Figure 6.8 and Figure 6.9 show the elemental compositions of the magnetite media and the slime, respectively. It is interesting to note the presence of titanium found in these media, particularly in magnetite #2. As mentioned previously, magnetite #2 was supplied by RBM, who produce titanium from ilmenite. Hence, the magnetite from this site will have a considerable amount of ilmenite. The slime came from a diamond processing plant.

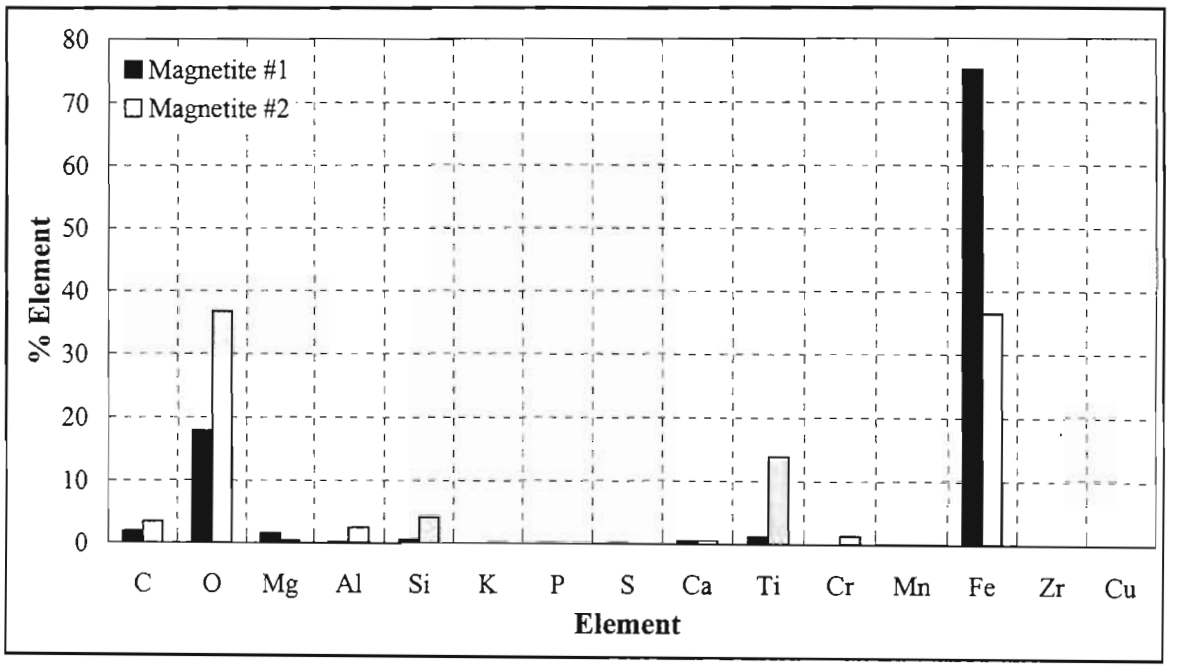

Figure 6.8 Elemental analysis of magnetite media

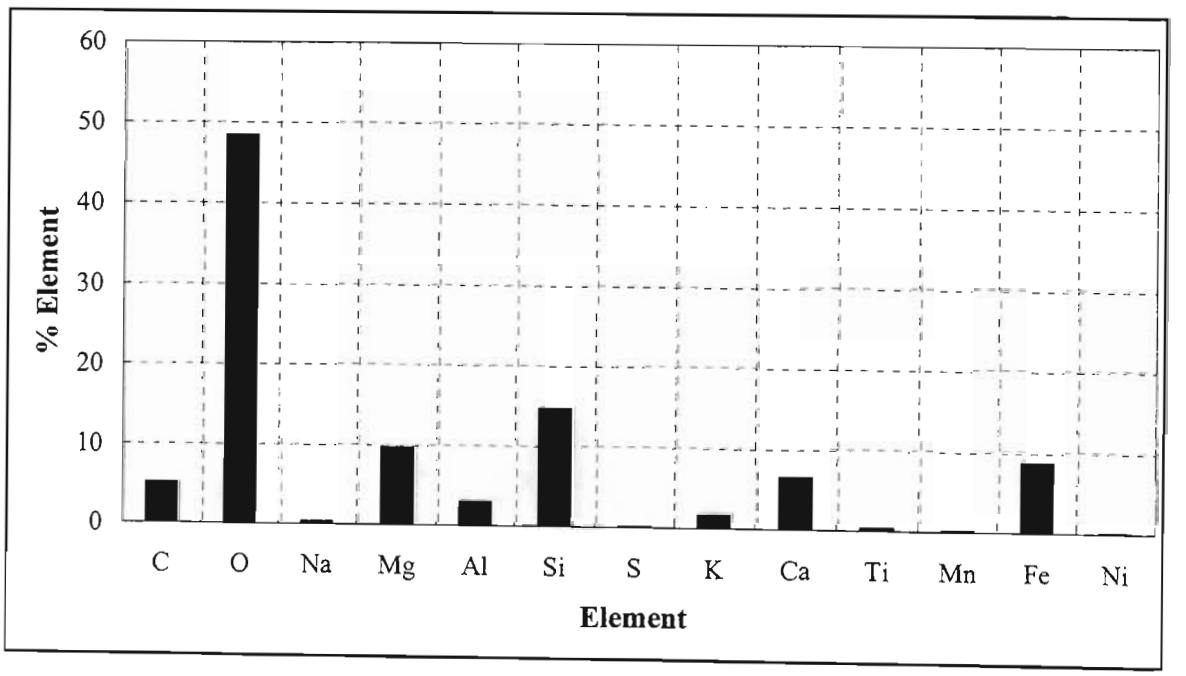

Figure 6.9 Elemental analysis of smectite clay / slime

6.1.3 Preliminary Rheological Tests

6.1.3.1 Aim of the Experiment

The aim of the experiments was to measure the rheological properties of uncontaminated ferrosilicon and magnetite suspensions. The viscosity of the suspensions could then be ascertained from the results of the investigation.

6.1.3.2 Experimental Method and Equipment

The rheology measurement tests were carried out using the rotational viscometer described in Chapter 5. The preparation method for the mediums was similar to that used by Govier et al. (1957). The experimental procedure is given in Appendix A2. Essentially, each medium was prepared by adding dry mineral solids to distilled water and mixing / shaking until a homogenous suspension of the desired density was achieved. A portion of this was then poured into the measuring cup. The measuring bob was first lowered into the cup, and set at an initial rotational speed before the medium was added. The peristaltic pump was switched on prior to the addition of the medium. This was all done to reduce settling out of the media particles.

The addition of a peristaltic pump was to keep the medium in suspension. This technique is similar to that presented by Ferrini et al. (1979). In their experiment a centrifugal pump was used. The main problem with a centrifugal pump is that it results in a temperature increase of the medium. The temperature has to be regulated by placing a cooling jacket around the measuring cup. In the experimental set up used in these investigations, there was no appreciable energy imparted by the peristaltic pump to the medium. All measurements were carried out at room temperature (22-26 °C).

The viscometer used in the measurement of the medium properties was calibrated using glycerol / water mixtures. The rheograms of glycerol / water mixtures, between 1.0 to 0.70 w/w (in steps of 0.05 w/w), were determined using the rotational viscometer. These were then compared to viscosity measurements made using a Brookfield viscometer in order to calculate the rheometer correction factor. The calibration results are given in Appendix A1.

6.1.3.3 Experimental Results and Discussion

The results discussed in this section are for ferrosilicon and magnetite #1 suspensions only. Ferrosilicon suspensions are used in the heavy medium separations of ores having a specific gravity in the range of approximately 2.5 to 4.0 [Collins et al. (1974)]. It is important to know the behaviour of these suspensions at different specific gravities, as this will influence the separation efficiency in the vessels. These tests were carried out to investigate the flow behaviour of the suspensions by measuring their shear stress versus shear rate in the rotational viscometer.

Ferrosilicon measurements were carried out at range of specific gravities between 2.0 and 3.0. Below a specific gravity of 2.0 the suspensions became unstable, making measurement very difficult. Above a specific gravity of 3.0, the viscosity measurements also became difficult due to the much higher solids volume concentration, which resulted in clogging of the annular region between the bob and cup. An interesting observation was the fluctuation and irreproducibility of the results at the low and high specific gravities. At high specific gravities lower than expected viscosity readings were observed. This is due to the settling out of suspension of the media particles. This results in a supernatant in the region around the measuring bob. The viscosity of the suspension then becomes lower because of reduction in the solid content in that region. Sometimes, if the settling rate of the solid particles is too high, the solids accumulate at the bottom of the cup and result in some resistance to the rotation of the bob. This has the effect of simulating high viscosities, resulting in inaccurate results. This was one of the motivations of adding a chamfer at the base of the rheometer cup.

Magnetite measurements were made at specific gravities ranging from 1.5 to 2.6. Above 2.6 the viscosity measurement became difficult because of the high viscosities associated with magnetite suspensions in this region. Because of this, magnetite suspensions are seldom used at specific gravities above 2.5 [Wills (1997)]. The stability of magnetite suspensions at lower specific gravities is much higher than that of ferrosilicon. This is due to its much lower density, which results in a higher solids volume percentage at similar specific gravities [Aplan et al. (1964)]. At specific gravities in excess of 2.6, viscosity measurement became difficult due to the same reasons as those for ferrosilicon.

Table 6.3 shows the solids volume percentage for ferrosilicon and magnetite #1 at the measured specific gravities.

Table 6.3 Ferrosilicon and Magnetite #1 solids volume percentage

Specific gravity	Φ (%)	
	Ferrosilicon	Magnetite #1
1.5	-	13.7
1.6	-	16.5
1.7	-	19.2
1.8	-	22.0
1.9	-	24.7
2.0	17.4	27.5
2.1	19.1	30.2
2.2	20.8	33.0
2.3	22.6	35.7
2.4	24.3	38.5
2.5	26.0	41.2
2.6	27.8	44.0
2.7	29.5	-
2.8	31.5	-
2.9	33.0	-
3.0	34.7	-

Figure 6.10 and Figure 6.11 show the rheograms for the ferrosilicon suspensions at the specific gravities given in Table 6.3. Figure 6.12 shows the effect of specific gravity on the shear stress of the suspensions. These results were plotted by taking the shear stress of each of the suspensions at a shear rate of 1200 s^{-1}. The results illustrate that there is an increase in the viscosity of the suspensions with specific gravity. This is due to an increase in the solids volume percentage. Figure 6.13 and Figure 6.14 show the rheograms for the magnetite #1 media. Figure 6.15 shows the effect of specific gravity on magnetite #1 suspensions at a constant shear rate equal to 1000 s^{-1}. The rheograms for both mediums were plotted on two separate graphs for the sake of clarity.

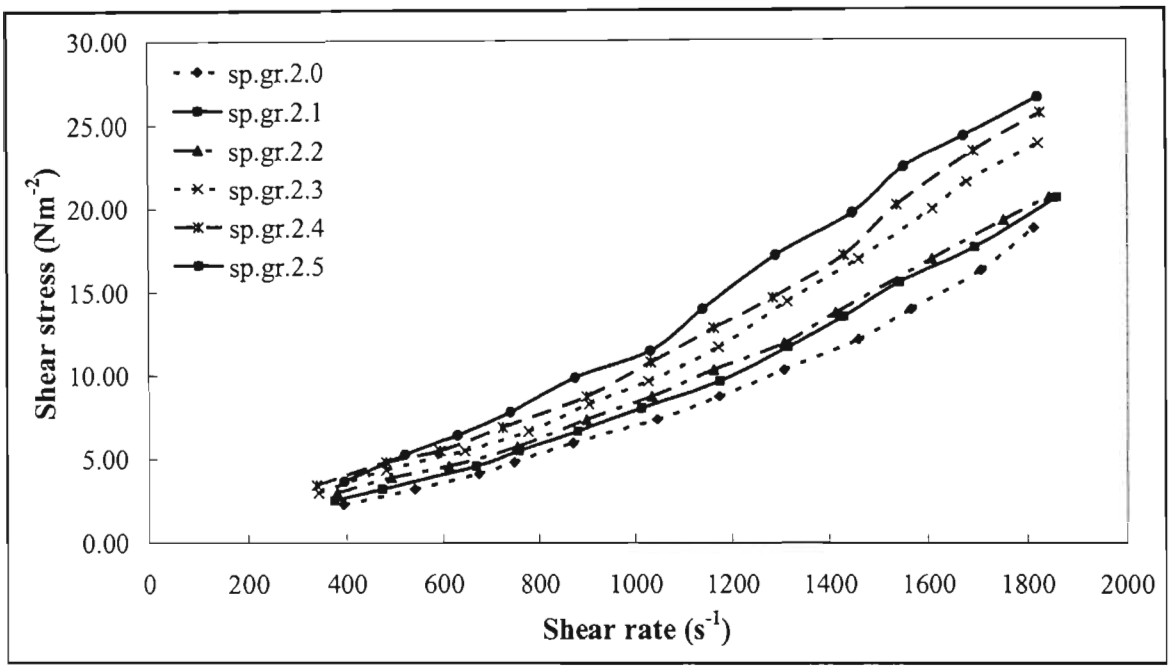

Figure 6.10 Ferrosilicon rheograms (sp.gr. 2.0-2.5)

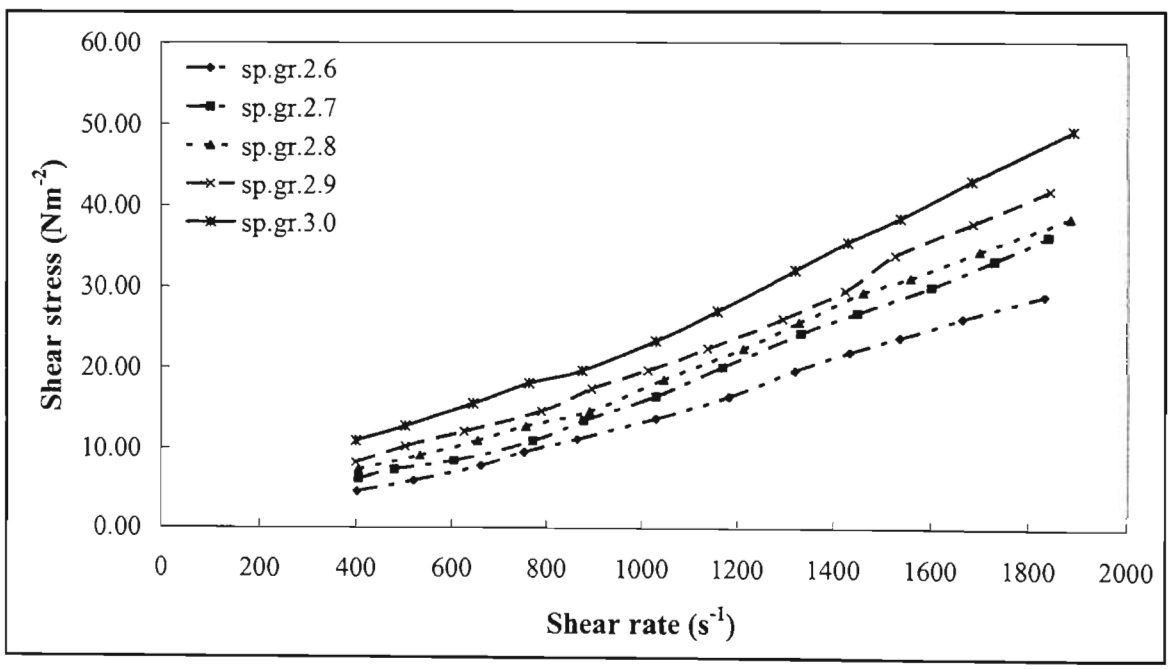

Figure 6.11 Ferrosilicon rheograms (sp.gr. 2.6-3.0)

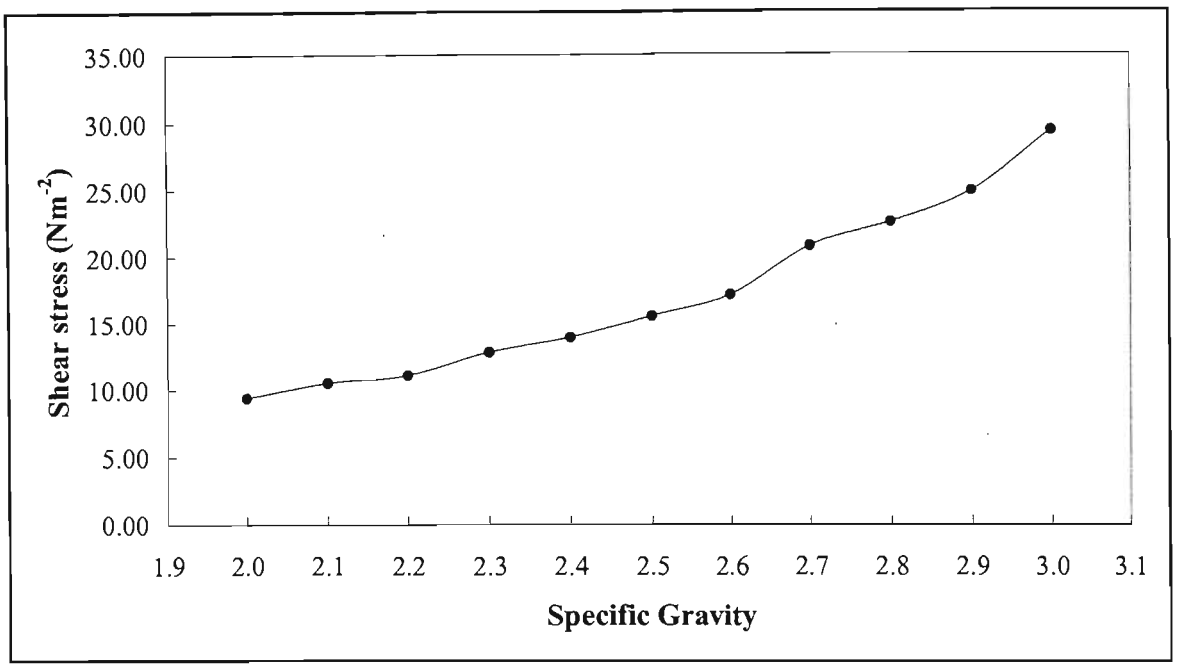

Figure 6.12 Shear stress versus specific gravity for ferrosilicon suspensions at a shear rate of 1200 s^{-1}

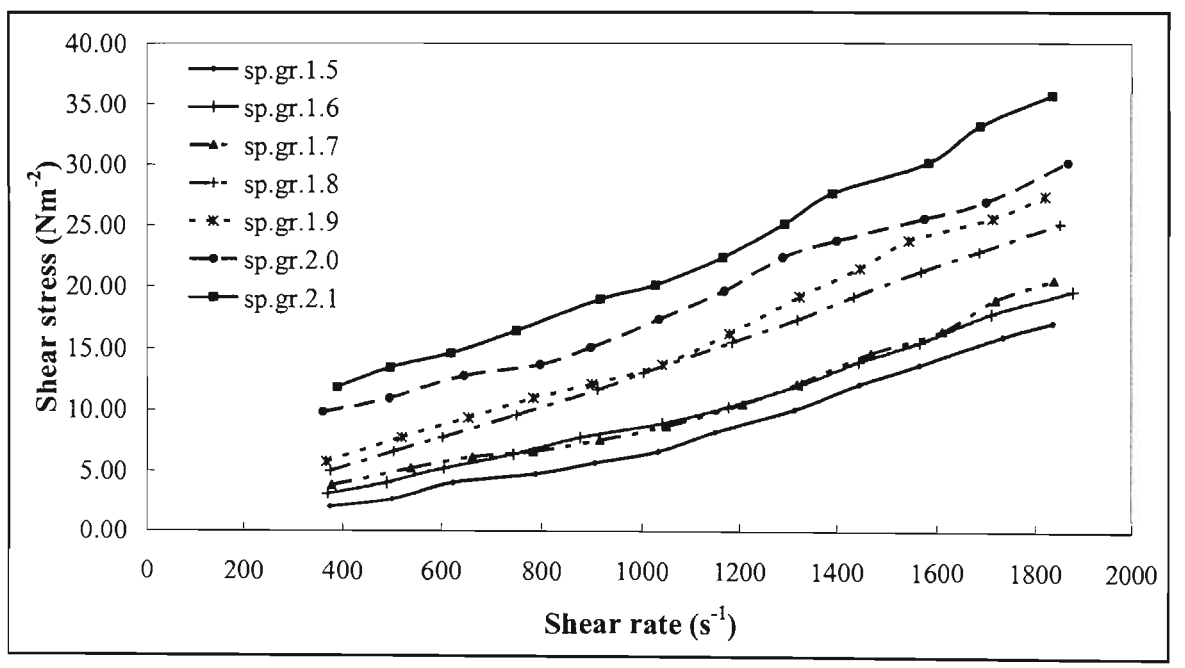

Figure 6.13 Magnetite #1 rheograms (sp.gr. 1.5-2.1)

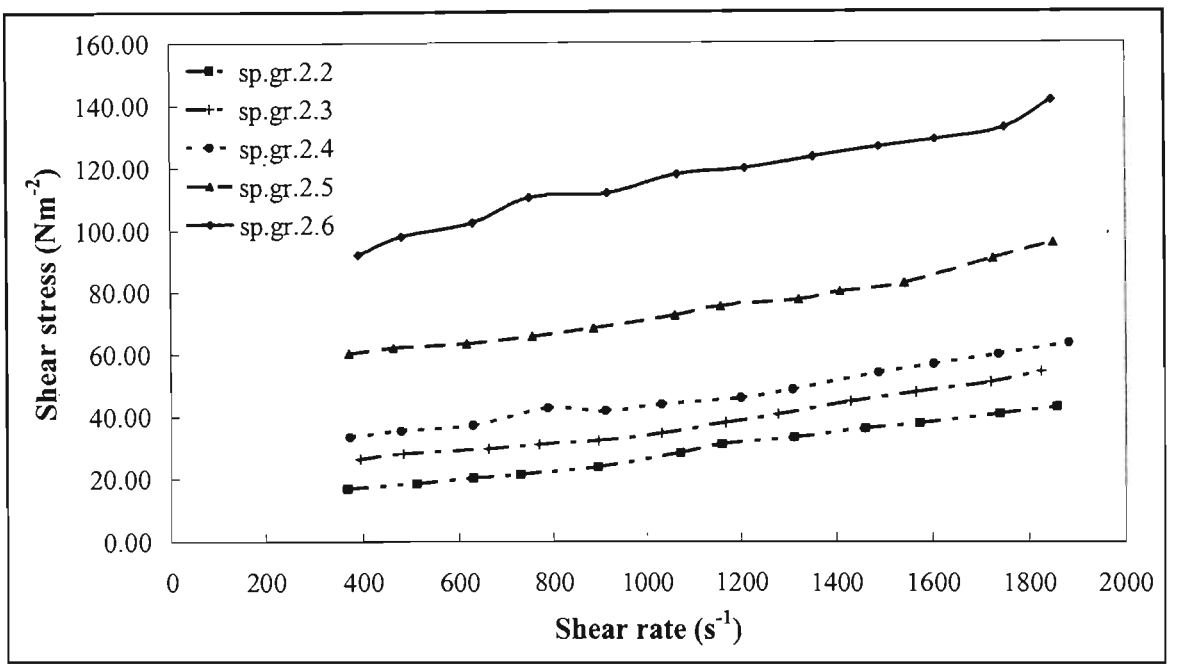

Figure 6.14 Magnetite #1 rheograms (sp.gr. 2.2-2.6)

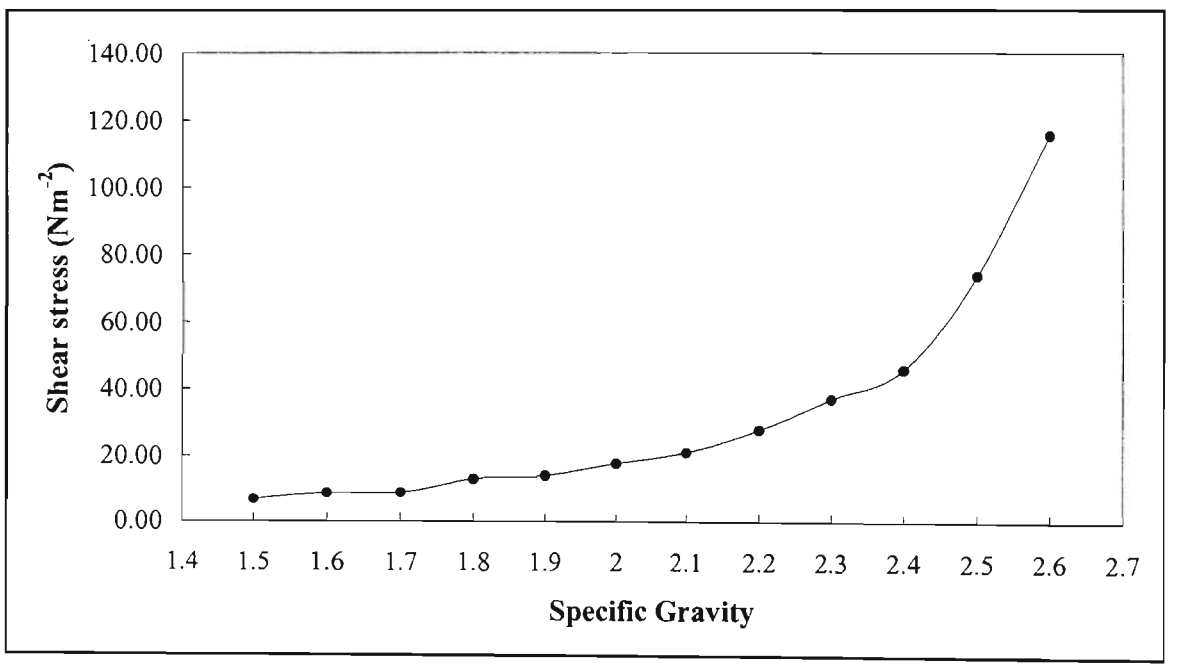

Figure 6.15 Shear stress versus specific gravity for magnetite #1 suspensions at a shear rate of 1000 s^{-1}

The ferrosilicon results show that the behaviour of the ferrosilicon suspensions ranges from Newtonian behaviour at low specific gravities, to dilatant behaviour at higher specific gravities. Figure 6.10 shows that at a specific gravity equal to 2.0, the ferrosilicon medium is Newtonian. There is an increase in viscosity with an increase in specific gravity. This is expected, since an increase in medium specific gravity results in an increase in the solids volume percentage, as illustrated in Table 6.3. The degree of dilatant behaviour appears to be increasing with specific gravity. Figure 6.11 also shows an increase in the dilatant behaviour of the medium as the specific gravity increases. Wills (1997), states that at a solid volume percentage above 30 %, heavy medium suspensions begin to exhibit non-Newtonian behaviour. This is evidenced from the results. In this case however, the onset of non-Newtonian behaviour begins at a specific gravity around 2.5, which has a solid volume percentage of 26.0 %. The onset of non-Newtonian behaviour at these specific gravities is due in part to the instability of the medium at low specific gravities. The solid particles settle out of the medium and accumulate at the base of the cup, slightly hindering the rotation of the measuring bob [Klein et al. (1990)]. This falsifies the results by giving the impression that a higher viscous medium is being tested. It will be shown later that measurement at these values begins to improve through the addition of slime, which acts as a stabilising agent.

The dilatant behaviour observed for the ferrosilicon suspensions is similar to that observed by Collins et al. (1976) and Ferrara et al. (1986). Both these authors found that milled ferrosilicon suspensions behave as pseudo-Newtonian fluids at low shear rates and specific gravities, and become dilatant at higher specific gravities. Collins et al. (1983) also showed that at specific gravities below 2.8 the behaviour of ferrosilicon suspensions is Newtonian, becoming dilatant at much higher specific gravities.

Figure 6.13 and Figure 6.14 show the shear stress versus shear rate relationship for the magnetite #1 media. At specific gravities ranging from 1.5 to 2.0, the behaviour of the media is pseudo-Newtonian. At these specific gravities, the solid volume percentages are below 30 %. For specific gravities in excess of 2.0, the pseudo-plastic behaviour of the media increases. As shown in Figure 6.14, the viscosity rises sharply from a specific gravity of 2.5 to 2.6, the latter being the maximum specific gravity which could be handled by the viscometer. Although measurements were not made at zero shear rates, the graphs seem to suggest the existence of a yield stress with an increase in specific gravity. These results are similar to those observed by Lapsin et al. (1988).

The viscosities of the magnetite suspensions appear to be greater than ferrosilicon viscosities at the same specific gravity. However, this is not the most realistic way of comparing the viscosities, since the solid volume percentages are different for these media at the same specific gravity. A much better method is to compare the viscosities of the two media at the same solids volume concentration. Figure 6.16 and Figure 6.17 compare the rheograms of magnetite and ferrosilicon media at a solids volume percentage of 24 % and 33 %, respectively. At the solid volume percentage of 24 % the specific gravity of magnetite is 1.9, and the ferrosilicon specific gravity is 2.4. For 33 % solids volume the specific gravities are 2.2 and 2.9 for magnetite and ferrosilicon, respectively.

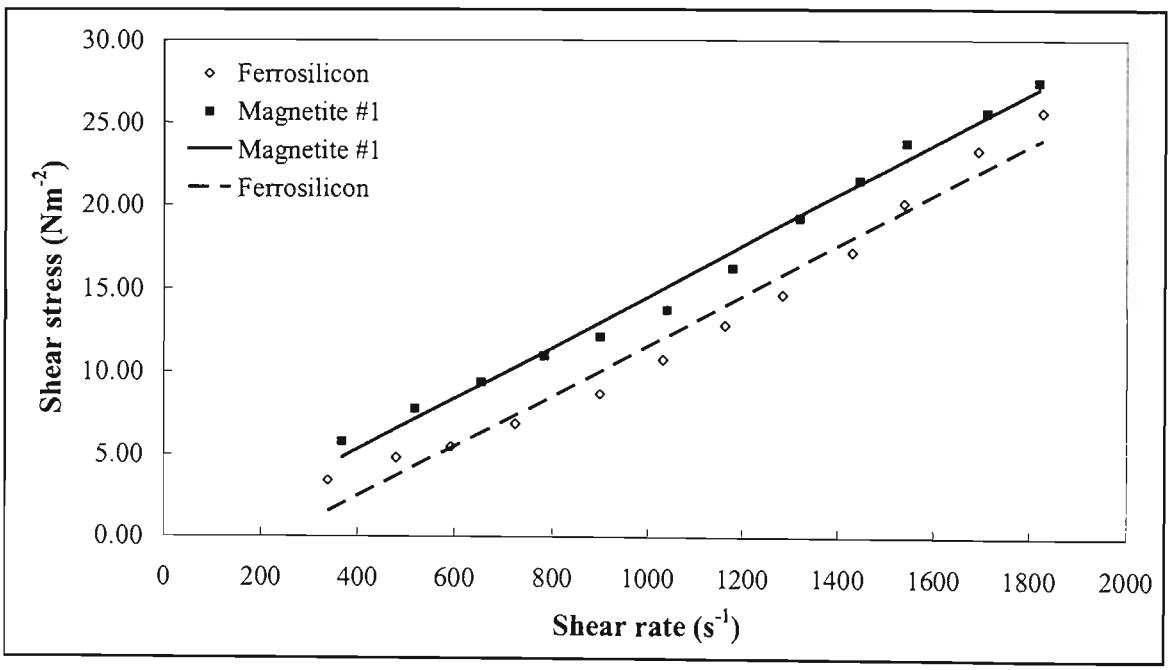

Figure 6.16 Shear stress vs shear rate at 24% volume solids

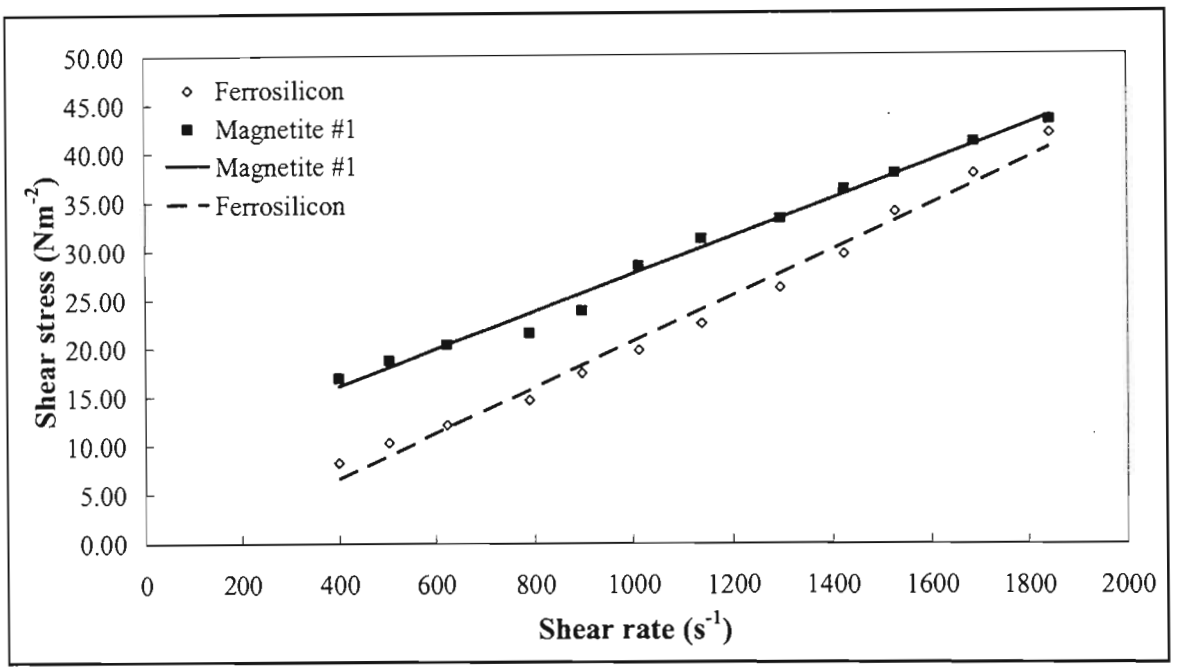

Figure 6.17 Shear stress vs shear rate at 33% volume solids

Both of the above graphs show that at equal solid volume concentrations the magnetite media have a much higher viscosity than ferrosilicon media. This is one of the reasons why ferrosilicon media are used at higher densities, irrespective of the fact that they cost more than magnetite media. The higher viscosities of magnetite media are associated with the higher fines content. This was also illustrated in the size distribution curves in Figure 6.1.

The preliminary rheological tests showed what type of behaviour magnetite and ferrosilicon suspensions followed. The results observed were similar to those found in literature. One of the biggest industrial challenges is the use of these suspensions at their critical specific gravities. For industrial separations using ferrosilicon suspensions, the presence of slimes presents a problem by increasing the acquired viscosity of the suspensions. For magnetite suspensions the challenge is working mediums of this type at specific gravities greater than the conventional ones. It was thus required to look at the different methods available for viscosity reductions in heavy medium suspensions. The two methods chosen for this project are the use of a surface active agent, and the use of coarser media size distributions. These form the basis of Experiment series A, B and C.

In some industrial heavy medium separations mixtures of ferrosilicon and magnetite are used to make up the suspensions. The amount of ferrosilicon and magnetite used depends on the

separating vessel, as well as the ore being separated. As mentioned above, magnetite media have high fines content, thus mixtures used should not result in viscosities that affect the separation efficiency. However, the presence of moderate amounts of magnetite improves the stability of ferrosilicon suspensions.

Collins et al. (1983) did some experiments using, ferrosilicon/magnetite suspensions, to evaluate the separation efficiency in dense media cyclones. Viscosity measurement was undertaken with cyclone 60 ferrosilicon and various mixtures of ferrosilicon with magnetite. Measurements were undertaken with a concentric cylinder rotational viscometer, at a temperature of 20 °C. They found that mixtures of ferrosilicon and magnetite were essentially pseudo-plastic at low magnetite levels (□ 25% magnetite), but showed Bingham plastic conditions at higher magnetite levels (□ 50% magnetite), yield stress increasing with the magnetite content of the medium. Their results indicated the large increase in viscosity caused by the use of magnetite with ferrosilicon and the problem of using magnetite at high separation densities and low shear rates.

Figure 6.18 shows the effect of specific gravity on the viscosity of FeSi/Mag #1 suspensions at ratios 1:1, 2:1, and 1:2. These graphs were plotted by taking the viscosity of each of the suspensions at a shear rate equal to 1200 s^{-1}. The results show that the viscosity of the suspensions increases with specific gravity. This effect becomes more pronounced at high specific gravities. The viscosities of the suspensions also increase with the amount of magnetite #1 present in the suspension. This is due mainly to the amount fines introduced with the addition of magnetite #1.

Figure 6.19 to Figure 6.25 show the effect of shear rate on viscosity of 270D ferrosilicon-magnetite #1 mixtures at specific gravities 2.2-2.8, for FeSi/Mag #1 ratios 1:1, 2:1, and 1:2.

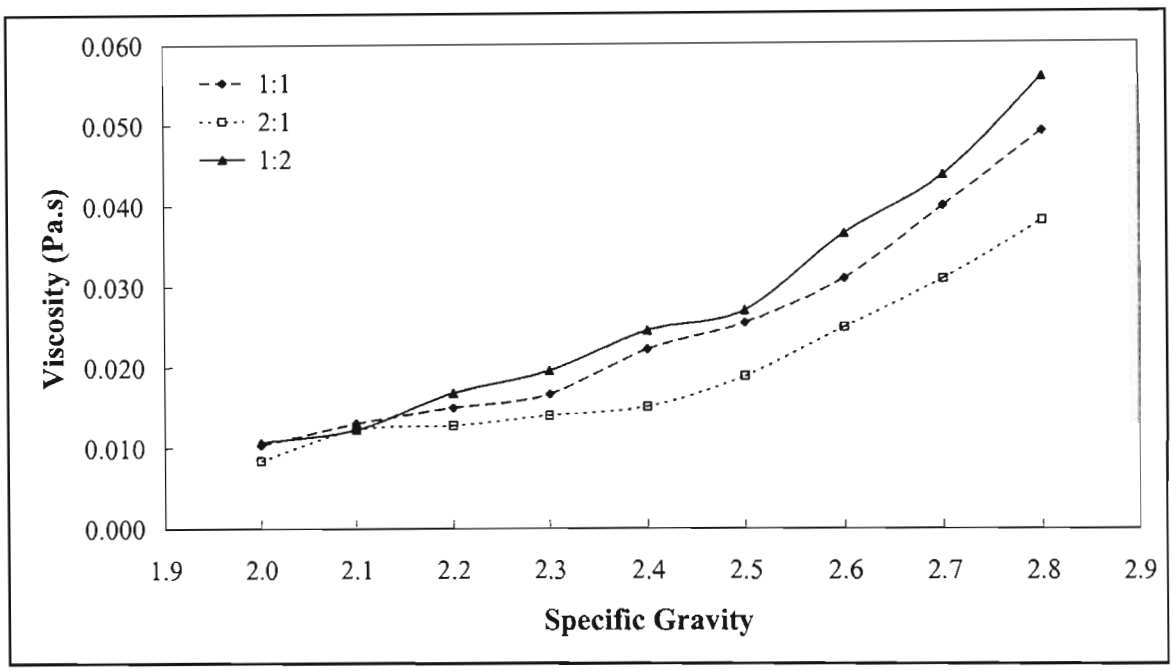

Figure 6.18 Effect of specific gravity on the viscosity of FeSi/Mag #1 suspensions at a shear rate of 1200 s^{-1}

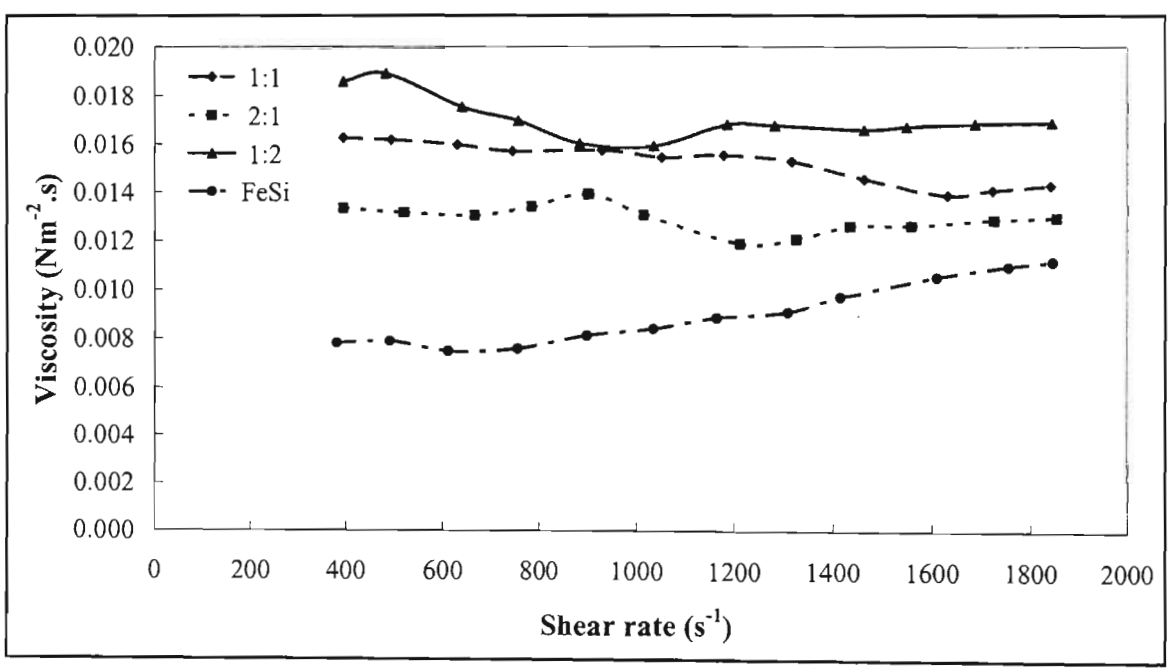

Figure 6.19 Effect of shear rate on viscosity for 270D ferrosilicon-magnetite #1 mixtures (sp.gr.2.2)

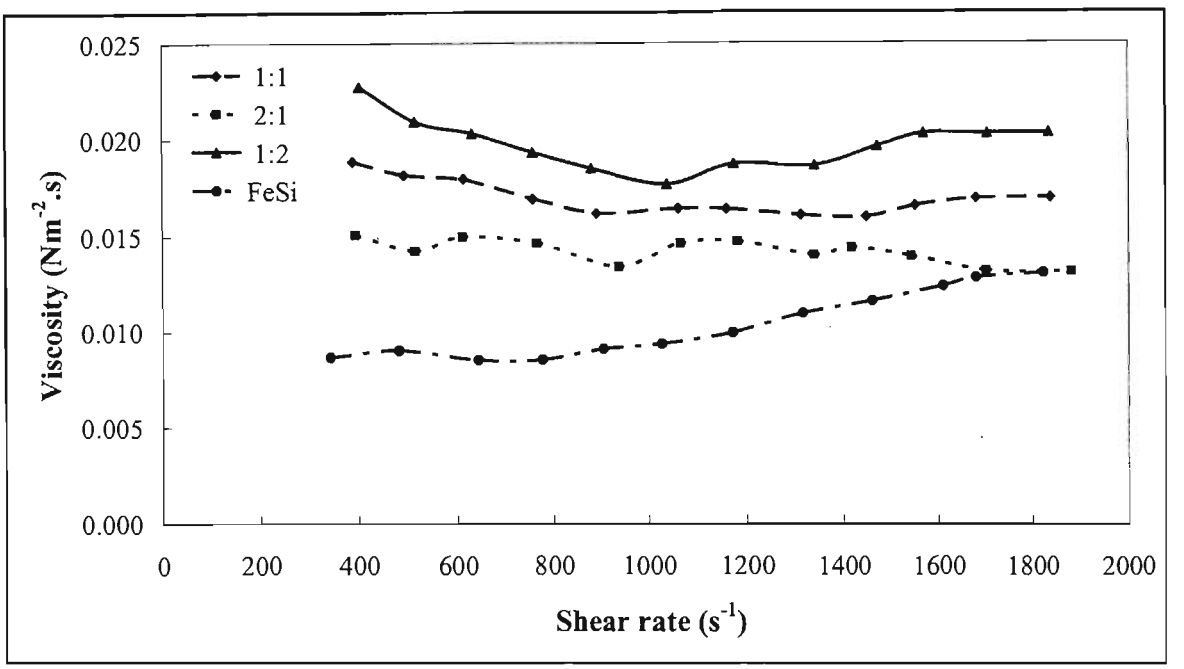

Figure 6.20 Effect of shear rate on viscosity for 270D ferrosilicon-magnetite #1 mixtures (sp.gr.2.3)

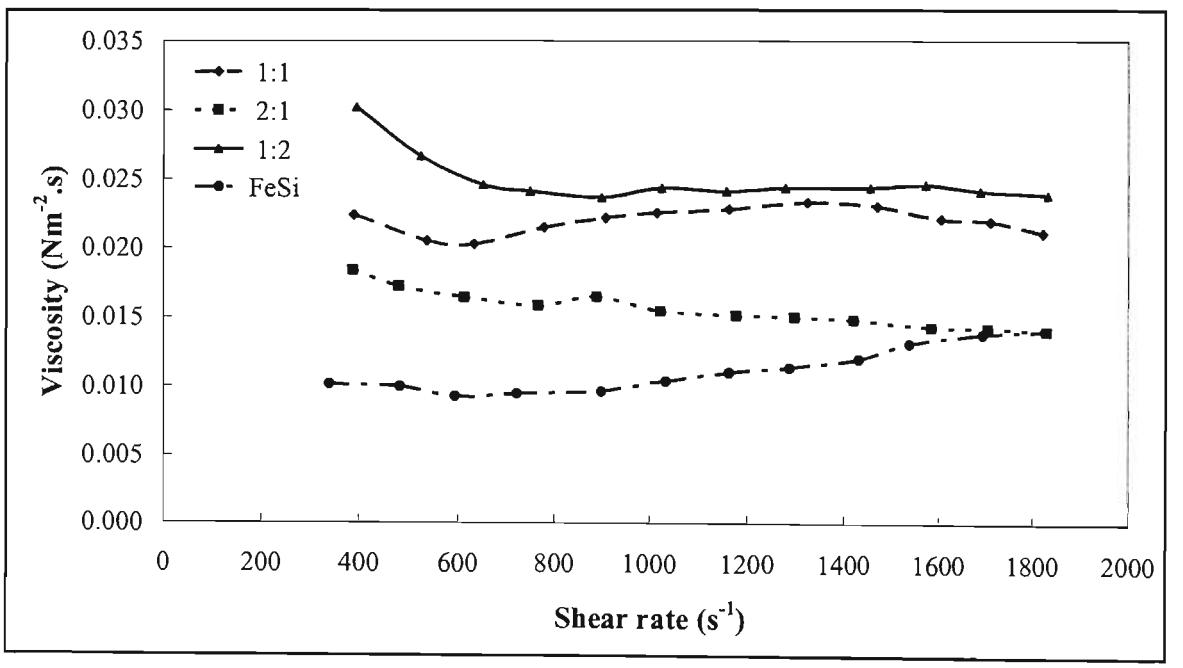

Figure 6.21 Effect of shear rate on viscosity for 270D ferrosilicon-magnetite #1 mixtures (sp.gr.2.4)

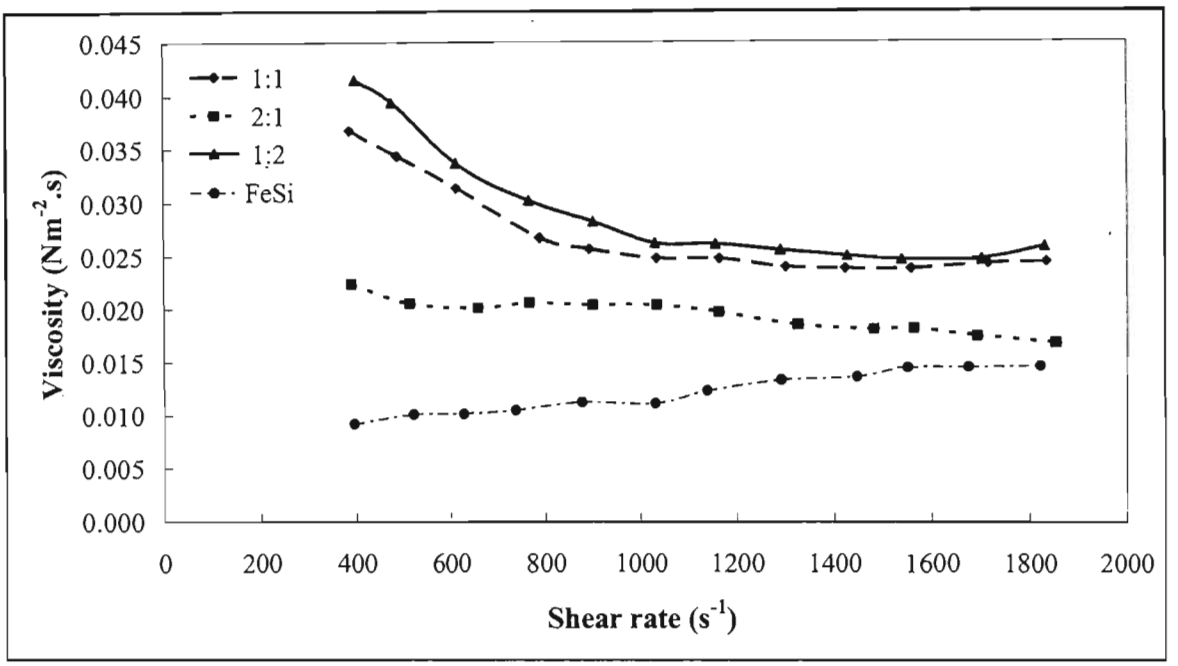

Figure 6.22 Effect of shear rate on viscosity for 270D ferrosilicon-magnetite mixtures #1 (sp.gr.2.5)

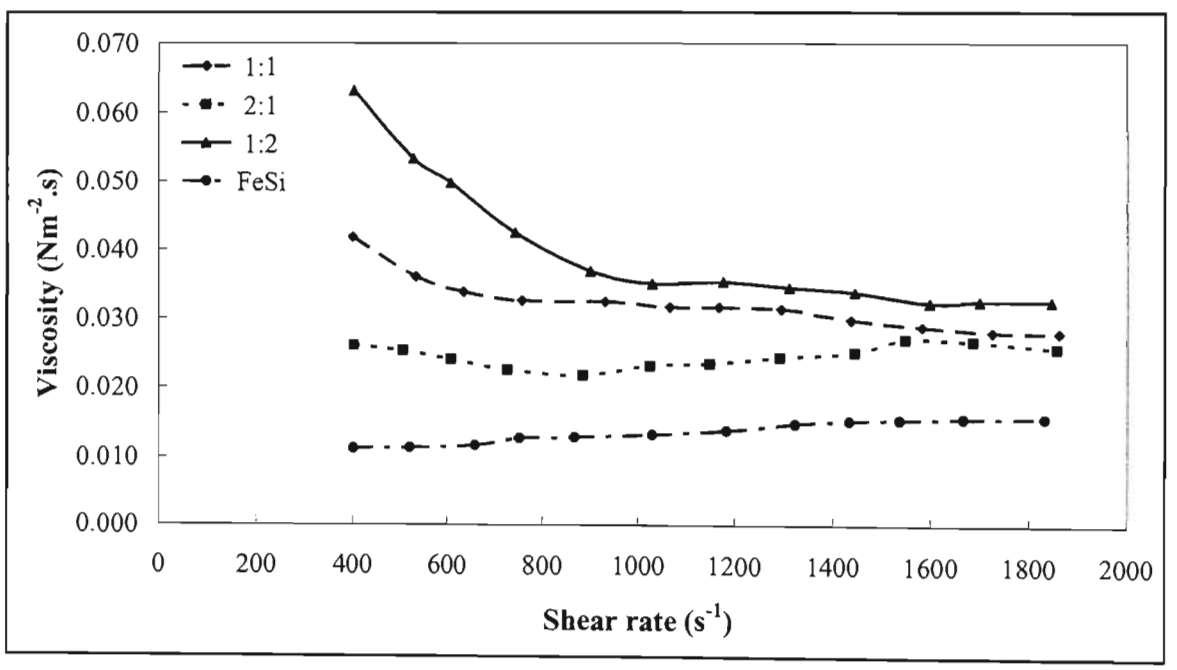

Figure 6.23 Effect of shear rate on viscosity for 270D ferrosilicon-magnetite #1 mixtures (sp.gr.2.6)

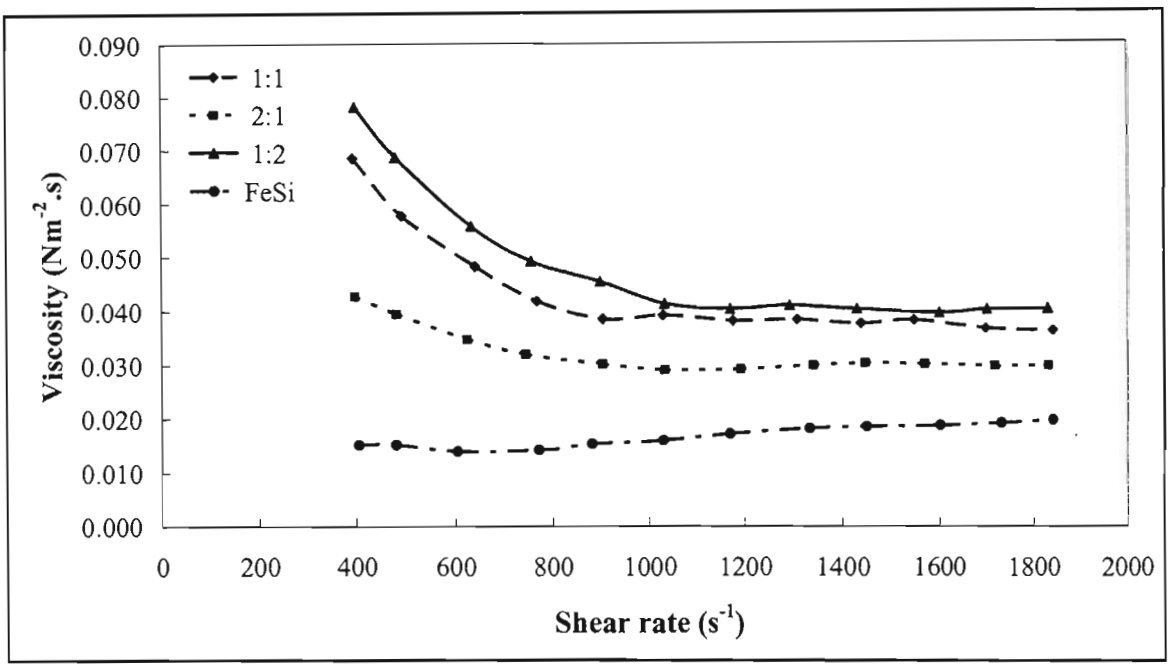

Figure 6.24 Effect of shear rate on viscosity for 270D ferrosilicon-magnetite #1 mixtures (sp.gr.2.7)

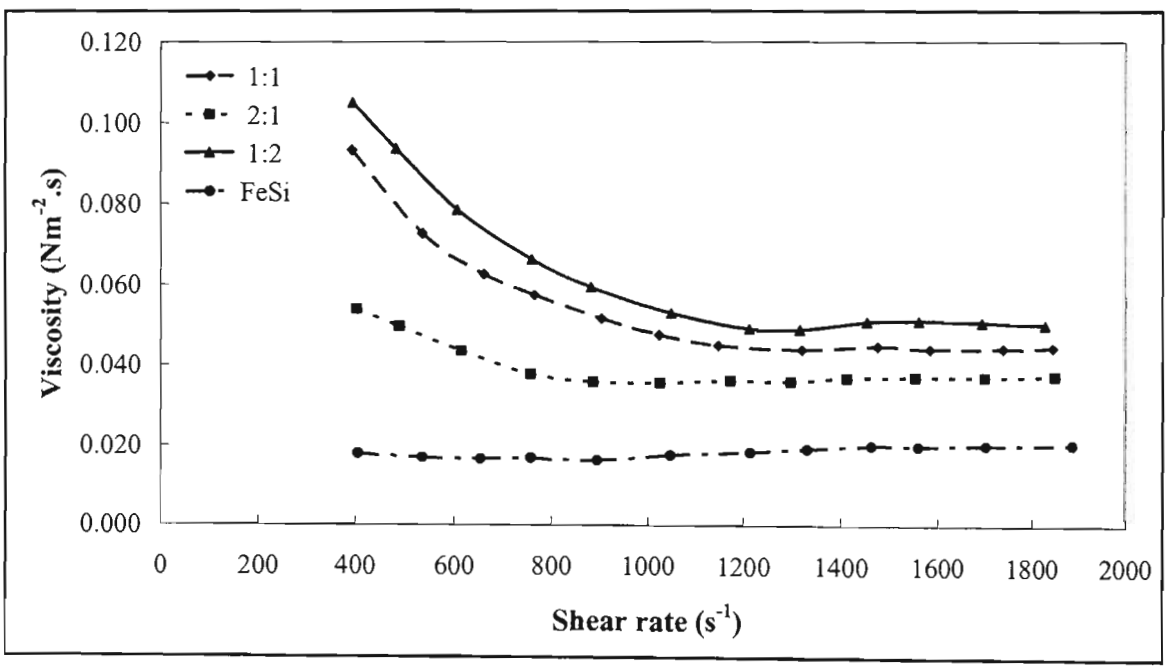

Figure 6.25 Effect of shear rate on viscosity for 270D ferrosilicon-magnetite #1 mixtures (sp.gr.2.8)

The graphs above were plotted together with viscosity values of pure ferrosilicon suspensions at the same specific gravity, in order to illustrate the increase in viscosity caused by the presence of magnetite. All the graphs show that there is an increase in the viscosity of suspensions due to the magnetite media. The graphs also show, for a constant specific gravity, an increase in viscosity as the amount of magnetite is increased. At a specific gravity of 2.2 the behaviour of the ferrosilicon-magnetite mixtures is close to Newtonian. At a specific gravity of 2.3, the behaviour of the mixtures begins to resemble that of a pseudo-plastic fluid, especially at higher magnetite content. From a specific gravity of 2.4 and above, the presence of a yield stress becomes prominent. As the amount of magnetite is increased, the yield stress value also increases. At these higher specific gravities, and higher magnetite ratios, the suspensions behave as Bingham plastic fluids. These results are similar to those found by Collins et al. (1983) and Lilge et al. (1958). This illustrates the large increase in viscosity caused by the use of magnetite with ferrosilicon, particularly at high specific gravities.

6.2 Experiment Series A: The effect of DP001 on the viscosity of heavy medium suspensions

This section discusses the effect of a surface active agent on the rheology of heavy medium suspensions. As mentioned earlier, stability and viscosity are the two most important rheological parameters in heavy medium separations. In these tests, however, only the viscosity of the suspensions was measured. All tests were carried out using the same viscometer used for the preliminary rheological tests.

Various chemical additives, both organic and inorganic, have been used to reduce viscosity and to increase stability of the suspensions [He et al. (1999)]. The general effect of these chemical additives is believed to reduce the yield stress rather than the plastic viscosity. However, the results of Valentylk et al. (1972) seemed to indicate that the addition of chemical additives resulted in an increase in both the yield stress and plastic viscosity.

The surface active agent used in these investigations is a development product supplied by Lignotech SA, under the manufacturing code DP001. DP001 is an orange-brown calcium lignosulphonate powder recovered from the paper and pulp industry. DP001 is a medium chain length anionic polymer with a high affinity for water. Lignosulphonates such as DP001 are used in as dispersing agents in concrete, textile dyes, pesticides, and ceramics. They are also used as binging agents in animal feed and for dust suppression.

The results in this section are divided into three sections:

i. The effect of DP001 on contaminated ferrosilicon suspensions

ii. The effect of DP001 on uncontaminated magnetite suspensions

iii. The effect of DP001 on various mixtures of ferrosilicon / magnetite suspensions

6.2.1 The effect of DP001 on ferrosilicon suspensions

This section discusses the results obtained from the rheological tests carried out on ferrosilicon suspensions. The range of specific gravities tested was from 2.0 to 3.0. The lower specific gravities were not tested because of the high instability experienced at these specific gravities. It should also be noted that ferrosilicon suspensions are seldom used at these low specific gravities. The conventional specific gravities for industrial separations using ferrosilicon media is from 2.5 upwards. Collins et al. (1974) stated that the critical density of ferrosilicon suspensions with the milled grade is in the region of 3.0, as used in these experiments. Above this critical density, the viscosity rises sharply. They state that, in general, it is not usual to employ milled ferrosilicon at a pulp specific gravity in excess of 3.0. Figure 6.12 showed the effect of specific gravity on the shear stress and viscosity of ferrosilicon suspensions. From the graph it can be deduced that there is an increase in suspension viscosity with specific gravity.

The presence of slimes in industrial separations can cause large increases in viscosity, with deleterious effects on separation and pumping characteristics. Slimes cannot be practically excluded from the separating vessel because an increase in the preparation screen efficiency would be costly and result in reduced capacity [Aplan et al. (1964)]. Particle abrasion with the heavy medium circuit also produces some sliming in the system. The most logical step is to reduce the viscosity of the media through the use of chemical dispersants, or surface active agents.

The size distribution of the slime used in this investigation is shown in Figure 6.1. The slime is a smectite clay obtained from a diamond processing operation. The slime particles were screened using a 75 μm sieve, and the undersize was used in these investigations. This was done because the majority of the slime is in this range, and also because the larger sizes cause damage to the rheometer by clogging the annular space between the bob and cup. The additions of slime were 10 % (kg /kg FeSi) at specific gravities 2.0 and 2.1, and 5 % (kg/kg FeSi) for specific gravities 2.2 upwards. The slime has an effect of increasing the stability of the medium at the expense of an increased viscosity. The optimum slime concentration for reasonable stability at a moderate viscosity is generally between 3-6 % by weight concentration of solids [Valentyik (1972)]. It has been observed by Aplan et al. (1964) that uncontaminated ferrosilicon suspensions are not affected by surface active agents. It is for this reason that DP001 additions were only made after the slime had been introduced to the medium.

6.2.1.1 Experimental Results and Discussion

Initially experiments were carried out on uncontaminated ferrosilicon suspensions at a specific gravity of 2.2. These results are illustrated in Figure 6.26.

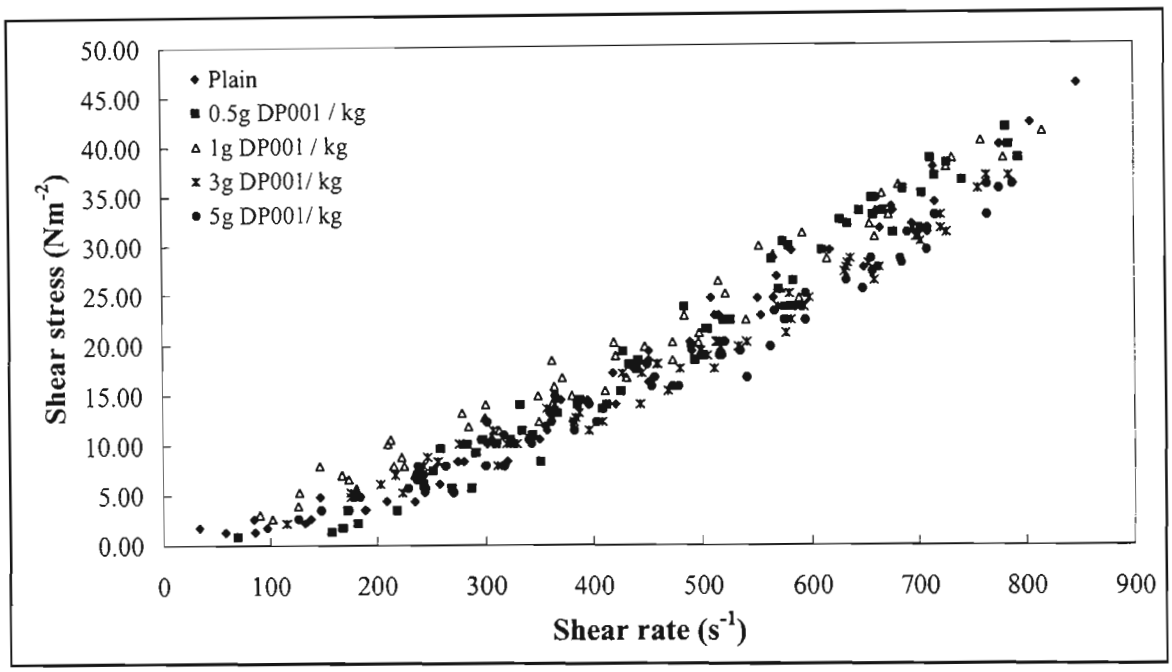

Figure 6.26 Rheograms for uncontaminated FeSi suspensions at sp.gr.2.2

The results show that DP001 has a negligible effect, if any. DP001 additions as high as 5 g / kg FeSi have little effect on the viscosity of the suspensions. This result is similar to the observations of Aplan and Spedden (1964), who stated that surface active agents have little effect on uncontaminated ferrosilicon suspensions, except for a minor amount of suspension of the finest particles, which is quite negligible in the case of the media used in this project.

From the above results, and the observations of Aplan and Spedden (1964), it was inferred that DP001 would have no effect on uncontaminated ferrosilicon suspensions at all specific gravities. It was then decided that the remainder of the experiments would be carried out on ferrosilicon suspensions contaminated with the slime. Figure 6.27 to Figure 6.37 show the rheograms for ferrosilicon media contaminated with the slime. Additions of DP001 were made at 1 and 2 g DP001/kg solids.

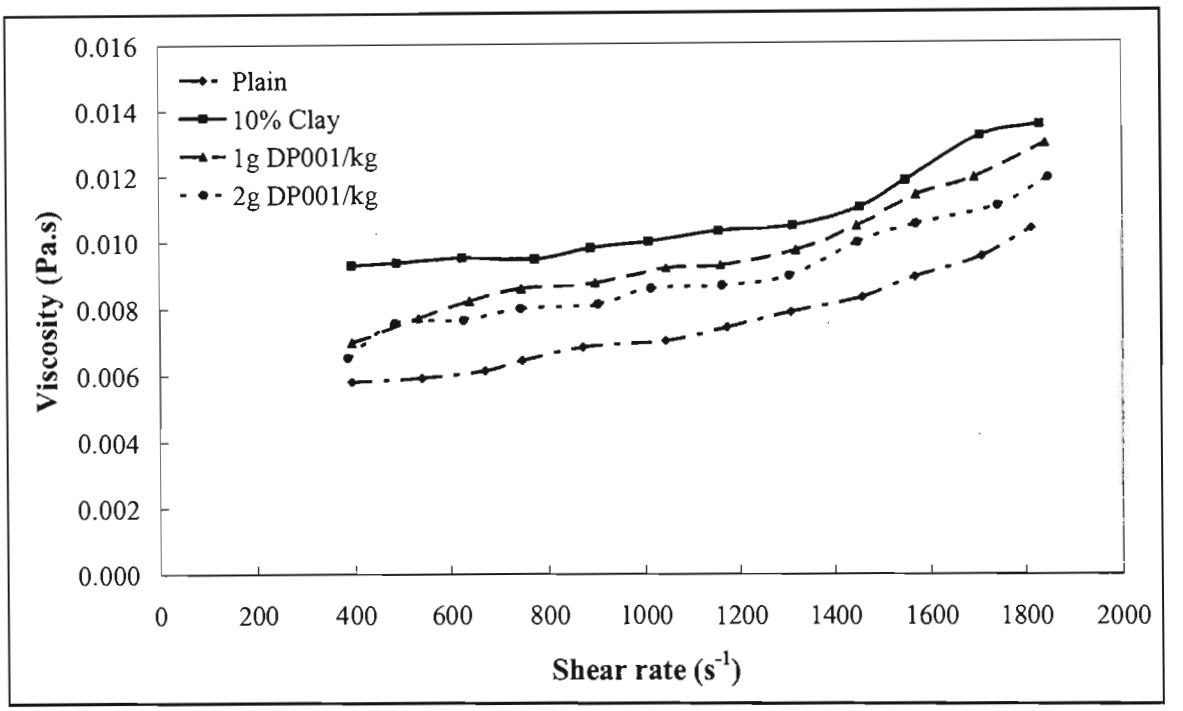

Figure 6.27 Effect of DP001 on contaminated ferrosilicon suspensions (sp.gr. 2.0)

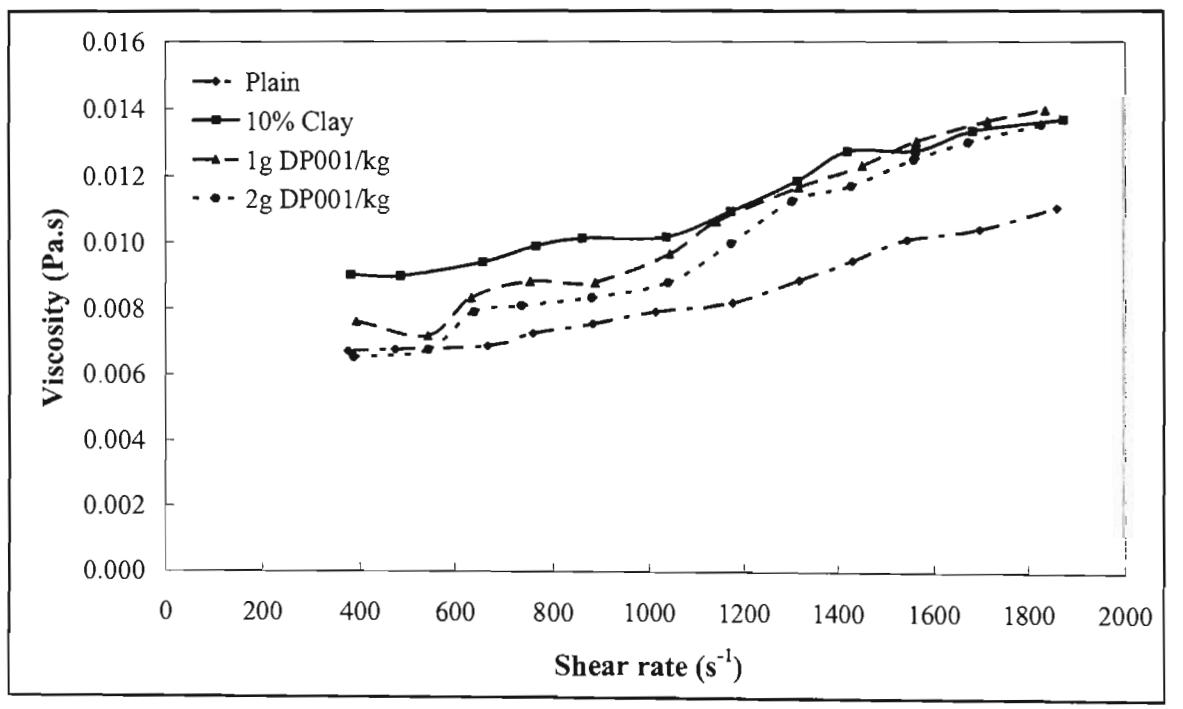

Figure 6.28 Effect of DP001 on contaminated ferrosilicon suspensions (sp.gr. 2.1)

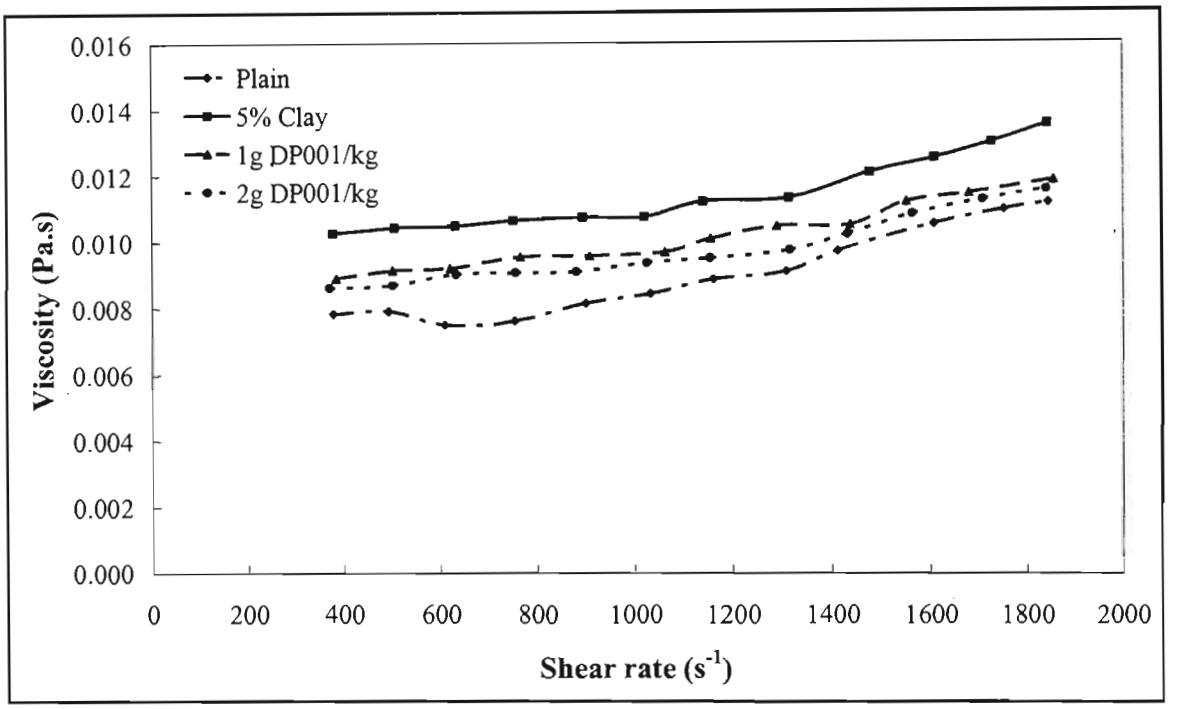

Figure 6.29 Effect of DP001 on contaminated ferrosilicon suspensions (sp.gr. 2.2)

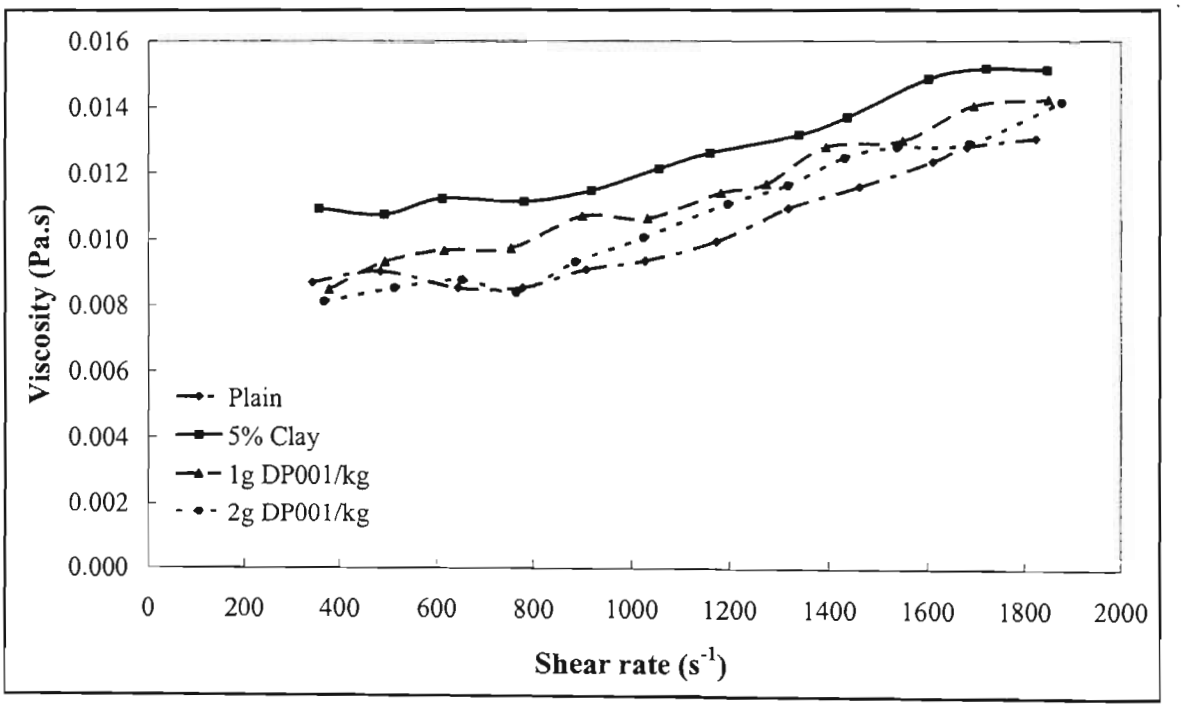

Figure 6.30 Effect of DP001 on contaminated ferrosilicon suspensions (sp.gr. 2.3)

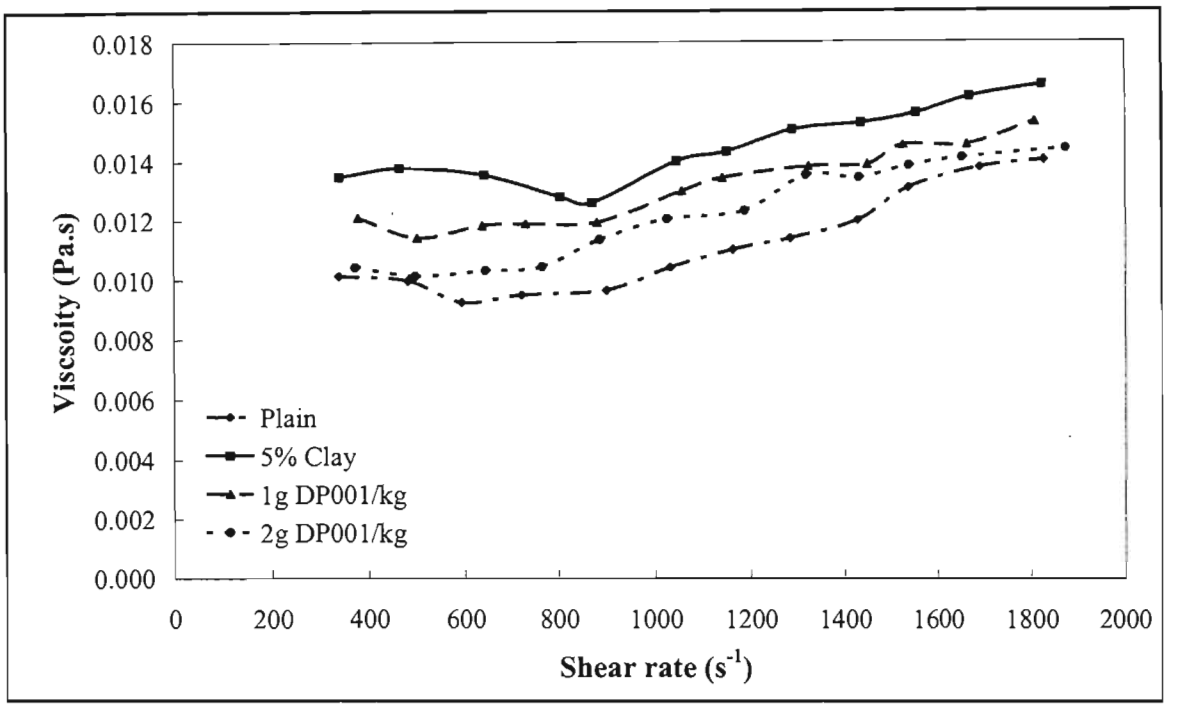

Figure 6.31 Effect of DP001 on contaminated ferrosilicon suspensions (sp.gr. 2.4)

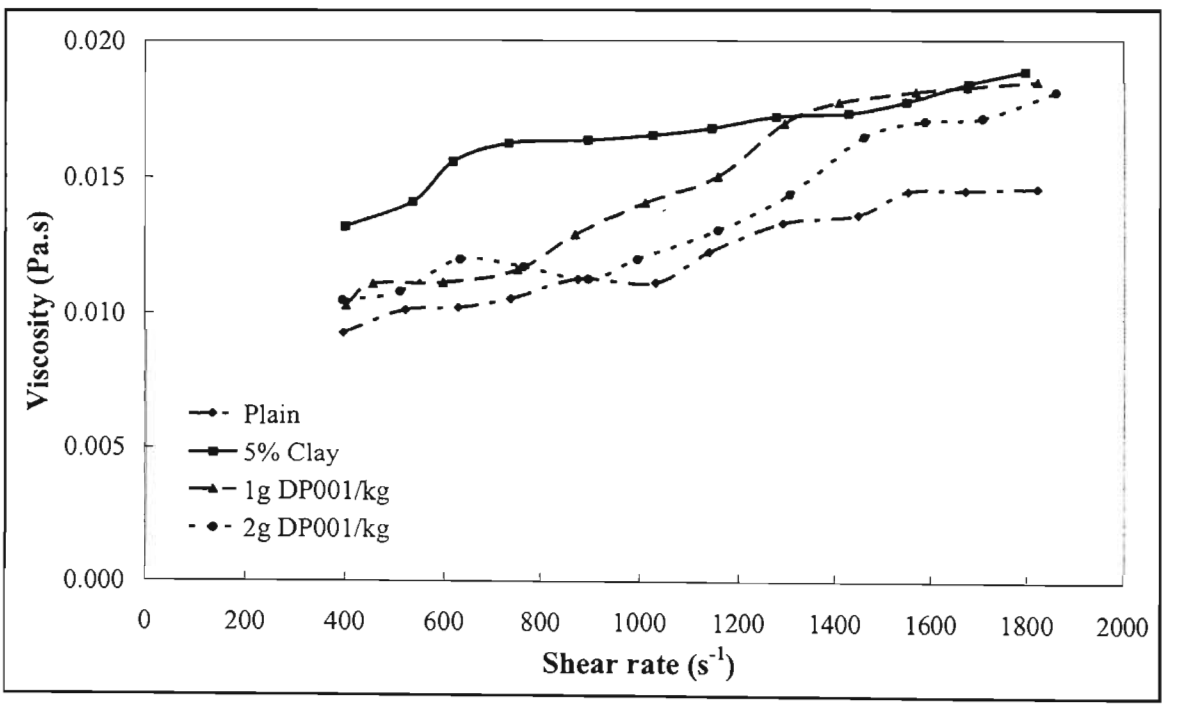

Figure 6.32 Effect of DP001 on contaminated ferrosilicon suspensions (sp.gr. 2.5)

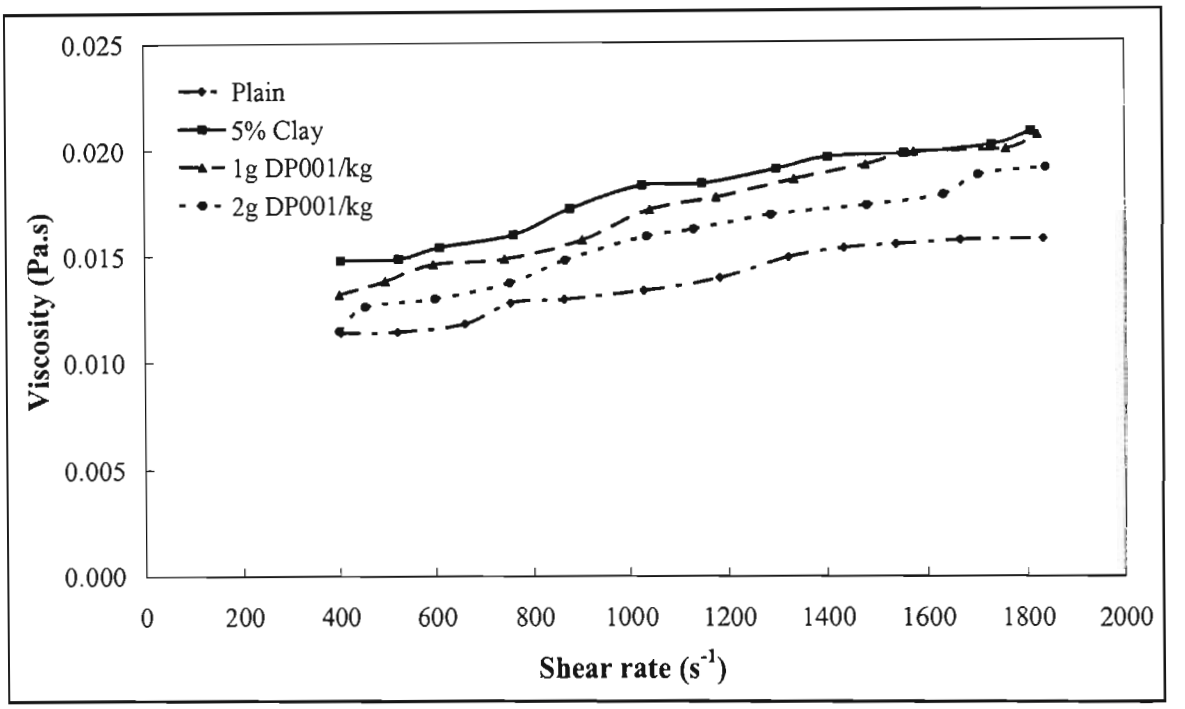

Figure 6.33 Effect of DP001 on contaminated ferrosilicon suspensions (sp.gr. 2.6)

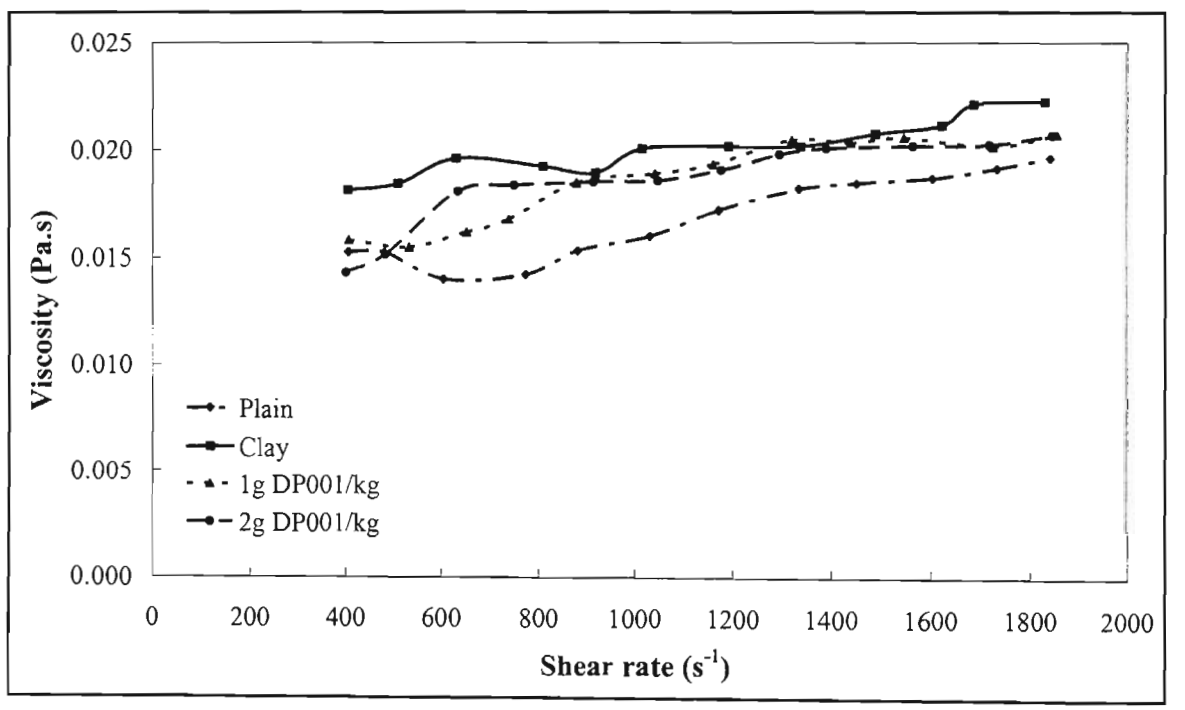

Figure 6.34 Effect of DP001 on contaminated ferrosilicon suspensions (sp.gr. 2.7)

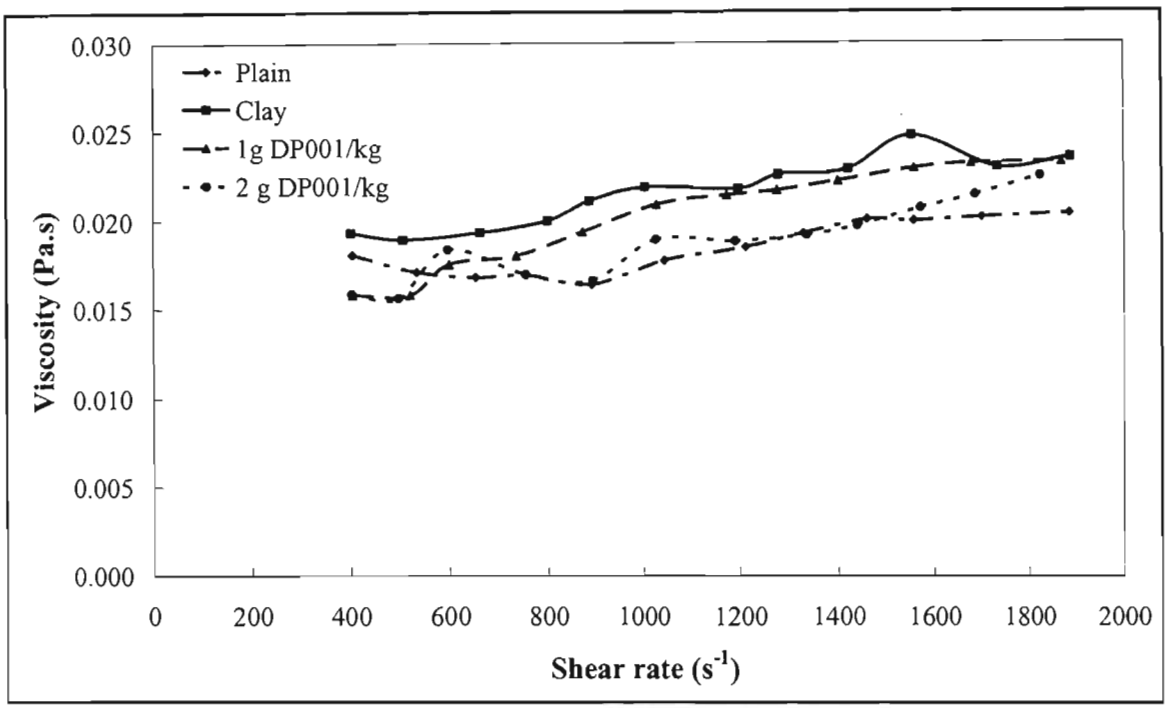

Figure 6.35 Effect of DP001 on contaminated ferrosilicon suspensions (sp.gr. 2.8)

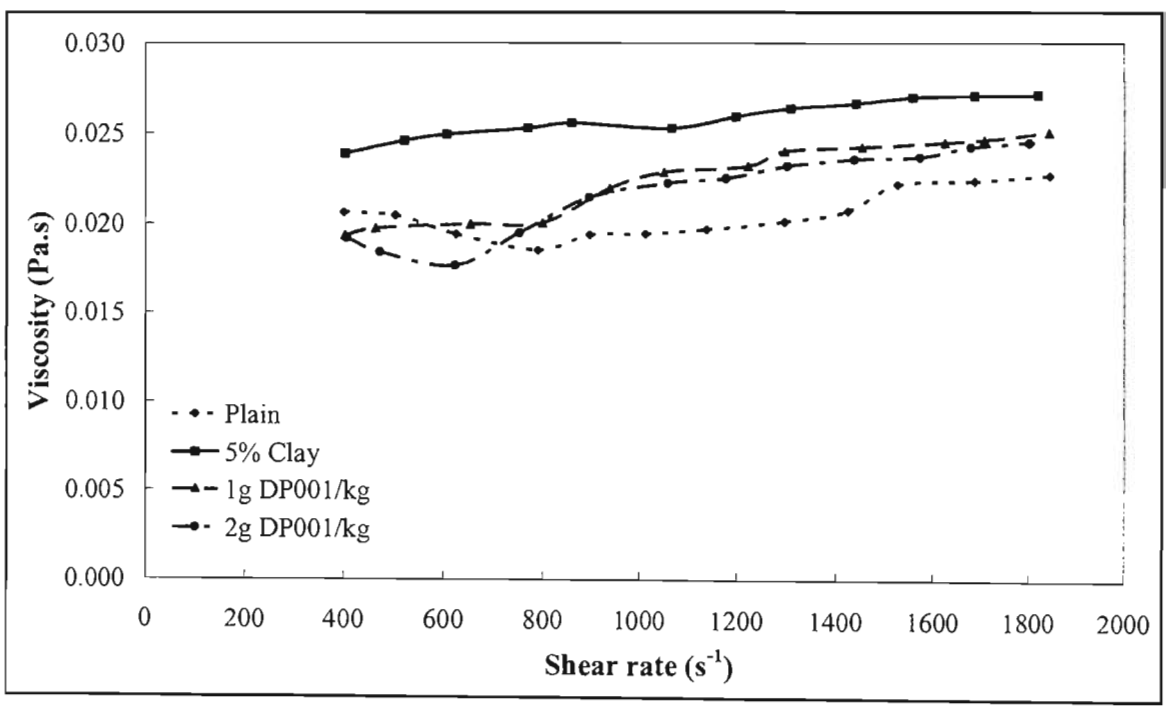

Figure 6.36 Effect of DP001 on contaminated ferrosilicon suspensions (sp.gr. 2.9)

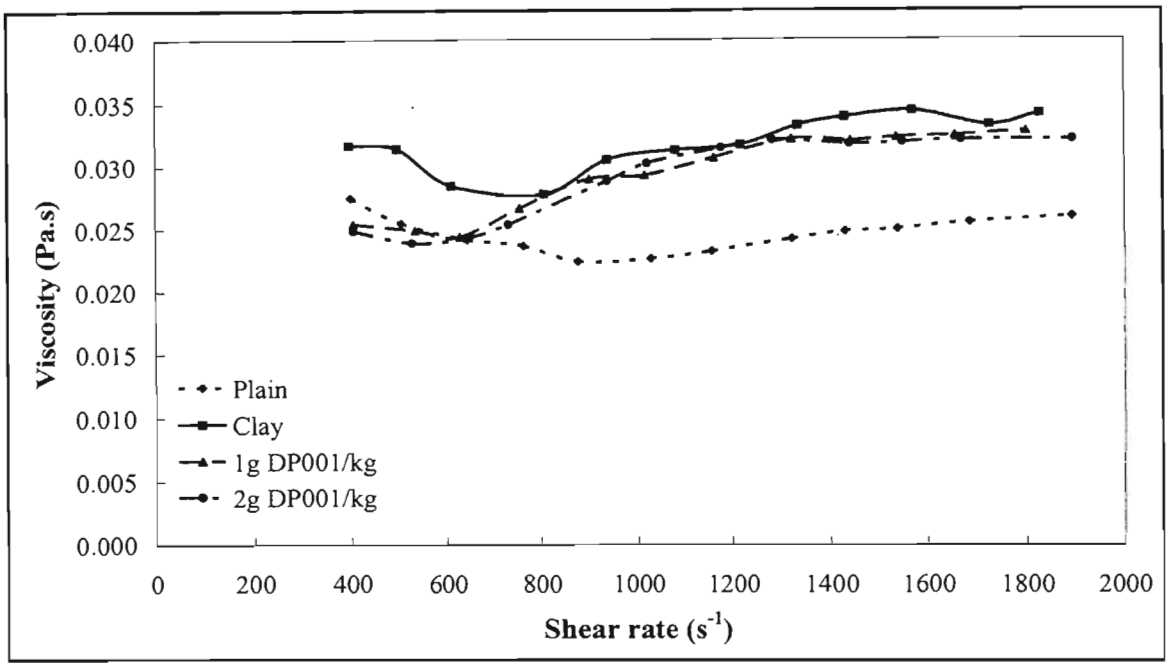

Figure 6.37 Effect of DP001 on contaminated ferrosilicon suspensions (sp.gr. 3.0)

All the graphs show an increase in the viscosity of the suspensions upon addition of the slime. Table 6.4 gives a summary of the increase in viscosity due to the presence of slime. The values in the table were calculated by taking the average increase in the viscosity of the suspensions over the entire range of shear rates i.e across all shear rate values..

Table 6.4 Percentage viscosity increase due to presence of slimes

Specific gravity	% Viscosity Increase
2.0	41.1
2.1	31.5
2.2	27.2
2.3	22.9
2.4	29.0
2.5	36.6
2.6	30.0
2.7	19.7
2.8	17.0
2.9	26.2
3.0	29.6

The table above shows that the highest increase in viscosity occurs at specific gravities 2.0 and 2.1. This is because of the higher percentage of clay added at these specific gravities in comparison to the others. The slime increases the viscosity of the suspensions in two ways. Firstly, it was observed during experimentation that the slime had a clay-like nature to it. Clays, or colloidal particles, reduce the viscosity of suspensions by absorbing some water, thereby resulting in less water available to associate with the rest of solid particles. This results in apparent increase in the solid volume concentration [Eirich (1960), and He et al. (1999)]. Secondly, the non-magnetic particles introduced by the slimes increase the solid volume concentration of the suspensions. These finer particles increase the surface area of the suspension, meaning that there is a lot more association between the solids and the water. This also results in an increase the apparent solid volume concentration.

Table 6.5 Ferrosilicon viscosity reduction due to DP001 addition

	% Viscosity Reduction	
Specific Gravity	**1 g DP001/kg**	**2 g DP001/kg**
2.0	9.9	15.9
2.1	5.5	11.0
2.2	11.2	14.6
2.3	10.9	15.8
2.4	8.9	15.5
2.5	11.6	17.1
2.6	4.2	12.5
2.7	7.4	7.4
2.8	6.5	13.3
2.9	13.0	16.0
3.0	7.8	8.7

The graphs also show that the basic trend of the graphs does not change. This means that both the addition of slime and DP001 do not change the behaviour of the suspensions from one form to another, e.g. from Newtonian to pseudoplastic. Most of the graphs do not show an appreciable presence of a yield stress. The reduction in viscosity shown in the graphs is thus probably due to a reduction in the apparent viscosity of the suspensions.

The graphs also show that reduction in suspensions viscosity is higher at high shear rates. This is a promising result because the reduction in viscosity occurs at shear rates in the region industrial separators operate under (approximately 100 s^{-1} to 600 s^{-1}). Upon addition of 1 g DP001/kg FeSi, there is a reduction in the viscosity of the suspensions. Addition of a further 1 g / kg FeSi results in a further reduction for some of the suspensions. Table 6.5 is a summary of the average viscosity reduction in contaminated ferrosilicon suspensions with DP001 at various specific gravities. The percentage viscosity reduction in the table was also calculated by taking the average values over the entire range of shear rates.

Rheological measurements were also carried out at constant speeds and different slimes additions to simulate build up in a heavy medium separation circuit. These tests were carried at specific gravities from 2.5 to 3.0, and DP001 additions of 2 g / kg solids. The results are illustrated in Figure 6.38 to Figure 6.43, for a constant shear rate equal to 500 s^{-1}.

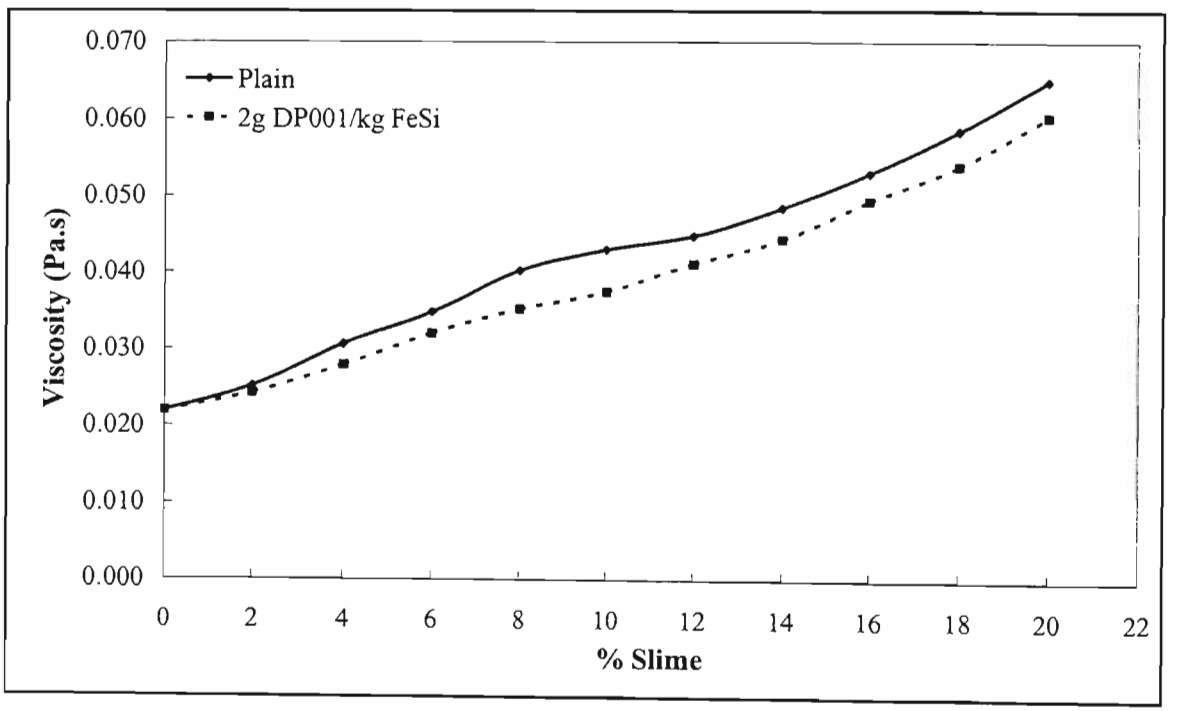

Figure 6.38 Effect of DP001 at 500 s^{-1} shear rate (sp.gr. 2.5)

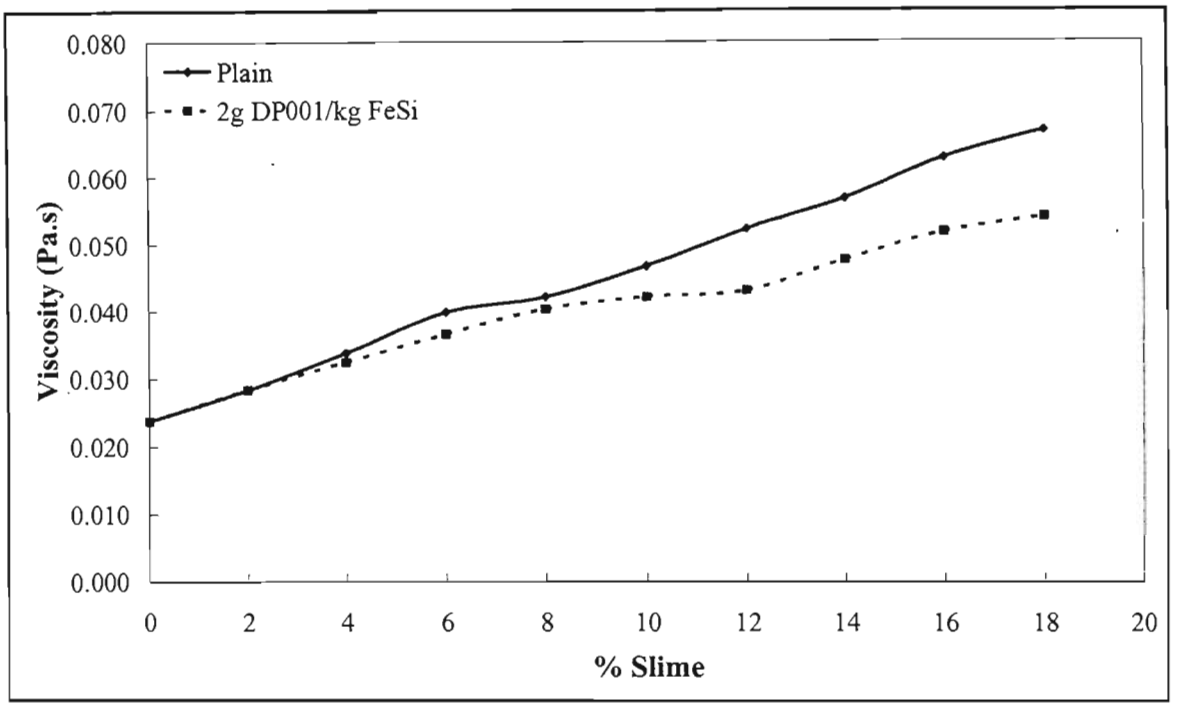

Figure 6.39 Effect of DP001 at 500 s^{-1} shear rate (sp.gr. 2.6)

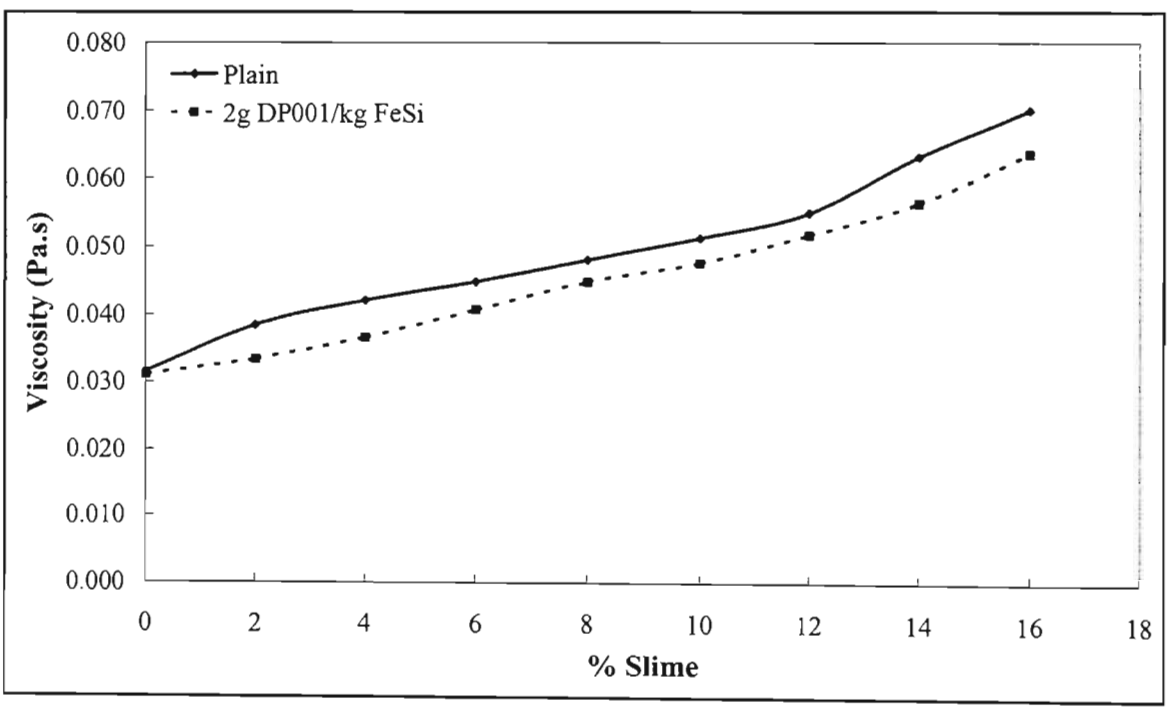

Figure 6.40 Effect of DP001 at 500 s-1 shear rate (sp.gr.2.7)

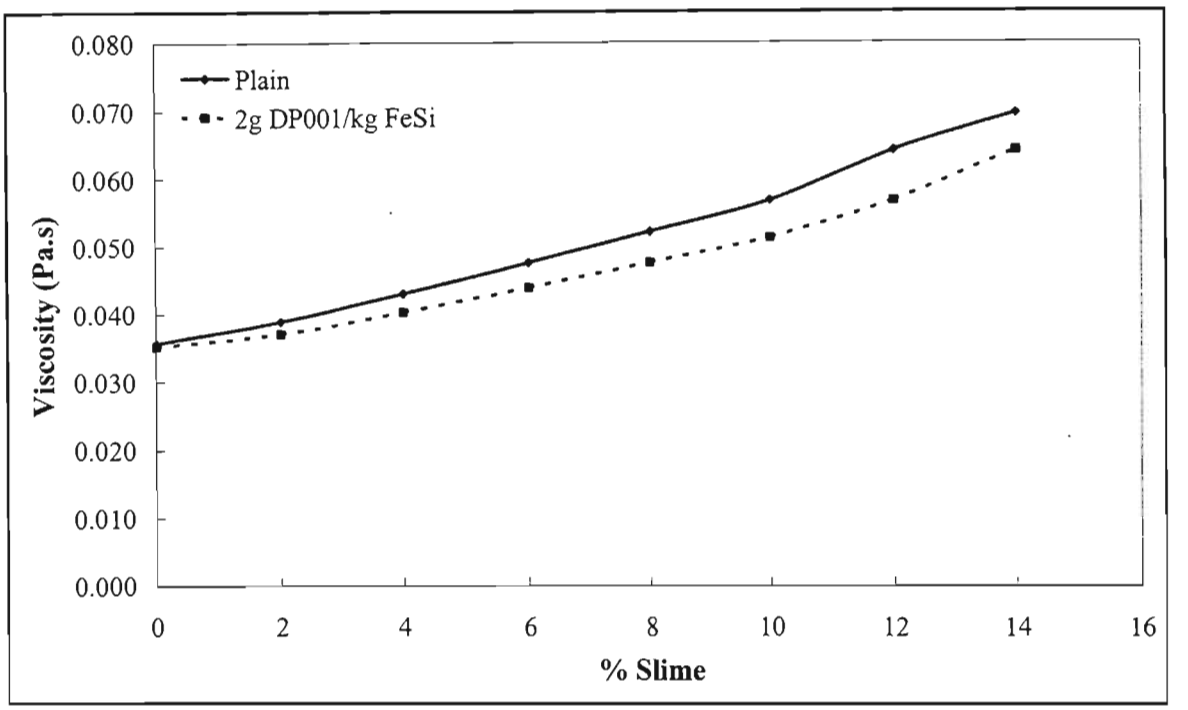

Figure 6.41 effect of DP001 at 500 s^{-1} shear rate (sp.gr. 2.8)

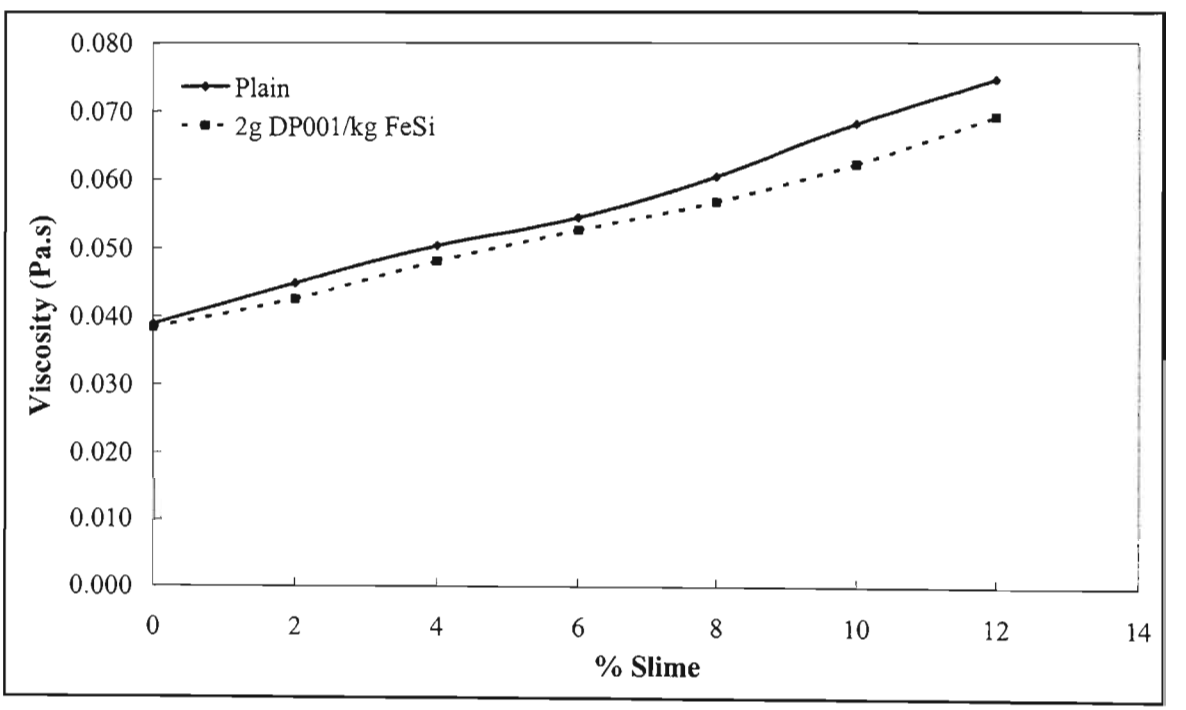

Figure 6.42 Effect of DP001 at 500 s^{-1} shear rate (sp.gr. 2.9)

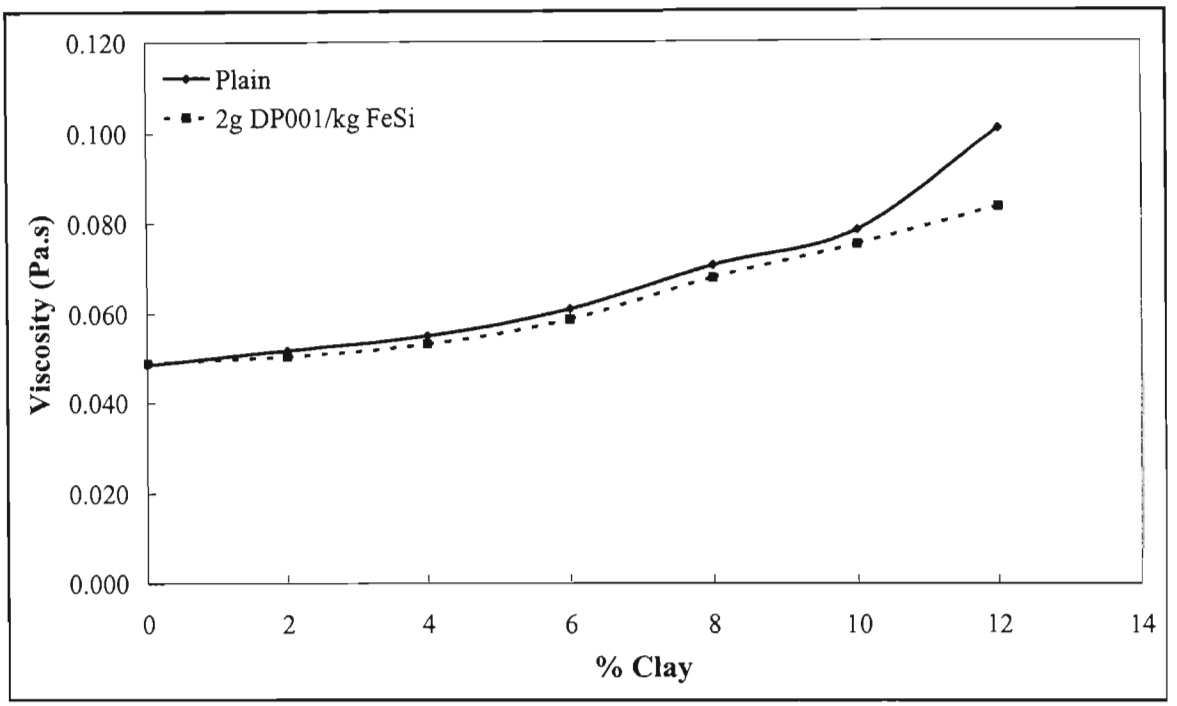

Figure 6.43 Effect of DP001 at 500 s^{-1} shear rate (sp.gr. 3.0)

At a specific gravity of 2.5 it can be seen that the viscosities for suspensions with DP001 are lower than that of plain suspensions at a given % slime. This reflects that there is a reduction the viscosity of the suspensions, even upon increasing the slime content. Even at high slime content, the effect of DP001 is still clearly visible. The same results were observed at a specific gravity of 2.6. At low slimes content the effect of DP001 appears to be less defined than that at higher slimes content. As the slime content is increases the effect of DP001 becomes modified, levelling off at slimes content from 10 % upwards. What can be seen from the above figures is that the extent of viscosity reduction by DP001 decreases as the specific gravity increases. The viscosity reduction at specific gravity 3.0 is much less than that at other specific gravities. This means that to reduce the viscosity at higher specific gravities, a higher dosage of DP001 may be required.

The results above are very significant to the viscosity reduction in heavy medium separations where slimes can cause problems. The results show that a small amount of DP001 is capable of reducing the viscosity of the suspensions even when there is an increase in slimes content. This means that if an operator observes an increase in slimes content, they can add the appropriate amount of DP001 based on the mass flowrate of the feed stream.

Rheological tests were also carried out at a constant shear rate of 240 s^{-1}, and specific gravity from 2.9 to 3.4. The reason for carrying out these tests at a low shear rate was to investigate whether DP001 could reduce the viscosity of ferrosilicon suspensions at shear rates similar to those at start up. When heavy medium suspensions have been shutdown for a while, the stored ferrosilicon suspensions sometimes cement and agglomerate, making pumping of the suspension to the separating vessels very difficult [Rodis et al. (1960)]. Figure 6.44 to Figure 6.49 show the results for these investigations.

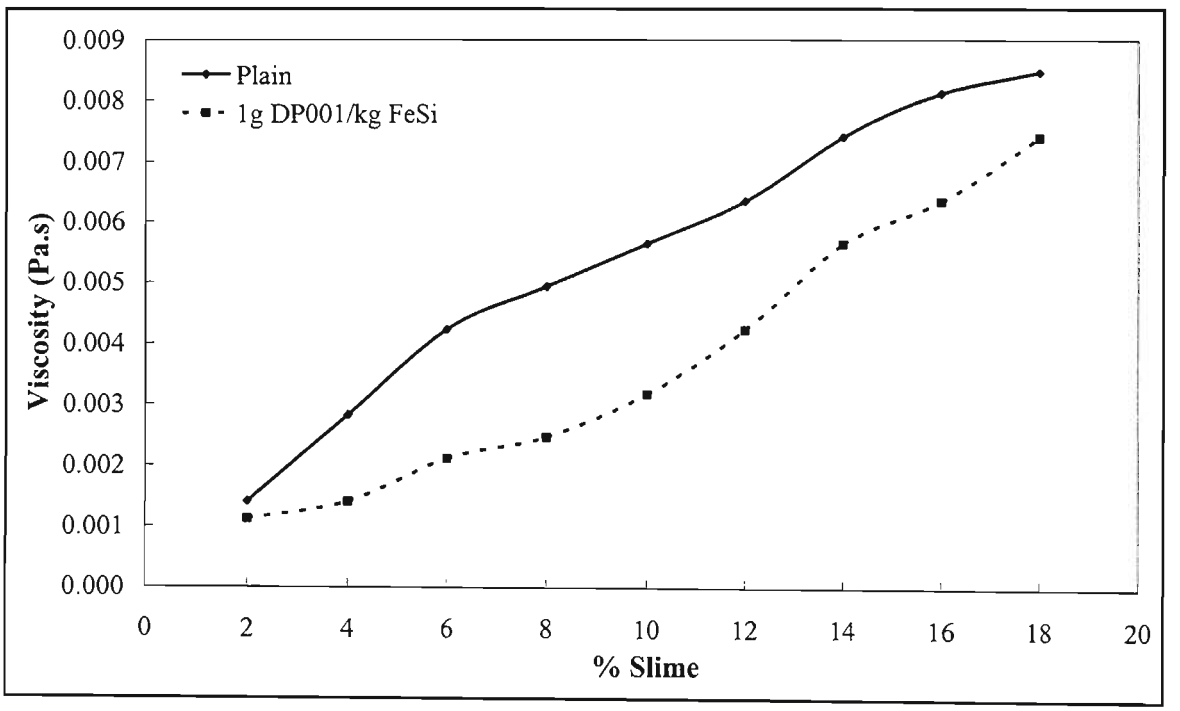

Figure 6.44 Effect of DP001 at 240 s^{-1} shear rate (sp.gr. 2.9)

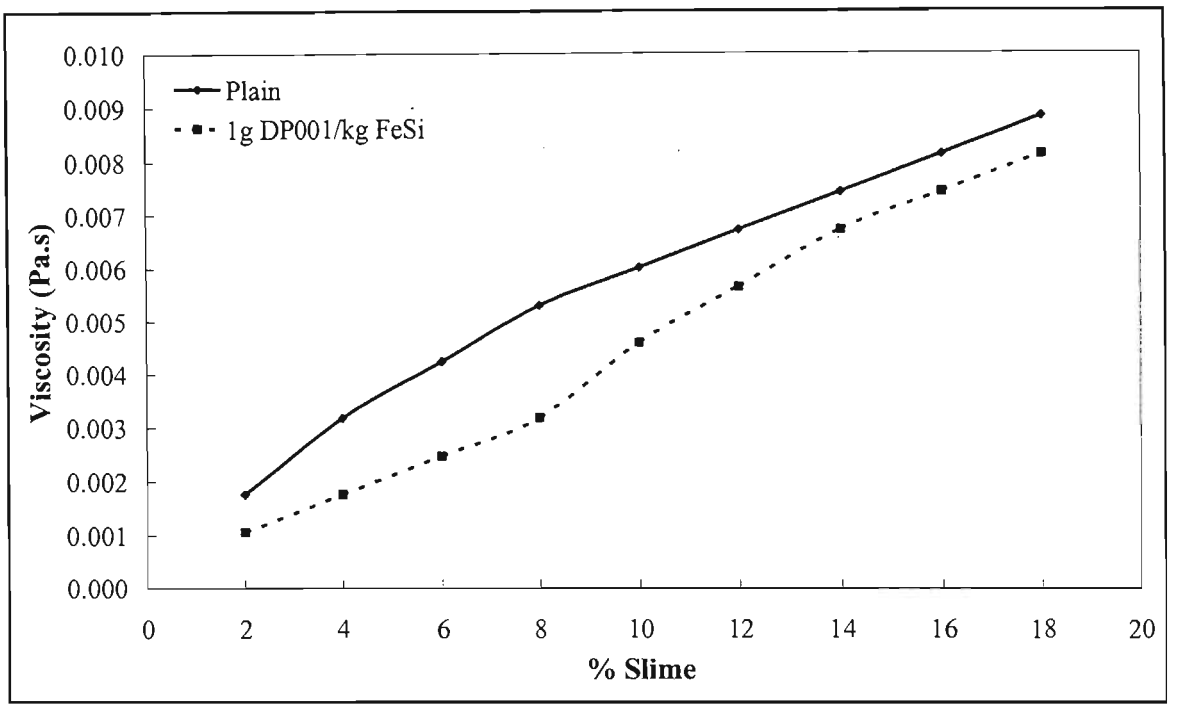

Figure 6.45 Effect of DP001 at 240 s^{-1} shear rate (sp.gr. 3.0)

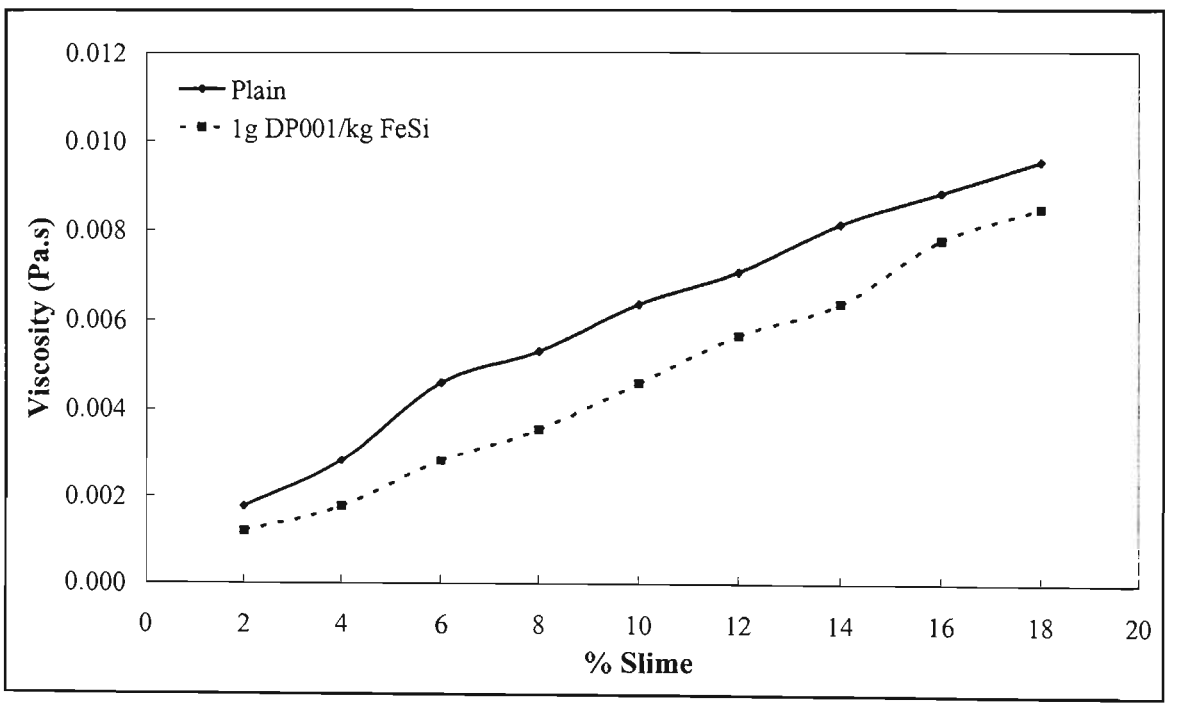

Figure 6.46 Effect of DP001 at 240 s^{-1} shear rate 9sp.gr. 3.1)

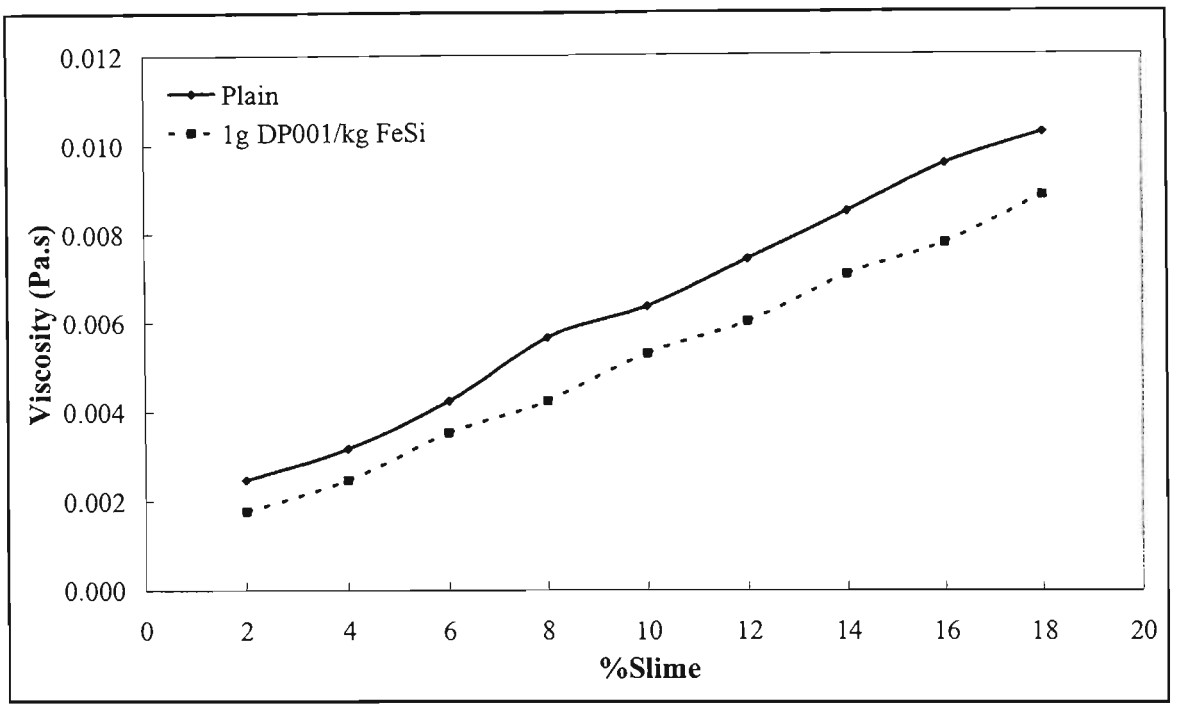

Figure 6.47 Effect of DP001 at 240 s^{-1} shear rate (sp.gr. 3.2)

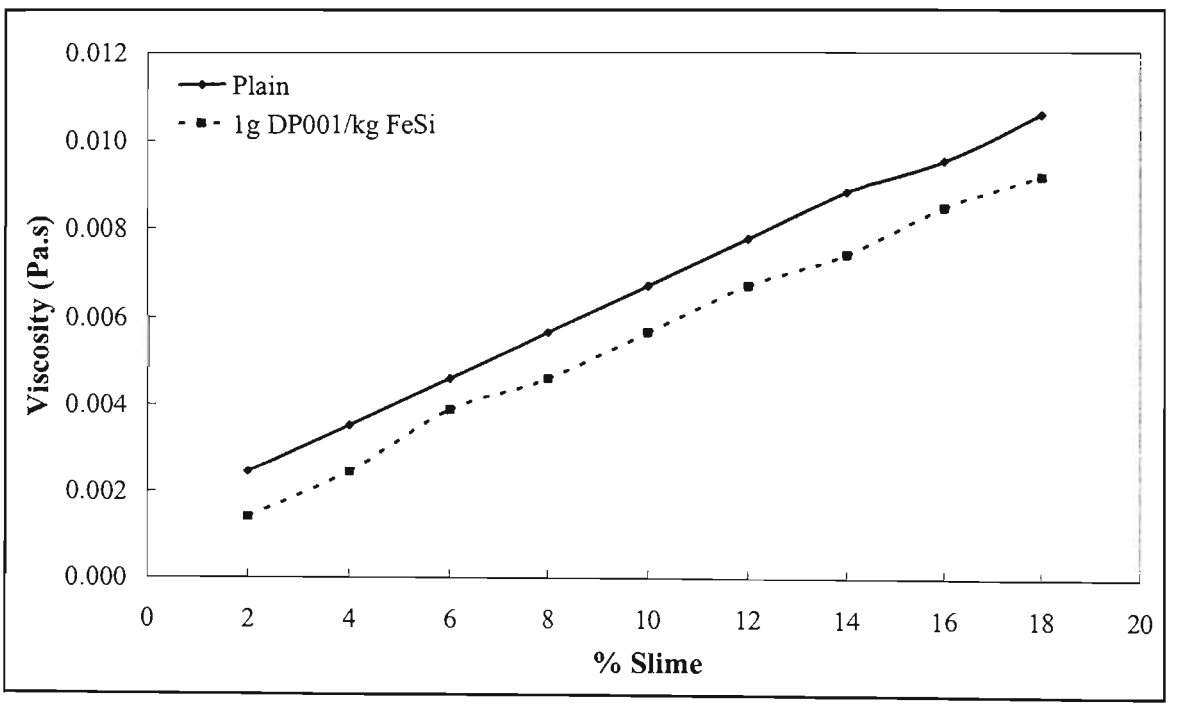

Figure 6.48 Effect of DP001 at 240 s^{-1} shear rate (sp.gr. 3.3)

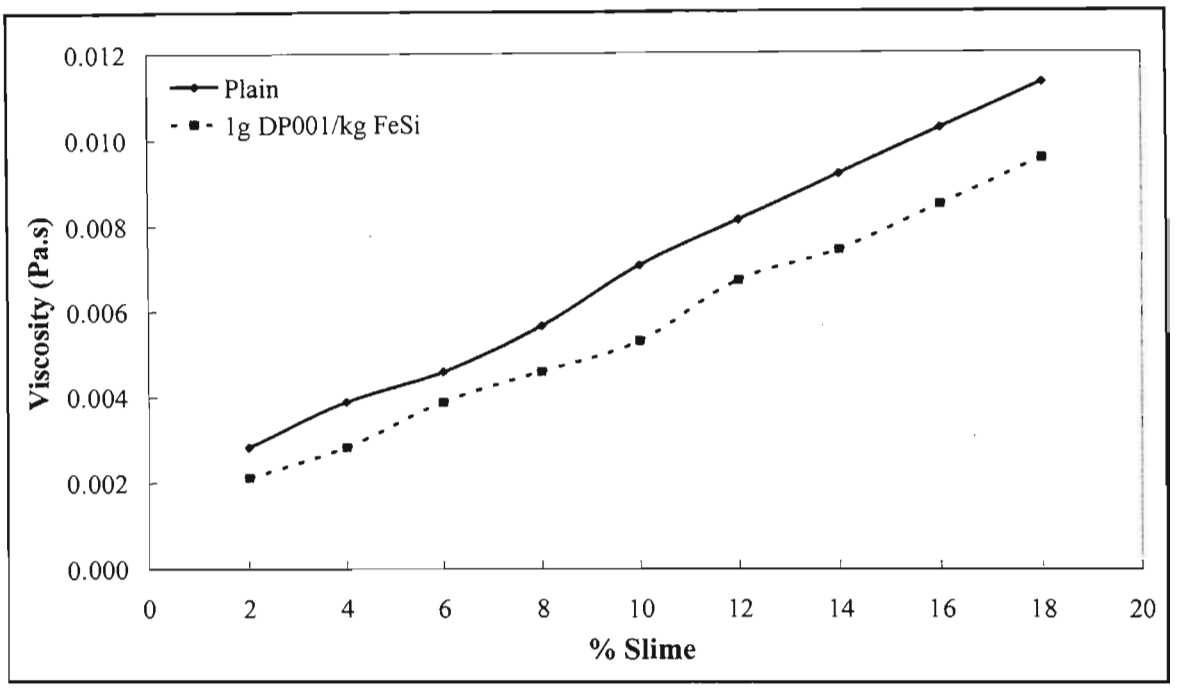

Figure 6.49 Effect of DP001 at 240 s^{-1} shear rate (sp.gr. 3.4)

The results from this investigation are summarised in Table 6.6. The percentage viscosity reduction was taken as an average over the entire range of slimes and DP001 additions i.e.not at any specific % slime, but over the entire range.

Table 6.6 Percentage viscosity reduction with DP001 at 240 s^{-1} shear rate

Specific Gravity	% Viscosity Reduction
2.9	32.1
3.0	20.5
3.1	23.4
3.2	18.4
3.3	16.6
3.4	19.1

All tested specific gravities showed a reduction in suspension viscosity on addition of DP001. This reduction at a low shear rate shows that viscosity reduction can be achieved in processes where there has been a long shutdown. Thereby, improving the pumping characteristics of the suspensions, resulting in reduced energy costs.

Aplan et al. (1964), using spherical ferrosilicon media suspensions contaminated with manganese ore slimes, also found a reduction in viscosity upon the addition of a chemical dispersant. The chemical dispersant they used for their investigations was sodium hexametaphosphate. Between 0.01 and 0.03 % (0.1 and 0.3 grams / kg solids) sodium hexametaphosphate additions, the viscosity reductions achievable were as high as fifty per cent. However, beyond a critical dosage, they observed a reduction in the stability of the suspensions. They showed that there is region between which a reduction in viscosity can be achieved without reducing the stability of the suspensions.

6.2.2 The Effect of DP001 on Magnetite Suspensions

Magnetite suspensions are commonly used in the separation of coal organic matter from its associated mineral matter [Collins et al. (1983), and He et al. (1999)]. Separations are carried out using specific gravities from 1.5 to 2.5. Above the specific gravity of 2.5 the viscosity of the magnetite suspensions become too high, resulting in reduced efficiency of separation.

This section looks at the effect of DP001 on the viscosity of magnetite suspensions. The results can then be used to asses whether or not magnetite suspensions can be used at higher specific gravities without having to deal with the large viscosities experienced at these specific gravities.

6.2.2.1 Experimental Results and Discussion

Investigations were carried out at specific gravities from 2.2 to 2.6, at DP001 additions of 1gram, 2 gram, and 5 gram DP001 per kilogram magnetite #1. The experimental methods were similar to those used for the ferrosilicon suspensions. Figure 6.50 to Figure 6.54 show the results obtained from the rheological measurements.

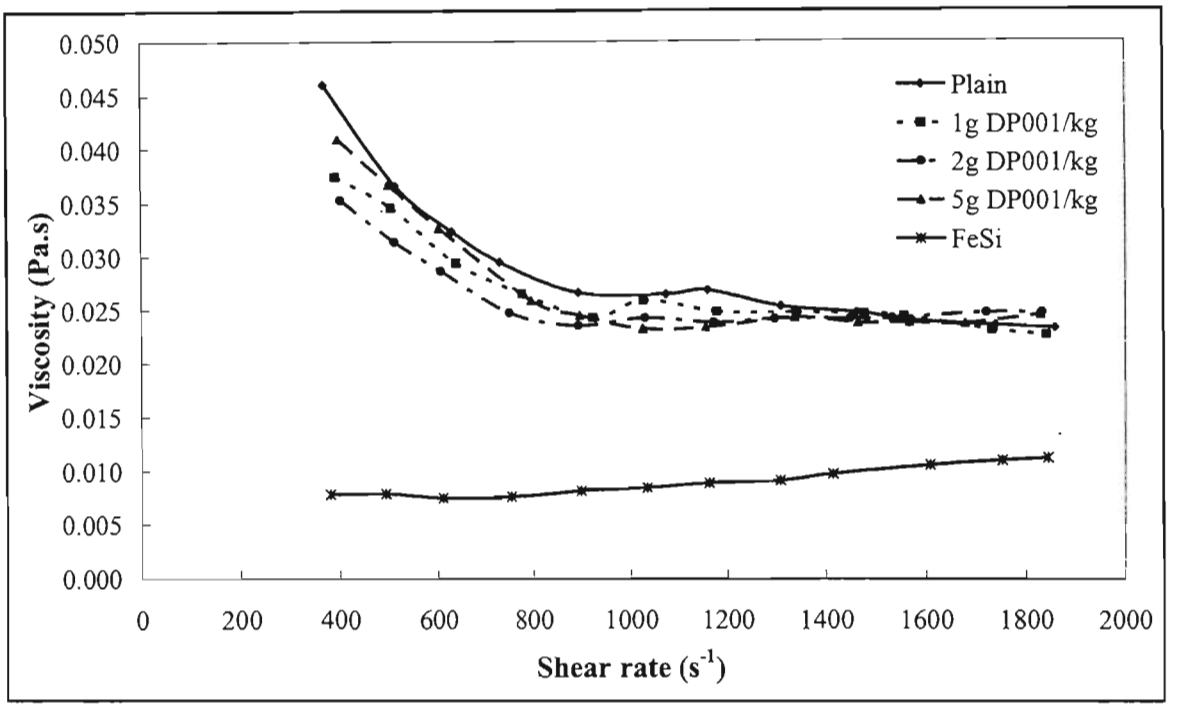

Figure 6.50 Effect of DP001 on magnetite suspensions (sp.gr. 2.2)

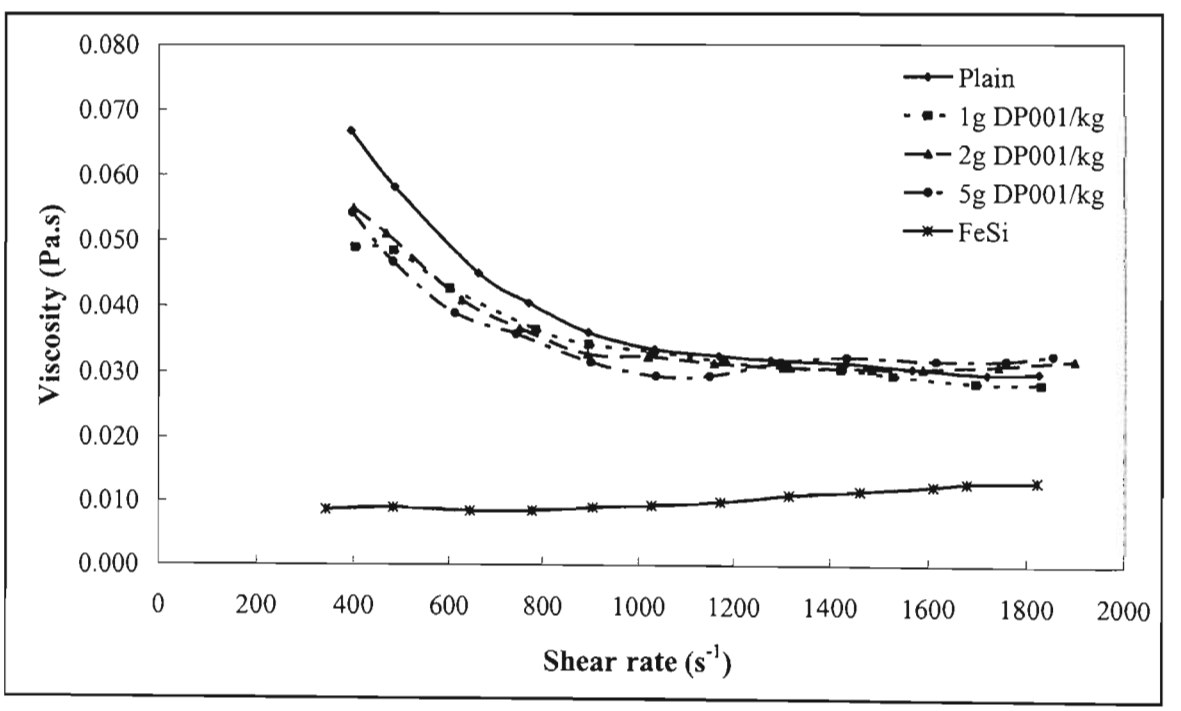

Figure 6.51 Effect of DP001 on magnetite suspensions (sp.gr. 2.3)

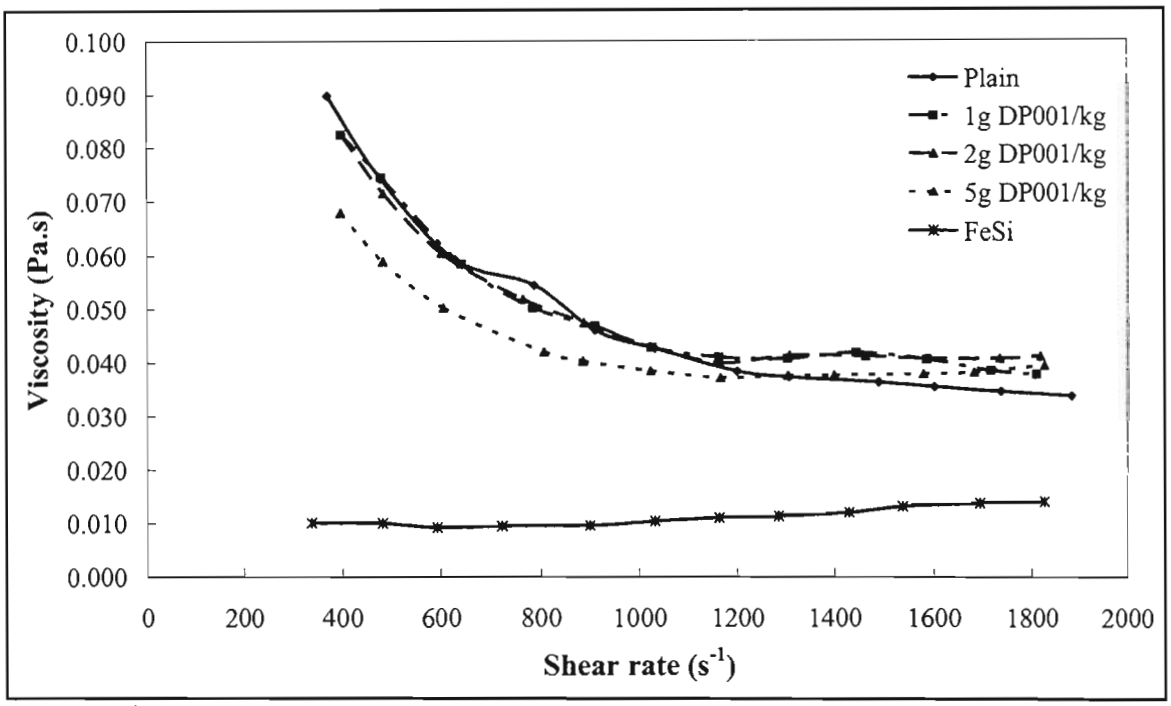

Figure 6.52 Effect of DP001 on magnetite suspensions (sp.gr. 2.4)

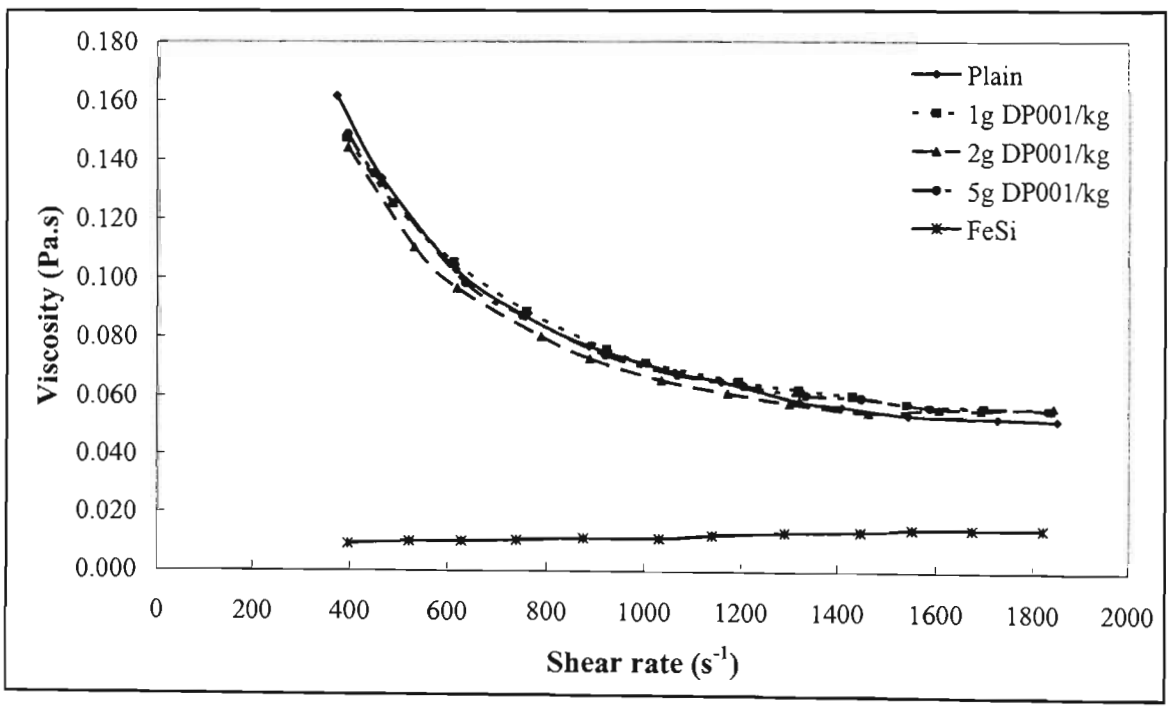

Figure 6.53 Effect of DP001 on magnetite suspensions (sp.gr. 2.5)

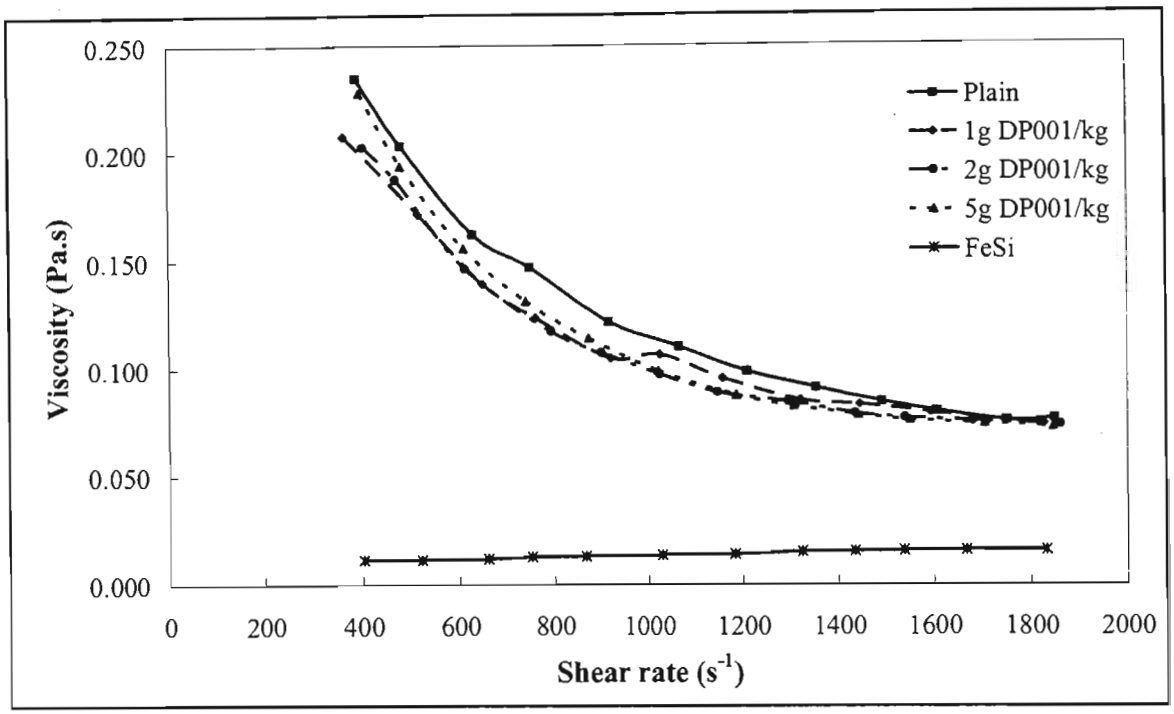

Figure 6.54 Effect of DP001 on magnetite suspensions (sp.gr. 2.6)

The graphs for magnetite are plotted together with those of plain ferrosilicon at the same specific gravity. The reason for this is to see how capable DP001 is in bringing the magnetite viscosity to that of ferrosilicon. Figure 6.50 shows the results obtained for a magnetite suspension with a specific gravity of 2.2. The graph shows that at an addition of 1g DP001/kg reduces the viscosity of the suspensions only slightly. An addition of another 1g DP001/kg further educes the viscosity of the suspensions. The greatest reduction is obtained at addition of 5g DP001/kg. However, at shear rates in excess of 1500 s^{-1}, the graphs appear to level, with some of them showing a much higher viscosity than the plain suspensions. this gives the impression that the DP001 only reduces the yield stress, as shown by the lower viscosities at low shear rates, and does not reduce the plastic viscosity. The graph also illustrates the much greater viscosity of the magnetite suspensions compared to the ferrosilicon suspensions. Even at the DP001 additions, the viscosity of the magnetite suspensions is still much higher than that for ferrosilicon.

Similar results as those stated above were observed at higher magnetite suspensions. All the graphs show a decrease in viscosity at low shear rates, but a sudden increase at much higher shear rates. Figure 6.51 and Figure 6.52 show a much larger increase in suspension viscosity for the DP001 magnetite suspensions after a certain shear rate. In Figure 6.52, only additions of 5g DP001/kg show any reduction in suspension viscosity. The suspensions viscosity is much lower

than the plain suspensions up to a shear rate of around 1200 s^{-1}, beyond which the viscosity increases substantially. Figure 6.53 shows a similar trend for a specific gravity of 2.5. In this case the effect of 5 g DP001/kg magnetite #1 appears to be lower than that at specific gravity 2.4. The suspensions viscosity is reduced up to a shear rate of 1500 s^{-1}, above which an increase in suspension viscosity is observed.

Figure 6.54 shows the results obtained for magnetite suspensions at a specific gravity of 2.6.The graph shows that a reduction in suspension viscosity is achieved at all DP001 additions. In this case, although the 5g DP001/kg magnetite #1 additions show the highest initial reduction, their viscosity increases above those for 1g and 2g DP001/kg magnetite #1 additions at a shear rate of 900 s^{-1}. All the DP001 graphs begin to approach the plain suspension graph, and no discernable viscosity difference is observed at shear rates 1800 s^{-1} and above.

6.2.3 The Effect of DP001 on Ferrosilicon / Magnetite suspensions

As mentioned in Section 6.1.3.3, some heavy medium separations are carried out using ferrosilicon-magnetite suspensions. It was also shown that the presence of magnetite results in high viscosities due to their lower density and high fines content. This section examines the results obtained from the use of DP001 in ferrosilicon-magnetite suspensions. The experimental methods are similar to those used earlier. Tests were carried out on ferrosilicon-magnetite mixtures with ratios 1:1, 2:1, and 1:2, on a mass basis. The results for each ratio will be presented separately.

6.2.3.1 Experimental Results and Discussion

6.2.3.2 Ferrosilicon-Magnetite #1 Mixtures at a Ratio of 1:1

Figure 6.55 to Figure 6.61 show the results obtained for DP001 additions on ferrosilicon-magnetite mixtures with a ratio of 1:1 FeSi to Mag#1.

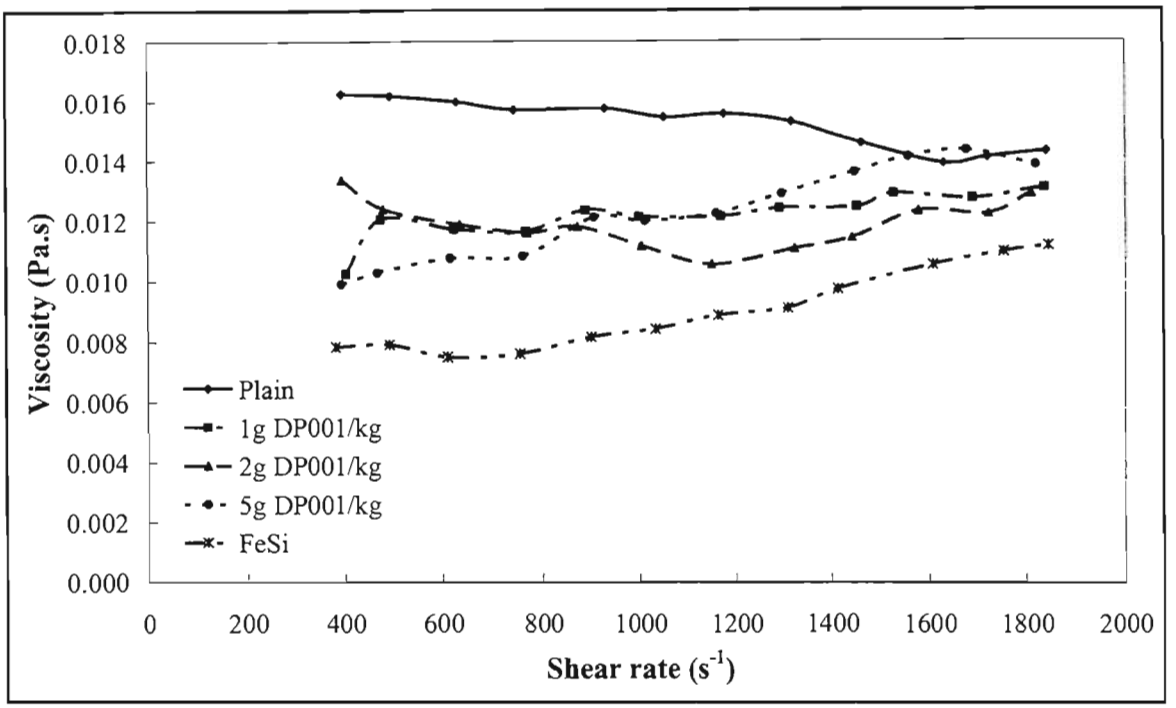

Figure 6.55 Effect of DP001 on ferrosilicon-magnetite #1 mixtures (1:1) at sp.gr.2.2

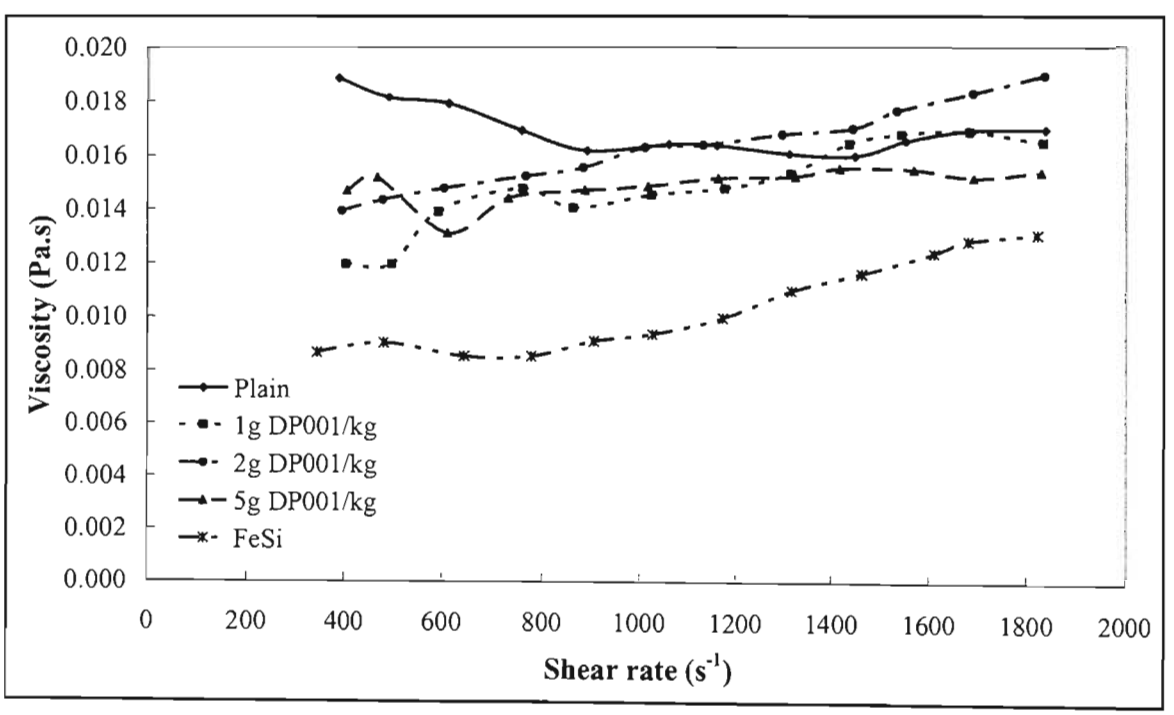

Figure 6.56 Effect of DP001 on ferrosilicon-magnetite #1 mixtures (1:1) at sp.gr.2.3

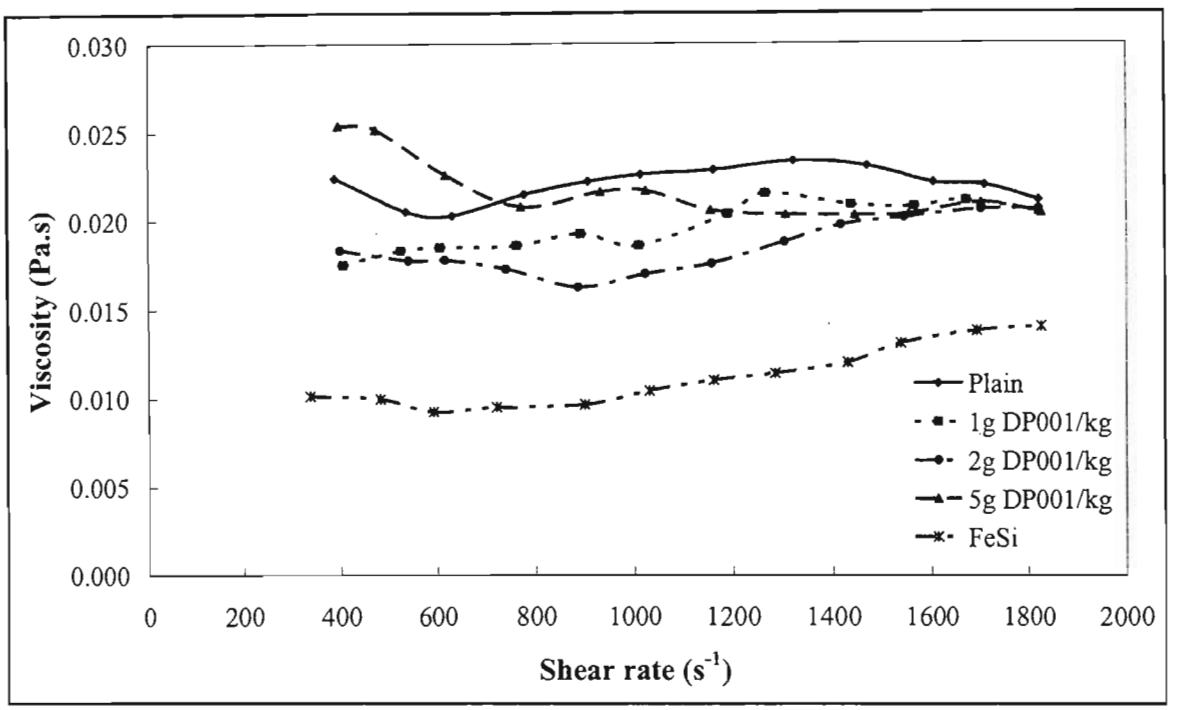

Figure 6.57 Effect of DP001 on ferrosilicon-magnetite #1 mixtures (1:1) at sp.gr.2.4

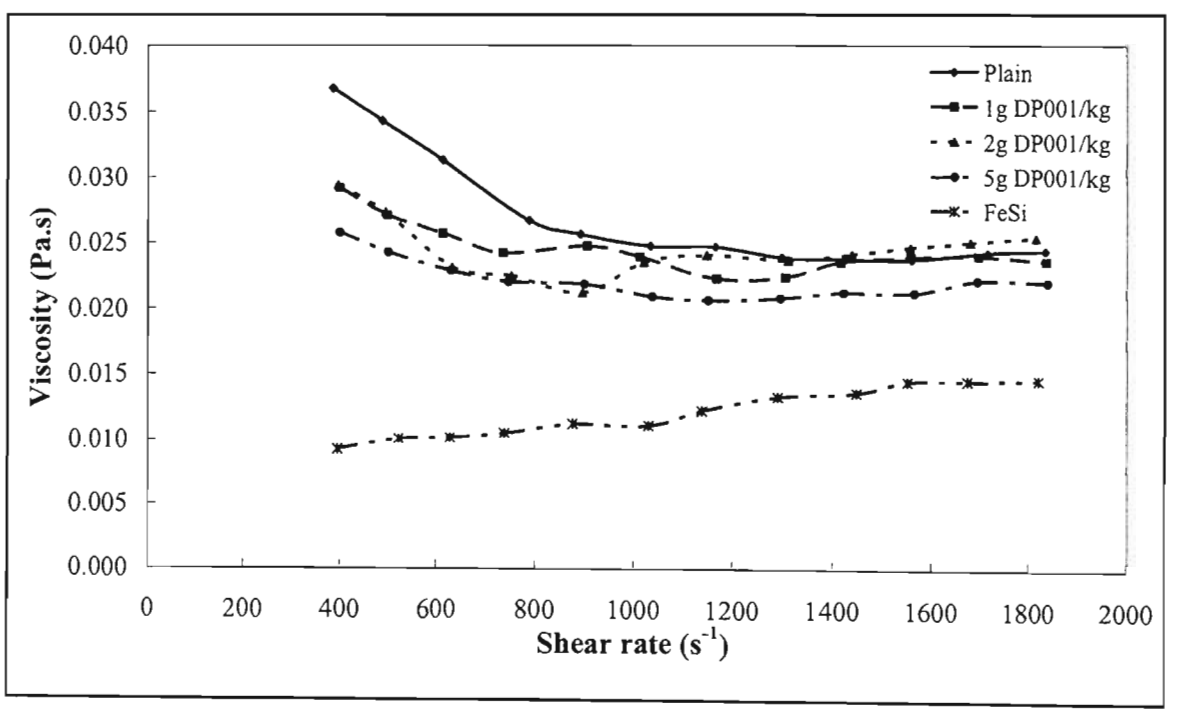

Figure 6.58 Effect of DP001 on ferrosilicon-magnetite #1 mixtures (1:1) at sp.gr.2.5

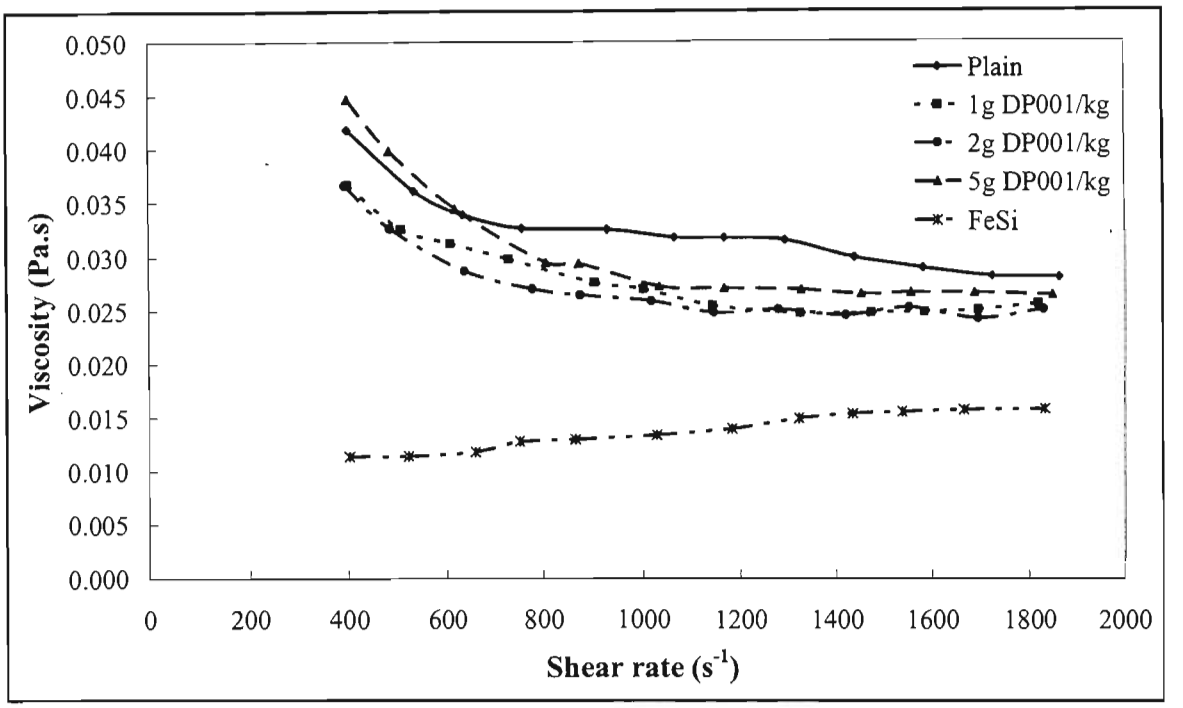

Figure 6.59 Effect of DP001 on ferrosilicon-magnetite #1 mixtures (1:1) at sp.gr.2.6

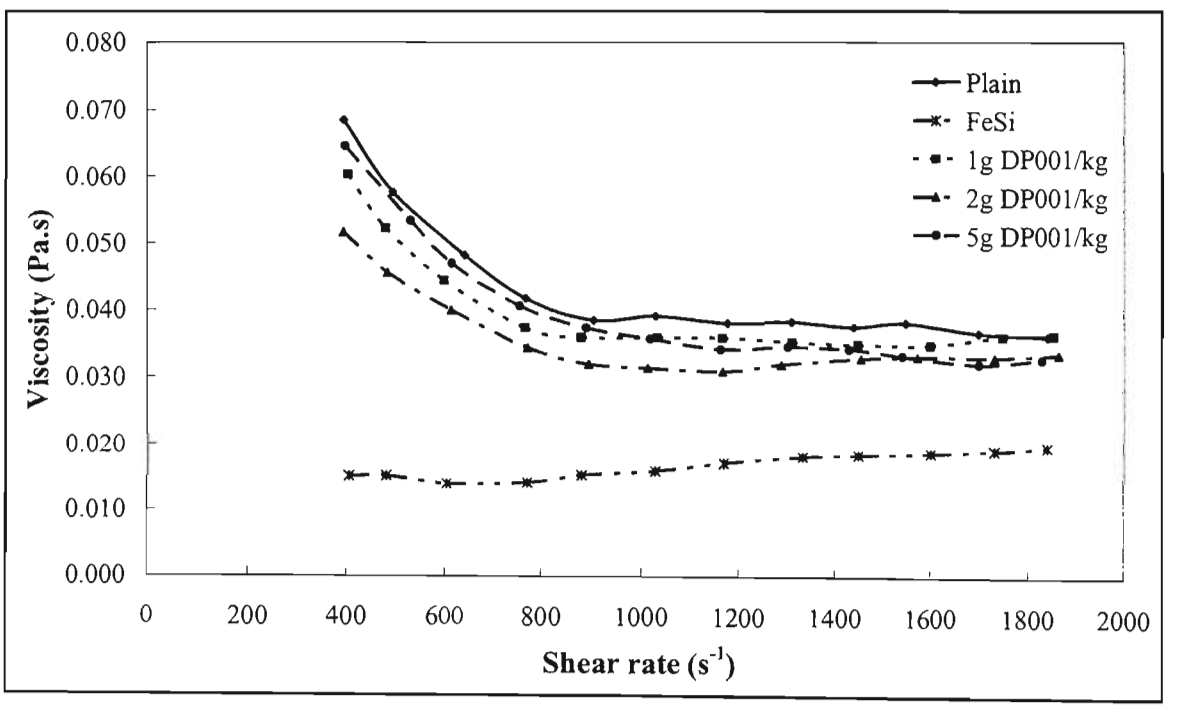

Figure 6.60 Effect of DP001 on ferrosilicon-magnetite #1 mixtures (1:1) at sp.gr.2.7

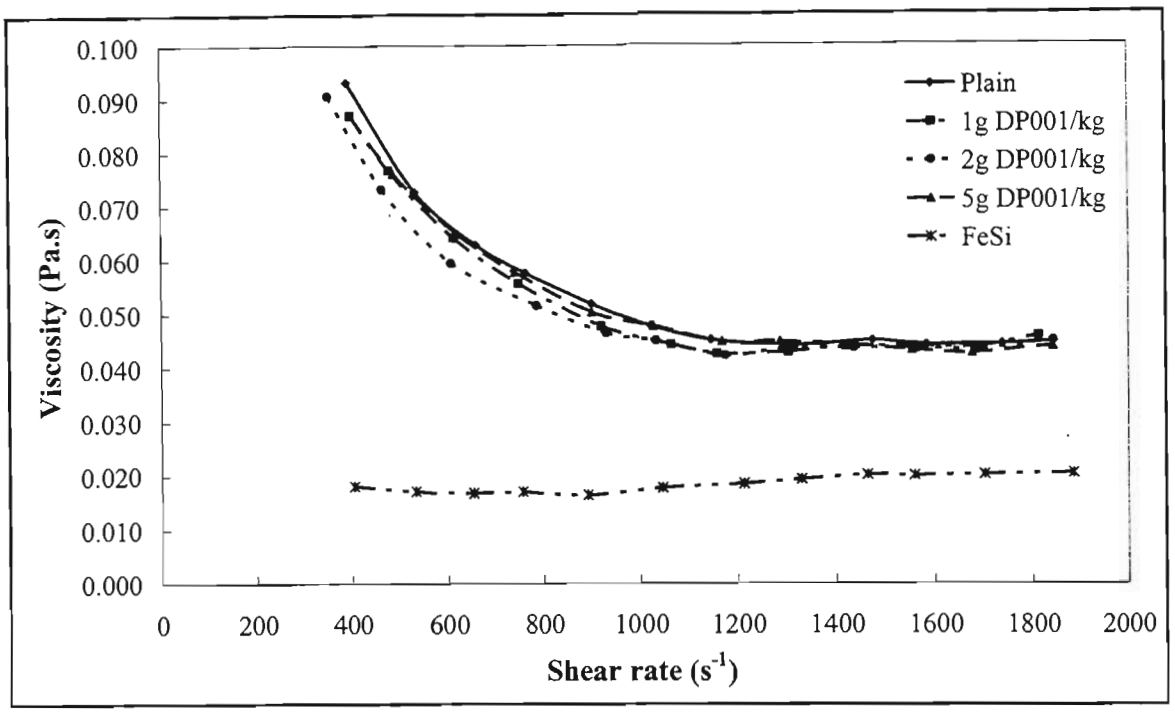

Figure 6.61 Effect of DP001 on ferrosilicon-magnetite #1 mixtures (1:1) at sp.gr.2.8

Table 6.7 summarises the results taken from the figures above. The percentage viscosity reduction is calculated by taking the average decrease in viscosity over the entire range of shear rates.

Table 6.7 Viscosity reduction on Ferrosilicon/Magnetite #1 (1:1) mixtures

Specific Gravity	% Viscosity Reduction		
	1g DP001/kg	2g DP001/kg	5g DP001/kg
2.2	20.3	22.1	19.8
2.3	12.4	3.9	12.0
2.4	10.6	15.9	1.4
2.5	9.1	9.3	18.1
2.6	13.4	15.8	5.7
2.7	7.5	17.0	7.5
2.8	2.3	3.9	0.9

The results show that the addition of DP001 reduces the viscosity of the suspensions. Figure 6.55 illustrates that the addition of DP001 to a ferrosilicon-magnetite suspension at a specific gravity of 2.2 reduces the viscosity of the suspensions by a considerable amount. The addition of 1g DP001/kg reduces the viscosity by up to 20%. Addition of a further 1 gram and 3 g DP001/kg does not appear to further reduce the viscosity of the suspensions by much. A similar trend is observed for some of the other specific gravities. At a specific gravity of 2.3 the reduction in the viscosity of the suspensions at DP001 additions equal to 2g DP001/kg is not as pronounced as at 1g DP001/kg. However, additions of 5g DP001/kg results in a further reduction of the viscosity. At a specific gravity of 2.4 the viscosity reduction for both 1g and 2g DP001 additions is relatively high. But at 5g DP001/kg additions, the viscosity reduction observed was much lower than that observed at the 1 and 2 g DP001/kg additions. At specific gravity 2.5 there appears to be little difference between the viscosity reductions at 1 and 2 g DP001/kg additions. A much larger drop in suspensions viscosity was observed at 5 g DP001/kg additions. From a specific gravity 2.6 to 2.8, the drop in viscosity increases between 1g and 2g DP001/kg additions. There appears to be little benift in increasing the dosage of DP001 additions to 5g DP001/kg.

The results above show that DP001 is capable of reducing the viscosity of suspensions of ferrosilicon-magnetite mixtures. At low specific gravities (2.2 to 2.4), some of the graphs with DP001 additions are close to the plain ferrosilicon graph at the same specific gravity. The results show that DP001 has an effect of bringing the viscosities of the ferrosilicon-magnetite suspensions towards those of plain ferrosilicon suspensions. However, it is not quite clear from the results which dosage of DP001 is more effective. It appears at though the optimum dosage lies somewhere between 1g and 2g DP001/kg additions.

6.2.3.3 Ferrosilicon-Magnetite #1 Mixtures at a Ratio of 2:1

Figure 6.62 to Figure 6.68 show the results for DP001 additions in ferrosilicon-magnetite suspensions at a ratio of ferrosilicon/magnetite equal to 2:1.

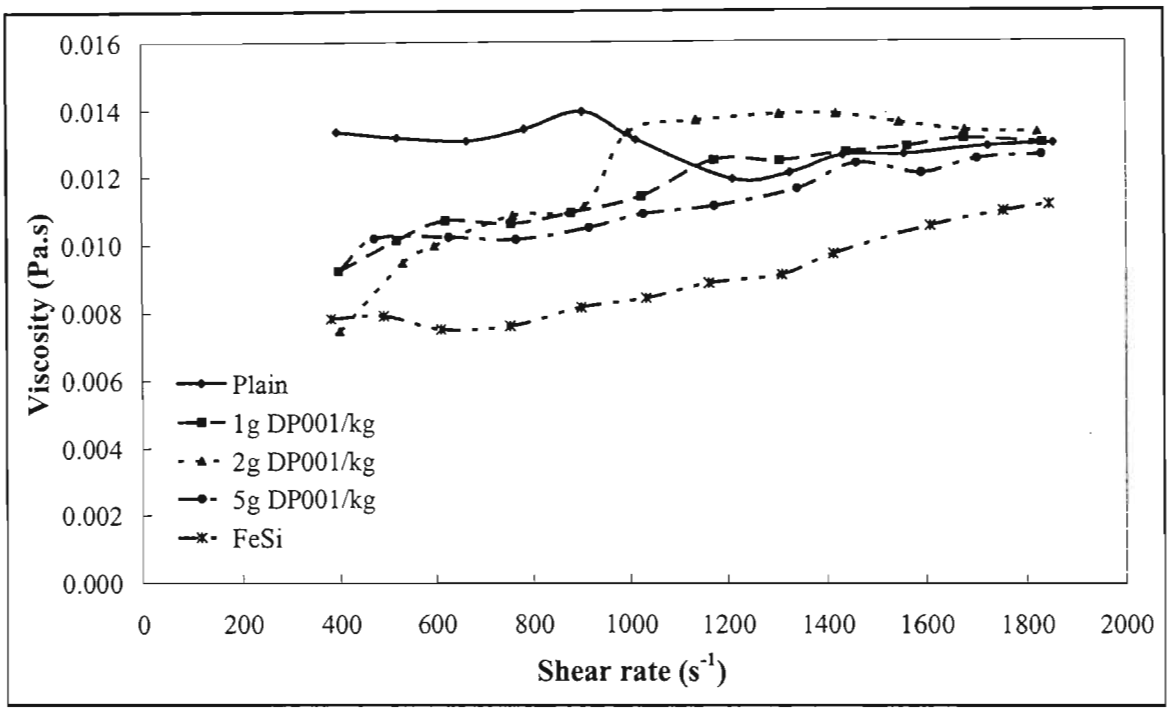

Figure 6.62 Effect of DP001 on ferrosilicon-magnetite #1 mixtures (2:1) at sp.gr.2.2

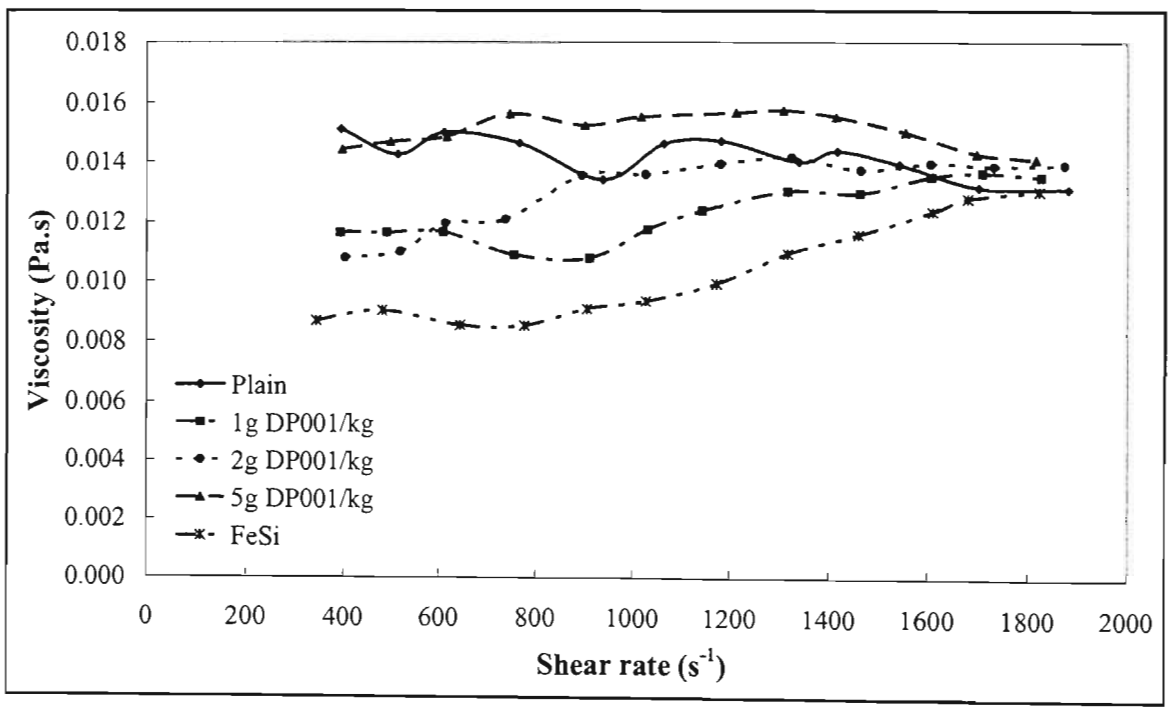

Figure 6.63 Effect of DP001 on ferrosilicon-magnetite #1 mixtures (2:1) at sp.gr.2.3

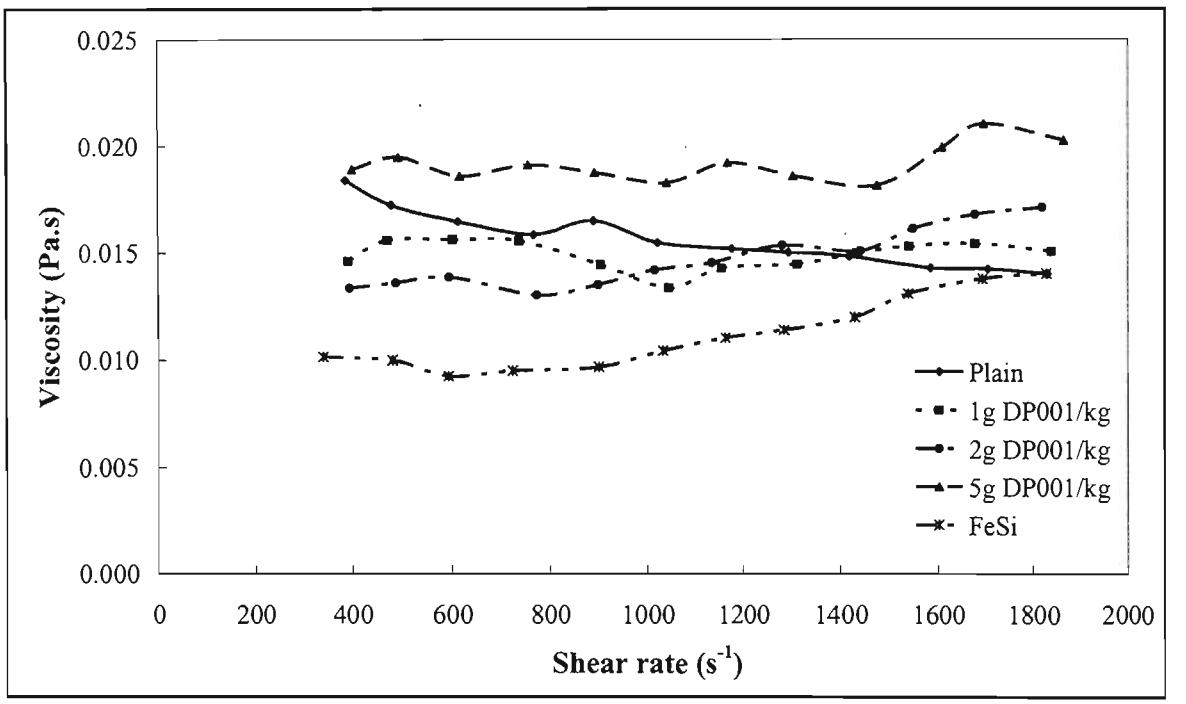

Figure 6.64 Effect of DP001 on ferrosilicon-magnetite #1 mixtures (2:1) at sp.gr.2.4

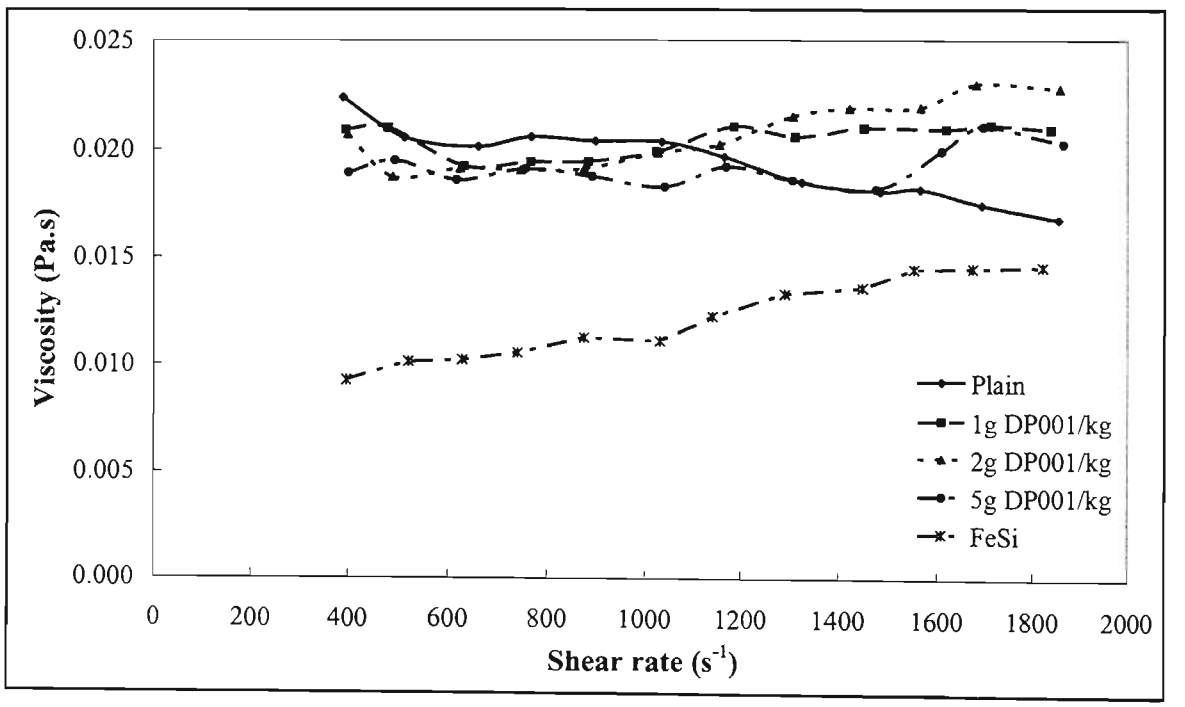

Figure 6.65 Effect of DP001 on ferrosilicon-magnetite #1 mixtures (2:1) at sp.gr.2.5

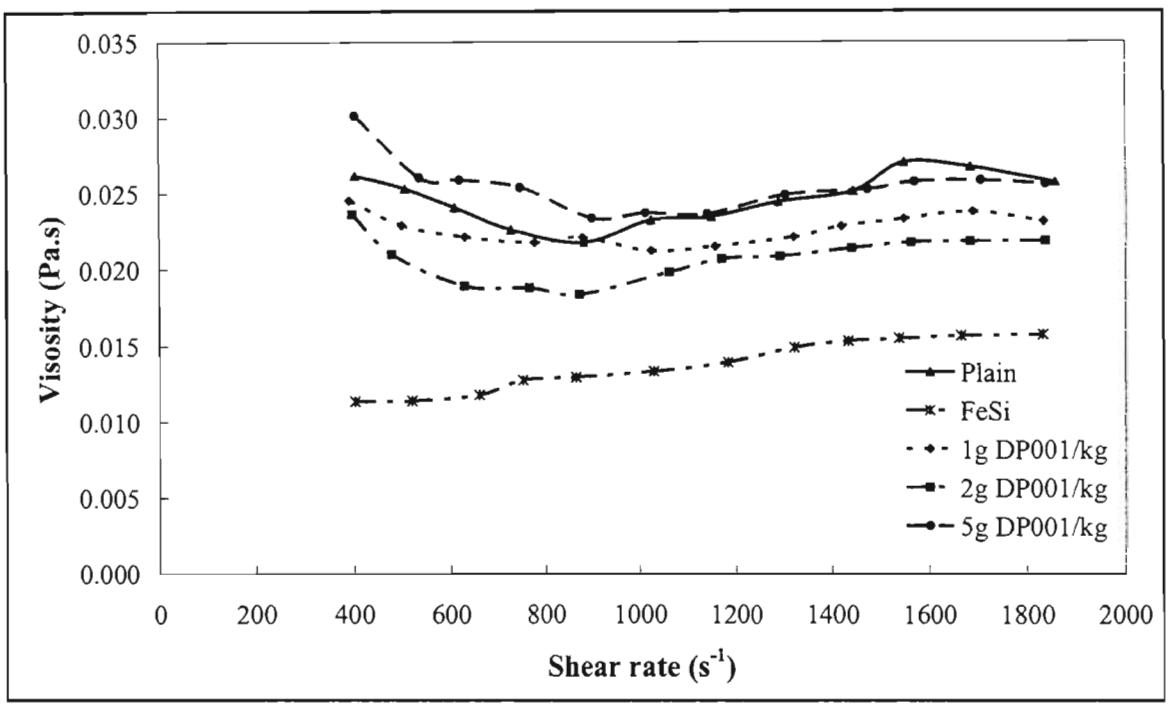

Figure 6.66 Effect of DP001 on ferrosilicon-magnetite #1 mixtures (2:1) at sp.gr.2.6

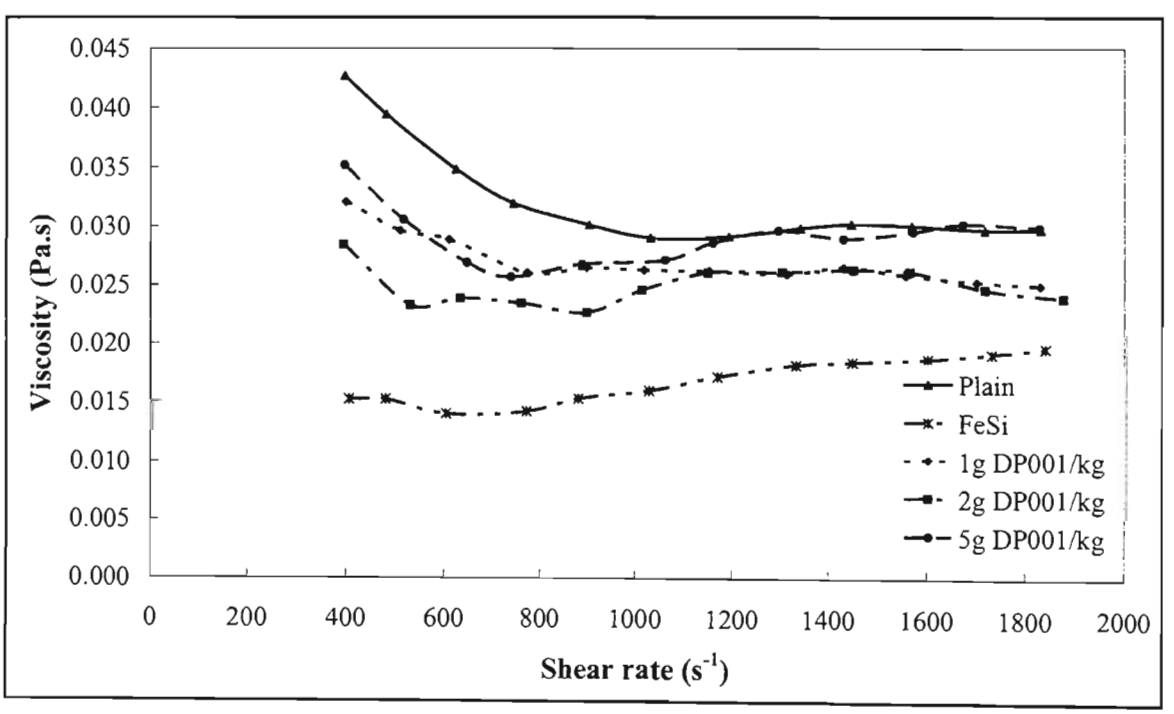

Figure 6.67 Effect of DP001 on ferrosilicon-magnetite #1 mixtures (2:1) at sp.gr.2.7

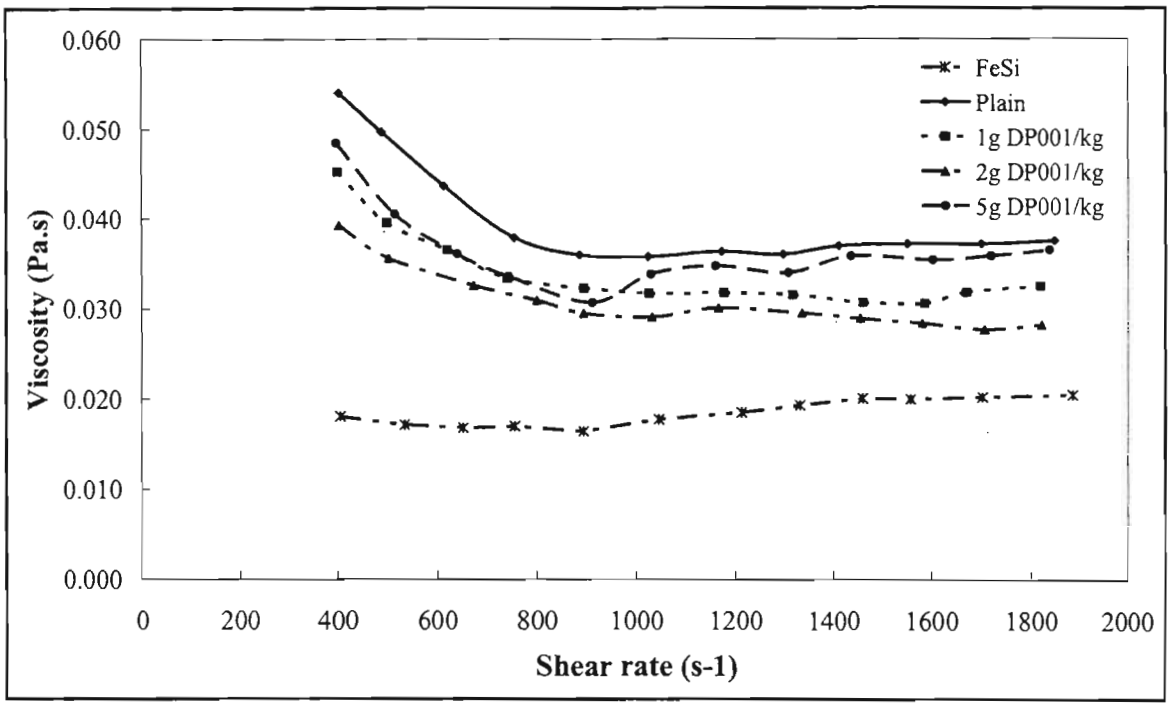

Figure 6.68 Effect of DP001 on ferrosilicon-magnetite #1 mixtures (2:1) at sp.gr.2.8

Table 6.8 summarises the results shown in the above figures. Again the percentage viscosity reduction was taken as an average over the entire range of shear rates.

Table 6.8 Viscosity reduction on Ferrosilicon/Magnetite #1 (2:1) mixtures

Specific Gravity	% Viscosity Reduction		
	1g DP001/kg	2g DP001/kg	5g DP001/kg
2.2	10.0	7.3	14.0
2.3	13.4	8.0	-6.1
2.4	4.7	5.8	-22.8
2.5	-5.4	-6.4	-14.8
2.6	8.2	15.8	-3.2
2.7	16.2	22.5	9.7
2.8	14.8	22.7	9.0

The figures above also show that the viscosity of the suspensions is reduced at some of DP001 additions. At a specific gravity of 2.2 the addition of 1gram DP001 / kilogram reduces the viscosity of the suspensions by up to 10%. There is not much difference observed through the addition of a further 1 gram. Additions of 5grams DP001 / kilogram reduce the viscosity by

14.0%. At a specific gravity of 2.3, the viscosity begins to increase after additions of 1gram DP001 / kilogram. At 5grams DP001 / kilogram additions the viscosity of the suspensions exceeds that of the pure suspensions. a similar sort of trend is observed at specific gravities 2.4 to 2.6. At a specific gravity of 2.5 there appears to be no reduction in viscosity. In fact, there is an increase in the viscosity of the suspensions at all DP001 additions. At specific gravities 2.7 and 2.8 the viscosity is reduced by additions up to 2grams DP001 / kilogram. At 5grams DP001 / kilogram additions, the viscosity appears to also increase.

For the ferrosilicon-magnetite suspensions at a ratio of 2:1, the presence of magnetite is much lower than ferrosilicon. The stability of the suspensions is thus not as stable as ferrosilicon-magnetite mixtures at a ratio of 1:1. The measurements of these suspensions were much more difficult at the lower specific gravities. The presence of DP001 could have also added to the higher settling rates of the media particles. The accumulation of solid particles at the base of the cup could have resulted in the simulation of viscosities in excess of plain suspensions at the lower specific gravities.

The graphs above also show that the viscosities of suspensions at some DP001 additions are close to those of ferrosilicon suspensions at the same specific gravities, particularly at low shear rates. At specific gravities 2.7 and 2.8, DP001 reduces the difference in viscosity between ferrosilicon-magnetite suspensions and pure ferrosilicon suspensions by as much 50% at high shear rates.

6.2.3.3 Ferrosilicon-magnetite #1 Mixtures at a Ratio of 1:2

Figure 6.69 to Figure 6.75 show the results for DP001 additions in ferrosilicon-magnetite suspensions at a ratio of ferrosilicon/magnetite equal to 1:2.

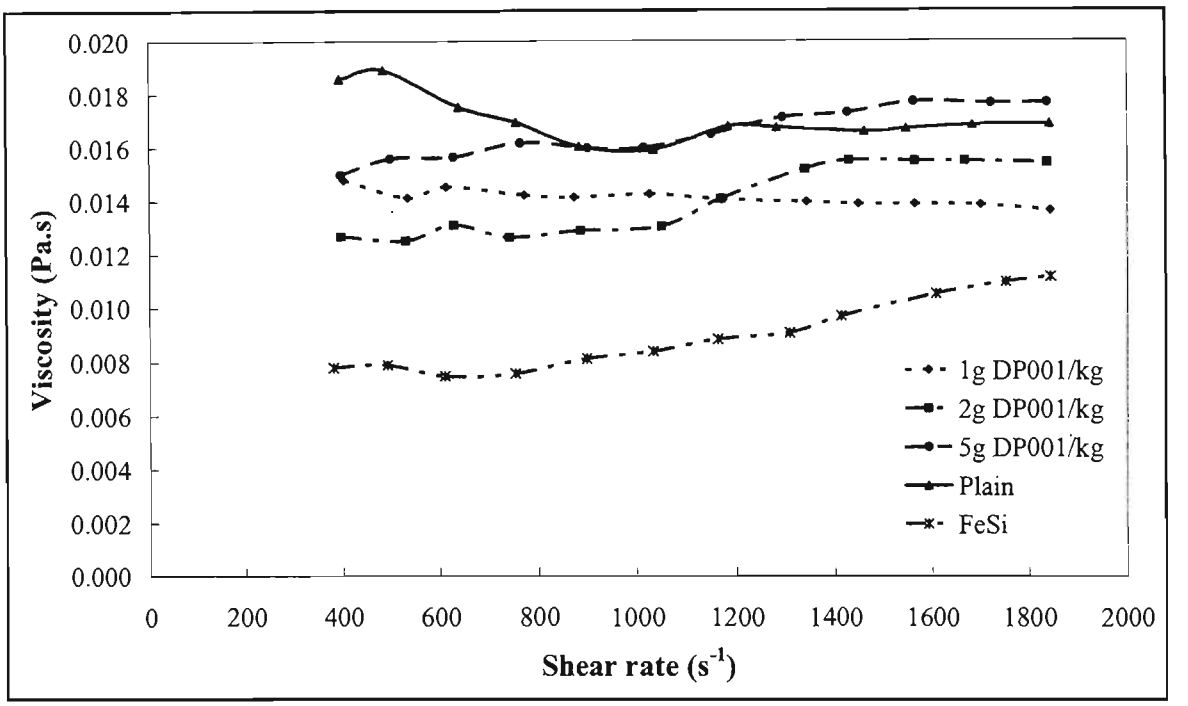

Figure 6.69 Effect of DP001 on ferrosilicon-magnetite #1 mixtures (1:2) at sp.gr.2.2

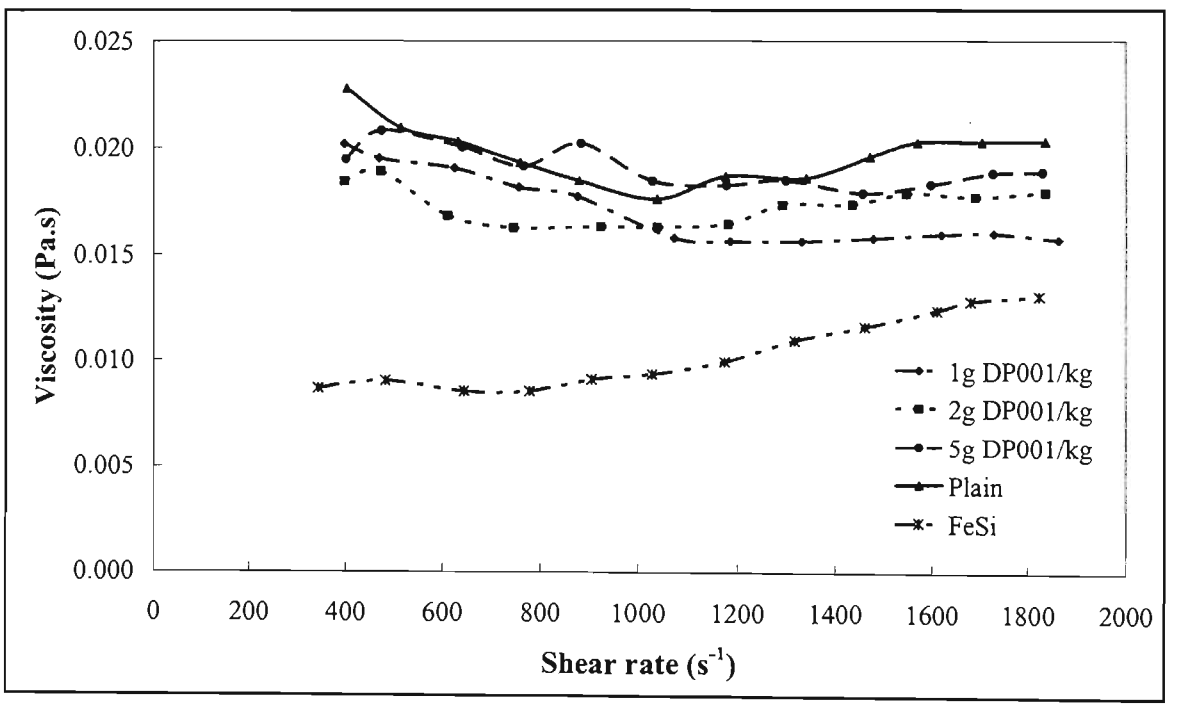

Figure 6.70 Effect of DP001 on ferrosilicon-magnetite #1 mixtures (1:2) at sp.gr.2.3

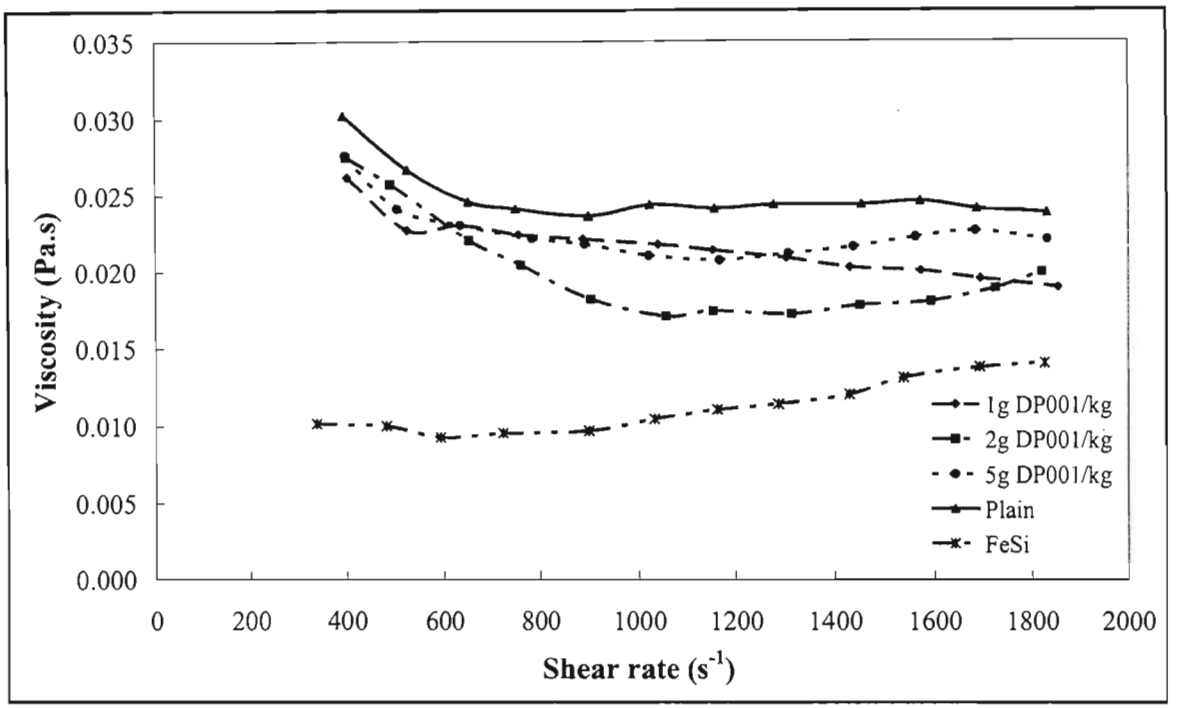

Figure 6.71 Effect of DP001 on ferrosilicon-magnetite #1 mixtures (1:2) at sp.gr.2.4

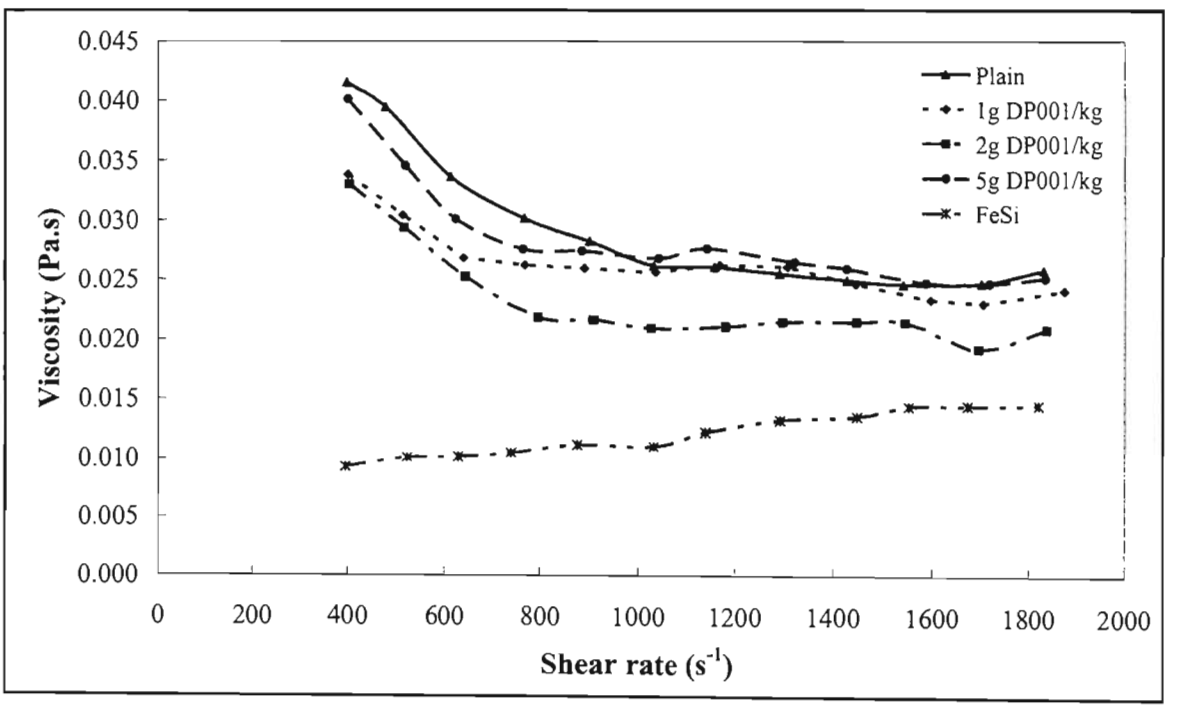

Figure 6.72 Effect of DP001 on ferrosilicon-magnetite #1 mixtures (1:2) at sp.gr.2.5

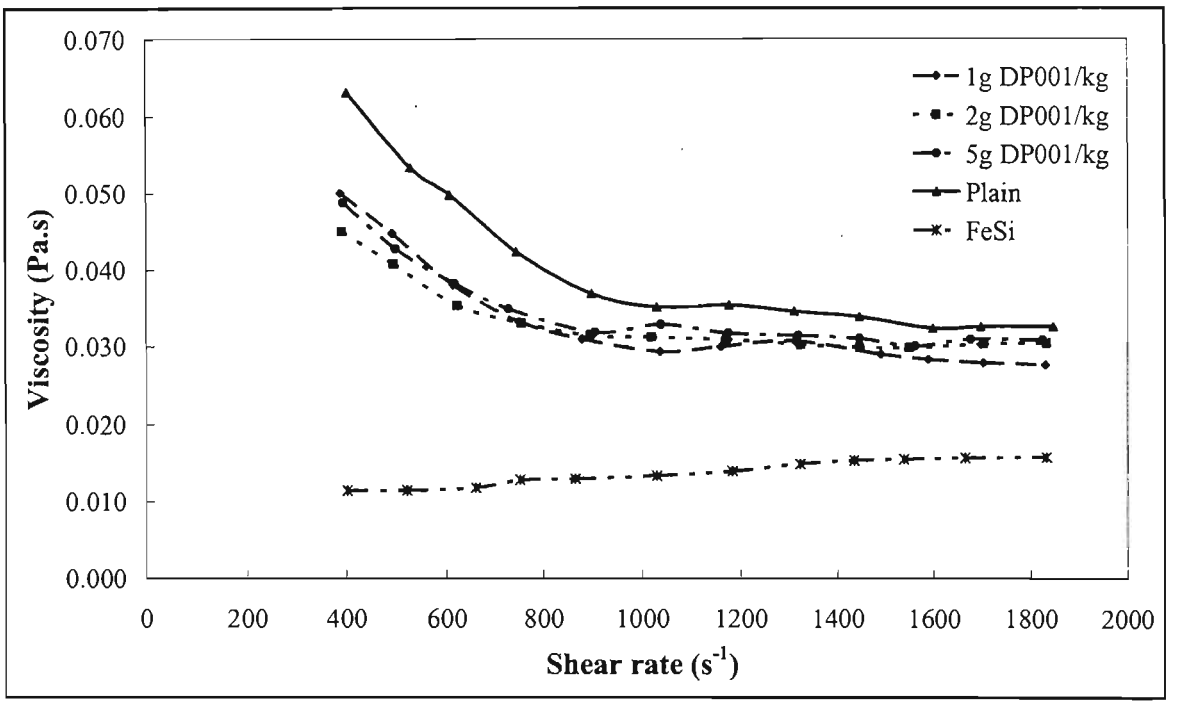

Figure 6. 73 Effect of DP001 on ferrosilicon-magnetite #1 mixtures (1:2) at sp.gr.2.6

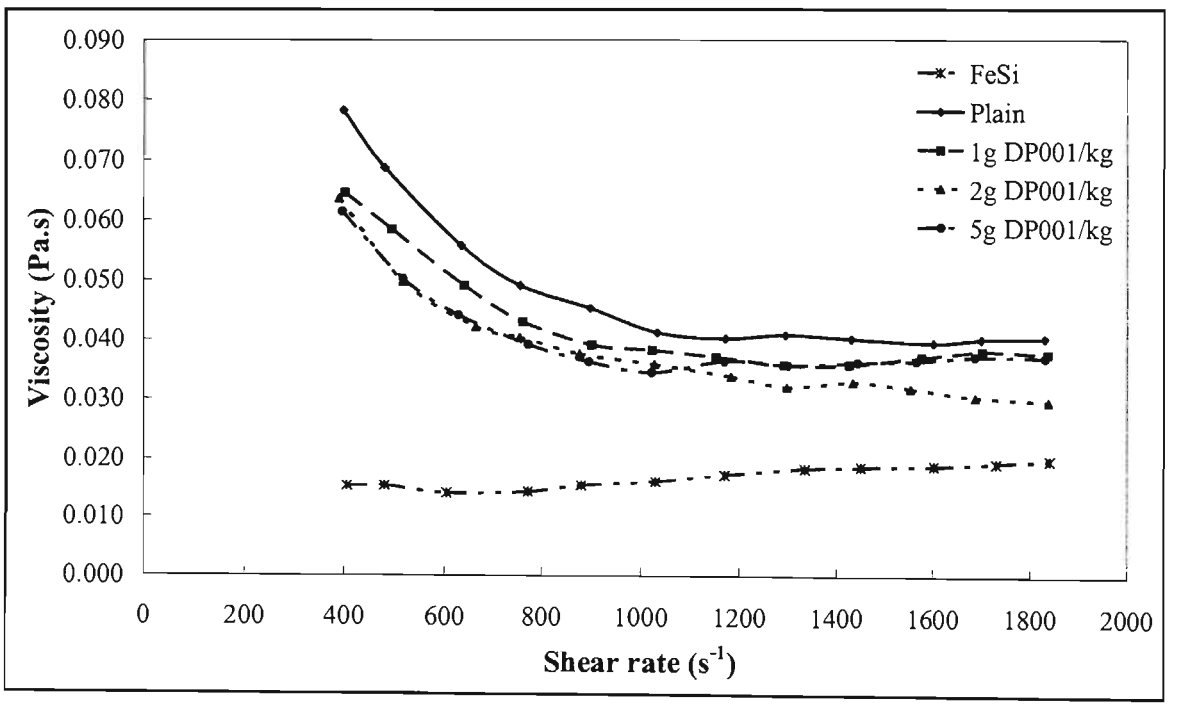

Figure 6.74 Effect of DP001 on ferrosilicon-magnetite #1 mixtures (1:2) at sp.gr.2.7

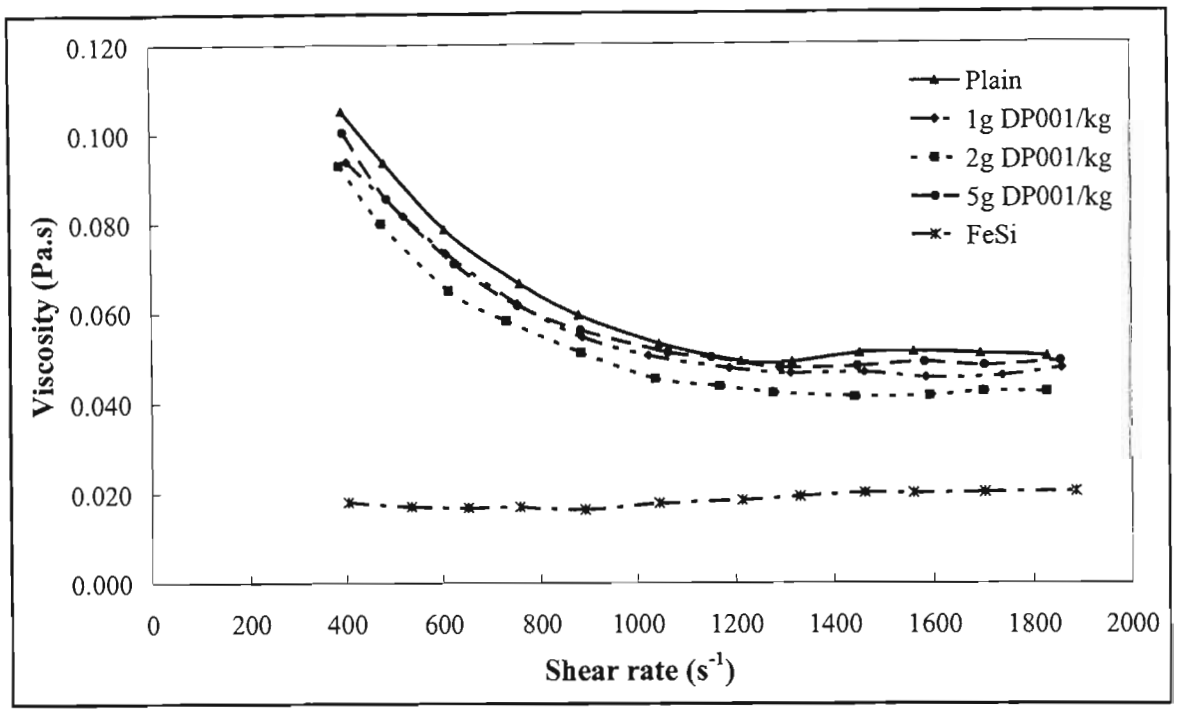

Figure 6.75 Effect of DP001 on ferrosilicon-magnetite #1 mixtures (1:2) at sp.gr.2.8

Table 6.9 summarises the average percentage viscosity reduction obtained from the above experiments.

Table 6.9 Viscosity reduction on Ferrosilicon/Magnetite #1 (1:2) mixtures

Specific Gravity	% Viscosity Reduction		
	1g DP001/kg	2g DP001/kg	5g DP001/kg
2.2	17.2	17.8	3.0
2.3	13.5	12.3	3.5
2.4	13.2	19.5	9.6
2.5	9.8	20.8	2.8
2.6	17.0	17.3	13.8
2.7	11.3	20.6	16.4
2.8	8.2	14.7	5.3

The results observed for these experiments also show a decrease in suspension viscosity due to DP001 additions. Most of the suspensions show an initial decrease in suspension viscosity upon the addition of 1gram DP001/kilogram. There appears to be little effect upon the addition of a further 1g DP001/kg. The viscosity begins to increase at additions of 5grams DP001 / kilogram. For specific gravities 2.2 to 2.4 DP001 reduces the difference in viscosity between the ferrosilicon-magnetite suspensions and pure ferrosilicon suspensions, at the same specific gravity, by as much as 50%. For specific gravities 2.5 to 2.8 the reduction is about 25%. At low shear rates the viscosities of the suspensions with DP001 are lower than those of the pure suspensions. This implies that there is a reduction in the yield stress due to the effect of DP001.

All the above results show that DP001 does have an effect on the viscosity of ferrosilicon-magnetite suspensions at all ratios. The effect of DP001 appears to increase with an increase in the ratio of magnetite in the suspensions, particularly at high specific gravities Ferrosilicon-magnetite suspensions at a ratio of 1:2 appear to be most affected by DP001 at high specific gravities.

Johnson et al. (2000) observed that mineral particles brought into contact with an aqueous environment often acquire a substantial charge. This can be caused by ion adsorption, isomorphous ion substitution, differential ion dissolution and ionization of surface sites. These processes are of particular importance to oxide minerals. They did tests on silica-iron oxide slurries, using sodium tripolyphosphate as a chemical dispersant. They found that sodium tripolyphosphate selectively binds to the iron oxide particles, and because the polyphosphate is a multi charged anion, the surface charge of the iron oxide becomes negative and the interaction with silica particles is destroyed. This resulted in a dispersed medium, with a lower viscosity.

Since magnetite is an iron oxide, it should be more susceptible to DP001 than ferrosilicon media. As mentioned earlier, DP001 is a medium chain anionic calcium lignosulphonate. Since it is a calcium salt, it means that it is soluble in water. Therefore, interaction between DP001 and magnetite can occur through the adsorption of anionic portion onto the surface of the magnetite particles. This would result in charged particles that would repel each other when in close proximity. This repulsion results in the dispersion of the particles, hence, a much lower viscosity.

However, there is a limit of particle adsorption, beyond which the onset of particle agglomeration could occur. Particle agglomeration results in rigid suspensions, which have a much higher

viscosity than dispersed particles. Particle agglomeration increases the viscosity of the suspensions by retaining a portion of the continuous phase, in this case water. This results in an increase in the apparent solids volume fraction. This could explain why there is a sudden increase in the viscosity for most of the suspensions at additions of 5 grams DP001 / kilogram.

A similar conclusion can be drawn from the effect of DP001 on suspensions of DP001 contaminated with the slime. Clay and colloidal particles have small surface charges which can interact with the DP001 anions. As mentioned earlier, clay particles also reduce the viscosity of suspension by absorbing water, resulting in higher apparent solid volume fractions. The presence of DP001 can neutralise these charges such that their affinity for water is reduced, resulting in much lower viscosities. A similar case can be drawn for colloidal particles, where the presence of DP001 could be to neutralise the particle surface charge.

6.3 Experiment Series B: The effect of media particle size and shape on the viscosity of heavy medium suspensions

This section presents the results obtained from experiments using magnetite #1 / magnetite #2 and ferrosilicon / magnetite #2 suspensions. The size distribution of these particles was presented in Section 6.1. Size analysis showed that magnetite #2 is much coarser than the other media particles. Using the SEM, it was also shown that the magnetite #2 particles were spherical in shape, unlike the other media which were rough and angular in shape. The combination of being much coarser and more spherical, it can be expected that magnetite #2 media particles will lower the viscosities of the ferrosilicon and magnetite #1 suspensions.

6.3.1 Aim of the Experiment

To evaluate the effect of media particle size distribution and shape on the viscosity of heavy medium suspension through the use of magnetite #2.

6.3.2 Experimental Methods and Equipment

The experimental methods and equipment used for Experiment Series B are similar to those used for Experiment Series A. Separate tests were carried out on magnetite #1 and ferrosilicon

suspensions. The required mass of each media were measured, mixed, and shaken until a homogeneous suspension was obtained. A portion of this was then poured into the viscometer. Initially, tests were performed on magnetite #2 suspensions only, but these proved to be too unstable, resulting in inconsistent, irreproducible results. It was then decided to combine the magnetite #2 particles, at different ratios, together with the ferrosilicon and magnetite #1 particles, in order to determine the reduction in viscosity of the latter suspensions. During the experiments it was observed that there was a reduction in the stability of the suspensions at low specific gravities and low shear rates, particularly for the ferrosilicon-magnetite #2 suspensions.

The results would also be used to determine the type behaviour of these suspensions. The presence of coarser particles could result in a shift in the type of behaviour shown by the pure suspensions. The results could also be compared to those obtained in Experiment series A, to evaluate the better option for viscosity reduction in heavy medium separators.

6.3.3 Experimental Results and Discussion

The viscosity of heavy medium suspensions is highly dependant on the media particle size distribution and media particle shape. For a constant pulp specific gravity the selection of a spherical or coarser medium type will reduce the viscosity and stability of the suspensions [Collins et al. (1983)]. Thus, although the choice of using a more spherical or coarser media type may reduce the viscosity of the suspensions, care needs to be taken to ensure that the stability of the suspensions does not become too low, as this will encourage the settling out of media particles from the suspensions.

The results presented in this section are divided into two small sections. The first section deals with the effect of the introduction of magnetite #2 media particles on the viscosity of magnetite #1 suspensions. The second section deals with the effect of magnetite #2 particles on ferrosilicon suspensions.

6.3.3.1 Effect of Magnetite #2 Media Particles on the Viscosity of Magnetite #1 Suspensions

This section presents the results for magnetite #1 / magnetite #2 suspensions at ratios of 1:1, 2:1, and 1:2 (magnetite #1:magnetite #2).

The values for plain magnetite #1 and ferrosilicon suspensions at the same specific gravity are also plotted on the graphs. This is done for comparative reasons, such that the deviation from each of the plain suspensions can be seen. Figure 6.76 to Figure 6.85 show the results of shear stress versus shear rate for magnetite #1-magnetite #2 suspensions for specific gravities 2.0 to 2.9. For specific gravities 2.7-2.9 there was no data available for plain magnetite suspensions. At specific gravities 2.7 and 2.9, no date was available for magnetite #1 / magnetite #2 suspension with a ratio of 2:1. For specific gravity 2.8 only data for a ratio of 1:2 magnetite #1 / magnetite #2 were available. This was due to the high viscosities experienced at these ratios.

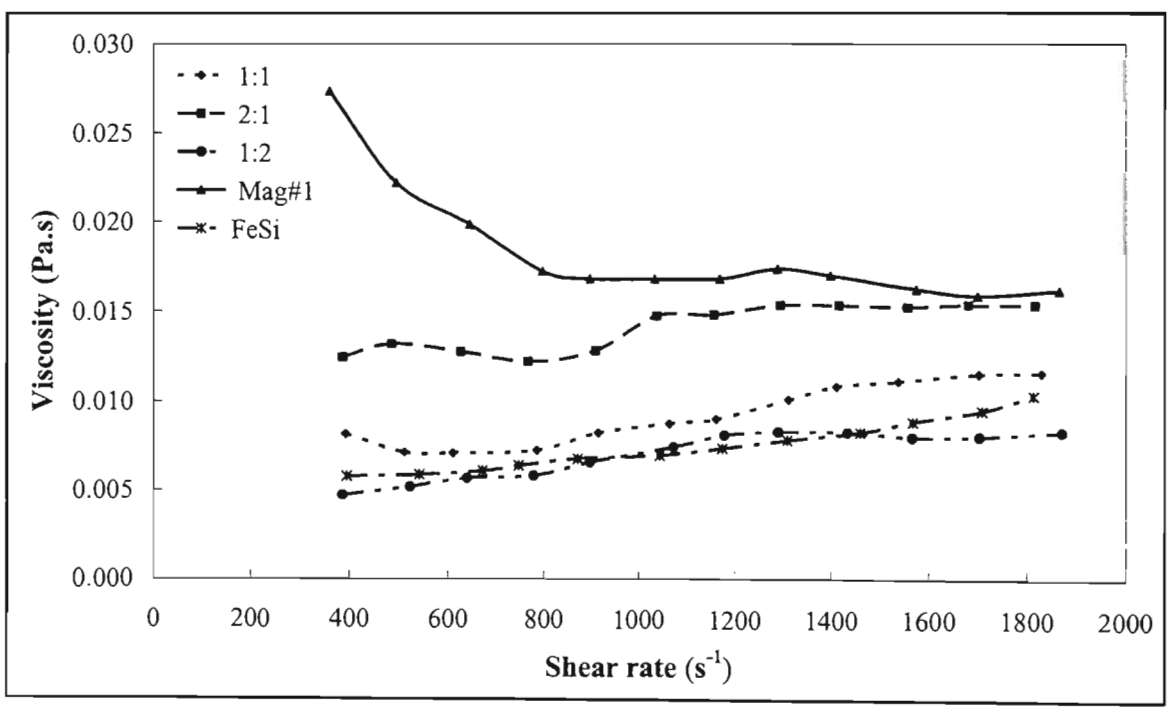

Figure 6.76 Effect of magnetite #2 on magnetite #1 suspensions (sp.gr.2.0)

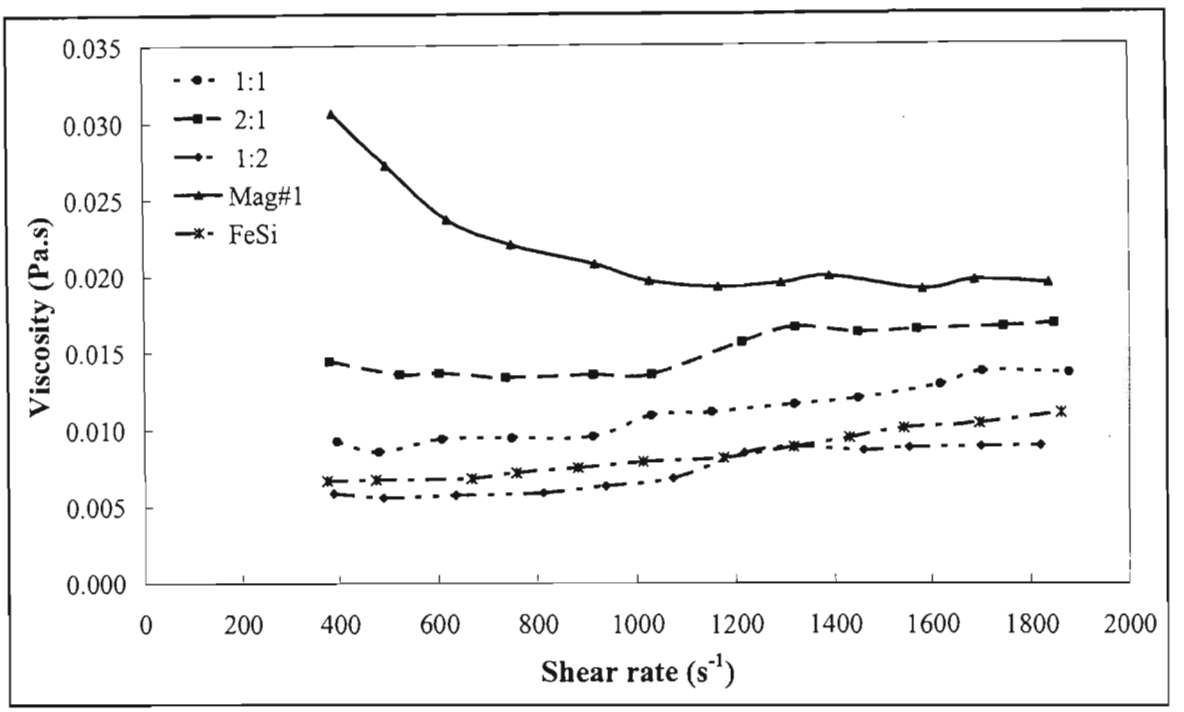

Figure 6.77 Effect of magnetite #2 on magnetite #1 suspensions (sp.gr.2.1)

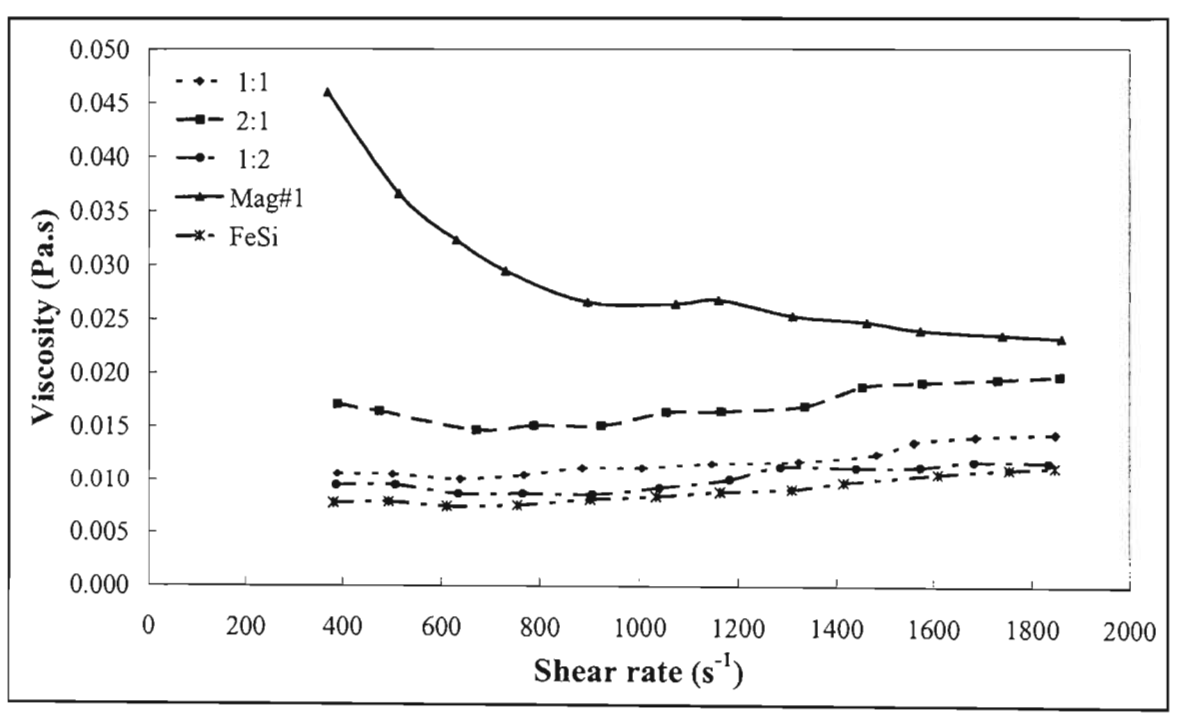

Figure 6.78 Effect of magnetite #2 on magnetite #1 suspensions (sp.gr.2.2)

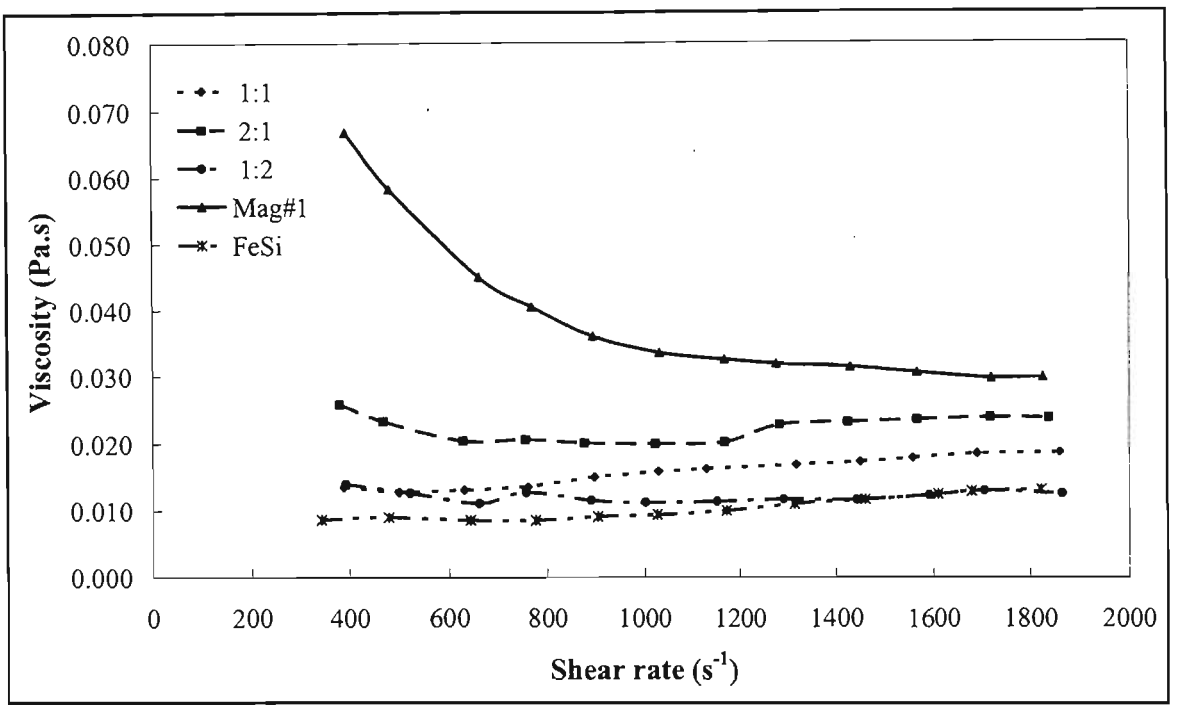

Figure 6.79 Effect of magnetite #2 on magnetite #1 suspensions (sp.gr.2.3)

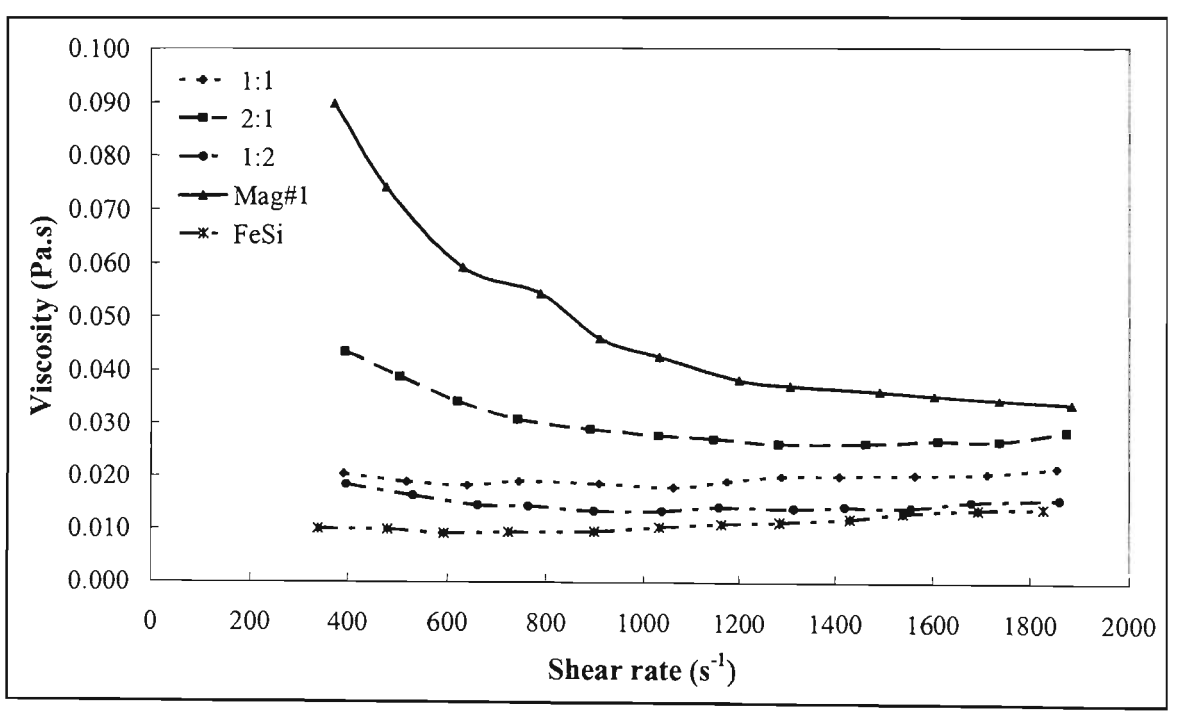

Figure 6.80 Effect of magnetite #2 on magnetite #1 suspensions (sp.gr.2.4)

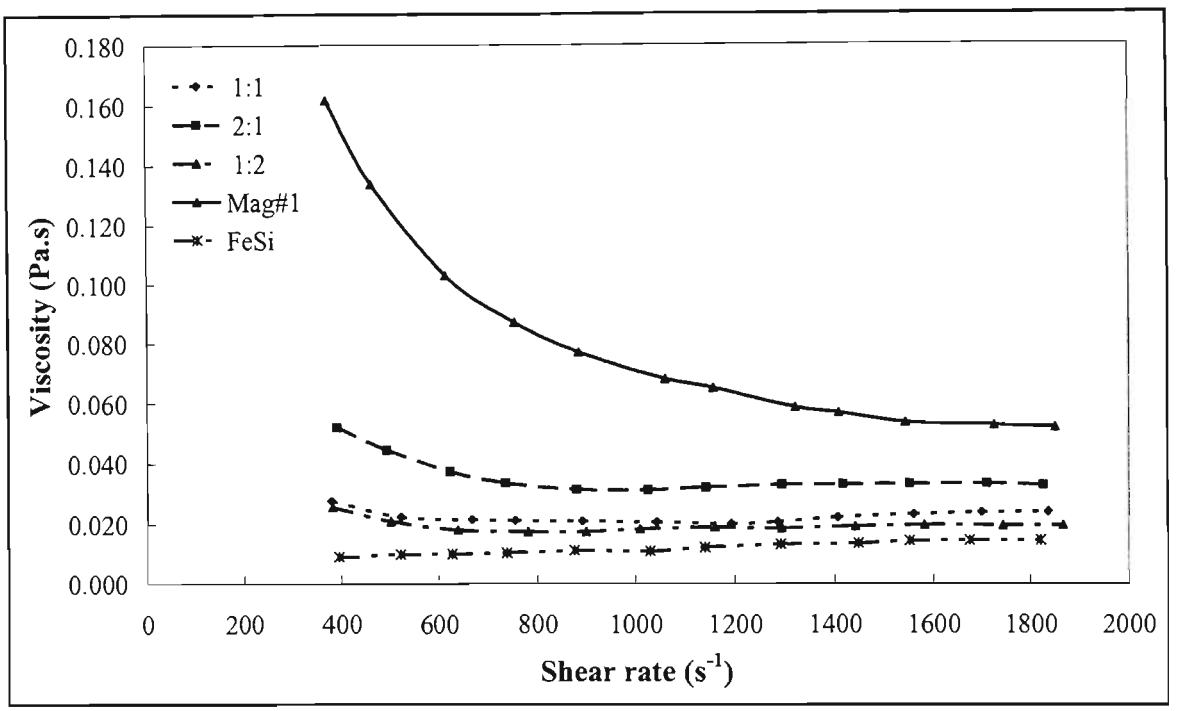

Figure 6.81 Effect of magnetite #2 on magnetite #1 suspensions (sp.gr.2.5)

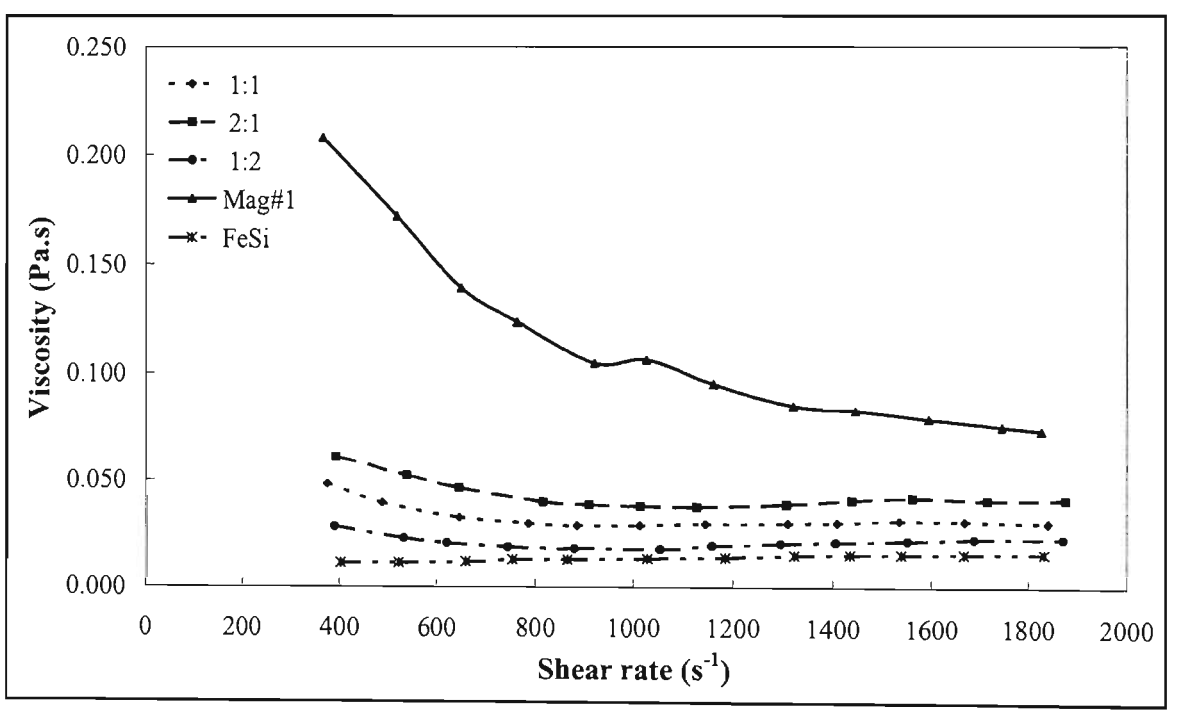

Figure 6.82 Effect of magnetite #2 on magnetite #1 suspensions (sp.gr.2.6)

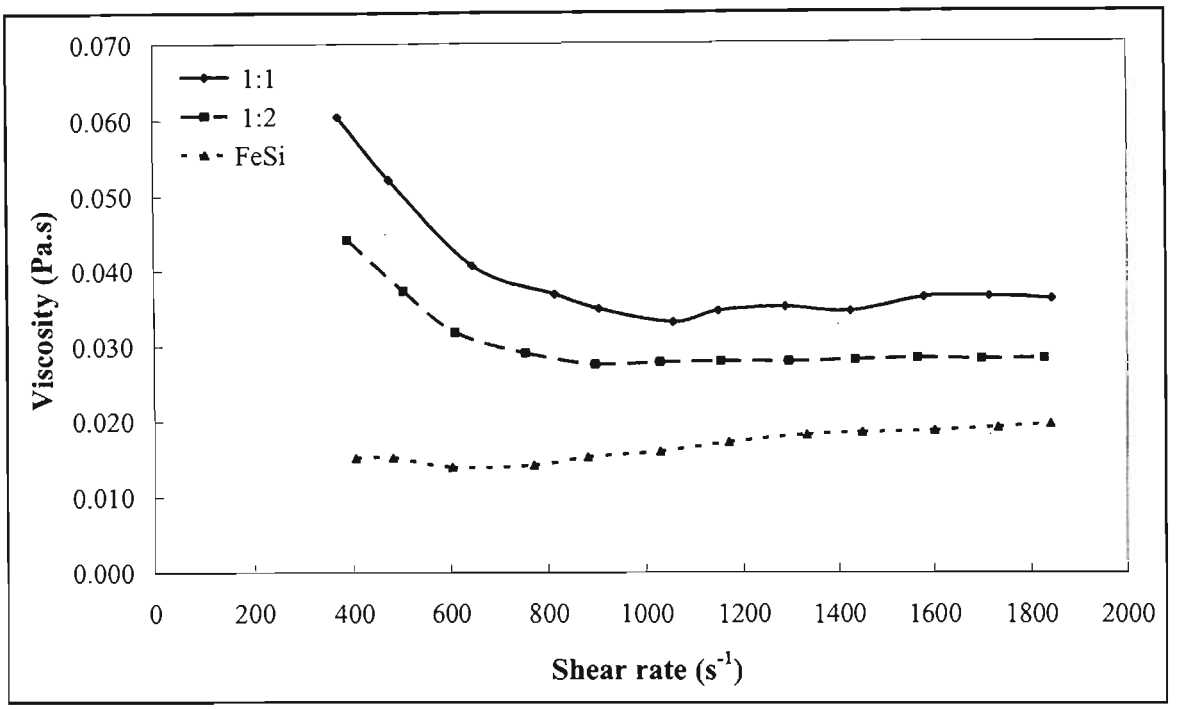

Figure 6.83 Effect of magnetite #2 on magnetite #1 suspensions (sp.gr.2.7)

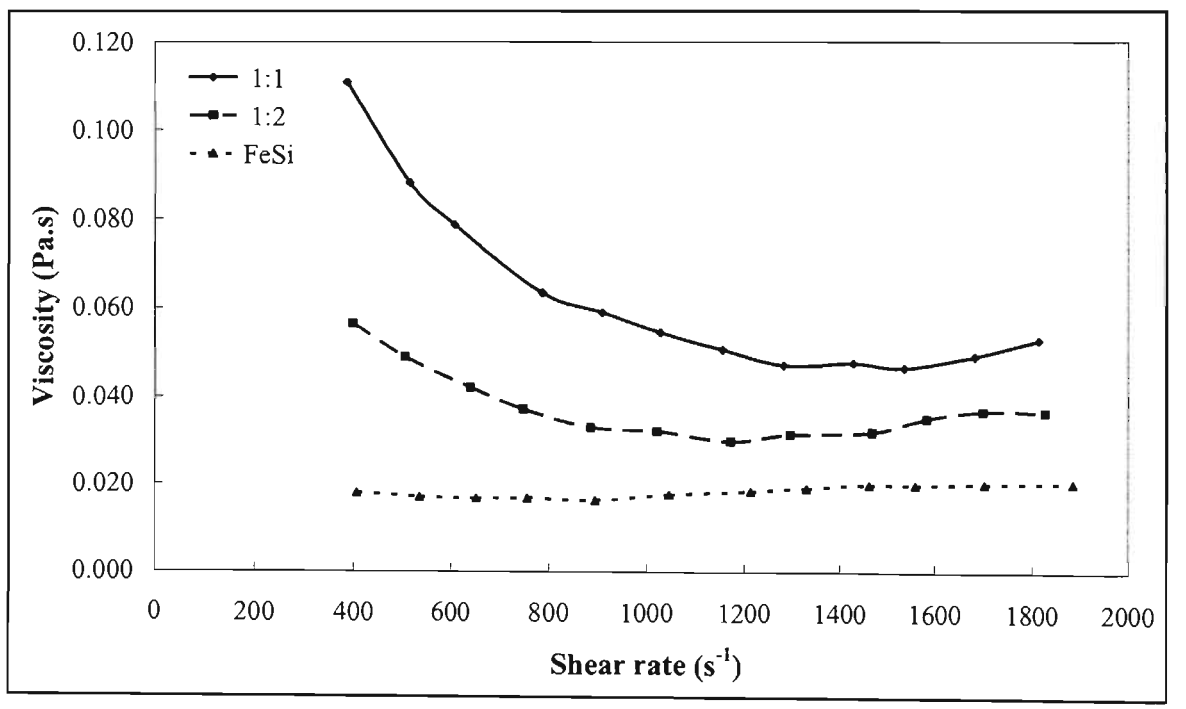

Figure 6.84 Effect of magnetite #2 on magnetite #1 suspensions (sp.gr.2.8)

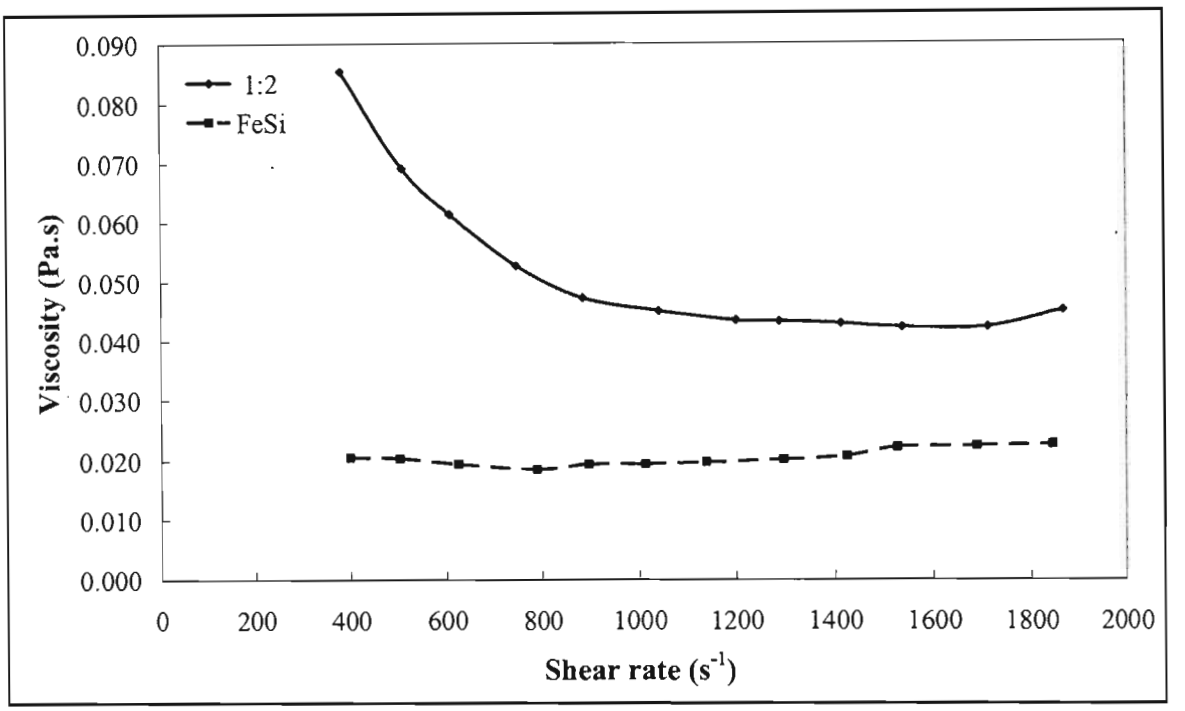

Figure 6.85 Effect of magnetite #2 on magnetite #1 suspensions (sp.gr.2.9)

All the above results show a decrease in the viscosity of the suspensions upon the addition of magnetite #2 media particles. The decrease in suspensions viscosity increases with the ratio of magnetite #2 particles.

Table 6.10 shows the average viscosity reduction of magnetite #1-magnetite #2 in comparison to plain magnetite #1 suspensions at the same specific gravity.

Table 6.10 Reduction in viscosity of magnetite #1 suspensions due to magnetite # 2 particles at different ratios

Specific Gravity	% Viscosity Reduction at Ratio		
	1:1	2:1	1:2
2.0	49.4	22.7	61.4
2.1	49.3	30.7	65.9
2.2	58.9	40.5	64.9
2.3	59.5	42.6	68.8
2.4	59.6	37.0	69.4
2.5	72.3	55.9	75.9
2.6	73.8	65.2	82.9

The results above show that magnetite #2 reduces the viscosity of the suspensions by a large amount. The decrease in viscosity increases as the ratio of magnetite #2 increases. Suspensions at a ratio of 1:2 show the largest decrease in suspension viscosity. The graphs also show that the rheograms for suspensions at this ratio are very close to the ferrosilicon rheograms. The viscosity reduction at a ratio of 1:1 is more than 50% for almost all specific gravities tested. At a specific gravity of 2.6, the viscosity reduction is close to 75%. Even at the higher magnetite #1 ratio, the viscosity reduction achieved is high. With the exception of the results at specific gravity 2.4, all the results show an increase in the viscosity reduction with specific gravity.

The graphs show that the difference in viscosity of suspensions with a ratio of 1:2 and ferrosilicon suspensions increases with specific gravity. Measurements at lower specific gravities, and lower shear rates, were more difficult because of the much higher settling rates under these conditions. At high specific gravities, and high magnetite #1 ratio, the viscosities of the suspensions became high, making measurements at these values extremely difficult.

In Section 6.1 it was shown that the density of magnetite #1 and magnetite #2 are identical. This means that the results plotted for the plain magnetite #1 and the magnetite #1-magnetite #2 suspensions at the same specific gravity are also at the same solids volume percentage. This shows that the viscosity reduction achieved is essentially due to both particle size and shape. The large particle size of magnetite #2 particles reduces the viscosity by reducing the surface area of

the particles in contact with the continuous phase. This segregates the suspensions into zones, or pockets, of particles with higher surface area (due to the finer magnetite #1 media particles). These zones are separated from one another by the coarser magnetite #2 particles. The interaction between theses zones decreases as the content of the larger particles is increased. This results in lower viscosities than would otherwise be experienced if the zones were not segregated.

The particle shape reduces the viscosity of the suspensions by increasing the particle slippage. Inter-particle interactions are minimised through the use of smoother particles, since the surfaces of the particles do not lock onto each other. In suspensions with rough-angular shaped particles, each particle does not rotate or move independently to those close to it. Instead, what happens is that if it moves it locks onto the particle next to it (analogous to mechanical gears), which in turn locks onto another, and so on. It becomes difficult for an ore being separated to penetrate such a network. For smooth particles there is a breakdown in this network. The movement of each particle becomes less dependent on those close to it. The particles are able to slip over one another, resulting in much lower viscosities, and making it easier for ore particles to penetrate the medium.

6.3.3.2 Effect of Magnetite #2 Media Particles on the Viscosity of ferrosilicon Suspensions

This section presents the results from measurements made with ferrosilicon-magnetite #2 suspensions. Rheological measurements on these suspensions were made very difficult by the high settling rates of the suspensions. Ferrosilicon particles, because of their high particle density, are very unstable. Addition of a coarser media to these suspensions further increases the instability of the suspensions. At specific gravities below 2.8, no meaningful results were possible. The results only began to make little sense from specific gravities 2.8 to 3.2. Even at these specific gravities, some of the results were not easily reproducible. Difficulties in measurement were largely experienced at low shear rates. Figure 6.86 to Figure 6.90 show the shear stress versus shear rate for these suspensions at specific gravities 2.8 to 3.2.

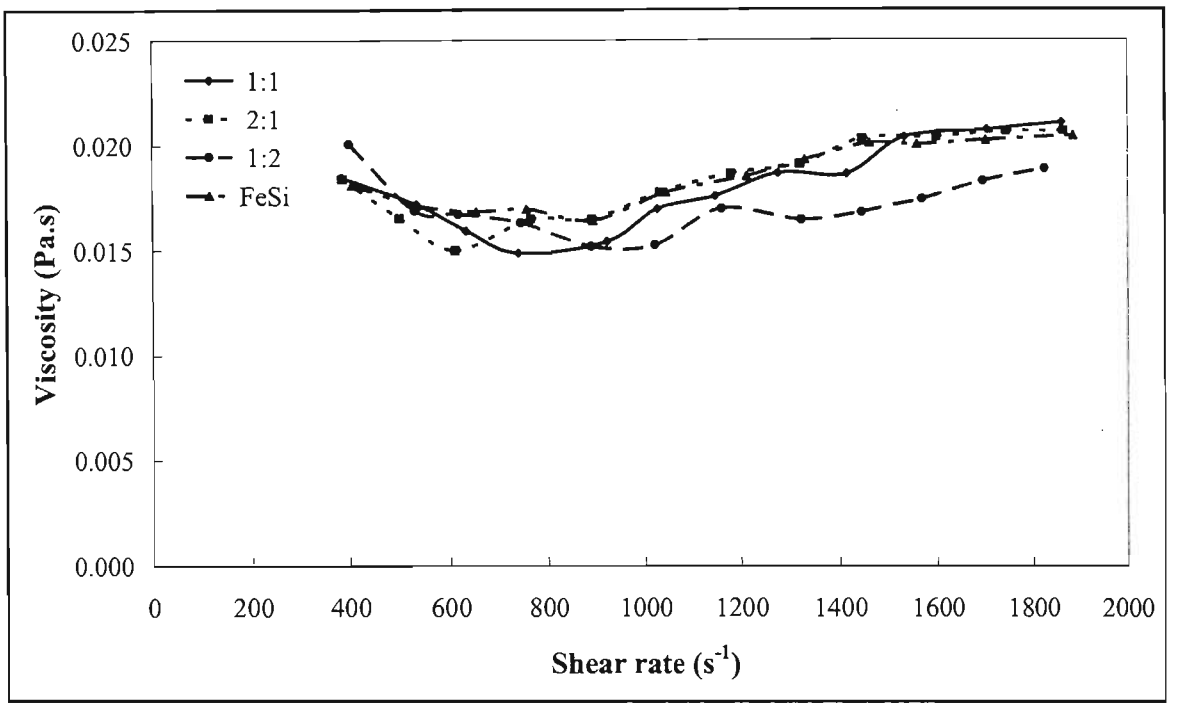

Figure 6.86 Effect of magnetite #2 on ferrosilicon suspensions (sp.gr.2.8)

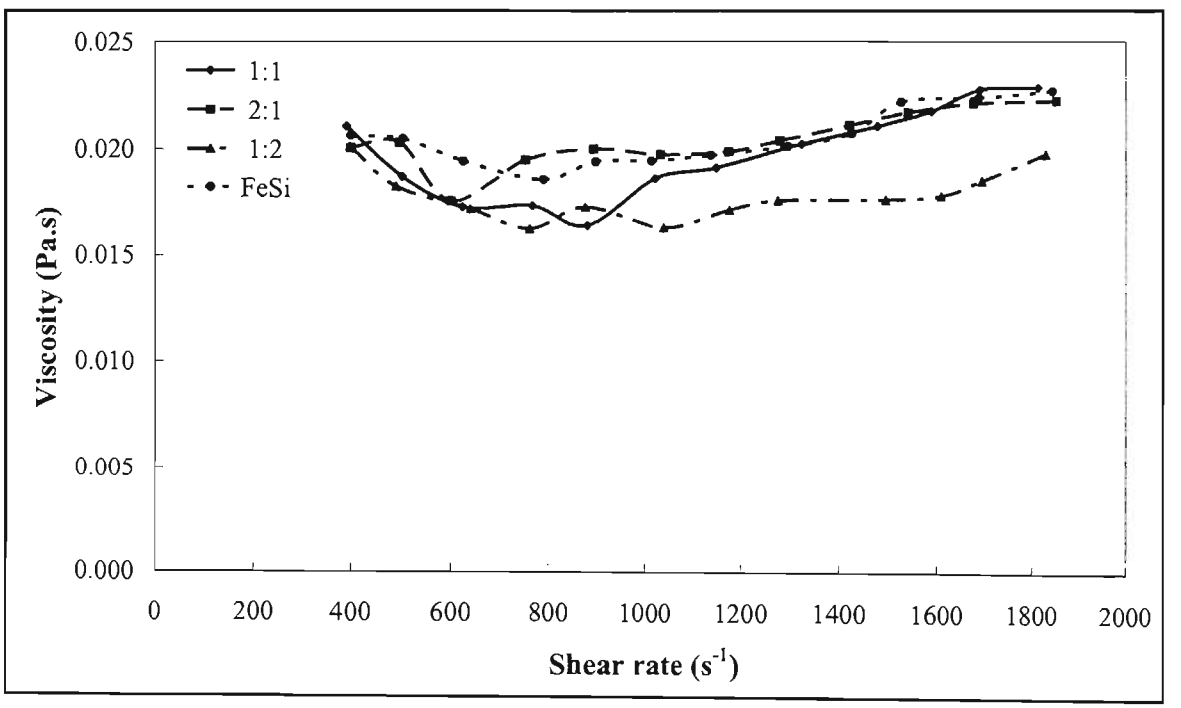

Figure 6.87 Effect of magnetite #2 on ferrosilicon suspensions (sp.gr.2.9)

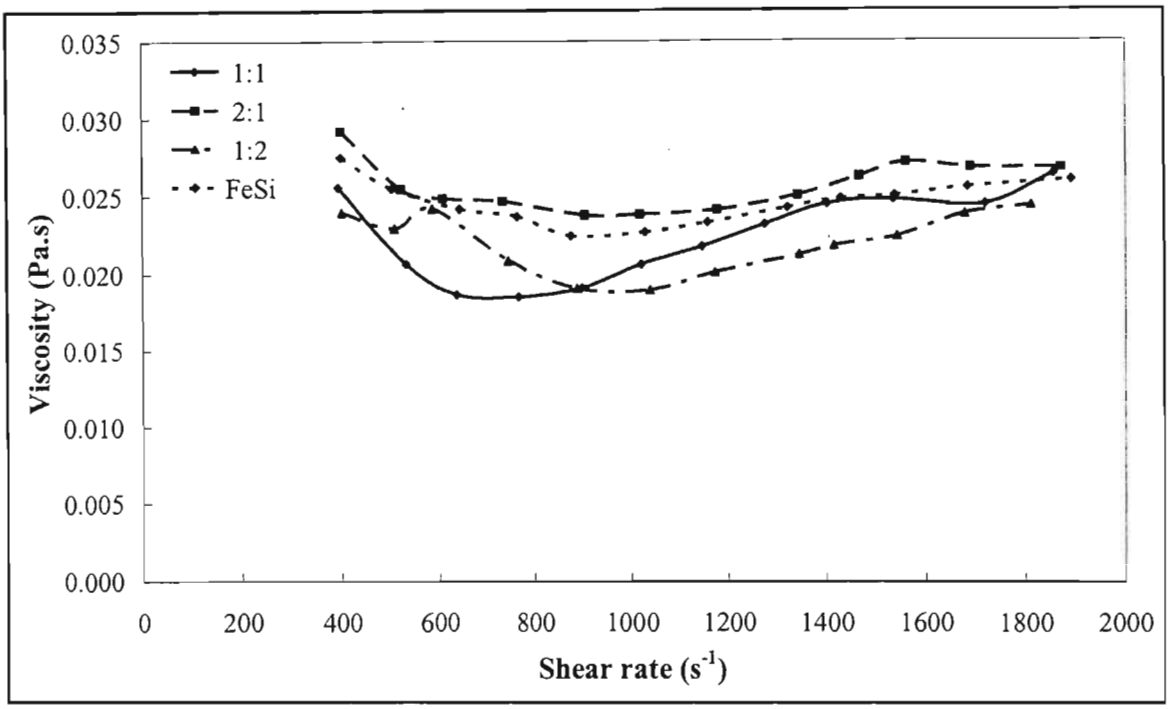

Figure 6.88 Effect of magnetite #2 on ferrosilicon suspensions (sp.gr.3.0)

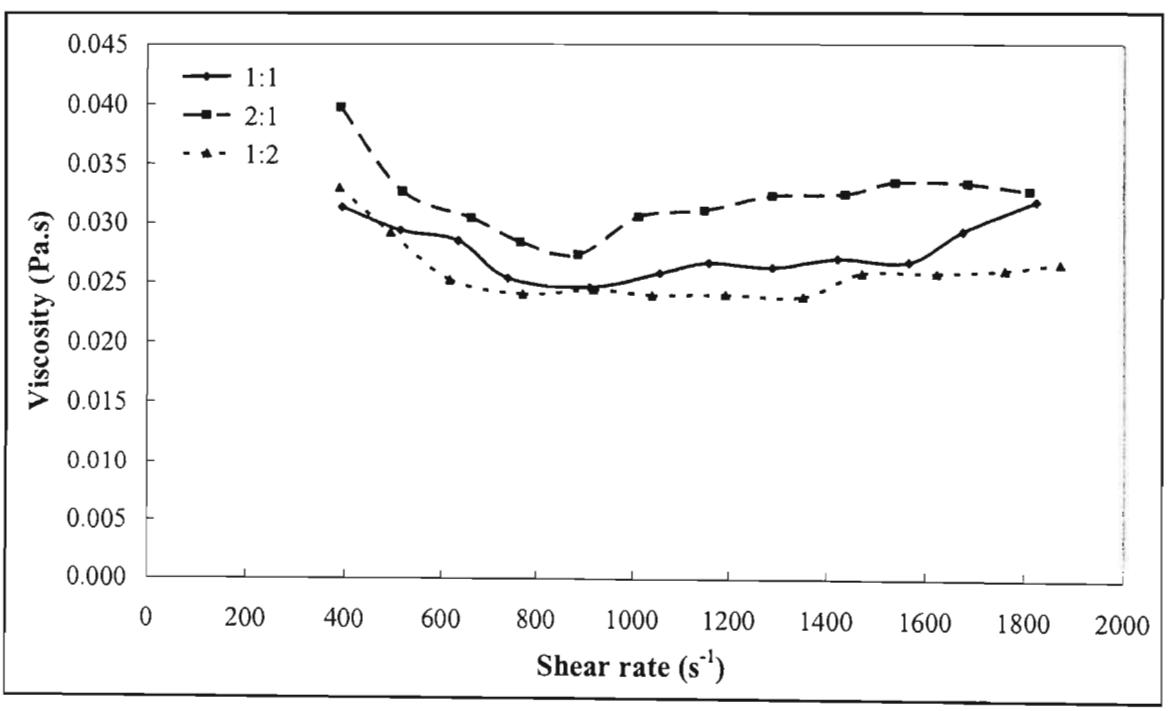

Figure 6.89 Effect of magnetite #2 on ferrosilicon suspensions (sp.gr.3.1)

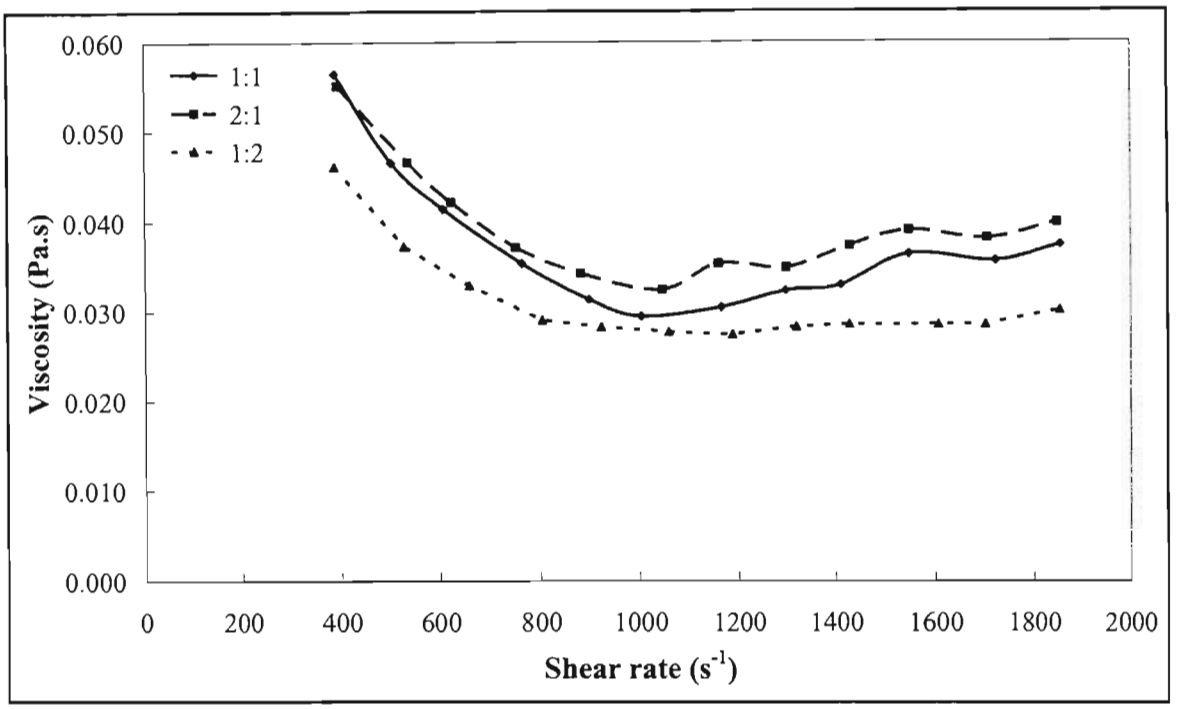

Figure 6.90 Effect of magnetite #2 on ferrosilicon suspensions (sp.gr.3.2)

When evaluating the effect of media particle size distribution and particle shape on the rheology of heavy medium suspensions, it is common practise to compare particles of the same form i.e. particles with similar densities. The reason for this is that proper comparison can only be made at the same solid volume concentration. In this work this principle was followed for the magnetite #1-magnetite #2 suspensions. For the ferrosilicon-magnetite #2 suspensions, the density of ferrosilicon is much greater than that of magnetite #2. Hence, the comparison between plain ferrosilicon and ferrosilicon-magnetite #2 suspensions is done at different solid volume concentrations. However, these results are useful in their own right.

From the results it can be seen that there is little difference in the viscosity of ferrosilicon-magnetite #2 at ratios 1:1 and 2:1, with plain ferrosilicon suspensions at specific gravities 2.8 to 3.0. The reason for this is that there are two opposing forces acting on the suspensions, which both influence the viscosity of the suspensions. The lower density of the magnetite should result in higher viscosity, since this would result in a higher solids volume concentration compared to plain ferrosilicon suspensions. At very same time, the particle size and shape of the magnetite #2 particles have the effect of reducing the viscosity of the suspensions. Depending on which factors outweigh the other, the viscosity of the suspensions will either be lower, higher, or equal to those

of plain ferrosilicon. For specific gravities 2.8 to 3.0, suspensions at ratios 1:1 and 2:1, these factors appear to have balanced themselves out. Only at ratios of 1:2 do we begin to see the effect of particle size and shape outweighing the density differential factor. Hence, lower viscosities are experienced at these ratios.

Because of the dilatant nature of ferrosilicon suspensions, rheology measurements over the entire range of shear rates used in this project (0-2000 s^{-1}) were difficult and erratic at specific gravites above 3.0. Hence, no plain ferrosilicon data was available at specific gravities 3.1 and 3.2. The suspensions were compared according to the ratio of magnetite #2 present. Both graphs show that the viscosity is lower at higher ratios of magnetite #2. This also illustrates the much greater effect of particle size and shape, compared to the much lower density of the magnetite particles.

The results in this section show that the viscosity reduction of ferrosilicon suspensions at high specific gravities is possible through the use of coarser-smoother particles with a density lower than that of ferrosilicon. The behaviour of the suspensions was found to be pseudo-Newtonian at all specific gravities and ratios tested. However, the stability of the suspensions has to be taken into consideration when drawing conclusions from this work. The suspensions were very unstable at all the specific gravities and ratios tested. This instability can have adverse effects on the separation efficiency in industrial processes.

6.4 Experiment Series C: The effect of DP001 and media particle size and shape on the separation efficiency in a dense medium cyclone

6.4.1 Aim of Experiment

The aim of these experiments was to measure the effect of DP001 and media particle size and shape on the efficiency of a heavy medium cyclone separating coal at different size ranges.

6.4.2 Experimental Method and Equipment

The dense medium cyclone used in these experiments was described in Chapter 5. Separation tests were conducted on a pilot scale dense medium cyclone loop similar to that of He et al. (1994). The diameter of the cyclone was 150 mm, and it was operated at a cone angle of 20°.The cyclone was gravity fed at a pressure head of 1.5 m.

Coal samples in the following size ranges were separated: -4 mm + 1mm; -1 mm + 500 μm; and -4 mm + 500 μm. The coal samples were introduced in the Headbox and allowed to pass through the system for at least 2 minutes, after which they were collected hand-held screens of appropriate sizes under the overflow and underflow. Prior to the addition of the coal samples, the feed rates of the overflow and underflow were measured. The density of the feed, overflow and underflow were also determined.

Two sets of experiments were carried out during these experiments. In both sets of experiments, magnetite #1 was used as the separating medium. The first set of experiments was to investigate the effect of DP001 in the separation efficiency of the cyclone. DP001 was added at 1 gram / kilogram solids, and 5 grams / kilogram solids. The second set of experiments was to investigate the effect of particle size and shape, through the addition of magnetite #2 to magnetite #1 suspensions, on the separation efficiency of the cyclone. The mass fraction of magnetite #2 in the suspensions was 0.12. DP001 was also added in these experiments to investigate whether it the combination of magnetite #2 and DP001 improved the separation efficiency. For the first set of experiments, separations were carried out at specific gravities 1.57 and 1.83. For the second set the separation was carried out at a specific gravity of 1.70. The operating densities were decided

from an ash analysis on the coal samples. The experimental procedures for these experiments are contained in Appendix A2.

After each of the coal samples had been introduced into the system, they were collected from the hand-held screens, washed, and then dried in oven at 30 °C. After being dried, sink-float analysis was carried out in order to determine the amount of misplaced material. These results were used to calculate the separation efficiency of the cyclone at the different operating conditions.

6.4.3 Experimental Results and Discussion

Magnetite media are the most commonly used media in the separation of coal by heavy medium separations. Because of this, and their ease of availability, magnetite #1 was chosen as the media to use in these experiments. What was left was to determine the suspension density to use. The operating density is dependant on the coal being separated. For coals with a large proportion of impurities, the separation must be performed at lower densities, to produce an acceptable coal quality. Ash analysis is the most common method used to determine the operating density range. By using the combined product and ash product, described in Appendix A2, the following results were obtained:

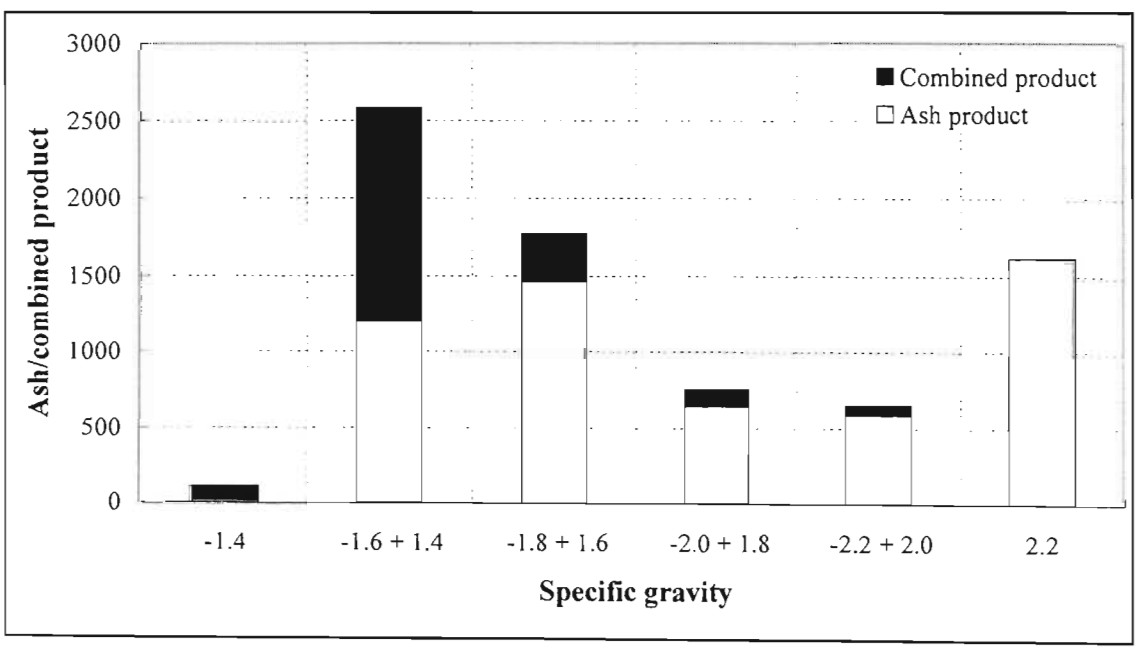

Figure 6.91 Ash-analysis of -4mm + 1mm coal sample

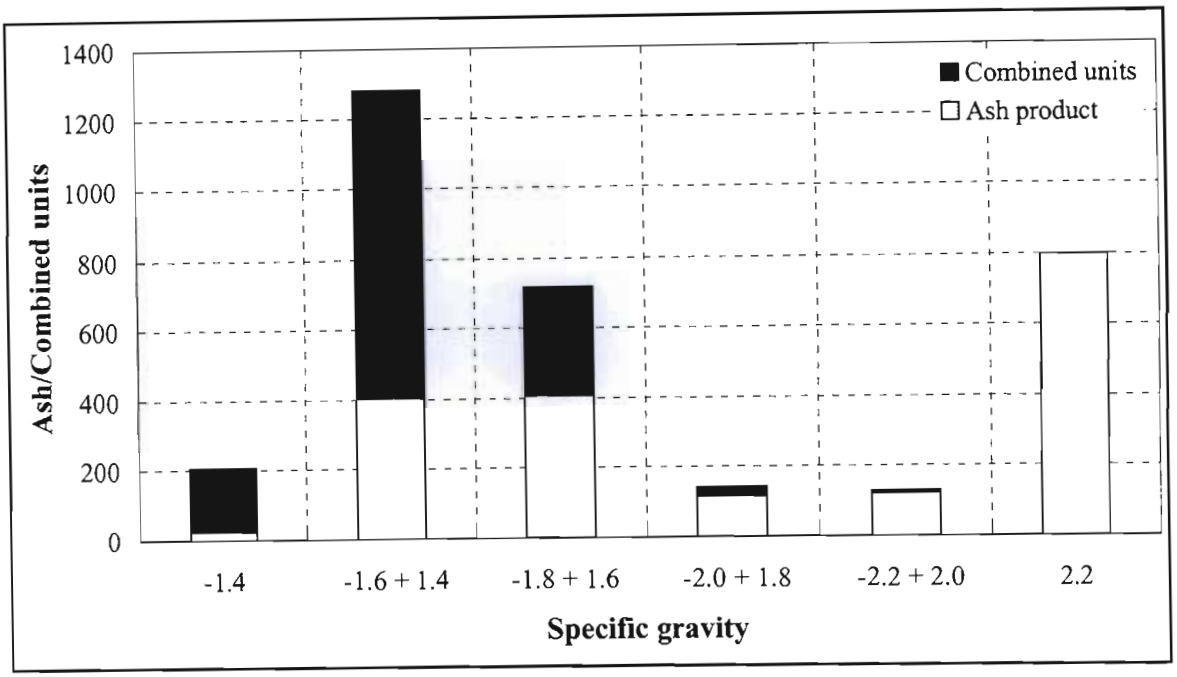

Figure 6.92 Ash-analysis of -1mm + 500 µm coal sample

The graphs above show that at an operating density less than 2.0 will result in a clean product with lowered ash content. The densities used for the experiment sets were given above.

6.4.3.1 Experiment Set 1: Effect of DP001 on Separation Efficiency

This section discusses the results of the separation efficiency of magnetite #1 suspensions using DP001, at specific gravities 1.57 and 1.83. At each coal size range, the separation efficiency was evaluated for plain, 1 gram DP001 / kilogram solids, and 5 grams / kilogram suspensions.

For coal size range sink-float analysis was carried out in order to be able to construct partition curves for each sample. The separation efficiency was calculated from the partition curves using the equations described in Chapter 4. The partition curves for these separations are given in Appendix A1. The results from these separations are given below. The Ecart probable (Ep) is plotted against percentage DP001 for each of the coal samples. The percentage DP001 is the mass DP001 in grams per kilogram media used, expressed as a percentage (i.e. DP001 (g) / kg solids x 100). For example, 0.1 % DP001 is equivalent to 1 g DP001 / kg solids.

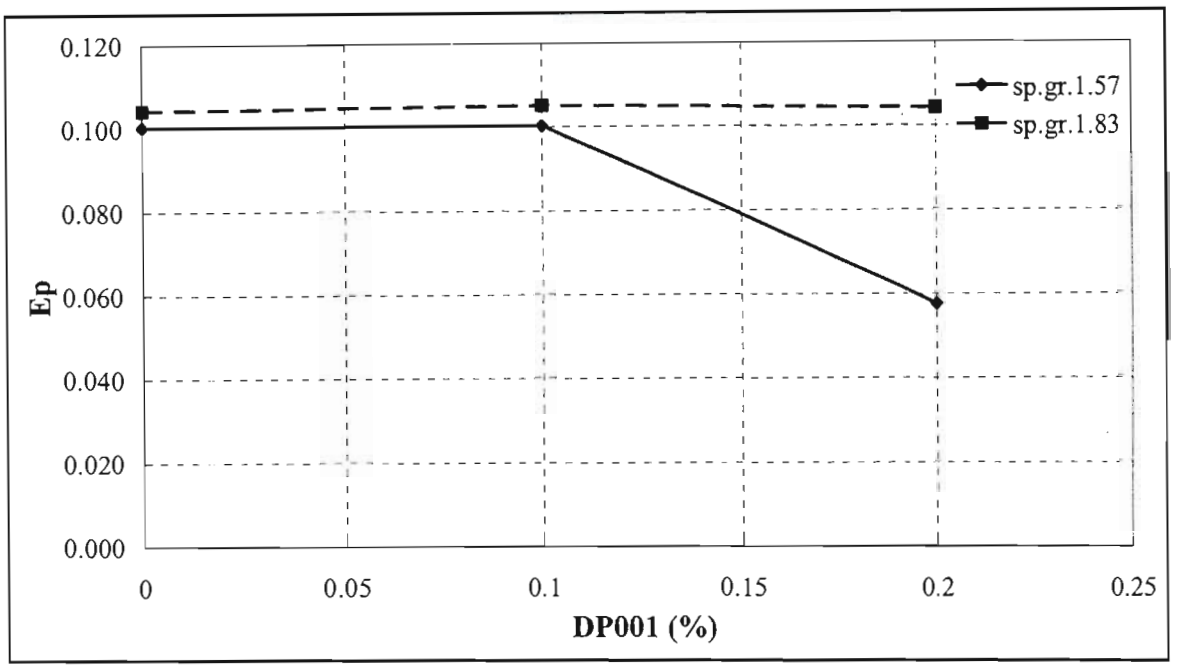

Figure 6.93 Ep versus % DP001 for -4 mm + 1 mm coal samples

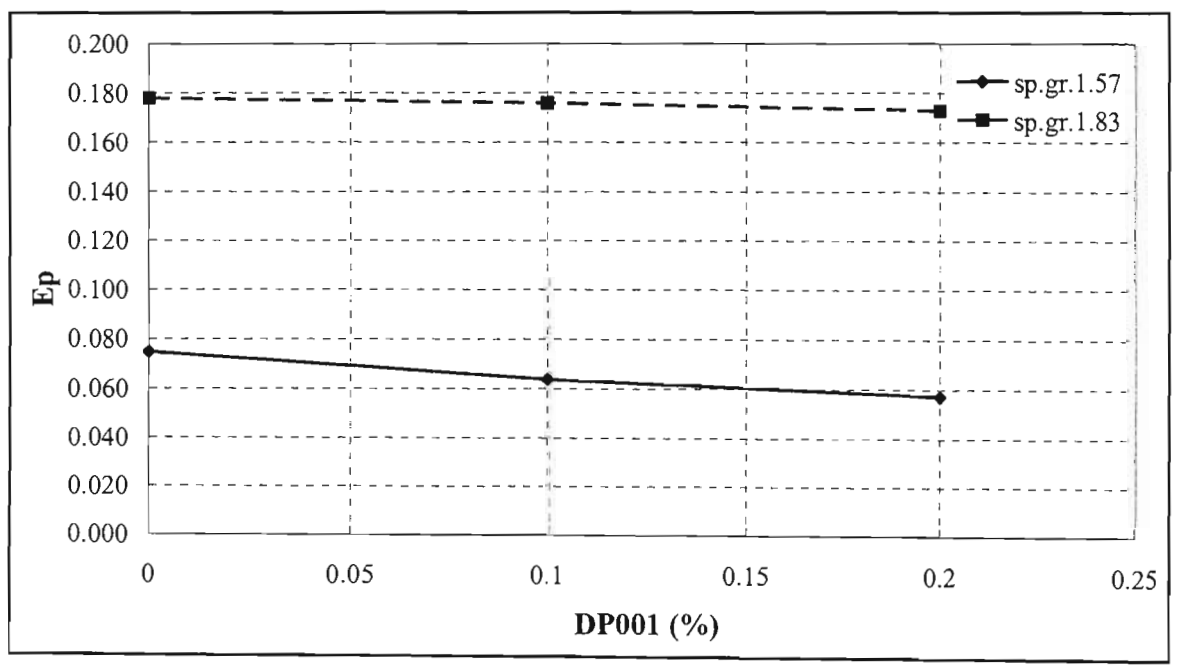

Figure 6.94 Ep versus % DP001 for -1 mm + 500 µm coal samples

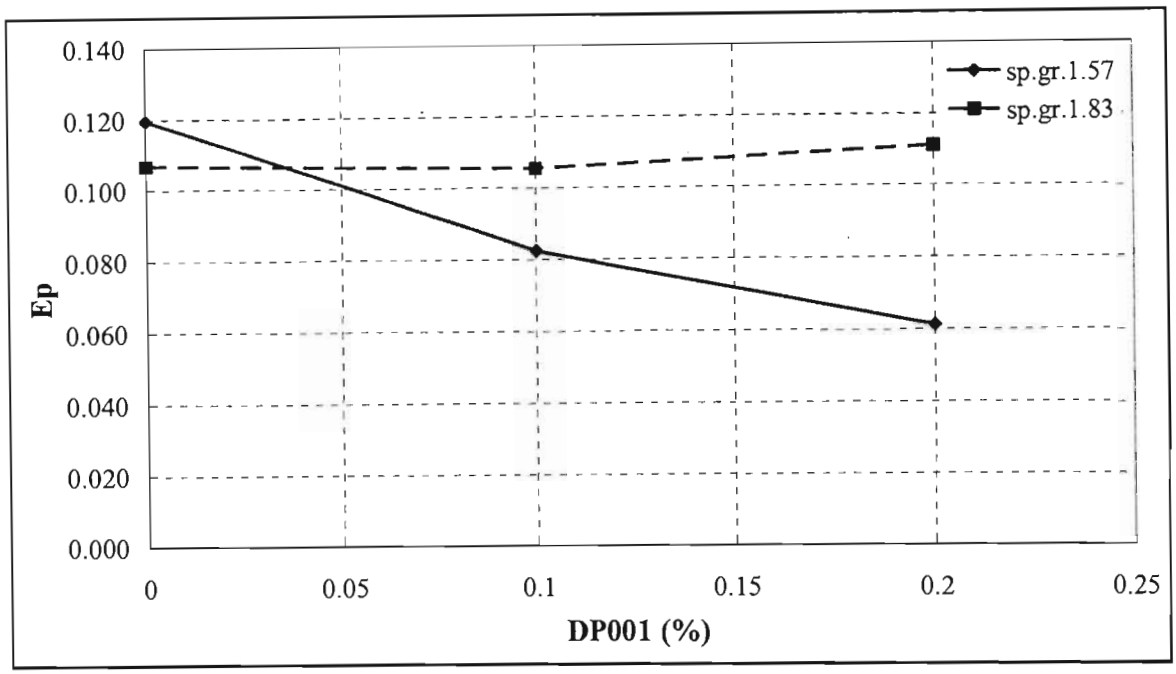

Figure 6.95 Ep versus % DP001 for -4 mm + 500 μm coal samples

The separation efficiency of heavy medium suspensions is dependant upon a lot of variables. These may include the type of separating, the ore being separated, or the properties of the separating medium. In this section both the properties of the separating medium and the size range of the coal particles are what define the separation efficiency. Napier-Munn (1990) showed that the viscosity of heavy medium suspensions resulted in less efficient separations. He also showed that ore particle size affected the separation efficiency.

In heavy medium suspensions a high Ep value translates to a less efficient separation, whilst a low Ep value translates to good separation efficiency. It ca be seen from Figure 6.93 that the separation efficiency at specific gravity 1.83 is lower than that at 1.57. An increase in suspension specific gravity results in an increase in the suspensions viscosity, and Napier-Munn (1990) stated that higher viscosities usually result in lower separation efficiencies. The graph shows that the separation efficiency at specific gravity 1.57 is not affected at 0.1 % DP001, but improves by 42 % at 0.2 % DP001. At specific gravity 1.83, there appears to be no effect.

Figure 6.94 shows the results for separation of the -1mm + 500 μm coal samples. The results also show that the separation efficiency at the higher specific gravity is much lower than that at lower specific gravity. The difference between these values is accentuated by the much smaller particle

size range of the coal particles. Smaller particles are more affected by viscosity than larger particles [Napier-Munn (1990)]. At specific gravity 1.57 the efficiency increases by 14 % at 0.1 % DP001 additions, and 24 % at 0.2 % DP001. Again, the efficiency at 1.87 appears to be unaffected by the addition of DP001, with only a slight increase of about 3 % at 0.2 % DP001 additions.

Figure 6.95 shows the separation efficiency for the -4 mm + 500 μm coal samples. The previous separations were carried at narrow size ranges. Industrial separations are usually carried at broad coal size ranges, where particle entrainment of the smaller particles becomes a concern. It is thus important to know how the separation efficiency is affected by DP001 at size ranges analogous to industrial separations. The graph shows that initially, the efficiency at 1.57 is lower than that at 1.83. This could be a result of particle entrainment, with either low density particles reporting to the underflow, or high density particles reporting to the overflow. The graph also shows that the suspensions at 1.57 are affected more by DP001 than those at 1.83. At 1.57 the separation efficiency increases by 31 % at 0.1 % DP001, and 49 % at 0.2 % DP001. At 1.83 there is no considerable change in the separation efficiency with DP001, although there is a slight increase at 0.2 % DP001.

6.4.3.2 Experiment Set 2: The effect of particle size and shape on separation efficiency

This section investigates the effect of adding magnetite #2 on the separation efficiency. As shown in the previous section, magnetite #2 has the effect of decreasing the viscosity of the suspensions. Tests were carried out using magnetite #1- magnetite #2 suspensions, with 12 % magnetite #2. The operating specific gravity was 1.7. For each of the coal size ranges, DP001 was also added to see the combined effect of particle size and shape, together with DP001.

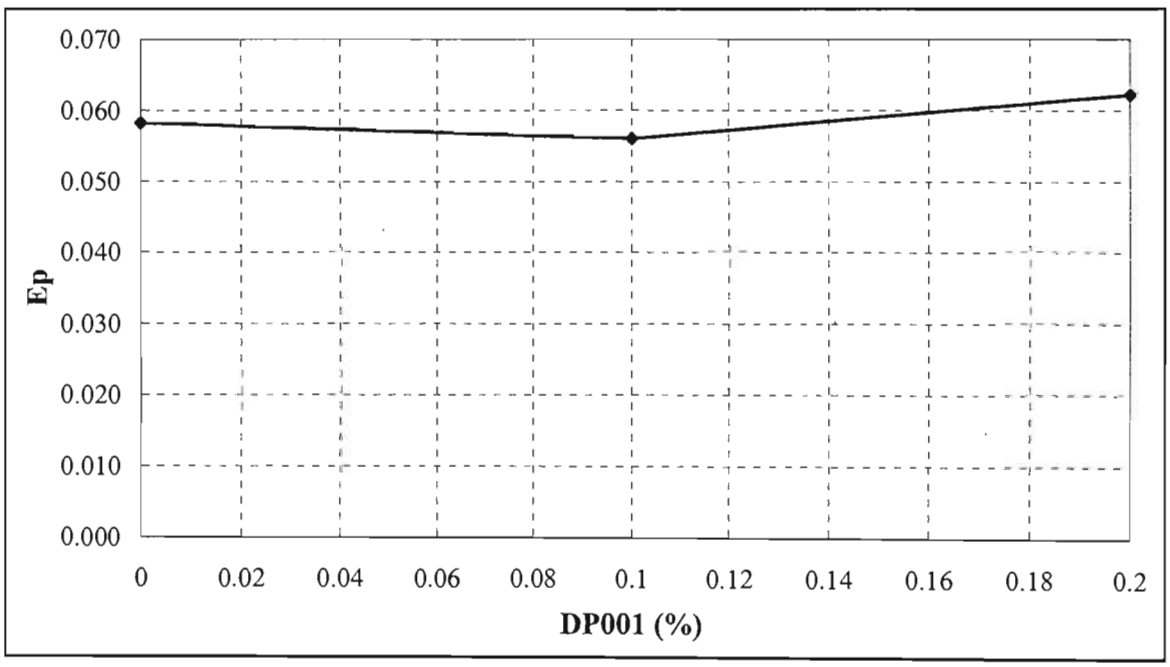

Figure 6.96 Combined effect of magnetite #2 and DP001 on the Ep of -4 mm + 1mm coal samples

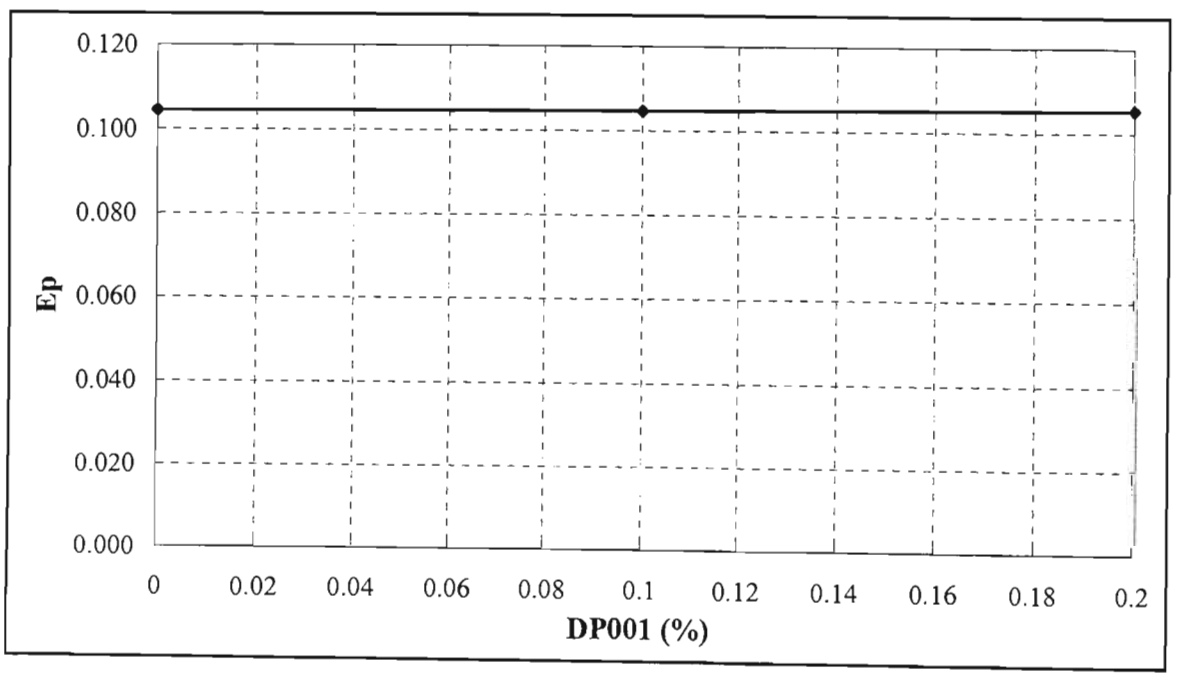

Figure 6.97 Combined effect of magnetite #2 and DP001 on the Ep of -1 mm + 500 µm coal samples

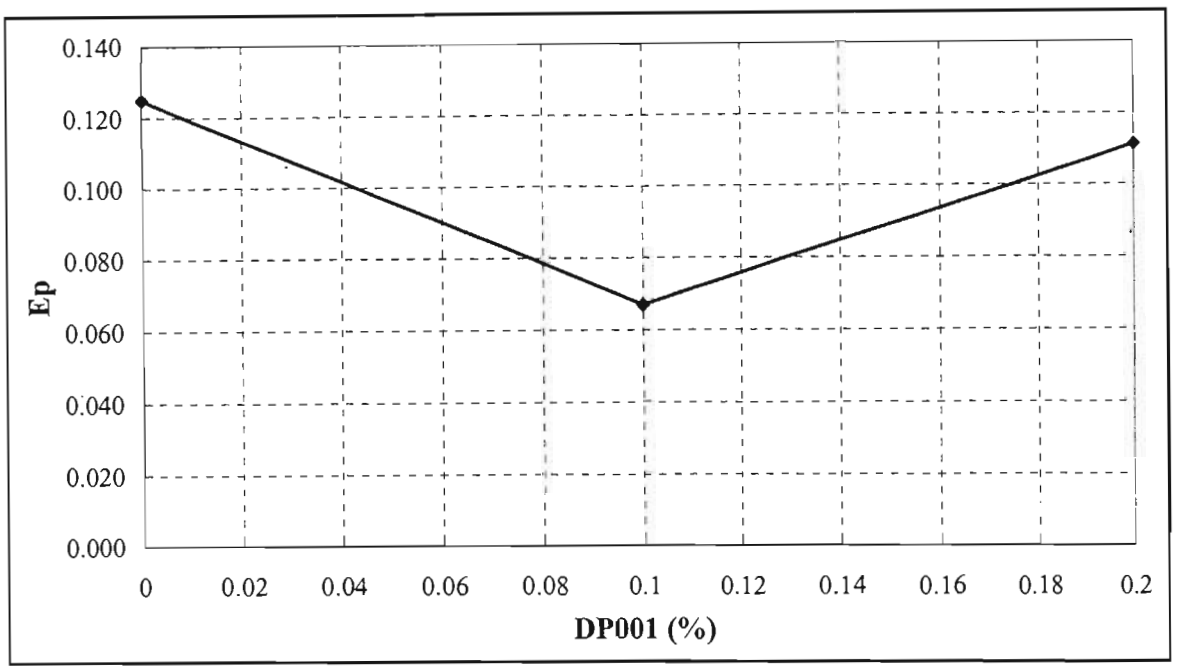

Figure 6.98 Combined effect of magnetite #2 and DP001 on the Ep of -4 mm + 500 μm coal samples

Figure 6.96 shows the results for the -4 mm + 1 mm coal samples. The separation efficiency of the process is generally lower at 0 % DP001 in comparison to that without magnetite #2 at a specific gravity of 1.6 (Table 6.11). This illustrates the fact that magnetite #2 has a viscosity reducing effect on the suspensions, thereby improving the separation efficiency. There appears to be little effect of DP001 at 0.1 %. However, there is an increase in the Ep value at 0.2 % DP001. This reduction in separation efficiency could be due to an increase in the stability of the suspensions. The presence of magnetite #2 results in an unstable suspension. The presence of DP001 could be accentuating this instability. From Figure 6.97 it can be seen that DP001 has no effect on the –1 mm +500 μm coal samples. The separation efficiency is, however, much higher than it would be without magnetite # 2.

Figure 6.98 gives the results for the -4 mm + 500 μm coal samples. It can be seen that the addition of 0.1 % DP001 reduces the Ep value by 65 %. This is probably due to the combined effect of magnetite and DP001 resulting in a better separation of these particles. An addition of a further 0.1 % DP001, however, increases the Ep by 65 %. This illustrates at this concentration the stability of the suspensions is further compromised, although the separation efficiency is still lower than it is at 0 % DP001.

Table 6.11 Comparison of Ep at all densities with no DP001 for the different coal size ranges

Coal Size Range	Ep		
	Mag #1 at sp.gr.1.57	Mag #1 at sp.gr.1.83	Mag #1/Mag#2 at sp.gr.1.70
-4mm +1mm	0.100	0.104	0.058
-1mm +500 μm	0.075	0.178	0.105
-4mm +500 μm	0.120	0.107	0.125

Table 6.11 compares the Ep values at the three coal size ranges for suspensions with no DP001 additions. The usual trend in heavy medium separations is that there should be an increase in the Ep Value, corresponding to an increase in suspension viscosity, with an increase in suspension specific gravity [Napier-Munn (1990)]. This basically means that there is a direct relation between the Ep value and the specific gravity of the suspension. As stated earlier, an increase in specific gravity increases the solids volume fraction, resulting in an increase in suspension viscosity. This, in turn, results in lower separation efficiencies. The results in the table above show that for magnetite #1 only suspensions, the separation efficiency is higher at a specific gravity of 1.6 for –4mm +1mm and -1mm +500 μm coal samples. However, the separation efficiency is higher for the -4mm +500 μm coal sample at specific gravity 1.8. The lower separation efficiency at specific gravity 1.6 is probably due to coal particle entrainment which is common at broader particle size ranges.

The presence of magnetite #2 improves the separation efficiency of the -4mm +1mm coal samples. Although the specific gravity (1.70) is higher than that at 1.57, the Ep value is lower. This is due to the surface shape of magnetite #2 particles, which have the effect of reducing the viscosity of the suspensions at high specific gravities. For the other coal size ranges the efficiency for magnetite #1 suspensions at specific gravity 1.57 is higher than that of magnetite #1 / magnetite #2 suspensions at specific gravity 1.70, irrespective of the reduction in suspensions viscosity caused by surface shape of magnetite #2. This is due to the instability of the suspensions caused by the presence of magnetite #2. This instability has a more pronounced effect on fine particles than on coarse particles [Collins et al. (1983)]. The same is also true for ore particles with a much broader size range. The separation efficiency is higher for the magnetite #1 / magnetite #2 suspensions at specific gravity 1.70 than for magnetite #1 suspensions at specific

gravity 1.8 at all the coal size ranges. This is due both to the lower specific gravity, and the magnetite #2 surface shape.

The above results show that DP001 has the ability of reducing the separation efficiency in heavy medium cyclones. It must be noted, however, that the separation efficiencies reported here are much lower than those encountered in Industry, which are in the region 0.02-0.08 [Wills (1997)]. These much higher values are mostly due to the design of the cyclone used in this project. It must also be noted that although both DP001 and magnetite #2 improve the separation efficiency, their effect on the stability of the suspensions must also be taken into account when evaluating these results.

The difference in underflow and overflow density is usually used as a measure of particle segregation occurring within a cyclone. Collins et al. (1983) reported that the best working range for heavy medium cyclones is with a density differential of 200-500 kgm^{-3}, the optimum being at about 400 kgm^{-3}.These values were 169 kgm^{-3} and 224 kgm^{-3} for the plain magnetite #1 suspensions at specific gravities 1.57 and 1.83, respectively. For the magnetite #1-magnetite #2 suspensions at specific gravity 1.7, this density differential was 251 kgm^{-3}. As can be seen from the results, at a specific gravity of 1.57 the density differential within the cyclone falls outside the specified optimum operating range. Collins et al. (1983) showed that the separation efficiency in heavy medium separations with a density differential in the region of 100 kgm-3 dropped off, and the viscosity effects were more pronounced. Since the specific gravity 1.57 samples fall within this range, they should be more affected by viscosity than samples at the other specific gravities. This is shown by the extent to which they are affected by DP001 compared to the other suspensions. The effect of DP001 on these suspensions is more pronounced compared to the other suspensions.

These authors also showed that for fine particles, the efficiency was higher at higher density differentials, and higher at low differentials for coarser particles. From this one would expect that the efficiency, at specific gravity1.83, for magnetite #1 suspensions to be higher than at the coarser size range than that of the magnetite #1-magnetite #2 suspensions. However, the lower viscosity due to particle size and shape, combined with the presence of DP001, results in much lower values for the magnetite #1-magnetite #2 suspensions. However, the higher density differential observed for these suspensions is an illustration of their lower stability compared to the plain magnetite #1 suspensions.

Chapter 7

Further Analysis

This section is an overview of the results and discussions of the previous section. In essence, the objective of this section is to further expound the factors which are important to the analysis of the results found. The two main point of focus are: the data regression of the experimental raw data; and the analysis of the methods by which DP001 is perceived as viscosity reducer in heavy medium suspensions.

In the data regression of the experimental data, rheological models of choice were fitted to the shear stress shear rate curves of the plain and uncontaminated heavy media used for this project. Data regression is important in that it can be used as a tool for inferring certain rheological parameters. It provides plant operators with information which can be used to make informative choices of what the effect of changes in either upward or downward streams may have on the separation efficiencies within the plant. It can also be used to extrapolate the properties of certain suspensions without the need of having to make laborious measurements.

Thus far the method by which DP001 affects the rheological properties of heavy medium suspensions has not be fully explained. Some of the theories behind this were elaborated on in Chapter 2, but there has still not been any explanation with regard to how they principally affect the viscosity of these suspensions. To address this adsorption tests were carried out on the media particles to examine the extent of DP001 adsorption on the media particles. The results were then used to explain and support some of the rheological changes observed in this project.

The first section will deal the data regression of the experimental data. And the second section will deal with the adsorption of DP001 onto the surfaces of the media particles.

7.1 Raw Data Regression

The raw data from the rheometry tests was regressed and fitted to the rheological models shown in Table 7.1. The models fitted were the Newton, Bingham, Ostwald, Herschel-Bulkley, and the Casson model. These models were fitted to the uncontaminated rheometry results, where no slime or DP001 added. These results are contained in Appendix A1.

Table 7.1 Rheological Models for Heavy Medium Suspensions [Laskowski et al. (1999)]

Name	Model
Newton	$\tau = \mu.D$
Bingham	$\tau = \tau_{pl} + \mu_{pl}.D$
Ostwald	$\tau = K.D^n$
Herschel-Bulkley	$\tau = \tau_o + K.D^n$
Casson	$\tau = [\tau^{1/2} + (\mu_c.D)^{1/2}]^2$

where τ is the shear stress, τ_{pl} and τ_o is the yield stress, μ is the suspension viscosity, K is a constant, D is the shear rate, and n is the power law index.

These models were chosen based on the work carried out by Laskowski et al. (1999), who fitted these models to experimental results they obtained from magnetite suspensions. All models in the table above were fitted to rheometry results of all the media suspensions used in this project.

The models were first used to try to parameterise the results from the rheological measurement of ferrosilicon suspensions. A sample graph is shown in Figure 7.1, for the adapt regression of ferrosilicon suspensions at specific gravity 2.9. A full set of graphs is contained in Appendix A1.

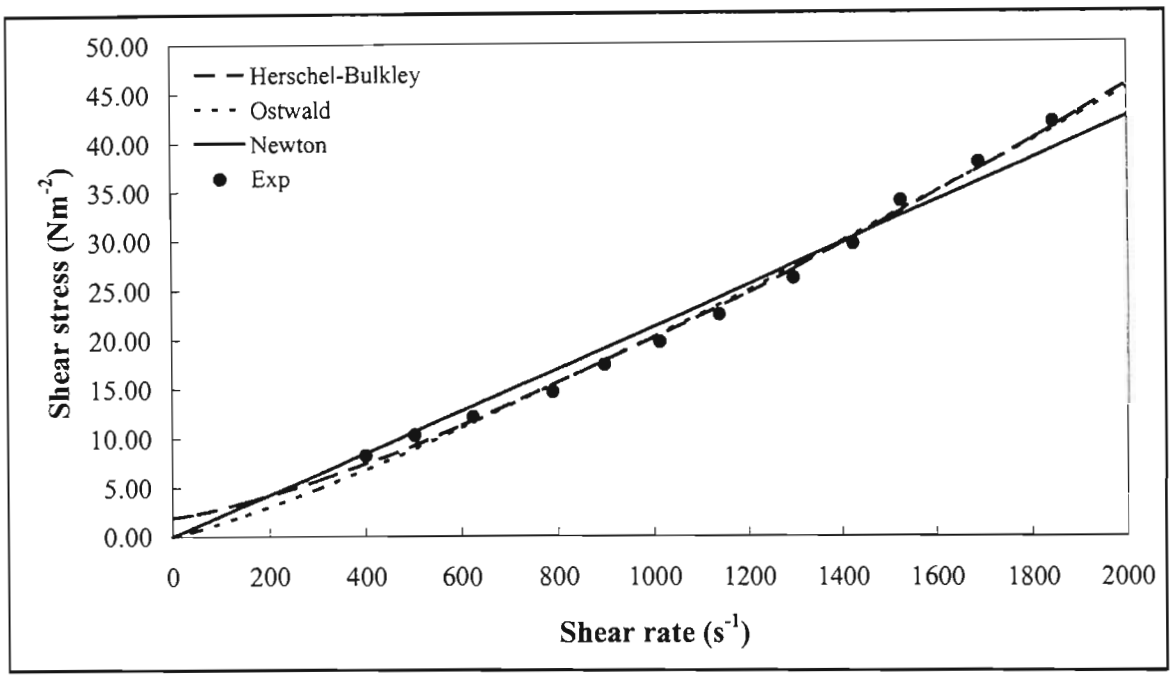

Figure 7.1 Regressed Ferrosilicon data at specific gravity 2.9.

The regressed ferrosilicon results showed that the ferrosilicon suspensions are described by the Herschel-Bulkley and Ostwald models at specific gravities from 2.0 to 2.4. At specific gravities 2.5 to 2.8 it appears as though the only the Ostwald model adequately describes the suspensions. The Herschel-Bulkley model best describes the data at specific gravities 2.9 and 3.0. The suspensions show dilatant behaviour at the high specific gravities. At lower specific gravities, the Newton model comes very close to describing the behaviour of the suspensions. One would have expected the Newton model to best describe the data points for all specific gravities with a solids volume percentage less than 30 %. However, the measured results are not only a function of the suspension properties, but are also dependant on the type of instrument and fluid used to calibrate the viscometer. At specific gravities 2.9 and 3.0, the Herschel-Bulkley model appeared to indicate the presence of yield stress. The value of this yield stress was 1.93 Nm^{-2} and 3.16 Nm^{-2} at specific gravities 2.9 and 3.0, respectively. This non-Newtonian behaviour is consistent with what one would expect for these suspensions [Collins et al. (1974) and Wills (1997)], as the solids volume percentages are 33.0 and 34.7 for specific gravities 2.9 and 3.0, respectively. The general behaviour of the suspensions, as shown by the models, appears to be dilatant.

The interpretation of the ferrosilicon data regression results was made difficult by the fact that these suspensions tended to settle very quickly. This undesirable property of these suspensions resulted in inconsistent results, particularly at specific gravities below 2.8. This is one of the reasons why industrial separations operating with ferrosilicon as the separating medium sometimes have slimes added to them, to try and stabilise the suspensions. As mentioned above, some of the models were not perfect at fitting the data at the various specific gravities, while others were. At low and high specific gravities it was observed that Herschel-Bulkley model fitted the results quite well. However, this model failed at intermediate specific gravities. The major drawback of the Herschel-Bulkley model is that the two parameters, k and n, do not have clear rheological meaning [Laskowski et al. (1999)]. This model, however, has a yield stress term which can be used to infer the yield stress of the suspensions. The Ostwald model is similar to the Herschel-Bulkley model, without the yield stress term. The extent of particle segregation and its effects on the rheology of the ferrosilicon suspensions can be better understood by comparing the results obtained for these two models. At low specific gravities the regression results showed the possibility of the presence of a yield stress in the suspensions. At intermediate specific gravities the results showed that there was no yield stress present in the suspension because only the Newton and the Ostwald model were capable of describing these suspensions. At high specific gravities the presence of a yield stress was once again observed. From the solid volume percentage, one would not expect there to be a yield stress at low specific gravities. However, the instability of the suspensions could have resulted in the solid particles accumulating at the base of the cup, thus retarding the motion of the bob. This would have the effect of inducing an apparent increase in suspension viscosity. This could be one of the reasons why there appears to be a yiled stress at the low specific gravities. The results for the intermediate specific gravities, which show no yield stress, are in direct agreement with what should be expected for these solid volume percentages. This result shows that the stability of the suspensions improves as the specific gravity increases. For the suspensions at high specific gravities, a yield stress values is expected since the solids volume percentage at these specific gravities suggests non-Newtonian behaviour.

For magnetite #1 suspensions it was found that either the Herschel-Bulkley or the Ostwald model are able to describe the suspensions at specific gravities 1.5 to 1.7. However, the measurements at these specific gravities were also made difficult by the instability of the suspensions. Hence, instead of the expected Newtonian behaviour being shown, the suspensions showed non-Newtonian behaviour. The stability of the suspensions improved as the solid volume percentage increased. For suspensions with specific gravities 1.8 and 1.9, all five models were able to

describe the suspensions. The Bingham and the Casson models both showed no yield stress, and their viscosity terms were equal to the viscosity calculated for the Newtonian model. These values were 0.0134 Pa.s and 0.0147 Pa.s for specific gravities 1.8 and 1.9, respectively. The Herschel-Bulkley and Ostwald models also showed no yield stress, and their power indices were 1.05 and 1.01 respectively at specific gravity 1.8, and both equal to 1.08 at specific gravity 1.9. At specific gravity 2.0 all the models, except the Newton model, are able to describe the behaviour of the suspensions at high shear rates. A sample graph for the regression at specific gravity 2.6 is given below.

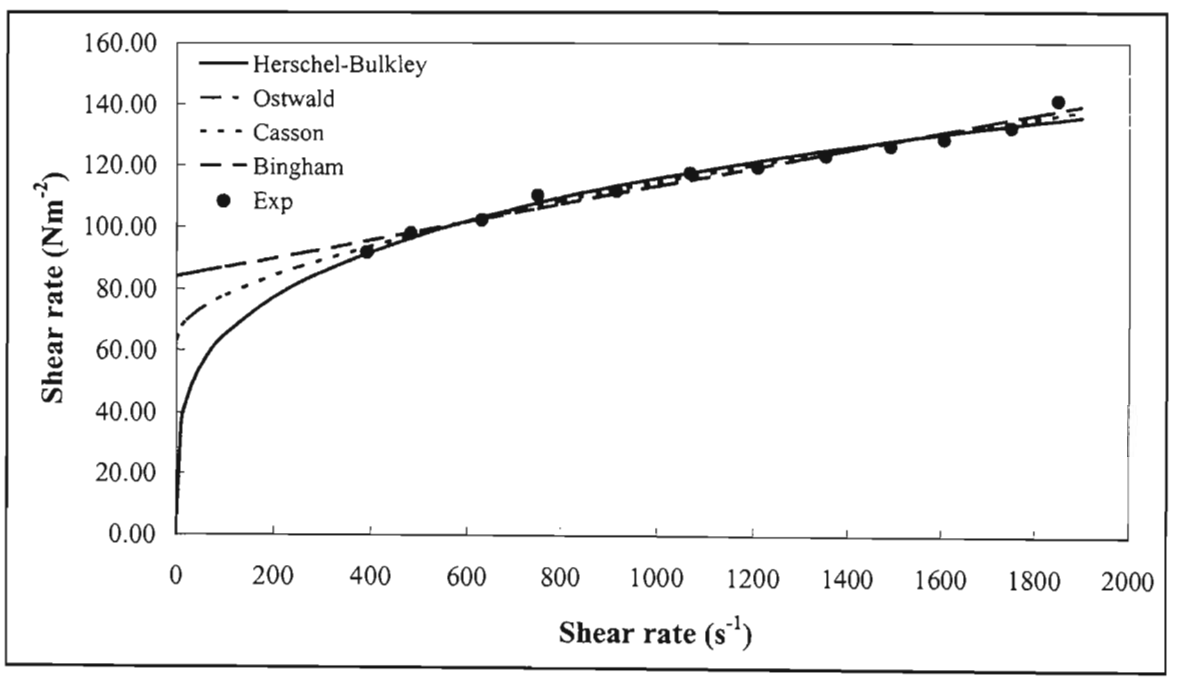

Figure 7.2 Regressed Magnetite #1 data at specific gravity 2.6

At low shear rates it appears as though the Bingham model comes closest to describing the behaviour. Unfortunately, the rheometer used was not able to make meaningful measurements at shear rates below 100 s^{-1} to accurately show this. The Bingham yield stress at this specific gravity was 3.73 Nm^{-2}. A similar trend is shown at specific gravity 2.1, which has a Bingham yield stress equal to 4.42 Nm^{-2}. At a specific gravity of 2.2 both the Casson model and the Newton model fail to describe the results at all shear rates tested. Again, the Bingham model appears to best describe the suspension at low shear rates. The Bingham yield stress at this specific gravity was 9.01 Nm^{-2}. For specific gravities 2.3 to 2.5, only the Newton model fails to describe the data. All other models appear to be able to describe the data at high shear rates. At low shear rates the Bingham

models also appears best able to describe the data. The Bingham yield stress obtained was 16.68 Nm^{-2}, 25.30 Nm^{-2}, and 49.37 Nm^{-2} at specific gravities 2.3, 2.4, and 2.5, respectively. At a specific gravity of 2.6 it appeared as though the Casson model was best at describing the data at low shear rates. The parameters of the Bingham models over the entire range of specific gravities were then plotted, to see the effect of specific of specific gravity on both the yield stress and viscosity of the suspensions. These graphs are shown below:

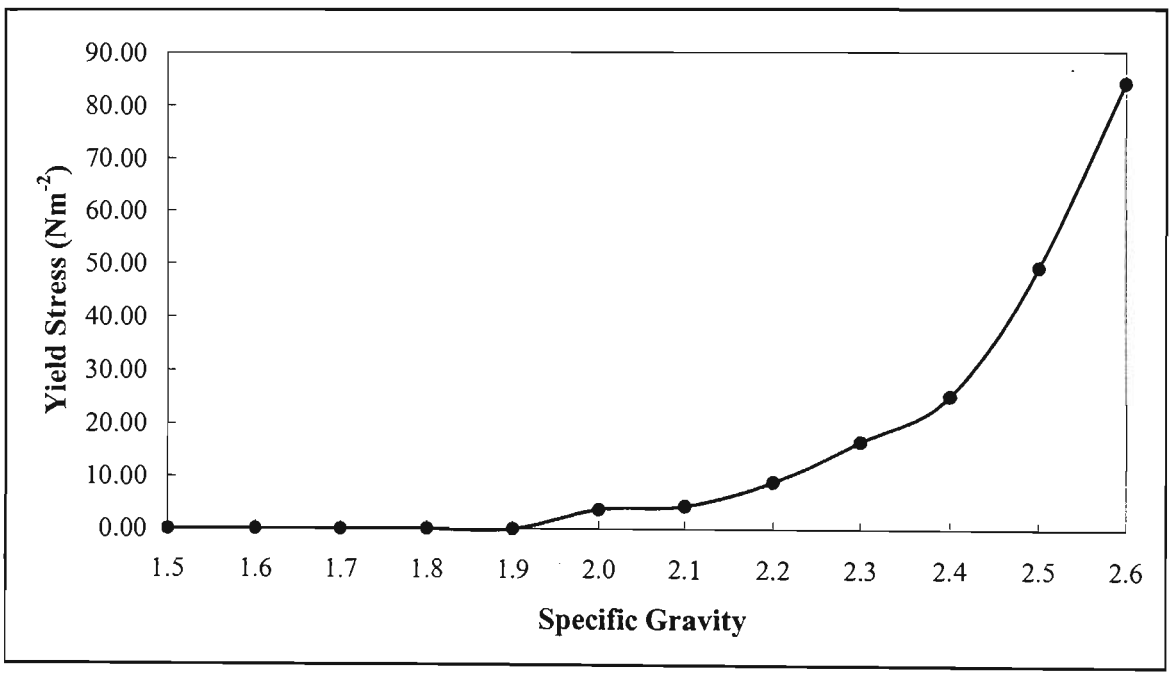

Figure 7.3 Yield stress versus specific gravity as predicted by Bingham model for magnetite #1 suspensions

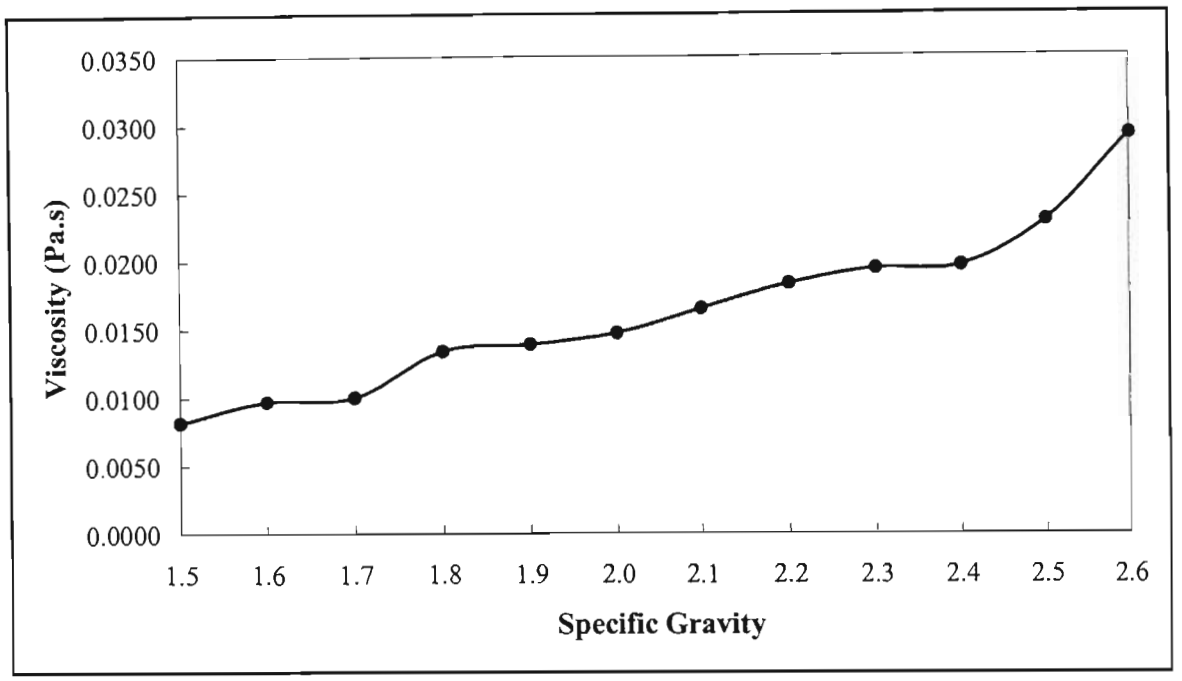

Figure 7.4 Viscosity versus specific gravity as predicted by the Bingham model for magnetite #1 suspensions

The graphs show that the Bingham yield stress predicted for the magnetite #1 suspensions increase with specific gravity. A similar trend is also observed for the viscosity if the suspensions. These results are consistent with those of Burt (1984) who showed that there was a non-linear relationship between both the yield stress and viscosity with specific gravity. He showed that for magnetite suspensions, the viscosity gradually increased up to the critical specific gravity. Above this critical viscosity, the viscosity of the suspensions increased almost exponentially. He showed that the critical specific gravity for most magnetite suspensions occurred between 2.2 and 2.4. The Bingham model results reveal that for the magnetite suspensions used in this project, the critical specific gravity occurred between 2.4 and 2.6.

Thus, it can be concluded that the data regression results obtained for the magnetite #1 suspensions showed that in general, at low specific gravities the suspensions can be considered to behave as Newtonian fluids. At specific gravities beyond 2.0 the suspensions begin to show non-Newtonian behaviour. Klein et al. (1999) found that the Bingham, Herschel-Bulkley, and Casson models described their experimental flow curves well. They found that the Bingham model inadequately described the flow curve data at the low shear rate region (below 100 s^{-1}), and the Herschel-Bulkley tended to underestimate the shear stress in the high shear rate region (above

250 s^{-1}). They found the Casson model to be very effective in describing their flow curves in a broad range of magnetite particle sizes. The shear stress of heavy medium suspensions which behave as Bingham plastics at moderately high shear rates usually bend downward as the flow curves approach the stress axis, due to plug flow [Perry et al. (1997)]. The flow curves show that of all models, the Casson model is the only which shows this type of behaviour.

The magnetite #1 / magnetite #2 suspensions appeared to be best described by the Herschel-Bulkley model over a broader range of magnetite #2 content. The presence of a yield stress was observed for suspensions with much higher levels of magnetite #1 from specific gravities of about 2.3 upwards. Examples of the regressed results are shown below:

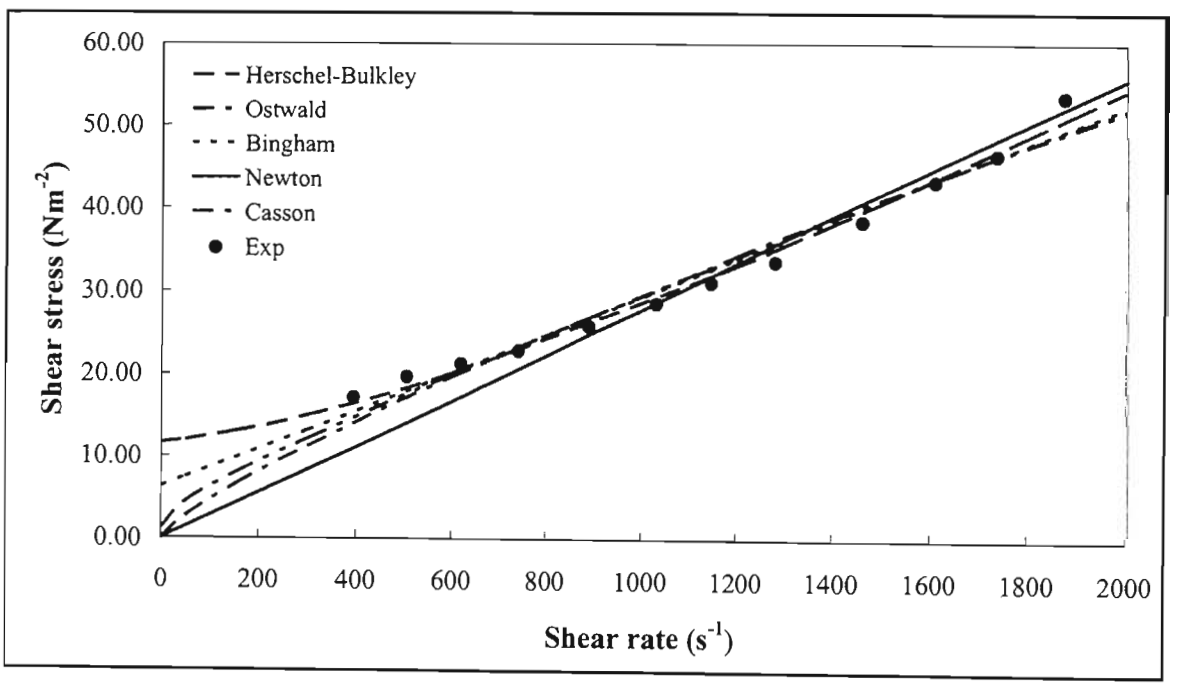

Figure 7.5 Regressed Mag #1 / Mag #2 data for ratio 2:1 at specific gravity 2.4

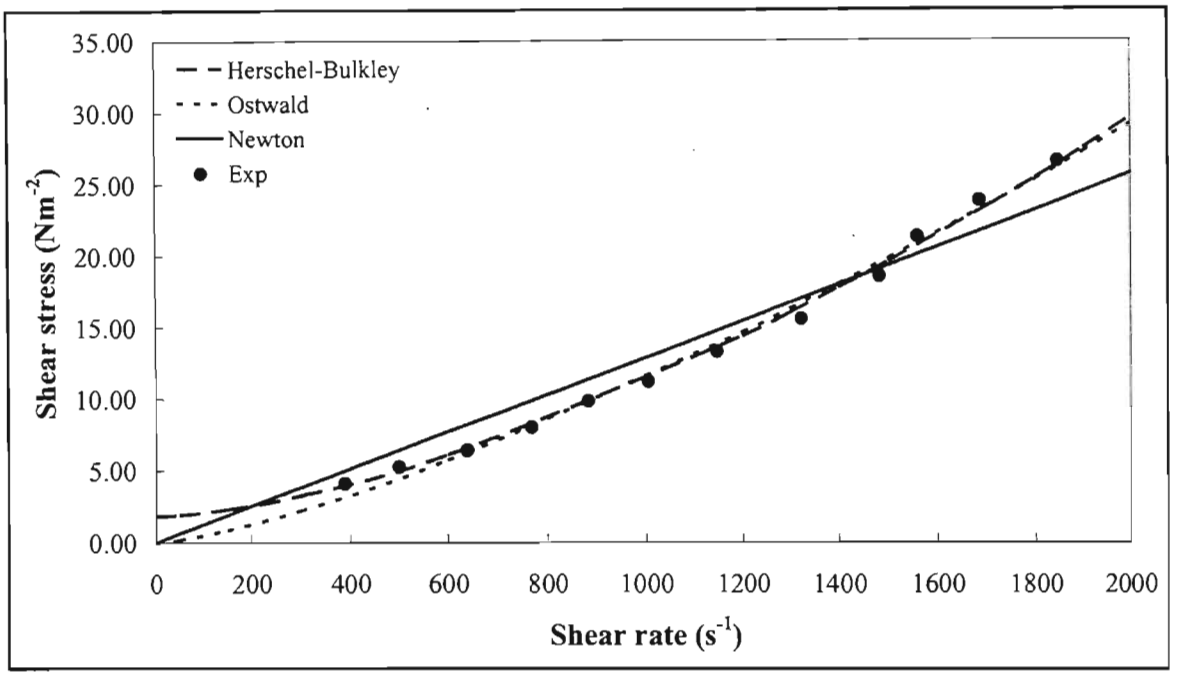

Figure 7.6 Regressed Mag #1 / Mag #2 data for ratio 1:1 at specific gravity 2.2

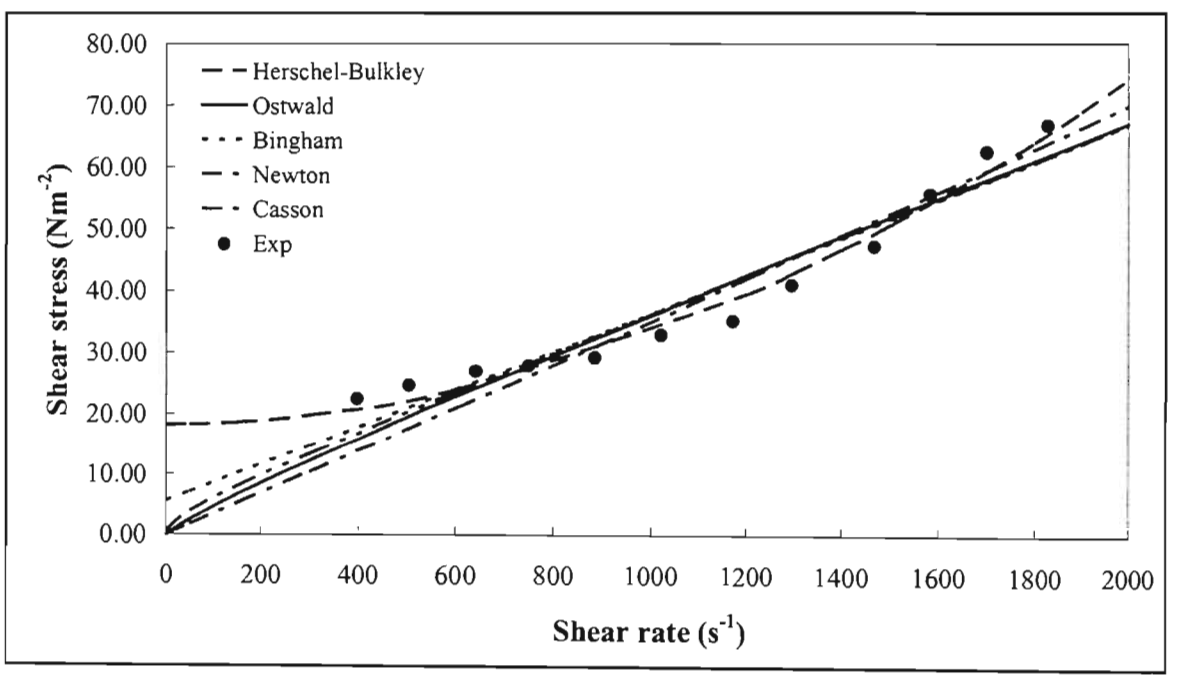

Figure 7.7 Regressed Mag #1 / Mag #2 data for ratio 1:2 at specific gravity 2.2

The Herschel-Bulkley yield stresses for the suspensions at the different ratio were plotted against specific gravity. This was done for Mag #1 / Mag #2 ratios of 1:1 and 1:2. The results at a ratio of 2:1 were not very clear, and as such were not plotted. The results are shown below:

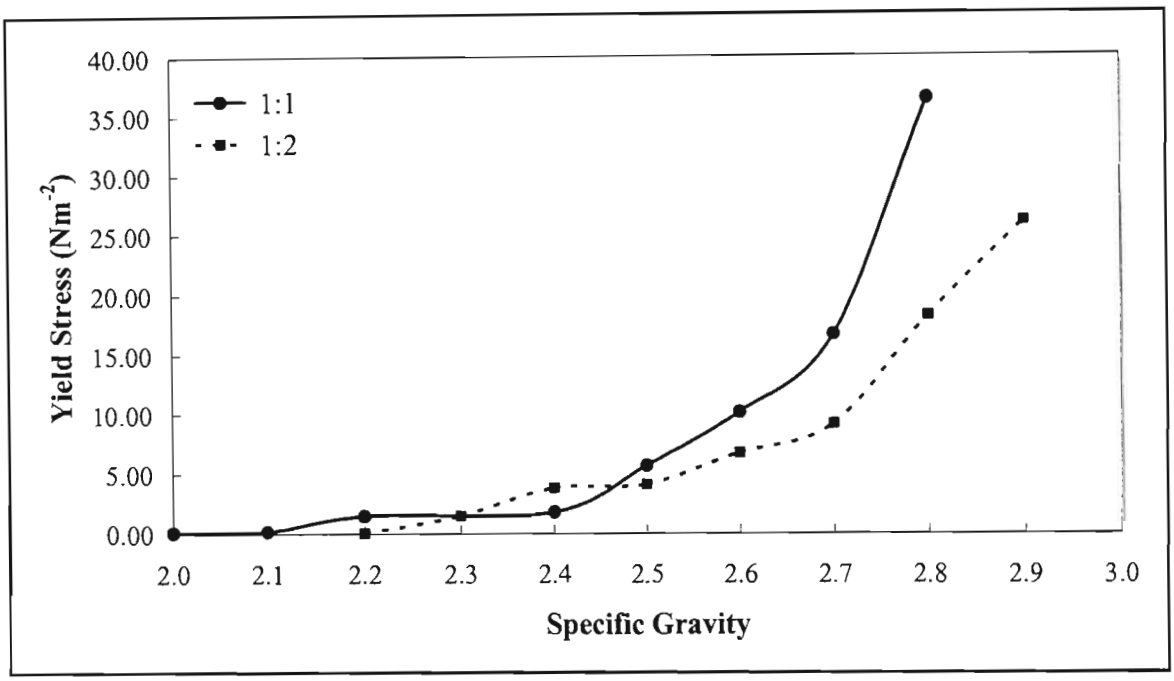

Figure 7. 8 Herschel-Bulkley yield stress versus specific gravity for Mag #1 / Mag #2 suspensions

The results show that for both ratios, the effect of increasing suspension specific gravity results in an increase in yield stress. The yield stress for suspensions with a ratio Mag #1 / Mag #2 of 1:1 generally have a higher yield stress than those with ratio 1:2. Except at specific gravity 2.4, where the yield stress of the 1:2 suspensions is greater. The higher yield stress of the 1:1 suspensions is due to the much finer size distribution of the media.

For mixtures of FeSi / Mag # 1 suspensions at a ratio of 1:1, the data is well defined by the Newton model at specific gravities from 2.0 to 2.4. For specific gravities 2.5 upwards, the Herschel-Bulkley model best describes the data. There regressed data showed an increase in yield stress with specific gravity. For suspensions with a FeSi / Mag #1 ratio of 2:1, the Newton model describes the data well for specific gravities 2.0 to 2.4. The Ostwald model best describes the data at specific gravities 2.5 to 2.7. At a specific gravity of 2.8 the Herschel-Bulkley model describes the data well. For suspensions with a FeSi / Mag #1 ratio of 1:2, the Newton model describes the

data well only for specific gravities 2.0 to 2.2. For specific gravities 2.3 upwards the Herschel-Bulkley model describes the model well. Samples of the results are plotted below:

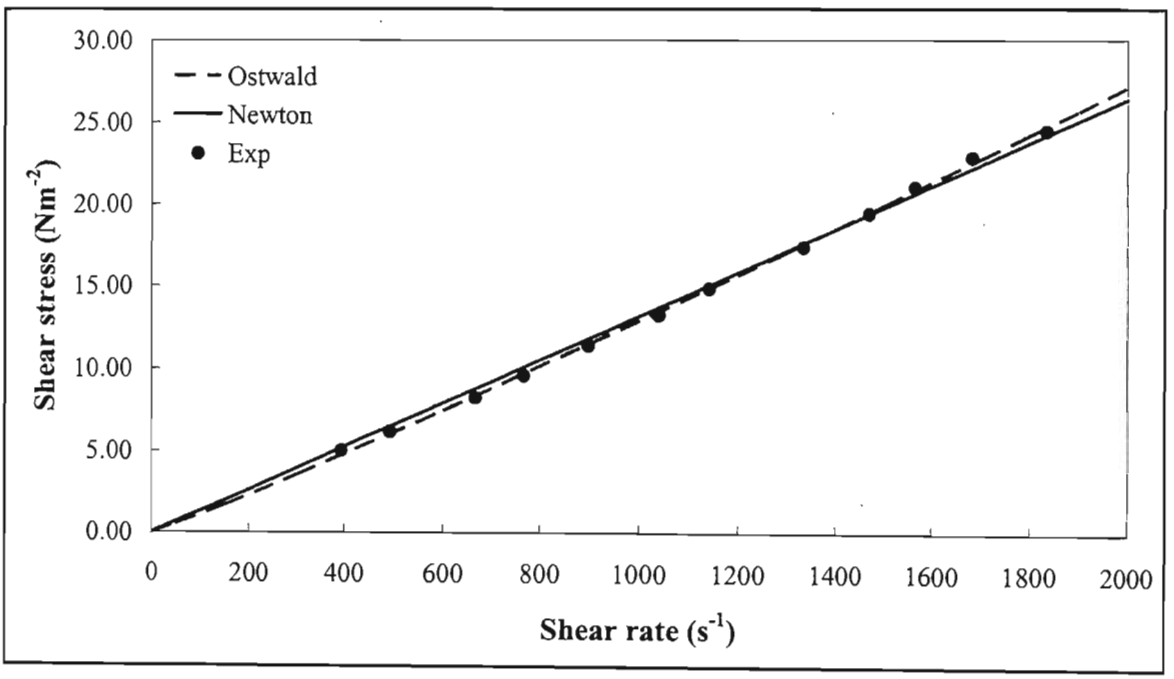

Figure 7.9 Regressed FeSi / Mag #1 data for ratio 1:1 at specific gravity 2.1

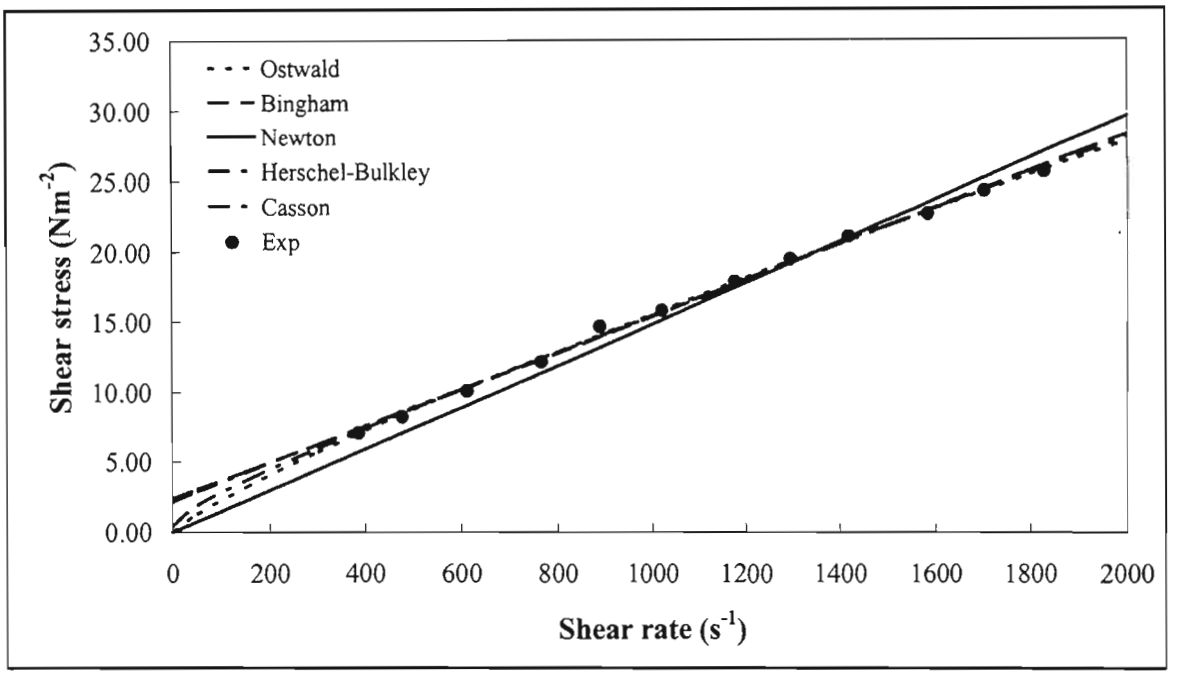

Figure 7.10 Regressed FeSi / Mag #1 data for ratio 2:1 at specific gravity 2.4

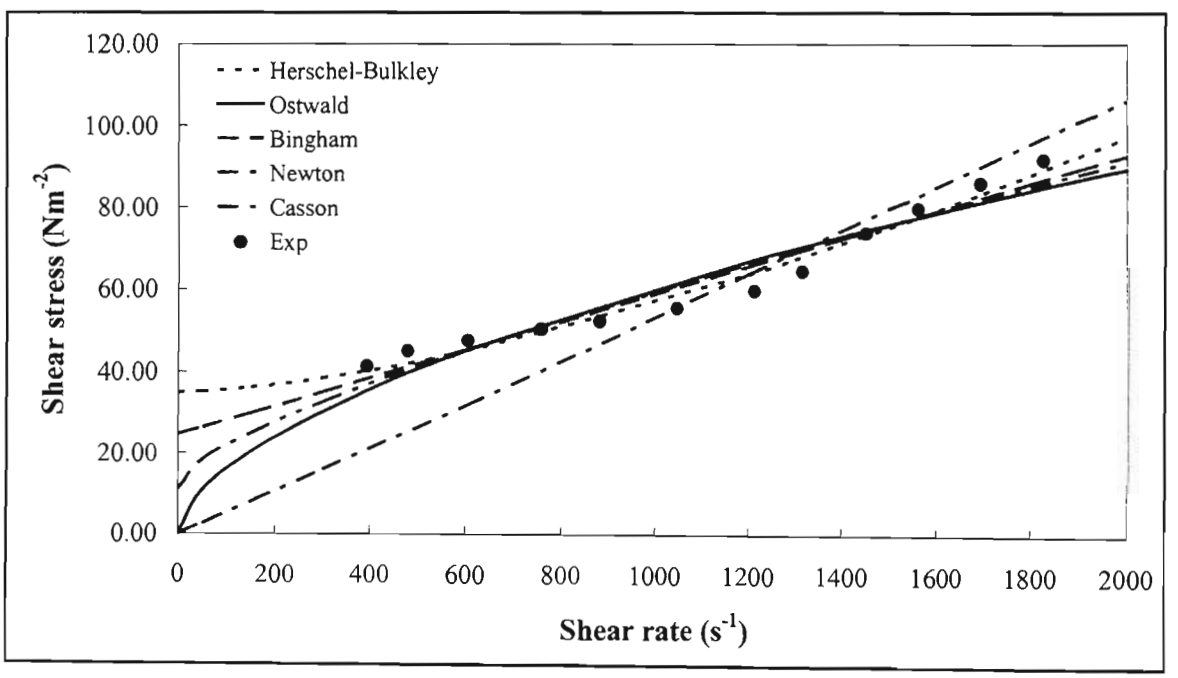

Figure 7.11 Regressed FeSi / Mag #1 data for ratio 1:2 at specific gravity 2.8

The results show that there is a development of a yield stress as the specific gravity is increased. Initially, for all the ratios, the yield stress is zero at low specific gravity, becoming fully developed at high specific gravities. The Herschel-Bulkley model was then used to measure the yield stress of the suspensions. And these were plotted against specific gravity for all FeSi / Mag #1 ratios. The results also showed that the yield stress at each specific gravity is a function of the amount of magnetite #1 present. The higher the amount of magnetite #1, the higher the yield stresses. These results are illustrated in the graph below. Also plotted on the graph are the Herschel-Bulkley yield stress for the ferrosilicon suspensions, and the Bingham yield stress for the magnetite #1 suspensions. The results illustrate that magnetite #1 has the highest yield stress, whereas ferrosilicon suspensions show the least yield stress.

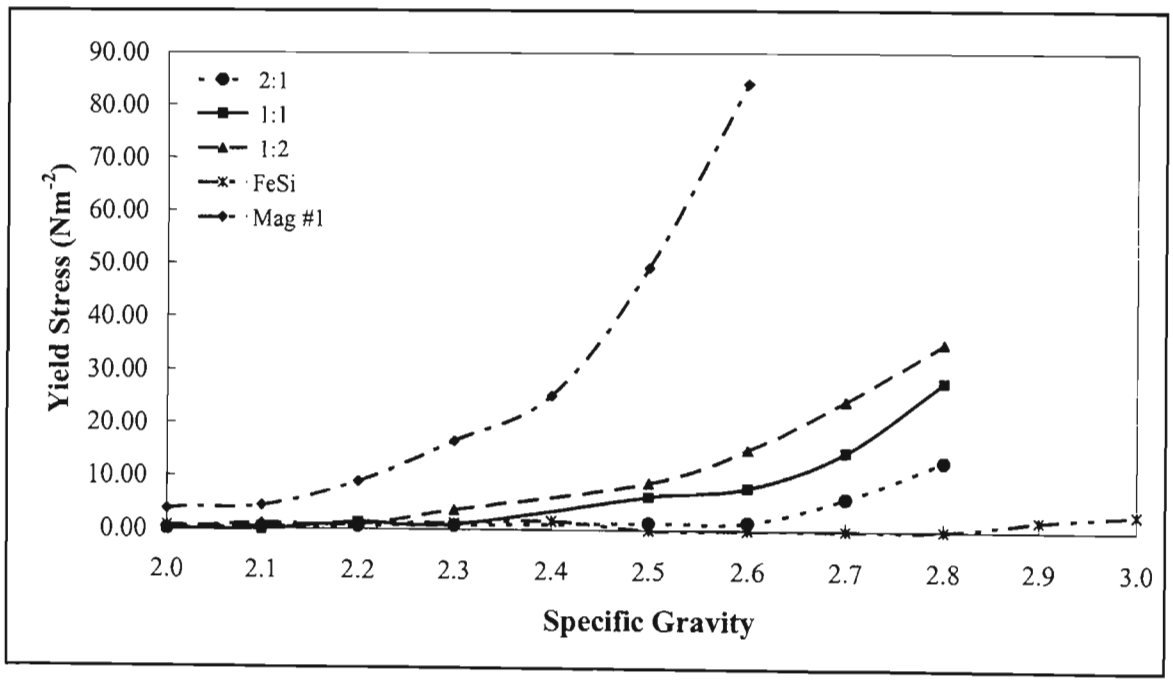

Figure 7.12 Herschel-Bulkley yield stress versus specific gravity for FeSi / Mag #1 suspensions

FeSi / Mag #2 suspensions were best described by the Herschel-Bulkley model at all ratios for the specific gravities tested (3.0 to 3.2). At lower specific gravities the stability of the suspension was too low to give meaningful results, due to both the high density of the ferrosilicon media particles and the shape and size of the magnetite #2 media particles. The regression graphs for these suspensions are contained in Appendix A1.

Finally, it must be stressed that the viscometers used for the rheometry tests were not able to get accurate results at low shear rates. As such, it was not possible to accurately describe what type of models best described the data at these shear rates. The effectiveness of each model was determined by evaluating which model gave the lowest least squares error. One of the aims of the data regression was to show that the data could be described by some of the rheological models used to define heavy medium suspensions. The ability of the data to be described by these models also shows the effectiveness of the rheometer in measuring the properties of the suspensions at moderate shear rates.

7.2 Effectiveness of DP001 on the Rheology of the Suspensions

This section discusses the use of DP001, and the effect it had on the viscosity of the heavy medium suspensions used in this work. The question one has to ask is how DP001 alters the viscosity of the heavy medium suspensions. As stated previously, DP001 is a medium chain length anionic calcium lignosulphonate. Which means that it dissolves when mixed with water, resulting in a solution containing negatively charged medium chain anionic polymers in it. How do these chains then interact with the solid particles, thereby altering the viscosity of the suspensions? It is believed that lignosulphonates, or surface active agents, are adsorbed onto the surfaces of heavy media particles [Jones et al. (1999)].

Adsorption tests were carried out on the media particles to determine how much DP001, if any, was adsorbed onto the surfaces of the particles. The experimental procedure for these experiments is contained on Appendix A2. The experiments involved measuring the absorbance of the solutions before and after the media particles were added to DP001 solutions using a UV spectrometer. However, only ferrosilicon and magnetite #1 media particles were tested. Magnetite #2 and the slimes causing clay proved too difficult to test because of the fine clay like particles they contained. Magnetite #2 was supplied by Richards Bay Mines, which mines the sand dunes of the coast of Kwa-Zulu Natal. Contamination of these media particles with other materials and some fines made them difficult to filter.

The first experiment investigated the effect of DP001 on ferrosilicon suspensions. Initial rheometry results showed that uncontaminated ferrosilicon suspensions were hardly affected by the presence of DP001. These results are similar to those observed by Aplan and Spedden (1964). Adsorption tests were then carried out using a UV spectrometer to determine whether any DP001

was adsorbed onto the ferrosilicon particle surfaces. These tests were carried out at a specific gravity of 2.4, and DP001 additions of 1 g DP001 / kg FeSi. The DP001 was first added to 100 grams water, and the absorbance measured. The correct amount of ferrosilicon was then added to the solution and shaken for a couple of minutes. The suspension was allowed to settle, and then filtered. The absorbance of the filtrate was then measured to determine whether any DP001 adsorption occurred. The adsorption before and after were 1.343 and 1.332, respectively. Using the calibration graph (Appendix A2), this corresponded to a mass of 0.209 g and 0.207 g of DP001 before and after the shake test, respectively. This corresponds to 0.96 g DP001/kg FeSi and 0.95 g DP001/kg FeSi before and after, respectively. This showed that there was very little, if any, DP001 adsorbed onto the media particles. The results show that only 0.01 g DP001 / kg FeSi was adsorbed onto the surfaces of the ferrosilicon particles i.e. there was no real effect, as seen earlier.

Aplan and Spedden (1964) showed that the addition of a dispersant (sodium hexametaphosphate) reduced the viscosity and increased the stability of the suspension they tested. They showed that there was a dosage region where there was a decrease in suspension viscosity without a decrease in suspension stability. However, for dosages beyond this region, they showed that the viscosity and stability of the suspensions both decreased, making the suspensions difficult to handle. Another conclusion reached on the effect of polymer modifiers on heavy medium suspensions was that both the viscosity and yield stress initially decreased with polymer addition, until a plateau was reached. They then started to increase with the amount of polymer added [Klein et al. (1999)]. This observation is similar to what was observed for the magnetite #1 suspensions tested in this project. There appeared to be an initial decrease in the viscosity of the suspensions with DP001 additions. This levelled off, with some suspensions showing no effect of DP001 at certain dosages. There was then an increase in the suspension viscosity, as observed at dosages of 5 g DP001 / kg. However, there is no clear indication of what the optimum DP001 dosage should be. It appears that additions of 5 g DP001 / kg are beyond the plateau region. Therefore, the optimum DP001 dosage appears to be somewhere between 1 g and 2 g DP001 / kg.

Adsorption tests were also carried out on magnetite #1 suspensions. Tests were carried out at specific gravity 2.2. This specific gravity was chosen because the solids volume fraction at this specific gravity for magnetite suspensions is equal to that at specific gravity 2.4 for ferrosilicon suspensions. DP001 additions were also carried out at 1 g DP001 / kg Mag #1. The same procedure used for the ferrosilicon suspensions were also used for magnetite #1 suspensions. The

measured absorbance was 1.376 and 0.547 before and after, respectively. This corresponded to a DP001 mass of 0.214 g and 0.085 g / 100 g water before and after, respectively. This was equivalent to 0.94 g DP001/ kg Mag #1 and 0.37 g DP001/ kg Mag #1 before and after mixing the magnetite media with the DP001 solutions, respectively. The results showed that the amount of DP001 adsorbed onto the magnetite suspensions was 0.129 g. This mass is equivalent to 0.57 g DP001 / kg Mag #1 being adsorbed onto the magnetite media particle surfaces. This actually shows that the maximum loading for DP001 onto the magnetite media particles occurs at DP001 loading below 1 g DP001 / kg Mag #1. Hence, the optimum amount of DP001 needed to reduce the viscosity of the suspensions is about 0.6 g DP001 / kg Mag #1. Values higher than this would first fall into the plateau region, and finally an increase in the viscosity of the suspensions could be observed.

The magnetite #1 rheograms were also compared to ferrosilicon rheograms at the same specific gravity. It was observed that the viscosity of the magnetite suspensions was much higher than that of ferrosilicon. At the same specific gravity, this is due to the higher volume percentage of the solid particles. At the same solid volume percentage, this is due to the much higher fines content of the magnetite particles, which increases their surface area. Even the addition of DP001 did not reduce the viscosity of the suspensions to that of ferrosilicon. Although there was a decrease in suspensions viscosity for some of the suspensions, this decrease does not appear large enough to warrant the use of magnetite #1 suspensions in place of ferrosilicon suspensions at high specific gravities. The results showed that magnetite suspensions are more affected by DP001 than uncontaminated ferrosilicon suspensions. This result is consistent with the observations of Johnson et al. (2000), who stated that metal oxide media particles are more affected by surface active chemicals. And since magnetite particles are an iron oxide, whereas ferrosilicon particles are not, it follows that the rheology of magnetite particles will be more affected by surface active chemicals.

Mixtures of ferrosilicon and magnetite #1 were prepared at FeSi / Mag #1 ratios equal to 2:1, 1:1, and 1:2. The rheograms for these suspensions were also compared to ferrosilicon rheograms at the same specific gravity.

For suspensions with a FeSi / Mag #1 ratio of 2:1 (Figure 6.62 to Figure 6.68), a decrease in suspension viscosity was observed for some DP001 additions. For some of the suspensions there was also a particular shear rate above which the effect of DP001 appeared to increase the

viscosity of the suspensions. At a specific gravity of 2.2 (Figure 6.62) there was a decrease in suspension viscosity for shear rates below 1000 s^{-1}. Addition of 1 g DP001 / kg solids (FeSi + Mag #1) decreased the viscosity of the suspensions. However, there appeared to be no further decrease with the addition of 2 g and 5 g DP001 / kg solids. Above 1000 s^{-1} shear rate, the effect of 1g and 2 g DP001 / kg solids diminished, and there appeared to be an increase in viscosity for 5 g DP001 / kg solids addition. This result showed that the optimum DP001 loading for the magnetite particles had been exceeded. And as such, the viscosity of the suspensions increased. In comparing these results to those of uncontaminated ferrosilicon at the same specific gravity, it was shown that the addition of magnetite #1 to ferrosilicon resulted in an increase in the viscosity of the suspensions. Below 1000 s^{-1} shear rate, the addition of DP001 reduced the viscosities of the mixtures close to those of uncontaminated ferrosilicon.

For specific gravities 2.3 (Figure 6.63) and 2.4 (Figure 6.64), a decrease in viscosity was observed for 1 g and 2 g DP001 / kg additions. There was large increase in suspension viscosity upon the addition of 5 g DP001 /kg. This result seems to illustrate that the effect of DP001 at high dosages acts as a stabilizing agent, rather than a viscosity reducer. This is similar to what was observed for the magnetite #1 suspensions. For both specific gravities, there is an increase in the viscosity of the suspensions at all DP001 additions after a shear rate of 1700 s^{-1} for specific gravity 2.3, and 1500 s^{-1} for specific gravity 2.4. At specific gravity 2.5 (Figure 6.65) DP001 additions appeared to have no effect on the viscosity of the suspensions. This was possibly due to experimental error, where the DP001 did not effectively interact with the media particles, or it could have been due to the settling out of the ferrosilicon particles from the suspensions. The suspensions viscosity was also observed to increase for shear rates in excess of 1200 s^{-1} for all DP001 additions. At specific gravities 2.6 to 2.8 there was a decrease in the suspension viscosity for all DP001 additions. Again, it was observed that the suspension viscosity increased slightly at 5 g DP001 / kg solids. The addition of 2 g DP001 / kg solids brought down the viscosity to values close to those of uncontaminated ferrosilicon suspensions at the same specific gravity.

For suspensions with a mixture of FeSi / Mag #1 of 1:1 (Figure 6.55 to Figure 6.61), a decrease in suspension viscosity was also observed. At a specific gravity of 2.2 (Figure 6.55) the viscosity of the suspensions was lower than that of the plain suspensions for all DP001 additions. Addition of 1 g DP001 / kg reduced the viscosity of the suspensions, bringing it close to that of ferrosilicon suspensions at the same specific gravity. There appeared to be little difference in the suspension viscosity between 1g and 2 g DP001 / kg additions. This seems to illustrate that the plateau region

for the DP001 had been reached. Addition of 5 g DP001 / kg slightly increased the viscosity of the suspensions above that at 1 g DP001 / kg additions. This result is similar to the one observed for the magnetite #1 suspensions. This also shows the plateau region had now been exceeded, and the region where the both the yield stress and plastic viscosity had been reached. A similar effect was observed for all other specific gravities. There was an initial decrease in suspensions viscosity for 1 g DP001 / kg, followed by the plateau region for 2 g DP001 / kg, and then an increase in suspension viscosity for 5 g DP001 / kg. Suspensions at a specific gravity of 2.8 (Figure 6.61) showed little on DP001 additions. It was also observed that the difference in viscosity between the uncontaminated suspensions and the FeSi / Mag #1 suspensions with DP001 increased with specific gravity.

The results for FeSi / Mag #1 suspensions at a ratio of 1:2 (Figure 6.69 to Figure 6.75) also showed similar results to suspensions with a ratio of 1:1. At a specific gravity of 2.2 (Figure 6.69) there was a decrease in the suspensions viscosity upon the addition of 1 g DP001 / kg. There was a further reduction for 2 g DP001 / kg, although the viscosity exceeded that at 1 g DP001 / kg for shear rates above 1200 s^{-1}. The addition of 5 g DP001 / kg increased the viscosity of the suspensions, pushing above that of the plain suspension at shear rates above 1300 s^{-1}. A similar trend was observed for the rest of the specific gravities. This again showed that the effect of DP001 was to initially decrease the viscosity of the suspensions, reaching a plateau, and then increasing it after that. The exact dosage DP001 at which the plateau is reached, and at which the viscosity begins to increase cannot be accurately determined from these results. This value can be expected to be around 0.6 g DP001 / kg Mag #1.

All the FeSi / Mag #1 results appear to show an increase in the effect of DP001 with the amount of magnetite present in the suspensions. Suspensions with a FeSi / Mag #1 ratio of 2:1 were the least affected by DP001 additions, with suspensions at ratios 1:1 and 1:2 showing almost equal effects. As discussed earlier, the adsorption of DP001 on the surface of the ferrosilicon particles is small when compared to the adsorption on magnetite #1 suspensions. This much higher adsorption on magnetite suspensions means that the more the amount of magnetite present, the more the amount of DP001 adsorbed on the particle surfaces will be. Hence the hydrodynamic repulsive forces will be much higher at higher magnetite #1 concentrations, resulting in more dispersed suspension at these levels. Hence, an increase in the magnitude of viscosity reductions was achieved.

7.3 The Importance of Reynolds Number

Thus far the Reynolds numbers of the suspensions tested using the rheometers have not been elaborated on. In the development of the equations governing the movement of particles in heavy medium separations (Chapter 4), the nature and type of drag force is of great importance to the analysis of the results in this section. It was shown in Chapter 4 that, depending on whether laminar flow or turbulent flow prevails, the viscosity of the suspensions may or may not be responsible for the drag force induced on the particles. It was shown that only under laminar conditions will the viscosities of the suspensions result in the particle drag force. Thus, if one is to conclude that DP001 does in fact reduce the viscosity of the heavy medium suspensions, one has to show that the flow regime prevailing within the rheometers was in fact laminar flow.

The flow conditions in the annulus were determined using the modified Reynolds number for concentric cylinders. This equation is given below [Govier et al. (1957)]:

$$\mathrm{Re} = \frac{N\rho}{\mu} \tag{7.1}$$

where N = rotational speed (revs per sec); ρ = density of the medium (g / cm^{-3}); and μ = apparent viscosity (Poise).

For Reynolds numbers less than 467, the suspensions can be considered to be in the laminar flow regime.

Table 7.2 Maximum annulus Reynolds number for the heavy medium suspensions

	Re (Max)	$Re_{Max}(1000\ s^{-1})$
FeSi	428	400
Mag #1	360	275
FeSi / Mag #1	545	291
Mag #1 / Mag #2	550	323
FeSi / Mag #2	332	214

The above table shows the maximum Reynolds numbers in the rheometer annulus of the heavy medium suspensions used in this project. The Reynolds is a function of not only shear rate, specific gravity, or apparent viscosity, but also a function of the type of behaviour exhibited by the suspensions. For Newtonian suspensions the Reynolds number will be independent of the shear rate at a particular specific gravity. For pseudo-plastic suspensions at constant specific gravity, the Reynolds number will be higher at higher shear rates. While for dilatant suspensions, the Reynolds number will be lower for higher shear rates at a constant specific gravity.

The values in the above table were calculated using Equation 7.1. The apparent viscosities used were calculated from the shear stress and shear rate values measured using the rheometer. As mentioned above, Reynolds number is inversely proportional to viscosity. Hence, the maximum Reynolds for all the suspensions occurred at low specific gravities, where the viscosity of the suspensions is minimal. For ferrosilicon suspensions this occurred at suspensions with specific gravity equal to 2.0. And since the ferrosilicon suspensions were dilatant, the maximum Re occurred at the lowest shear rate. The same was true for FeSi / Mag #2 suspensions, where Re_{Max} occurred at a specific gravity of 2.8 and low shear rate. This value occurred at a FeSi / Mag #2 ratio of 1:2, since low viscosities were observed at these mixtures. The rest of the suspensions behaved as pseudo-plastic fluids. Thus, Re_{Max} occurred at high shear rates for constant specific gravities. These values also occurred at ratios which gave the least viscosity. For FeSi / Mag #1 and Mag #1 / Mag #2 suspensions this was for suspensions with less magnetite #1 present.

The results show that for some of the suspensions the Reynolds criterion for laminar flow conditions to prevail is not satisfied. These high Re values occur at shear rates in excess of 1300 s^{-1}. However, the results showed that all the suspensions satisfy the Reynolds criterion for shear rates less than, or equal to 1000 s^{-1}. These results show that, since laminar flow conditions prevail, the drag forces experienced in the cup are a function of viscosity. Hence, it is reasonable to conclude that DP001 does affect the viscosity of the suspensions tested, and that the Reynolds criterion is satisfied. Thus, DP001 should affect drag forces, and ultimately separation efficiency.

7.4 The Effect of DP001 and Media Particle Size and Shape on the Separation Efficiency

The separation efficiency of heavy medium separators was calculated by determining the Ecart probable (Ep). The calculation of the Ep value was described in Chapter 4. It is equal to the half the densities at partition coefficients 75 % and 25 % on the partition curve. The closer this value is to zero, the more efficient the separator. This section discusses the Ep values obtained when using DP001 and magnetite #2 to reduce the viscosity of the suspensions.

The dense medium separation cycle was described in Chapter 5. The particles separated were coal particles in three different size ranges. These particle size ranges were -4mm + 1mm, -1mm + 500 μm, and -4mm + 500 μm. Initial separations involved only magnetite #1 suspensions at specific gravities 1.57 and 1.83. DP001 was added at a mass of 1 g DP0001 and 2 g DP001 / kg Mag #1. The second set of experiments involved the use of a mixture of magnetite #1 and magnetite #2 at a ratio of 12 % magnetite #2, and specific gravity 1.7. The operating specific gravities were determined sink – float analysis of the coal samples. The results showed that a specific gravity between 1.4 and 1.9 would recover a clean product with lowered ash.

The first set of results for coal samples in size range -4mm + 1mm showed that the separation efficiency at specific gravity 1.57 was slightly better than that at 1.83. The addition of DP001 appeared to improve the separation of suspensions at specific gravity 1.57, whereas those at specific gravity 1.83 were unaffected. For coal samples with size range -1mm + 500 μm, a similar result was obtained. These results showed that the separation efficiency at specific gravity 1.57 was more than two times better than that 1.83. The suspensions at both specific gravities showed a slight improvement in separation efficiency with DP001 addition. For the -4mm + 500 μm coal samples, the separation efficiency at no DP001 additions was higher at specific gravity 1.83 than at specific gravity 1.57. This was probably due to particle entrainment common at broader ore particle size ranges. As DP001 was added to the suspensions, the separation efficiency of the 1.57 suspensions improved, becoming higher than that at specific gravity 1.83. The separation efficiency at 2 g DP001 / kg Mag #1 (0.2 %) was double the efficiency at 0 % DP001. For suspensions at specific gravity 1.83, the separation efficiency is initially unaffected by DP001 additions, and the separation efficiency begins to get lower at 0.2 % DP001 additions.

These results show that the separation efficiency decreases with specific gravity (at no DP001 addition). This is consistent with the results of Collins et al. (1983) and Napier-Munn (1990). The results also show the effectiveness of DP001 in improving the separation efficiency. However, it appears that the effectiveness of DP001 is much higher at low specific gravities. The results obtained from the separation tests seem to tally well the rheological results obtained from the rheometry measurements. However, it was not possible to relate the shear rates experienced in the rheometer with those in the cyclone, mianly because the cyclone used in this project did not allow for the measurements of shear rates within the cyclone. This would have given a better interpretation of the separation results. For now it is safe to say that DP001 does indeed improve the separation efficiency, since almost other variable which could affect the efficiency were kept constant. These include the feed rate, cone shape, and underflow and overflow diameters. The Ep values obtained for separations with no DP001 additions show that the cyclone is inefficient. In practice the Ep usually lies in the range 0.02 – 0.08 [Wills (1997)], whereas for the cyclone used in this project the range was 0.05 – 0.125.

As mentioned, separation tests were also carried out using magnetite #1 and magnetite #2 suspensions. These separations were carried out at a suspension specific gravity equal to 1.70. DP001 was also added to suspension to see whether it would improve the separation efficiency. Since magnetite #1 and magnetite #2 have similar chemical composition, it can be assumed that DP001 is adsorbed onto both magnetite #1 and magnetite #2 surfaces. The results obtained showed that for the -4 mm + 1mm coal samples, the addition of DP001 slightly improved the separation efficiency. The Ep value decreased from 0.058 at 0 %, to 0.056 with the addition of 0.2 % DP001. The -1mm + 500 μm coal samples were not affected by DP001. The -4mm + 500 μm coal samples showed an improvement in efficiency of more than 60 % with the addition of 0.1 % DP001. The Ep value decreased from 0.125 at 0 % DP001, to 0.067 at 0.1 % DP001. However, the separation efficiency decreased when 0.2 % DP001 was added to the suspensions. The Ep value increased to 0.111 at these additions. The results showed that at no DP001 additions the separation efficiency was highest (corresponding to lowest Ep value) for the -4 mm + 1mm coal samples. This is due to the larger particle size range, which is much easier to separate. The -4mm + 500 μm coal samples showed the lowest separation efficiency. This was once again due to particle entrainment.

One of the biggest challenges with heavy medium separations is trying to correlate the results obtained from the rheometry tests to those obtained from the separation tests. The difficulty arises

because the shear rates occurring in the cyclone are difficult to quantify. To overcome this problem, Lilge et al. (1958) determined the speeds with a cyclone using anemometer and stroboscope. From the rotational speeds measured by the anemometer, the shear rates within the cyclone were determined. Shear rates within the cyclone decrease from a maximum at the centre of the cyclone, to a minimum at cyclone outer wall. Thus, shear rates within the cyclone decrease with radius. The above authors carried out experiments on a 6 inch cyclone (150 mm), which was equivalent in size to the one used in this project. The maximum shear rates which they achieved were approximately equal to 502 s^{-1} and 143 s^{-1}, at inlet pressures 552 kPa and 69 kPa, respectively. The shear rates within the cyclone were compared to the results obtained from a rotational viscometer, and the viscosities within the cyclone could be inferred. However, it was not possible to do this in these experiments, and such the actual viscosities within the cyclone were not known. If these values could have been determined it would have given a clear indication the optimum dosage required to reduce the viscosity of the suspensions.

Chapter 8

Conclusions

The understanding of the viscosity of heavy medium suspensions is important in the evaluation of the separation efficiency in heavy medium suspensions. It is important to know what the properties of the heavy media have on the rheology of heavy medium suspensions, and how this, in turn, will affect separation efficiency. During the course of this investigation, the properties of heavy medium suspensions were adequately measured using a laboratory scale device, and the effect of a dispersant called DP001 was also investigated. The effects of both particle shape and media size were also investigated through the use of a much coarser and smoother media type. Suspensions were then prepared to evaluate the separation efficiency in a pilot size dense medium cyclone. The heavy media used in this project were: 270D ferrosilicon; a fine magnetite grade, labelled as magnetite #1; and a coarse magnetite grade, labelled as magnetite #2. A slime causing smectite clay was used to simulate slimes build in the ferrosilicon suspensions.

One of the biggest challenges with measuring the properties of heavy medium suspensions using rotational rheometers is the settling nature of the suspensions. Because of the relatively high density of the media particles, the particles tend to settle out easily from the suspensions. One then has to design a rheometer which can counteract this. The rheometers used in this project were modifications of the DIN 53 019 and ISO 3219 rheometers. The suspension in the rheometer cup was kept in constant motion through recirculation with a peristaltic pump. This was found to reduce the settling of the suspensions. To further minimise the settling effect, a chamfer was added to the base of the cup, such that any settling solids do not accumulate at the base of the cup, which were found to induce an apparent increase in suspension viscosity.

Initial measurements carried out on uncontaminated ferrosilicon, with specific gravities ranging from 2.0 to 3.0, showed that these suspensions behaved as Newtonian fluids at low specific gravities, and as dilatant fluids at high specific gravities. The biggest challenge during these experiments was to try and minimise the settling of the media particles from the suspension. Magnetite #1 suspensions were tested from specific gravities ranging from 1.5 to 2.6. These

suspensions also showed Newtonian behaviour at low specific gravities, and pseudo-plastic behaviour at high specific gravities. As the specific gravity increased above 2.0, the development of a yield stress was observed. The magnitude of this yield stress increased with specific gravity, showing maximum values at specific gravity 2.6. When comparing the viscosity of the ferrosilicon suspensions to that of magnetite #1 at equal percentage volume solids (24 % and 33 %), it was found that the viscosity of the magnetite suspensions was reasonably higher. This was attributed to the much higher fines content of the magnetite #1 media particles, as illustrated by size distribution tests carried out using a Malvern Metsizer 2000.

Suspensions of ferrosilicon and magnetite #1 mixtures were also prepared and tested. The results showed that at equal specific gravities, the viscosity of the suspensions was higher for suspensions with a high magnetite #1 content. The specific gravities were from 2.2 to 2.8, and it was found that the behaviour of the suspensions varied from pseudo-Newtonian at low specific gravities, to pseudo-plastic at high specific gravity. It was found that the onset of non-Newtonian behaviour occurred at much lower specific gravities for the suspensions with a high magnetite #1 content. When comparing the viscosities of these suspensions to those of ferrosilicon at the same specific gravity, it was found that the viscosity of suspensions with a FeSi / Mag #1 ratio of 2:1 was very close to that of uncontaminated ferrosilicon, particularly at high shear rates.

Adsorption tests carried out on uncontaminated ferrosilicon suspensions showed that DP001 had little effect these suspensions. When DP001 was added to suspensions contaminated with slime, it was observed that here was a considerable decrease in the viscosity of the suspensions. For DP001 additions equal to 2 g DP001 / kg FeSi, viscosity reductions as high as 16 % were achievable. DP001 additions at constant shear rates and different slimes additions also revealed the effectiveness of DP001 in reducing the viscosity of the suspensions. For a constant shear rate equal to 240 s^{-1}, viscosity reduction as high as 32.1 % were achievable for specific gravity of 2.9. the results showed that the DP001 reduced the viscosity of the suspensions by interacting with the slime or clay particles. However, because of the amount of fines in the slime, it was not possible to perform any adsorption tests on them to verify this claim.

DP001 addition to magnetite #1 suspensions showed that DP001 was capable of reducing the viscosity of the suspensions. There was, however, an increase in viscosity for some of the suspensions with an increase in the amount of DP001 added. There appeared to an initial decrease in suspension viscosity, followed by a plateau region where there was no change in suspension

viscosity with more DP001 addition. After the plateau region there was an observed increase in suspension viscosity with DP001. These observations were in agreement with the observations from the adsorption tests. The adsorption tests showed that DP001 was adsorbed onto the surfaces of magnetite #1 media particles. The results also showed that the optimum loading for DP001 on magnetite #1 media particles was 0.6 g DP001 / kg Magnetite #1. The adsorption tests show that although the minimum amount of DP001 added during the rheometry tests was 1 g DP001 / Mag #1, this value is above the optimum loading, meaning that the plateau region had already been reached at 1g DP001 / kg Mag #1. This explained why there was an increase in suspensions viscosity for some of the suspensions for DP001 in excess of 1 g DP001 / kg Mag #1.

Rheometry tests on ferrosilicon / magnetite #1 mixtures also showed viscosity reductions with the addition of DP001. The observations from these experiments were similar to those of magnetite #1 suspensions. There was an increase in suspension viscosity for some DP001 additions. The adsorption results illustrate that the viscosity reduction is due to DP001 adsorbing onto the magnetite #1 surfaces, and not onto the ferrosilicon surfaces. The increase in suspension viscosity also illustrates that the optimum loading had been exceeded for some of the suspensions, and the either the plateau or viscosity increase region had been reached. The results showed that the effect of DP001 increased with the amount of magnetite #1 present in the suspensions, confirming again that DP001 adsorbed onto the magnetite #1 media particles.

During the DP001 tests it was important to know what the Reynolds number in the annular region of the rheometer was. It was found that, for most suspensions, the Reynolds criterion for laminar flow conditions was satisfied. At shear rates below 1000 s^{-1}, all the suspensions satisfied Reynolds criterion. This result was important because it showed that since laminar was prevalent in the annular space, the viscosity of the suspensions was responsible for the drag forces induced by the suspensions. Thus, it was concluded that DP001 did actually reduce the drag forces in the suspensions by reducing the viscosity of the suspensions.

Malvern analyzer tests and SEM tests showed that magnetite #2 media particles were much coarser and smoother than either the ferrosilicon or magnetite #1 media particles. When these suspensions were mixed at different ratios with both ferrosilicon and magnetite #1 media particles, the suspensions showed a significant decrease in suspension viscosity. The decrease in suspension viscosity was enhanced by the presence of magnetite #2 media particles, the viscosity decreasing with the amount of magnetite #2 present. When the viscosity reductions caused by

magnetite #2 were compared to those due to DP001 additions, the effect of the former was much greater. However, magnetite #2 resulted in a decrease in the suspension stability, particularly with ferrosilicon suspensions. It can thus be concluded that the introduction of a much coarser size distribution reduce the viscosity of the suspensions more than the dispersant DP001.

Separation tests using magnetite #1 suspensions at specific gravities 1.57 and 1.83 showed that the separation efficiency was much higher at the lower specific gravity. The results also showed that the separation efficiency was much higher for the coarser ore coal size range. The separation efficiency decreased for coal samples with a larger size range. The addition of DP001 to these suspensions resulted in an increase of the separation efficiency for some DP001 additions. A mixture of magnetite #1 and magnetite #2 suspensions at specific gravity 1.70 showed much higher separation efficiency compared to those for magnetite #1 only suspensions. Addition of DP001 to these suspensions resulted in an increase in separation efficiency for some of the coal size ranges, but the separation efficiency decreased upon the further addition of DP001. It can be concluded from these results that DP001 generally improves the separation efficiency in the heavy medium separations, and that the presence of a coarser size distribution media also improves the separation efficiency.

Chapter 9

Recommendations

9.1 Rheometer Design

- The rheometer used in this project could not adequately measure the shear stress of the suspensions at low shear rates, due to the settling nature of the suspensions. This shortfall meant that the yield stresses of the suspensions, if present, at high specific gravities could not be determined. The yield stress values are important in the evaluation of the properties of heavy medium suspensions. Thus, the rheometer would have to be re-designed such that it was able to measure these values.

- The rheometer should also be designed such that measurements at various suspensions temperatures are possible. This can be achieved through the use of a water jacket or water bath. It is a known fact that viscosity is highly dependant on temperature, and since the temperatures in industrial separations may vary, it is important to know what effect this could have on the viscosity of the suspensions. Adsorption is also a function of temperature. In most adsorption tests, the adsorption rate decreases with temperature. Since it has been postulated that DP001 affects the viscosity of the suspensions by adsorbing onto the media surfaces, it is important to know what the effect of DP001 at various temperatures would be. During the separation tests it was observed that the suspension temperature was as high as 37 ^{0}C. Hence, knowing what the effect of DP001 is at these temperatures would help relate the separation tests to the rheometry tests more efficiently. All this is dependant on the ability of the rheometer to make measurements at wider range temperatures.

9.2 Adsorption Tests

- Adsorption tests should be carried out on all the suspensions, including those with high fines content. This means that a more appropriate filter would have to be used, such that no fine particles end up in the filtrate. Adsorption should also be carried out at a range of temperatures, such that it is possible to construct isotherms for DP001 adsorption on the media particle surfaces. These results could then be compared to the rheometry tests to determine the maximum DP001 loading or dosage at a particular temperature.

- Alternatively, a zeta-potential meter can be used to measure the extent of DP001 adsorption the media particle surfaces. Zeta meters are extensivley used to in industrial processes to measure the extent of solid particle dispersion or agglomeration due to a surface active chemical.

9.3 Dense Medium Cyclone Loop

- A flow meter or pressure gauge should be installed at the inlet pipe of the cyclone to accurately measure the cyclone inlet flowrate or pressure. The inlet flowrate or pressure is important to the separation efficiency. The magnitude of these values is important because they determine the tangential velocity at the cyclone inlet, which in turn determines the average shear rate within the cyclone. It is thus important to make sure that these values are carefully monitored during experimentation. And this can only be done through accurate measurement.

- The cyclone loop should be redesigned such that it is capable of handling suspensions with high specific gravities. The set up used for this project could not handle magnetite suspensions with specific gravities in excess of 2.0. A more powerful pump, together with a redesign of the pipe circuitry would have to be used to achieve this. Separation measurements with slime contaminated ferrosilicon should also be made using the cyclone. Measurements with DP001 additions would have to be done at specific gravities in excess of 3.0. Thus, the cyclone loop should be capable of handling such a high solids loading.

REFERENCES

Aplan F.F., Spedden H.R., "Viscosity Control in Heavy-Media suspensions", *VII International Mineral Processing Congress*: Vol.1, AIM (American Institute of Mining), Presented 20-24 September 1964 AIM

Barnes H.A., 2000. Measuring the viscosity of large-particle (and flocculated) suspensions-a note on the necessary gap size of rotational viscometers, *Journal of non-Newtonian fluid mechanics* **94 (2)**, 213-217.

Barnes H.A., Hutton J.F., Walters K., 1989. An Introduction to Rheology, 3, Elsevier.

Blair G.W.S., 1969. Elementary Rheology. Academic Press (London and New York).

Boardman G., Whitmore R.L., 1960. Yield Stress exerted on a body immersed in a Bingham Fluid. *Nature* **187**, 50-51.

Bozzato P., Bevilacqua P., Ferrara G., 2000. Static and Dynamic Stability in Dense Medium Separation Processes. *Mineral Processing and Extractive Metallurgy Review* **20 (1-3)**, 197-214.

Burt R.O., 1984. Gravity concentration techniques, Developments in Mineral processing, 5, Elsevier.

Collins B., Napier-Munn T.J., Sciarone M., 1974. The production, properties, and selection of ferrosilicon powders for heavy-medium separation. *Journal of the South African Institute of Mining and Metallurgy (December)*, 103-115.

Collins D.N., Turnbull T., Wright B.A., Ngan W., 1983. Separation efficiency in dense medium cyclones, *Transactions of the Institution of Mining and Metallurgy Section C* **92**, 39-51.

Dunglison M.E., Napier-Munn T.J., Shi F.N., 1999. The Rheology of ferrosilicon dense medium suspensions. *Mineral Processing and Extractive Metallurgy Review* **20 (1)**, 183-196.

Eirich F.R., 1956. Rheology: Theory and Applications, Volume 1. Academic Press Publishers Inc., New York.

Ferrara G., Bevilacqua P., De Lorenzi L., Zanin M., 2000. The influence of particle shape on the dynamic dense medium separation of plastics, *International Journal of Minerals Processing* **59**, 225-235.

Ferrara G., Lapsin R., Bevilacqua P., 1992. Modelling the rheological behaviour of dense media and design of medium circuits in dynamic DMS processes, *Minerals Engineering* **9 (10-12)**, 1123-1134.

Ferrara G., De Lorenzi L., Bevilacqua P., 1999. Rheology of low density suspensions in dense medium separation of post-consumer plastics. *Coal Preparation* **21 (2)**, 197-209

Ferrara G., Schena G.D., 1986. Influence of contamination and type of ferrosilicon on viscosity and stability of dense media. *Transactions of the Institution of Mining and Metallurgy* **95**, C211-C215.

Ferrini F., Ercolani D., de Cindio B., Nicodemo L., Nicolais L., Ranaudo S., 1979 Shear viscosity of settling suspensions. *Rheologica Acta* **18**, 289-296.

Geer M.R., Sokaski M., West J.M., Yancey H.F., 1957. The role of viscosity in Dense-Medium Coal Cleaning, United Bureau of Mines, R.I. 5354.

Goosen P., du Toit J., 2004. Development of a novel viscometer for use with FeSi and Magnetite Dense Medium Slurries, Mineral Processing 5-6 August 2004, Somerset West, South Africa

Govier G.W., Shook C.A., Lilge E.O., 1957. The rheological properties of water suspensions of finely subdivided magnetite, galena, and ferrosilicon, *Transaction of the Canadian Institute of Mining and Metallurgy* **60**, 147-154.

Grobler J.D., Sandenbergh R.F., Pistorius P.C., 2002. The stability of ferrosilicon dense medium suspensions, *Journal of the South African Institute of Mining and Metallurgy* **102 (2)**, 83-86.

Harris J., 1977. Rheology and non-Newtonian flow, Longman, London and New York.

He Y.B., Laskowski J.S., 1995. Dense Medium cyclone separation of fine particles Part 1: The effect of medium split ratio on dense medium cyclone performance. *Coal Preparation* **6**, 1-25.

He Y.B., Laskowski J.S., 1995. Dense Medium cyclone separation of fine particles Part 2: The effect of medium composition on dense medium cyclone performance, *Coal Preparation* **16**, 27-49.

He Y.B., Laskowski J.S., Klein B., 2001. Particle movement in non-Newtonian slurries: The effect of yield stress on dense medium separation. *Chemical Engineering Science* 56 (9), 2001
He Y.B., Laskowski J.S., 1999. Rheological Properties of Magnetite Suspensions. *Mineral processing and extractive metallurgy review* **20**, 167-182.

He Y.B., Laskowski J.S., Effect of dense medium properties on the separation of a dense medium cyclone, Minerals Engineering, Vol. 7, No. 2-3, pp 209-221, 1994

Horsfall D.W., 1993. Coal preparation and usage-Coal processing for management, Volume 2, Coal Publications (Pty) Ltd.

Jinescu V.V., 1974. The rheology of suspensions. *International Chemical Engineering* **14**, 397-420.

Johnson S.B., Franks G.V., Scales P.J., Boger D.V., Healy T.W., 2000. Surface chemistry-rheology relationship in concentrated mineral suspensions, *International Journal of Mineral Processing* **58**, 267-304.

Jones R.L., Horsely R.R., 1999. Viscosity Modifiers in the mining industry, *Mineral Processing and Extractive Metallurgy Review* 20 (1), 215-223.

Klein B., Laskowski J.S., Partridge S.J., 1990. Rheology of Unstable Mineral Suspensions. *Coal Preparation* **8**, 123-134.

Lapsin R., 1988. Rheological Characterization of Magnetite Dense Media. *Coal preparation* **5**, 167-183.

Lapsin R., Ferrara G., Ruscio E., Schena G.D., 1990. Modelling the rheological behaviour of dense media for coal processing. *Coal Preparation* **8**, 167-183.

Lilge E.O., Fregen T.E., Purdy G.R., 1958. Apparent viscosities of heavy media and the Driessen cone. *Transactions of the Institution of Mining and Metallurgy*, **67**, 229-249.

Laskowski J.S., Evaluation of flocculants and dispersants through rheological tests, Polymers in Mineral Processing, Met Soc, pp 541-555

Laskowski J.S., Ralston J., Colloid chemistry in Mineral Processing. *Developments in Mineral Processing*, **12**, 150-171.

Mabuza N.T., Pocock J., Loveday B.K., 2005. The use of surface active chemicals in heavy medium viscosity reduction. *Minerals Engineering* **18 (1)**, 25-31.

Mooney M., 1951. The viscosity of a concentrated suspension of spherical particles. *Journal of Colloid Science* **6**, 162-170.

Myburgh H.A., 1966. Influence of quality of ferrosilicon on rheology of dense medium and ability to reach higher densities. *Mineral processing and extractive metallurgy* **112**, C39-C43.

Napier-Munn T.J., 1990. The effect of dense medium viscosity on separation efficiency. *Coal Preparation* **8**, 145-165.

Napier-Munn T.J., Shi F.N., 1996. Measuring the rheology of slurries using an on-line viscometer. *International Journal of Minerals Processing* **47**, 153-176.

Napier-Munn T.J., Shi F.N., 1996. A model for slurry rheology. *International Journal of Minerals Processing*. **47 (1-2)**, 103-124.

Perry R.H., Green D.W., 1999. Perry's Chemical Engineers' Handbook, McGraw Hill.

Pryor E.J., 1965. Mineral Processing, 3rd Edition, Elsevier Publishing Co Ltd.

Reeves T.J., 1985. On-line viscometer for mineral slurries. *Transactions of the Institution of Mining and Metallurgy* **94**, C201-208.

Reeves T.J., 1990. On-line viscosity measurement under industrial conditions. *Coal Preparation* **8**, 135-144.

Rodis F., Cremer J., 1960. Why an Atomized ferrosilicon proves superior for heavy media plants. *Mining World* **22**, 36-39.

Scott Blair G.W., 1969. Elementary Rheology, Academic Press London and New York,.

Slatter P., Knowlton J., Masalova I., Perret D., 2000. Practical Rheology Course, Cape Technikon Rheology Centre, November 2000

Valentyik L., 1972, Rheological Properties of Heavy Media Suspensions Stabilized by Polymers. *Transactions of the American Institute of Mining, Metallurgical, and Petroleum Engineers, Incorporated* **252**, 99-105.

Valentyik L., Patton T., 1976, Rheological Properties of Heavy Media Suspensions Stabilized by Polymers and Bentonites. *Transactions of the American Institute of Mining, Metallurgical, and Petroleum Engineers, Incorporated* **260**, 113-118.

Whitmore R.L., Boardman G., 1960. Yield Stress exerted on a body immersed in a Bingham Fluid. *Nature: International weekly journal of science* **187**, 50-51.

Whorlow R.W., 1980. Rheological Techniques, Ellis Horwood Publishers.

Williams R.A., Kelsall G.H., Gochin R.J., 1986. Differences in physical properties of milled and atomised ferrosilicon powders. *Transactions of the Institution of Mining and Metallurgy* **95**, C215-C221.

Wills B.A., 1997. Mineral Processing Technology, 6th Edition, Butterworth-Heinemann, Oxford.

Appendices

Appendix 1

Raw Data and Experimental Results

A1.1 Viscometer Calibration

A1.1.1 Aim of the Experiment

The aim of these experiments was to calibrate the viscometer using glycerol-water solutions. The design of most viscometers does not enable them to give the true viscosities of any fluid. Therefore it is important to calibrate these viscometers against solutions of known viscosity. From these results a correction factor can be obtained, which can be multiplied to the values obtained by the viscometer, thereby giving a more accurate value of the viscosity of the fluid being measured.

A1.1.2 Experimental Conditions

Glycerol-water solutions with glycerol mass fractions equal to 0.95, 0.90, 0.85, and 0.80 were used in the calibration of the viscometer. All measurements were taken at a room temperature of 26 °C. The viscosity of the solutions was measured using both Rheometer 1 and Rheometer 2. Independent measurements were also carried out using a calibrated Brookfield viscometer. The Brookfield viscometer results were taken as the true viscosity of the solutions. These results were then compared to those obtained from Rheometer 1and Rheometer 2 in order to get a correction factor for the latter viscometers. The calibration experimental procedure is contained in Appendix A2.

The Brookfield viscometer (model: RVT) comes equipped with different size spindles for measurement of fluid viscosity, ranging from large spindles to small spindles. For suspensions with lower viscosities the larger spindles are used because they have a much larger surface area. This enables measurement of meaningful shear stress results for these fluids at the set rotational speeds. In these experiments spindle #1 was used, with spindle #1 being the largest of the available spindles. As will be explained in Appendix A2, measurements are taken at different spindle rotational speeds, and the viscosity is obtained by multiplying the viscometer dial reading at a particular speed with a spindle factor. The factors for the spindle used are given below.

Table A1.1 Multiplication factors for Spindle #1

Spindle # 1	
Speed	**Factor**
0.5	200
1	100
2.5	40
5	20
10	10
20	5
50	2
100	1

A1.1.3 Experimental Results

A1.1.3.1 Brookfield Viscometer Results

Using the multiplication factors in Table A1.1, the following viscosities were obtained from the Brookfield viscometer.

Table A1.2 Brookfield viscosities for 0.95 w/w glycerol solution

Speed	Factor	Dial reading	Viscosity (Pa.s)
2.5	40	4.00	0.160
5	20	8.00	0.160
10	10	16.00	0.160
20	5	31.50	0.158
50	2	80.00	0.160
		Average	0.160

Table A1.3 Brookfield viscosities for 0.90 w/w glycerol solution

Speed	Factor	Dial reading	Viscosity (Pa.s)
2.5	40	2.50	0.100
5	20	5.00	0.100
10	10	9.50	0.095
20	5	18.50	0.093
50	2	45.50	0.091
		Average	0.096

Table A1.4 Brookfield viscosities for 0.85 w/w glycerol solution

Speed	Factor	Dial reading	Viscosity (Pa.s)
2.5	40	1.50	0.060
5	20	3.00	0.060
10	10	6.00	0.060
20	5	11.00	0.055
50	2	26.00	0.052
		Average	0.057

Table A1.5 Brookfield viscosities for 0.80 w/w glycerol solution

Speed	Factor	Dial reading	Viscosity (Pa.s)
2.5	40	1.25	0.050
5	20	2.00	0.040
10	10	4.00	0.040
20	5	6.50	0.033
50	2	21.75	0.044
		Average	0.041

A1.1.3.2 Rheometer #1 Calibration Results

The results in this section show the shear stress versus shear rate curves for glycerol-water solutions measured using Rheometer #1. The results show that all the solutions behave as Newtonian fluids.

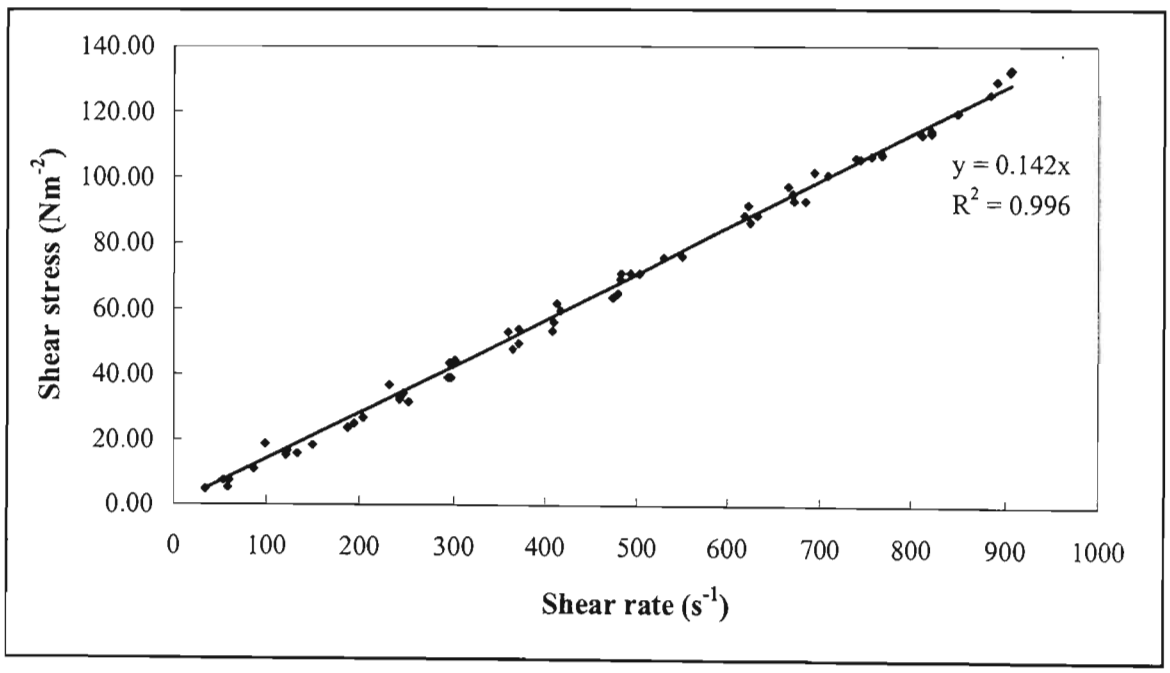

Figure A1.1 Rheometer #1 rheogram at 0.80 w/w glycerol

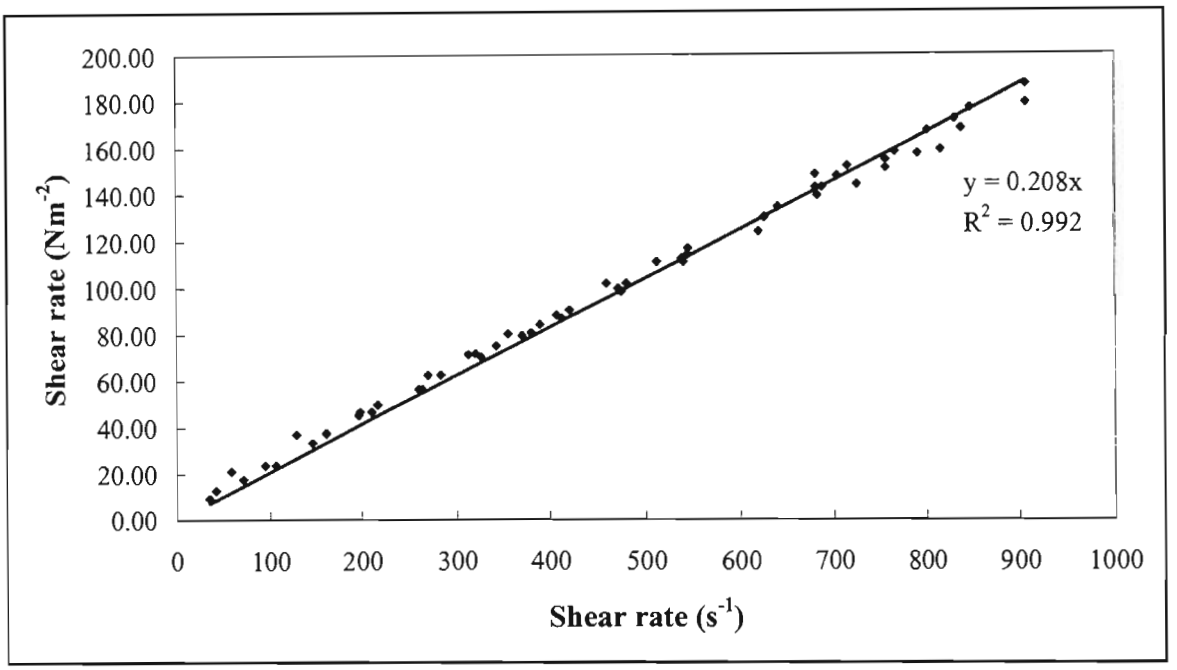

Figure A1.2 Rheometer #1 rheogram at 0.85 w/w glycerol

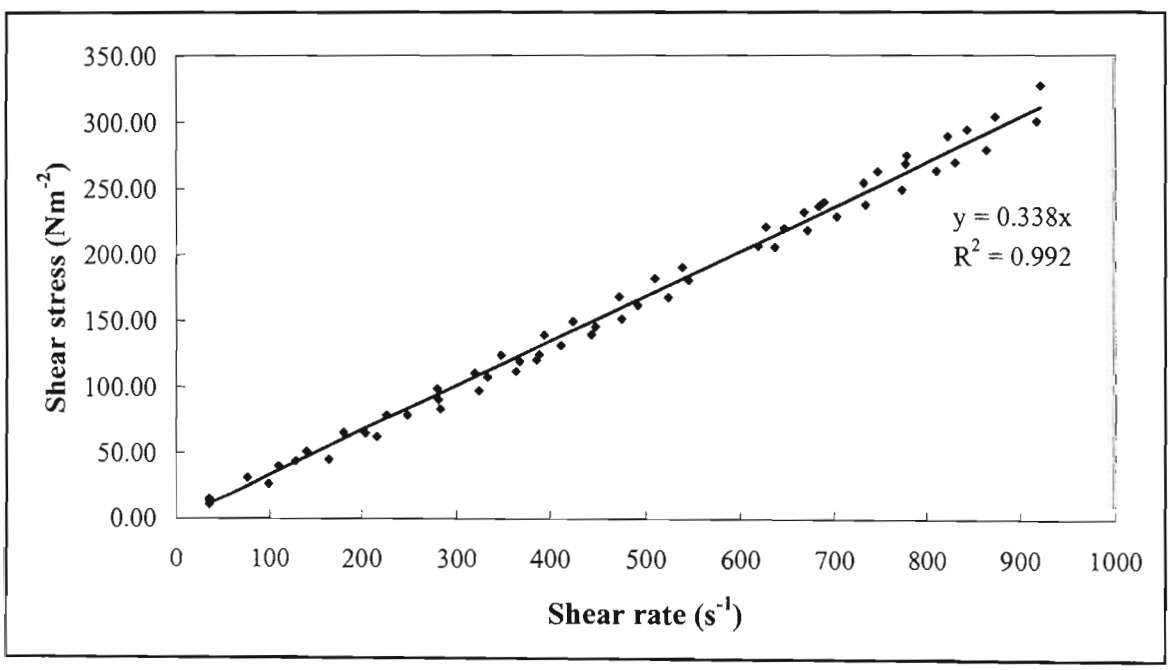

Figure A1.3 Rheometer #1 rheogram at 0.90 w/w glycerol

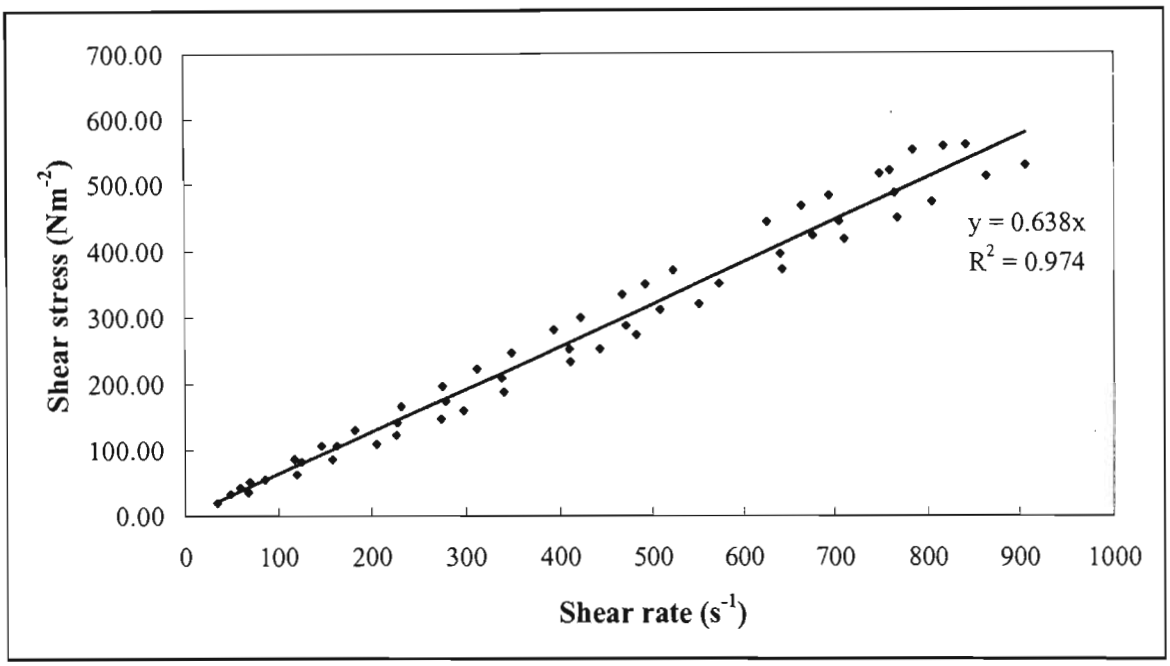

Figure A1.4 Rheometer #1 rheogram at 0.95 w/w glycerol

The gradients of the graphs above were taken as the viscosity of the solutions. Using these values, together with the Brookfield viscometer results, the following correction factors were obtained:

Table A1.6 Correction factors for Rheometer #1

Mass fraction (w/w)	μ (Pa.s)		Correction factor ($1/c_L$)
	Rheometer	Brookfield	
0.95	0.638	0.160	0.25
0.90	0.338	0.097	0.29
0.85	0.208	0.057	0.27
0.80	0.142	0.041	0.29

The viscosities obtained using the Brookfield viscometer were then plotted against those obtained using Rheometer #1. These results are illustrated in Figure A1.5.

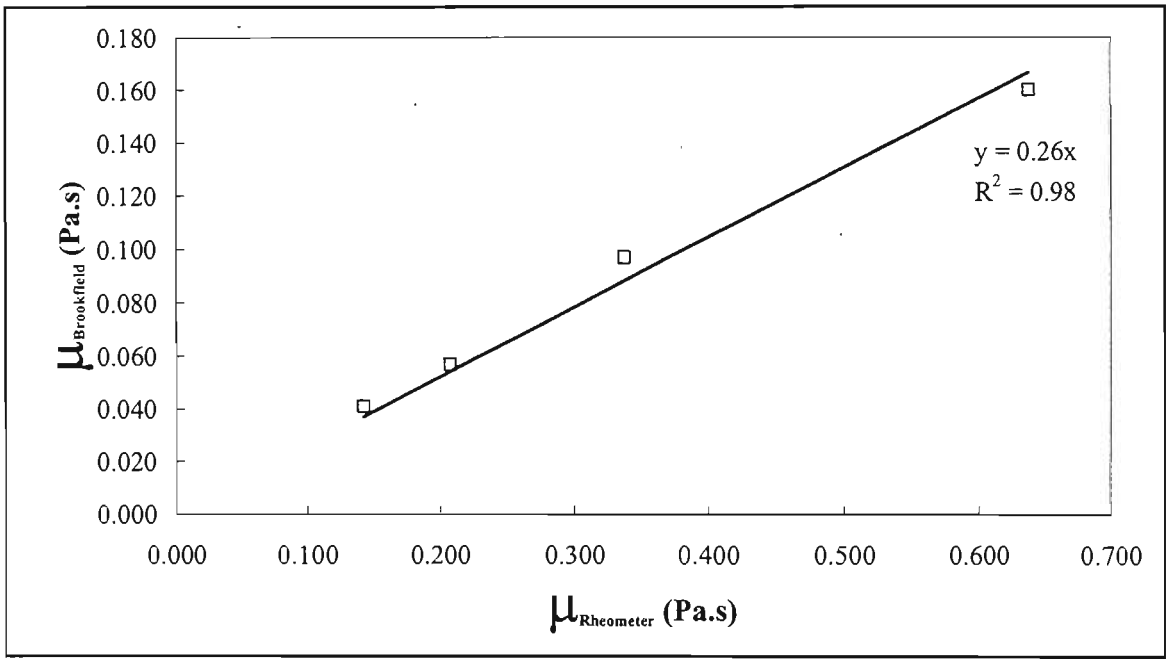

Figure A1.5 Rheometer #1 calibration graph

The gradient of the above graph gives the average correction factor ($1/c_L$) for Rheometer #1. For Rheometer #1, this value is equal to 0.26.

A1.1.3.3 Rheometer #2 Calibration Results

The methods used in this section are similar to those used in the previous section.

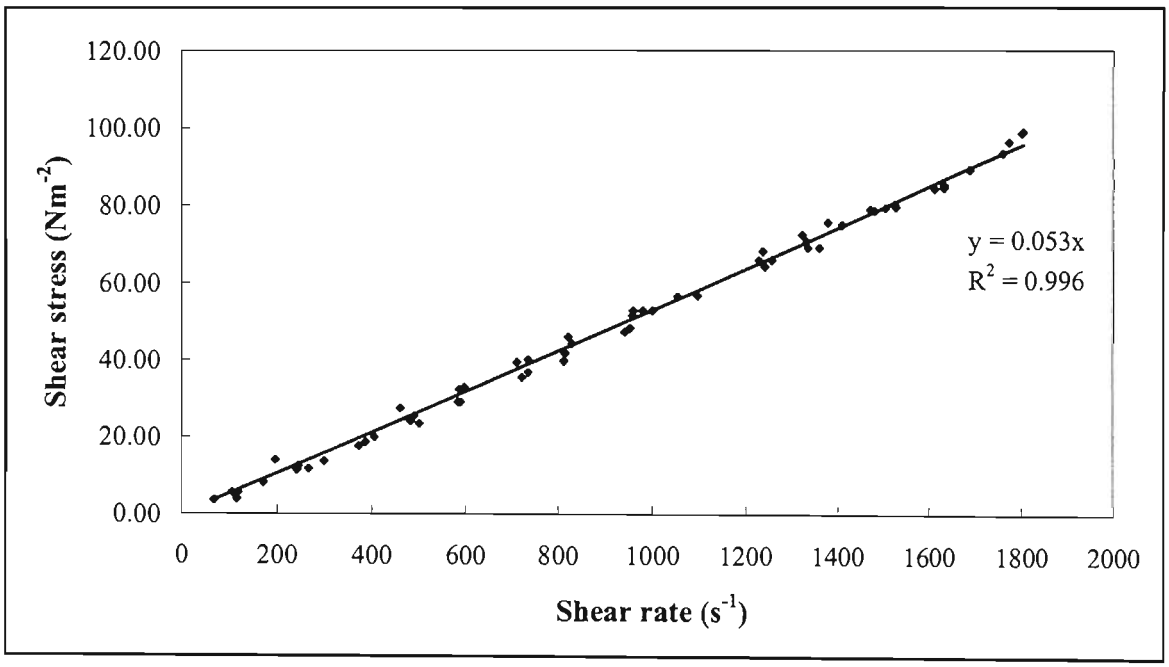

Figure A1.6 Rheometer #2 rheogram at 0.80 w/w glycerol

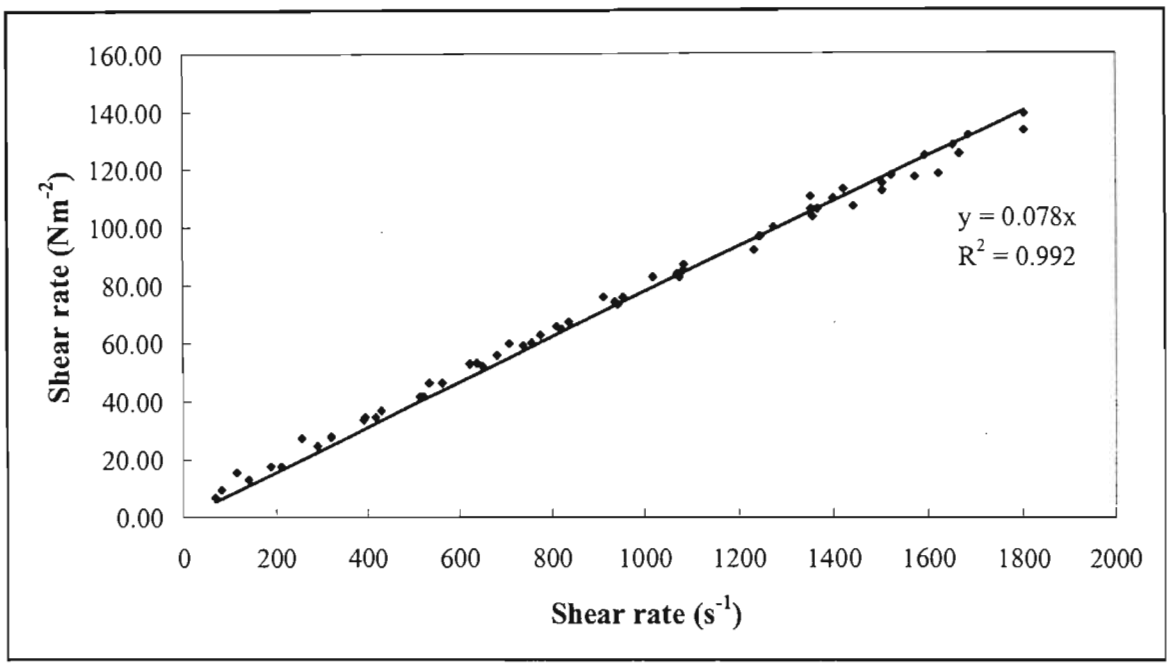

Figure A1.7 Rheometer #2 rheogram at 0.85 w/w glycerol

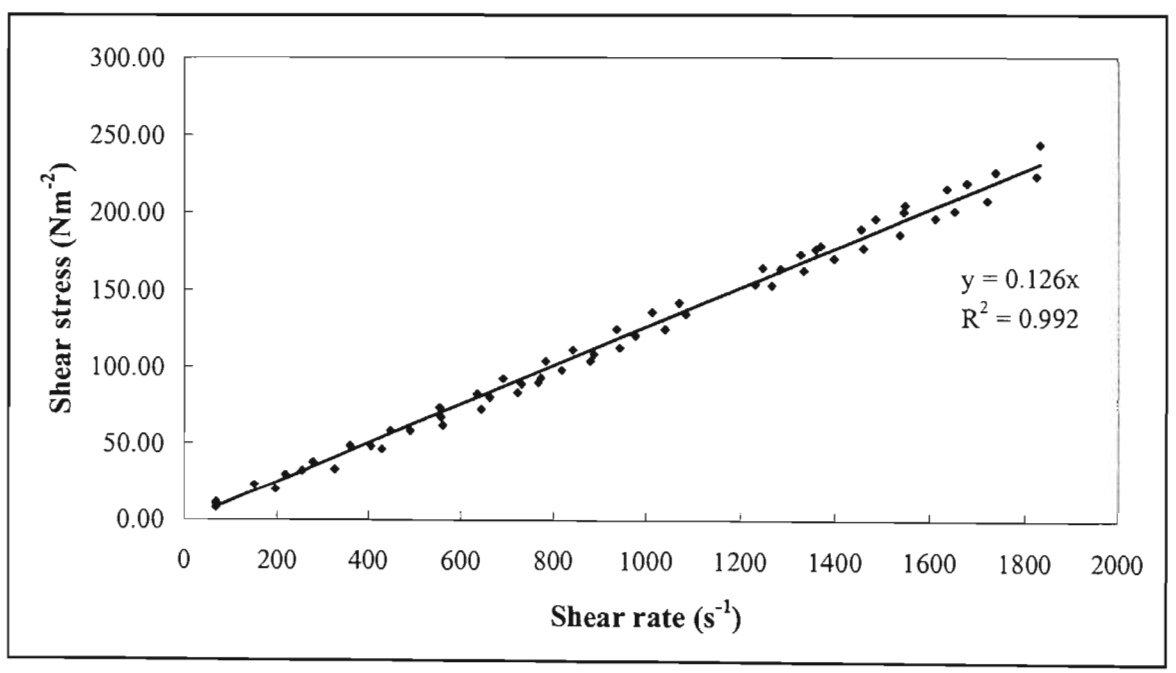

Figure A1.8 Rheometer #2 rheogram at 0.90 w/w glycerol

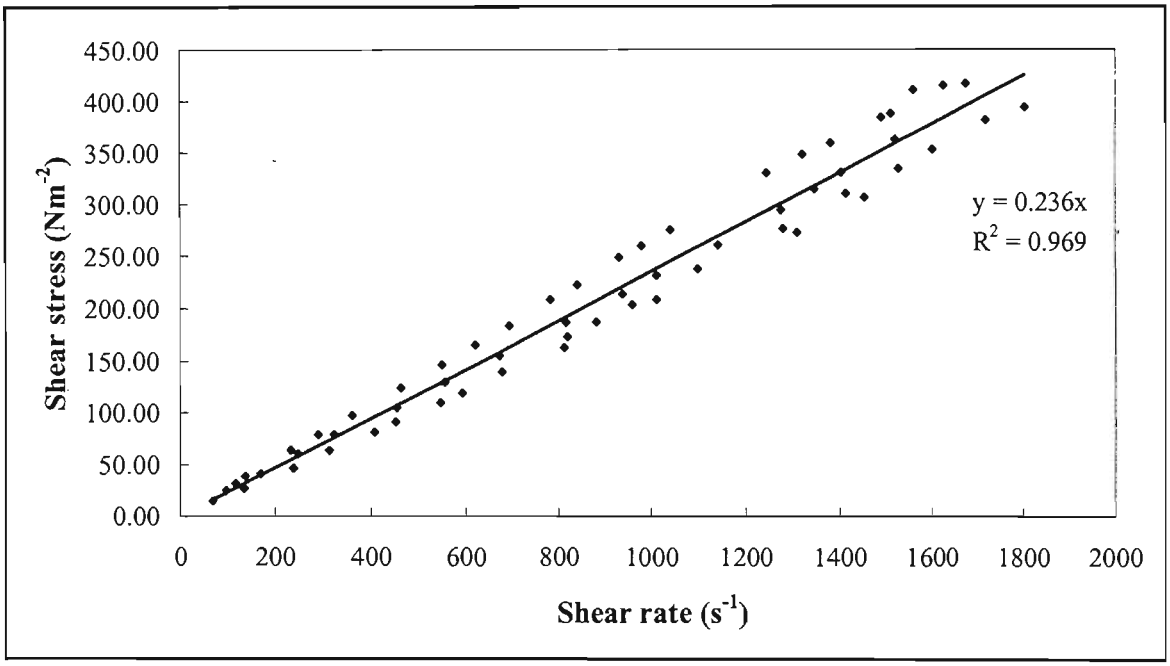

Figure A1.9 Rheometer #2 rheogram at 0.95 w/w glycerol

The viscosities obtained using Rheometer #2 were also compared to those obtained using the Brookfield viscometer. These are illustrated in Table A1.7.

Table A1.7 Correction factors for Rheometer #2

Mass fraction	μ (Pa.s)		Correction factor
(w/w)	Rheometer	Brookfield	(c_L)
0.95	0.236	0.160	0.68
0.90	0.126	0.097	0.77
0.85	0.078	0.057	0.73
0.80	0.053	0.041	0.77

The calibration graph for Rheometer #2 is shown below.

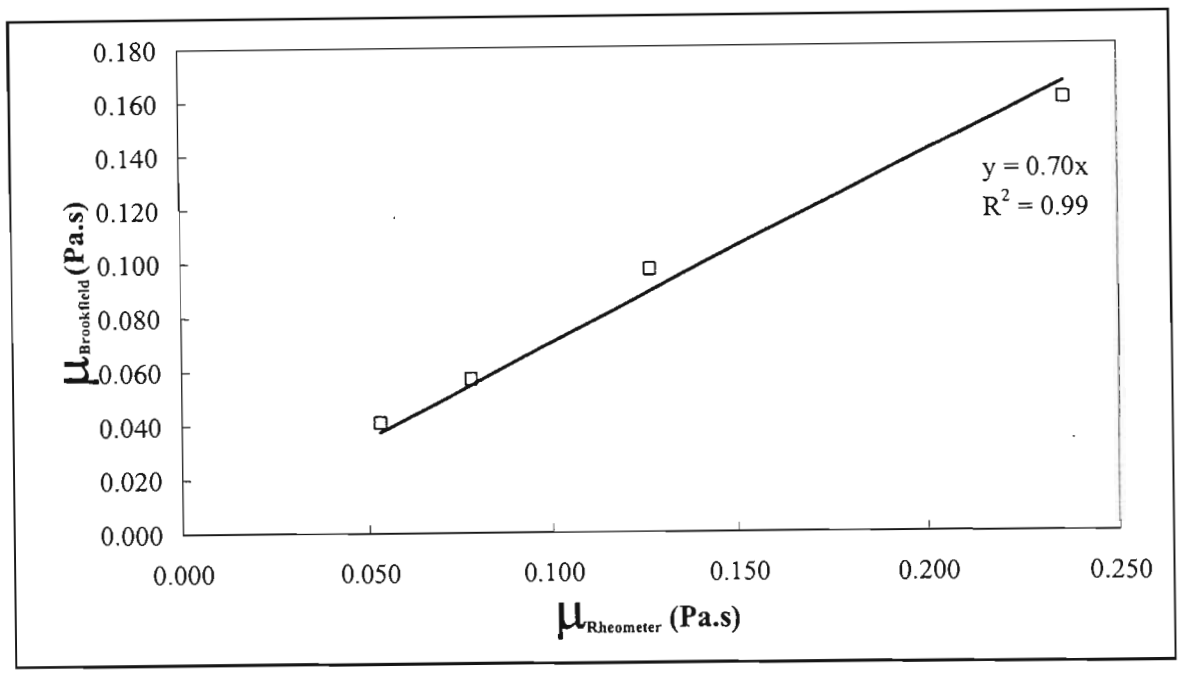

Figure A1.10 Rheometer #2 Calibration graph

The graph shows that the correction factor (1/cL) for Rheometer #2 is equal to 0.70.

A1.2 Experiment Series A: The Effect of DP001 on the Viscosity of Heavy Medium Suspensions

A1.2.1 The Effect of DP001 on ferrosilicon suspensions

A1.2.1.1 Aim of the Experiment

The purpose of these experiments was to investigate the effect of DP001 on ferrosilicon suspensions contaminated with smectite slime. The shear stress and shear rate were measured for plain suspension, suspensions contaminated with the slime, and suspension with different concentrations of DP001. The rheograms obtained from these results could then be used to evaluate the effect of DP001 by evaluating the difference in viscosity of the suspensions. Ferrosilicon suspensions with specific gravities 2.0-3.0 were used. The amount of clay added was 5 % and 10 % of the mass ferrosilicon used to make up the suspension. DP001 additions were made at 1 gram / kilogram ferrosilicon.

A1.2.1.2 Experimental Conditions

All rheological measurements were carried out at an average room temperature between 24-28 °C. The mass of water used to prepare the ferrosilicon suspensions was 100 grams. The mass of the ferrosilicon needed to prepare each sample was calculated from Equation A1.1.

$$x = \frac{100s(D-1000)}{D(s-1000)} \qquad \text{(A1.1)}$$

where x is the percentage solids, s is the solids density (kgm^{-3}), and D is the suspension density (kgm^{-3}).

Using x and the mass water, the mass ferrosilicon mass needed at each specific gravity could be determined. The amount of ferrosilicon, slime, and DP001 are given below:

Table A1.8 Mass ferrosilicon used in suspensions

D / kgm^{-3}	x / %	M_{FeSi} / g
2000	59	142
2100	61	160
2200	64	178
2300	66	197
2400	68	217
2500	70	238
2600	72	260
2700	74	283
2800	75	307
2900	77	333
3000	78	360

Table A1.9 Mass of slime added to ferrosilicon suspensions

	Mass clay / slime (g)	
D / kgm^{-3}	5%	10%
2000	7.1	14.2
2100	8.0	16.0
2200	8.9	-
2300	9.9	-
2400	10.9	-
2500	11.9	-
2600	13.0	-
2700	14.2	-
2800	15.4	-
2900	16.6	-
3000	18.0	-

Table A1.10 Mass DP001 added to ferrosilicon suspensions

	Mass DP001(g) / kg FeSi		
D / kgm^{-3}	1g	2g	5g
2000	0.14	0.28	0.71
2100	0.16	0.32	0.80
2200	0.18	0.36	0.89
2300	0.20	0.39	0.99
2400	0.22	0.43	1.09
2500	0.24	0.48	1.19
2600	0.26	0.52	1.30
2700	0.28	0.57	1.42
2800	0.31	0.61	1.54
2900	0.33	0.67	1.66
3000	0.36	0.72	1.80

A1.1.1.3 Experimental Results

Table A1.11 Plain ferrosilicon (sp.gr.2.0)

ϕ (rpm)	Force (N)	σ (Nm)	σ_c (Nm)	τ (Nm^{-2})	ω (rad/s)	γ (s^{-1})	μ (Pa.s)
289	0.010	0.0008	0.0005	2.29	30	394	0.0058
397	0.014	0.0011	0.0007	3.20	42	541	0.0059
493	0.018	0.0014	0.0009	4.12	52	672	0.0061
548	0.021	0.0016	0.0011	4.81	57	747	0.0064
639	0.026	0.0020	0.0014	5.95	67	871	0.0068
766	0.032	0.0024	0.0017	7.33	80	1044	0.0070
861	0.038	0.0029	0.0020	8.70	90	1174	0.0074
960	0.045	0.0034	0.0024	10.30	101	1309	0.0079
1071	0.053	0.0040	0.0028	12.13	112	1460	0.0083
1150	0.061	0.0046	0.0032	13.96	120	1568	0.0089
1253	0.071	0.0053	0.0037	16.25	131	1709	0.0095
1330	0.082	0.0062	0.0043	18.77	139	1814	0.0104

Table A1.12 Plain ferrosilicon + 10% slime (sp.gr.2.0)

ϕ (rpm)	Force (N)	σ (Nm)	σ_c (Nm)	τ (Nm^{-2})	ω (rad/s)	γ (s^{-1})	μ (Pa.s)
289	0.016	0.0012	0.0008	3.66	30	394	0.0093
358	0.020	0.0015	0.0011	4.58	37	488	0.0094
459	0.026	0.0020	0.0014	5.95	48	626	0.0095
567	0.032	0.0024	0.0017	7.33	59	773	0.0095
651	0.038	0.0029	0.0020	8.70	68	888	0.0098
740	0.044	0.0033	0.0023	10.07	77	1009	0.0100
848	0.052	0.0039	0.0027	11.90	89	1156	0.0103
963	0.060	0.0045	0.0032	13.73	101	1313	0.0105
1068	0.070	0.0053	0.0037	16.02	112	1456	0.0110
1136	0.080	0.0060	0.0042	18.31	119	1549	0.0118
1251	0.098	0.0074	0.0051	22.43	131	1706	0.0132
1343	0.108	0.0081	0.0057	24.72	141	1831	0.0135

Table A1.13 Plain ferrosilicon + 10% slime + 1g DP001/kg (sp.gr.2.0)

ϕ (rpm)	Force (N)	σ (Nm)	σ_c (Nm)	τ (Nm^{-2})	ω (rad/s)	γ (s^{-1})	μ (Pa.s)
289	0.012	0.0009	0.0006	2.75	30	394	0.0070
392	0.018	0.0014	0.0009	4.12	41	535	0.0077
470	0.023	0.0017	0.0012	5.27	49	641	0.0082
547	0.028	0.0021	0.0015	6.41	57	746	0.0086
658	0.034	0.0026	0.0018	7.85	69	897	0.0088
767	0.042	0.0032	0.0022	9.61	80	1046	0.0092
851	0.047	0.0035	0.0025	10.76	89	1160	0.0093
968	0.056	0.0042	0.0029	12.82	101	1320	0.0097
1063	0.066	0.0050	0.0035	15.11	111	1449	0.0104
1152	0.078	0.0059	0.0041	17.86	121	1571	0.0114
1242	0.088	0.0066	0.0046	20.14	130	1694	0.0119
1352	0.104	0.0078	0.0055	23.81	142	1844	0.0129

Table A1.14 Plain ferrosilicon + 10% slime + 2g DP001/kg (sp.gr.2.0)

ϕ (rpm)	Force (N)	σ (Nm)	σ_c (Nm)	τ (Nm^{-2})	ω (rad/s)	γ (s^{-1})	μ (Pa.s)
283	0.011	0.0008	0.0006	2.52	30	386	0.00653
355	0.016	0.0012	0.0008	3.66	37	484	0.0076
461	0.021	0.0016	0.0011	4.81	48	629	0.0076
546	0.026	0.0020	0.0014	5.95	57	744	0.0080
662	0.032	0.0024	0.0017	7.33	69	903	0.0081
743	0.038	0.0029	0.0020	8.70	78	1013	0.0086
853	0.044	0.0033	0.0023	10.07	89	1163	0.0087
958	0.051	0.0038	0.0027	11.67	100	1306	0.0089
1064	0.063	0.0047	0.0033	14.42	111	1451	0.0099
1152	0.072	0.0054	0.0038	16.48	121	1571	0.0105
1278	0.084	0.0063	0.0044	19.23	134	1743	0.0110
1356	0.096	0.0072	0.0050	21.98	142	1849	0.0119

Table A1.15 Plain ferrosilicon (sp.gr.2.1)

ϕ (rpm)	Force (N)	σ (Nm)	σ_c (Nm)	τ (Nm^{-2})	ω (rad/s)	γ (s^{-1})	μ (Pa.s)
275	0.011	0.0008	0.0006	2.52	29	375	0.0067
347	0.014	0.0011	0.0007	3.20	36	473	0.0068
489	0.020	0.0015	0.0011	4.58	51	667	0.0069
556	0.024	0.0018	0.0013	5.49	58	758	0.0072
646	0.029	0.0022	0.0015	6.64	68	881	0.0075
743	0.035	0.0026	0.0018	8.01	78	1013	0.0079
862	0.042	0.0032	0.0022	9.61	90	1175	0.0082
966	0.051	0.0038	0.0027	11.67	101	1317	0.0089
1049	0.059	0.0044	0.0031	13.51	110	1430	0.0094
1132	0.068	0.0051	0.0036	15.57	119	1544	0.0101
1244	0.077	0.0058	0.0040	17.63	130	1696	0.0104
1364	0.090	0.0067	0.0047	20.56	143	1860	0.0111

Table A1.16 Plain ferrosilicon + 10% slime (sp.gr.2.1)

ϕ (rpm)	Force (N)	σ (Nm)	σ_c (Nm)	τ (Nm^{-2})	ω (rad/s)	γ (s^{-1})	μ (Pa.s)
279	0.015	0.0011	0.0008	3.43	29	380	0.0090
355	0.019	0.0014	0.0010	4.35	37	484	0.0090
482	0.027	0.0020	0.0014	6.18	50	657	0.0094
560	0.033	0.0025	0.0017	7.55	59	764	0.0099
630	0.038	0.0029	0.0020	8.70	66	859	0.0101
759	0.046	0.0035	0.0024	10.53	79	1035	0.0102
859	0.056	0.0042	0.0029	12.82	90	1171	0.0109
963	0.068	0.0051	0.0036	15.57	101	1313	0.0119
1041	0.079	0.0059	0.0041	18.08	109	1419	0.0127
1145	0.087	0.0065	0.0046	19.92	120	1561	0.0128
1233	0.098	0.0074	0.0051	22.43	129	1681	0.0133
1374	0.112	0.0084	0.0059	25.64	144	1874	0.0137

Table A1.17 Plain ferrosilicon + 10% slime + 1g DP001/kg (sp.gr.2.1)

ϕ (rpm)	Force (N)	σ (Nm)	σ_c (Nm)	τ (Nm^{-2})	ω (rad/s)	γ (s^{-1})	μ (Pa.s)
287	0.013	0.0010	0.0007	2.98	30	391	0.0076
398	0.017	0.0013	0.0009	3.89	42	543	0.0072
464	0.023	0.0017	0.0012	5.27	49	633	0.0083
552	0.029	0.0022	0.0015	6.64	58	753	0.0088
649	0.034	0.0026	0.0018	7.78	68	885	0.0088
765	0.044	0.0033	0.0023	10.07	80	1043	0.0097
837	0.053	0.0040	0.0028	12.13	88	1141	0.0106
965	0.067	0.0050	0.0035	15.34	101	1316	0.0117
1064	0.078	0.0059	0.0041	17.86	111	1451	0.0123
1146	0.089	0.0067	0.0047	20.37	120	1563	0.0130
1256	0.102	0.0077	0.0054	23.35	132	1713	0.0136
1346	0.112	0.0084	0.0059	25.64	141	1835	0.0140

Table A1.18 Plain ferrosilicon + 10% slime + 2g DP001/kg (sp.gr.2.1)

ϕ (rpm)	Force (N)	σ (Nm)	σ_c (Nm)	τ (Nm^{-2})	ω (rad/s)	γ (s^{-1})	μ (Pa.s)
283	0.011	0.0008	0.0006	2.52	30	386	0.0065
398	0.016	0.0012	0.0008	3.66	42	543	0.0067
468	0.022	0.0017	0.0012	5.04	49	638	0.0079
540	0.026	0.0020	0.0014	5.95	57	736	0.0081
644	0.032	0.0024	0.0017	7.33	67	878	0.0083
763	0.040	0.0030	0.0021	9.16	80	1040	0.0088
859	0.051	0.0038	0.0027	11.67	90	1171	0.0100
955	0.064	0.0048	0.0034	14.65	100	1302	0.0113
1047	0.073	0.0055	0.0038	16.71	110	1428	0.0117
1142	0.085	0.0064	0.0045	19.46	120	1557	0.0125
1226	0.095	0.0071	0.0050	21.75	128	1672	0.0130
1340	0.108	0.0081	0.0057	24.72	140	1827	0.0135

Table A1.19 Plain ferrosilicon (sp.gr.2.2)

ϕ (rpm)	Force (N)	σ (Nm)	σ_c (Nm)	τ (Nm^{-2})	ω (rad/s)	γ (s^{-1})	μ (Pa.s)
279	0.013	0.0010	0.0007	2.98	29	380	0.0078
361	0.017	0.0013	0.0009	3.89	38	492	0.0079
448	0.020	0.0015	0.0011	4.58	47	611	0.0075
553	0.025	0.0019	0.0013	5.72	58	754	0.0076
660	0.032	0.0024	0.0017	7.33	69	900	0.0081
758	0.038	0.0029	0.0020	8.70	79	1034	0.0084
853	0.045	0.0034	0.0024	10.30	89	1163	0.0089
960	0.052	0.0039	0.0027	11.90	101	1309	0.0091
1037	0.060	0.0045	0.0032	13.73	109	1414	0.0097
1180	0.074	0.0056	0.0039	16.94	124	1609	0.0105
1286	0.084	0.0063	0.0044	19.23	135	1754	0.0110
1353	0.090	0.0068	0.0047	20.60	142	1845	0.0112

Table A1.20 Plain ferrosilicon + 5% slime (sp.gr.2.2)

ϕ (rpm)	Force (N)	σ (Nm)	σ_c (Nm)	τ (Nm^{-2})	ω (rad/s)	γ (s^{-1})	μ (Pa.s)
278	0.017	0.0013	0.0009	3.89	29	379	0.0103
370	0.023	0.0017	0.0012	5.27	39	505	0.0104
464	0.029	0.0022	0.0015	6.64	49	633	0.0105
552	0.035	0.0026	0.0018	8.01	58	753	0.0106
656	0.042	0.0032	0.0022	9.61	69	894	0.0107
749	0.048	0.0036	0.0025	10.99	78	1021	0.0108
838	0.056	0.0042	0.0029	12.82	88	1143	0.0112
964	0.065	0.0049	0.0034	14.88	101	1314	0.0113
1084	0.078	0.0059	0.0041	17.86	114	1478	0.0121
1181	0.088	0.0066	0.0046	20.14	124	1610	0.0125
1267	0.098	0.0074	0.0051	22.43	133	1728	0.0130
1352	0.109	0.0082	0.0057	24.95	142	1844	0.0135

Table A1. 21 Plain ferrosilicon + 5% slime + 1g DP001/kg (sp.gr.2.2)

ϕ (rpm)	Force (N)	σ (Nm)	σ_c (Nm)	τ (Nm^{-2})	ω (rad/s)	γ (s^{-1})	μ (Pa.s)
283	0.015	0.0011	0.0008	3.43	30	386	0.0089
367	0.020	0.0015	0.0011	4.58	38	500	0.0091
456	0.025	0.0019	0.0013	5.72	48	622	0.0092
563	0.032	0.0024	0.0017	7.33	59	768	0.0095
666	0.038	0.0029	0.0020	8.70	70	908	0.0096
780	0.045	0.0034	0.0024	10.30	82	1064	0.0097
849	0.051	0.0038	0.0027	11.67	89	1158	0.0101
946	0.059	0.0044	0.0031	13.51	99	1290	0.0105
1055	0.066	0.0050	0.0035	15.11	110	1439	0.0105
1139	0.076	0.0057	0.0040	17.40	119	1553	0.0112
1232	0.084	0.0063	0.0044	19.23	129	1680	0.0114
1361	0.096	0.0072	0.0050	21.98	143	1856	0.0118

Table A1.22 Plain ferrosilicon + 5% slime + 2g DP001/kg (sp.gr.2.2)

ϕ (rpm)	Force (N)	σ (Nm)	σ_c (Nm)	τ (Nm^{-2})	ω (rad/s)	γ (s^{-1})	μ (Pa.s)
273	0.014	0.0011	0.0007	3.20	29	372	0.0086
367	0.019	0.0014	0.0010	4.35	38	500	0.0087
465	0.025	0.0019	0.0013	5.72	49	634	0.0090
556	0.030	0.0023	0.0016	6.87	58	758	0.0091
646	0.035	0.0026	0.0018	8.01	68	881	0.0091
753	0.042	0.0032	0.0022	9.61	79	1027	0.0094
848	0.048	0.0036	0.0025	10.99	89	1156	0.0095
965	0.056	0.0042	0.0029	12.82	101	1316	0.0097
1051	0.064	0.0048	0.0034	14.65	110	1433	0.0102
1148	0.074	0.0056	0.0039	16.94	120	1565	0.0108
1253	0.084	0.0063	0.0044	19.23	131	1709	0.0113
1350	0.093	0.0070	0.0049	21.29	141	1841	0.0116

Table A1.23 Plain ferrosilicon (sp.gr.2.3)

ϕ (rpm)	Force (N)	σ (Nm)	σ_c (Nm)	τ (Nm^{-2})	ω (rad/s)	γ (s^{-1})	μ (Pa.s)
251	0.013	0.0010	0.0007	2.98	26	342	0.0087
353	0.019	0.0014	0.0010	4.35	37	481	0.0090
472	0.024	0.0018	0.0013	5.49	49	644	0.0085
570	0.029	0.0022	0.0015	6.64	60	777	0.0085
664	0.036	0.0027	0.0019	8.24	70	905	0.0091
753	0.042	0.0032	0.0022	9.61	79	1027	0.0094
860	0.051	0.0038	0.0027	11.67	90	1173	0.0100
965	0.063	0.0047	0.0033	14.42	101	1316	0.0110
1071	0.074	0.0056	0.0039	16.94	112	1460	0.0116
1181	0.087	0.0065	0.0046	19.92	124	1610	0.0124
1232	0.094	0.0071	0.0049	21.52	129	1680	0.0128
1337	0.104	0.0078	0.0055	23.81	140	1823	0.0131

Table A1.24 Plain ferrosilicon + 5% slime (sp.gr.2.3)

ϕ (rpm)	Force (N)	σ (Nm)	σ_c (Nm)	τ (Nm^{-2})	ω (rad/s)	γ (s^{-1})	μ (Pa.s)
261	0.017	0.0013	0.0009	3.89	27	356	0.0109
359	0.023	0.0017	0.0012	5.27	38	490	0.0108
448	0.030	0.0023	0.0016	6.87	47	611	0.0112
572	0.038	0.0029	0.0020	8.70	60	780	0.0112
672	0.046	0.0035	0.0024	10.53	70	916	0.0115
774	0.056	0.0042	0.0029	12.82	81	1055	0.0121
851	0.064	0.0048	0.0034	14.65	89	1160	0.0126
981	0.077	0.0058	0.0040	17.63	103	1338	0.0132
1053	0.086	0.0065	0.0045	19.69	110	1436	0.0137
1174	0.104	0.0078	0.0055	23.81	123	1601	0.0149
1261	0.114	0.0086	0.0060	26.10	132	1719	0.0152
1354	0.122	0.0092	0.0064	27.93	142	1846	0.0151

Table A1.25 Plain ferrosilicon + 5% slime + 1g DP001/kg (sp.gr.2.3)

ϕ (rpm)	Force (N)	σ (Nm)	σ_c (Nm)	τ (Nm^{-2})	ω (rad/s)	γ (s^{-1})	μ (Pa.s)
277	0.014	0.0011	0.0007	3.20	29	378	0.0085
360	0.020	0.0015	0.0011	4.58	38	491	0.0093
451	0.026	0.0020	0.0014	5.95	47	615	0.0097
552	0.032	0.0024	0.0017	7.33	58	753	0.0097
658	0.042	0.0032	0.0022	9.61	69	897	0.0107
757	0.048	0.0036	0.0025	10.99	79	1032	0.0106
867	0.059	0.0044	0.0031	13.51	91	1182	0.0114
933	0.065	0.0049	0.0034	14.88	98	1272	0.0117
1022	0.078	0.0059	0.0041	17.86	107	1394	0.0128
1136	0.088	0.0066	0.0046	20.14	119	1549	0.0130
1242	0.104	0.0078	0.0055	23.81	130	1694	0.0141
1356	0.115	0.0086	0.0060	26.33	142	1849	0.0142

Table A1.26 Plain ferrosilicon + 5% slime + 2g DP001/kg (sp.gr.2.3)

ϕ (rpm)	Force (N)	σ (Nm)	σ_c (Nm)	τ (Nm^{-2})	ω (rad/s)	γ (s^{-1})	μ (Pa.s)
269	0.013	0.0010	0.0007	2.98	28	367	0.0081
374	0.019	0.0014	0.0010	4.35	39	510	0.0085
478	0.025	0.0019	0.0013	5.72	50	652	0.0088
560	0.028	0.0021	0.0015	6.41	59	764	0.0084
648	0.036	0.0027	0.0019	8.24	68	884	0.0093
751	0.045	0.0034	0.0024	10.30	79	1024	0.0101
877	0.058	0.0044	0.0030	13.28	92	1196	0.0111
965	0.067	0.0050	0.0035	15.34	101	1316	0.0117
1049	0.078	0.0059	0.0041	17.86	110	1430	0.0125
1127	0.086	0.0065	0.0045	19.69	118	1537	0.0128
1235	0.095	0.0071	0.0050	21.75	129	1684	0.0129
1376	0.116	0.0087	0.0061	26.55	144	1876	0.0142

Table A1.27 Plain ferrosilicon (sp.gr.2.4)

ϕ (rpm)	Force (N)	σ (Nm)	σ_c (Nm)	τ (Nm^{-2})	ω (rad/s)	γ (s^{-1})	μ (Pa.s)
248	0.015	0.0011	0.0008	3.43	26	338	0.0102
353	0.021	0.0016	0.0011	4.81	37	481	0.0100
435	0.024	0.0018	0.0013	5.49	46	593	0.0093
530	0.030	0.0023	0.0016	6.87	56	723	0.0095
660	0.038	0.0029	0.0020	8.70	69	900	0.0097
757	0.047	0.0035	0.0025	10.76	79	1032	0.0104
853	0.056	0.0042	0.0029	12.82	89	1163	0.0110
943	0.064	0.0048	0.0034	14.65	99	1286	0.0114
1049	0.075	0.0056	0.0039	17.17	110	1430	0.0120
1128	0.088	0.0066	0.0046	20.14	118	1538	0.0131
1242	0.102	0.0077	0.0054	23.35	130	1694	0.0138
1340	0.112	0.0084	0.0059	25.64	140	1827	0.0140

Table A1.28 Plain ferrosilicon + 5% slime (sp.gr.2.4)

ϕ (rpm)	Force (N)	σ (Nm)	σ_c (Nm)	τ (Nm^{-2})	ω (rad/s)	γ (s^{-1})	μ (Pa.s)
249	0.020	0.0015	0.0011	4.58	26	340	0.0135
341	0.028	0.0021	0.0015	6.41	36	465	0.0138
471	0.038	0.0029	0.0020	8.70	49	642	0.0135
590	0.045	0.0034	0.0024	10.30	62	804	0.0128
639	0.048	0.0036	0.0025	10.99	67	871	0.0126
767	0.064	0.0048	0.0034	14.65	80	1046	0.0140
844	0.072	0.0054	0.0038	16.48	88	1151	0.0143
947	0.085	0.0064	0.0045	19.46	99	1291	0.0151
1054	0.096	0.0072	0.0050	21.98	110	1437	0.0153
1140	0.106	0.0080	0.0056	24.27	119	1554	0.0156
1226	0.118	0.0089	0.0062	27.01	128	1672	0.0162
1338	0.132	0.0099	0.0069	30.22	140	1824	0.0166

Table A1.29 Plain ferrosilicon + 5% slime + 1g DP001 (sp.gr.2.4)

ϕ (rpm)	Force (N)	σ (Nm)	σ_c (Nm)	τ (Nm^{-2})	ω (rad/s)	γ (s^{-1})	μ (Pa.s)
277	0.020	0.0015	0.0011	4.58	29	378	0.0121
367	0.025	0.0019	0.0013	5.72	38	500	0.0114
468	0.033	0.0025	0.0017	7.55	49	638	0.0118
536	0.038	0.0029	0.0020	8.70	56	731	0.0119
646	0.046	0.0035	0.0024	10.53	68	881	0.0120
775	0.060	0.0045	0.0032	13.73	81	1057	0.0130
837	0.067	0.0050	0.0035	15.34	88	1141	0.0134
972	0.080	0.0060	0.0042	18.31	102	1325	0.0138
1064	0.088	0.0066	0.0046	20.14	111	1451	0.0139
1120	0.097	0.0073	0.0051	22.20	117	1527	0.0145
1222	0.106	0.0080	0.0056	24.27	128	1666	0.0146
1326	0.121	0.0091	0.0064	27.70	139	1808	0.0153

Table A1.30 Plain ferrosilicon + 5% slime + 2g DP001/kg (sp.gr.2.4)

ϕ (rpm)	Force (N)	σ (Nm)	σ_c (Nm)	τ (Nm^{-2})	ω (rad/s)	γ (s^{-1})	μ (Pa.s)
273	0.017	0.0013	0.0009	3.89	29	372	0.0105
364	0.022	0.0017	0.0012	5.04	38	496	0.0101
472	0.029	0.0022	0.0015	6.64	49	644	0.0103
562	0.035	0.0026	0.0018	8.01	59	766	0.0105
650	0.044	0.0033	0.0023	10.07	68	886	0.0114
752	0.054	0.0041	0.0028	12.36	79	1025	0.0121
871	0.064	0.0048	0.0034	14.65	91	1188	0.0123
968	0.078	0.0059	0.0041	17.86	101	1320	0.0135
1050	0.084	0.0063	0.0044	19.23	110	1432	0.0134
1128	0.093	0.0070	0.0049	21.29	118	1538	0.0138
1214	0.102	0.0077	0.0054	23.35	127	1655	0.0141
1374	0.118	0.0089	0.0062	27.01	144	1874	0.0144

Table A1.31 Plain ferrosilicon (sp.gr.2.5)

ϕ (rpm)	Force (N)	σ (Nm)	σ_c (Nm)	τ (Nm^{-2})	ω (rad/s)	γ (s^{-1})	μ (Pa.s)
290	0.016	0.0012	0.0008	3.66	30	395	0.0093
382	0.023	0.0017	0.0012	5.27	40	521	0.0101
461	0.028	0.0021	0.0015	6.41	48	629	0.0102
542	0.034	0.0026	0.0018	7.78	57	739	0.0105
642	0.043	0.0032	0.0023	9.84	67	875	0.0112
756	0.050	0.0038	0.0026	11.45	79	1031	0.0111
836	0.061	0.0046	0.0032	13.96	88	1140	0.0122
947	0.075	0.0056	0.0039	17.17	99	1291	0.0133
1062	0.086	0.0065	0.0045	19.69	111	1448	0.0136
1138	0.098	0.0074	0.0051	22.43	119	1552	0.0145
1228	0.106	0.0080	0.0056	24.27	129	1674	0.0145
1336	0.116	0.0087	0.0061	26.55	140	1822	0.0146

Table A1.32 Plain ferrosilicon + 5% slime (sp.gr.2.5)

ϕ (rpm)	Force (N)	σ (Nm)	σ_c (Nm)	τ (Nm^{-2})	ω (rad/s)	γ (s^{-1})	μ (Pa.s)
293	0.023	0.0017	0.0012	5.27	31	400	0.0132
393	0.033	0.0025	0.0017	7.55	41	536	0.0141
453	0.042	0.0032	0.0022	9.61	47	618	0.0156
538	0.052	0.0039	0.0027	11.90	56	734	0.0162
657	0.064	0.0048	0.0034	14.65	69	896	0.0164
752	0.074	0.0056	0.0039	16.94	79	1025	0.0165
840	0.084	0.0063	0.0044	19.23	88	1145	0.0168
937	0.096	0.0072	0.0050	21.98	98	1278	0.0172
1047	0.108	0.0081	0.0057	24.72	110	1428	0.0173
1136	0.120	0.0090	0.0063	27.47	119	1549	0.0177
1232	0.135	0.0101	0.0071	30.90	129	1680	0.0184
1318	0.148	0.0111	0.0078	33.88	138	1797	0.0189

Table A1.33 Plain ferrosilicon + 5% slime + 1g DP001/kg (sp.gr.2.5)

ϕ (rpm)	Force (N)	σ (Nm)	σ_c (Nm)	τ (Nm^{-2})	ω (rad/s)	γ (s^{-1})	μ (Pa.s)
294	0.018	0.0014	0.0009	4.12	31	401	0.0103
334	0.022	0.0017	0.0012	5.04	35	455	0.0111
438	0.029	0.0022	0.0015	6.64	46	597	0.0111
551	0.038	0.0029	0.0020	8.70	58	751	0.0116
638	0.049	0.0037	0.0026	11.22	67	870	0.0129
741	0.062	0.0047	0.0033	14.19	78	1010	0.0140
849	0.076	0.0057	0.0040	17.40	89	1158	0.0150
950	0.096	0.0072	0.0050	21.98	99	1295	0.0170
1033	0.109	0.0082	0.0057	24.95	108	1409	0.0177
1150	0.124	0.0093	0.0065	28.39	120	1568	0.0181
1231	0.134	0.0101	0.0070	30.67	129	1679	0.0183
1336	0.147	0.0110	0.0077	33.65	140	1822	0.0185

Table A1.34 Plain ferrosilicon + 5% slime + 2g DP001/kg (sp.gr.2.5)

ϕ (rpm)	Force (N)	σ (Nm)	σ_c (Nm)	τ (Nm^{-2})	ω (rad/s)	γ (s^{-1})	μ (Pa.s)
289	0.018	0.0014	0.0009	4.12	30	394	0.0105
374	0.024	0.0018	0.0013	5.49	39	510	0.0108
463	0.033	0.0025	0.0017	7.55	48	631	0.0120
560	0.039	0.0029	0.0020	8.93	59	764	0.0117
657	0.044	0.0033	0.0023	10.07	69	896	0.0112
729	0.052	0.0039	0.0027	11.90	76	994	0.0120
849	0.066	0.0050	0.0035	15.11	89	1158	0.0131
958	0.082	0.0062	0.0043	18.77	100	1306	0.0144
1071	0.105	0.0079	0.0055	24.04	112	1460	0.0165
1164	0.118	0.0089	0.0062	27.01	122	1587	0.0170
1254	0.128	0.0096	0.0067	29.30	131	1710	0.0171
1364	0.147	0.0110	0.0077	33.65	143	1860	0.0181

Table A1.35 Plain ferrosilicon (sp.gr.2.6)

ϕ (rpm)	Force (N)	σ (Nm)	σ_c (Nm)	τ (Nm^{-2})	ω (rad/s)	γ (s^{-1})	μ (Pa.s)
295	0.020	0.0015	0.0011	4.58	31	402	0.0114
382	0.026	0.0020	0.0014	5.95	40	521	0.0114
484	0.034	0.0026	0.0018	7.78	51	660	0.0118
552	0.042	0.0032	0.0022	9.61	58	753	0.0128
635	0.049	0.0037	0.0026	11.22	66	866	0.0130
755	0.060	0.0045	0.0032	13.73	79	1029	0.0133
868	0.072	0.0054	0.0038	16.48	91	1184	0.0139
970	0.086	0.0065	0.0045	19.69	102	1323	0.0149
1052	0.096	0.0072	0.0050	21.98	110	1434	0.0153
1128	0.104	0.0078	0.0055	23.81	118	1538	0.0155
1222	0.114	0.0086	0.0060	26.10	128	1666	0.0157
1344	0.126	0.0095	0.0066	28.84	141	1833	0.0157

Table A1.36 Plain ferrosilicon + 5% slime (sp.gr.2.6)

ϕ (rpm)	Force (N)	σ (Nm)	σ_c (Nm)	τ (Nm^{-2})	ω (rad/s)	γ (s^{-1})	μ (Pa.s)
295	0.026	0.0020	0.0014	5.95	31	402	0.0148
384	0.034	0.0026	0.0018	7.78	40	524	0.0149
447	0.041	0.0031	0.0022	9.39	47	610	0.0154
557	0.053	0.0040	0.0028	12.13	58	759	0.0160
644	0.066	0.0050	0.0035	15.11	67	878	0.0172
753	0.082	0.0062	0.0043	18.77	79	1027	0.0183
842	0.092	0.0069	0.0048	21.06	88	1148	0.0183
953	0.108	0.0081	0.0057	24.72	100	1299	0.0190
1029	0.120	0.0090	0.0063	27.47	108	1403	0.0196
1140	0.134	0.0101	0.0070	30.67	119	1554	0.0197
1268	0.152	0.0114	0.0080	34.80	133	1729	0.0201
1326	0.164	0.0123	0.0086	37.54	139	1808	0.0208

Table A1.37 Plain ferrosilicon + 5% slime + 1g DP001/kg (sp.gr.2.6)

ϕ (rpm)	Force (N)	σ (Nm)	σ_c (Nm)	τ (Nm^{-2})	ω (rad/s)	γ (s^{-1})	μ (Pa.s)
293	0.023	0.0017	0.0012	5.27	31	400	0.0132
364	0.030	0.0023	0.0016	6.87	38	496	0.0138
437	0.038	0.0029	0.0020	8.70	46	596	0.0146
543	0.048	0.0036	0.0025	10.99	57	740	0.0148
662	0.062	0.0047	0.0033	14.19	69	903	0.0157
764	0.078	0.0059	0.0041	17.86	80	1042	0.0171
863	0.091	0.0068	0.0048	20.83	90	1177	0.0177
979	0.108	0.0081	0.0057	24.72	103	1335	0.0185
1084	0.124	0.0093	0.0065	28.39	114	1478	0.0192
1154	0.136	0.0102	0.0071	31.13	121	1574	0.0198
1289	0.153	0.0115	0.0080	35.02	135	1758	0.0199
1336	0.164	0.0123	0.0086	37.54	140	1822	0.0206

Table A1.38 Plain ferrosilicon + 5% slime + 2g DP001/kg (sp.gr.2.6)

ϕ (rpm)	Force (N)	σ (Nm)	σ_c (Nm)	τ (Nm^{-2})	ω (rad/s)	γ (s^{-1})	μ (Pa.s)
293	0.020	0.0015	0.0011	4.58	31	400	0.0115
333	0.025	0.0019	0.0013	5.72	35	454	0.0126
440	0.034	0.0026	0.0018	7.78	46	600	0.0130
551	0.045	0.0034	0.0024	10.30	58	751	0.0137
636	0.056	0.0042	0.0029	12.82	67	867	0.0148
760	0.072	0.0054	0.0038	16.48	80	1036	0.0159
829	0.080	0.0060	0.0042	18.31	87	1130	0.0162
945	0.095	0.0071	0.0050	21.75	99	1289	0.0169
1086	0.112	0.0084	0.0059	25.64	114	1481	0.0173
1198	0.127	0.0095	0.0067	29.07	125	1634	0.0178
1248	0.139	0.0104	0.0073	31.82	131	1702	0.0187
1348	0.153	0.0115	0.0080	35.02	141	1838	0.0191

Table A1.39 Plain ferrosilicon (sp.gr.2.7)

ϕ (rpm)	Force (N)	σ (Nm)	σ_c (Nm)	τ (Nm^{-2})	ω (rad/s)	γ (s^{-1})	μ (Pa.s)
297	0.027	0.0020	0.0014	6.18	31	405	0.0153
352	0.032	0.0024	0.0017	7.33	37	480	0.0153
443	0.037	0.0028	0.0019	8.47	46	604	0.0140
566	0.048	0.0036	0.0025	10.99	59	772	0.0142
646	0.059	0.0044	0.0031	13.51	68	881	0.0153
755	0.072	0.0054	0.0038	16.48	79	1029	0.0160
858	0.088	0.0066	0.0046	20.14	90	1170	0.0172
978	0.106	0.0080	0.0056	24.27	102	1334	0.0182
1063	0.117	0.0088	0.0061	26.78	111	1449	0.0185
1175	0.131	0.0098	0.0069	29.99	123	1602	0.0187
1270	0.145	0.0109	0.0076	33.19	133	1732	0.0192
1350	0.158	0.0119	0.0083	36.17	141	1841	0.0196

Table A1.40 Plain ferrosilicon + 5% slime (sp.gr.2.7)

ϕ (rpm)	Force (N)	σ (Nm)	σ_c (Nm)	τ (Nm^{-2})	ω (rad/s)	γ (s^{-1})	μ (Pa.s)
296	0.032	0.0024	0.0017	7.33	31	404	0.0181
373	0.041	0.0031	0.0022	9.39	39	509	0.0185
462	0.054	0.0041	0.0028	12.36	48	630	0.0196
593	0.068	0.0051	0.0036	15.57	62	809	0.0193
673	0.076	0.0057	0.0040	17.40	70	918	0.0190
744	0.089	0.0067	0.0047	20.37	78	1014	0.0201
873	0.105	0.0079	0.0055	24.04	91	1190	0.0202
981	0.118	0.0089	0.0062	27.01	103	1338	0.0202
1091	0.135	0.0101	0.0071	30.90	114	1488	0.0208
1189	0.150	0.0113	0.0079	34.34	125	1621	0.0212
1236	0.163	0.0122	0.0086	37.31	129	1685	0.0221
1342	0.178	0.0134	0.0093	40.75	141	1830	0.0223

Table A1.41 Plain ferrosilicon + 5% slime + 1g DP001/kg (sp.gr.2.7)

ϕ (rpm)	Force (N)	σ (Nm)	σ_c (Nm)	τ (Nm^{-2})	ω (rad/s)	γ (s^{-1})	μ (Pa.s)
297	0.028	0.0021	0.0015	6.41	31	405	0.0158
390	0.036	0.0027	0.0019	8.24	41	532	0.0155
477	0.046	0.0035	0.0024	10.53	50	650	0.0162
540	0.054	0.0041	0.0028	12.36	57	736	0.0168
644	0.071	0.0053	0.0037	16.25	67	878	0.0185
763	0.086	0.0065	0.0045	19.69	80	1040	0.0189
850	0.098	0.0074	0.0051	22.43	89	1159	0.0194
967	0.118	0.0089	0.0062	27.01	101	1319	0.0205
1055	0.128	0.0096	0.0067	29.30	110	1439	0.0204
1133	0.139	0.0104	0.0073	31.82	119	1545	0.0206
1264	0.152	0.0114	0.0080	34.80	132	1724	0.0202
1360	0.168	0.0126	0.0088	38.46	142	1854	0.0207

Table A1.42 Plain ferrosilicon + 5% slime + 2g DP001/kg (sp.gr.2.7)

ϕ (rpm)	Force (N)	σ (Nm)	σ_c (Nm)	τ (Nm^{-2})	ω (rad/s)	γ (s^{-1})	μ (Pa.s)
293	0.025	0.0019	0.0013	5.72	31	400	0.0143
354	0.032	0.0024	0.0017	7.33	37	483	0.0152
464	0.050	0.0038	0.0026	11.45	49	633	0.0181
548	0.060	0.0045	0.0032	13.73	57	747	0.0184
670	0.074	0.0056	0.0039	16.94	70	914	0.0185
767	0.085	0.0064	0.0045	19.46	80	1046	0.0186
862	0.098	0.0074	0.0051	22.43	90	1175	0.0191
949	0.112	0.0084	0.0059	25.64	99	1294	0.0198
1019	0.122	0.0092	0.0064	27.93	107	1389	0.0201
1146	0.138	0.0104	0.0072	31.59	120	1563	0.0202
1259	0.152	0.0114	0.0080	34.80	132	1717	0.0203
1353	0.167	0.0125	0.0088	38.23	142	1845	0.0207

Table A1.43 Plain ferrosilicon (sp.gr.2.8)

ϕ (rpm)	Force (N)	σ (Nm)	σ_c (Nm)	τ (Nm^{-2})	ω (rad/s)	γ (s^{-1})	μ (Pa.s)
297	0.032	0.0024	0.0017	7.33	31	405	0.0181
392	0.040	0.0030	0.0021	9.16	41	535	0.0171
479	0.048	0.0036	0.0025	10.99	50	653	0.0168
555	0.056	0.0042	0.0029	12.82	58	757	0.0169
655	0.064	0.0048	0.0034	14.65	69	893	0.0164
767	0.081	0.0061	0.0043	18.54	80	1046	0.0177
890	0.098	0.0074	0.0051	22.43	93	1214	0.0185
976	0.112	0.0084	0.0059	25.64	102	1331	0.0193
1072	0.128	0.0096	0.0067	29.30	112	1462	0.0200
1143	0.136	0.0102	0.0071	31.13	120	1559	0.0200
1248	0.150	0.0113	0.0079	34.34	131	1702	0.0202
1383	0.168	0.0126	0.0088	38.46	145	1886	0.0204

Table A1.44 Plain ferrosilicon + 5% slime (sp.gr.2.8)

ϕ (rpm)	Force (N)	σ (Nm)	σ_c (Nm)	τ (Nm^{-2})	ω (rad/s)	γ (s^{-1})	μ (Pa.s)
295	0.034	0.0026	0.0018	7.78	31	402	0.0193
372	0.042	0.0032	0.0022	9.61	39	507	0.0190
486	0.056	0.0042	0.0029	12.82	51	663	0.0193
587	0.070	0.0053	0.0037	16.02	61	800	0.0200
652	0.082	0.0062	0.0043	18.77	68	889	0.0211
737	0.096	0.0072	0.0050	21.98	77	1005	0.0219
879	0.114	0.0086	0.0060	26.10	92	1199	0.0218
939	0.126	0.0095	0.0066	28.84	98	1280	0.0225
1043	0.142	0.0107	0.0075	32.51	109	1422	0.0229
1140	0.168	0.0126	0.0088	38.46	119	1554	0.0247
1272	0.174	0.0131	0.0091	39.83	133	1734	0.0230
1385	0.194	0.0146	0.0102	44.41	145	1889	0.0235

Table A1.45 Plain ferrosilicon + 5% slime + 1g DP001/kg (sp.gr.2.8)

ϕ (rpm)	Force (N)	σ (Nm)	σ_c (Nm)	τ (Nm^{-2})	ω (rad/s)	γ (s^{-1})	μ (Pa.s)
297	0.028	0.0021	0.0015	6.41	31	405	0.0158
382	0.036	0.0027	0.0019	8.24	40	521	0.0158
440	0.046	0.0035	0.0024	10.53	46	600	0.0176
540	0.058	0.0044	0.0030	13.28	57	736	0.0180
641	0.074	0.0056	0.0039	16.94	67	874	0.0194
755	0.094	0.0071	0.0049	21.52	79	1029	0.0209
862	0.110	0.0083	0.0058	25.18	90	1175	0.0214
937	0.121	0.0091	0.0064	27.70	98	1278	0.0217
1028	0.136	0.0102	0.0071	31.13	108	1402	0.0222
1144	0.156	0.0117	0.0082	35.71	120	1560	0.0229
1232	0.170	0.0128	0.0089	38.92	129	1680	0.0232
1371	0.190	0.0143	0.0100	43.49	144	1869	0.0233

Table A1.46 Plain ferrosilicon + 5% slime + 2g DP001/kg (sp.gr.2.8)

ϕ (rpm)	Force (N)	σ (Nm)	σ_c (Nm)	τ (Nm^{-2})	ω (rad/s)	γ (s^{-1})	μ (Pa.s)
296	0.028	0.0021	0.0015	6.41	31	404	0.0159
365	0.034	0.0026	0.0018	7.78	38	498	0.0156
438	0.048	0.0036	0.0025	10.99	46	597	0.0184
554	0.056	0.0042	0.0029	12.82	58	755	0.0170
656	0.065	0.0049	0.0034	14.88	69	894	0.0166
754	0.085	0.0064	0.0045	19.46	79	1028	0.0189
874	0.098	0.0074	0.0051	22.43	92	1192	0.0188
981	0.112	0.0084	0.0059	25.64	103	1338	0.0192
1057	0.124	0.0093	0.0065	28.39	111	1441	0.0197
1153	0.142	0.0107	0.0075	32.51	121	1572	0.0207
1238	0.158	0.0119	0.0083	36.17	130	1688	0.0214
1338	0.179	0.0134	0.0094	40.98	140	1824	0.0225

Table A1.47 Plain ferrosilicon (sp.gr.2.9)

ϕ (rpm)	Force (N)	σ (Nm)	σ_c (Nm)	τ (Nm^{-2})	ω (rad/s)	γ (s^{-1})	μ (Pa.s)
293	0.036	0.0027	0.0019	8.24	31	400	0.0206
369	0.045	0.0034	0.0024	10.30	39	503	0.0205
458	0.053	0.0040	0.0028	12.13	48	625	0.0194
579	0.064	0.0048	0.0034	14.65	61	789	0.0186
658	0.076	0.0057	0.0040	17.40	69	897	0.0194
743	0.086	0.0065	0.0045	19.69	78	1013	0.0194
835	0.098	0.0074	0.0051	22.43	87	1139	0.0197
951	0.114	0.0086	0.0060	26.10	100	1297	0.0201
1045	0.129	0.0097	0.0068	29.53	109	1425	0.0207
1120	0.148	0.0111	0.0078	33.88	117	1527	0.0222
1238	0.165	0.0124	0.0087	37.77	130	1688	0.0224
1353	0.183	0.0137	0.0096	41.87	142	1845	0.0227

Table A1.48 Plain ferrosilicon + 5% slime (sp.gr.2.9)

ϕ (rpm)	Force (N)	σ (Nm)	σ_c (Nm)	τ (Nm^{-2})	ω (rad/s)	γ (s^{-1})	μ (Pa.s)
295	0.042	0.0032	0.0022	9.61	31	402	0.0239
382	0.056	0.0042	0.0029	12.82	40	521	0.0246
444	0.066	0.0050	0.0035	15.11	46	605	0.0250
564	0.085	0.0064	0.0045	19.46	59	769	0.0253
630	0.096	0.0072	0.0050	21.98	66	859	0.0256
783	0.118	0.0089	0.0062	27.01	82	1068	0.0253
879	0.136	0.0102	0.0071	31.13	92	1199	0.0260
960	0.151	0.0113	0.0079	34.57	101	1309	0.0264
1057	0.168	0.0126	0.0088	38.46	111	1441	0.0267
1143	0.184	0.0138	0.0097	42.12	120	1559	0.0270
1238	0.200	0.0150	0.0105	45.78	130	1688	0.0271
1335	0.216	0.0162	0.0113	49.45	140	1820	0.0272

Table A1.49 Plain ferrosilicon + 5% slime + 1g DP001/kg (sp.gr.2.9)

ϕ (rpm)	Force (N)	σ (Nm)	σ_c (Nm)	τ (Nm^{-2})	ω (rad/s)	γ (s^{-1})	μ (Pa.s)
295	0.034	0.0026	0.0018	7.78	31	402	0.0193
340	0.040	0.0030	0.0021	9.16	36	464	0.0198
479	0.057	0.0043	0.0030	13.05	50	653	0.0200
586	0.070	0.0053	0.0037	16.02	61	799	0.0201
688	0.090	0.0068	0.0047	20.60	72	938	0.0220
771	0.105	0.0079	0.0055	24.04	81	1051	0.0229
897	0.124	0.0093	0.0065	28.39	94	1223	0.0232
951	0.136	0.0102	0.0071	31.13	100	1297	0.0240
1066	0.154	0.0116	0.0081	35.25	112	1454	0.0243
1192	0.174	0.0131	0.0091	39.83	125	1625	0.0245
1253	0.184	0.0138	0.0097	42.12	131	1709	0.0247
1352	0.202	0.0152	0.0106	46.24	142	1844	0.0251

Table A1.50 Plain ferrosilicon + 5% slime + 2g DP001/kg (sp.gr.2.9)

ϕ (rpm)	Force (N)	σ (Nm)	σ_c (Nm)	τ (Nm^{-2})	ω (rad/s)	γ (s^{-1})	μ (Pa.s)
297	0.034	0.0026	0.0018	7.78	31	405	0.0192
346	0.038	0.0029	0.0020	8.70	36	472	0.0184
456	0.048	0.0036	0.0025	10.99	48	622	0.0177
551	0.064	0.0048	0.0034	14.65	58	751	0.0195
657	0.084	0.0063	0.0044	19.23	69	896	0.0215
777	0.103	0.0077	0.0054	23.58	81	1059	0.0223
864	0.116	0.0087	0.0061	26.55	90	1178	0.0225
955	0.132	0.0099	0.0069	30.22	100	1302	0.0232
1054	0.148	0.0111	0.0078	33.88	110	1437	0.0236
1154	0.163	0.0122	0.0086	37.31	121	1574	0.0237
1232	0.178	0.0134	0.0093	40.75	129	1680	0.0243
1322	0.193	0.0145	0.0101	44.18	138	1803	0.0245

Table A1.51 Plain ferrosilicon (sp.gr.3.0)

ϕ (rpm)	Force (N)	σ (Nm)	σ_c (Nm)	τ (Nm^{-2})	ω (rad/s)	γ (s^{-1})	μ (Pa.s)
293	0.048	0.0036	0.0025	10.99	31	400	0.0275
369	0.056	0.0042	0.0029	12.82	39	503	0.0255
472	0.068	0.0051	0.0036	15.57	49	644	0.0242
560	0.079	0.0059	0.0041	18.08	59	764	0.0237
643	0.086	0.0065	0.0045	19.69	67	877	0.0225
755	0.102	0.0077	0.0054	23.35	79	1029	0.0227
850	0.118	0.0089	0.0062	27.01	89	1159	0.0233
970	0.140	0.0105	0.0074	32.05	102	1323	0.0242
1049	0.155	0.0116	0.0081	35.48	110	1430	0.0248
1128	0.168	0.0126	0.0088	38.46	118	1538	0.0250
1236	0.188	0.0141	0.0099	43.04	129	1685	0.0255
1388	0.215	0.0161	0.0113	49.22	145	1893	0.0260

Table A1.52 Plain ferrosilicon + 5% slime (sp.gr.3.0)

ϕ (rpm)	Force (N)	σ (Nm)	σ_c (Nm)	τ (Nm^{-2})	ω (rad/s)	γ (s^{-1})	μ (Pa.s)
291	0.055	0.0041	0.0029	12.59	30	397	0.0317
363	0.068	0.0051	0.0036	15.57	38	495	0.0314
448	0.076	0.0057	0.0040	17.40	47	611	0.0285
592	0.098	0.0074	0.0051	22.43	62	807	0.0278
687	0.125	0.0094	0.0066	28.61	72	937	0.0305
793	0.148	0.0111	0.0078	33.88	83	1081	0.0313
894	0.169	0.0127	0.0089	38.69	94	1219	0.0317
979	0.194	0.0146	0.0102	44.41	103	1335	0.0333
1049	0.212	0.0159	0.0111	48.53	110	1430	0.0339
1151	0.236	0.0177	0.0124	54.02	121	1569	0.0344
1265	0.251	0.0188	0.0132	57.46	132	1725	0.0333
1340	0.273	0.0205	0.0143	62.49	140	1827	0.0342

Table A1.53 Plain ferrosilicon + 5% slime + 1g DP001/kg (sp.gr.3.0)

ϕ (rpm)	Force (N)	σ (Nm)	σ_c (Nm)	τ (Nm^{-2})	ω (rad/s)	γ (s^{-1})	μ (Pa.s)
297	0.045	0.0034	0.0024	10.30	31	405	0.0254
391	0.058	0.0044	0.0030	13.28	41	533	0.0249
461	0.067	0.0050	0.0035	15.34	48	629	0.0244
554	0.088	0.0066	0.0046	20.14	58	755	0.0267
660	0.114	0.0086	0.0060	26.10	69	900	0.0290
745	0.130	0.0098	0.0068	29.76	78	1016	0.0293
853	0.156	0.0117	0.0082	35.71	89	1163	0.0307
970	0.186	0.0140	0.0098	42.58	102	1323	0.0322
1058	0.202	0.0152	0.0106	46.24	111	1443	0.0321
1127	0.217	0.0163	0.0114	49.67	118	1537	0.0323
1215	0.235	0.0176	0.0123	53.80	127	1657	0.0325
1320	0.258	0.0194	0.0135	59.06	138	1800	0.0328

Table A1. 54 Plain ferrosilicon + 5% slime + 2g DP001/kg (sp.gr.3.0)

ϕ (rpm)	Force (N)	σ (Nm)	σ_c (Nm)	τ (Nm^{-2})	ω (rad/s)	γ (s^{-1})	μ (Pa.s)
297	0.044	0.0033	0.0023	10.07	31	405	0.0249
386	0.055	0.0041	0.0029	12.59	40	526	0.0239
470	0.068	0.0051	0.0036	15.57	49	641	0.0243
536	0.081	0.0061	0.0043	18.54	56	731	0.0254
687	0.118	0.0089	0.0062	27.01	72	937	0.0288
749	0.135	0.0101	0.0071	30.90	78	1021	0.0303
864	0.162	0.0122	0.0085	37.08	90	1178	0.0315
941	0.180	0.0135	0.0095	41.20	99	1283	0.0321
1056	0.200	0.0150	0.0105	45.78	111	1440	0.0318
1136	0.216	0.0162	0.0113	49.45	119	1549	0.0319
1224	0.234	0.0176	0.0123	53.57	128	1669	0.0321
1389	0.266	0.0200	0.0140	60.89	145	1894	0.0322

A1.2.1.4 Effect of DP001 on Ferrosilicon-Slime Suspensions at Constant Shear Rate

A1.2.1.4.1 Aim of Experiment

The aim of these experiments was to investigate the effect of DP001 on increasing slimes level in ferrosilicon suspensions at constant speed. The constant shear rates tested in these experiments were 500 s^{-1} and 240 s^{-1}. These fall within the range of shear rates experienced in heavy medium cyclones [Lilge et al. (1958)]. Higher shear rates are experienced at the centre of the cyclone, while lower shear rates are experienced at the outer walls of the cyclone.

A1.2.1.4.2 Experimental Conditions

For a constant shear rate of 500 s^{-1}, tests were carried out specific gravities 2.5-3.0. For 240 s^{-1} tests were carried out from a specific gravity of 2.9 to 3.4. The amount of slime used ranged from 0-20 %, depending on the specific gravity of the suspensions. For higher suspensions, the maximum slimes loading were about 12%, whereas for lower specific gravities it was 20 %. The amount of material used was calculated using the same methods as above. These values will not be shown here, since most of them are similar to the values used for the plain ferrosilicon suspensions above. The amount of DP001 added was 1g DP001/kg and 2g DP001/kg at shear rates 241 s^{-1} and 500 s^{-1}, respectively. It should be noted that Rheometer 1 was used for measurements at 240 s^{-1}, and Rheometer 2 was used for the measurements at 500 s^{-1}. The correction factors were 1.17 and 0.29 for Rheometer 1 and Rheometer 2, respectively.

A1.2.1.4.3 Experimental Results

Table A1.55 Plain ferrosilicon-slime at shear rate 500 s^{-1} (sp.gr.2.5)

% Clay	M_{clay} /g	Force (N)	σ (Nm)	σ_c (Nm)	τ (Nm^{-2})	μ (Pa.s)
0	0	0.048	0.0036	0.0025	10.99	0.0220
2	5	0.055	0.0041	0.0029	12.59	0.0252
4	10	0.067	0.0050	0.0035	15.34	0.0307
6	14	0.076	0.0057	0.0040	17.40	0.0348
8	19	0.088	0.0066	0.0046	20.14	0.0403
10	24	0.094	0.0071	0.0049	21.52	0.0430
12	29	0.098	0.0074	0.0051	22.43	0.0449
14	33	0.106	0.0080	0.0056	24.27	0.0485
16	38	0.116	0.0087	0.0061	26.55	0.0531
18	43	0.128	0.0096	0.0067	29.30	0.0586
20	48	0.142	0.0107	0.0075	32.51	0.0650

Table A1.56 Plain ferrosilicon-slime + 2g DP001/kg at shear rate 500 s^{-1} (sp.gr.2.5)

% Clay	M_{clay} /g	Force (N)	σ (Nm)	σ_c (Nm)	τ (Nm^{-2})	μ (Pa.s)
0	0.0	0.048	0.0036	0.0025	10.99	0.0220
2	5.2	0.053	0.0040	0.0028	12.13	0.0243
4	10.4	0.061	0.0046	0.0032	13.96	0.0279
6	15.6	0.070	0.0053	0.0037	16.02	0.0320
8	20.8	0.077	0.0058	0.0040	17.63	0.0353
10	26.0	0.082	0.0062	0.0043	18.77	0.0375
12	31.2	0.090	0.0068	0.0047	20.60	0.0412
14	36.4	0.097	0.0073	0.0051	22.20	0.0444
16	41.6	0.108	0.0081	0.0057	24.72	0.0494
18	46.8	0.118	0.0089	0.0062	27.01	0.0540
20	52.0	0.132	0.0099	0.0069	30.22	0.0604

Table A1.57 Plain ferrosilicon-slime at shear rate 500 s^{-1} (sp.gr.2.6)

% Clay	M_{clay} /g	Force (N)	σ (Nm)	σ_c (Nm)	τ (Nm^{-2})	μ (Pa.s)
0	0.0	0.052	0.0039	0.0027	11.90	0.0238
2	5.2	0.062	0.0047	0.0033	14.19	0.0284
4	10.4	0.074	0.0056	0.0039	16.94	0.0339
6	15.6	0.087	0.0065	0.0046	19.92	0.0398
8	20.8	0.092	0.0069	0.0048	21.06	0.0421
10	26.0	0.102	0.0077	0.0054	23.35	0.0467
12	31.2	0.114	0.0086	0.0060	26.10	0.0522
14	36.4	0.124	0.0093	0.0065	28.39	0.0568
16	41.6	0.137	0.0103	0.0072	31.36	0.0627
18	46.8	0.146	0.0110	0.0077	33.42	0.0668

Table A1.58 Plain ferrosilicon-slime + 2g DP001/kg at shear rate 500 s^{-1} (sp.gr.2.6)

% Clay	M_{clay} /g	Force (N)	σ (Nm)	σ_c (Nm)	τ (Nm^{-2})	μ (Pa.s)
0	0.0	0.052	0.0039	0.0027	11.90	0.0238
2	5.2	0.062	0.0047	0.0033	14.19	0.0284
4	10.4	0.071	0.0053	0.0037	16.25	0.0325
6	15.6	0.080	0.0060	0.0042	18.31	0.0366
8	20.8	0.088	0.0066	0.0046	20.14	0.0403
10	26.0	0.092	0.0069	0.0048	21.06	0.0421
12	31.2	0.094	0.0071	0.0049	21.52	0.0430
14	36.4	0.104	0.0078	0.0055	23.81	0.0476
16	41.6	0.113	0.0085	0.0059	25.87	0.0517
18	46.8	0.118	0.0089	0.0062	27.01	0.0540

Table A1.59 Plain ferrosilicon-slime at shear rate 500 s^{-1} (sp.gr.2.7)

% Clay	M_{clay} /g	Force (N)	σ (Nm)	σ_c (Nm)	τ (Nm^{-2})	μ (Pa.s)
0	0.0	0.069	0.0052	0.0036	15.80	0.032
2	5.7	0.084	0.0063	0.0044	19.23	0.038
4	11.3	0.092	0.0069	0.0048	21.06	0.042
6	17.0	0.098	0.0074	0.0051	22.43	0.045
8	22.6	0.105	0.0079	0.0055	24.04	0.048
10	28.3	0.112	0.0084	0.0059	25.64	0.051
12	34.0	0.120	0.0090	0.0063	27.47	0.055
14	39.6	0.138	0.0104	0.0072	31.59	0.063
16	45.3	0.153	0.0115	0.0080	35.02	0.070

Table A1.60 Plain ferrosilicon-slime + 2g DP001/kg at shear rate 500 s^{-1} (sp.gr.2.7)

% Clay	M_{clay} /g	Force (N)	σ (Nm)	σ_c (Nm)	τ (Nm^{-2})	μ (Pa.s)
0	0.0	0.068	0.0051	0.0036	15.57	0.0311
2	5.7	0.073	0.0055	0.0038	16.71	0.0334
4	11.3	0.080	0.0060	0.0042	18.31	0.0366
6	17.0	0.089	0.0067	0.0047	20.37	0.0407
8	22.6	0.098	0.0074	0.0051	22.43	0.0449
10	28.3	0.104	0.0078	0.0055	23.81	0.0476
12	34.0	0.113	0.0085	0.0059	25.87	0.0517
14	39.6	0.123	0.0092	0.0065	28.16	0.0563
16	45.3	0.139	0.0104	0.0073	31.82	0.0636

Table A1.61 Plain ferrosilicon-slime at shear rate 500 s^{-1} (sp.gr.2.8)

% Clay	M_{clay} /g	Force (N)	σ (Nm)	σ_c (Nm)	τ (Nm^{-2})	μ (Pa.s)
0	0.0	0.078	0.0059	0.0041	17.86	0.0357
2	6.1	0.085	0.0064	0.0045	19.46	0.0389
4	12.3	0.094	0.0071	0.0049	21.52	0.0430
6	18.4	0.104	0.0078	0.0055	23.81	0.0476
8	24.6	0.114	0.0086	0.0060	26.10	0.0522
10	30.7	0.124	0.0093	0.0065	28.39	0.0568
12	36.9	0.140	0.0105	0.0074	32.05	0.0641
14	43.0	0.152	0.0114	0.0080	34.80	0.0696

Table A1.62 Plain ferrosilicon-slime + 2g DP001/kg at shear rate 500 s^{-1} (sp.gr.2.8)

% Clay	M_{clay} /g	Force (N)	σ (Nm)	σ_c (Nm)	τ (Nm^{-2})	μ (Pa.s)
0	0.0	0.077	0.0058	0.0040	17.63	0.0353
2	6.1	0.081	0.0061	0.0043	18.54	0.0371
4	12.3	0.088	0.0066	0.0046	20.14	0.0403
6	18.4	0.096	0.0072	0.0050	21.98	0.0440
8	24.6	0.104	0.0078	0.0055	23.81	0.0476
10	30.7	0.112	0.0084	0.0059	25.64	0.0513
12	36.9	0.124	0.0093	0.0065	28.39	0.0568
14	43.0	0.140	0.0105	0.0074	32.05	0.0641

Table A1.63 Plain ferrosilicon-slime at shear rate 500 s^{-1} (sp.gr.2.9)

% Clay	M_{clay} /g	Force (N)	σ (Nm)	σ_c (Nm)	τ (Nm^{-2})	μ (Pa.s)
0	0.0	0.085	0.0064	0.0045	19.46	0.0389
2	6.7	0.098	0.0074	0.0051	22.43	0.0449
4	13.3	0.110	0.0083	0.0058	25.18	0.0504
6	20.0	0.119	0.0089	0.0062	27.24	0.0545
8	26.6	0.132	0.0099	0.0069	30.22	0.0604
10	33.3	0.149	0.0112	0.0078	34.11	0.0682
12	39.9	0.163	0.0122	0.0086	37.31	0.0746

Table A1.64 Plain ferrosilicon-slime + 2g DP001/kg at shear rate 500 s^{-1} (sp.gr.2.9)

% Clay	M_{clay} /g	Force (N)	σ (Nm)	σ_c (Nm)	τ (Nm^{-2})	μ (Pa.s)
0	0.0	0.084	0.0063	0.0044	19.23	0.0385
2	6.7	0.093	0.0070	0.0049	21.29	0.0426
4	13.3	0.105	0.0079	0.0055	24.04	0.0481
6	20.0	0.115	0.0086	0.0060	26.33	0.0527
8	26.6	0.124	0.0093	0.0065	28.39	0.0568
10	33.3	0.136	0.0102	0.0071	31.13	0.0623
12	39.9	0.151	0.0113	0.0079	34.57	0.0691

Table A1.65 Plain ferrosilicon-slime at shear rate 500 s^{-1} (sp.gr.3.0)

% Clay	M_{clay} /g	Force (N)	σ (Nm)	σ_c (Nm)	τ (Nm^{-2})	μ (Pa.s)
0	0.0	0.106	0.0080	0.0056	24.27	0.0485
2	7.2	0.113	0.0085	0.0059	25.87	0.0517
4	14.4	0.120	0.0090	0.0063	27.47	0.0549
6	21.6	0.133	0.0100	0.0070	30.45	0.0609
8	28.8	0.154	0.0116	0.0081	35.25	0.0705
10	36.0	0.171	0.0128	0.0090	39.14	0.0783
12	43.1	0.220	0.0165	0.0116	50.36	0.1007

Table A1.66 Plain ferrosilicon-slime + 2g DP001/kg at shear rate 500 s^{-1} (sp.gr.3.0)

% Clay	M_{clay} /g	Force (N)	σ (Nm)	σ_c (Nm)	τ (Nm^{-2})	μ (Pa.s)
0	0.0	0.107	0.0080	0.0056	24.49	0.0490
2	7.2	0.110	0.0083	0.0058	25.18	0.0504
4	14.4	0.116	0.0087	0.0061	26.55	0.0531
6	21.6	0.128	0.0096	0.0067	29.30	0.0586
8	28.8	0.148	0.0111	0.0078	33.88	0.0678
10	36.0	0.164	0.0123	0.0086	37.54	0.0751
12	43.1	0.182	0.0137	0.0096	41.66	0.0833

Table A1.67 Plain ferrosilicon-slime at shear rate 241 s^{-1} (sp.gr.2.9)

% clay	Force (N)	σ (Nm)	σ_c (Nm)	τ (Nm^{-2})	μ (Pa.s)
2	0.004	0.00030	0.00008	0.34	0.0014
4	0.008	0.00060	0.00016	0.68	0.0028
6	0.012	0.00090	0.00023	1.02	0.0042
8	0.014	0.00105	0.00027	1.19	0.0049
10	0.016	0.00120	0.00031	1.36	0.0057
12	0.018	0.00135	0.00035	1.53	0.0064
14	0.021	0.00158	0.00041	1.79	0.0074
16	0.023	0.00173	0.00045	1.96	0.0081
18	0.024	0.00180	0.00047	2.04	0.0085

Table A1.68 Plain ferrosilicon-slime + 1g DP001/kg at shear rate 241 s^{-1} (sp.gr.2.9)

% clay	Force (N)	σ (Nm)	σ_c (Nm)	τ (Nm^{-2})	μ (Pa.s)
2	0.0032	0.00024	0.00006	0.27	0.0011
4	0.004	0.00030	0.00008	0.34	0.0014
6	0.006	0.00045	0.00012	0.51	0.0021
8	0.007	0.00053	0.00014	0.60	0.0025
10	0.009	0.00068	0.00018	0.77	0.0032
12	0.012	0.00090	0.00023	1.02	0.0042
14	0.016	0.00120	0.00031	1.36	0.0057
16	0.018	0.00135	0.00035	1.53	0.0064
18	0.021	0.00158	0.00041	1.79	0.0074

Table A1.69 Plain ferrosilicon-slime at shear rate 241 s^{-1} (sp.gr.3.0)

% clay	Force (N)	σ (Nm)	σ_c (Nm)	τ (Nm^{-2})	μ (Pa.s)
2	0.005	0.00038	0.00010	0.43	0.0018
4	0.009	0.00068	0.00018	0.77	0.0032
6	0.012	0.00090	0.00023	1.02	0.0042
8	0.015	0.00113	0.00029	1.28	0.0053
10	0.017	0.00128	0.00033	1.45	0.0060
12	0.019	0.00143	0.00037	1.62	0.0067
14	0.021	0.00158	0.00041	1.79	0.0074
16	0.023	0.00173	0.00045	1.96	0.0081
18	0.025	0.00188	0.00049	2.13	0.0088

Table A1.70 Plain ferrosilicon-slime + 1g DP001/kg at shear rate 241 s^{-1} (sp.gr.3.0)

% clay	Force (N)	σ (Nm)	σ_c (Nm)	τ (Nm^{-2})	μ (Pa.s)
2	0.003	0.00023	0.000059	0.26	0.0011
4	0.005	0.00038	0.000098	0.43	0.0018
6	0.007	0.00053	0.000137	0.60	0.0025
8	0.009	0.00068	0.000176	0.77	0.0032
10	0.013	0.00098	0.000254	1.11	0.0046
12	0.016	0.00120	0.000312	1.36	0.0057
14	0.019	0.00143	0.000371	1.62	0.0067
16	0.021	0.00158	0.000410	1.79	0.0074
18	0.023	0.00173	0.000449	1.96	0.0081

Table A1.71 Plain ferrosilicon-slime at shear rate 241 s^{-1} (sp.gr.3.1)

% clay	Force (N)	σ (Nm)	σ_c (Nm)	τ (Nm^{-2})	μ (Pa.s)
2	0.005	0.00038	0.00010	0.43	0.0018
4	0.008	0.00060	0.00016	0.68	0.0028
6	0.013	0.00098	0.00025	1.11	0.0046
8	0.015	0.00113	0.00029	1.28	0.0053
10	0.018	0.00135	0.00035	1.53	0.0064
12	0.020	0.00150	0.00039	1.70	0.0071
14	0.023	0.00173	0.00045	1.96	0.0081
16	0.025	0.00188	0.00049	2.13	0.0088
18	0.027	0.00203	0.00053	2.30	0.0095

Table A1.72 Plain ferrosilicon-slime + 1g DP001/kg at shear rate 241 s^{-1} (sp.gr.3.1)

% clay	Force (N)	σ (Nm)	σ_c (Nm)	τ (Nm^{-2})	μ (Pa.s)
2	0.0034	0.00026	0.000066	0.29	0.0012
4	0.005	0.00038	0.000098	0.43	0.0018
6	0.008	0.00060	0.000156	0.68	0.0028
8	0.010	0.00075	0.000195	0.85	0.0035
10	0.013	0.00098	0.000254	1.11	0.0046
12	0.016	0.00120	0.000312	1.36	0.0057
14	0.018	0.00135	0.000351	1.53	0.0064
16	0.022	0.00165	0.000429	1.87	0.0078
18	0.024	0.00180	0.000468	2.04	0.0085

Table A1.73 Plain ferrosilicon-slime at shear rate 241 s^{-1} (sp.gr.3.2)

% clay	Force (N)	σ (Nm)	σ_c (Nm)	τ (Nm^{-2})	μ (Pa.s)
2	0.007	0.00053	0.00014	0.60	0.0025
4	0.009	0.00068	0.00018	0.77	0.0032
6	0.012	0.00090	0.00023	1.02	0.0042
8	0.016	0.00120	0.00031	1.36	0.0057
10	0.018	0.00135	0.00035	1.53	0.0064
12	0.021	0.00158	0.00041	1.79	0.0074
14	0.024	0.00180	0.00047	2.04	0.0085
16	0.027	0.00203	0.00053	2.30	0.0095
18	0.029	0.00218	0.00057	2.47	0.0102

Table A1.74 Plain ferrosilicon-slime + 1g DP001/kg at shear rate 241 s^{-1} (sp.gr.3.2)

% clay	Force (N)	σ (Nm)	σ_c (Nm)	τ (Nm^{-2})	μ (Pa.s)
2	0.005	0.00038	0.000098	0.43	0.0018
4	0.007	0.00053	0.000137	0.60	0.0025
6	0.010	0.00075	0.000195	0.85	0.0035
8	0.012	0.00090	0.000234	1.02	0.0042
10	0.015	0.00113	0.000293	1.28	0.0053
12	0.017	0.00128	0.000332	1.45	0.0060
14	0.020	0.00150	0.000390	1.70	0.0071
16	0.022	0.00165	0.000429	1.87	0.0078
18	0.025	0.00188	0.000488	2.13	0.0088

Table A1.75 Plain ferrosilicon-slime at shear rate 241 s^{-1} (sp.gr.3.3)

% clay	Force (N)	σ (Nm)	σ_c (Nm)	τ (Nm^{-2})	μ (Pa.s)
2	0.007	0.00053	0.00014	0.60	0.0025
4	0.010	0.00075	0.00020	0.85	0.0035
6	0.013	0.00098	0.00025	1.11	0.0046
8	0.016	0.00120	0.00031	1.36	0.0057
10	0.019	0.00143	0.00037	1.62	0.0067
12	0.022	0.00165	0.00043	1.87	0.0078
14	0.025	0.00188	0.00049	2.13	0.0088
16	0.027	0.00203	0.00053	2.30	0.0095
18	0.030	0.00225	0.00059	2.55	0.0106

Table A1.76 Plain ferrosilicon-slime + 1g DP001/kg at shear rate 241 s^{-1} (sp.gr.3.3)

% clay	Force (N)	σ (Nm)	σ_c (Nm)	τ (Nm^{-2})	μ (Pa.s)
2	0.004	0.00030	0.00008	0.34	0.0014
4	0.007	0.00053	0.00014	0.60	0.0025
6	0.011	0.00083	0.00021	0.94	0.0039
8	0.013	0.00098	0.00025	1.11	0.0046
10	0.016	0.00120	0.00031	1.36	0.0057
12	0.019	0.00143	0.00037	1.62	0.0067
14	0.021	0.00158	0.00041	1.79	0.0074
16	0.024	0.00180	0.00047	2.04	0.0085
18	0.026	0.00195	0.00051	2.21	0.0092

Table A1.167 Plain ferrosilicon-magnetite #1 + 1g DP001 at Ratio 2:1 (sp.gr.2.7)

ϕ (rpm)	Force (N)	σ (Nm)	σ_c (Nm)	τ (Nm^{-2})	ω (rad/s)	γ (s^{-1})	μ (Pa.s)
293	0.056	0.0042	0.0029	12.82	31	400	0.0321
374	0.066	0.0050	0.0035	15.11	39	510	0.0296
448	0.077	0.0058	0.0040	17.63	47	611	0.0289
567	0.088	0.0066	0.0046	20.14	59	773	0.0261
659	0.104	0.0078	0.0055	23.81	69	899	0.0265
747	0.117	0.0088	0.0061	26.78	78	1019	0.0263
845	0.132	0.0099	0.0069	30.22	88	1152	0.0262
964	0.149	0.0112	0.0078	34.11	101	1314	0.0259
1049	0.166	0.0125	0.0087	38.00	110	1430	0.0266
1142	0.176	0.0132	0.0092	40.29	120	1557	0.0259
1248	0.188	0.0141	0.0099	43.04	131	1702	0.0253
1342	0.200	0.0150	0.0105	45.78	141	1830	0.0250

Table A1.168 Plain ferrosilicon-magnetite #1 + 2g DP001/kg at Ratio 2:1 (sp.gr.2.7)

ϕ (rpm)	Force (N)	σ (Nm)	σ_c (Nm)	τ (Nm^{-2})	ω (rad/s)	γ (s^{-1})	μ (Pa.s)
289	0.049	0.0037	0.0026	11.22	30	394	0.0285
389	0.054	0.0041	0.0028	12.36	41	530	0.0233
464	0.066	0.0050	0.0035	15.11	49	633	0.0239
558	0.078	0.0059	0.0041	17.86	58	761	0.0235
659	0.089	0.0067	0.0047	20.37	69	899	0.0227
744	0.109	0.0082	0.0057	24.95	78	1014	0.0246
843	0.131	0.0098	0.0069	29.99	88	1149	0.0261
957	0.149	0.0112	0.0078	34.11	100	1305	0.0261
1064	0.167	0.0125	0.0088	38.23	111	1451	0.0264
1148	0.179	0.0134	0.0094	40.98	120	1565	0.0262
1260	0.185	0.0139	0.0097	42.35	132	1718	0.0246
1376	0.196	0.0147	0.0103	44.87	144	1876	0.0239

Table A1.169 Plain ferrosilicon-magnetite #1 + 5g DP001/kg at Ratio 2:1 (sp.gr.2.7)

ϕ (rpm)	Force (N)	σ (Nm)	σ_c (Nm)	τ (Nm^{-2})	ω (rad/s)	γ (s^{-1})	μ (Pa.s)
291	0.061	0.0046	0.0032	13.96	30	397	0.0352
379	0.069	0.0052	0.0036	15.80	40	517	0.0306
474	0.076	0.0057	0.0040	17.40	50	646	0.0269
542	0.083	0.0062	0.0044	19.00	57	739	0.0257
652	0.104	0.0078	0.0055	23.81	68	889	0.0268
779	0.126	0.0095	0.0066	28.84	82	1062	0.0272
851	0.145	0.0109	0.0076	33.19	89	1160	0.0286
951	0.168	0.0126	0.0088	38.46	100	1297	0.0297
1049	0.181	0.0136	0.0095	41.43	110	1430	0.0290
1153	0.203	0.0152	0.0107	46.47	121	1572	0.0296
1228	0.221	0.0166	0.0116	50.59	129	1674	0.0302
1341	0.239	0.0179	0.0125	54.71	140	1829	0.0299

Table A1.170 Plain ferrosilicon-magnetite #1 at Ratio 2:1 (sp.gr.2.8)

ϕ (rpm)	Force (N)	σ (Nm)	σ_c (Nm)	τ (Nm^{-2})	ω (rad/s)	γ (s^{-1})	μ (Pa.s)
295	0.095	0.0071	0.0050	21.75	31	402	0.0541
358	0.106	0.0080	0.0056	24.27	37	488	0.0497
450	0.117	0.0088	0.0061	26.78	47	614	0.0436
554	0.125	0.0094	0.0066	28.61	58	755	0.0379
649	0.139	0.0104	0.0073	31.82	68	885	0.0360
751	0.160	0.0120	0.0084	36.63	79	1024	0.0358
860	0.186	0.0140	0.0098	42.58	90	1173	0.0363
951	0.204	0.0153	0.0107	46.70	100	1297	0.0360
1035	0.228	0.0171	0.0120	52.19	108	1411	0.0370
1138	0.252	0.0189	0.0132	57.69	119	1552	0.0372
1246	0.276	0.0207	0.0145	63.18	130	1699	0.0372
1355	0.303	0.0227	0.0159	69.36	142	1848	0.0375

Table A1.171 Plain ferrosilicon-magnetite #1 + 1g DP001/kg at Ratio 2:1 (sp.gr.2.8)

ϕ (rpm)	Force (N)	σ (Nm)	σ_c (Nm)	τ (Nm^{-2})	ω (rad/s)	γ (s^{-1})	μ (Pa.s)
293	0.079	0.0059	0.0041	18.08	31	400	0.0453
365	0.086	0.0065	0.0045	19.69	38	498	0.0396
455	0.099	0.0074	0.0052	22.66	48	620	0.0365
544	0.108	0.0081	0.0057	24.72	57	742	0.0333
656	0.126	0.0095	0.0066	28.84	69	894	0.0322
753	0.142	0.0107	0.0075	32.51	79	1027	0.0317
863	0.163	0.0122	0.0086	37.31	90	1177	0.0317
965	0.181	0.0136	0.0095	41.43	101	1316	0.0315
1072	0.196	0.0147	0.0103	44.87	112	1462	0.0307
1164	0.212	0.0159	0.0111	48.53	122	1587	0.0306
1225	0.232	0.0174	0.0122	53.11	128	1670	0.0318
1334	0.258	0.0194	0.0135	59.06	140	1819	0.0325

Table A1.172 Plain ferrosilicon-magnetite #1 + 2g DP001/kg at Ratio 2:1 (sp.gr.2.8)

ϕ (rpm)	Force (N)	σ (Nm)	σ_c (Nm)	τ (Nm^{-2})	ω (rad/s)	γ (s^{-1})	μ (Pa.s)
295	0.069	0.0052	0.0036	15.80	31	402	0.0393
368	0.078	0.0059	0.0041	17.86	39	502	0.0356
495	0.096	0.0072	0.0050	21.98	52	675	0.0326
587	0.108	0.0081	0.0057	24.72	61	800	0.0309
655	0.115	0.0086	0.0060	26.33	69	893	0.0295
757	0.131	0.0098	0.0069	29.99	79	1032	0.0291
855	0.153	0.0115	0.0080	35.02	90	1166	0.0300
979	0.172	0.0129	0.0090	39.37	103	1335	0.0295
1068	0.184	0.0138	0.0097	42.12	112	1456	0.0289
1160	0.196	0.0147	0.0103	44.87	121	1582	0.0284
1251	0.206	0.0155	0.0108	47.16	131	1706	0.0276
1336	0.224	0.0168	0.0118	51.28	140	1822	0.0281

Table A1.173 Plain ferrosilicon-magnetite #1 + 5g DP001/kg at Ratio 2:1 (sp.gr.2.8)

ϕ (rpm)	Force (N)	σ (Nm)	σ_c (Nm)	τ (Nm^{-2})	ω (rad/s)	γ (s^{-1})	μ (Pa.s)
291	0.084	0.0063	0.0044	19.23	30	397	0.0485
377	0.091	0.0068	0.0048	20.83	39	514	0.0405
470	0.101	0.0076	0.0053	23.12	49	641	0.0361
546	0.109	0.0082	0.0057	24.95	57	744	0.0335
668	0.122	0.0092	0.0064	27.93	70	911	0.0307
755	0.152	0.0114	0.0080	34.80	79	1029	0.0338
851	0.176	0.0132	0.0092	40.29	89	1160	0.0347
959	0.194	0.0146	0.0102	44.41	100	1308	0.0340
1054	0.225	0.0169	0.0118	51.51	110	1437	0.0358
1176	0.248	0.0186	0.0130	56.77	123	1604	0.0354
1260	0.269	0.0202	0.0141	61.58	132	1718	0.0358
1348	0.293	0.0220	0.0154	67.07	141	1838	0.0365

A1.2.3.3.3 Ferrosilicon-Magnetite #1 Ratio 1:2

Table A1.174 Plain ferrosilicon-magnetite #1 at Ratio 1:2 (sp.gr.2.0)

ϕ (rpm)	Force (N)	σ (Nm)	σ_c (Nm)	τ (Nm^{-2})	ω (rad/s)	γ (s^{-1})	μ (Pa.s)
291	0.014	0.0011	0.0007	3.20	30	397	0.0081
391	0.022	0.0017	0.0012	5.04	41	533	0.0094
468	0.029	0.0022	0.0015	6.64	49	638	0.0104
549	0.034	0.0026	0.0018	7.78	57	749	0.0104
658	0.040	0.0030	0.0021	9.16	69	897	0.0102
795	0.049	0.0037	0.0026	11.22	83	1084	0.0103
884	0.054	0.0041	0.0028	12.36	93	1205	0.0103
969	0.062	0.0047	0.0033	14.19	101	1321	0.0107
1055	0.068	0.0051	0.0036	15.57	110	1439	0.0108
1130	0.075	0.0056	0.0039	17.17	118	1541	0.0111
1241	0.086	0.0065	0.0045	19.69	130	1692	0.0116
1341	0.094	0.0071	0.0049	21.52	140	1829	0.0118

Table A1.175 Plain ferrosilicon-magnetite #1 at Ratio 1:2 (sp.gr.2.1)

ϕ (rpm)	Force (N)	σ (Nm)	σ_c (Nm)	τ (Nm^{-2})	ω (rad/s)	γ (s^{-1})	μ (Pa.s)
291	0.022	0.0017	0.0012	5.04	30	397	0.0127
341	0.027	0.0020	0.0014	6.18	36	465	0.0133
449	0.034	0.0026	0.0018	7.78	47	612	0.0127
546	0.041	0.0031	0.0022	9.39	57	744	0.0126
657	0.046	0.0035	0.0024	10.53	69	896	0.0118
751	0.055	0.0041	0.0029	12.59	79	1024	0.0123
878	0.062	0.0047	0.0033	14.19	92	1197	0.0119
991	0.068	0.0051	0.0036	15.57	104	1351	0.0115
1072	0.075	0.0056	0.0039	17.17	112	1462	0.0117
1137	0.084	0.0063	0.0044	19.23	119	1550	0.0124
1250	0.096	0.0072	0.0050	21.98	131	1704	0.0129
1344	0.104	0.0078	0.0055	23.81	141	1833	0.0130

Table A1.176 Plain ferrosilicon-magnetite #1 at Ratio 1:2 (sp.gr.2.2)

ϕ (rpm)	Force (N)	σ (Nm)	σ_c (Nm)	τ (Nm^{-2})	ω (rad/s)	γ (s^{-1})	μ (Pa.s)
289	0.032	0.0024	0.0017	7.33	30	394	0.0186
355	0.040	0.0030	0.0021	9.16	37	484	0.0189
469	0.049	0.0037	0.0026	11.22	49	639	0.0175
554	0.056	0.0042	0.0029	12.82	58	755	0.0170
649	0.062	0.0047	0.0033	14.19	68	885	0.0160
759	0.072	0.0054	0.0038	16.48	79	1035	0.0159
869	0.087	0.0065	0.0046	19.92	91	1185	0.0168
941	0.094	0.0071	0.0049	21.52	99	1283	0.0168
1072	0.106	0.0080	0.0056	24.27	112	1462	0.0166
1135	0.113	0.0085	0.0059	25.87	119	1548	0.0167
1236	0.124	0.0093	0.0065	28.39	129	1685	0.0168
1352	0.136	0.0102	0.0071	31.13	142	1844	0.0169

Table A1.177 Plain ferrosilicon-magnetite #1 + 1g DP001/kg at Ratio 1:2 (sp.gr.2.2)

ϕ (rpm)	Force (N)	σ (Nm)	σ_c (Nm)	τ (Nm^{-2})	ω (rad/s)	γ (s^{-1})	μ (Pa.s)
295	0.026	0.0020	0.0014	5.95	31	402	0.0148
392	0.033	0.0025	0.0017	7.55	41	535	0.0141
450	0.039	0.0029	0.0020	8.93	47	614	0.0145
566	0.048	0.0036	0.0025	10.99	59	772	0.0142
641	0.054	0.0041	0.0028	12.36	67	874	0.0141
753	0.064	0.0048	0.0034	14.65	79	1027	0.0143
859	0.072	0.0054	0.0038	16.48	90	1171	0.0141
985	0.082	0.0062	0.0043	18.77	103	1343	0.0140
1063	0.088	0.0066	0.0046	20.14	111	1449	0.0139
1148	0.095	0.0071	0.0050	21.75	120	1565	0.0139
1248	0.103	0.0077	0.0054	23.58	131	1702	0.0139
1353	0.110	0.0083	0.0058	25.18	142	1845	0.0136

Table A1.178 Plain ferrosilicon-magnetite #1 + 2g DP001/kg at Ratio 1:2 (sp.gr.2.2)

ϕ (rpm)	Force (N)	σ (Nm)	σ_c (Nm)	τ (Nm^{-2})	ω (rad/s)	γ (s^{-1})	μ (Pa.s)
291	0.022	0.0017	0.0012	5.04	30	397	0.0127
389	0.029	0.0022	0.0015	6.64	41	530	0.0125
461	0.036	0.0027	0.0019	8.24	48	629	0.0131
544	0.041	0.0031	0.0022	9.39	57	742	0.0127
651	0.050	0.0038	0.0026	11.45	68	888	0.0129
771	0.060	0.0045	0.0032	13.73	81	1051	0.0131
858	0.072	0.0054	0.0038	16.48	90	1170	0.0141
983	0.089	0.0067	0.0047	20.37	103	1340	0.0152
1049	0.097	0.0073	0.0051	22.20	110	1430	0.0155
1148	0.106	0.0080	0.0056	24.27	120	1565	0.0155
1224	0.113	0.0085	0.0059	25.87	128	1669	0.0155
1348	0.124	0.0093	0.0065	28.39	141	1838	0.0154

Table A1.179 Plain ferrosilicon-magnetite #1 + 5g DP001/kg at Ratio 1:2 (sp.gr.2.2)

ϕ (rpm)	Force (N)	σ (Nm)	σ_c (Nm)	τ (Nm^{-2})	ω (rad/s)	γ (s^{-1})	μ (Pa.s)
291	0.026	0.0020	0.0014	5.95	30	397	0.0150
366	0.034	0.0026	0.0018	7.78	38	499	0.0156
461	0.043	0.0032	0.0023	9.84	48	629	0.0157
560	0.054	0.0041	0.0028	12.36	59	764	0.0162
662	0.063	0.0047	0.0033	14.42	69	903	0.0160
745	0.071	0.0053	0.0037	16.25	78	1016	0.0160
844	0.083	0.0062	0.0044	19.00	88	1151	0.0165
950	0.097	0.0073	0.0051	22.20	99	1295	0.0171
1047	0.108	0.0081	0.0057	24.72	110	1428	0.0173
1146	0.121	0.0091	0.0064	27.70	120	1563	0.0177
1264	0.133	0.0100	0.0070	30.45	132	1724	0.0177
1348	0.142	0.0107	0.0075	32.51	141	1838	0.0177

Table A1.180 Plain ferrosilicon-magnetite #1 at Ratio 1:2 (sp.gr.2.3)

ϕ (rpm)	Force (N)	σ (Nm)	σ_c (Nm)	τ (Nm^{-2})	ω (rad/s)	γ (s^{-1})	μ (Pa.s)
295	0.040	0.0030	0.0021	9.16	31	402	0.0228
377	0.047	0.0035	0.0025	10.76	39	514	0.0209
463	0.056	0.0042	0.0029	12.82	48	631	0.0203
556	0.064	0.0048	0.0034	14.65	58	758	0.0193
645	0.071	0.0053	0.0037	16.25	68	879	0.0185
761	0.080	0.0060	0.0042	18.31	80	1038	0.0176
862	0.096	0.0072	0.0050	21.98	90	1175	0.0187
983	0.109	0.0082	0.0057	24.95	103	1340	0.0186
1079	0.126	0.0095	0.0066	28.84	113	1471	0.0196
1151	0.139	0.0104	0.0073	31.82	121	1569	0.0203
1250	0.151	0.0113	0.0079	34.57	131	1704	0.0203
1346	0.163	0.0122	0.0086	37.31	141	1835	0.0203

Table A1.181 Plain ferrosilicon-magnetite #1 + 1g DP001/kg at Ratio 1:2 (sp.gr.2.3)

ϕ (rpm)	Force (N)	σ (Nm)	σ_c (Nm)	τ (Nm^{-2})	ω (rad/s)	γ (s^{-1})	μ (Pa.s)
291	0.035	0.0026	0.0018	8.01	30	397	0.0202
344	0.040	0.0030	0.0021	9.16	36	469	0.0195
458	0.052	0.0039	0.0027	11.90	48	625	0.0191
554	0.060	0.0045	0.0032	13.73	58	755	0.0182
643	0.068	0.0051	0.0036	15.57	67	877	0.0178
786	0.074	0.0056	0.0039	16.94	82	1072	0.0158
869	0.081	0.0061	0.0043	18.54	91	1185	0.0156
976	0.091	0.0068	0.0048	20.83	102	1331	0.0157
1084	0.102	0.0077	0.0054	23.35	114	1478	0.0158
1188	0.113	0.0085	0.0059	25.87	124	1620	0.0160
1268	0.121	0.0091	0.0064	27.70	133	1729	0.0160
1366	0.128	0.0096	0.0067	29.30	143	1863	0.0157

Table A1.182 Plain ferrosilicon-magnetite #1 + 2g DP001/kg at Ratio 1:2 (sp.gr.2.3)

ϕ (rpm)	Force (N)	σ (Nm)	σ_c (Nm)	τ (Nm^{-2})	ω (rad/s)	γ (s^{-1})	μ (Pa.s)
291	0.032	0.0024	0.0017	7.33	30	397	0.0185
346	0.039	0.0029	0.0020	8.93	36	472	0.0189
448	0.045	0.0034	0.0024	10.30	47	611	0.0169
546	0.053	0.0040	0.0028	12.13	57	744	0.0163
678	0.066	0.0050	0.0035	15.11	71	924	0.0163
761	0.074	0.0056	0.0039	16.94	80	1038	0.0163
866	0.085	0.0064	0.0045	19.46	91	1181	0.0165
947	0.098	0.0074	0.0051	22.43	99	1291	0.0174
1052	0.109	0.0082	0.0057	24.95	110	1434	0.0174
1134	0.121	0.0091	0.0064	27.70	119	1546	0.0179
1240	0.131	0.0098	0.0069	29.99	130	1691	0.0177
1346	0.144	0.0108	0.0076	32.96	141	1835	0.0180

Table A1.183 Plain ferrosilicon-magnetite #1 + 5g DP001/kg at Ratio 1:2 (sp.gr.2.3)

ϕ (rpm)	Force (N)	σ (Nm)	σ_c (Nm)	τ (Nm^{-2})	ω (rad/s)	γ (s^{-1})	μ (Pa.s)
293	0.034	0.0026	0.0018	7.78	31	400	0.0195
347	0.043	0.0032	0.0023	9.84	36	473	0.0208
469	0.056	0.0042	0.0029	12.82	49	639	0.0200
561	0.064	0.0048	0.0034	14.65	59	765	0.0192
648	0.078	0.0059	0.0041	17.86	68	884	0.0202
754	0.083	0.0062	0.0044	19.00	79	1028	0.0185
863	0.094	0.0071	0.0049	21.52	90	1177	0.0183
952	0.105	0.0079	0.0055	24.04	100	1298	0.0185
1068	0.114	0.0086	0.0060	26.10	112	1456	0.0179
1173	0.128	0.0096	0.0067	29.30	123	1599	0.0183
1266	0.142	0.0107	0.0075	32.51	133	1726	0.0188
1342	0.151	0.0113	0.0079	34.57	141	1830	0.0189

Table A1.184 Plain ferrosilicon-magnetite #1 at Ratio 1:2 (sp.gr.2.4)

ϕ (rpm)	Force (N)	σ (Nm)	σ_c (Nm)	τ (Nm^{-2})	ω (rad/s)	γ (s^{-1})	μ (Pa.s)
289	0.052	0.0039	0.0027	11.90	30	394	0.0302
384	0.061	0.0046	0.0032	13.96	40	524	0.0267
478	0.070	0.0053	0.0037	16.02	50	652	0.0246
550	0.079	0.0059	0.0041	18.08	58	750	0.0241
660	0.093	0.0070	0.0049	21.29	69	900	0.0237
751	0.109	0.0082	0.0057	24.95	79	1024	0.0244
849	0.122	0.0092	0.0064	27.93	89	1158	0.0241
937	0.136	0.0102	0.0071	31.13	98	1278	0.0244
1067	0.155	0.0116	0.0081	35.48	112	1455	0.0244
1153	0.169	0.0127	0.0089	38.69	121	1572	0.0246
1238	0.178	0.0134	0.0093	40.75	130	1688	0.0241
1344	0.191	0.0143	0.0100	43.72	141	1833	0.0239

Table A1.185 Plain ferrosilicon-magnetite #1 + 1g DP001/kg at Ratio 1:2 (sp.gr.2.4)

ϕ (rpm)	Force (N)	σ (Nm)	σ_c (Nm)	τ (Nm^{-2})	ω (rad/s)	γ (s^{-1})	μ (Pa.s)
295	0.046	0.0035	0.0024	10.53	31	402	0.0262
384	0.052	0.0039	0.0027	11.90	40	524	0.0227
466	0.064	0.0048	0.0034	14.65	49	635	0.0231
554	0.074	0.0056	0.0039	16.94	58	755	0.0224
652	0.086	0.0065	0.0045	19.69	68	889	0.0221
763	0.099	0.0074	0.0052	22.66	80	1040	0.0218
847	0.108	0.0081	0.0057	24.72	89	1155	0.0214
955	0.119	0.0089	0.0062	27.24	100	1302	0.0209
1050	0.127	0.0095	0.0067	29.07	110	1432	0.0203
1154	0.138	0.0104	0.0072	31.59	121	1574	0.0201
1243	0.145	0.0109	0.0076	33.19	130	1695	0.0196
1361	0.154	0.0116	0.0081	35.25	143	1856	0.0190

Table A1.186 Plain ferrosilicon-magnetite #1 + 2g DP001/kg at Ratio 1:2 (sp.gr.2.4)

ϕ (rpm)	Force (N)	σ (Nm)	σ_c (Nm)	τ (Nm^{-2})	ω (rad/s)	γ (s^{-1})	μ (Pa.s)
293	0.048	0.0036	0.0025	10.99	31	400	0.0275
359	0.055	0.0041	0.0029	12.59	38	490	0.0257
479	0.063	0.0047	0.0033	14.42	50	653	0.0221
558	0.068	0.0051	0.0036	15.57	58	761	0.0205
663	0.072	0.0054	0.0038	16.48	69	904	0.0182
775	0.079	0.0059	0.0041	18.08	81	1057	0.0171
847	0.088	0.0066	0.0046	20.14	89	1155	0.0174
963	0.099	0.0074	0.0052	22.66	101	1313	0.0173
1064	0.113	0.0085	0.0059	25.87	111	1451	0.0178
1169	0.126	0.0095	0.0066	28.84	122	1594	0.0181
1266	0.143	0.0107	0.0075	32.73	133	1726	0.0190
1336	0.159	0.0119	0.0083	36.40	140	1822	0.0200

Table A1.187 Plain ferrosilicon-magnetite #1 + 5g DP001/kg at Ratio 1:2 (sp.gr.2.4)

ϕ (rpm)	Force (N)	σ (Nm)	σ_c (Nm)	τ (Nm^{-2})	ω (rad/s)	γ (s^{-1})	μ (Pa.s)
292	0.048	0.0036	0.0025	10.99	31	398	0.0276
369	0.053	0.0040	0.0028	12.13	39	503	0.0241
466	0.064	0.0048	0.0034	14.65	49	635	0.0231
575	0.076	0.0057	0.0040	17.40	60	784	0.0222
654	0.085	0.0064	0.0045	19.46	68	892	0.0218
749	0.094	0.0071	0.0049	21.52	78	1021	0.0211
857	0.106	0.0080	0.0056	24.27	90	1169	0.0208
958	0.121	0.0091	0.0064	27.70	100	1306	0.0212
1055	0.136	0.0102	0.0071	31.13	110	1439	0.0216
1146	0.152	0.0114	0.0080	34.80	120	1563	0.0223
1236	0.167	0.0125	0.0088	38.23	129	1685	0.0227
1344	0.177	0.0133	0.0093	40.52	141	1833	0.0221

Table A1.188 Plain ferrosilicon-magnetite #1 at Ratio 1:2 (sp.gr.2.5)

ϕ (rpm)	Force (N)	σ (Nm)	σ_c (Nm)	τ (Nm^{-2})	ω (rad/s)	γ (s^{-1})	μ (Pa.s)
291	0.072	0.0054	0.0038	16.48	30	397	0.0415
349	0.082	0.0062	0.0043	18.77	37	476	0.0394
449	0.090	0.0068	0.0047	20.60	47	612	0.0337
562	0.101	0.0076	0.0053	23.12	59	766	0.0302
660	0.111	0.0083	0.0058	25.41	69	900	0.0282
756	0.118	0.0089	0.0062	27.01	79	1031	0.0262
849	0.132	0.0099	0.0069	30.22	89	1158	0.0261
946	0.144	0.0108	0.0076	32.96	99	1290	0.0256
1047	0.156	0.0117	0.0082	35.71	110	1428	0.0250
1130	0.166	0.0125	0.0087	38.00	118	1541	0.0247
1248	0.184	0.0138	0.0097	42.12	131	1702	0.0248
1343	0.207	0.0155	0.0109	47.39	141	1831	0.0259

Table A1.189 Plain ferrosilicon-magnetite #1 + 1g DP001/kg at Ratio 1:2 (sp.gr.2.5)

ϕ (rpm)	Force (N)	σ (Nm)	σ_c (Nm)	τ (Nm^{-2})	ω (rad/s)	γ (s^{-1})	μ (Pa.s)
293	0.059	0.0044	0.0031	13.51	31	400	0.0338
375	0.068	0.0051	0.0036	15.57	39	511	0.0304
469	0.075	0.0056	0.0039	17.17	49	639	0.0268
563	0.088	0.0066	0.0046	20.14	59	768	0.0262
653	0.101	0.0076	0.0053	23.12	68	890	0.0260
759	0.116	0.0087	0.0061	26.55	79	1035	0.0257
857	0.134	0.0101	0.0070	30.67	90	1169	0.0263
958	0.149	0.0112	0.0078	34.11	100	1306	0.0261
1060	0.156	0.0117	0.0082	35.71	111	1445	0.0247
1171	0.163	0.0122	0.0086	37.31	123	1597	0.0234
1251	0.172	0.0129	0.0090	39.37	131	1706	0.0231
1376	0.198	0.0149	0.0104	45.33	144	1876	0.0242

Table A1.190 Plain ferrosilicon-magnetite #1 + 2g DP001/kg at Ratio 1:2 (sp.gr.2.5)

ϕ (rpm)	Force (N)	σ (Nm)	σ_c (Nm)	τ (Nm^{-2})	ω (rad/s)	γ (s^{-1})	μ (Pa.s)
295	0.058	0.0044	0.0030	13.28	31	402	0.0330
377	0.066	0.0050	0.0035	15.11	39	514	0.0294
472	0.071	0.0053	0.0037	16.25	49	644	0.0253
583	0.076	0.0057	0.0040	17.40	61	795	0.0219
666	0.086	0.0065	0.0045	19.69	70	908	0.0217
752	0.094	0.0071	0.0049	21.52	79	1025	0.0210
866	0.109	0.0082	0.0057	24.95	91	1181	0.0211
951	0.122	0.0092	0.0064	27.93	100	1297	0.0215
1061	0.136	0.0102	0.0071	31.13	111	1447	0.0215
1132	0.145	0.0109	0.0076	33.19	119	1544	0.0215
1244	0.143	0.0107	0.0075	32.73	130	1696	0.0193
1348	0.168	0.0126	0.0088	38.46	141	1838	0.0209

Table A1.191 plain ferrosilicon-magnetite #1 + 5g DP001/kg at Ratio 1:2 (sp.gr.2.5)

ϕ (rpm)	Force (N)	σ (Nm)	σ_c (Nm)	τ (Nm^{-2})	ω (rad/s)	γ (s^{-1})	μ (Pa.s)
293	0.070	0.0053	0.0037	16.02	31	400	0.0401
379	0.078	0.0059	0.0041	17.86	40	517	0.0346
457	0.082	0.0062	0.0043	18.77	48	623	0.0301
560	0.092	0.0069	0.0048	21.06	59	764	0.0276
649	0.106	0.0080	0.0056	24.27	68	885	0.0274
764	0.122	0.0092	0.0064	27.93	80	1042	0.0268
838	0.138	0.0104	0.0072	31.59	88	1143	0.0276
969	0.153	0.0115	0.0080	35.02	101	1321	0.0265
1047	0.162	0.0122	0.0085	37.08	110	1428	0.0260
1164	0.172	0.0129	0.0090	39.37	122	1587	0.0248
1261	0.186	0.0140	0.0098	42.58	132	1719	0.0248
1346	0.202	0.0152	0.0106	46.24	141	1835	0.0252

Table A1.192 Plain ferrosilicon-magnetite #1 at Ratio 1:2 (sp.gr.2.6)

ϕ (rpm)	Force (N)	σ (Nm)	σ_c (Nm)	τ (Nm^{-2})	ω (rad/s)	γ (s^{-1})	μ (Pa.s)
295	0.111	0.0083	0.0058	25.41	31	402	0.0632
387	0.123	0.0092	0.0065	28.16	41	528	0.0534
445	0.132	0.0099	0.0069	30.22	47	607	0.0498
546	0.138	0.0104	0.0072	31.59	57	744	0.0424
659	0.145	0.0109	0.0076	33.19	69	899	0.0369
755	0.158	0.0119	0.0083	36.17	79	1029	0.0351
863	0.182	0.0137	0.0096	41.66	90	1177	0.0354
961	0.198	0.0149	0.0104	45.33	101	1310	0.0346
1060	0.214	0.0161	0.0112	48.99	111	1445	0.0339
1172	0.226	0.0170	0.0119	51.73	123	1598	0.0324
1246	0.242	0.0182	0.0127	55.40	130	1699	0.0326
1354	0.263	0.0197	0.0138	60.20	142	1846	0.0326

Table A1.193 Plain ferrosilicon-magnetite #1 + 1g DP001/kg at Ratio 1:2 (sp.gr.2.6)

ϕ (rpm)	Force (N)	σ (Nm)	σ_c (Nm)	τ (Nm^{-2})	ω (rad/s)	γ (s^{-1})	μ (Pa.s)
285	0.085	0.0064	0.0045	19.46	30	389	0.0501
360	0.096	0.0072	0.0050	21.98	38	491	0.0448
450	0.102	0.0077	0.0054	23.35	47	614	0.0381
550	0.109	0.0082	0.0057	24.95	58	750	0.0333
645	0.119	0.0089	0.0062	27.24	68	879	0.0310
760	0.133	0.0100	0.0070	30.45	80	1036	0.0294
851	0.152	0.0114	0.0080	34.80	89	1160	0.0300
962	0.176	0.0132	0.0092	40.29	101	1312	0.0307
1093	0.189	0.0142	0.0099	43.26	114	1490	0.0290
1165	0.197	0.0148	0.0103	45.10	122	1589	0.0284
1250	0.208	0.0156	0.0109	47.61	131	1704	0.0279
1342	0.221	0.0166	0.0116	50.59	141	1830	0.0276

Table A1.194 Plain ferrosilicon-magnetite #1 + 2g DP001/kg at Ratio 1:2 (sp.gr.2.6)

ϕ (rpm)	Force (N)	σ (Nm)	σ_c (Nm)	τ (Nm^{-2})	ω (rad/s)	γ (s^{-1})	μ (Pa.s)
287	0.077	0.0058	0.0040	17.63	30	391	0.0450
362	0.088	0.0066	0.0046	20.14	38	494	0.0408
456	0.096	0.0072	0.0050	21.98	48	622	0.0353
554	0.109	0.0082	0.0057	24.95	58	755	0.0330
657	0.123	0.0092	0.0065	28.16	69	896	0.0314
747	0.139	0.0104	0.0073	31.82	78	1019	0.0312
859	0.158	0.0119	0.0083	36.17	90	1171	0.0309
971	0.175	0.0131	0.0092	40.06	102	1324	0.0303
1060	0.189	0.0142	0.0099	43.26	111	1445	0.0299
1136	0.202	0.0152	0.0106	46.24	119	1549	0.0299
1250	0.226	0.0170	0.0119	51.73	131	1704	0.0304
1344	0.244	0.0183	0.0128	55.86	141	1833	0.0305

Table A1.195 plain ferrosilicon-magnetite #1 + 5g DP001/kg at Ratio 1:2 (sp.gr.2.6)

ϕ (rpm)	Force (N)	σ (Nm)	σ_c (Nm)	τ (Nm^{-2})	ω (rad/s)	γ (s^{-1})	μ (Pa.s)
289	0.084	0.0063	0.0044	19.23	30	394	0.0488
365	0.093	0.0070	0.0049	21.29	38	498	0.0428
452	0.103	0.0077	0.0054	23.58	47	616	0.0383
534	0.111	0.0083	0.0058	25.41	56	728	0.0349
664	0.126	0.0095	0.0066	28.84	70	905	0.0319
761	0.149	0.0112	0.0078	34.11	80	1038	0.0329
862	0.163	0.0122	0.0086	37.31	90	1175	0.0317
967	0.181	0.0136	0.0095	41.43	101	1319	0.0314
1060	0.196	0.0147	0.0103	44.87	111	1445	0.0310
1145	0.205	0.0154	0.0108	46.93	120	1561	0.0301
1230	0.227	0.0170	0.0119	51.96	129	1677	0.0310
1338	0.246	0.0185	0.0129	56.31	140	1824	0.0309

Table A1.196 Plain ferrosilicon-magnetite #1 at Ratio 1:2 (sp.gr.2.7)

ϕ (rpm)	Force (N)	σ (Nm)	σ_c (Nm)	τ (Nm^{-2})	ω (rad/s)	γ (s^{-1})	μ (Pa.s)
292	0.136	0.0102	0.0071	31.13	31	398	0.0782
352	0.144	0.0108	0.0076	32.96	37	480	0.0687
464	0.154	0.0116	0.0081	35.25	49	633	0.0557
554	0.162	0.0122	0.0085	37.08	58	755	0.0491
659	0.178	0.0134	0.0093	40.75	69	899	0.0453
757	0.186	0.0140	0.0098	42.58	79	1032	0.0413
859	0.206	0.0155	0.0108	47.16	90	1171	0.0403
949	0.231	0.0173	0.0121	52.88	99	1294	0.0409
1049	0.251	0.0188	0.0132	57.46	110	1430	0.0402
1174	0.276	0.0207	0.0145	63.18	123	1601	0.0395
1248	0.298	0.0224	0.0156	68.22	131	1702	0.0401
1342	0.322	0.0242	0.0169	73.71	141	1830	0.0403

Table A1.197 Plain ferrosilicon-magnetite #1 + 1g DP001/kg at Ratio 1:2 (sp.gr.2.7)

ϕ (rpm)	Force (N)	σ (Nm)	σ_c (Nm)	τ (Nm^{-2})	ω (rad/s)	γ (s^{-1})	μ (Pa.s)
294	0.113	0.0085	0.0059	25.87	31	401	0.0645
362	0.126	0.0095	0.0066	28.84	38	494	0.0584
469	0.137	0.0103	0.0072	31.36	49	639	0.0490
558	0.143	0.0107	0.0075	32.73	58	761	0.0430
661	0.154	0.0116	0.0081	35.25	69	901	0.0391
750	0.171	0.0128	0.0090	39.14	79	1023	0.0383
845	0.187	0.0140	0.0098	42.81	88	1152	0.0372
947	0.202	0.0152	0.0106	46.24	99	1291	0.0358
1046	0.223	0.0167	0.0117	51.05	110	1426	0.0358
1156	0.255	0.0191	0.0134	58.37	121	1576	0.0370
1249	0.283	0.0212	0.0149	64.78	131	1703	0.0380
1347	0.302	0.0227	0.0159	69.13	141	1837	0.0376

Table A1.198 Plain ferrosilicon-magnetite #1 + 2g DP001/kg at Ratio 1:2 (sp.gr.2.7)

ϕ (rpm)	Force (N)	σ (Nm)	σ_c (Nm)	τ (Nm^{-2})	ω (rad/s)	γ (s^{-1})	μ (Pa.s)
285	0.108	0.0081	0.0057	24.72	30	389	0.0636
378	0.112	0.0084	0.0059	25.64	40	515	0.0497
486	0.122	0.0092	0.0064	27.93	51	663	0.0421
553	0.133	0.0100	0.0070	30.45	58	754	0.0404
643	0.144	0.0108	0.0076	32.96	67	877	0.0376
753	0.161	0.0121	0.0085	36.86	79	1027	0.0359
867	0.175	0.0131	0.0092	40.06	91	1182	0.0339
951	0.182	0.0137	0.0096	41.66	100	1297	0.0321
1051	0.206	0.0155	0.0108	47.16	110	1433	0.0329
1139	0.216	0.0162	0.0113	49.45	119	1553	0.0318
1238	0.224	0.0168	0.0118	51.28	130	1688	0.0304
1348	0.238	0.0179	0.0125	54.48	141	1838	0.0296

Table A1.199 Plain ferrosilicon-magnetite #1 + 5g DP001/kg at Ratio 1:2 (sp.gr.2.7)

ϕ (rpm)	Force (N)	σ (Nm)	σ_c (Nm)	τ (Nm^{-2})	ω (rad/s)	γ (s^{-1})	μ (Pa.s)
290	0.106	0.0080	0.0056	24.3	30	395	0.0614
378	0.113	0.0085	0.0059	25.9	40	515	0.0502
460	0.121	0.0091	0.0064	27.7	48	627	0.0442
566	0.132	0.0099	0.0069	30.2	59	772	0.0392
657	0.142	0.0107	0.0075	32.5	69	896	0.0363
749	0.154	0.0116	0.0081	35.3	78	1021	0.0345
857	0.186	0.0140	0.0098	42.6	90	1169	0.0364
953	0.203	0.0152	0.0107	46.5	100	1299	0.0358
1058	0.228	0.0171	0.0120	52.2	111	1443	0.0362
1148	0.249	0.0187	0.0131	57.0	120	1565	0.0364
1238	0.274	0.0206	0.0144	62.7	130	1688	0.0372
1343	0.296	0.0222	0.0155	67.8	141	1831	0.0370

Table A1.200 Plain ferrosilicon-magnetite #1 at Ratio 1:2 (sp.gr.2.8)

ϕ (rpm)	Force (N)	σ (Nm)	σ_c (Nm)	τ (Nm^{-2})	ω (rad/s)	γ (s^{-1})	μ (Pa.s)
289	0.181	0.0136	0.0095	41.43	30	394	0.1051
353	0.197	0.0148	0.0103	45.10	37	481	0.0937
444	0.208	0.0156	0.0109	47.61	46	605	0.0786
556	0.220	0.0165	0.0116	50.36	58	758	0.0664
646	0.229	0.0172	0.0120	52.42	68	881	0.0595
768	0.243	0.0182	0.0128	55.63	80	1047	0.0531
889	0.261	0.0196	0.0137	59.75	93	1212	0.0493
965	0.282	0.0212	0.0148	64.55	101	1316	0.0491
1065	0.323	0.0242	0.0170	73.94	112	1452	0.0509
1144	0.349	0.0262	0.0183	79.89	120	1560	0.0512
1242	0.376	0.0282	0.0197	86.07	130	1694	0.0508
1340	0.401	0.0301	0.0211	91.80	140	1827	0.0502

Table A1.201 Plain ferrosilicon-magnetite #1 + 1g DP001/kg at Ratio 1:2 (sp.gr.2.8)

ϕ (rpm)	Force (N)	σ (Nm)	σ_c (Nm)	τ (Nm^{-2})	ω (rad/s)	γ (s^{-1})	μ (Pa.s)
297	0.166	0.0125	0.0087	38.00	31	405	0.0938
382	0.186	0.0140	0.0098	42.58	40	521	0.0817
446	0.195	0.0146	0.0102	44.64	47	608	0.0734
552	0.204	0.0153	0.0107	46.70	58	753	0.0620
652	0.212	0.0159	0.0111	48.53	68	889	0.0546
752	0.226	0.0170	0.0119	51.73	79	1025	0.0505
872	0.248	0.0186	0.0130	56.77	91	1189	0.0477
963	0.267	0.0200	0.0140	61.12	101	1313	0.0465
1072	0.298	0.0224	0.0156	68.22	112	1462	0.0467
1162	0.315	0.0236	0.0165	72.11	122	1584	0.0455
1274	0.348	0.0261	0.0183	79.66	133	1737	0.0459
1362	0.386	0.0290	0.0203	88.36	143	1857	0.0476

Table A1.202 Plain ferrosilicon-magnetite #1 + 2g DP001/kg at Ratio 1:2 (sp.gr.2.8)

ϕ (rpm)	Force (N)	σ (Nm)	σ_c (Nm)	τ (Nm^{-2})	ω (rad/s)	γ (s^{-1})	μ (Pa.s)
285	0.158	0.0119	0.0083	36.17	30	389	0.0931
348	0.166	0.0125	0.0087	38.00	36	475	0.0801
450	0.174	0.0131	0.0091	39.83	47	614	0.0649
536	0.186	0.0140	0.0098	42.58	56	731	0.0583
649	0.198	0.0149	0.0104	45.33	68	885	0.0512
762	0.206	0.0155	0.0108	47.16	80	1039	0.0454
857	0.223	0.0167	0.0117	51.05	90	1169	0.0437
937	0.236	0.0177	0.0124	54.02	98	1278	0.0423
1057	0.260	0.0195	0.0137	59.52	111	1441	0.0413
1168	0.289	0.0217	0.0152	66.16	122	1593	0.0415
1246	0.315	0.0236	0.0165	72.11	130	1699	0.0424
1340	0.338	0.0254	0.0177	77.37	140	1827	0.0423

Table A1.203 Plain ferrosilicon-magnetite #1 + 5g DP001/kg at Ratio 1:2 (sp.gr.2.8)

ϕ (rpm)	Force (N)	σ (Nm)	σ_c (Nm)	τ (Nm^{-2})	ω (rad/s)	γ (s^{-1})	μ (Pa.s)
291	0.174	0.0131	0.0091	39.8	30	397	0.1004
357	0.182	0.0137	0.0096	41.7	37	487	0.0856
459	0.194	0.0146	0.0102	44.4	48	626	0.0710
553	0.203	0.0152	0.0107	46.5	58	754	0.0616
649	0.217	0.0163	0.0114	49.7	68	885	0.0561
781	0.238	0.0179	0.0125	54.5	82	1065	0.0512
845	0.252	0.0189	0.0132	57.7	88	1152	0.0501
948	0.270	0.0203	0.0142	61.8	99	1293	0.0478
1062	0.304	0.0228	0.0160	69.6	111	1448	0.0481
1160	0.338	0.0254	0.0177	77.4	121	1582	0.0489
1248	0.358	0.0269	0.0188	82.0	131	1702	0.0482
1360	0.398	0.0299	0.0209	91.1	142	1854	0.0491

A1.3 Experimental Series B: The Effect of Particle Size and Shape on the Viscosity of Heavy Medium Suspensions

A1.3.1 Aim of the Experiment

The aim of these experiments was to investigate the effect of the addition coarser particles on the viscosity of heavy medium suspensions. The rheological properties of heavy medium suspensions are highly dependant on the media particles size distribution and shape of the particles. Thus, it is of great importance to know what the effect coarser and smoother particles are on the rheology of heavy medium suspensions.

A1.3.2 Experimental Conditions

Magnetite #2 was added at different ratios to both magnetite #1 and ferrosilicon suspensions. Magnetite #2 additions were made at ratios 1:1, 2:1; and 1:2 for both magnetite #1 and ferrosilicon suspensions. The mass of magnetite #2 used with ferrosilicon was the same as that given in Table A1.108 to Table A1.110. Because of the instability of the suspensions at low specific gravities, measurements were only done at specific gravities 2.8 to 3.2. The mass of magnetite #2 used with magnetite #1 is given below, for specific gravities 2.0-2.8, 2.0-2.6, and 2.0-2.8 for ratios 1:1, 2:1 and 1:2, respectively.

Table A1.204 Mass magnetite #1 and #2 at Ratio 1:1

D / kgm^{-3}	x / %	M_{Solids} / g	$M_{Mag\#1}$ / g	$M_{Mag\#2}$ / g
2000	64	177	88	88
2100	67	202	101	101
2200	70	229	115	115
2300	72	259	130	130
2400	74	292	146	146
2500	77	327	164	164
2600	79	367	183	183
2700	80	410	205	205
2800	82	458	229	229
2900	84	512	256	256

Table A1.205 Mass magnetite #1 and #2 at Ratio 2:1

D / kgm^{-3}	x / %	M_{Solids} / g	$M_{Mag\#1}$ / g	$M_{Mag\#2}$ / g
2000	64	176	118	59
2100	67	202	134	67
2200	70	229	153	76
2300	72	259	173	86
2400	74	291	194	97
2500	77	327	218	109
2600	79	366	244	122
2700	80	409	273	136
2800	82	457	305	152
2900	84	510	340	170

The amount magnetite used at a ratio 2:1 is similar to that given in Table A1.205, with the masses reversed for magnetite #1 and #2.

A1.3.3 Experimental Results

A1.3.3.1 Magnetite #1 and Magnetite #2 Suspensions

Table A1.206 Plain magnetite #1-magnetite #2 at Ratio 1:1 (sp.gr.2.0)

ϕ (rpm)	Force (N)	σ (Nm)	σ_c (Nm)	τ (Nm^{-2})	ω (rad/s)	γ (s^{-1})	μ (Pa.s)
287	0.014	0.0011	0.0007	3.20	30	391	0.0082
375	0.016	0.0012	0.0008	3.66	39	511	0.0072
448	0.019	0.0014	0.0010	4.35	47	611	0.0071
576	0.025	0.0019	0.0013	5.72	60	785	0.0073
670	0.033	0.0025	0.0017	7.55	70	914	0.0083
781	0.041	0.0031	0.0022	9.39	82	1065	0.0088
852	0.046	0.0035	0.0024	10.53	89	1162	0.0091
961	0.058	0.0044	0.0030	13.28	101	1310	0.0101
1034	0.067	0.0050	0.0035	15.34	108	1410	0.0109
1128	0.075	0.0056	0.0039	17.17	118	1538	0.0112
1248	0.086	0.0065	0.0045	19.69	131	1702	0.0116
1342	0.093	0.0070	0.0049	21.29	141	1830	0.0116

Table A1.207 Plain magnetite #1-magnetite #2 at Ratio 1:1 (sp.gr.2.1)

ϕ (rpm)	Force (N)	σ (Nm)	σ_c (Nm)	τ (Nm^{-2})	ω (rad/s)	γ (s^{-1})	μ (Pa.s)
290	0.016	0.0012	0.0008	3.66	30	395	0.0093
352	0.018	0.0014	0.0009	4.12	37	480	0.0086
446	0.025	0.0019	0.0013	5.72	47	608	0.0094
549	0.031	0.0023	0.0016	7.10	57	749	0.0095
668	0.038	0.0029	0.0020	8.70	70	911	0.0096
755	0.049	0.0037	0.0026	11.22	79	1029	0.0109
845	0.056	0.0042	0.0029	12.82	88	1152	0.0111
967	0.067	0.0050	0.0035	15.34	101	1319	0.0116
1062	0.076	0.0057	0.0040	17.40	111	1448	0.0120
1186	0.091	0.0068	0.0048	20.83	124	1617	0.0129
1248	0.102	0.0077	0.0054	23.35	131	1702	0.0137
1376	0.112	0.0084	0.0059	25.64	144	1876	0.0137

Table A1.208 Plain magnetite #1-magnetite #2 at Ratio 1:1 (sp.gr.2.2)

ϕ (rpm)	Force (N)	σ (Nm)	σ_c (Nm)	τ (Nm^{-2})	ω (rad/s)	γ (s^{-1})	μ (Pa.s)
285	0.018	0.0014	0.0009	4.12	30	389	0.0106
367	0.023	0.0017	0.0012	5.27	38	500	0.0105
468	0.028	0.0021	0.0015	6.41	49	638	0.0100
563	0.035	0.0026	0.0018	8.01	59	768	0.0104
648	0.043	0.0032	0.0023	9.84	68	884	0.0111
737	0.049	0.0037	0.0026	11.22	77	1005	0.0112
841	0.058	0.0044	0.0030	13.28	88	1147	0.0116
970	0.068	0.0051	0.0036	15.57	102	1323	0.0118
1087	0.081	0.0061	0.0043	18.54	114	1482	0.0125
1144	0.093	0.0070	0.0049	21.29	120	1560	0.0136
1236	0.104	0.0078	0.0055	23.81	129	1685	0.0141
1354	0.116	0.0087	0.0061	26.55	142	1846	0.0144

Table A1.209 Plain magnetite #1-magnetite #2 at Ratio 1:1 (sp.gr.2.3)

ϕ (rpm)	Force (N)	σ (Nm)	σ_c (Nm)	τ (Nm^{-2})	ω (rad/s)	γ (s^{-1})	μ (Pa.s)
285	0.023	0.0017	0.0012	5.27	30	389	0.0135
368	0.028	0.0021	0.0015	6.41	39	502	0.0128
463	0.036	0.0027	0.0019	8.24	48	631	0.0131
558	0.045	0.0034	0.0024	10.30	58	761	0.0135
659	0.059	0.0044	0.0031	13.51	69	899	0.0150
755	0.071	0.0053	0.0037	16.25	79	1029	0.0158
829	0.080	0.0060	0.0042	18.31	87	1130	0.0162
968	0.097	0.0073	0.0051	22.20	101	1320	0.0168
1064	0.109	0.0082	0.0057	24.95	111	1451	0.0172
1142	0.121	0.0091	0.0064	27.70	120	1557	0.0178
1240	0.136	0.0102	0.0071	31.13	130	1691	0.0184
1364	0.151	0.0113	0.0079	34.57	143	1860	0.0186

Table A1.210 Plain magnetite #1-magnetite #2 at Ratio 1:1 (sp.gr.2.4)

ϕ (rpm)	Force (N)	σ (Nm)	σ_c (Nm)	τ (Nm^{-2})	ω (rad/s)	γ (s^{-1})	μ (Pa.s)
287	0.035	0.0026	0.0018	8.01	30	391	0.0205
381	0.043	0.0032	0.0023	9.84	40	520	0.0189
469	0.051	0.0038	0.0027	11.67	49	639	0.0183
546	0.062	0.0047	0.0033	14.19	57	744	0.0191
667	0.074	0.0056	0.0039	16.94	70	909	0.0186
779	0.083	0.0062	0.0044	19.00	82	1062	0.0179
861	0.098	0.0074	0.0051	22.43	90	1174	0.0191
946	0.113	0.0085	0.0059	25.87	99	1290	0.0201
1033	0.124	0.0093	0.0065	28.39	108	1409	0.0202
1146	0.139	0.0104	0.0073	31.82	120	1563	0.0204
1256	0.154	0.0116	0.0081	35.25	132	1713	0.0206
1360	0.176	0.0132	0.0092	40.29	142	1854	0.0217

Table A1.211 Plain magnetite #1-magnetite #2 at Ratio 1:1 (sp.gr.2.5)

ϕ (rpm)	Force (N)	σ (Nm)	σ_c (Nm)	τ (Nm^{-2})	ω (rad/s)	γ (s^{-1})	μ (Pa.s)
279	0.046	0.0035	0.0024	10.53	29	380	0.0277
383	0.051	0.0038	0.0027	11.67	40	522	0.0224
491	0.063	0.0047	0.0033	14.42	51	669	0.0215
554	0.070	0.0053	0.0037	16.02	58	755	0.0212
654	0.082	0.0062	0.0043	18.77	68	892	0.0210
766	0.094	0.0071	0.0049	21.52	80	1044	0.0206
875	0.105	0.0079	0.0055	24.04	92	1193	0.0201
943	0.116	0.0087	0.0061	26.55	99	1286	0.0207
1031	0.136	0.0102	0.0071	31.13	108	1406	0.0221
1144	0.158	0.0119	0.0083	36.17	120	1560	0.0232
1246	0.176	0.0132	0.0092	40.29	130	1699	0.0237
1347	0.192	0.0144	0.0101	43.95	141	1837	0.0239

Table A1.212 Plain magnetite #1-magnetite #2 at Ratio 1:1 (sp.gr.2.6)

ϕ (rpm)	Force (N)	σ (Nm)	σ_c (Nm)	τ (Nm^{-2})	ω (rad/s)	γ (s^{-1})	μ (Pa.s)
275	0.079	0.0059	0.0041	18.08	29	375	0.0482
357	0.084	0.0063	0.0044	19.23	37	487	0.0395
475	0.092	0.0069	0.0048	21.06	50	648	0.0325
576	0.102	0.0077	0.0054	23.35	60	785	0.0297
649	0.111	0.0083	0.0058	25.41	68	885	0.0287
743	0.128	0.0096	0.0067	29.30	78	1013	0.0289
840	0.148	0.0111	0.0078	33.88	88	1145	0.0296
960	0.171	0.0128	0.0090	39.14	101	1309	0.0299
1033	0.186	0.0140	0.0098	42.58	108	1409	0.0302
1125	0.209	0.0157	0.0110	47.84	118	1534	0.0312
1224	0.224	0.0168	0.0118	51.28	128	1669	0.0307
1350	0.242	0.0182	0.0127	55.40	141	1841	0.0301

Table A1.213 Plain magnetite #1-magnetite #2 at Ratio 1:1 (sp.gr.2.7)

ϕ (rpm)	Force (N)	σ (Nm)	σ_c (Nm)	τ (Nm^{-2})	ω (rad/s)	γ (s^{-1})	μ (Pa.s)
272	0.098	0.0074	0.0051	22.43	28	371	0.0605
348	0.108	0.0081	0.0057	24.72	36	475	0.0521
475	0.115	0.0086	0.0060	26.33	50	648	0.0406
597	0.131	0.0098	0.0069	29.99	63	814	0.0368
663	0.138	0.0104	0.0072	31.59	69	904	0.0349
775	0.153	0.0115	0.0080	35.02	81	1057	0.0331
843	0.174	0.0131	0.0091	39.83	88	1149	0.0347
946	0.198	0.0149	0.0104	45.33	99	1290	0.0351
1045	0.215	0.0161	0.0113	49.22	109	1425	0.0345
1159	0.251	0.0188	0.0132	57.46	121	1580	0.0364
1257	0.273	0.0205	0.0143	62.49	132	1714	0.0365
1352	0.291	0.0218	0.0153	66.61	142	1844	0.0361

Table A1.214 Plain magnetite #1-magnetite #2 at Ratio 1:1 (sp.gr.2.8)

ϕ (rpm)	Force (N)	σ (Nm)	σ_c (Nm)	τ (Nm^{-2})	ω (rad/s)	γ (s^{-1})	μ (Pa.s)
283	0.187	0.0140	0.0098	42.81	30	386	0.1109
377	0.198	0.0149	0.0104	45.33	39	514	0.0882
446	0.209	0.0157	0.0110	47.84	47	608	0.0787
577	0.218	0.0164	0.0114	49.90	60	787	0.0634
666	0.234	0.0176	0.0123	53.57	70	908	0.0590
754	0.245	0.0184	0.0129	56.08	79	1028	0.0546
847	0.256	0.0192	0.0134	58.60	89	1155	0.0507
941	0.265	0.0199	0.0139	60.66	99	1283	0.0473
1047	0.298	0.0224	0.0156	68.22	110	1428	0.0478
1126	0.313	0.0235	0.0164	71.65	118	1535	0.0467
1234	0.362	0.0272	0.0190	82.87	129	1683	0.0492
1330	0.419	0.0314	0.0220	95.92	139	1814	0.0529

Table A1.215 Plain magnetite #1-magnetiet #2 at Ratio 2:1 (sp.gr.2.0)

ϕ (rpm)	Force (N)	σ (Nm)	σ_c (Nm)	τ (Nm^{-2})	ω (rad/s)	γ (s^{-1})	μ (Pa.s)
283	0.021	0.0016	0.0011	4.81	30	386	0.0125
356	0.028	0.0021	0.0015	6.41	37	485	0.0132
459	0.035	0.0026	0.0018	8.01	48	626	0.0128
562	0.041	0.0031	0.0022	9.39	59	766	0.0122
666	0.051	0.0038	0.0027	11.67	70	908	0.0129
761	0.067	0.0050	0.0035	15.34	80	1038	0.0148
848	0.075	0.0056	0.0039	17.17	89	1156	0.0148
949	0.087	0.0065	0.0046	19.92	99	1294	0.0154
1038	0.095	0.0071	0.0050	21.75	109	1415	0.0154
1142	0.104	0.0078	0.0055	23.81	120	1557	0.0153
1232	0.113	0.0085	0.0059	25.87	129	1680	0.0154
1332	0.122	0.0092	0.0064	27.93	139	1816	0.0154

Table A1.216 Plain magnetite #1-magnetite #2 at Ratio 2:1 (sp.gr.2.1)

ϕ (rpm)	Force (N)	σ (Nm)	σ_c (Nm)	τ (Nm^{-2})	ω (rad/s)	γ (s^{-1})	μ (Pa.s)
279	0.024	0.0018	0.0013	5.49	29	380	0.0144
383	0.031	0.0023	0.0016	7.10	40	522	0.0136
442	0.036	0.0027	0.0019	8.24	46	603	0.0137
540	0.043	0.0032	0.0023	9.84	57	736	0.0134
669	0.054	0.0041	0.0028	12.36	70	912	0.0136
756	0.061	0.0046	0.0032	13.96	79	1031	0.0135
890	0.083	0.0062	0.0044	19.00	93	1214	0.0157
969	0.096	0.0072	0.0050	21.98	101	1321	0.0166
1062	0.103	0.0077	0.0054	23.58	111	1448	0.0163
1152	0.113	0.0085	0.0059	25.87	121	1571	0.0165
1280	0.127	0.0095	0.0067	29.07	134	1745	0.0167
1354	0.136	0.0102	0.0071	31.13	142	1846	0.0169

Table A1. 217 Plain magnetite #1-magnetite #2 at Ratio 2:1 (sp.gr.2.2)

ϕ (rpm)	Force (N)	σ (Nm)	σ_c (Nm)	τ (Nm^{-2})	ω (rad/s)	γ (s^{-1})	μ (Pa.s)
285	0.029	0.0022	0.0015	6.64	30	389	0.0171
347	0.034	0.0026	0.0018	7.78	36	473	0.0164
491	0.043	0.0032	0.0023	9.84	51	669	0.0147
577	0.052	0.0039	0.0027	11.90	60	787	0.0151
676	0.061	0.0046	0.0032	13.96	71	922	0.0151
773	0.075	0.0056	0.0040	17.24	81	1054	0.0164
855	0.084	0.0063	0.0044	19.23	90	1166	0.0165
979	0.099	0.0074	0.0052	22.66	103	1335	0.0170
1065	0.119	0.0089	0.0062	27.24	112	1452	0.0188
1156	0.132	0.0099	0.0069	30.22	121	1576	0.0192
1269	0.147	0.0110	0.0077	33.65	133	1730	0.0194
1361	0.160	0.0120	0.0084	36.63	143	1856	0.0197

Table A1. 218 Plain magnetite #1-magnetite #2 at Ratio 2:1 (sp.gr.2.3)

ϕ (rpm)	Force (N)	σ (Nm)	σ_c (Nm)	τ (Nm^{-2})	ω (rad/s)	γ (s^{-1})	μ (Pa.s)
279	0.043	0.0032	0.0023	9.84	29	380	0.0259
345	0.048	0.0036	0.0025	10.99	36	470	0.0234
461	0.056	0.0042	0.0029	12.82	48	629	0.0204
554	0.068	0.0051	0.0036	15.57	58	755	0.0206
643	0.077	0.0058	0.0040	17.63	67	877	0.0201
750	0.089	0.0067	0.0047	20.37	79	1023	0.0199
857	0.103	0.0077	0.0054	23.58	90	1169	0.0202
942	0.128	0.0096	0.0067	29.30	99	1284	0.0228
1045	0.144	0.0108	0.0076	33.03	109	1425	0.0232
1149	0.161	0.0121	0.0085	36.86	120	1567	0.0235
1260	0.179	0.0134	0.0094	40.98	132	1718	0.0239
1348	0.191	0.0143	0.0100	43.72	141	1838	0.0238

Table A1.219 Plain magnetite #1-magnetite #2 at Ratio 2:1 (sp.gr.2.4)

ϕ (rpm)	Force (N)	σ (Nm)	σ_c (Nm)	τ (Nm^{-2})	ω (rad/s)	γ (s^{-1})	μ (Pa.s)
289	0.075	0.0056	0.0039	17.17	30	394	0.0436
371	0.086	0.0065	0.0045	19.69	39	506	0.0389
454	0.093	0.0070	0.0049	21.29	48	619	0.0344
544	0.100	0.0075	0.0053	22.89	57	742	0.0309
654	0.113	0.0085	0.0059	25.87	68	892	0.0290
756	0.125	0.0094	0.0066	28.61	79	1031	0.0278
841	0.136	0.0102	0.0071	31.13	88	1147	0.0271
941	0.147	0.0110	0.0077	33.65	99	1283	0.0262
1072	0.168	0.0126	0.0088	38.46	112	1462	0.0263
1181	0.189	0.0142	0.0099	43.26	124	1610	0.0269
1274	0.203	0.0152	0.0107	46.47	133	1737	0.0268
1374	0.234	0.0176	0.0123	53.57	144	1874	0.0286

Table A1.220 Plain magnetite #1-magnetite #2 at Ratio 2:1 (sp.gr.2.5)

ϕ (rpm)	Force (N)	σ (Nm)	σ_c (Nm)	τ (Nm^{-2})	ω (rad/s)	γ (s^{-1})	μ (Pa.s)
287	0.089	0.0067	0.0047	20.37	30	391	0.0521
362	0.096	0.0072	0.0050	21.98	38	494	0.0445
458	0.102	0.0077	0.0054	23.35	48	625	0.0374
540	0.108	0.0081	0.0057	24.72	57	736	0.0336
646	0.121	0.0091	0.0064	27.70	68	881	0.0314
753	0.140	0.0105	0.0074	32.05	79	1027	0.0312
838	0.160	0.0120	0.0084	36.63	88	1143	0.0321
949	0.186	0.0140	0.0098	42.58	99	1294	0.0329
1039	0.204	0.0153	0.0107	46.70	109	1417	0.0330
1138	0.225	0.0169	0.0118	51.51	119	1552	0.0332
1254	0.248	0.0186	0.0130	56.77	131	1710	0.0332
1340	0.261	0.0196	0.0137	59.75	140	1827	0.0327

Table A1.221 Plain magnetite #1-magnetite #2 at Ratio 2:1 (sp.gr.2.6)

ϕ (rpm)	Force (N)	σ (Nm)	σ_c (Nm)	τ (Nm^{-2})	ω (rad/s)	γ (s^{-1})	μ (Pa.s)
288	0.105	0.0079	0.0055	24.04	30	393	0.0612
394	0.123	0.0092	0.0065	28.16	41	537	0.0524
474	0.131	0.0098	0.0069	29.99	50	646	0.0464
598	0.142	0.0107	0.0075	32.51	63	815	0.0399
667	0.153	0.0115	0.0080	35.02	70	909	0.0385
744	0.168	0.0126	0.0088	38.46	78	1014	0.0379
827	0.185	0.0139	0.0097	42.35	87	1128	0.0376
958	0.222	0.0167	0.0117	50.82	100	1306	0.0389
1055	0.256	0.0192	0.0134	58.60	110	1439	0.0407
1145	0.286	0.0215	0.0150	65.47	120	1561	0.0419
1258	0.305	0.0229	0.0160	69.82	132	1715	0.0407
1376	0.336	0.0252	0.0176	76.92	144	1876	0.0410

Table A1.222 Plain magnetite #1-magnetite #2 at Ratio 1:2 (sp.gr.2.0)

ϕ (rpm)	Force (N)	σ (Nm)	σ_c (Nm)	τ (Nm^{-2})	ω (rad/s)	γ (s^{-1})	μ (Pa.s)
283	0.008	0.0006	0.00042	1.83	30	386	0.0047
384	0.012	0.0009	0.00063	2.75	40	524	0.0052
469	0.016	0.0012	0.00084	3.66	49	639	0.0057
571	0.020	0.0015	0.00105	4.58	60	779	0.0059
658	0.026	0.0020	0.00137	5.95	69	897	0.0066
787	0.035	0.0026	0.00184	8.01	82	1073	0.0075
864	0.042	0.0032	0.00221	9.61	90	1178	0.0082
946	0.047	0.0035	0.00247	10.76	99	1290	0.0083
1051	0.052	0.0039	0.00273	11.90	110	1433	0.0083
1149	0.055	0.0041	0.00289	12.59	120	1567	0.0080
1249	0.060	0.0045	0.00315	13.73	131	1703	0.0081
1373	0.068	0.0051	0.00357	15.57	144	1872	0.0083

Table A1.223 Plain magnetite #1-magnetite #2 at Ratio 1:2 (sp.gr.2.1)

ϕ (rpm)	Force (N)	σ (Nm)	σ_c (Nm)	τ (Nm^{-2})	ω (rad/s)	γ (s^{-1})	μ (Pa.s)
285	0.010	0.0008	0.0005	2.29	30	389	0.0059
358	0.012	0.0009	0.0006	2.75	37	488	0.0056
466	0.016	0.0012	0.0008	3.66	49	635	0.0058
596	0.021	0.0016	0.0011	4.81	62	813	0.0059
687	0.026	0.0020	0.0014	5.95	72	937	0.0064
787	0.032	0.0024	0.0017	7.33	82	1073	0.0068
893	0.045	0.0034	0.0024	10.30	94	1218	0.0085
966	0.051	0.0038	0.0027	11.67	101	1317	0.0089
1070	0.055	0.0041	0.0029	12.59	112	1459	0.0086
1140	0.060	0.0045	0.0032	13.73	119	1554	0.0088
1246	0.066	0.0050	0.0035	15.11	130	1699	0.0089
1334	0.071	0.0053	0.0037	16.25	140	1819	0.0089

Table A1.224 Plain magnetite #1-magnetite #2 at Ratio 1:2 (sp.gr.2.2)

ϕ (rpm)	Force (N)	σ (Nm)	σ_c (Nm)	τ (Nm^{-2})	ω (rad/s)	γ (s^{-1})	μ (Pa.s)
283	0.016	0.0012	0.0008	3.66	30	386	0.0095
371	0.021	0.0016	0.0011	4.81	39	506	0.0095
465	0.024	0.0018	0.0013	5.49	49	634	0.0087
561	0.029	0.0022	0.0015	6.64	59	765	0.0087
663	0.034	0.0026	0.0018	7.78	69	904	0.0086
763	0.042	0.0032	0.0022	9.61	80	1040	0.0092
867	0.052	0.0039	0.0027	11.90	91	1182	0.0101
943	0.063	0.0047	0.0033	14.42	99	1286	0.0112
1056	0.070	0.0053	0.0037	16.02	111	1440	0.0111
1154	0.077	0.0058	0.0040	17.63	121	1574	0.0112
1234	0.086	0.0065	0.0045	19.69	129	1683	0.0117
1344	0.093	0.0070	0.0049	21.29	141	1833	0.0116

Table A1.225 Plain magnetite #1-magnetite #2 at Ratio 1:2 (sp.gr.2.3)

ϕ (rpm)	Force (N)	σ (Nm)	σ_c (Nm)	τ (Nm^{-2})	ω (rad/s)	γ (s^{-1})	μ (Pa.s)
288	0.024	0.0018	0.0013	5.49	30	393	0.0140
384	0.029	0.0022	0.0015	6.64	40	524	0.0127
485	0.032	0.0024	0.0017	7.33	51	661	0.0111
555	0.042	0.0032	0.0022	9.61	58	757	0.0127
654	0.045	0.0034	0.0024	10.30	68	892	0.0116
735	0.049	0.0037	0.0026	11.22	77	1002	0.0112
845	0.057	0.0043	0.0030	13.05	88	1152	0.0113
948	0.066	0.0050	0.0035	15.11	99	1293	0.0117
1058	0.073	0.0055	0.0038	16.71	111	1443	0.0116
1167	0.085	0.0064	0.0045	19.46	122	1591	0.0122
1251	0.096	0.0072	0.0050	21.98	131	1706	0.0129
1368	0.102	0.0077	0.0054	23.35	143	1865	0.0125

Table A1.226 Plain magnetite #1-magnetite #2 at Ratio 1:2 (sp.gr.2.4)

ϕ (rpm)	Force (N)	σ (Nm)	σ_c (Nm)	τ (Nm^{-2})	ω (rad/s)	γ (s^{-1})	μ (Pa.s)
291	0.032	0.0024	0.0017	7.33	30	397	0.0185
390	0.038	0.0029	0.0020	8.70	41	532	0.0164
484	0.042	0.0032	0.0022	9.61	51	660	0.0146
560	0.048	0.0036	0.0025	10.99	59	764	0.0144
659	0.053	0.0040	0.0028	12.13	69	899	0.0135
761	0.061	0.0046	0.0032	13.96	80	1038	0.0135
849	0.072	0.0054	0.0038	16.48	89	1158	0.0142
964	0.080	0.0060	0.0042	18.31	101	1314	0.0139
1041	0.088	0.0066	0.0046	20.14	109	1419	0.0142
1140	0.096	0.0072	0.0050	21.98	119	1554	0.0141
1232	0.112	0.0084	0.0059	25.64	129	1680	0.0153
1364	0.128	0.0096	0.0067	29.30	143	1860	0.0158

Table A1.227 Plain magnetite #1-magnetite #2 at Ratio 1:2 (sp.gr.2.5)

ϕ (rpm)	Force (N)	σ (Nm)	σ_c (Nm)	τ (Nm^{-2})	ω (rad/s)	γ (s^{-1})	μ (Pa.s)
281	0.043	0.0032	0.0023	9.84	29	383	0.0257
368	0.046	0.0035	0.0024	10.53	39	502	0.0210
470	0.051	0.0038	0.0027	11.67	49	641	0.0182
573	0.060	0.0045	0.0032	13.73	60	781	0.0176
660	0.069	0.0052	0.0036	15.80	69	900	0.0176
741	0.081	0.0061	0.0043	18.54	78	1010	0.0184
851	0.096	0.0072	0.0050	21.98	89	1160	0.0189
949	0.105	0.0079	0.0055	24.04	99	1294	0.0186
1057	0.121	0.0091	0.0064	27.70	111	1441	0.0192
1160	0.136	0.0102	0.0071	31.13	121	1582	0.0197
1279	0.148	0.0111	0.0078	33.88	134	1744	0.0194
1369	0.159	0.0119	0.0083	36.40	143	1867	0.0195

Table A1.228 Plain magnetite #1-magnetite #2 at Ratio 1:2 (sp.gr.2.6)

ϕ (rpm)	Force (N)	σ (Nm)	σ_c (Nm)	τ (Nm^{-2})	ω (rad/s)	γ (s^{-1})	μ (Pa.s)
286	0.048	0.0036	0.0025	10.99	30	390	0.0282
390	0.053	0.0040	0.0028	12.13	41	532	0.0228
456	0.056	0.0042	0.0029	12.82	48	622	0.0206
546	0.061	0.0046	0.0032	13.96	57	744	0.0188
645	0.070	0.0053	0.0037	16.02	68	879	0.0182
773	0.082	0.0062	0.0043	18.77	81	1054	0.0178
849	0.098	0.0074	0.0051	22.43	89	1158	0.0194
950	0.116	0.0087	0.0061	26.55	99	1295	0.0205
1031	0.130	0.0098	0.0068	29.76	108	1406	0.0212
1138	0.148	0.0111	0.0078	33.88	119	1552	0.0218
1238	0.167	0.0125	0.0088	38.23	130	1688	0.0226
1372	0.186	0.0140	0.0098	42.58	144	1871	0.0228

Table A1.229 Plain magnetite #1-magnetite #2 at Ratio 1:2 (sp.gr.2.7)

ϕ (rpm)	Force (N)	σ (Nm)	σ_c (Nm)	τ (Nm^{-2})	ω (rad/s)	γ (s^{-1})	μ (Pa.s)
285	0.075	0.0056	0.0039	17.17	30	389	0.0442
369	0.082	0.0062	0.0043	18.77	39	503	0.0373
448	0.085	0.0064	0.0045	19.46	47	611	0.0319
554	0.096	0.0072	0.0050	21.98	58	755	0.0291
658	0.108	0.0081	0.0057	24.72	69	897	0.0276
755	0.125	0.0094	0.0066	28.61	79	1029	0.0278
847	0.141	0.0106	0.0074	32.28	89	1155	0.0279
951	0.158	0.0119	0.0083	36.17	100	1297	0.0279
1052	0.176	0.0132	0.0092	40.29	110	1434	0.0281
1149	0.194	0.0146	0.0102	44.41	120	1567	0.0283
1246	0.209	0.0157	0.0110	47.84	130	1699	0.0282
1340	0.226	0.0170	0.0119	51.73	140	1827	0.0283

Table A1.230 Plain magnetite #1-magnetite #2 at Ratio 1:2 (sp.gr.2.8)

ϕ (rpm)	Force (N)	σ (Nm)	σ_c (Nm)	τ (Nm^{-2})	ω (rad/s)	γ (s^{-1})	μ (Pa.s)
291	0.098	0.0074	0.0051	22.43	30	397	0.0565
370	0.108	0.0081	0.0057	24.72	39	505	0.0490
470	0.118	0.0089	0.0062	27.01	49	641	0.0421
549	0.122	0.0092	0.0064	27.93	57	749	0.0373
649	0.128	0.0096	0.0067	29.30	68	885	0.0331
749	0.144	0.0108	0.0076	32.96	78	1021	0.0323
859	0.154	0.0116	0.0081	35.25	90	1171	0.0301
951	0.179	0.0134	0.0094	40.98	100	1297	0.0316
1076	0.206	0.0155	0.0108	47.16	113	1467	0.0321
1161	0.243	0.0182	0.0128	55.63	122	1583	0.0351
1246	0.273	0.0205	0.0143	62.49	130	1699	0.0368
1340	0.292	0.0219	0.0153	66.84	140	1827	0.0366

Table A1.231 Plain magnetite #1-magnetite #2 at Ratio 1:2 (sp.gr.2.9)

ϕ (rpm)	Force (N)	σ (Nm)	σ_c (Nm)	τ (Nm^{-2})	ω (rad/s)	γ (s^{-1})	μ (Pa.s)
281	0.143	0.0107	0.0075	32.73	29	383	0.0854
374	0.154	0.0116	0.0081	35.25	39	510	0.0691
446	0.163	0.0122	0.0086	37.31	47	608	0.0614
548	0.172	0.0129	0.0090	39.37	57	747	0.0527
650	0.183	0.0137	0.0096	41.89	68	886	0.0473
764	0.205	0.0154	0.0108	46.93	80	1042	0.0450
881	0.228	0.0171	0.0120	52.19	92	1201	0.0434
946	0.244	0.0183	0.0128	55.86	99	1290	0.0433
1037	0.265	0.0199	0.0139	60.66	109	1414	0.0429
1128	0.284	0.0213	0.0149	65.01	118	1538	0.0423
1255	0.316	0.0237	0.0166	72.34	131	1711	0.0423
1369	0.368	0.0276	0.0193	84.24	143	1867	0.0451

A1.3.3.2 Ferrosilicon and Magnetite #2 Suspensions

Table A1.232 Plain ferrosilicon-magnetite #2 at Ratio 1:1 (sp.gr.2.8)

ϕ (rpm)	Force (N)	σ (Nm)	σ_c (Nm)	τ (Nm^{-2})	ω (rad/s)	γ (s^{-1})	μ (Pa.s)
282	0.031	0.0023	0.0016	7.10	30	385	0.018
391	0.040	0.0030	0.0021	9.16	41	533	0.017
464	0.044	0.0033	0.0023	10.07	49	633	0.016
542	0.048	0.0036	0.0025	10.99	57	739	0.015
676	0.062	0.0047	0.0033	14.19	71	922	0.015
753	0.076	0.0057	0.0040	17.40	79	1027	0.017
842	0.088	0.0066	0.0046	20.14	88	1148	0.018
937	0.104	0.0078	0.0055	23.81	98	1278	0.019
1038	0.115	0.0086	0.0060	26.33	109	1415	0.019
1124	0.136	0.0102	0.0071	31.13	118	1533	0.020
1250	0.154	0.0116	0.0081	35.25	131	1704	0.021
1365	0.171	0.0128	0.0090	39.14	143	1861	0.021

Table A1.233 Plain ferrosilicon-magnetite #2 at Ratio 1:1 (sp.gr.2.9)

ϕ (rpm)	Force (N)	σ (Nm)	σ_c (Nm)	τ (Nm^{-2})	ω (rad/s)	γ (s^{-1})	μ (Pa.s)
287	0.036	0.0027	0.0019	8.24	30	391	0.021
368	0.041	0.0031	0.0022	9.39	39	502	0.019
457	0.047	0.0035	0.0025	10.76	48	623	0.017
562	0.058	0.0044	0.0030	13.28	59	766	0.017
645	0.063	0.0047	0.0033	14.42	68	879	0.016
749	0.083	0.0062	0.0044	19.00	78	1021	0.019
843	0.096	0.0072	0.0050	21.98	88	1149	0.019
971	0.117	0.0088	0.0061	26.78	102	1324	0.020
1084	0.136	0.0102	0.0071	31.13	114	1478	0.021
1165	0.151	0.0113	0.0079	34.57	122	1589	0.022
1240	0.168	0.0126	0.0088	38.46	130	1691	0.023
1330	0.181	0.0136	0.0095	41.43	139	1814	0.023

Table A1.234 Plain ferrosilicon-magnetite #2 at Ratio 1:1 (sp.gr.3.0)

ϕ (rpm)	Force (N)	σ (Nm)	σ_c (Nm)	τ (Nm^{-2})	ω (rad/s)	γ (s^{-1})	μ (Pa.s)
289	0.044	0.0033	0.0023	10.07	30	394	0.026
390	0.048	0.0036	0.0025	10.99	41	532	0.021
467	0.052	0.0039	0.0027	11.90	49	637	0.019
562	0.062	0.0047	0.0033	14.19	59	766	0.019
660	0.075	0.0056	0.0039	17.17	69	900	0.019
749	0.092	0.0069	0.0048	21.06	78	1021	0.021
841	0.109	0.0082	0.0057	24.95	88	1147	0.022
935	0.129	0.0097	0.0068	29.53	98	1275	0.023
1029	0.150	0.0113	0.0079	34.34	108	1403	0.024
1126	0.166	0.0125	0.0087	38.00	118	1535	0.025
1262	0.184	0.0138	0.0097	42.12	132	1721	0.024
1362	0.214	0.0161	0.0112	48.99	143	1857	0.026

Table A1.235 Plain ferrosilicon-magnetite #2 at Ratio 1:1 (sp.gr.3.1)

ϕ (rpm)	Force (N)	σ (Nm)	σ_c (Nm)	τ (Nm^{-2})	ω (rad/s)	γ (s^{-1})	μ (Pa.s)
289	0.054	0.0041	0.0028	12.36	30	394	0.031
377	0.066	0.0050	0.0035	15.11	39	514	0.029
465	0.079	0.0059	0.0041	18.08	49	634	0.029
542	0.082	0.0062	0.0043	18.77	57	739	0.025
668	0.098	0.0074	0.0051	22.43	70	911	0.025
774	0.119	0.0089	0.0062	27.24	81	1055	0.026
849	0.135	0.0101	0.0071	30.90	89	1158	0.027
945	0.148	0.0111	0.0078	33.88	99	1289	0.026
1043	0.168	0.0126	0.0088	38.46	109	1422	0.027
1148	0.183	0.0137	0.0096	41.89	120	1565	0.027
1229	0.215	0.0161	0.0113	49.22	129	1676	0.029
1338	0.254	0.0191	0.0133	58.14	140	1824	0.032

Table A1.236 Plain ferrosilicon-magnetite #2 at Ratio 1:1 (sp.gr.3.2)

ϕ (rpm)	Force (N)	σ (Nm)	σ_c (Nm)	τ (Nm^{-2})	ω (rad/s)	γ (s^{-1})	μ (Pa.s)
285	0.096	0.0072	0.0050	21.98	30	389	0.057
368	0.102	0.0077	0.0054	23.35	39	502	0.047
446	0.110	0.0083	0.0058	25.18	47	608	0.041
560	0.118	0.0089	0.0062	27.01	59	764	0.035
659	0.123	0.0092	0.0065	28.16	69	899	0.031
736	0.129	0.0097	0.0068	29.53	77	1004	0.029
855	0.155	0.0116	0.0081	35.48	90	1166	0.030
952	0.183	0.0137	0.0096	41.89	100	1298	0.032
1035	0.203	0.0152	0.0107	46.47	108	1411	0.033
1136	0.246	0.0185	0.0129	56.31	119	1549	0.036
1263	0.268	0.0201	0.0141	61.35	132	1722	0.036
1361	0.303	0.0227	0.0159	69.36	143	1856	0.037

Table A1.237 Plain ferrosilicon-magnetite #2 at Ratio 2:1 (sp.gr.2.8)

ϕ (rpm)	Force (N)	σ (Nm)	σ_c (Nm)	τ (Nm^{-2})	ω (rad/s)	γ (s^{-1})	μ (Pa.s)
283	0.031	0.0023	0.0016	7.10	30	386	0.018
366	0.036	0.0027	0.0019	8.24	38	499	0.017
448	0.040	0.0030	0.0021	9.16	47	611	0.015
561	0.055	0.0041	0.0029	12.59	59	765	0.016
653	0.064	0.0048	0.0034	14.65	68	890	0.016
757	0.080	0.0060	0.0042	18.31	79	1032	0.018
866	0.096	0.0072	0.0050	21.98	91	1181	0.019
969	0.110	0.0083	0.0058	25.18	101	1321	0.019
1061	0.128	0.0096	0.0067	29.30	111	1447	0.020
1172	0.142	0.0107	0.0075	32.51	123	1598	0.020
1279	0.157	0.0118	0.0082	35.94	134	1744	0.021
1368	0.168	0.0126	0.0088	38.46	143	1865	0.021

Table A1.238 Plain ferrosilicon-magnetite #2 at Ratio 2:1 (sp.gr.2.9)

ϕ (rpm)	Force (N)	σ (Nm)	σ_c (Nm)	τ (Nm^{-2})	ω (rad/s)	γ (s^{-1})	μ (Pa.s)
293	0.035	0.0026	0.0018	8.01	31	400	0.020
364	0.044	0.0033	0.0023	10.07	38	496	0.020
440	0.046	0.0035	0.0024	10.53	46	600	0.018
552	0.064	0.0048	0.0034	14.65	58	753	0.019
655	0.078	0.0059	0.0041	17.86	69	893	0.020
757	0.089	0.0067	0.0047	20.37	79	1032	0.020
862	0.102	0.0077	0.0054	23.35	90	1175	0.020
939	0.114	0.0086	0.0060	26.10	98	1280	0.020
1042	0.131	0.0098	0.0069	29.99	109	1421	0.021
1130	0.146	0.0110	0.0077	33.42	118	1541	0.022
1230	0.162	0.0122	0.0085	37.08	129	1677	0.022
1359	0.180	0.0135	0.0095	41.20	142	1853	0.022

Table A1.239 Plain ferrosilicon-magnetite #2 at Ratio 2:1 (sp.gr.3.0)

ϕ (rpm)	Force (N)	σ (Nm)	σ_c (Nm)	τ (Nm^{-2})	ω (rad/s)	γ (s^{-1})	μ (Pa.s)
293	0.051	0.0038	0.0027	11.67	31	400	0.029
383	0.058	0.0044	0.0030	13.28	40	522	0.025
446	0.066	0.0050	0.0035	15.11	47	608	0.025
538	0.079	0.0059	0.0041	18.08	56	734	0.025
664	0.094	0.0071	0.0049	21.52	70	905	0.024
747	0.106	0.0080	0.0056	24.27	78	1019	0.024
864	0.124	0.0093	0.0065	28.39	90	1178	0.024
986	0.147	0.0110	0.0077	33.65	103	1344	0.025
1076	0.168	0.0126	0.0088	38.46	113	1467	0.026
1144	0.185	0.0139	0.0097	42.35	120	1560	0.027
1240	0.198	0.0149	0.0104	45.33	130	1691	0.027
1373	0.219	0.0164	0.0115	50.13	144	1872	0.027

Table A1.240 Plain ferrosilicon-magnetite #2 at Ratio 2:1 (sp.gr.3.1)

ϕ (rpm)	Force (N)	σ (Nm)	σ_c (Nm)	τ (Nm^{-2})	ω (rad/s)	γ (s^{-1})	μ (Pa.s)
287	0.068	0.0051	0.0036	15.57	30	391	0.040
380	0.074	0.0056	0.0039	16.94	40	518	0.033
485	0.088	0.0066	0.0046	20.14	51	661	0.030
561	0.095	0.0071	0.0050	21.75	59	765	0.028
650	0.106	0.0080	0.0056	24.27	68	886	0.027
742	0.135	0.0101	0.0071	30.90	78	1012	0.031
842	0.156	0.0117	0.0082	35.71	88	1148	0.031
945	0.182	0.0137	0.0096	41.66	99	1289	0.032
1054	0.204	0.0153	0.0107	46.70	110	1437	0.032
1128	0.225	0.0169	0.0118	51.51	118	1538	0.033
1236	0.246	0.0185	0.0129	56.31	129	1685	0.033
1328	0.259	0.0194	0.0136	59.29	139	1811	0.033

Table A1.241 Plain ferrosilicon-magnetite at Ratio 2:1 (sp.gr.3.2)

ϕ (rpm)	Force (N)	σ (Nm)	σ_c (Nm)	τ (Nm^{-2})	ω (rad/s)	γ (s^{-1})	μ (Pa.s)
289	0.095	0.0071	0.0050	21.75	30	394	0.055
393	0.109	0.0082	0.0057	24.95	41	536	0.047
458	0.115	0.0086	0.0060	26.33	48	625	0.042
551	0.122	0.0092	0.0064	27.93	58	751	0.037
647	0.132	0.0099	0.0069	30.22	68	882	0.034
767	0.148	0.0111	0.0078	33.88	80	1046	0.032
851	0.179	0.0134	0.0094	40.98	89	1160	0.035
953	0.198	0.0149	0.0104	45.33	100	1299	0.035
1049	0.233	0.0175	0.0122	53.34	110	1430	0.037
1136	0.264	0.0198	0.0139	60.43	119	1549	0.039
1251	0.284	0.0213	0.0149	65.01	131	1706	0.038
1356	0.322	0.0242	0.0169	73.71	142	1849	0.040

Table A1.242 Plain ferrosilicon-magnetite #2 at Ratio 1:2 (sp.gr.2.8)

ϕ (rpm)	Force (N)	σ (Nm)	σ_c (Nm)	τ (Nm^{-2})	ω (rad/s)	γ (s^{-1})	μ (Pa.s)
293	0.035	0.0026	0.0018	8.01	31	400	0.020
388	0.039	0.0029	0.0020	8.93	41	529	0.017
452	0.045	0.0034	0.0024	10.30	47	616	0.017
546	0.053	0.0040	0.0028	12.13	57	744	0.016
652	0.059	0.0044	0.0031	13.51	68	889	0.015
749	0.068	0.0051	0.0036	15.57	78	1021	0.015
852	0.086	0.0065	0.0045	19.69	89	1162	0.017
971	0.095	0.0071	0.0050	21.75	102	1324	0.016
1060	0.106	0.0080	0.0056	24.27	111	1445	0.017
1150	0.119	0.0089	0.0062	27.24	120	1568	0.017
1243	0.135	0.0101	0.0071	30.90	130	1695	0.018
1338	0.150	0.0113	0.0079	34.34	140	1824	0.019

Table A1.243 Plain ferrosilicon-magnetite #2 at Ratio 1:2 (sp.gr.2.9)

ϕ (rpm)	Force (N)	σ (Nm)	σ_c (Nm)	τ (Nm^{-2})	ω (rad/s)	γ (s^{-1})	μ (Pa.s)
292	0.035	0.0026	0.0018	8.01	31	398	0.020
359	0.039	0.0029	0.0020	8.93	38	490	0.018
469	0.048	0.0036	0.0025	10.99	49	639	0.017
558	0.054	0.0041	0.0028	12.36	58	761	0.016
642	0.066	0.0050	0.0035	15.11	67	875	0.017
762	0.074	0.0056	0.0039	16.94	80	1039	0.016
863	0.088	0.0066	0.0046	20.14	90	1177	0.017
936	0.098	0.0074	0.0051	22.43	98	1276	0.018
1096	0.115	0.0086	0.0060	26.33	115	1494	0.018
1180	0.125	0.0094	0.0066	28.61	124	1609	0.018
1243	0.137	0.0103	0.0072	31.36	130	1695	0.019
1342	0.158	0.0119	0.0083	36.17	141	1830	0.020

Table A1.244 Plain ferrosilicon-magnetite #2 at Ratio 1:2 (sp.gr.3.0)

ϕ (rpm)	Force (N)	σ (Nm)	σ_c (Nm)	τ (Nm^{-2})	ω (rad/s)	γ (s^{-1})	μ (Pa.s)
294	0.042	0.0032	0.0022	9.61	31	401	0.024
373	0.051	0.0038	0.0027	11.67	39	509	0.023
430	0.062	0.0047	0.0033	14.19	45	586	0.024
547	0.068	0.0051	0.0036	15.57	57	746	0.021
652	0.074	0.0056	0.0039	16.94	68	889	0.019
762	0.086	0.0065	0.0045	19.69	80	1039	0.019
861	0.103	0.0077	0.0054	23.58	90	1174	0.020
988	0.125	0.0094	0.0066	28.61	103	1347	0.021
1039	0.135	0.0101	0.0071	30.90	109	1417	0.022
1131	0.151	0.0113	0.0079	34.57	118	1542	0.022
1232	0.175	0.0131	0.0092	40.06	129	1680	0.024
1329	0.193	0.0145	0.0101	44.18	139	1812	0.024

Table A1.245 Plain ferrosilicon-magnetite #2 at Ratio 1:2 (sp.gr.3.1)

ϕ (rpm)	Force (N)	σ (Nm)	σ_c (Nm)	τ (Nm^{-2})	ω (rad/s)	γ (s^{-1})	μ (Pa.s)
285	0.056	0.0042	0.0029	12.82	30	389	0.033
362	0.063	0.0047	0.0033	14.42	38	494	0.029
452	0.068	0.0051	0.0036	15.57	47	616	0.025
565	0.081	0.0061	0.0043	18.54	59	770	0.024
674	0.098	0.0074	0.0051	22.43	71	919	0.024
763	0.109	0.0082	0.0057	24.95	80	1040	0.024
874	0.125	0.0094	0.0066	28.61	92	1192	0.024
992	0.141	0.0106	0.0074	32.28	104	1353	0.024
1079	0.166	0.0125	0.0087	38.00	113	1471	0.026
1190	0.183	0.0137	0.0096	41.89	125	1623	0.026
1292	0.201	0.0151	0.0106	46.01	135	1762	0.026
1374	0.218	0.0164	0.0114	49.90	144	1874	0.027

Table A1.246 Plain ferrosilicon-magnetite #2 at Ratio 1:2 (sp.gr.3.2)

ϕ (rpm)	Force (N)	σ (Nm)	σ_c (Nm)	τ (Nm^{-2})	ω (rad/s)	γ (s^{-1})	μ (Pa.s)
284	0.078	0.0059	0.0041	17.86	30	387	0.046
387	0.086	0.0065	0.0045	19.69	41	528	0.037
484	0.095	0.0071	0.0050	21.75	51	660	0.033
590	0.102	0.0077	0.0054	23.35	62	804	0.029
677	0.114	0.0086	0.0060	26.10	71	923	0.028
777	0.128	0.0096	0.0067	29.30	81	1059	0.028
871	0.142	0.0107	0.0075	32.51	91	1188	0.027
968	0.163	0.0122	0.0086	37.31	101	1320	0.028
1048	0.178	0.0134	0.0093	40.75	110	1429	0.029
1179	0.200	0.0150	0.0105	45.78	123	1608	0.028
1248	0.212	0.0159	0.0111	48.53	131	1702	0.029
1360	0.244	0.0183	0.0128	55.86	142	1854	0.030

A1.4 Experiment Series C: The effect of DP001 and media particle size and shape on the separation efficiency in a dense medium cyclone

A1.4.1 Aim of the Experiment

The aim of these experiments was to investigate the separation efficiency in a dense medium. The effect of DP001 and media particle size and shape, through the addition of magnetite #2, were investigated.

A1.4.2 Experimental Conditions

The separations were carried out using the dense medium cyclone loop described in Chapter 5. The cyclone was operated at an angle of 20° to the horizontal. The suspensions were prepared using magnetite #1 at specific gravities 1.57 and 1.83. DP001 was added at 1 and 2 grams/kilogram solids. To investigate the effect of particle size and shape, magnetite #2 was added to the magnetite #1 suspensions. The mass of magnetite #2 used was 12 % of the mass of magnetite used. The operating specific gravity for these experiments was 1.70.

Coal in three different size ranges was separated. The size ranges were: -4 mm + 1 mm; -1 mm + 500 μm; and -4 mm + 500 μm. The coal was added into the Headbox of the cyclone and allowed to circulate in the system for at least two minutes, after which it was collected on handheld sieves for both the overflow and underflow. For each coal size range and medium specific gravity, three separate tests were carried out. Firstly, tests were carried out on plain suspensions, suspensions with 1 gram DP001/kilogram, and finally with 2 grams DP001/kilogram.

The density of the overflow and underflow were measured using the density can method described by Wills (1997). The flow rates were measured by measuring the time it took for the product streams to fill a container of known volume. The density of the feed was then determined through a mass balance around the cyclone. The flow rates and density at each specific gravity tested are given below.

Table A1.247 Flow rate and density of cyclone product streams

Feed	Q (m^3s^{-1})		F (kgs^{-1})		density (kgm^{-3})	
density (kgm^{-3})	Float	Sink	Float	Sink	Float	Sink
1567	0.00122	0.00019	1.88	0.32	1545	1714
1701	0.00105	0.00044	1.71	0.82	1628	1879
1832	0.00128	0.00028	2.29	0.56	1791	2015

A1.4.3 Experimental Results

This section will present the experimental raw data for each of the coal samples, together with their partition curves, at the operating feed densities listed in Table A1.247. It is important to note that at the density 1701 kgm^{-3}, magnetite #2 was also used to make up the suspension.

The results in this section were determined by sampling the sink and float products and performing heavy liquids tests using tetrabromoethane to determine the amount of misplaced material in each of the products. The results are shown in Table A1.248 to Table A1.274. The column in the tables are calculated using a method similar to that described by Wills (1997). Columns 1 and 2 are the results of sink-float tests on the float on sink products and columns 3 and 4 relate these results to the total distribution of the feed material to floats and sink which must be determined by using the flow rates in Table A1.247. The weight fractions in columns 3 and 4 are added together to produce the reconstituted feed weight distribution in each density fraction (column 5). Column 6 gives the nominal specific gravity of each density range, i.e. material in the density range 1.4-1.6 is assumed to have a specific gravity lying midway between these densities-1.5.

The partition coefficient (column 7) is the percentage of feed material of a certain nominal specific gravity which reports to the sinks, i.e.

$$column-(7)=\frac{column-(4)}{column-(5)}\times 100\% \qquad \text{(A1.2)}$$

The partition curve is then constructed by plotting the partition coefficient against the nominal specific gravity, from which the probable error (Ep) of the vessel can be determined.

Table A1.248 Magnetite #1 coal separation analyses at sp.gr.1.57 (-4mm + 1mm)

Specific gravity fraction	(1) % In each fraction Floats	(2) Sinks	(3) % of Feed Floats	(4) Sinks	(5) Reconstituted feed (%)	(6) Nominal sp.gr	(7) Partition coefficient
-1.4	13.80	0.00	11.67	0.00	11.67	1.30	0.0
-1.6 + 1.4	78.89	0.89	66.69	0.14	66.82	1.50	0.2
-1.8 + 1.6	7.31	16.09	6.18	2.49	8.67	1.70	28.7
-2.0 + 1.8	0.00	30.11	0.00	4.66	4.66	1.90	100.0
-2.2 + 2.0	0.00	35.51	0.00	5.49	5.49	2.10	100.0
+2.2	0.00	17.40	0.00	2.69	2.69	2.30	100.0
Totals	100.00	100.00	84.53	15.47	100.00		

Table A1.249 Magnetite #1 + 1g DP001/kg coal separation analyses at sp.gr.1.57 (-4mm+1mm)

Specific gravity fraction	(1) % In each fraction Floats	(2) Sinks	(3) % of Feed Floats	(4) Sinks	(5) Reconstituted feed (%)	(6) Nominal sp.gr	(7) Partition coefficient
-1.4	14.41	0.00	12.18	0.00	12.18	1.30	0.0
-1.6 + 1.4	77.42	1.14	65.45	0.18	65.62	1.50	0.3
-1.8 + 1.6	8.17	21.58	6.91	3.34	10.25	1.70	32.6
-2.0 + 1.8	0.00	28.87	0.00	4.47	4.47	1.90	100.0
-2.2 + 2.0	0.00	23.77	0.00	3.68	3.68	2.10	100.0
+2.2	0.00	24.65	0.00	3.81	3.81	2.30	100.0
Totals	100.00	100.00	84.53	15.47	100.00		

Table A1.250 Magnetite #1 + 2g DP001/kg coal separation analyses at sp.gr.1.57 (-4mm + 1mm)

Specific gravity fraction	(1) % In each fraction Floats	(2) Sinks	(3) % of Feed Floats	(4) Sinks	(5) Reconstituted feed (%)	(6) Nominal sp.gr	(7) Partition coefficient
-1.4	10.79	0.00	9.12	0.00	9.12	1.30	0.0
-1.6 + 1.4	72.29	0.35	61.11	0.05	61.17	1.50	0.1
-1.8 + 1.6	16.91	13.60	14.30	2.10	16.40	1.70	12.8
-2.0 + 1.8	0.00	29.54	0.00	4.57	4.57	1.90	100.0
-2.2 + 2.0	0.00	34.15	0.00	5.28	5.28	2.10	100.0
+2.2	0.00	22.36	0.00	3.46	3.46	2.30	100.0
Totals	100.00	100.00	84.53	15.47	100.00		

Table A1.251 Magnetite #1 coal separation analyses at sp.gr.1.83 (-4mm + 1mm)

Specific gravity fraction	(1) % In each fraction Floats	(2) Sinks	(3) % of Feed Floats	(4) Sinks	(5) Reconstituted feed (%)	(6) Nominal sp.gr	(7) Partition coefficient
-1.4	5.86	0.00	4.70	0.00	4.70	1.30	0.0
-1.6 + 1.4	73.77	0.96	59.19	0.19	59.38	1.50	0.3
-1.8 + 1.6	16.30	2.80	13.08	0.55	13.63	1.70	4.1
-2.0 + 1.8	4.08	23.48	3.27	4.64	7.91	1.90	58.7
-2.2 + 2.0	0.00	40.37	0.00	7.98	7.98	2.10	100.0
+2.2	0.00	32.38	0.00	6.40	6.40	2.30	100.0
Totals	100.00	100.00	80.24	19.76	100.00		

Table A1.252 Magnetite #1 + 1g DP001/kg coal separation analyses at sp.gr.1.83 (-4mm + 1mm)

Specific gravity fraction	(1) % In each fraction Floats	(2) Sinks	(3) % of Feed Floats	(4) Sinks	(5) Reconstituted feed (%)	(6) Nominal sp.gr	(7) Partition coefficient
-1.4	26.97	0.00	21.64	0.00	21.64	1.30	0.0
-1.6 + 1.4	53.73	2.03	43.11	0.40	43.51	1.50	0.9
-1.8 + 1.6	16.05	3.36	12.88	0.66	13.54	1.70	4.9
-2.0 + 1.8	3.24	27.64	2.60	5.46	8.07	1.90	67.7
-2.2 + 2.0	0.00	36.82	0.00	7.28	7.28	2.10	100.0
+2.2	0.00	30.15	0.00	5.96	5.96	2.30	100.0
Totals	100.00	100.00	80.24	19.76	100.00		

Table A1.253 Magnetite #1 + 2g DP001/kg coal separation analyses at sp.gr.1.83 (-4mm + 1mm)

Specific gravity fraction	(1) % In each fraction Floats	(2) Sinks	(3) % of Feed Floats	(4) Sinks	(5) Reconstituted feed (%)	(6) Nominal sp.gr	(7) Partition coefficient
-1.4	19.00	0.00	15.24	0.00	15.24	1.30	0.0
-1.6 + 1.4	62.13	1.47	49.85	0.29	50.14	1.50	0.6
-1.8 + 1.6	13.68	2.38	10.97	0.47	11.44	1.70	4.1
-2.0 + 1.8	5.20	37.74	4.17	7.46	11.63	1.90	64.1
-2.2 + 2.0	0.00	40.05	0.00	7.92	7.92	2.10	100.0
+2.2	0.00	18.36	0.00	3.63	3.63	2.30	100.0
Totals	100.00	100.00	80.24	19.76	100.00		

Table A1.254 Magnetite #1 coal separation analyses at sp.gr.1.57 (-1mm + 500µm)

Specific gravity fraction	(1) % In each fraction Floats	(2) Sinks	(3) % of Feed Floats	(4) Sinks	(5) Reconstituted feed (%)	(6) Nominal sp.gr	(7) Partition coefficient
-1.4	40.10	4.65	33.90	0.72	34.62	1.30	2.1
-1.6 + 1.4	45.03	2.60	38.06	0.40	38.46	1.50	1.0
-1.8 + 1.6	13.57	9.02	11.47	1.39	12.86	1.70	10.8
-2.0 + 1.8	1.31	24.26	1.10	3.75	4.85	1.90	77.3
-2.2 + 2.0	0.00	23.27	0.00	3.60	3.60	2.10	100.0
+2.2	0.00	36.22	0.00	5.60	5.60	2.30	100.0
Totals	100.00	100.00	84.53	15.47	100.00		

Table A1.255 Magnetite #1 + 1g DP001/kg coal separation analyses at sp.gr.1.57 (-1mm + 500µm)

Specific gravity fraction	(1) % In each fraction Floats	(2) Sinks	(3) % of Feed Floats	(4) Sinks	(5) Reconstituted feed (%)	(6) Nominal sp.gr	(7) Partition coefficient
-1.4	54.21	1.27	45.83	0.20	46.02	1.30	0.4
-1.6 + 1.4	38.98	3.02	32.95	0.47	33.41	1.50	1.4
-1.8 + 1.6	6.81	10.02	5.76	1.55	7.31	1.70	21.2
-2.0 + 1.8	0.00	26.77	0.00	4.14	4.14	1.90	100.0
-2.2 + 2.0	0.00	25.61	0.00	3.96	3.96	2.10	100.0
+2.2	0.00	33.31	0.00	5.15	5.15	2.30	100.0
Totals	100.00	100.00	84.53	15.47	100.00		

Table A1.256 Magnetite #1 + 2g DP001/kg coal separation analyses at sp.gr.1.57 (-1mm + 500µm)

Specific gravity fraction	(1) % In each fraction Floats	(2) Sinks	(3) % of Feed Floats	(4) Sinks	(5) Reconstituted feed (%)	(6) Nominal sp.gr	(7) Partition coefficient
-1.4	44.86	5.18	37.92	0.80	38.72	1.30	2.1
-1.6 + 1.4	38.85	3.33	32.84	0.51	33.35	1.50	1.5
-1.8 + 1.6	16.29	12.34	13.77	1.91	15.68	1.70	12.2
-2.0 + 1.8	0.00	27.24	0.00	4.21	4.21	1.90	100.0
-2.2 + 2.0	0.00	23.57	0.00	3.65	3.65	2.10	100.0
+2.2	0.00	28.34	0.00	4.38	4.38	2.30	100.0
Totals	100.00	100.00	84.53	15.47	100.00		

Table A1.257 Magnetite #1 coal separation analyses at sp.gr.1.83 (-1mm + 500µm)

Specific gravity fraction	(1) % In each fraction Floats	(2) Sinks	(3) % of Feed Floats	(4) Sinks	(5) Reconstituted feed (%)	(6) Nominal sp.gr	(7) Partition coefficient
-1.4	20.88	1.22	16.75	0.24	16.99	1.30	1.4
-1.6 + 1.4	50.61	10.64	40.61	2.10	42.71	1.50	4.9
-1.8 + 1.6	17.38	7.88	13.94	1.56	15.50	1.70	10.0
-2.0 + 1.8	6.99	19.04	5.61	3.76	9.37	1.90	40.2
-2.2 + 2.0	4.14	33.02	3.32	6.53	9.85	2.10	66.3
+2.2	0.00	28.19	0.00	5.57	5.57	2.30	100.0
Totals	100.00	100.00	80.24	19.76	100.00	2.50	100.0

Table A1.258 Magnetite #1 + 1g DP001/kg coal separation analyses at sp.gr.1.83 (-1mm + 500µm)

Specific gravity fraction	(1) % In each fraction Floats	(2) Sinks	(3) % of Feed Floats	(4) Sinks	(5) Reconstituted feed (%)	(6) Nominal sp.gr	(7) Partition coefficient
-1.4	22.13	4.63	17.75	0.91	18.67	1.30	4.9
-1.6 + 1.4	53.48	11.99	42.91	2.37	45.28	1.50	5.2
-1.8 + 1.6	18.92	6.80	15.18	1.34	16.53	1.70	8.1
-2.0 + 1.8	4.69	30.33	3.76	5.99	9.76	1.90	61.4
-2.2 + 2.0	0.78	16.19	0.63	3.20	3.83	2.10	83.6
+2.2	0.00	30.06	0.00	5.94	5.94	2.30	100.0
Totals	100.00	100.00	80.24	19.76	100.00	2.50	100.0

Table A1.259 Magnetite #1 + 2g DP001/kg coal separation analyses at sp.gr.1.83 (-1mm + 500µm)

Specific gravity fraction	(1) % In each fraction Floats	(2) Sinks	(3) % of Feed Floats	(4) Sinks	(5) Reconstituted feed (%)	(6) Nominal sp.gr	(7) Partition coefficient
-1.4	18.71	4.34	15.01	0.86	15.87	1.30	5.4
-1.6 + 1.4	54.19	13.38	43.48	2.64	46.12	1.50	5.7
-1.8 + 1.6	19.81	12.24	15.90	2.42	18.32	1.70	13.2
-2.0 + 1.8	6.64	14.73	5.33	2.91	8.24	1.90	35.3
-2.2 + 2.0	0.65	18.59	0.52	3.67	4.20	2.10	87.5
+2.2	0.00	36.72	0.00	7.26	7.26	2.30	100.0
Totals	100.00	100.00	80.24	19.76	100.00	2.50	100.0

Table A1.260 Magnetite #1 coal separation analyses at sp.gr.1.57 (-4mm + 500µm)

Specific gravity fraction	(1) % In each fraction Floats	(2) Sinks	(3) % of Feed Floats	(4) Sinks	(5) Reconstituted feed (%)	(6) Nominal sp.gr	(7) Partition coefficient
-1.4	18.98	0.00	16.05	0.00	16.05	1.30	0.0
-1.6 + 1.4	73.08	2.82	61.78	0.44	62.22	1.50	0.7
-1.8 + 1.6	7.01	13.53	5.92	2.09	8.02	1.70	26.1
-2.0 + 1.8	0.93	26.03	0.78	4.03	4.81	1.90	83.7
-2.2 + 2.0	0.00	28.03	0.00	4.34	4.34	2.10	100.0
+2.2	0.00	29.59	0.00	4.58	4.58	2.30	100.0
Totals	100.00	100.00	84.53	15.47	100.00		

Table A1.261 Magnetite #1 + 1g DP001/kg coal separation analysis at sp.gr.1.57 (-4mm + 500µm)

Specific gravity fraction	(1) % In each fraction Floats	(2) Sinks	(3) % of Feed Floats	(4) Sinks	(5) Reconstituted feed (%)	(6) Nominal sp.gr	(7) Partition coefficient
-1.4	18.47	0.00	15.62	0.00	15.62	1.30	0.0
-1.6 + 1.4	72.67	4.28	61.43	0.66	62.09	1.50	1.1
-1.8 + 1.6	8.22	14.24	6.95	2.20	9.15	1.70	24.1
-2.0 + 1.8	0.64	19.73	0.54	3.05	3.59	1.90	85.0
-2.2 + 2.0	0.00	35.59	0.00	5.50	5.50	2.10	100.0
+2.2	0.00	26.15	0.00	4.04	4.04	2.30	100.0
Totals	100.00	100.00	84.53	15.47	100.00		

Table A1.262 Magnetite #1 + 2g DP001/kg coal separation analysis at sp.gr.1.57 (-4mm + 500µm)

Specific gravity fraction	(1) % In each fraction Floats	(2) Sinks	(3) % of Feed Floats	(4) Sinks	(5) Reconstituted feed (%)	(6) Nominal sp.gr	(7) Partition coefficient
-1.4	23.68	0.00	20.02	0.00	20.02	1.30	0.0
-1.6 + 1.4	70.30	1.92	59.43	0.30	59.73	1.50	0.5
-1.8 + 1.6	6.02	7.06	5.09	1.09	6.18	1.70	17.7
-2.0 + 1.8	0.00	22.07	0.00	3.41	3.41	1.90	100.0
-2.2 + 2.0	0.00	27.37	0.00	4.23	4.23	2.10	100.0
+2.2	0.00	41.58	0.00	6.43	6.43	2.30	100.0
Totals	100.00	100.00	84.53	15.47	100.00		

Table A1.263 Magnetite #1 coal separation analyses at sp.gr.1.83 (-4mm + 500μm)

Specific gravity fraction	(1) % In each fraction Floats	(2) Sinks	(3) % of Feed Floats	(4) Sinks	(5) Reconstituted feed (%)	(6) Nominal sp.gr	(7) Partition coefficient
-1.4	25.73	2.31	20.65	0.46	21.10	1.30	2.2
-1.6 + 1.4	60.50	7.43	48.54	1.47	50.01	1.50	2.9
-1.8 + 1.6	10.97	3.08	8.80	0.61	9.41	1.70	6.5
-2.0 + 1.8	2.79	29.06	2.24	5.74	7.98	1.90	71.9
-2.2 + 2.0	0.00	30.47	0.00	6.02	6.02	2.10	100.0
+2.2	0.00	27.66	0.00	5.47	5.47	2.30	100.0
Totals	100.00	100.00	80.24	19.76	100.00		

Table A1.264 Magnetite #1 + 1g DP001/kg coal separation analyses at sp.gr.1.83 (-4mm + 500μm)

Specific gravity fraction	(1) % In each fraction Floats	(2) Sinks	(3) % of Feed Floats	(4) Sinks	(5) Reconstituted feed (%)	(6) Nominal sp.gr	(7) Partition coefficient
-1.4	21.67	1.64	17.39	0.32	17.71	1.30	1.8
-1.6 + 1.4	57.09	4.27	45.80	0.84	46.65	1.50	1.8
-1.8 + 1.6	17.02	3.78	13.66	0.75	14.40	1.70	5.2
-2.0 + 1.8	4.22	34.17	3.39	6.75	10.14	1.90	66.6
-2.2 + 2.0	0.00	31.62	0.00	6.25	6.25	2.10	100.0
+2.2	0.00	24.53	0.00	4.85	4.85	2.30	100.0
Totals	100.00	100.00	80.24	19.76	100.00		

Table A1.265 Magnetite #1 + 2g DP001/kg coal separation analyses at sp.gr.1.83 (-4mm + 500μm)

Specific gravity fraction	(1) % In each fraction Floats	(2) Sinks	(3) % of Feed Floats	(4) Sinks	(5) Reconstituted feed (%)	(6) Nominal sp.gr	(7) Partition coefficient
-1.4	16.44	0.00	13.19	0.00	13.19	1.30	0.0
-1.6 + 1.4	70.32	6.91	56.42	1.37	57.79	1.50	2.4
-1.8 + 1.6	9.35	7.29	7.50	1.44	8.94	1.70	16.1
-2.0 + 1.8	3.89	27.77	3.12	5.49	8.61	1.90	63.7
-2.2 + 2.0	0.00	31.48	0.00	6.22	6.22	2.10	100.0
+2.2	0.00	26.55	0.00	5.25	5.25	2.30	100.0
Totals	100.00	100.00	80.24	19.76	100.00		

Table A1.266 Mag #1and Mag #2 coal separation analyses at sp.gr.1.70 (-4mm + 1mm)

Specific gravity fraction	(1) % In each fraction Floats	(2) Sinks	(3) % of Feed Floats	(4) Sinks	(5) Reconstituted feed (%)	(6) Nominal sp.gr	(7) Partition coefficient
-1.4	1.93	0.00	1.31	0.00	1.31	1.30	0.0
-1.6 + 1.4	30.56	0.00	20.67	0.00	20.67	1.50	0.0
-1.8 + 1.6	65.30	2.38	44.16	0.77	44.93	1.70	1.7
-2.0 + 1.8	2.21	32.29	1.49	10.45	11.94	1.90	87.5
-2.2 + 2.0	0.00	25.77	0.00	8.34	8.34	2.10	100.0
+2.2	0.00	39.57	0.00	12.81	12.81	2.30	100.0
Totals	100.00	100.00	67.63	32.37	100.00		

Table A1.267 Mag #1 and Mag #2 + 1g DP001/kg coal separation analyses at sp.gr.1.70 (-4mm + 1mm)

Specific gravity fraction	(1) % In each fraction Floats	(2) Sinks	(3) % of Feed Floats	(4) Sinks	(5) Reconstituted feed (%)	(6) Nominal sp.gr	(7) Partition coefficient
-1.4	2.35	0.27	1.59	0.09	1.68	1.30	5.2
-1.6 + 1.4	46.91	5.12	31.72	1.66	33.38	1.50	5.0
-1.8 + 1.6	49.43	8.63	33.43	2.79	36.22	1.70	7.7
-2.0 + 1.8	1.32	75.35	0.89	24.39	25.28	1.90	96.5
-2.2 + 2.0	0.00	8.67	0.00	2.81	2.81	2.10	100.0
+2.2	0.00	1.95	0.00	0.63	0.63	2.30	100.0
Totals	100.00	100.00	67.63	32.37	100.00		

Table A1.268 Mag #1 and Mag #2 + 1g DP001/kg coal separation analyses at sp.gr.1.70 (-4mm + 1mm)

Specific gravity fraction	(1) % In each fraction Floats	(2) Sinks	(3) % of Feed Floats	(4) Sinks	(5) Reconstituted feed (%)	(6) Nominal sp.gr	(7) Partition coefficient
-1.4	3.80	0.00	2.57	0.00	2.57	1.30	0.0
-1.6 + 1.4	54.51	2.50	36.87	0.81	37.68	1.50	2.2
-1.8 + 1.6	39.98	3.80	27.04	1.23	28.27	1.70	4.4
-2.0 + 1.8	1.70	32.99	1.15	10.68	11.83	1.90	90.3
-2.2 + 2.0	0.00	41.25	0.00	13.35	13.35	2.10	100.0
+2.2	0.00	19.46	0.00	6.30	6.30	2.30	100.0
Totals	100.00	100.00	67.63	32.37	100.00		

Table A1.269 Mag #1 and Mag #2 coal separation analyses at sp.gr.1.70 (-1mm + 500μm)

Specific gravity fraction	(1) % In each fraction Floats	(2) Sinks	(3) % of Feed Floats	(4) Sinks	(5) Reconstituted feed (%)	(6) Nominal sp.gr	(7) Partition coefficient
-1.4	13.15	1.00	8.89	0.32	9.22	1.30	3.5
-1.6 + 1.4	59.41	5.17	40.18	1.67	41.85	1.50	4.0
-1.8 + 1.6	23.96	2.55	16.20	0.83	17.03	1.70	4.8
-2.0 + 1.8	3.48	9.91	2.35	3.21	5.56	1.90	57.7
-2.2 + 2.0	0.00	19.44	0.00	6.29	6.29	2.10	100.0
+2.2	0.00	61.93	0.00	20.05	20.05	2.30	100.0
Totals	100.00	100.00	67.63	32.37	100.00		

Table A1.270 Mag #1 and Mag #2 + 1g DP001/kg coal separation analyses at sp.gr.1.70 (-1mm + 500μm)

Specific gravity fraction	(1) % In each fraction Floats	(2) Sinks	(3) % of Feed Floats	(4) Sinks	(5) Reconstituted feed (%)	(6) Nominal sp.gr	(7) Partition coefficient
-1.4	19.05	2.03	12.88	0.66	13.54	1.30	4.8
-1.6 + 1.4	17.79	3.08	12.03	1.00	13.03	1.50	7.6
-1.8 + 1.6	60.88	11.69	41.17	3.78	44.96	1.70	8.4
-2.0 + 1.8	2.28	11.93	1.54	3.86	5.40	1.90	71.5
-2.2 + 2.0	0.00	19.10	0.00	6.18	6.18	2.10	100.0
+2.2	0.00	52.17	0.00	16.89	16.89	2.30	100.0
Totals	100.00	100.00	67.63	32.37	100.00		

Table A1.271 Mag #1 and Mag #2 + 2g DP001/kg coal separation analyses at sp.gr.1.70 (-1mm + 500μm)

Specific gravity fraction	(1) % In each fraction Floats	(2) Sinks	(3) % of Feed Floats	(4) Sinks	(5) Reconstituted feed (%)	(6) Nominal sp.gr	(7) Partition coefficient
-1.4	28.03	1.79	18.96	0.58	19.54	1.30	3.0
-1.6 + 1.4	38.67	2.98	26.15	0.97	27.12	1.50	3.6
-1.8 + 1.6	31.56	6.85	21.35	2.22	23.56	1.70	9.4
-2.0 + 1.8	1.73	12.07	1.17	3.91	5.08	1.90	76.9
-2.2 + 2.0	0.00	21.58	0.00	6.99	6.99	2.10	100.0
+2.2	0.00	54.73	0.00	17.72	17.72	2.30	100.0
Totals	100.00	100.00	67.63	32.37	100.00		

Table A1.272 Mag #1 and Mag #2 coal separation analysis at sp.gr.1.70 (-4mm + 500µm)

Specific gravity fraction	(1) % In each fraction Floats	(2) Sinks	(3) % of Feed Floats	(4) Sinks	(5) Reconstituted feed (%)	(6) Nominal sp.gr	(7) Partition coefficient
-1.4	3.64	0.40	2.46	0.13	2.59	1.30	5.0
-1.6 + 1.4	35.17	10.50	23.79	3.40	27.18	1.50	12.5
-1.8 + 1.6	51.60	26.96	34.90	8.73	43.62	1.70	20.0
-2.0 + 1.8	9.58	22.51	6.48	7.29	13.77	1.90	52.9
-2.2 + 2.0	0.00	10.80	0.00	3.50	3.50	2.10	100.0
+2.2	0.00	28.84	0.00	9.33	9.33	2.30	100.0
Totals	100.00	100.00	67.63	32.37	100.00		

Table A1.273 Mag #1 and Mag #2 + 1g DP001/kg coal separation analyses at sp.gr.1.70 (-4mm + 500µm)

Specific gravity fraction	(1) % In each fraction Floats	(2) Sinks	(3) % of Feed Floats	(4) Sinks	(5) Reconstituted feed (%)	(6) Nominal sp.gr	(7) Partition coefficient
-1.4	3.06	0.00	2.07	0.00	2.07	1.30	0.0
-1.6 + 1.4	31.73	2.07	21.46	0.67	22.13	1.50	3.0
-1.8 + 1.6	50.14	8.63	33.91	2.79	36.70	1.70	7.6
-2.0 + 1.8	15.08	20.86	10.20	6.75	16.95	1.90	39.8
-2.2 + 2.0	0.00	20.19	0.00	6.54	6.54	2.10	100.0
+2.2	0.00	48.24	0.00	15.62	15.62	2.30	100.0
Totals	100.00	100.00	67.63	32.37	100.00		

Table A1.274 Mag #1 and Mag #2 + 2g DP001/kg coal separation analyses at sp.gr.1.70 (-4mm + 500µm)

Specific gravity fraction	(1) % In each fraction Floats	(2) Sinks	(3) % of Feed Floats	(4) Sinks	(5) Reconstituted feed (%)	(6) Nominal sp.gr	(7) Partition coefficient
-1.4	3.03	0.79	2.05	0.25	2.31	1.30	11.1
-1.6 + 1.4	48.01	13.71	32.47	4.44	36.90	1.50	12.0
-1.8 + 1.6	46.14	21.01	31.20	6.80	38.00	1.70	17.9
-2.0 + 1.8	2.82	18.72	1.91	6.06	7.97	1.90	76.1
-2.2 + 2.0	0.00	15.96	0.00	5.17	5.17	2.10	100.0
+2.2	0.00	29.82	0.00	9.65	9.65	2.30	100.0
Totals	100.00	100.00	67.63	32.37	100.00		

The partition curves obtained from the data above are plotted in figures below. The results were plotted for each sample at the given specific gravity. The graphs thus illustrate the effect of DP001 on the separation curves.

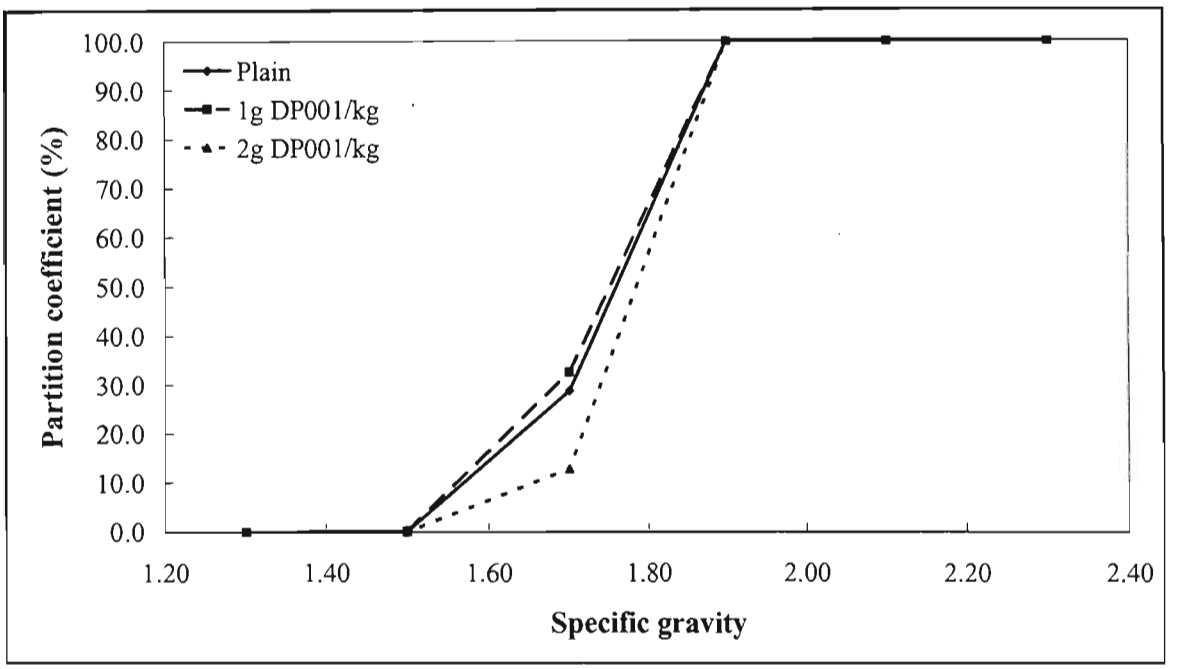

Figure A1.11 Magnetite #1 partition curves for coal size range -4mm + 1mm (sp.gr.1.57)

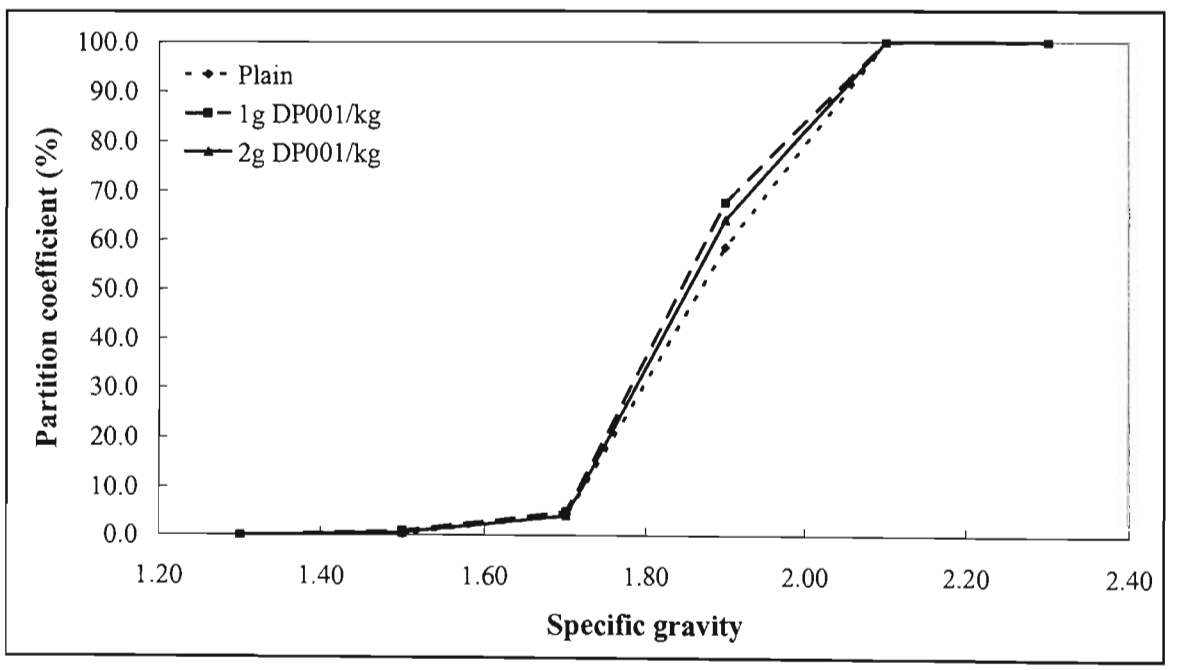

Figure A1.12 Magnetite #1 partition curves for coal size range -4mm + 1mm (sp.gr.1.83)

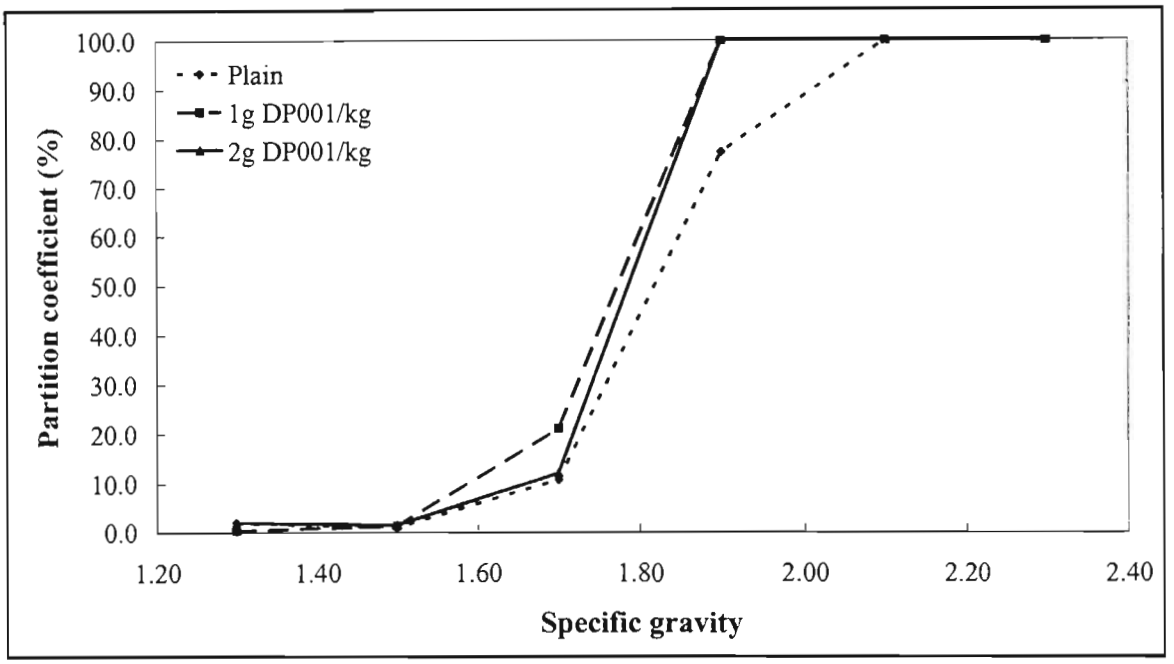

Figure A1.13 Magnetite #1 partition curves for coal size range -1mm + 500µm (sp.gr.1.57)

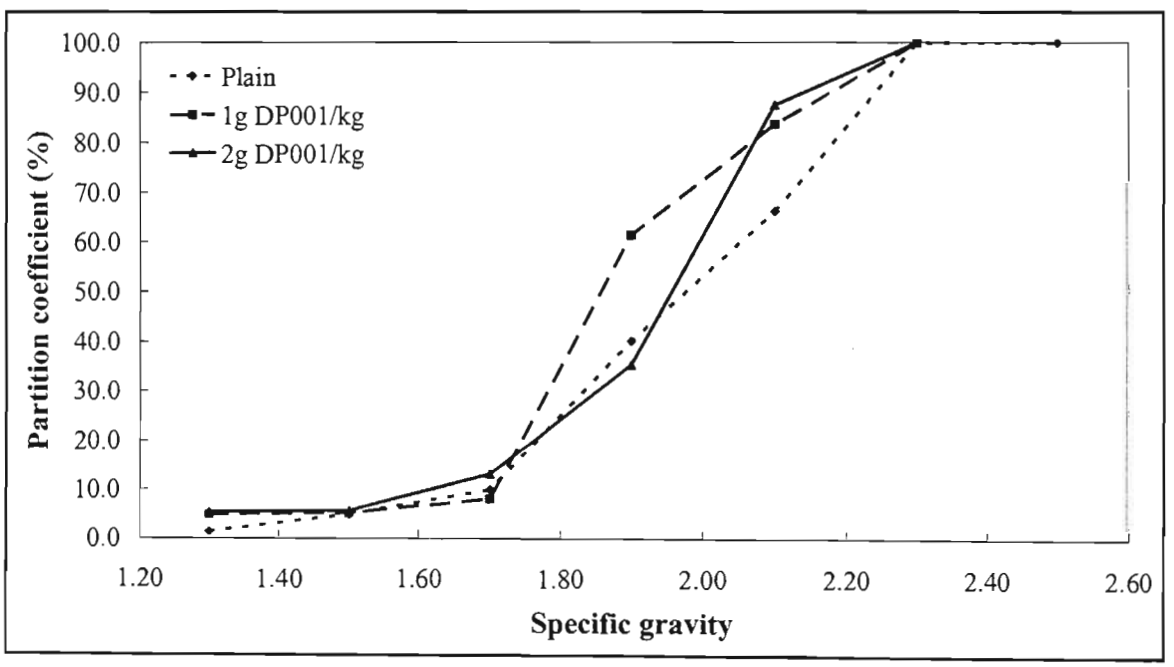

Figure A1.14 Magnetite #1 partition curves for coal size range -1mm + 500µm (sp.gr.1.83)

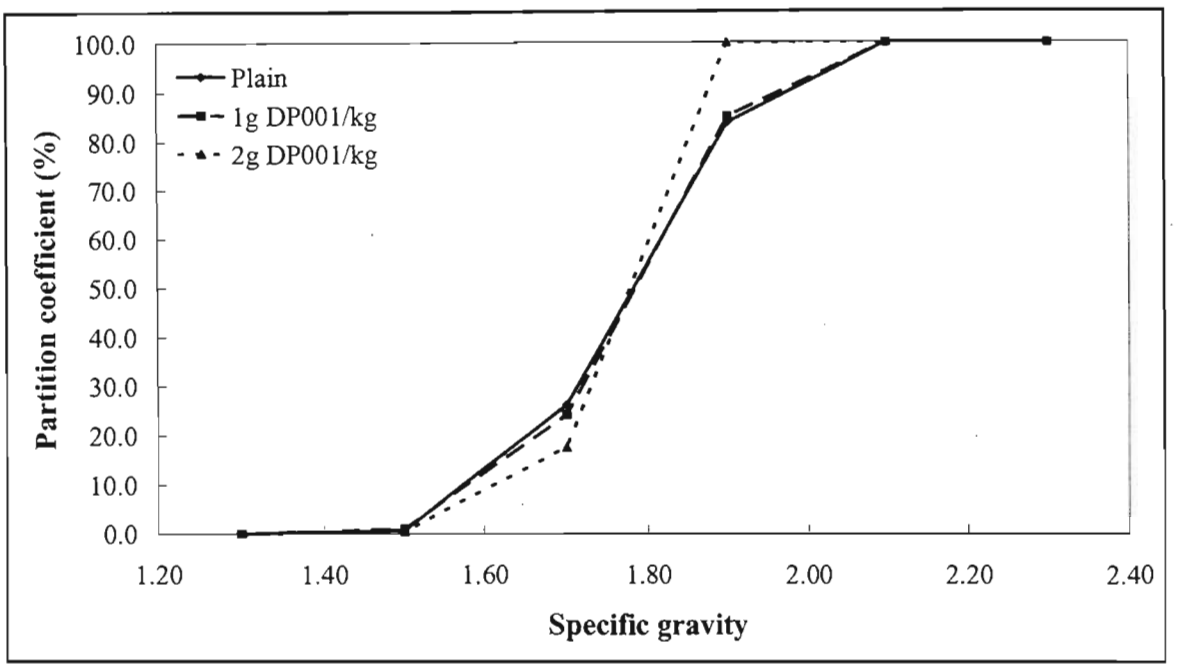

Figure A1.15 Magnetite #1 partition curves for coal size range -4mm + 500µm (sp.gr.1.57)

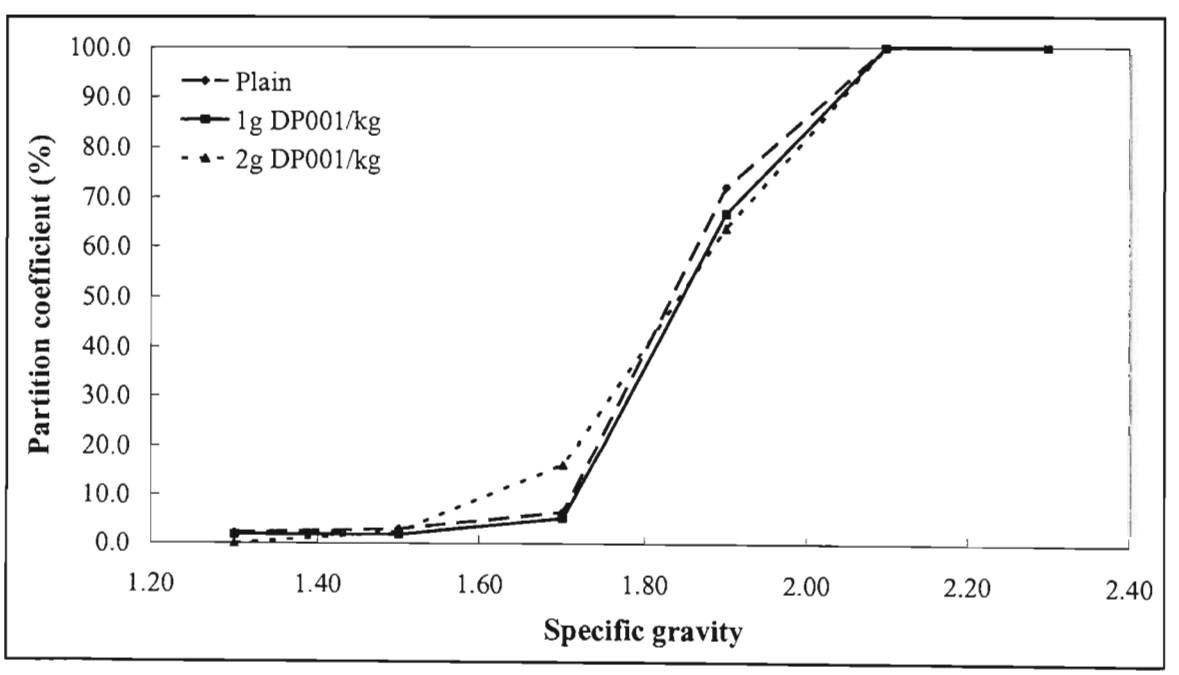

Figure A1.16 Magnetite #1 partition curves for coal size range -4mm + 500µm (sp.gr.1.83)

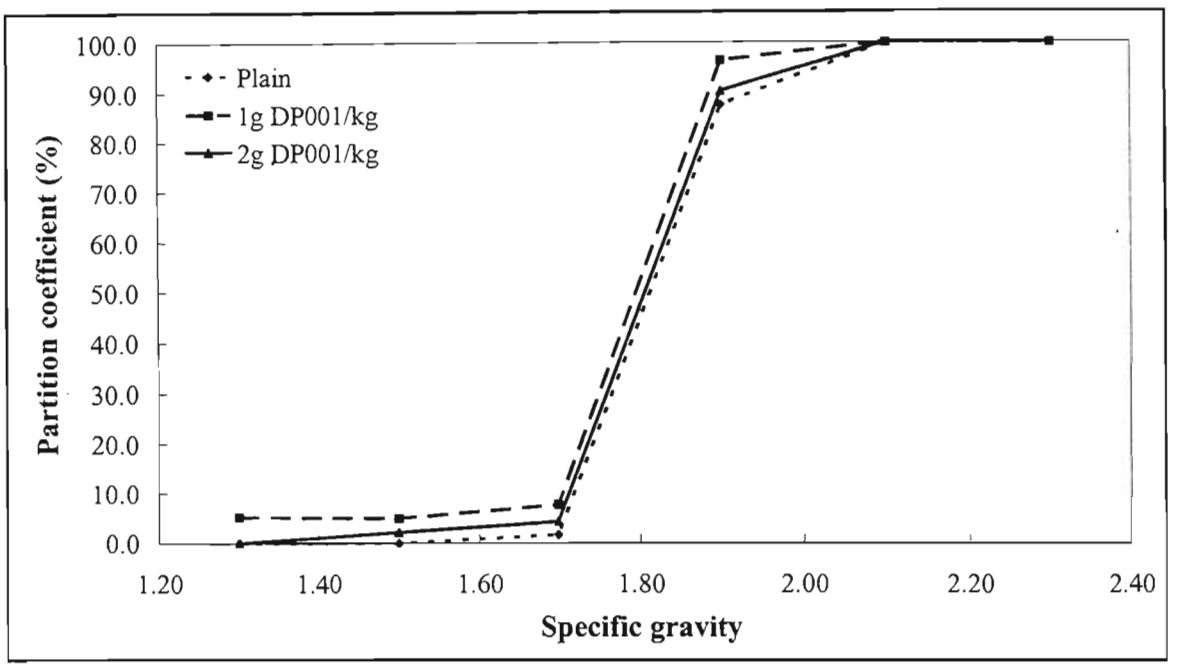

Figure A1.17 Mag #1-Mag #2 partition curves for coal size range -4mm +1mm (sp.gr.1.70)

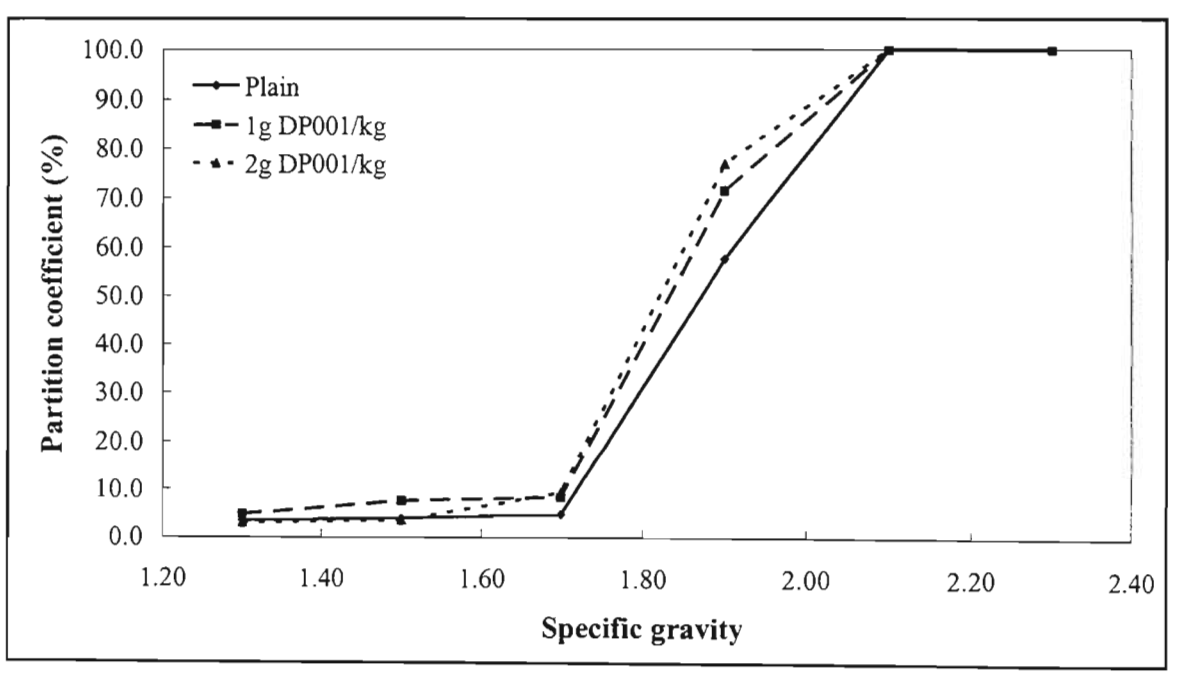

Figure A1.18 Mag #1-Mag #2 partition curves for coal size range -1mm +500μm (sp.gr.1.70)

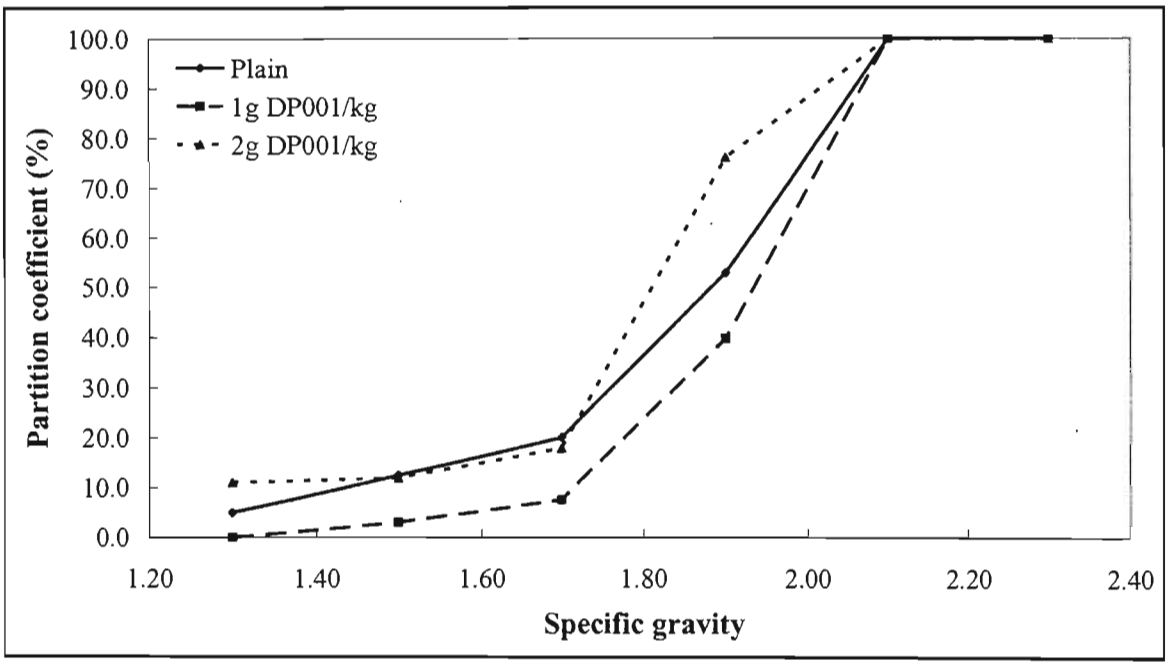

Figure A1.19 Mag #1-Mag #2 partition curves for coal size range -4mm +500μm (sp.gr.1.70)

A1.5 Scanning Electron Micrograph (SEM) Results

A1.5.1 Aim of the Experiment

The aim of these experiments was to determine the surface shape of the media used in these investigations. The media particle shape has a direct influence on the viscosity of heavy medium suspensions. Rougher particles result in higher viscosities, while smoother particles result in lower viscosities.

A1.5.2 Experimental Results

The media particles tested were: ferrosilicon; magnetite #1; magnetite #2; and the slime / clay. SEM measurements were done using the SEM unit in the Department of Applied Physics at the University of Kwa-Zulu Natal, Howard College Campus. The unit is described in Chapter 5, and some pictures of the unit are contained in Appendix A3. The shapes of each of the above media are given below.

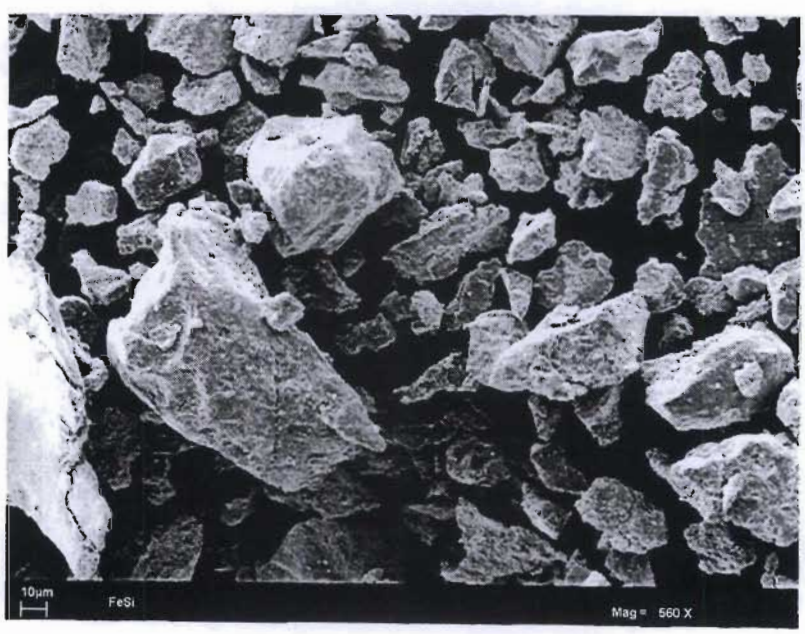

Figure A1.20 Ferrosilicon media particles at magnitude 560 X (b)

Figure A1.21 Ferrosilicon media particles at magnitude 560 X (b)

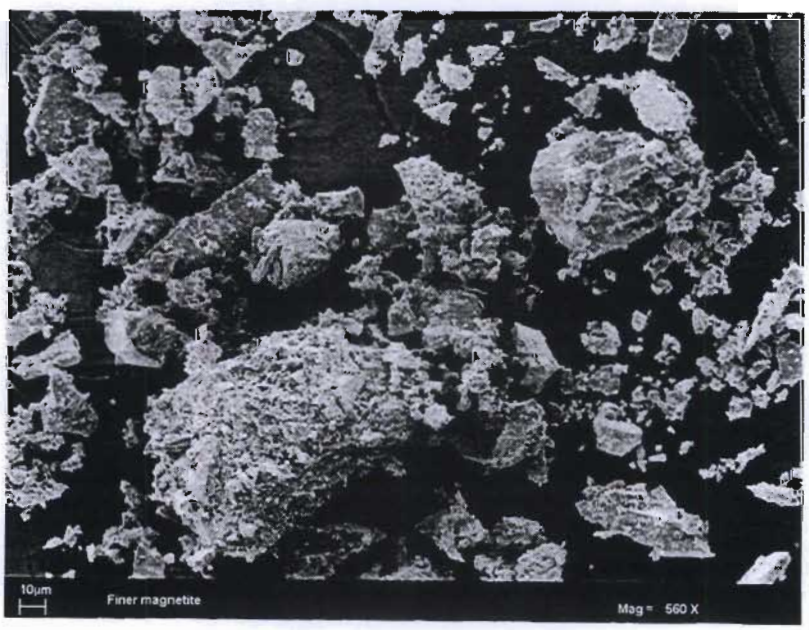

Figure A1.22 Magnetite #1 media particles at magnitude 560 X (a)

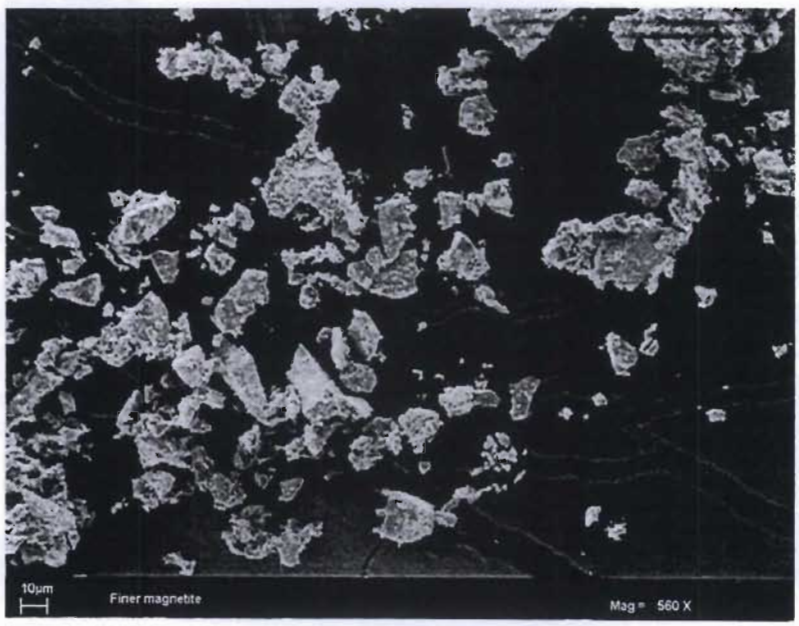

Figure A1.23 Magnetite #1 media particles at magnitude 560 X (b)

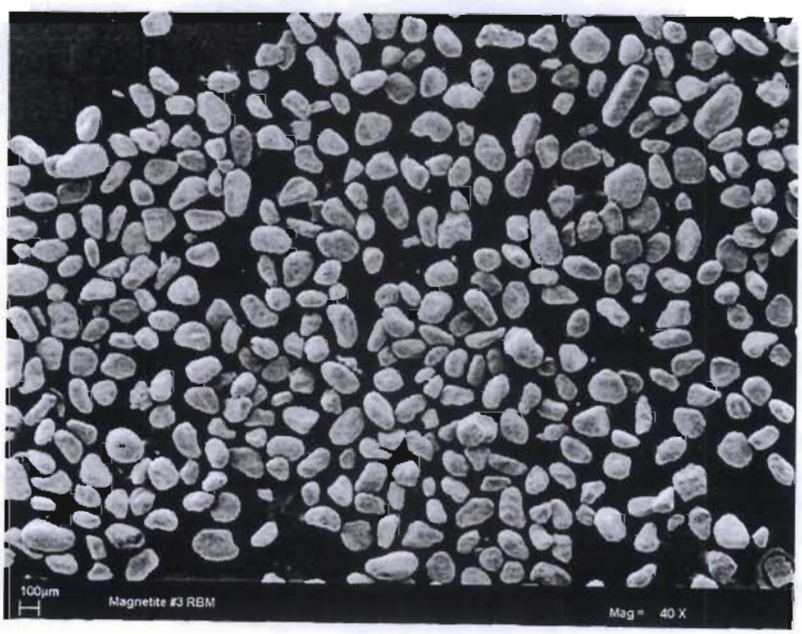

Figure A1.24 Magnetite #2 media particles at magnitude 40 X (a)

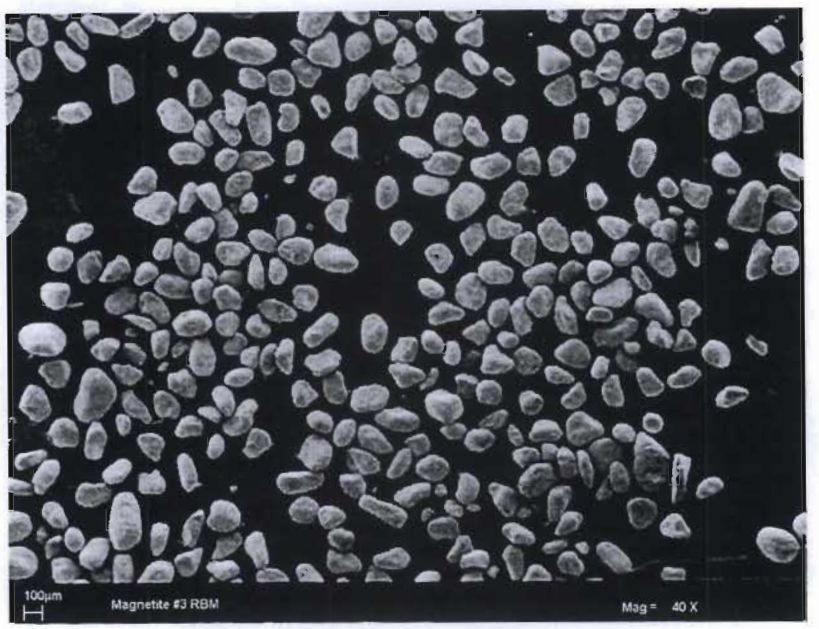

Figure A1.25 Magnetite #2 media particles at magnitude 40 X (b)

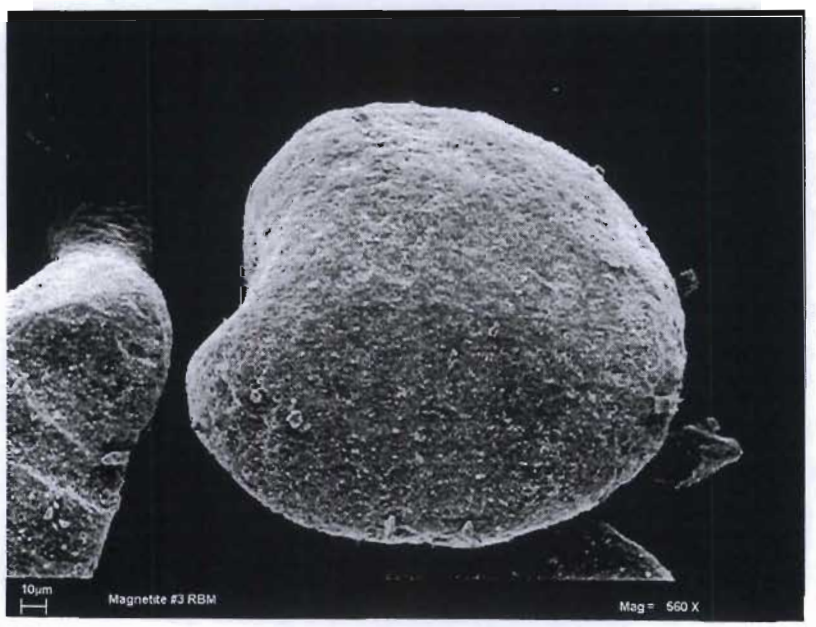

Figure A1.26 Magnetite #2 media particles at magnitude 560 X (a)

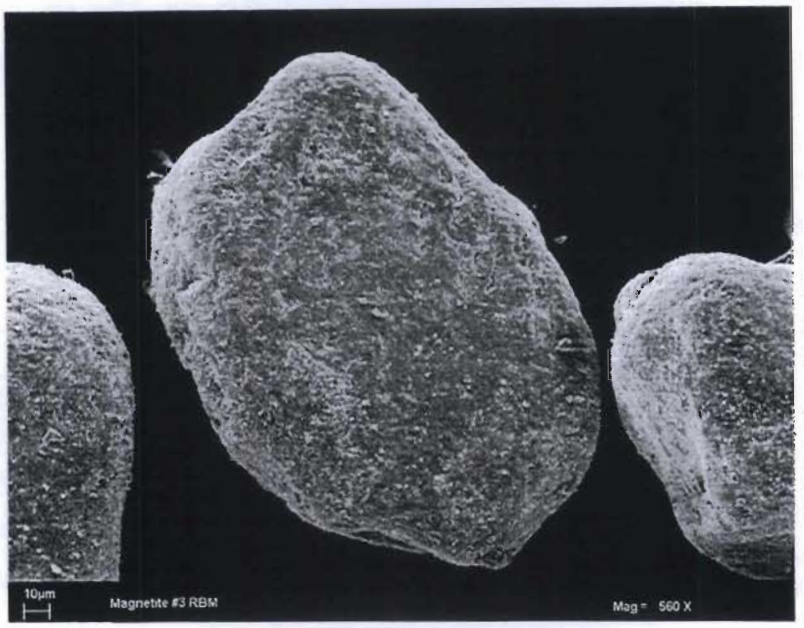

Figure A1.27 Magnetite #2 media particles at magnitude 560 X (b)

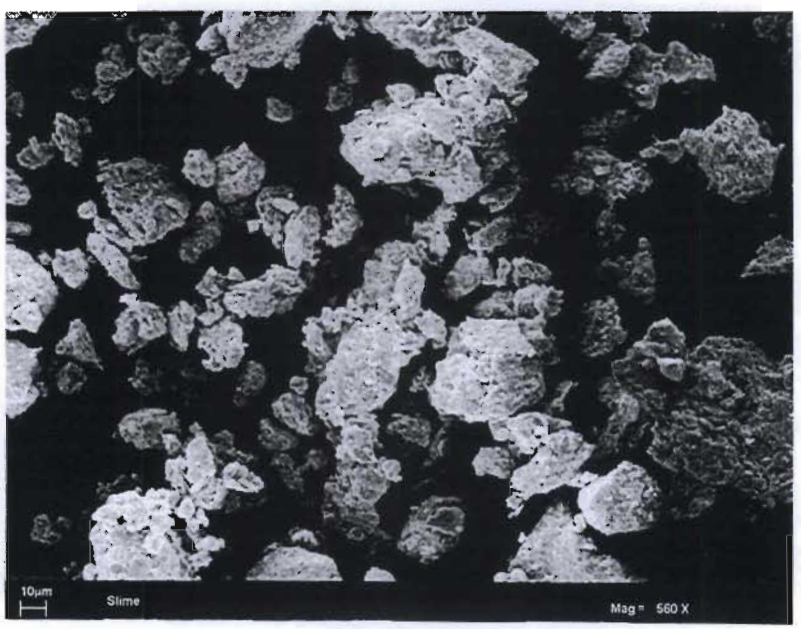

Figure A1.28 Slime / clay particles at magnitude 560 X (a)

Figure A1.29 Slime / clay particles at magnitude 560 X (b)

A1.6 Data Regression

A1.6.1 Objectives

The objective of this exercise was to fit the plain suspension results to rheological models, and to see which model best fitted the data. The models tested are similar to those given in Table A1.3. The tested models were the Herschel-Bulkley, Ostwald, Bingham, Casson, and Newton models. These models were fitted to the experimental results using Excel solver, in order to get the values of the parameters in the various equations. Once the parameters had been obtained, these were then used to plot the flow curves at arbitrary shear rates. This section presents the results obtained from the data regression. Only the models which gave meaningful results were plotted together with the experimental data points. For example, if the regressed parameters for some of the models (particularly those with yield stress terms) gave negative values, then these models were considered unfit and were not plotted together with the experimental data.

A1.6.2 Regression Results

The presentation of the regressed results will be similar to that of the rheometry tests, i.e. starting from ferrosilicon, magnetite #1, FeSi / Mag #1 mixtures, Mag #1 / Mag #2, and finally ending with FeSi / Mag #2 results.

A1.6.2.1 Regressed Ferrosilicon Suspension Data Results

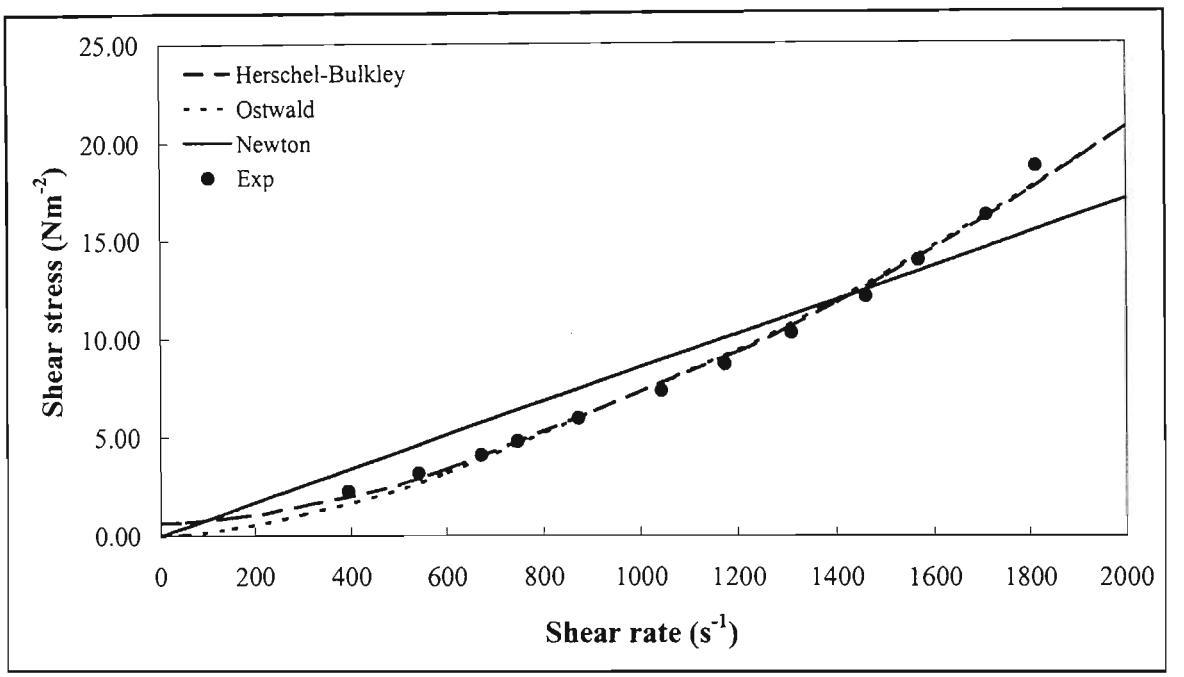

Figure A1.30 Regressed Ferrosilicon data at specific gravity 2.0

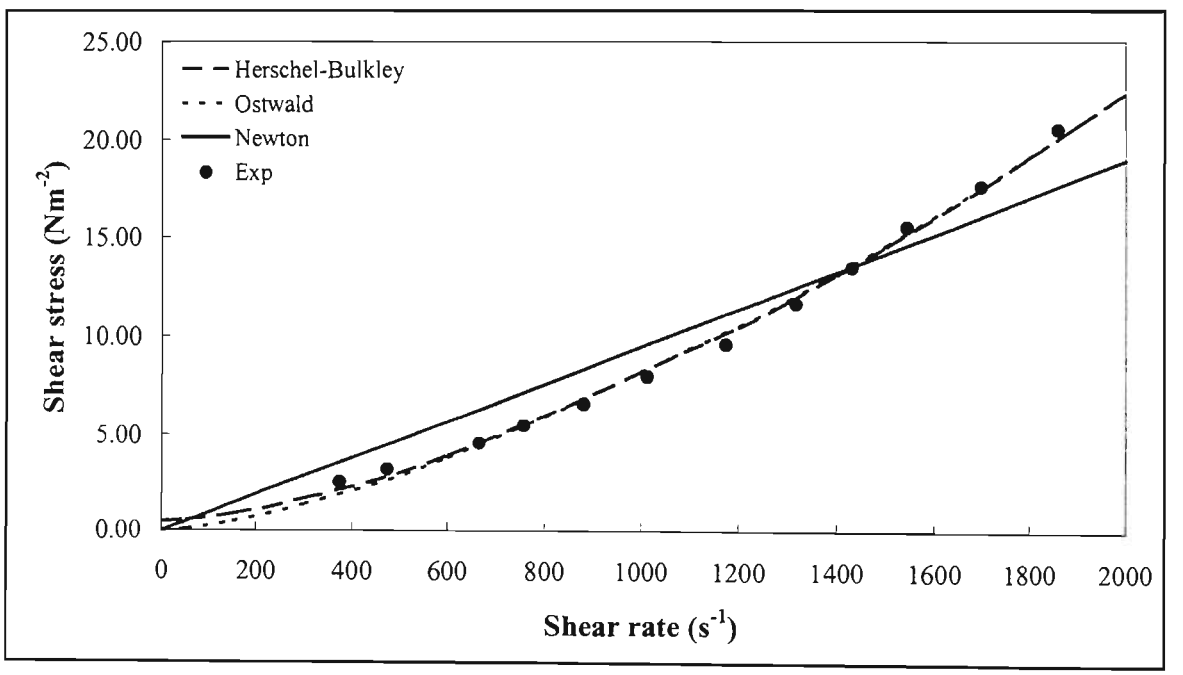

Figure A1.31 Regressed Ferrosilicon data at specific gravity 2.1

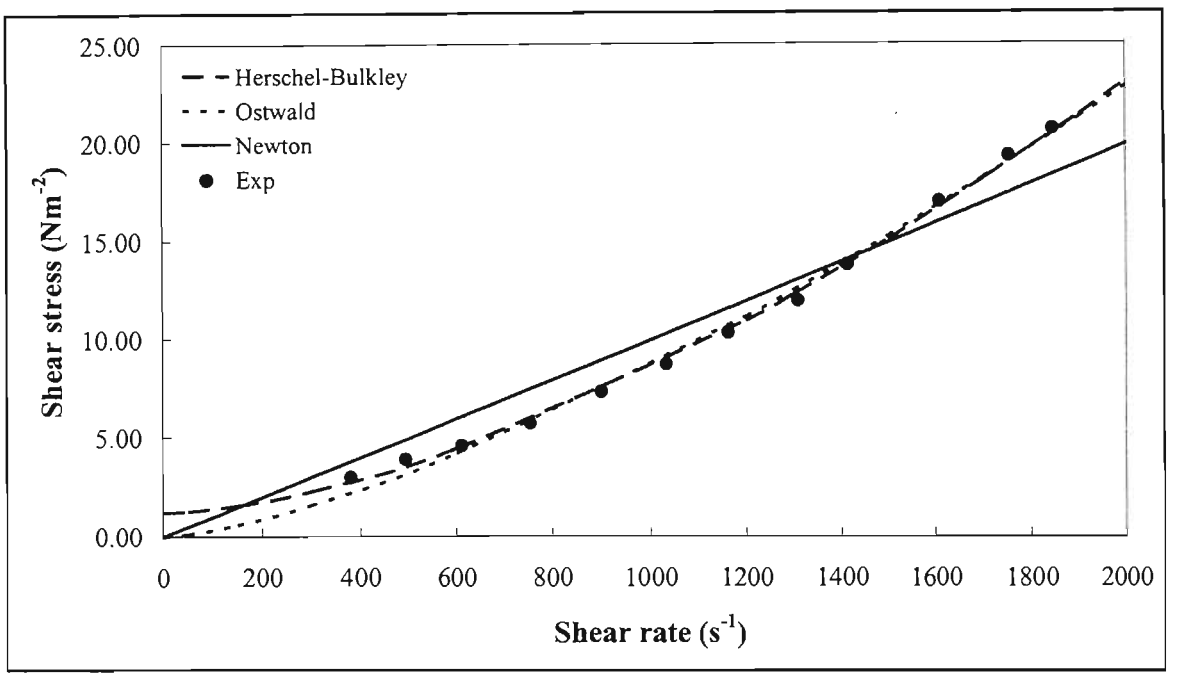

Figure A1.32 Regressed Ferrosilicon data at specific gravity 2.2

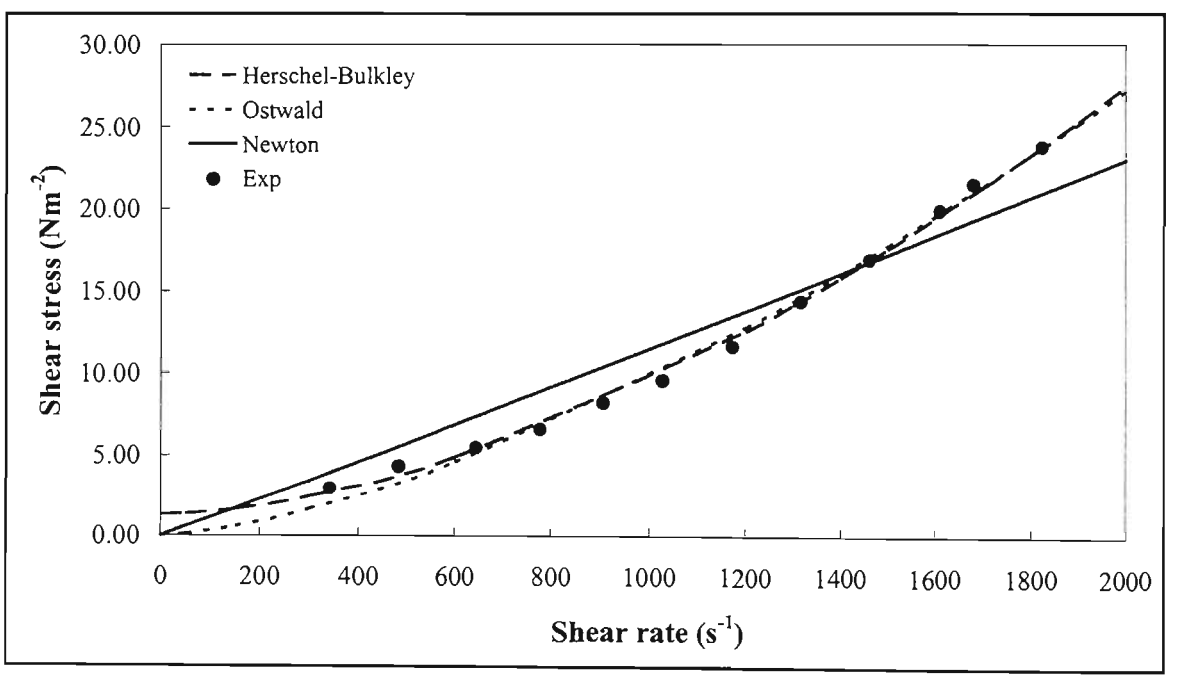

Figure A1.33 Regressed Ferrosilicon data at specific gravity 2.3

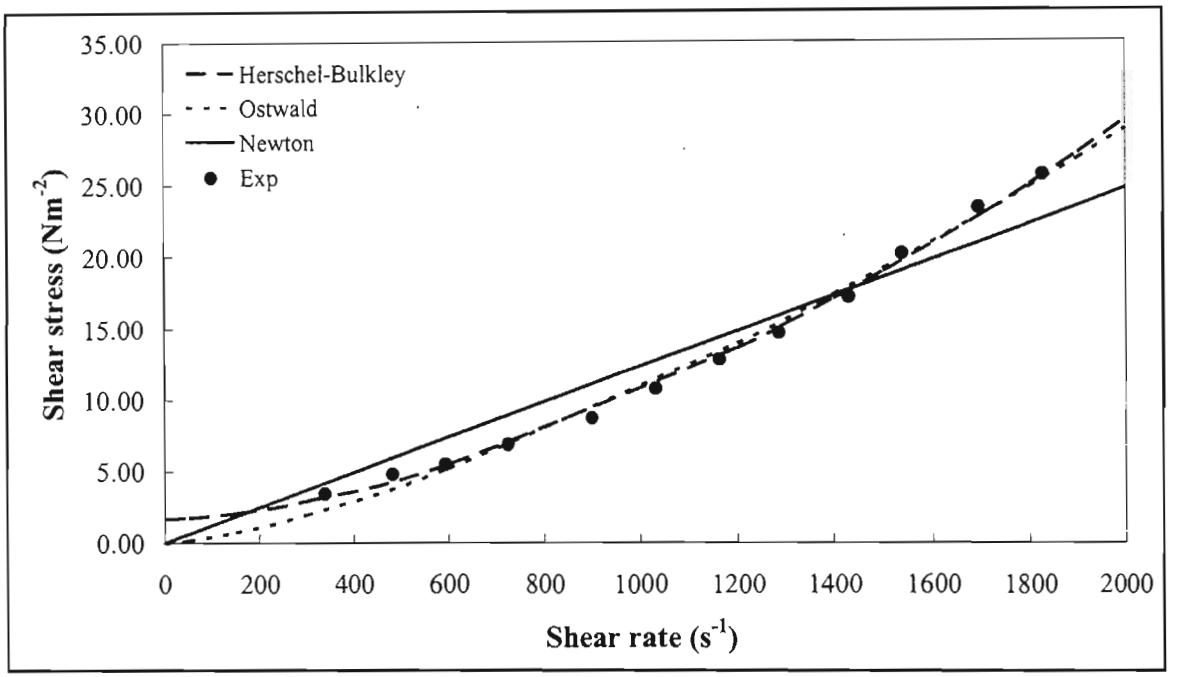

Figure A1.34 Regressed Ferrosilicon data at specific gravity 2.4

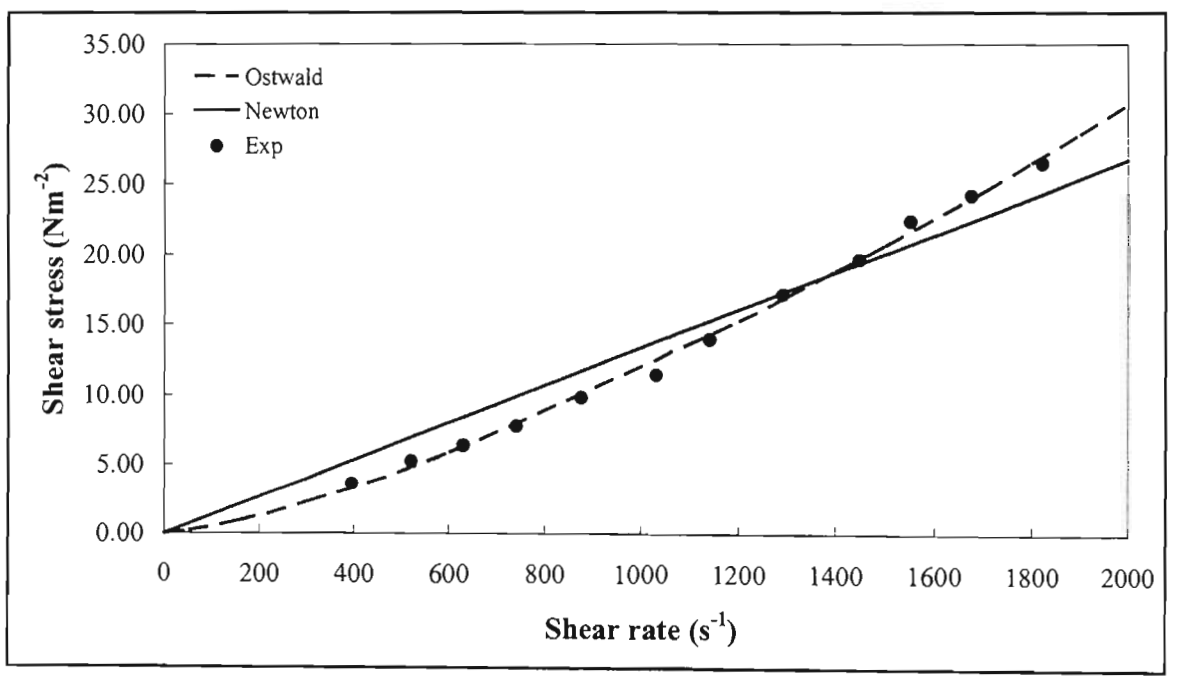

Figure A1.35 Regressed Ferrosilicon data at specific gravity 2.5

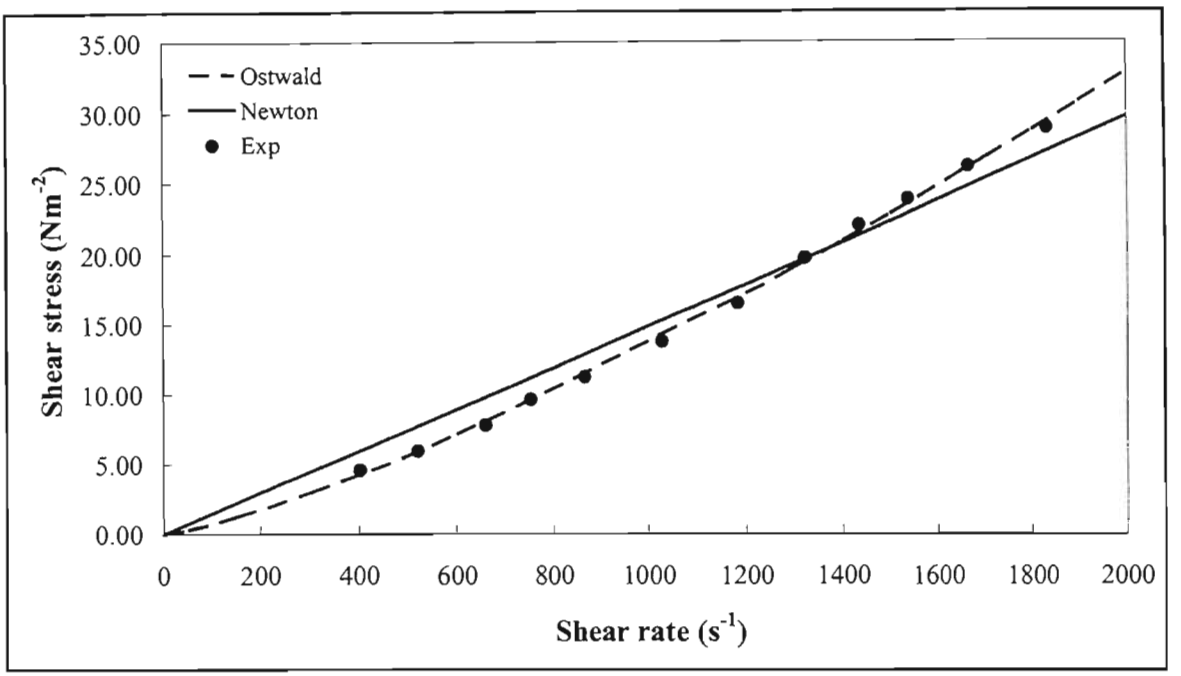

Figure A1.36 Regressed Ferrosilicon data at specific gravity 2.6

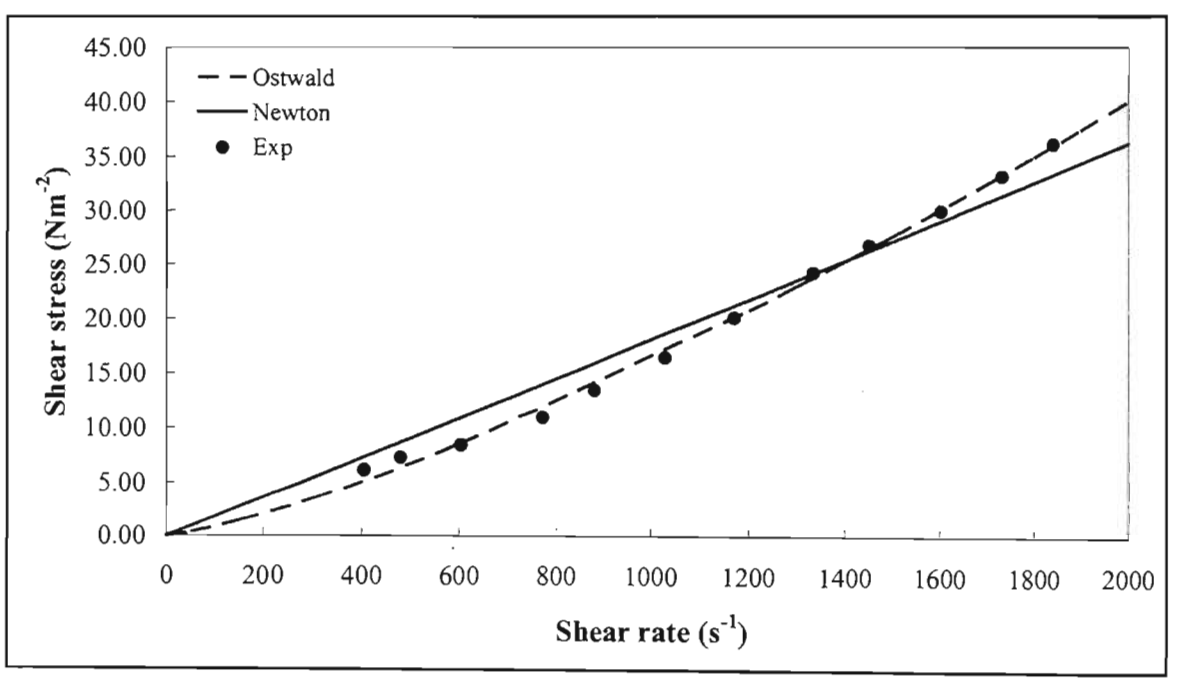

Figure A1.37 Regressed Ferrosilicon data at specific gravity 2.7

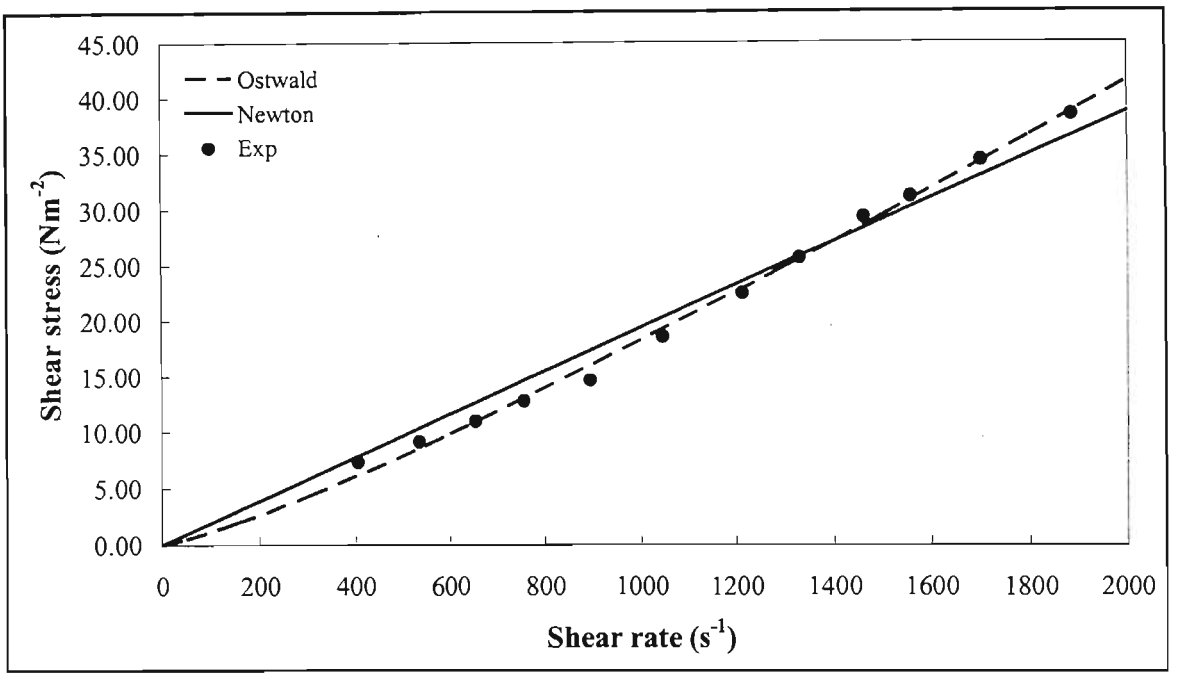

Figure A1.38 Regressed Ferrosilicon data at specific gravity 2.8

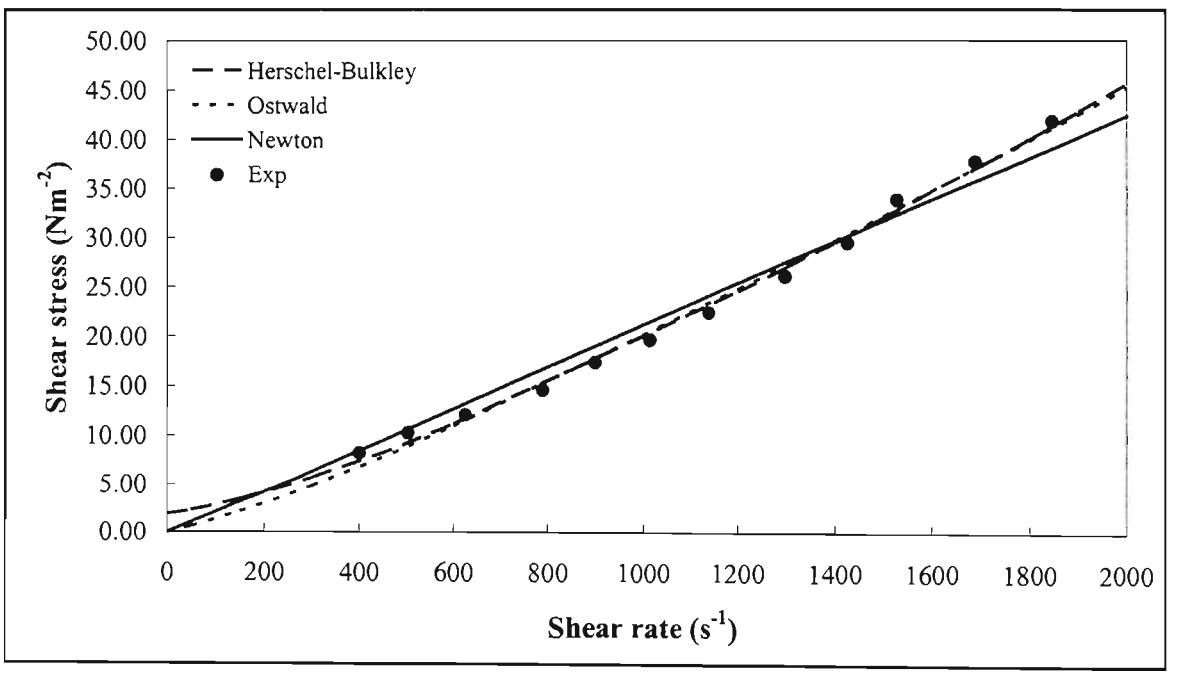

Figure A1.39 Regressed Ferrosilicon data at specific gravity 2.9

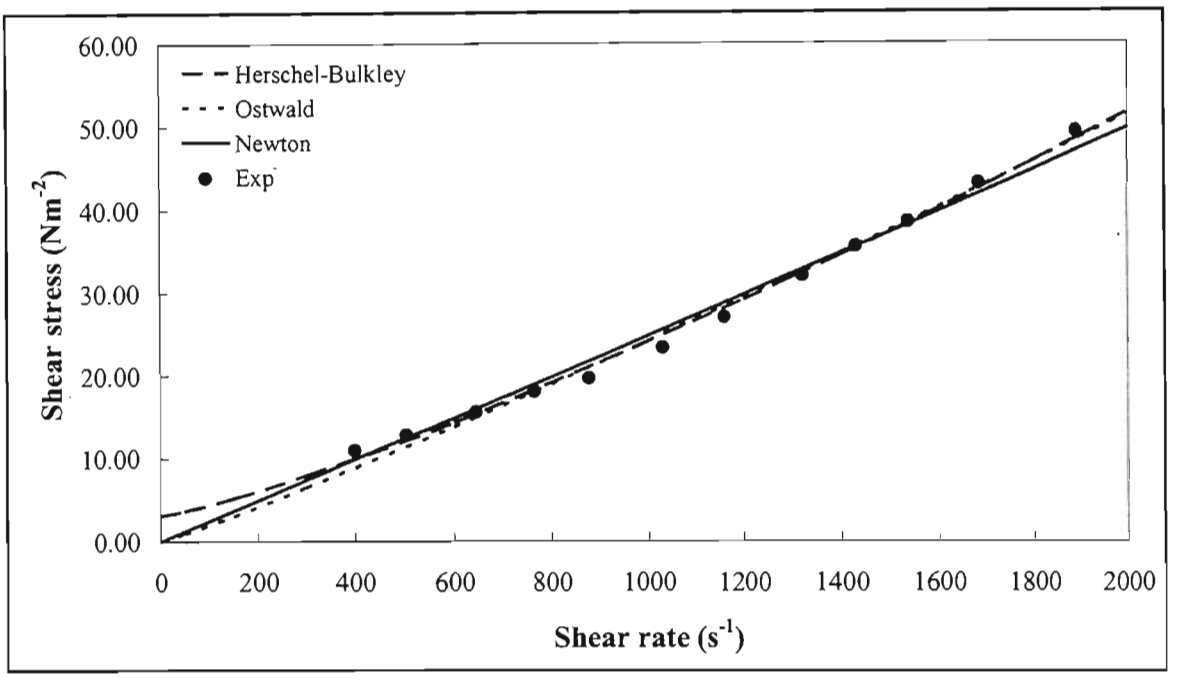

Figure A1.40 Regressed Ferrosilicon data at specific gravity 3.0

A1.6.2.2 Regressed Magnetite #1 Suspension Data Results

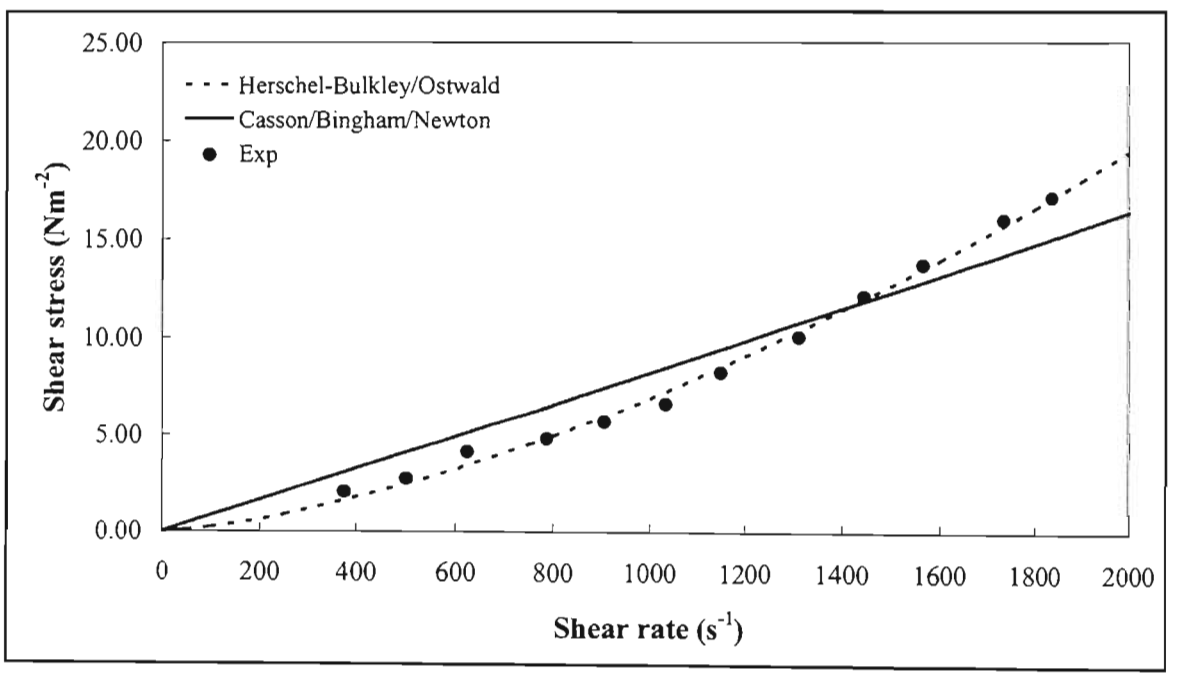

Figure A1.41 Regressed Magnetite #1 data at specific gravity 1.5

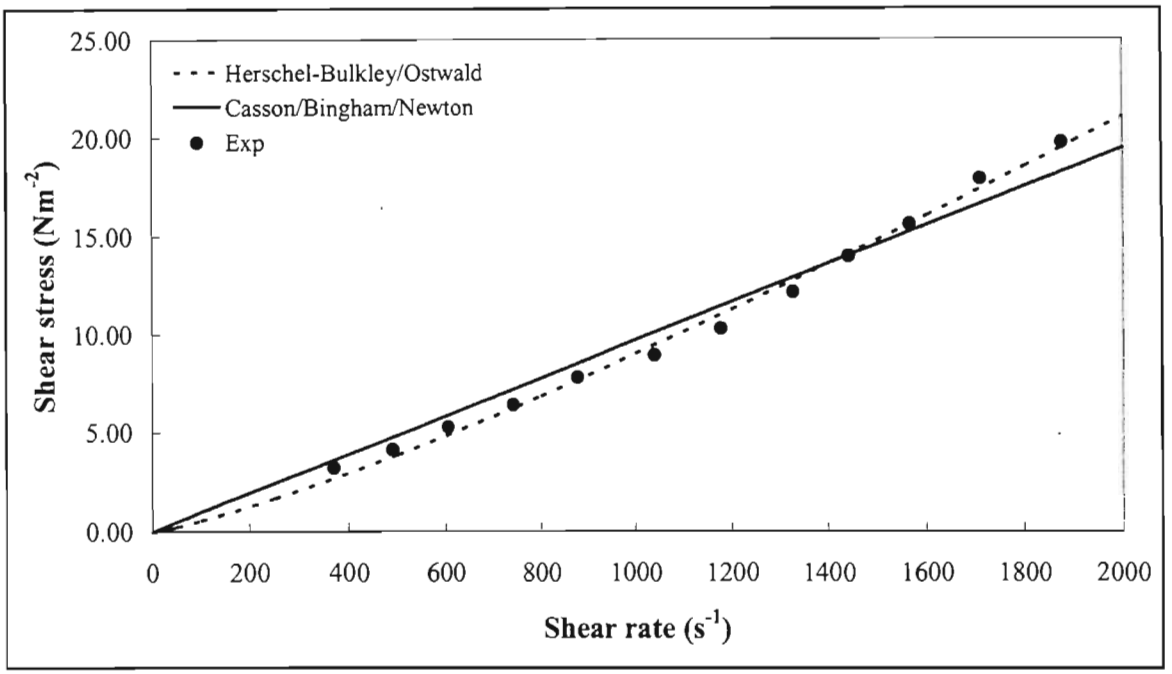

Figure A1.42 Regressed Magnetite #1 data at specific gravity 1.6

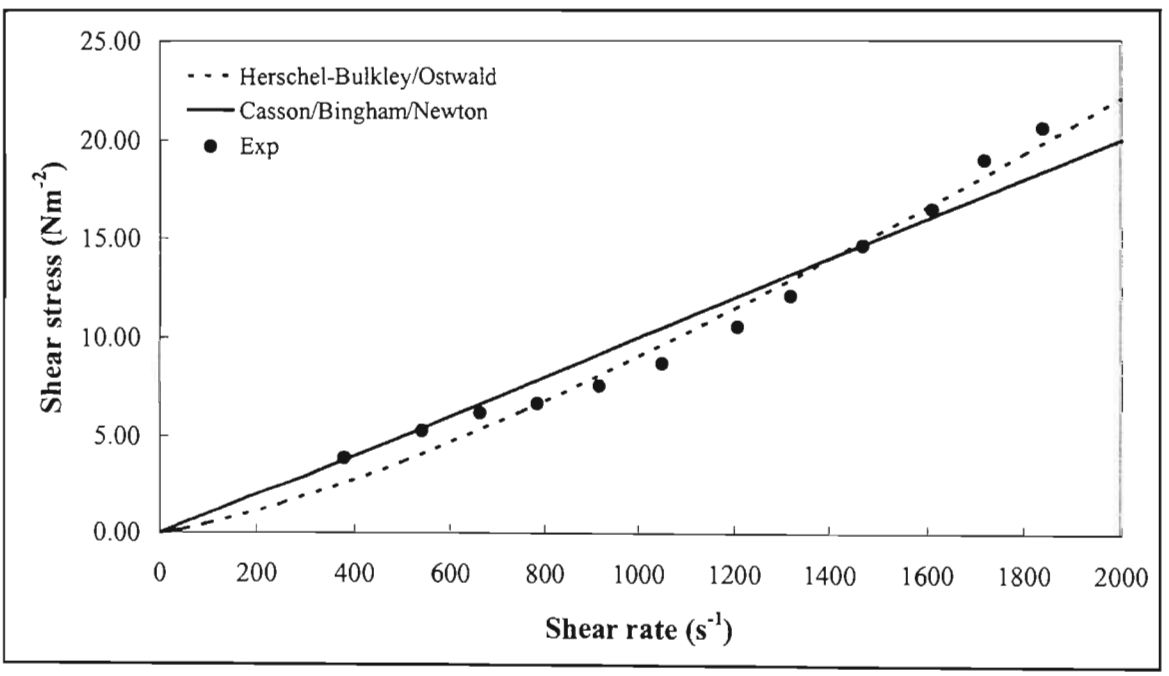

Figure A1.43 Regressed Magnetite #1 data at specific gravity 1.7

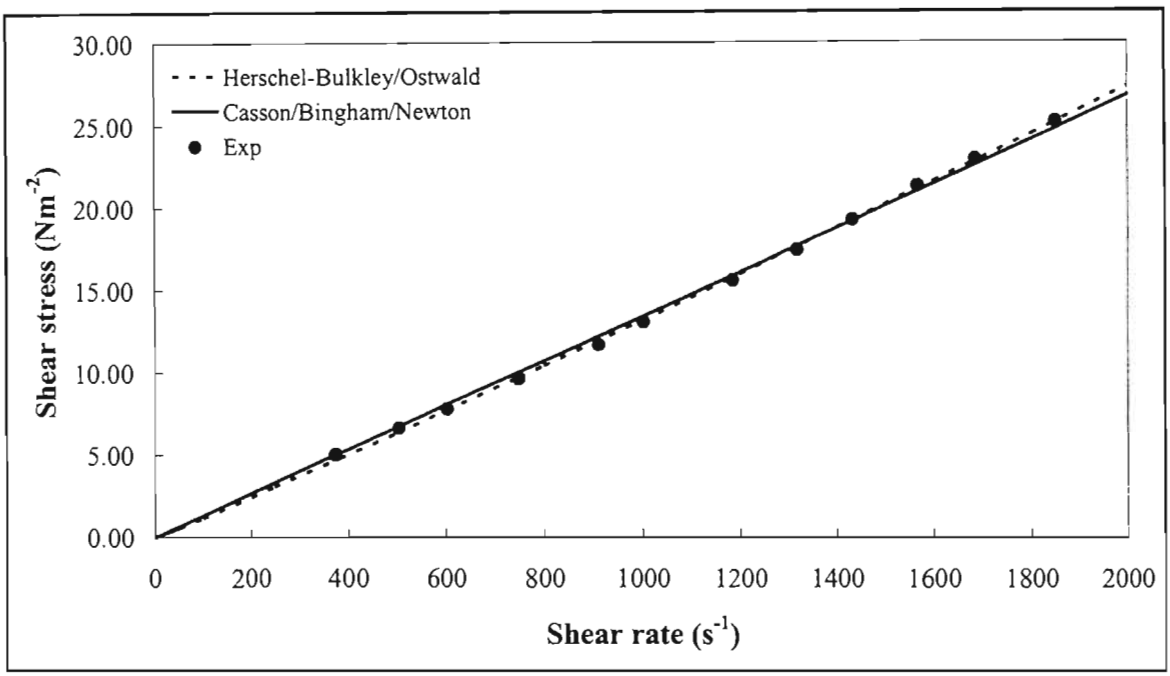

Figure A1.44 Regressed Magnetite #1 data at specific gravity 1.8

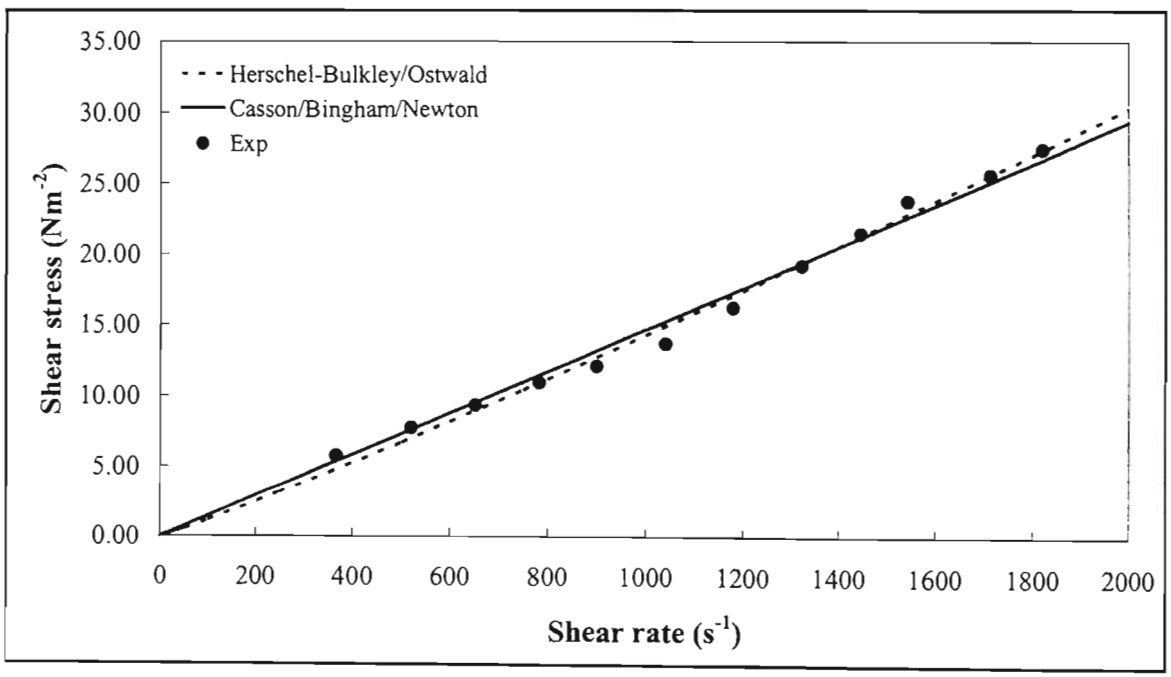

Figure A1.45 Regressed Magnetite #1 data at specific gravity 1.9

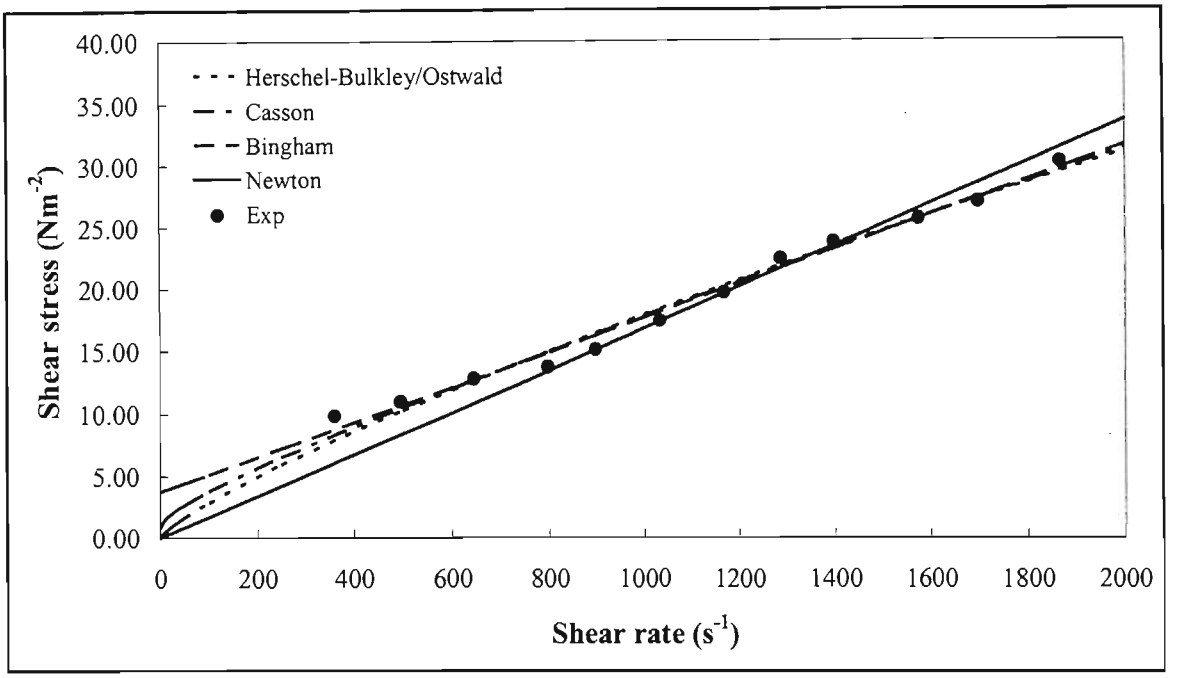

Figure A1.46 Regressed Magnetite #1 data at specific gravity 2.0

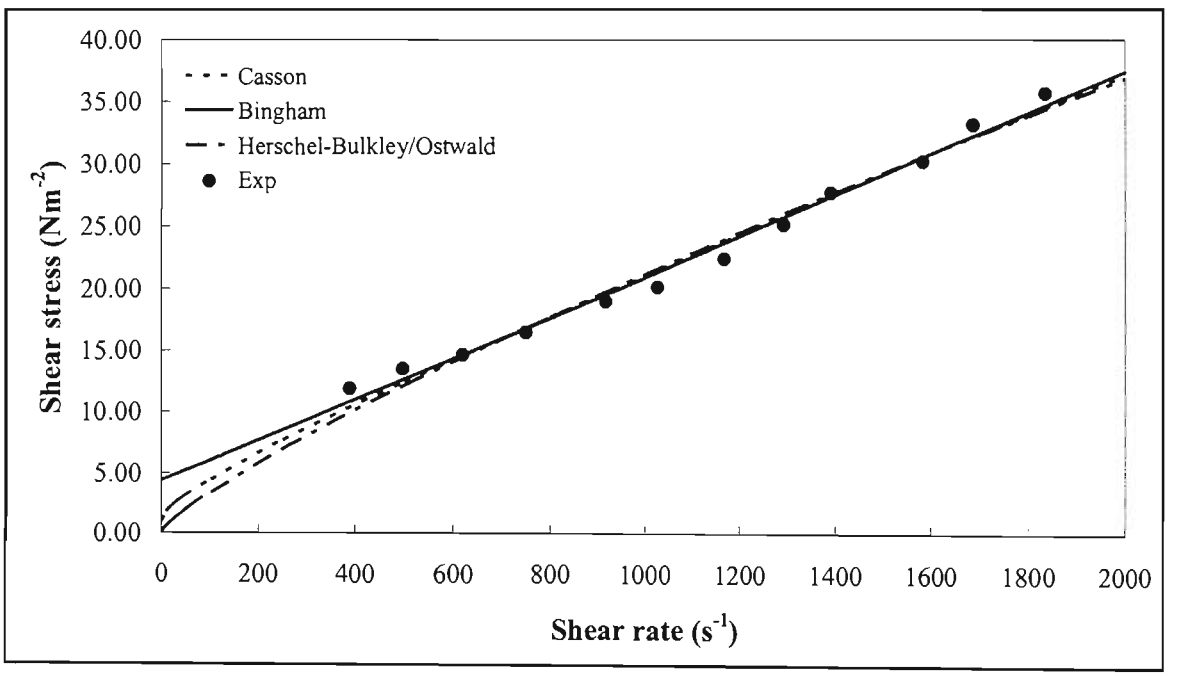

Figure A1.47 Regressed Magnetite #1 data at specific gravity 2.1

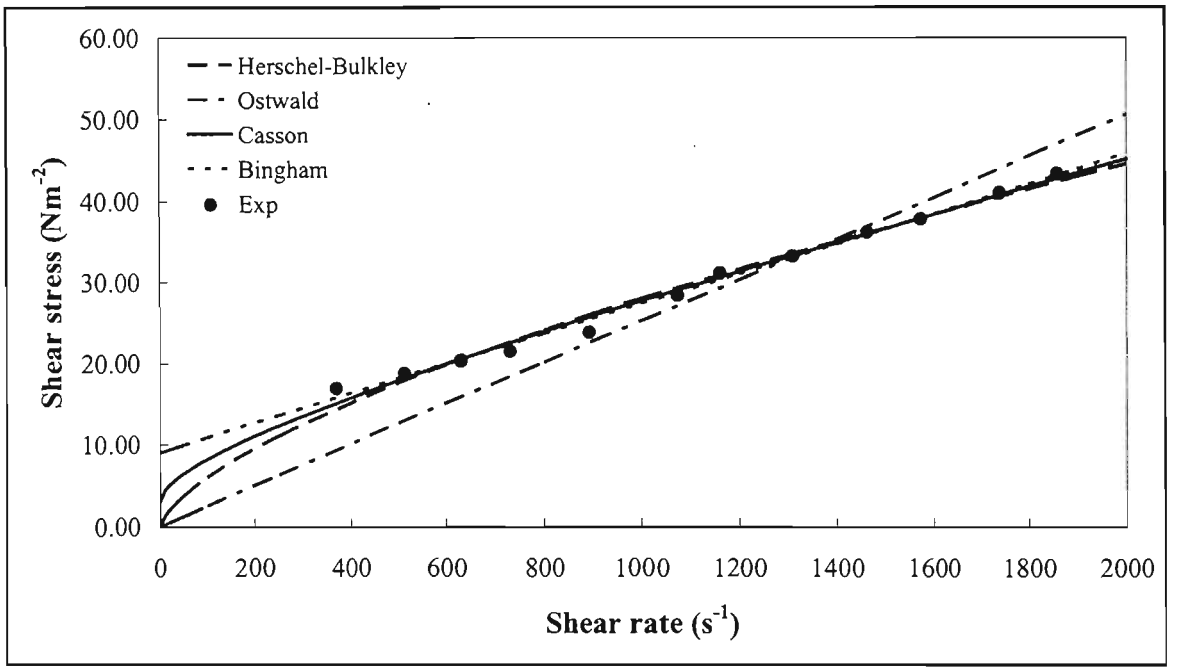

Figure A1.48 Regressed Magnetite #1 data at specific gravity 2.2

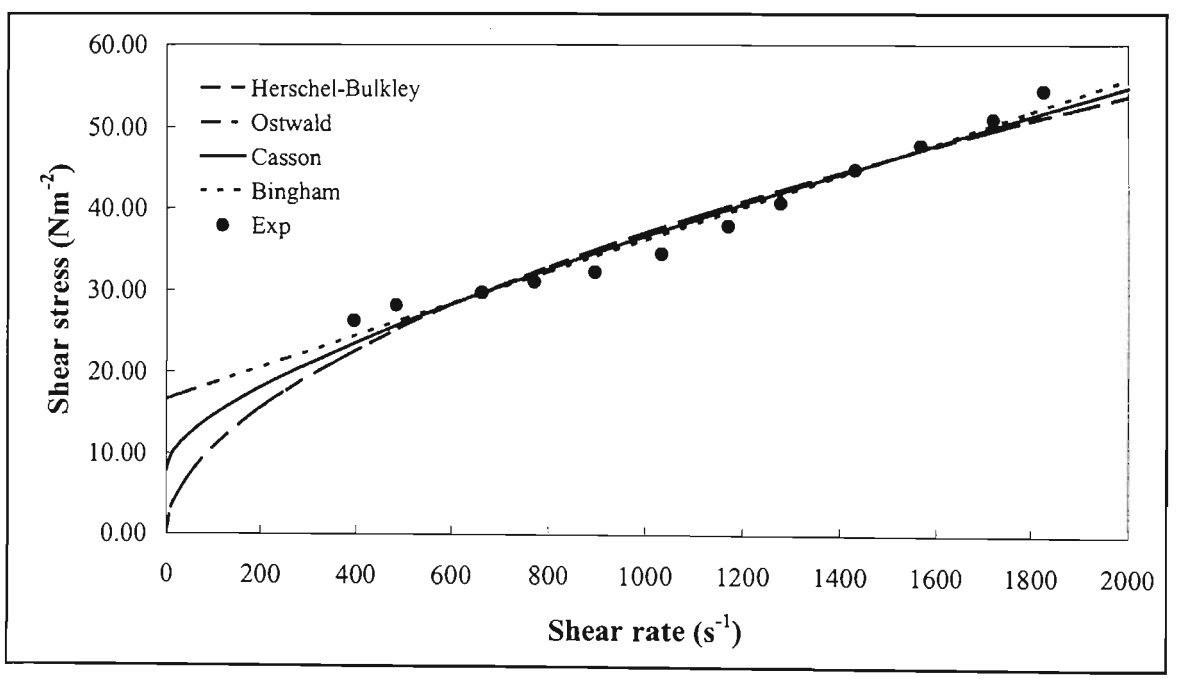

Figure A1.49 Regressed Magnetite #1 data at specific gravity 2.3

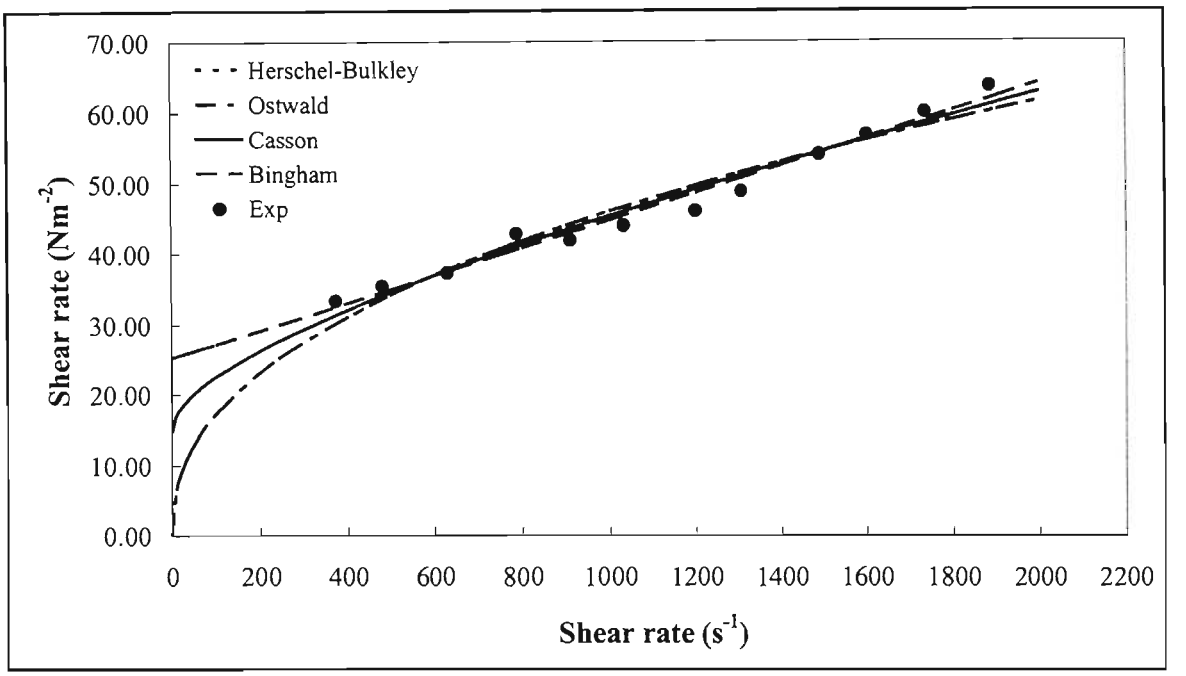

Figure A1.50 Regressed Magnetite #1 data at specific gravity 2.4

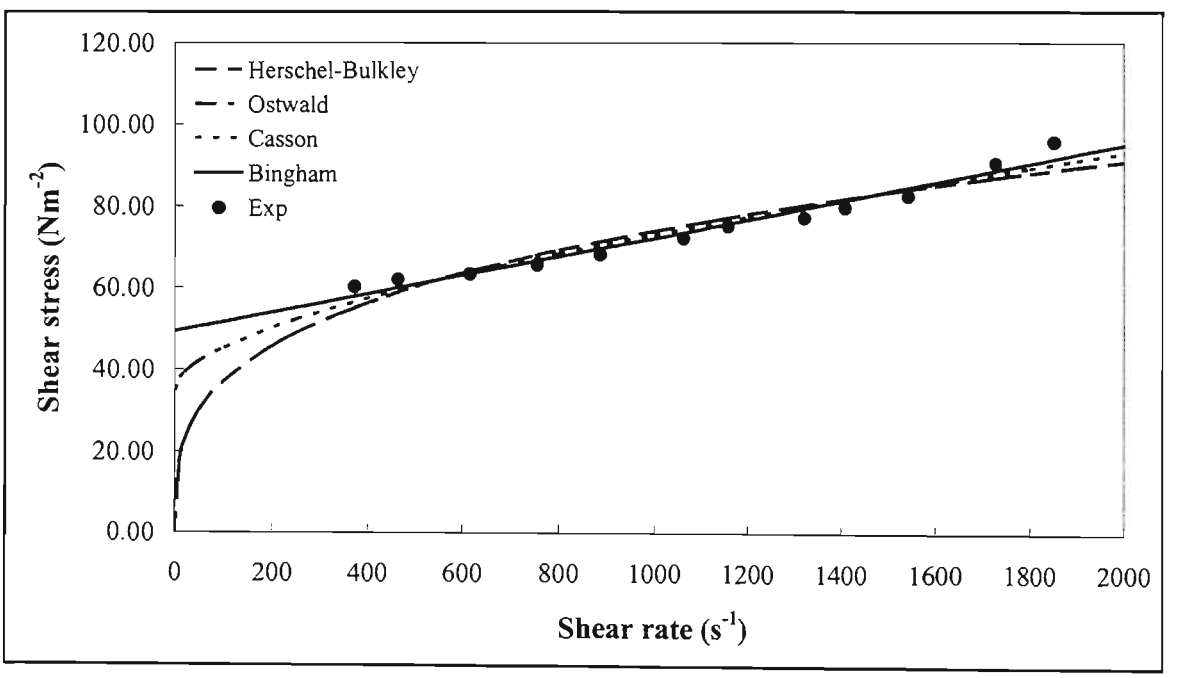

Figure A1.51 Regressed Magnetite #1 data at specific gravity 2.5

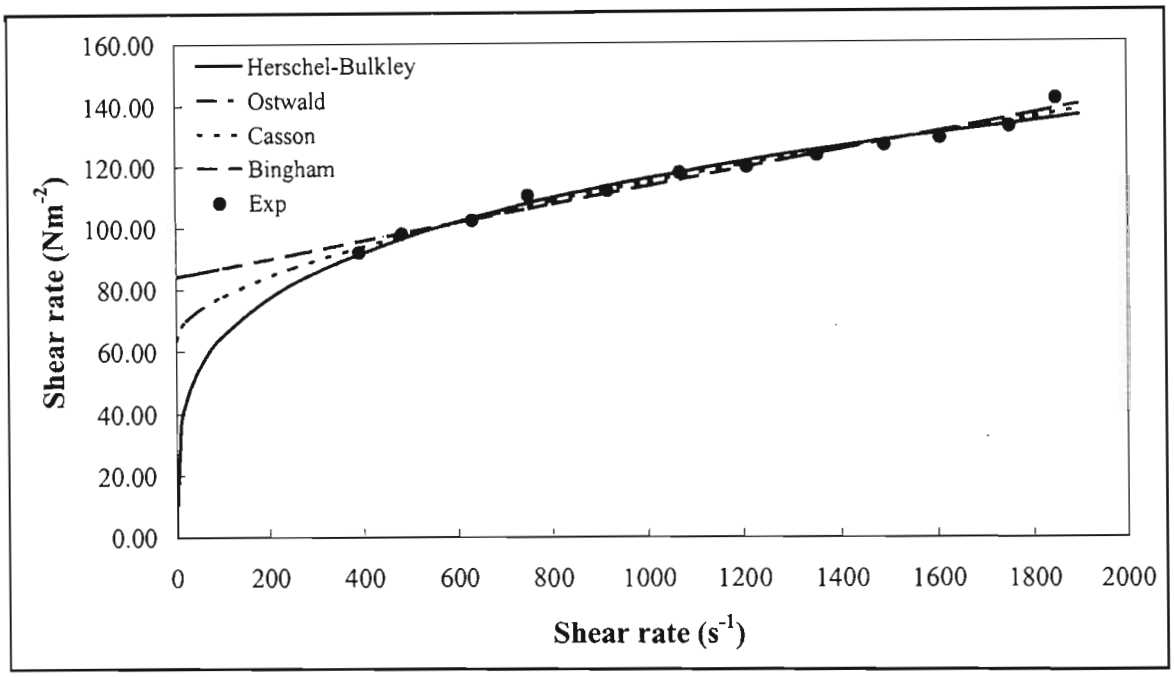

Figure A1.52 Regressed Magnetite #1 data at specific gravity 2.6

A1.6.2.3 Regressed Ferrosilicon / Magnetite #1 Data Results

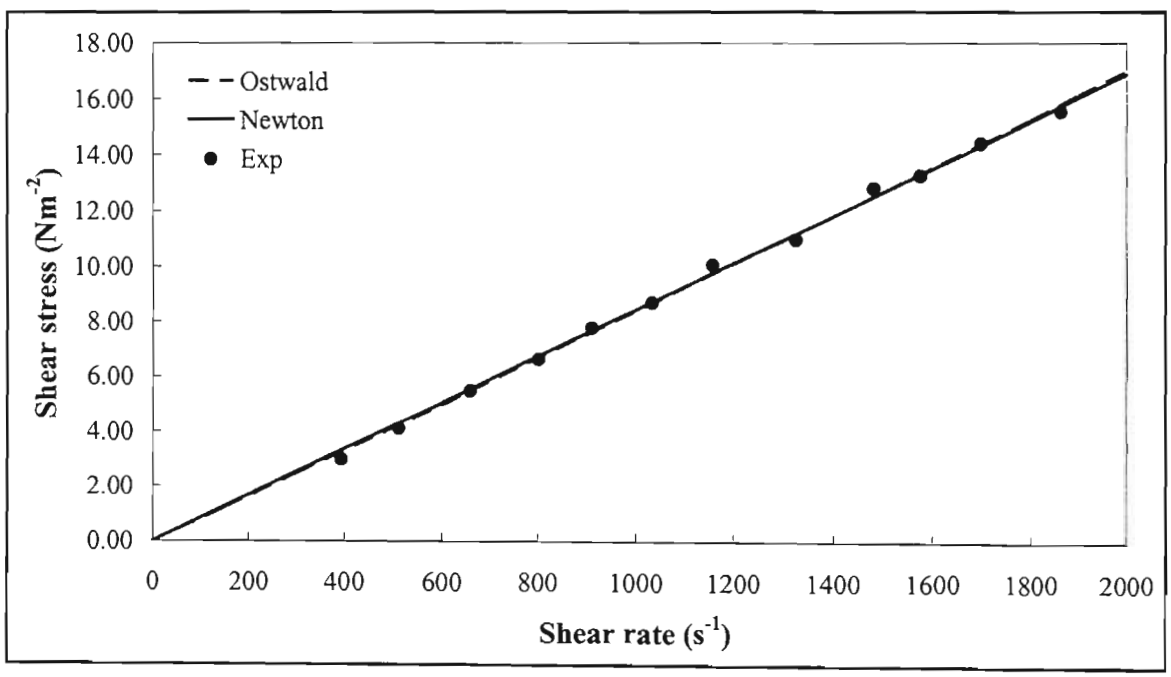

Figure A1.53 Regressed data for FeSi / Mag #1 for ratio 2:1 at specific gravity 2.0

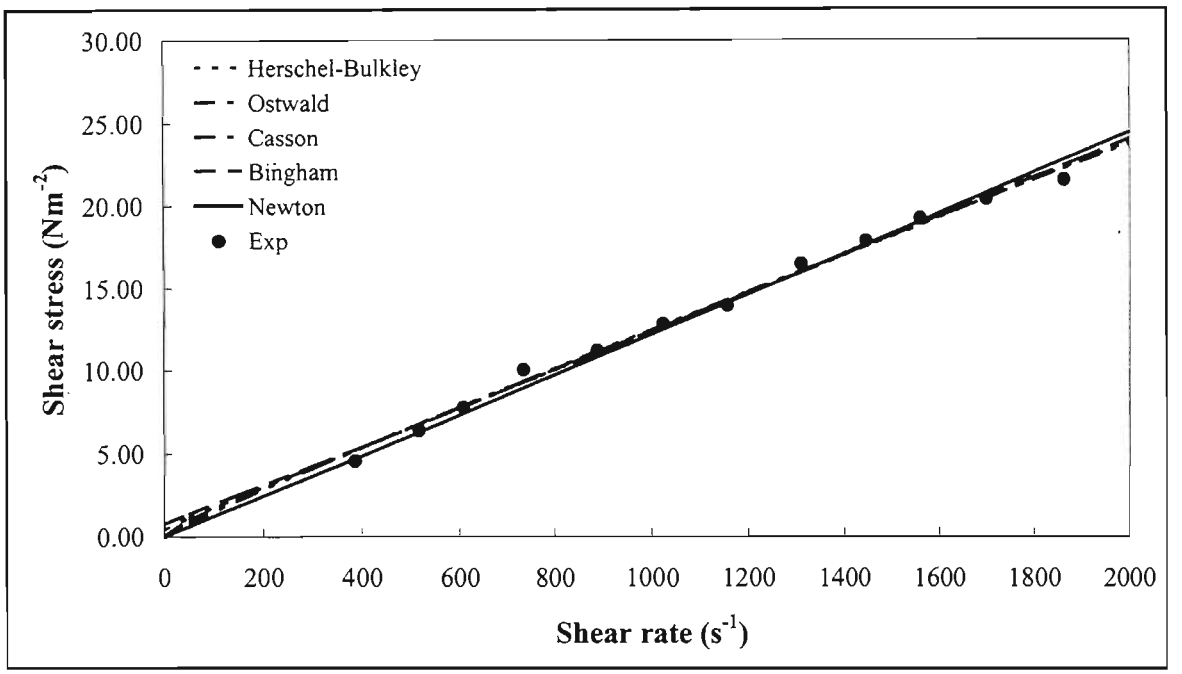

Figure A1.54 Regressed data for FeSi / Mag #1 for ratio 2:1 at specific gravity 2.1

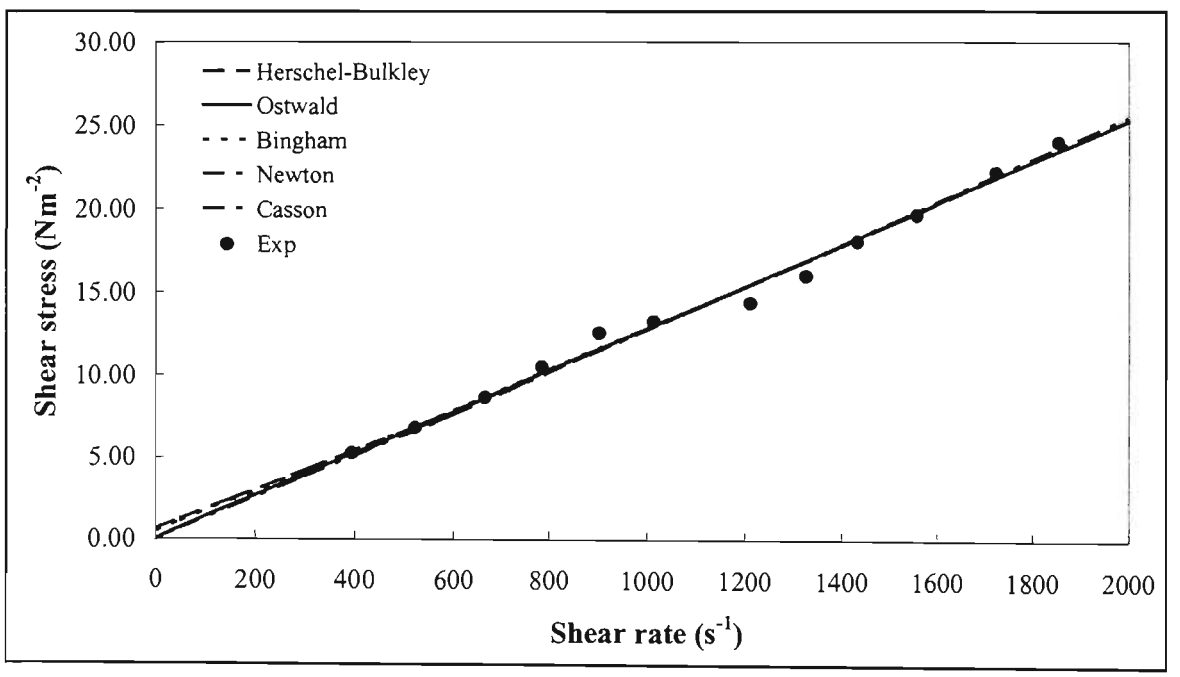

Figure A1.55 Regressed data for FeSi / Mag #1 for ratio 2:1 at specific gravity 2.2

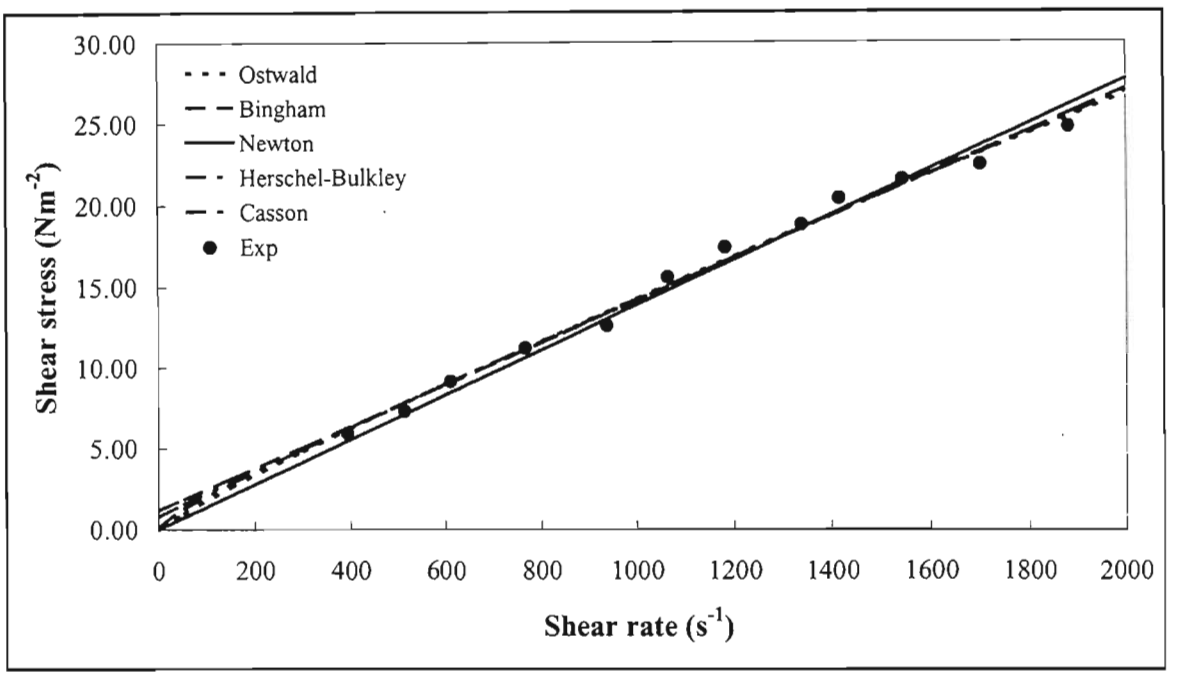

Figure A1.56 Regressed data for FeSi / Mag #1 for ratio 2:1 at specific gravity 2.3

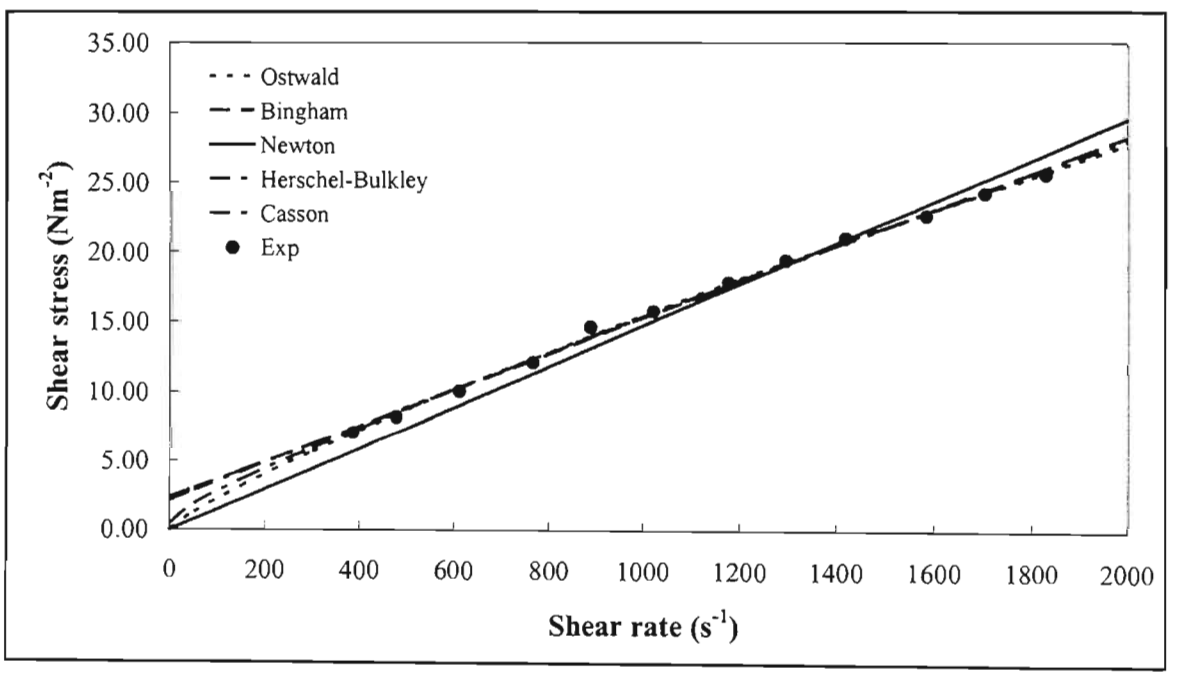

Figure A1.57 Regressed data for FeSi / Mag #1 for ratio 2:1 at specific gravity 2.4

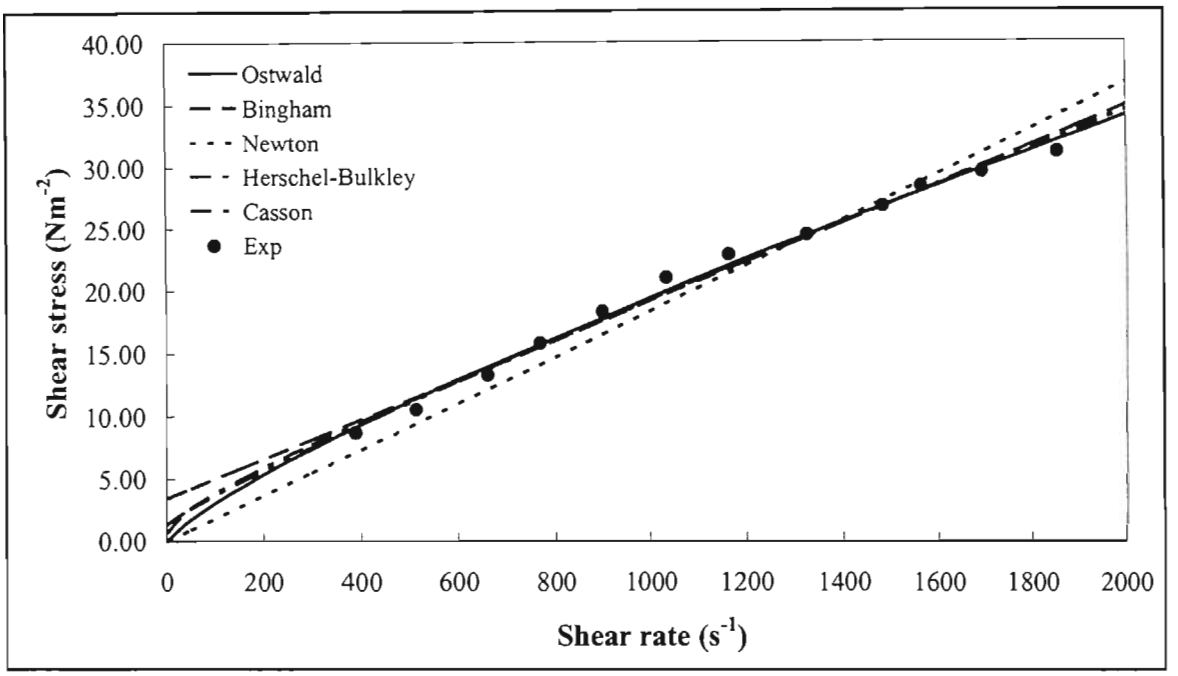

Figure A1.58 Regressed data for FeSi / Mag #1 for ratio 2:1 at specific gravity 2.5

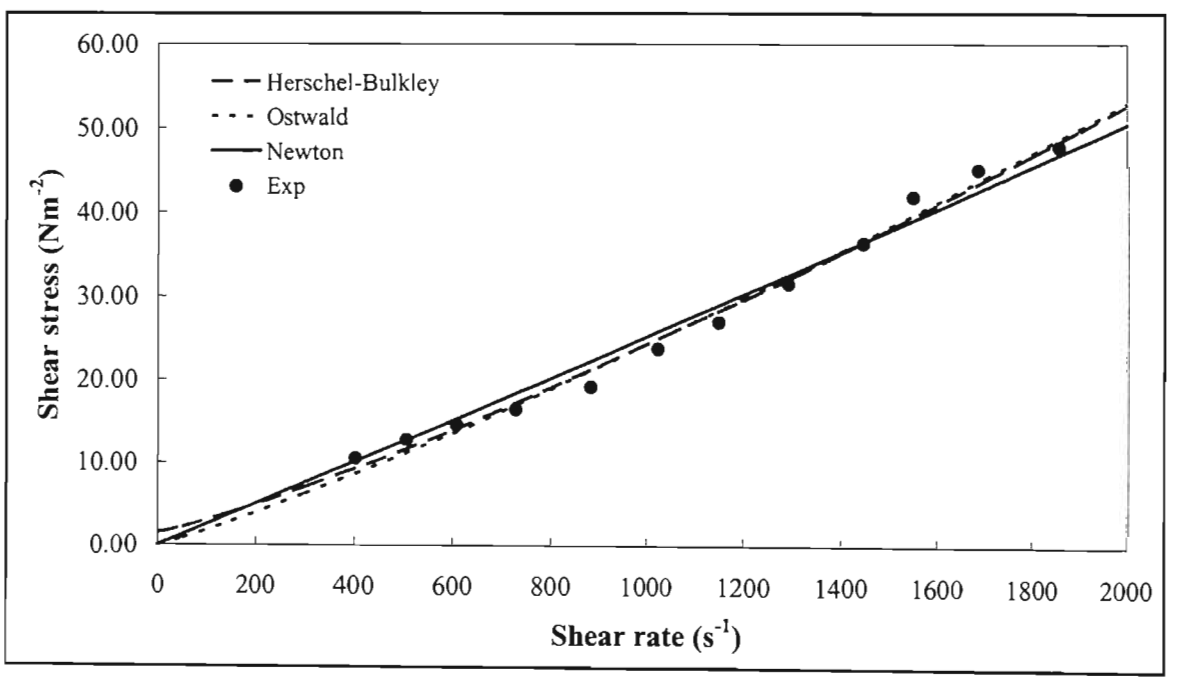

Figure A1.59 Regressed data for FeSi / Mag #1 for ratio 2:1 at specific gravity 2.6

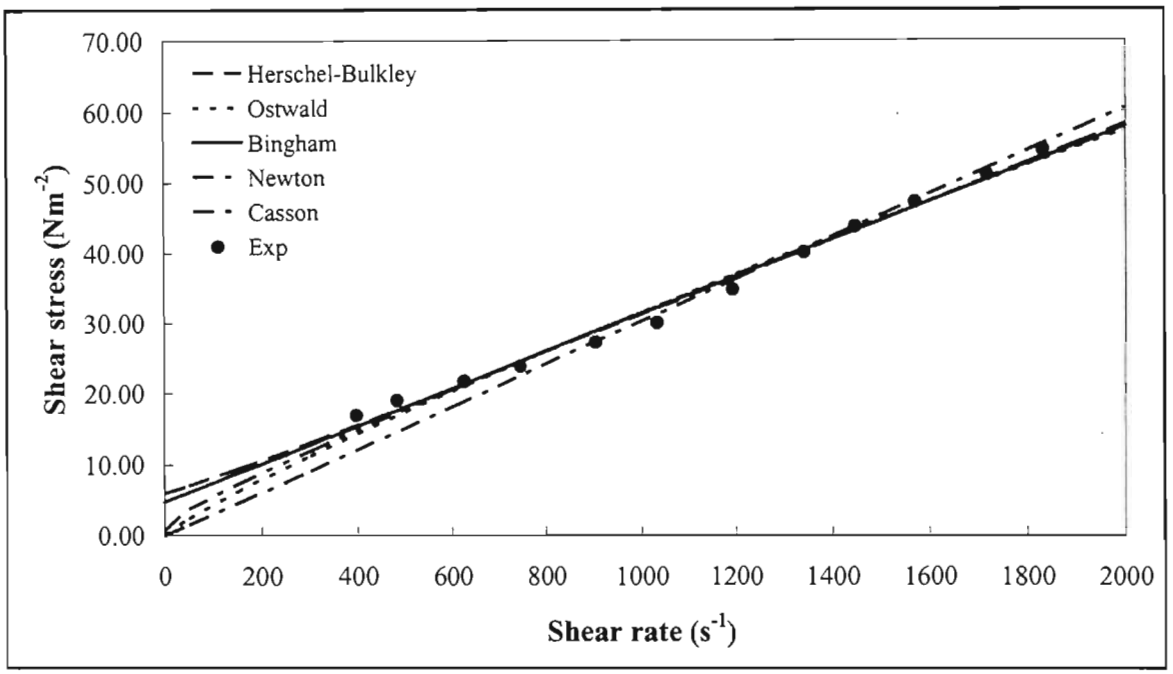

Figure A1.60 Regressed data for FeSi / Mag #1 for ratio 2:1 at specific gravity 2.7

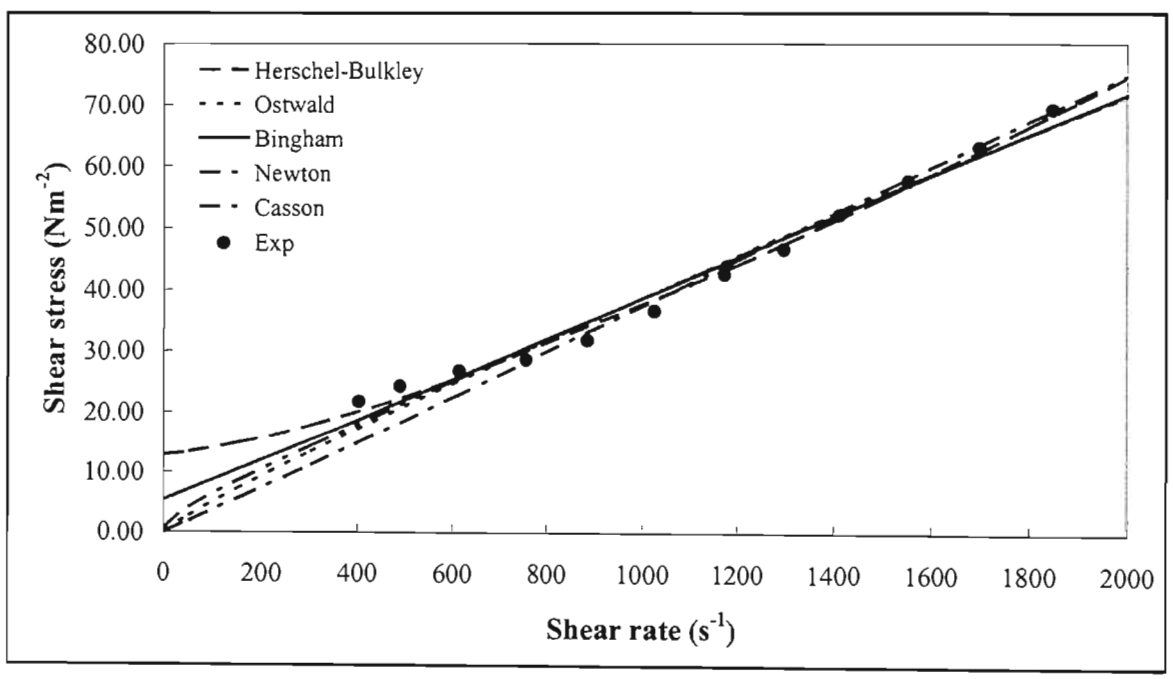

Figure A1.61 Regressed data for FeSi / Mag #1 for ratio 2:1 at specific gravity 2.8

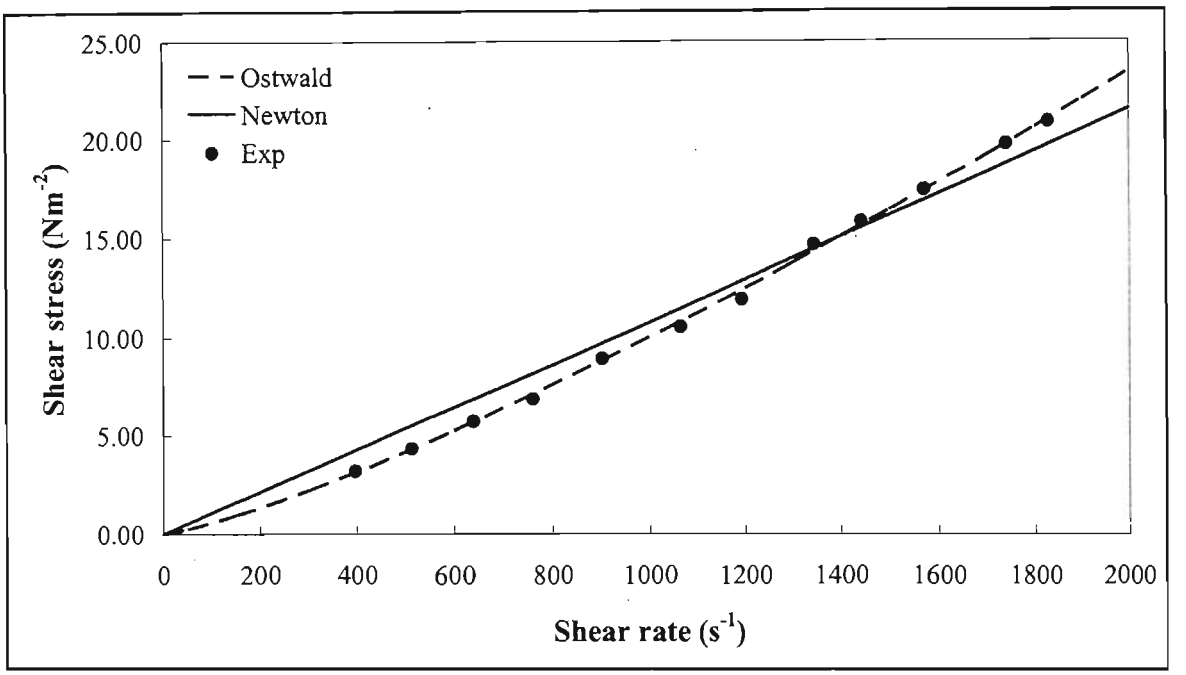

Figure A1.62 Regressed data for FeSi / Mag #1 for ratio 1:1 at specific gravity 2.0

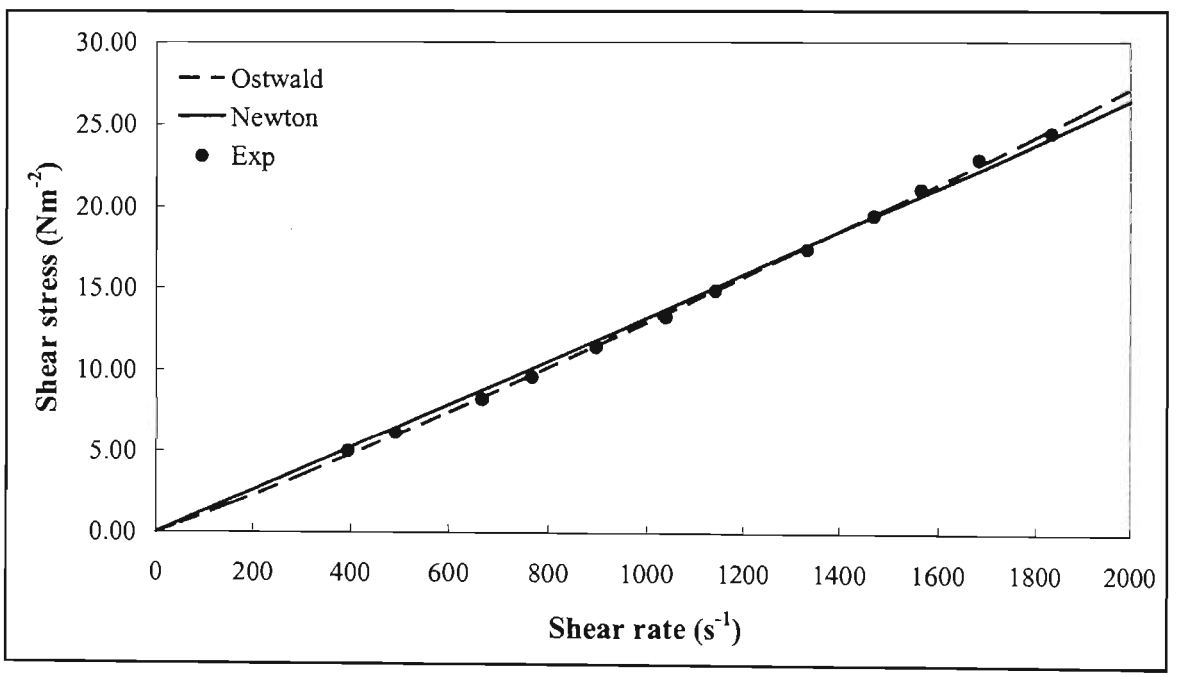

Figure A1.63 Regressed data for FeSi / Mag #1 for ratio 1:1 at specific gravity 2.1

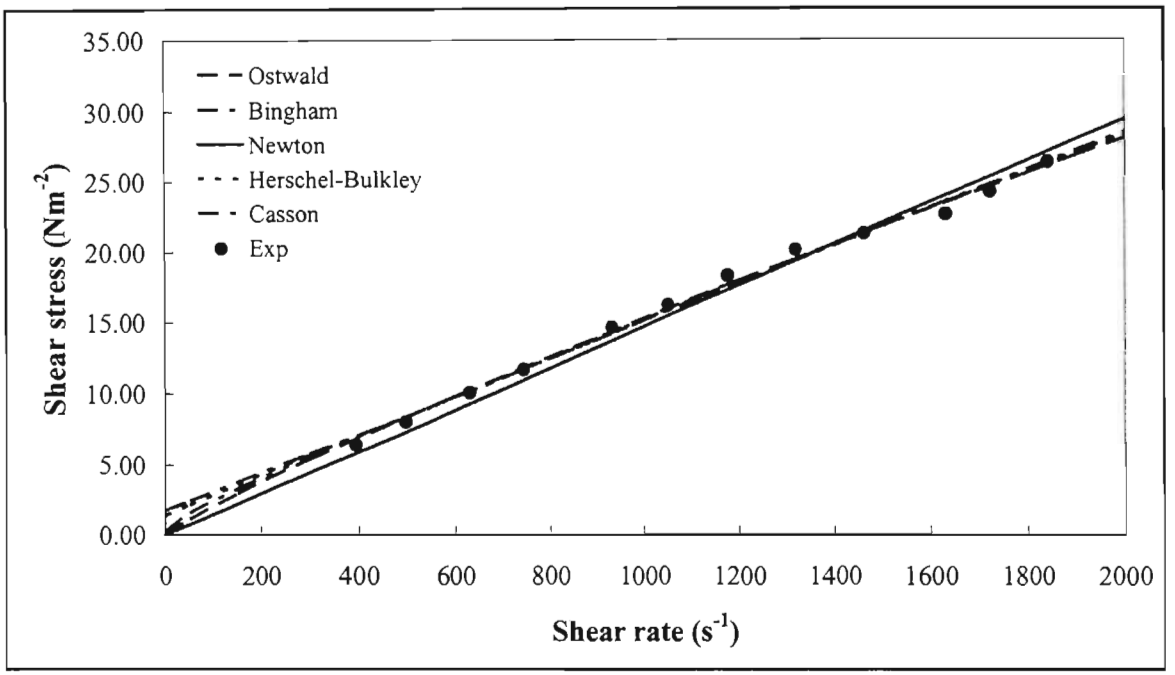

Figure A1.64 Regressed data for FeSi / Mag #1 for ratio 1:1 at specific gravity 2.2

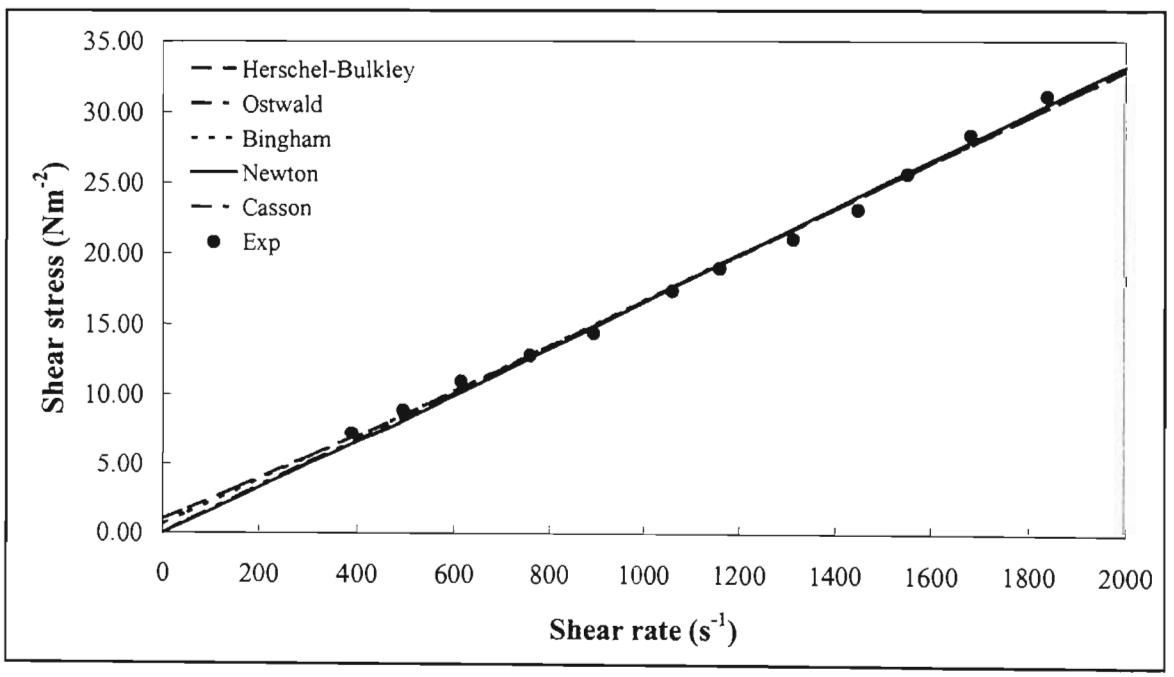

Figure A1.65 Regressed data for FeSi / Mag #1 for ratio 1:1 at specific gravity 2.3

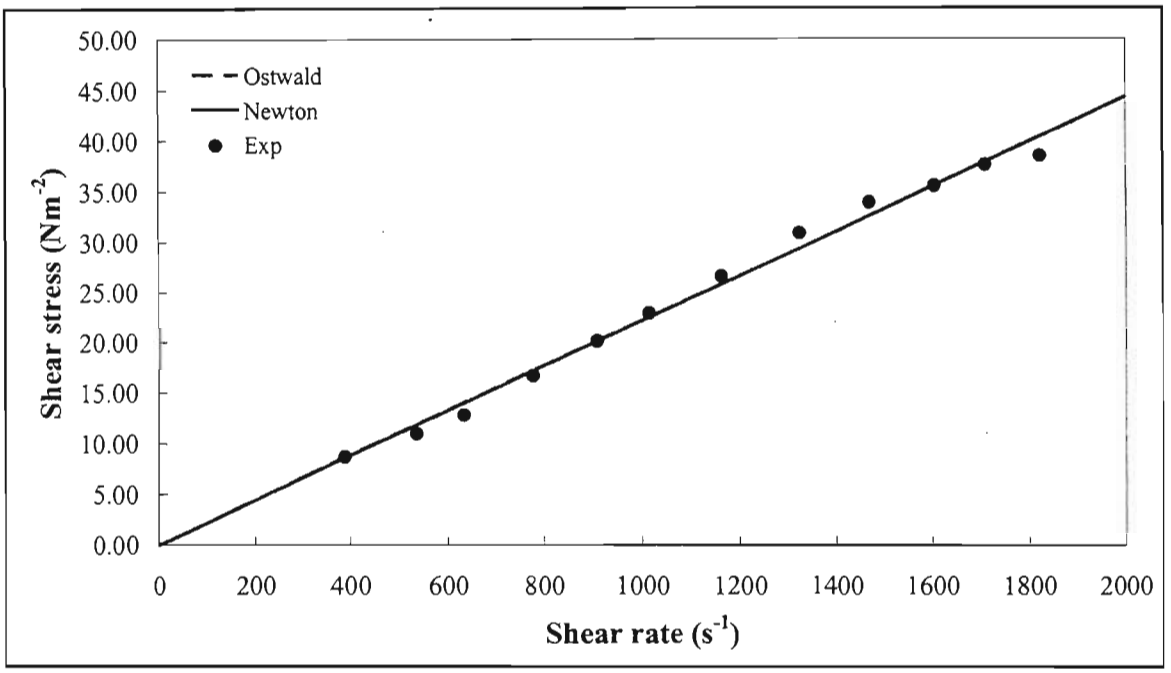

Figure A1.66 Regressed data for FeSi / Mag #1 for ratio 1:1 at specific gravity 2.4

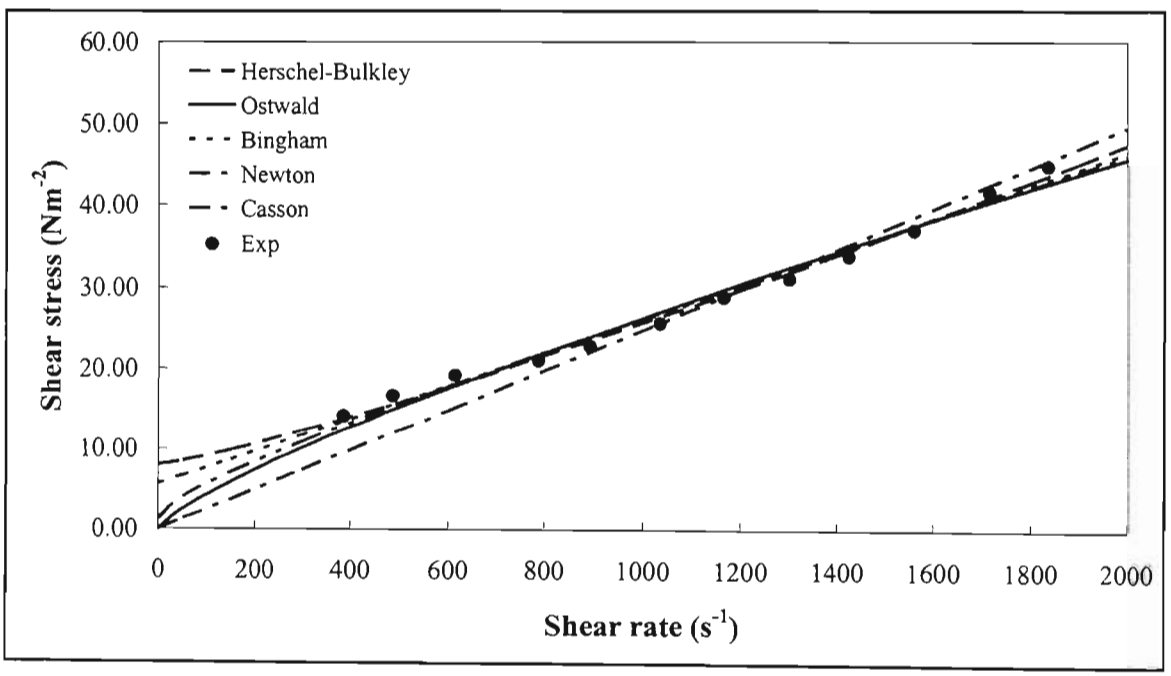

Figure A1.67 Regressed data for FeSi / Mag #`1 for ratio 1:1 at specific gravity 2.5

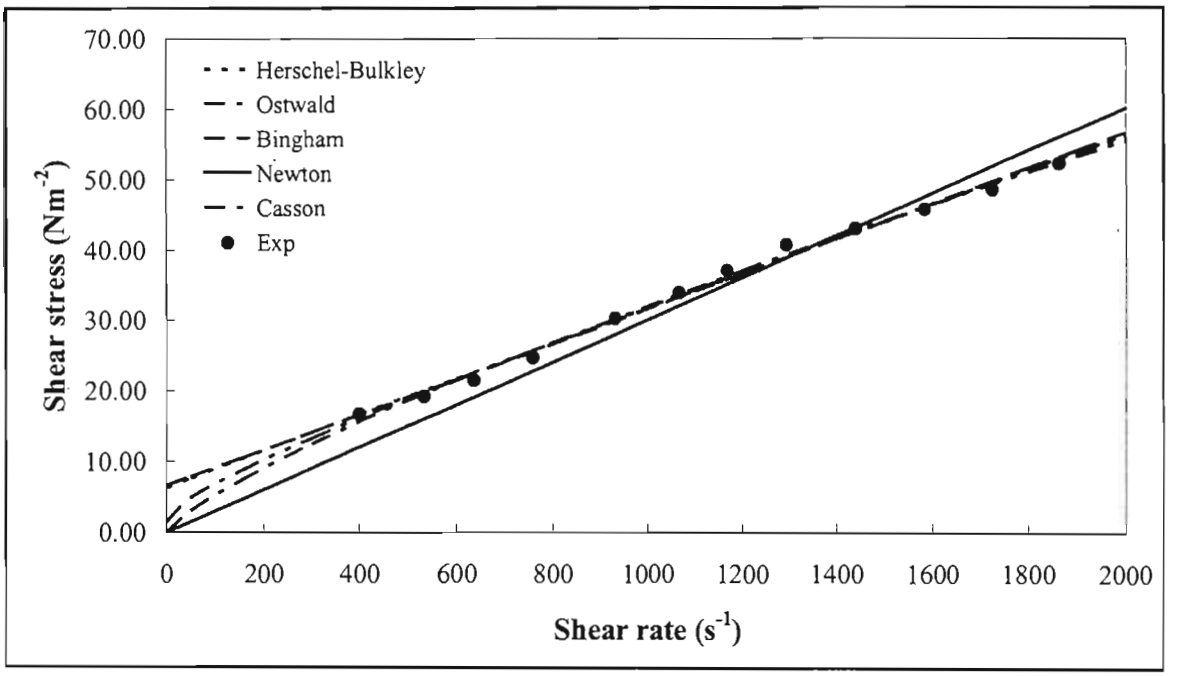

Figure A1.68 Regressed data for FeSi / Mag #1 for ratio 1:1 at specific gravity 2.6

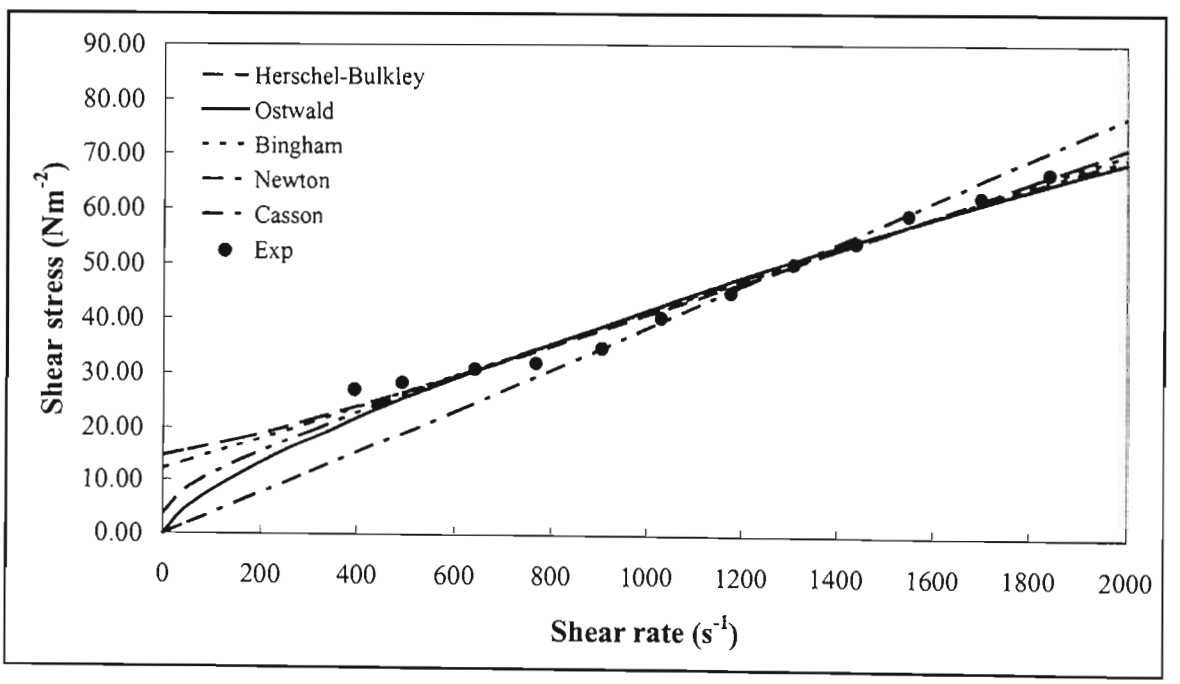

Figure A1.69 Regressed data for FeSi / Mag #1 for ratio 1:1 at specific gravity 2.7

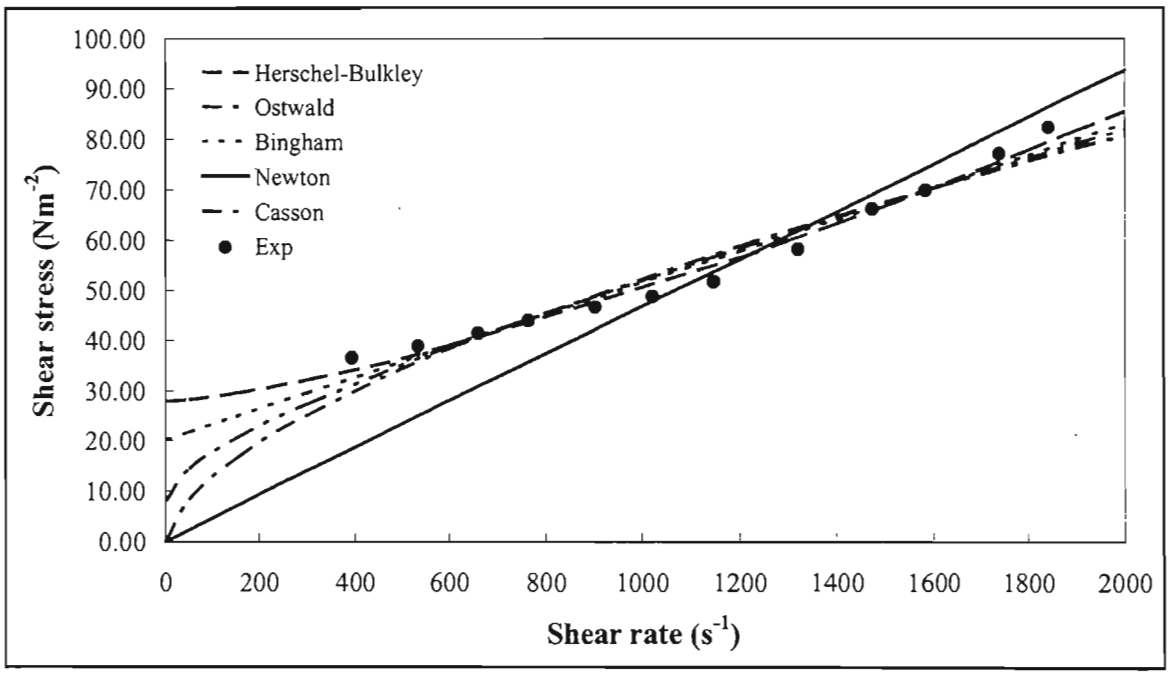

Figure A1.70 Regressed data for FeSi / Mag #1 for ratio 1:1 at specific gravity 2.8

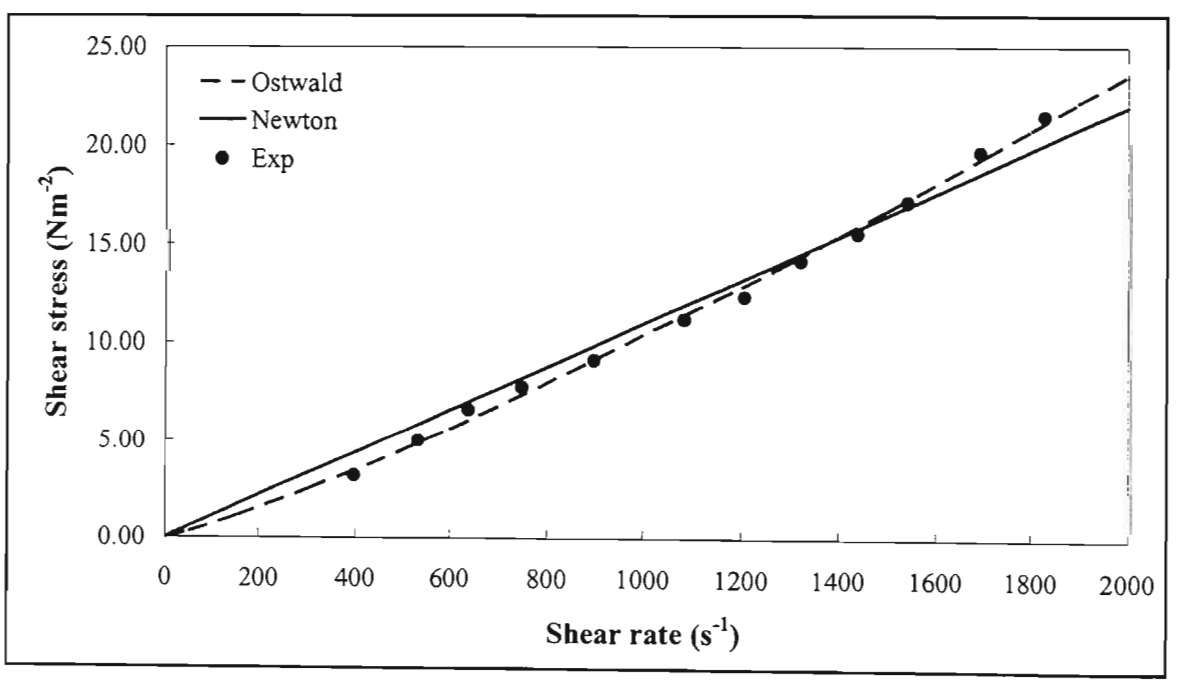

Figure A1.71 Regressed data for FeSi / Mag #1 for ratio 1:2 at specific gravity 2.0

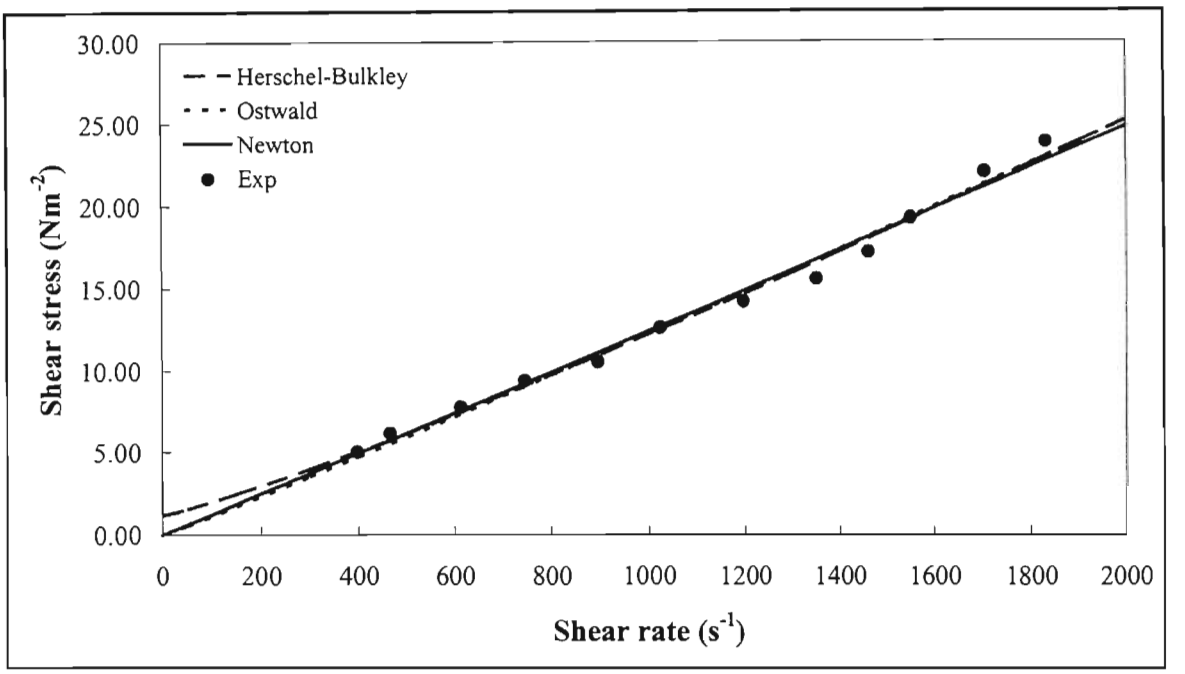

Figure A1.72 Regressed data for FeSi / Mag #1 for ratio 1:2 at specific gravity 2.1

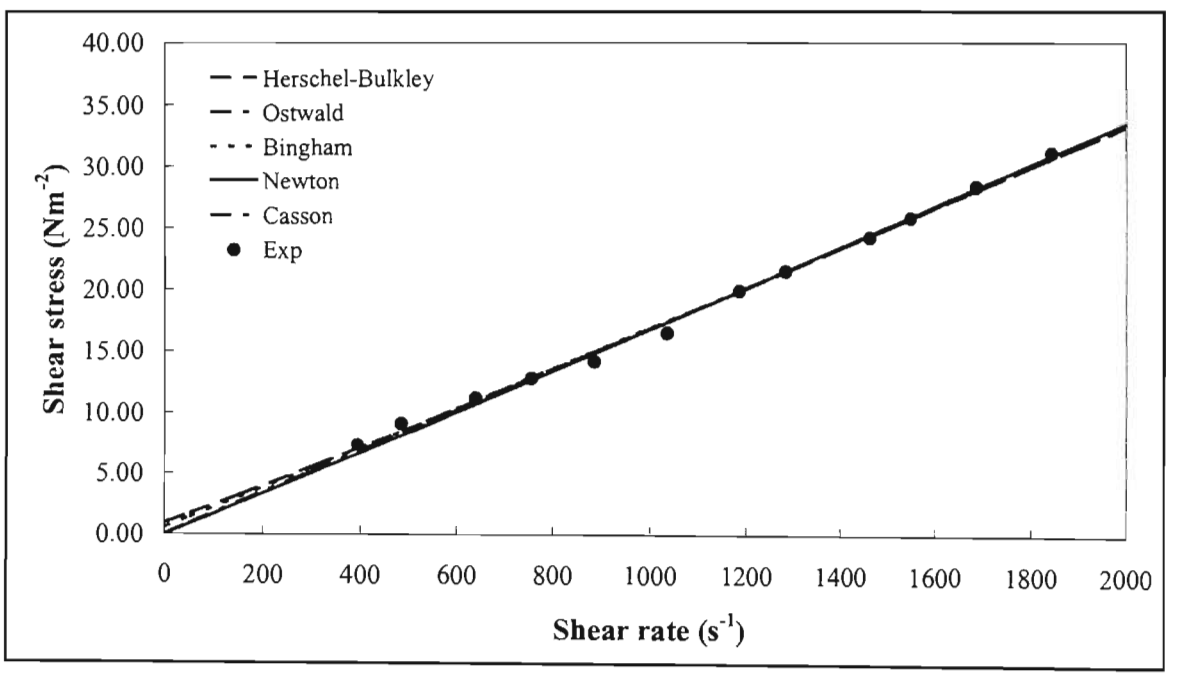

Figure A1.73 Regressed data for FeSi / Mag #1 for ratio 1:2 at specific gravity 2.2

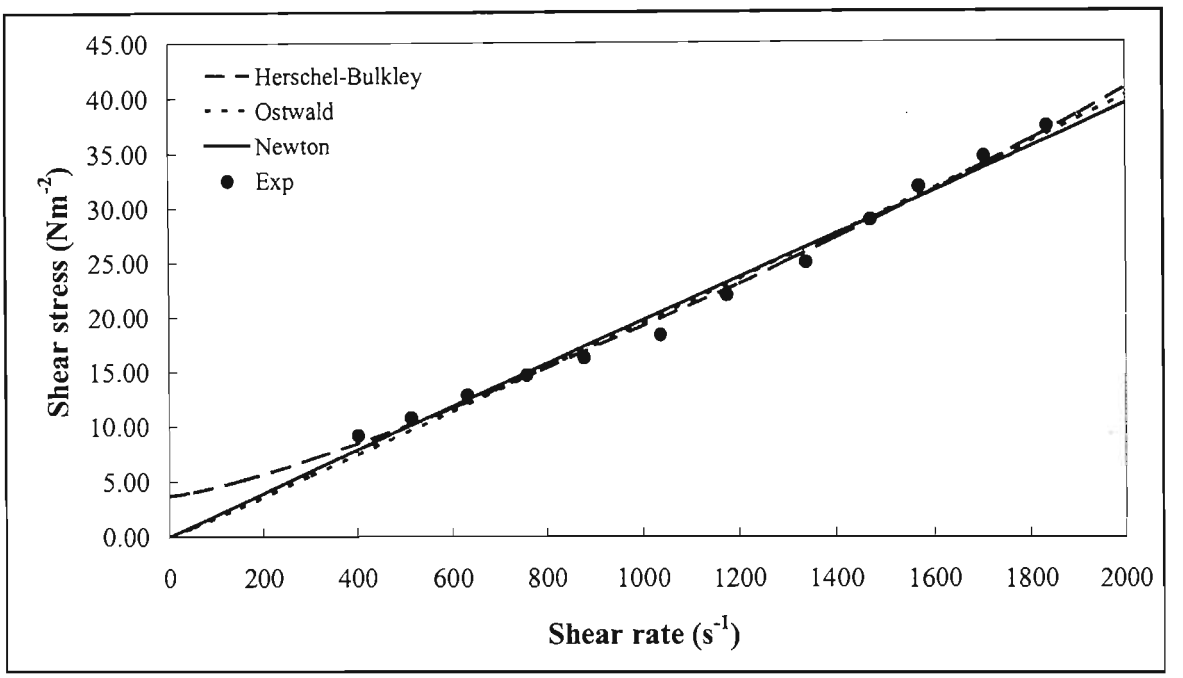

Figure A1.74 Regressed data for FeSi / Mag #1 for ratio 1:2 at specific gravity 2.3

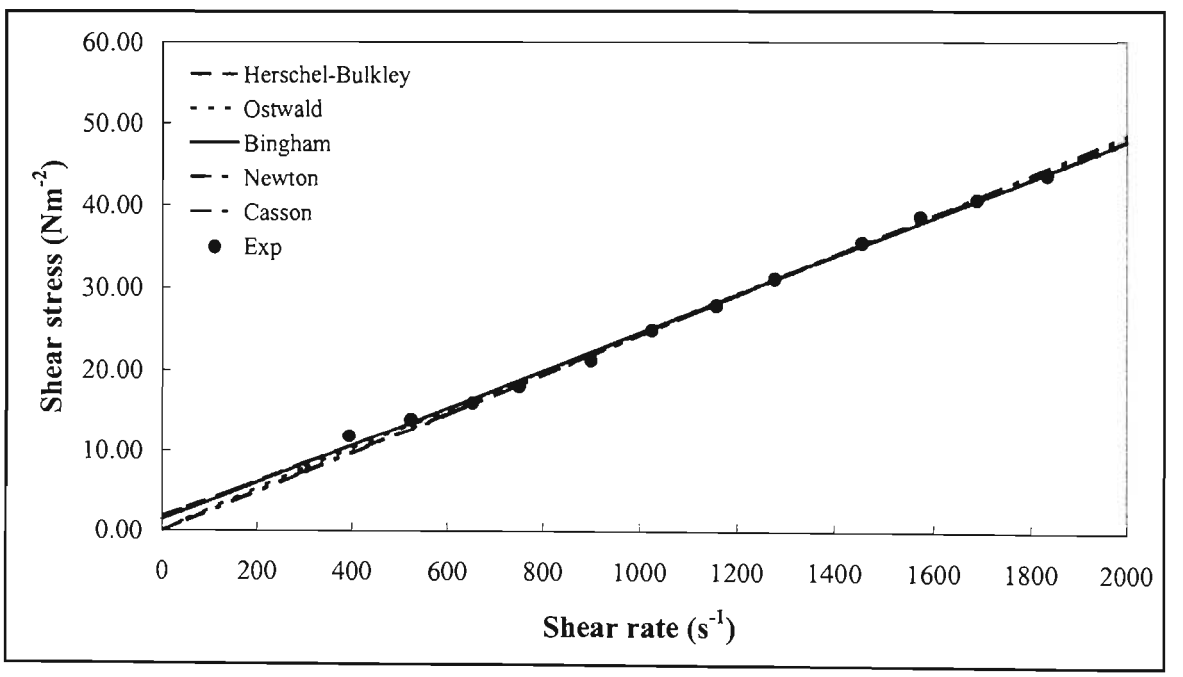

Figure A1.75 Regressed data for FeSi / Mag #1 for ratio 1:2 at specific gravity 2.4

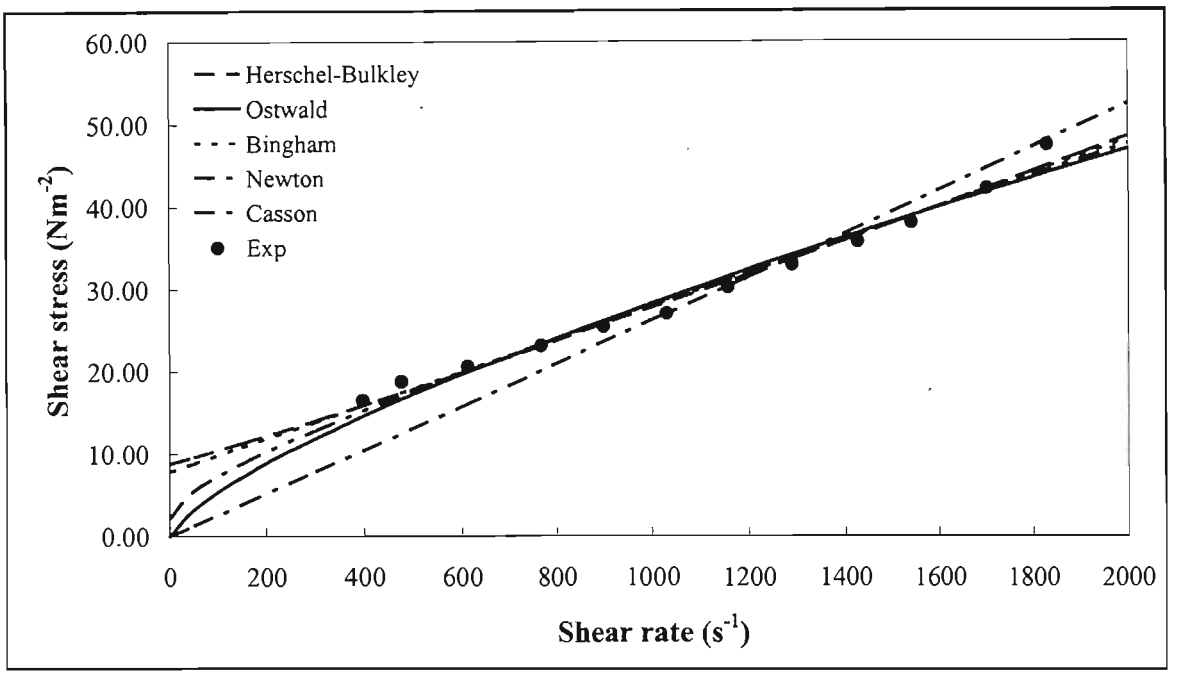

Figure A1.76 Regressed data for FeSi / Mag #1 for ratio 1:2 at specific gravity 2.5

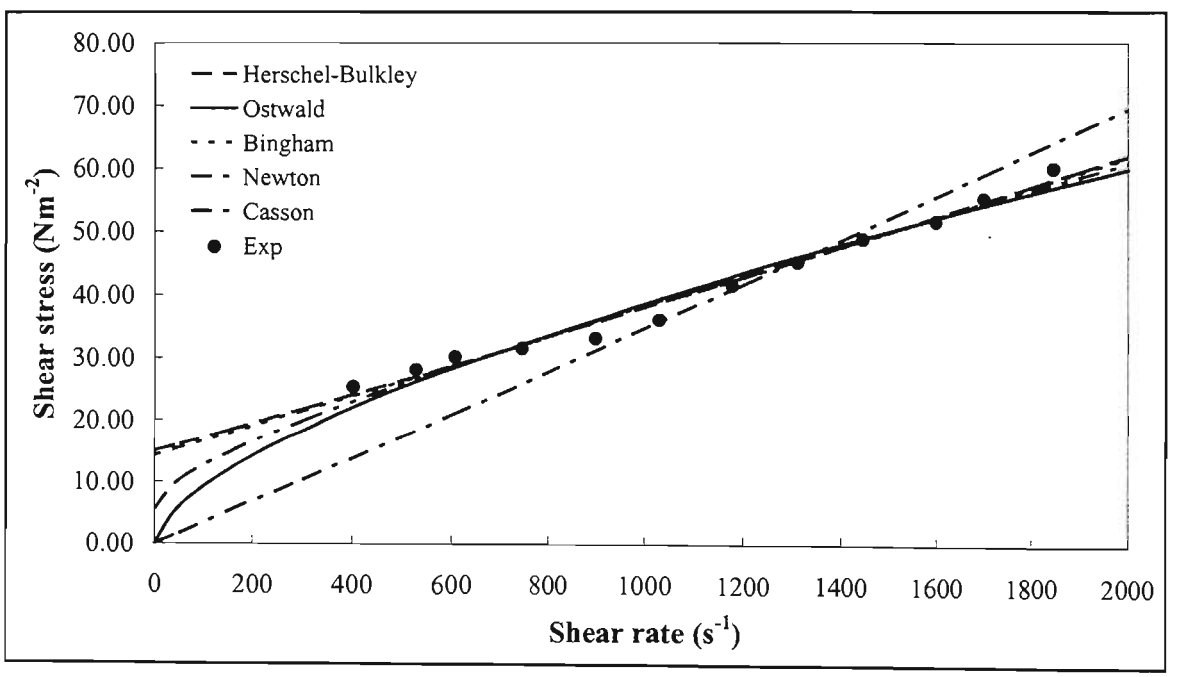

Figure A1.77 Regressed data for FeSi / Mag #1 for ratio 1:2 at specific gravity 2.6

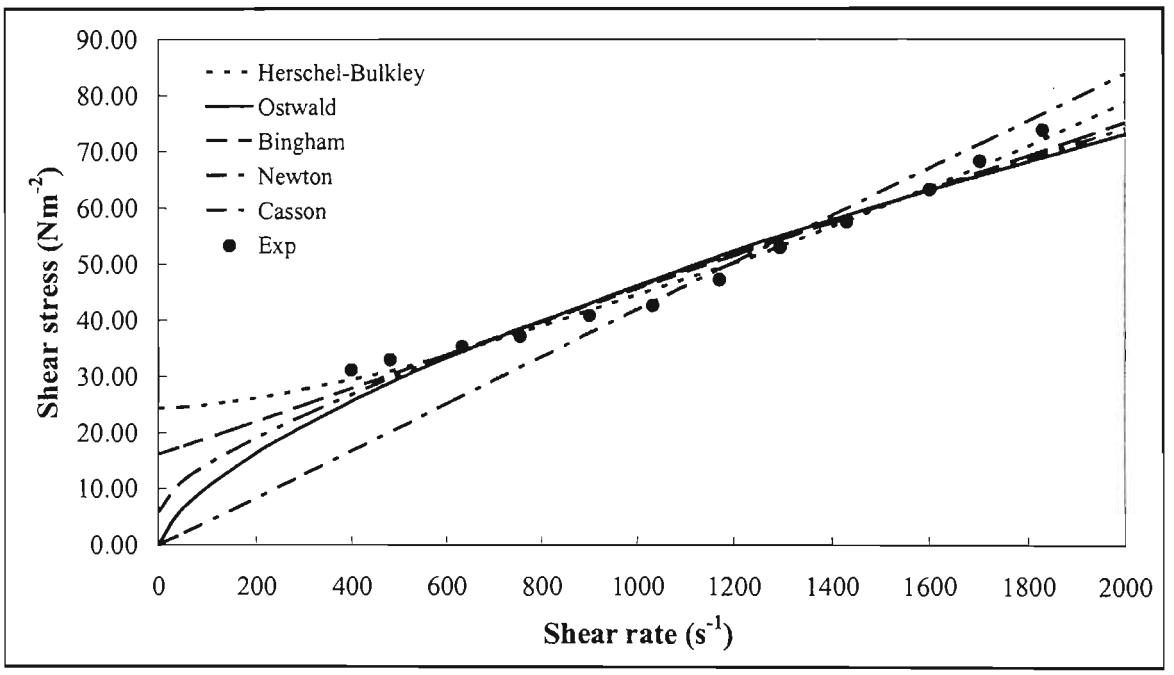

Figure A1.78 Regressed data for FeSi / Mag #1 for ratio 1:2 at specific gravity 2.7

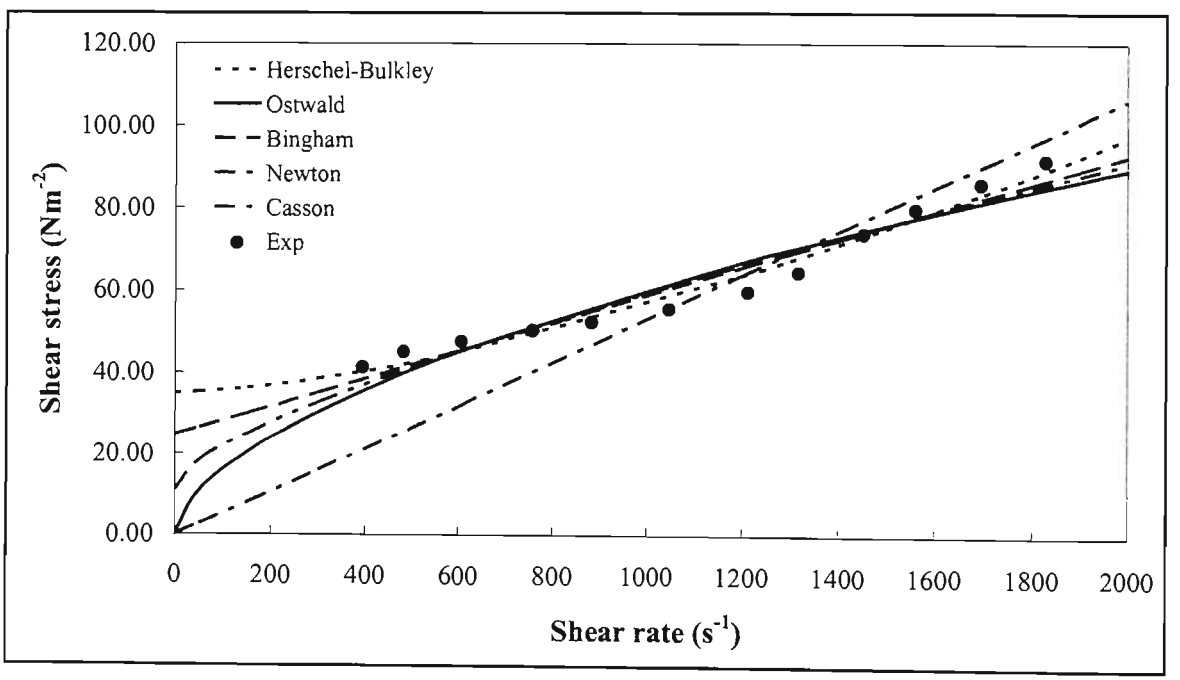

Figure A1.79 Regressed data for FeSi / Mag #1 for ratio 1:2 at specific gravity 2.8

A1.6.2.4 Regressed Magnetite #1 / Magnetite #2 Data Results

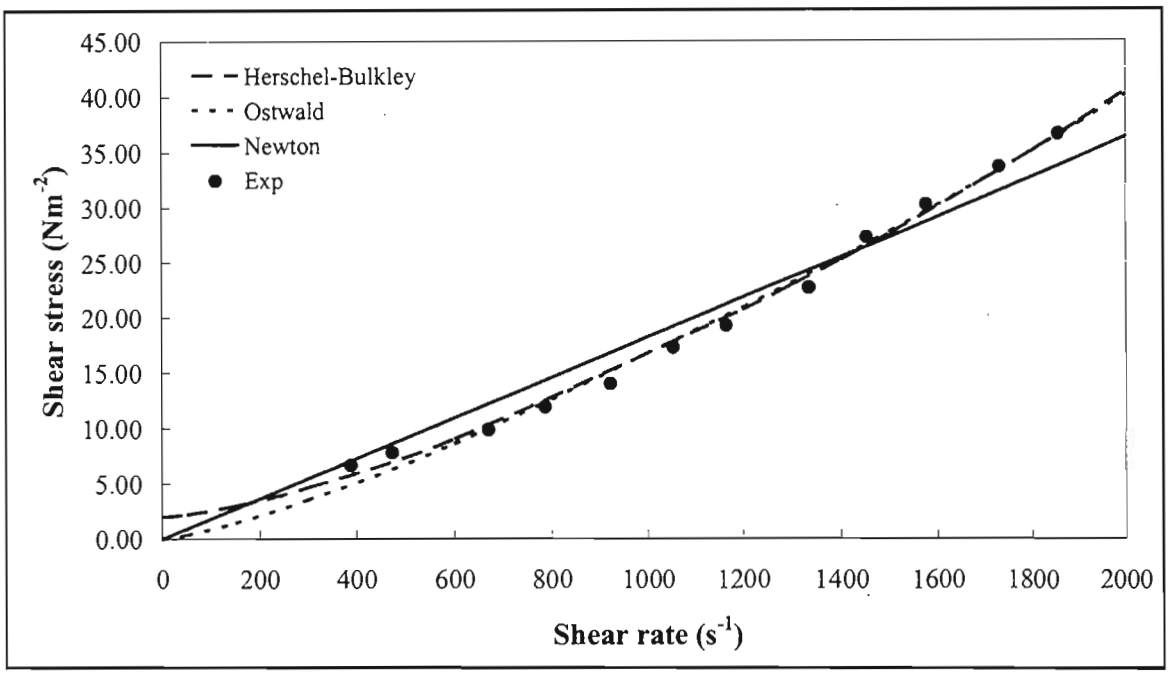

Figure A1.80 Regressed data for Mag #1 / Mag #2 for ratio 2:1 at specific gravity 2.2

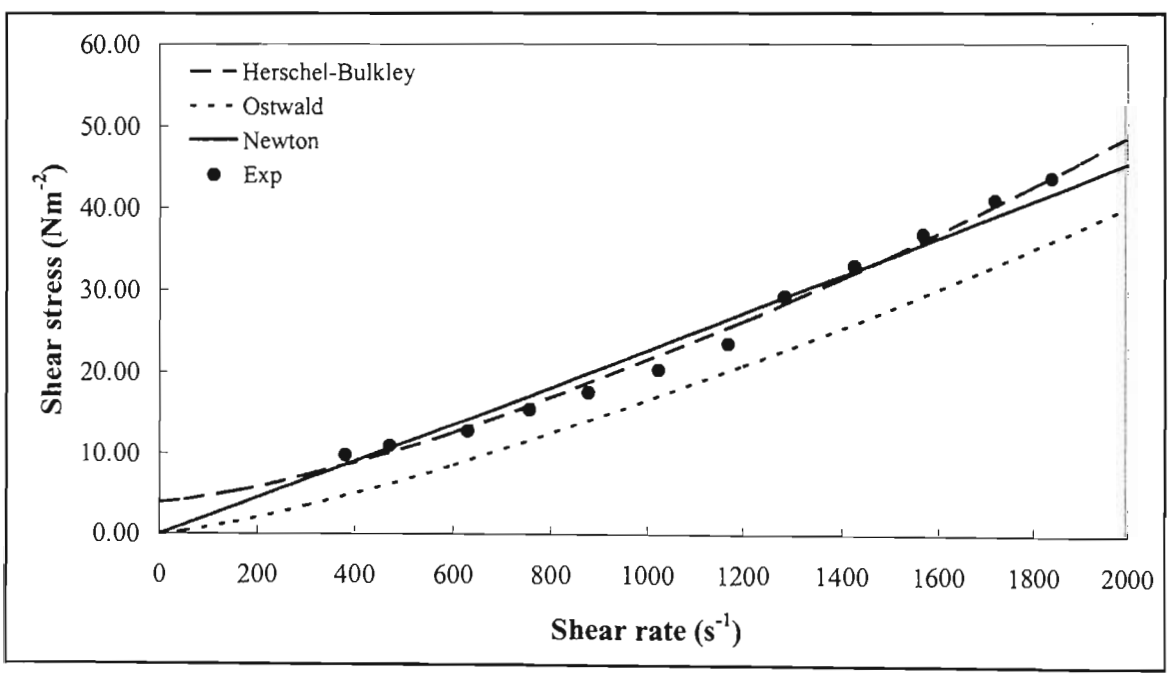

Figure A1.81 Regressed data for Mag #1 / Mag #2 for ratio 2:1 at specific gravity 2.3

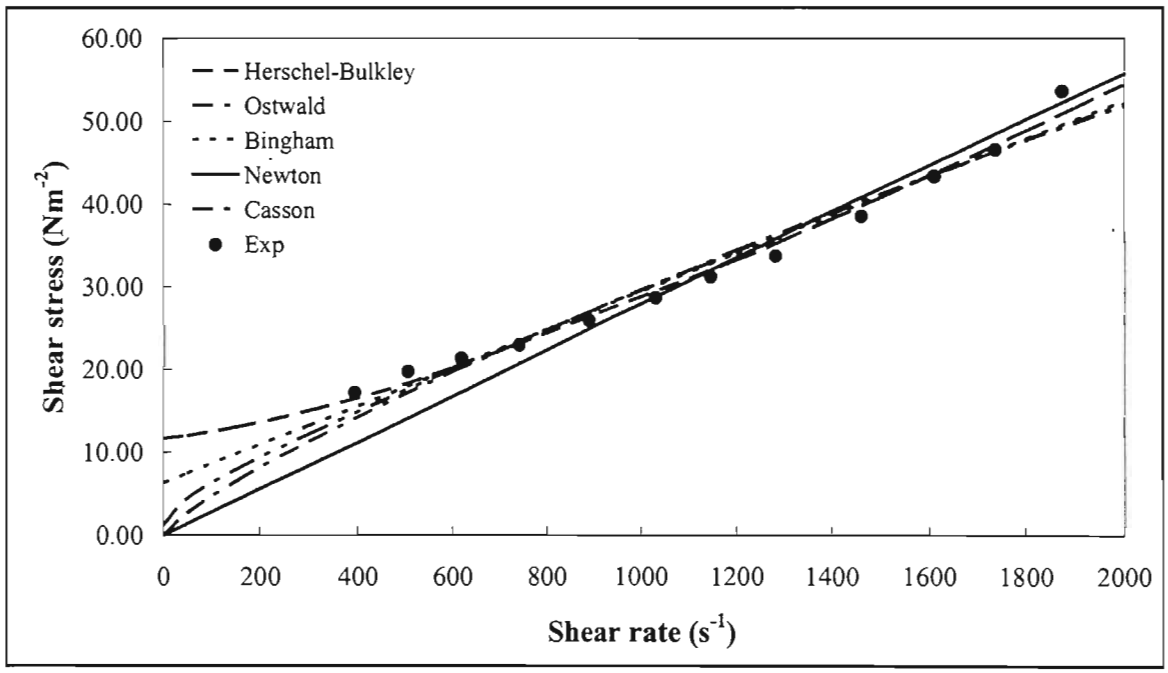

Figure A1.82 Regressed data for Mag #1 / Mag #2 for ratio 2:1 at specific gravity 2.4

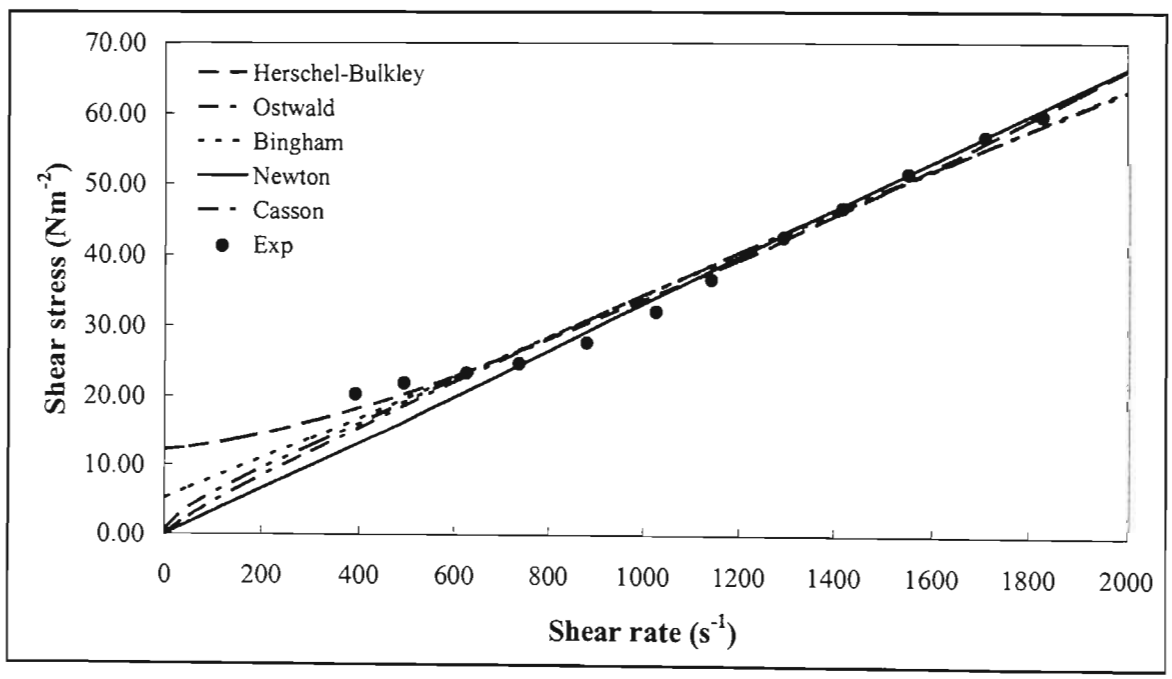

Figure A1.83 Regressed data for Mag #1 / Mag #2 for ratio 2:1 at specific gravity 2.5

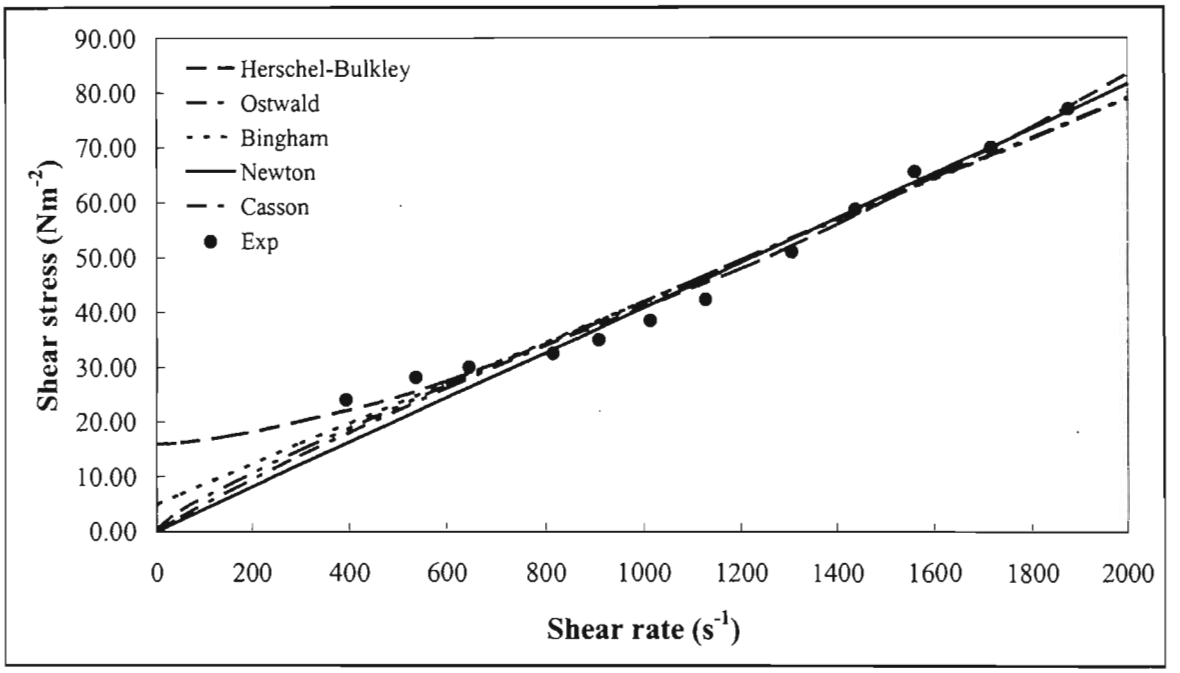

Figure A1.84 Regressed data for Mag #1 / Mag #2 for ratio 2:1 at specific gravity 2.6

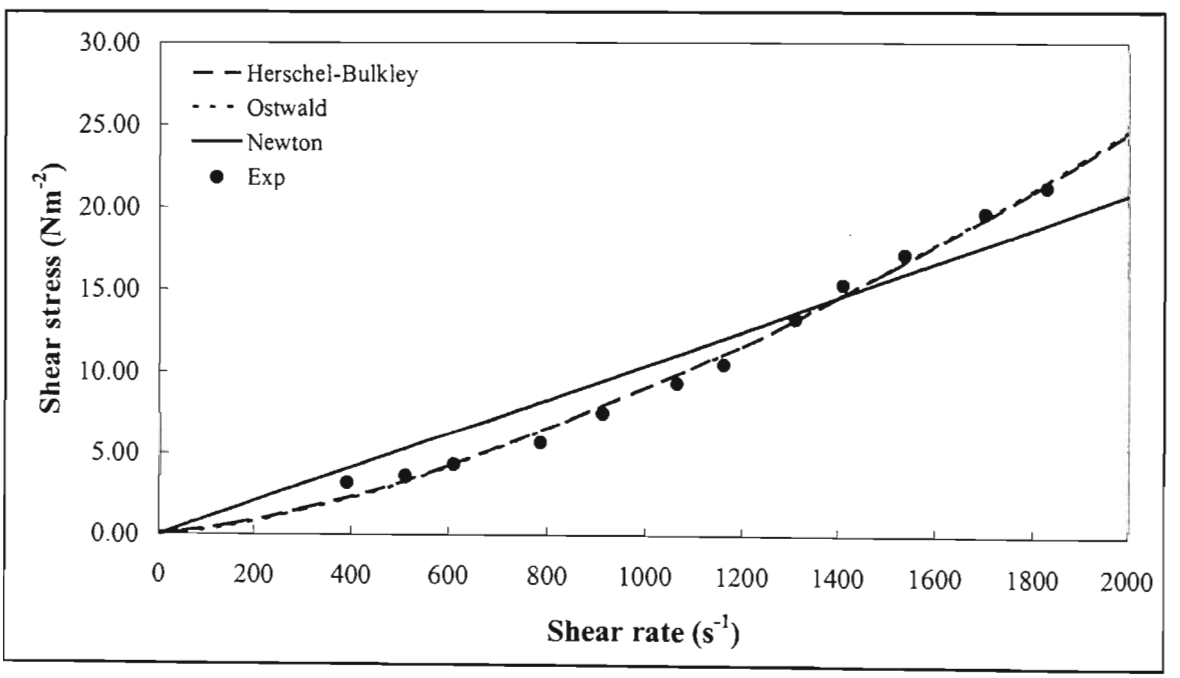

Figure A1.85 Regressed data for Mag #1 / Mag #2 for ratio 1:1 at specific gravity 2.0

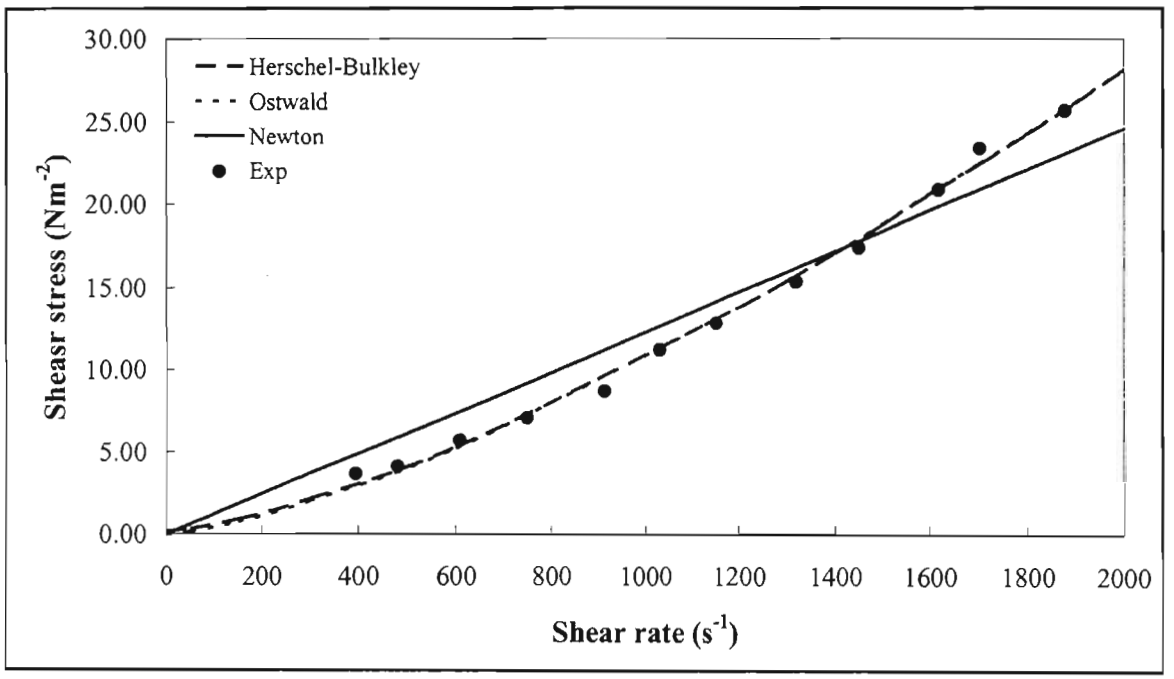

Figure A1.86 Regressed data for Mag #1 / Mag #2 for ratio 1:1 at specific gravity 2.1

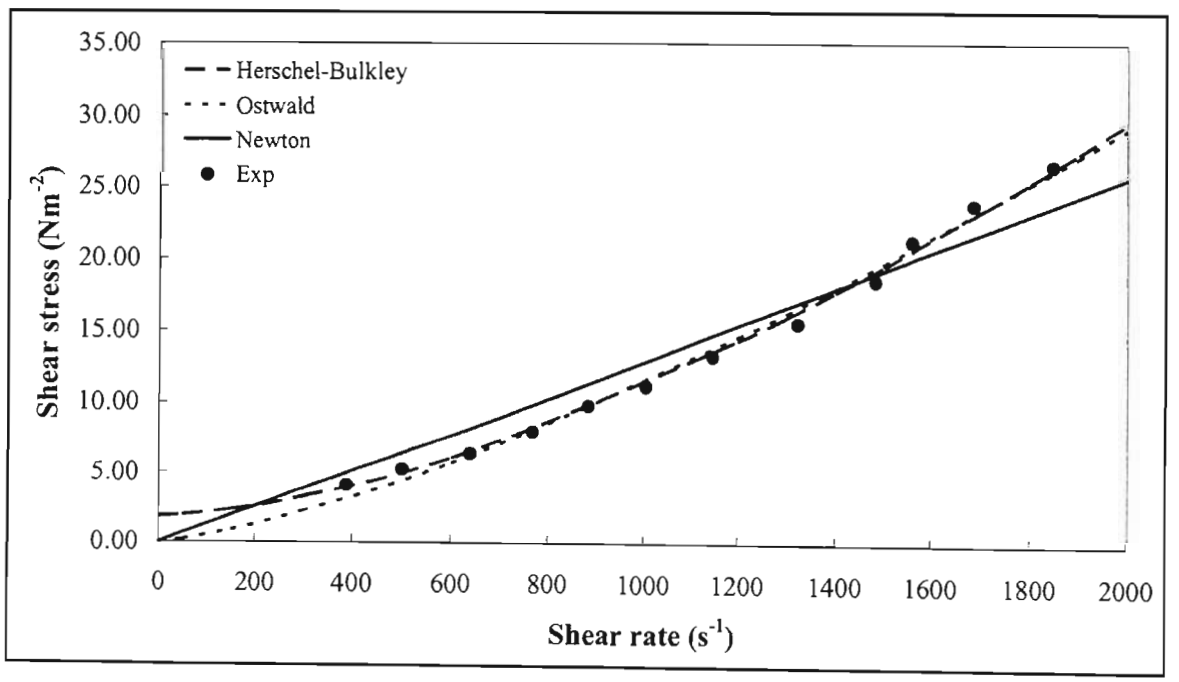

Figure A1.87 Regressed data for Mag #1 / Mag #2 for ratio 1:1 at specific gravity 2.2

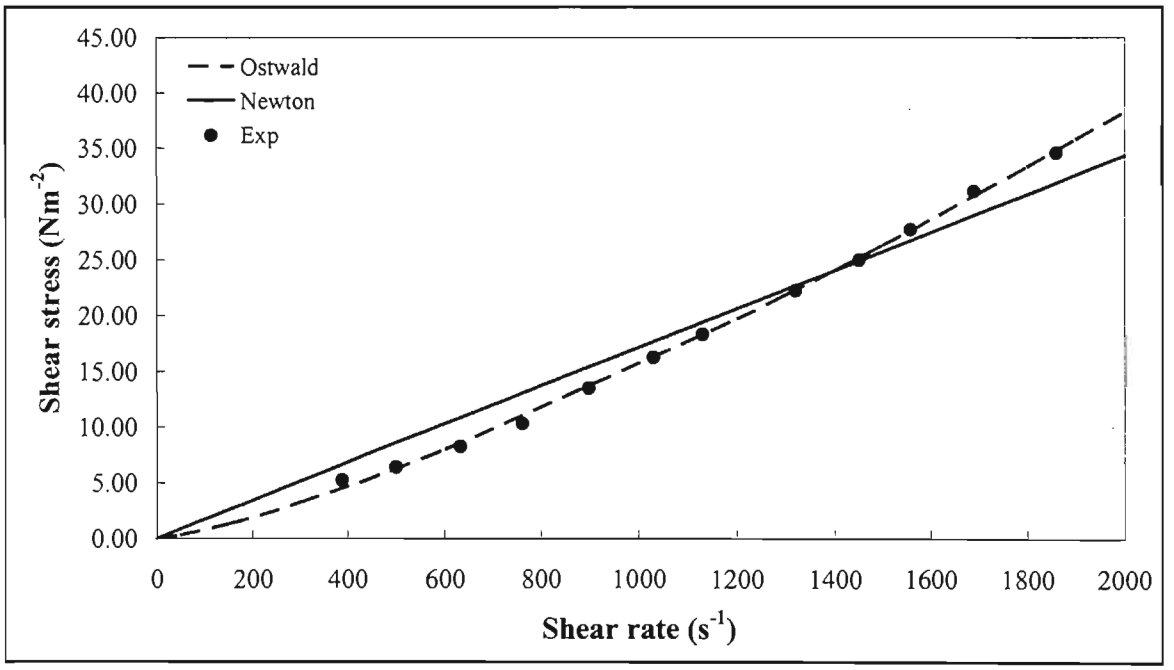

Figure A1.88 Regressed data for Mag #1 / Mag #2 for ratio 1:1 at specific gravity 2.3

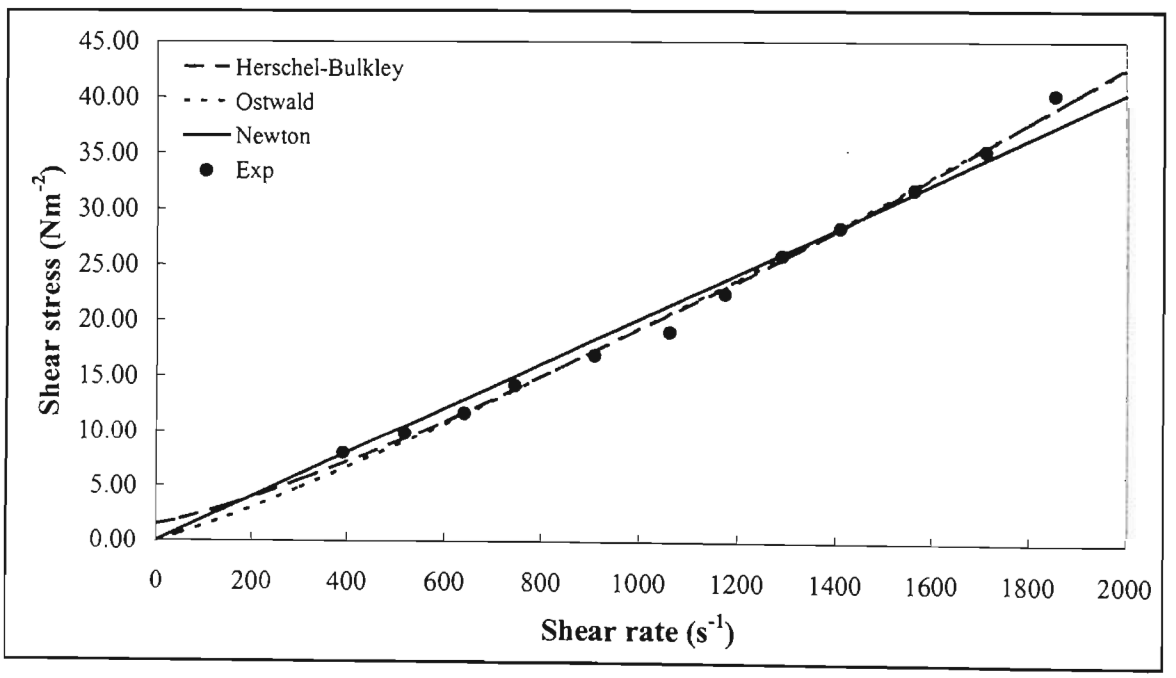

Figure A1.89 Regressed data for Mag #1 / Mag #2 for ratio 1:1 at specific gravity 2.4

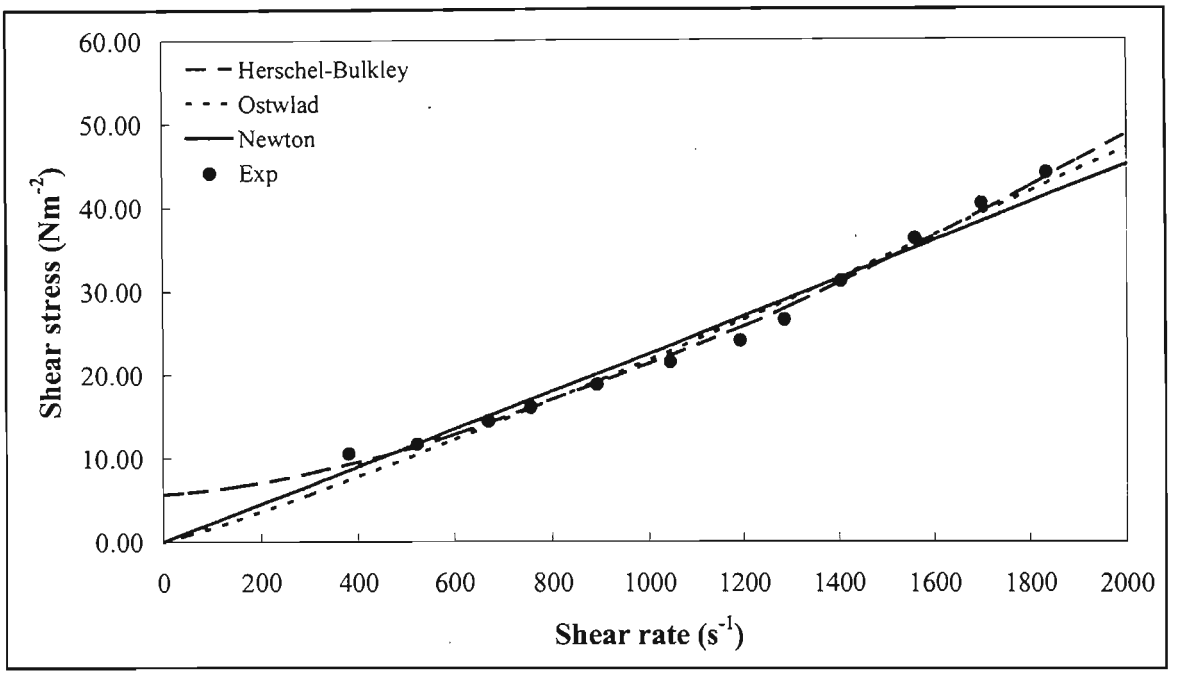

Figure A1.90 Regressed data for Mag #1 / Mag #2 for ratio 1:1 at specific gravity 2.5

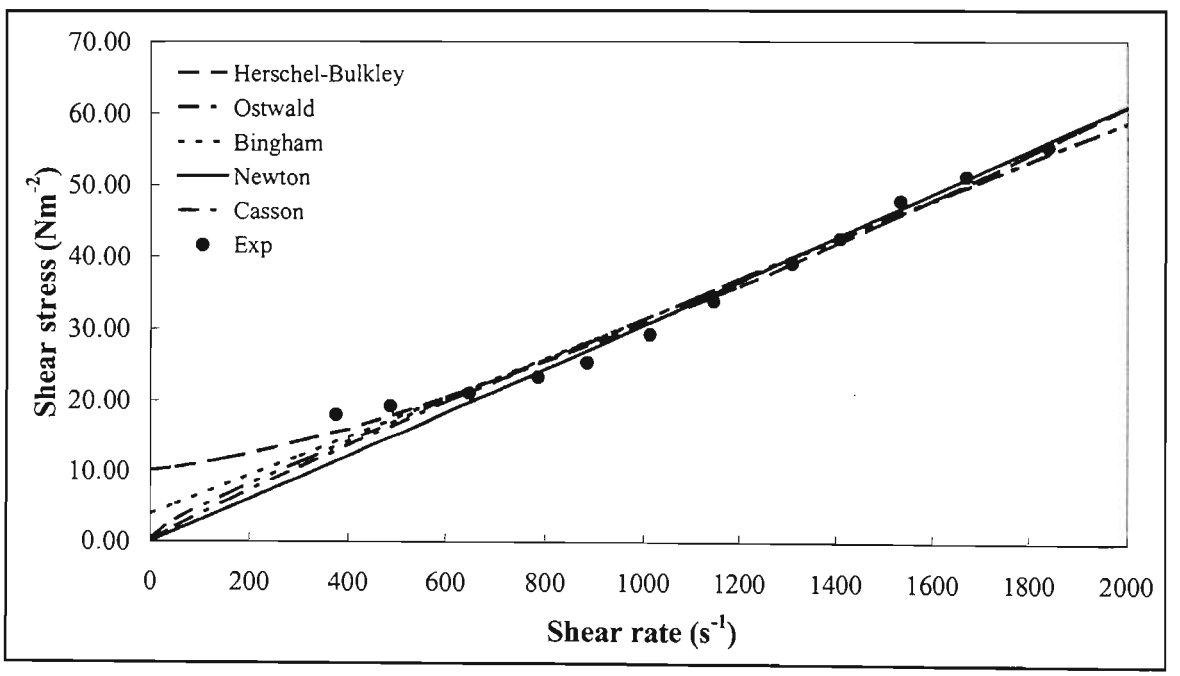

Figure A1.91 Regressed data for Mag #1 / Mag #2 for ratio 1:1 at specific gravity 2.6

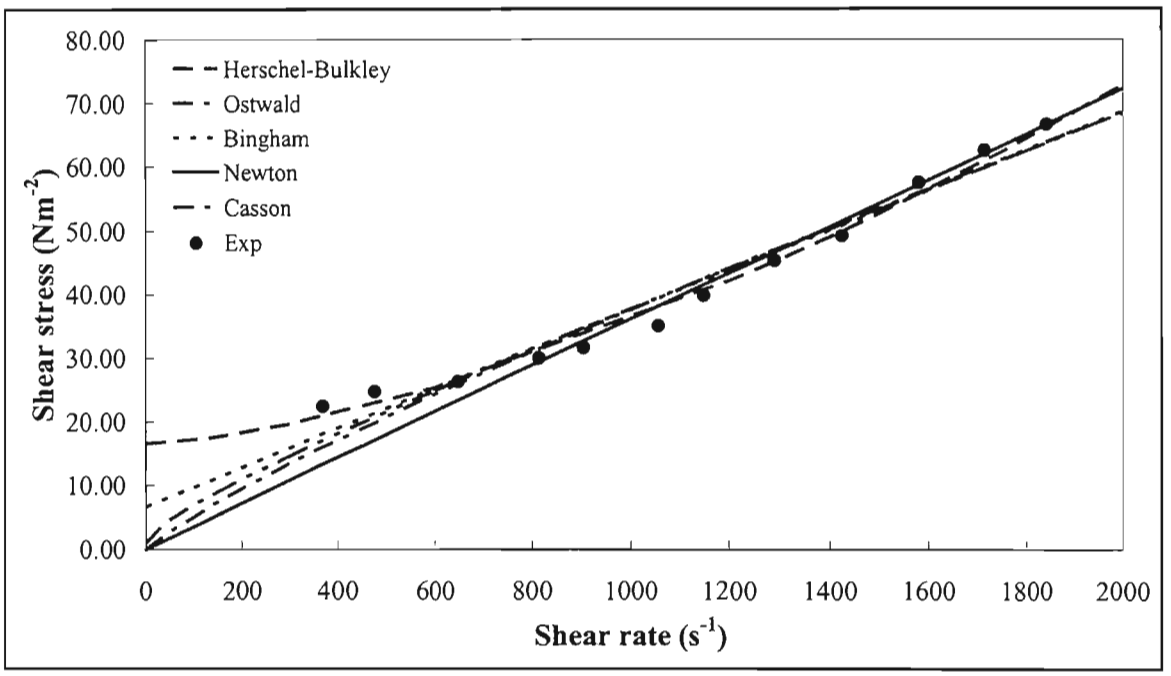

Figure A1.92 Regressed data for Mag #1 / Mag #2 for ratio 1:1 at specific gravity 2.7

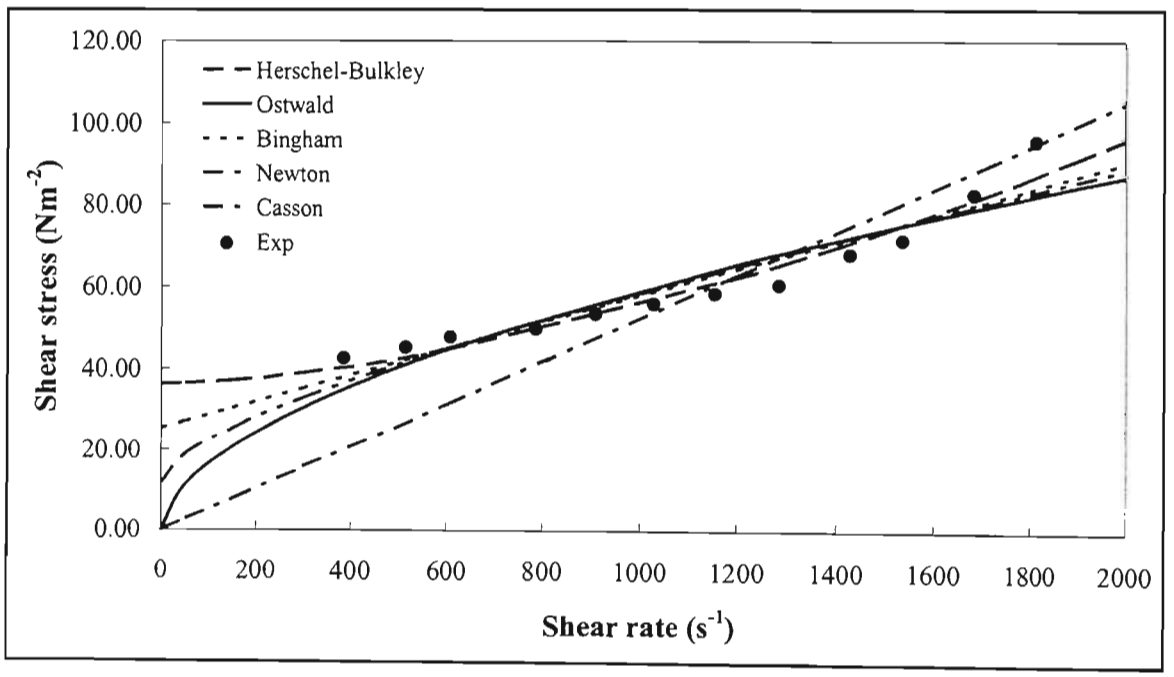

Figure A1.93 Regressed data for Mag #1 / Mag #2 for ratio 1:1 at specific gravity 2.8

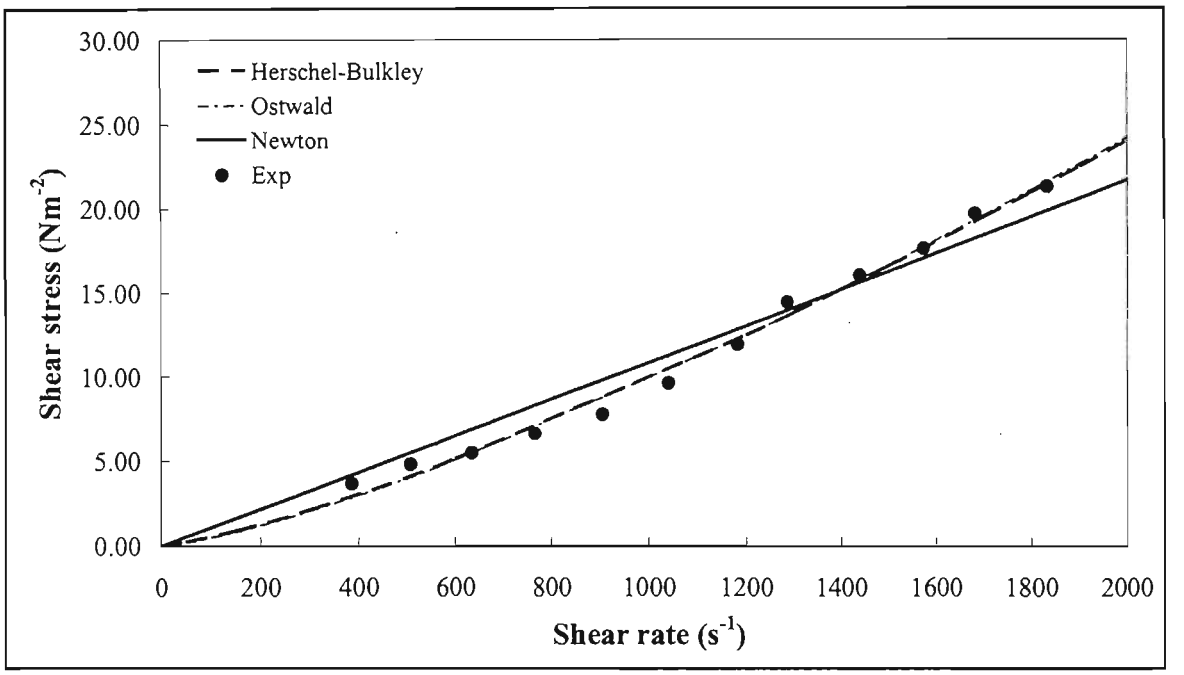

Figure A1.94 Regressed data for Mag #1 / Mag #2 for ratio 1:2 at specific gravity 2.2

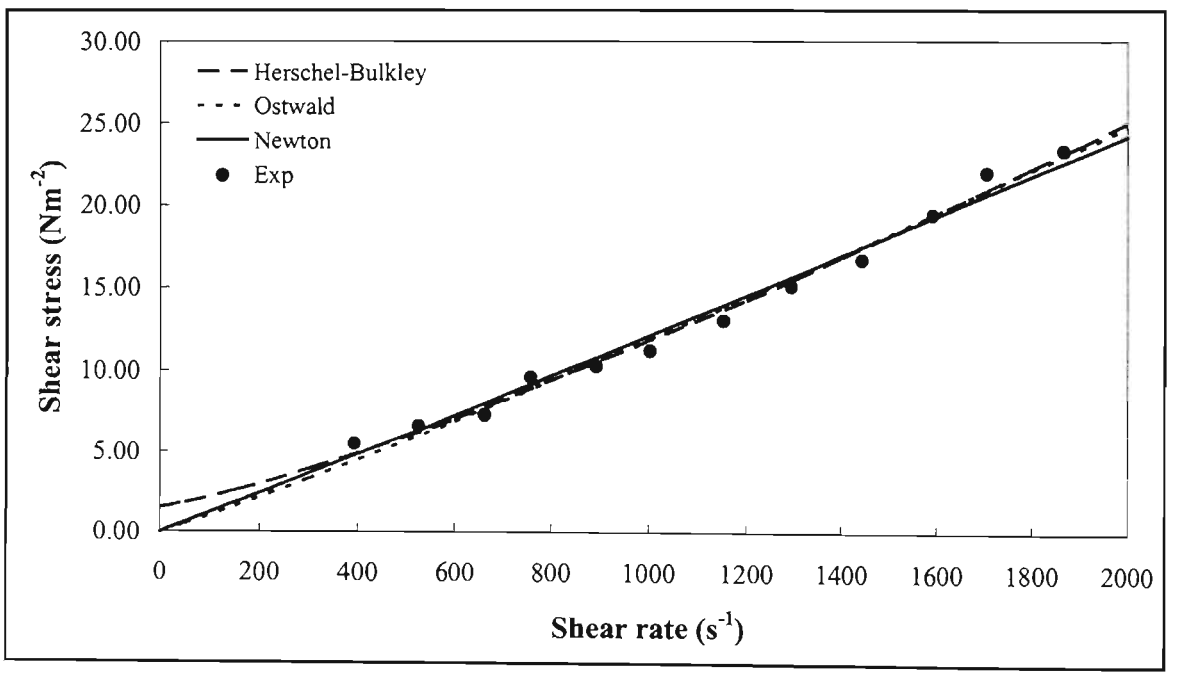

Figure A1.95 Regressed data for Mag #1 / Mag #2 for ratio 1:2 at specific gravity 2.3

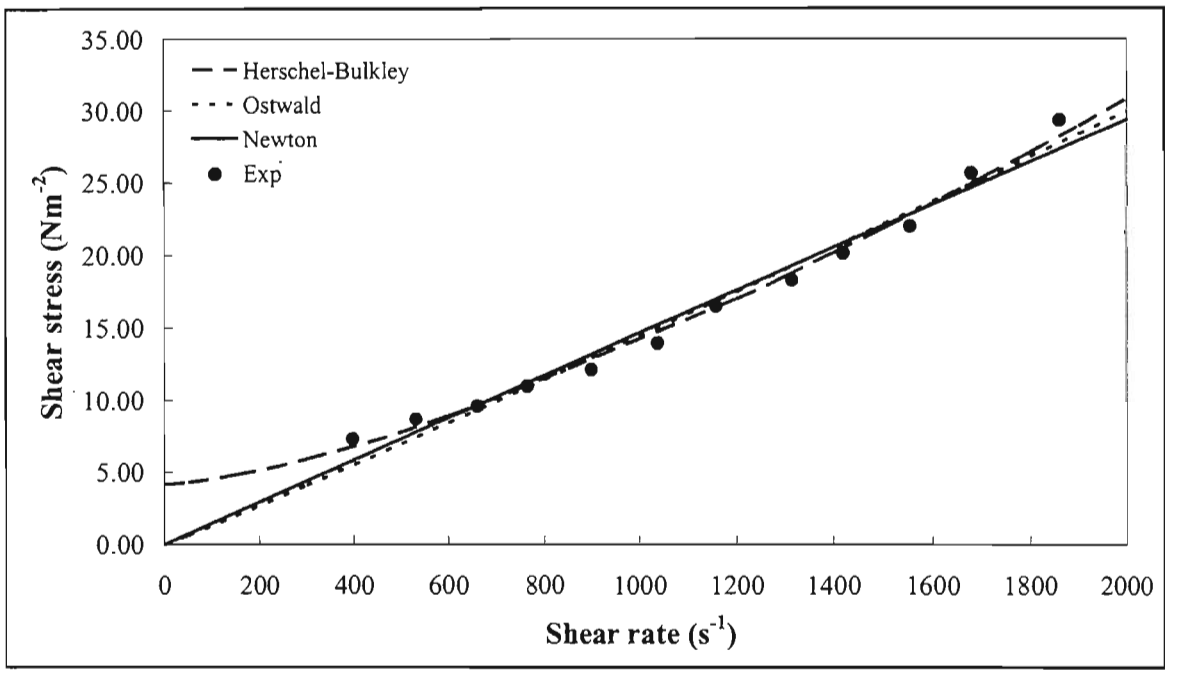

Figure A1.96 Regressed data for Mag #1 / Mag #2 for ratio 1:2 at specific gravity 2.4

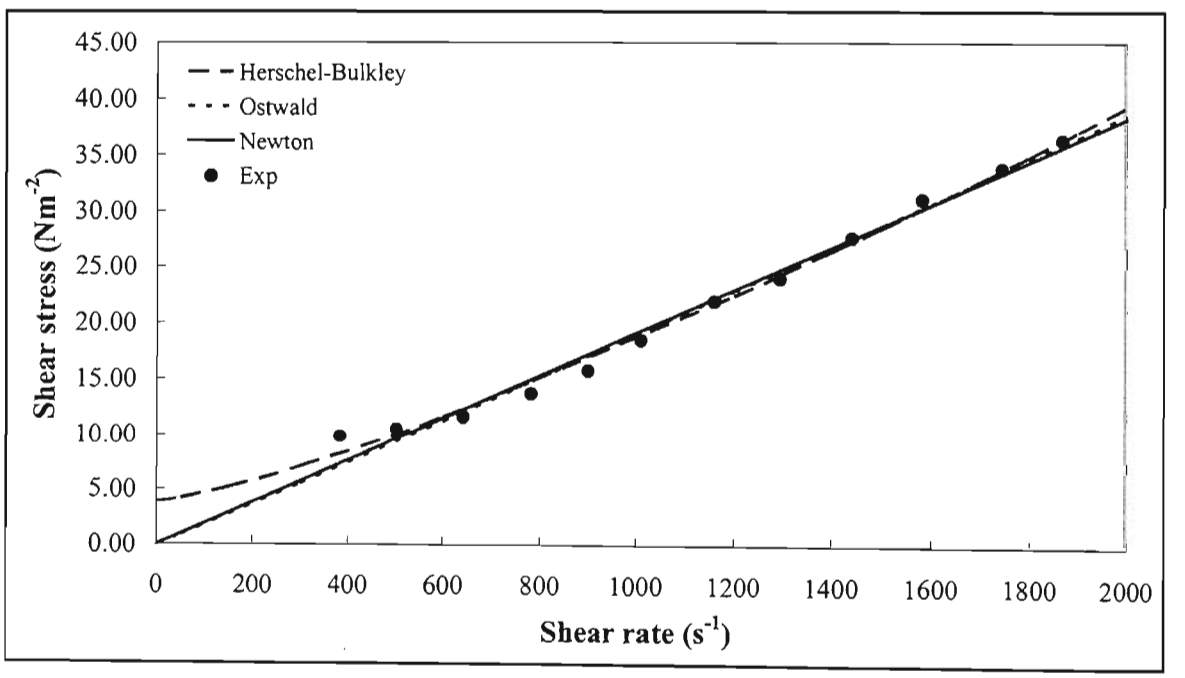

Figure A1.97 Regressed Mag #1 / Mag #2 for ratio 1:2 at specific gravity 2.5

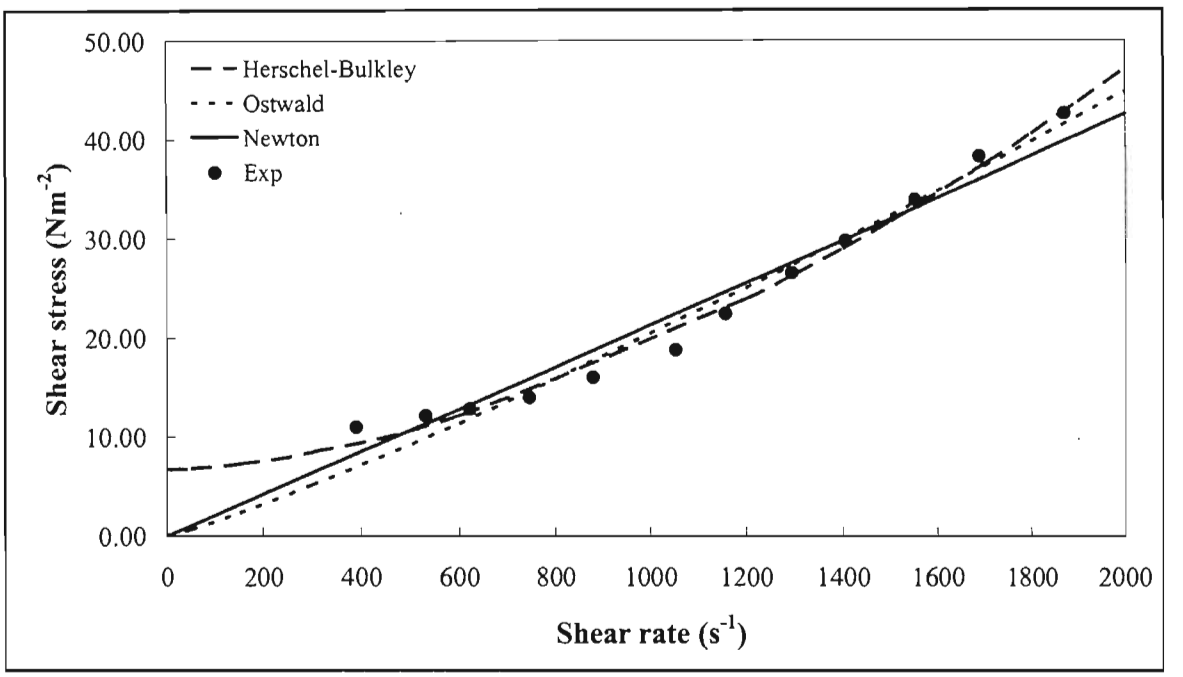

Figure A1.98 Regressed Mag #1 / Mag #2 for ratio 1:2 at specific gravity 2.6

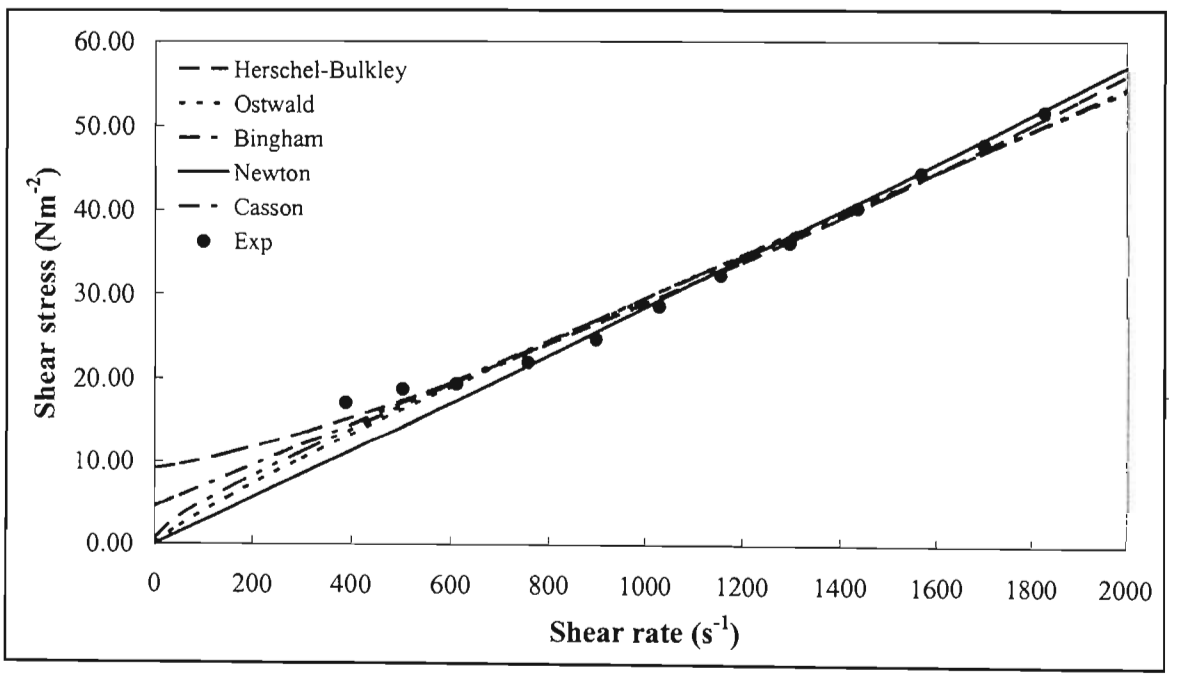

Figure A1.99 Regressed Mag #1 / Mag #2 for ratio 1:2 at specific gravity 2.7

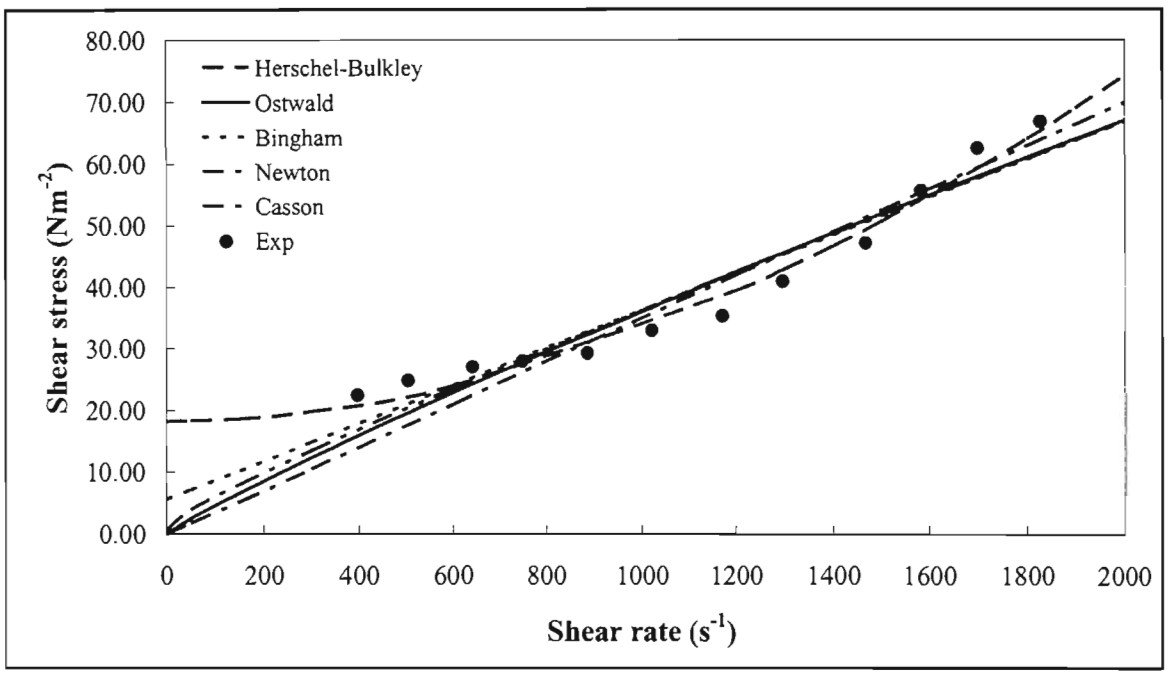

Figure A1.100 Regressed data for Mag #1 / Mag #2 for ratio 1:2 at specific gravity 2.8

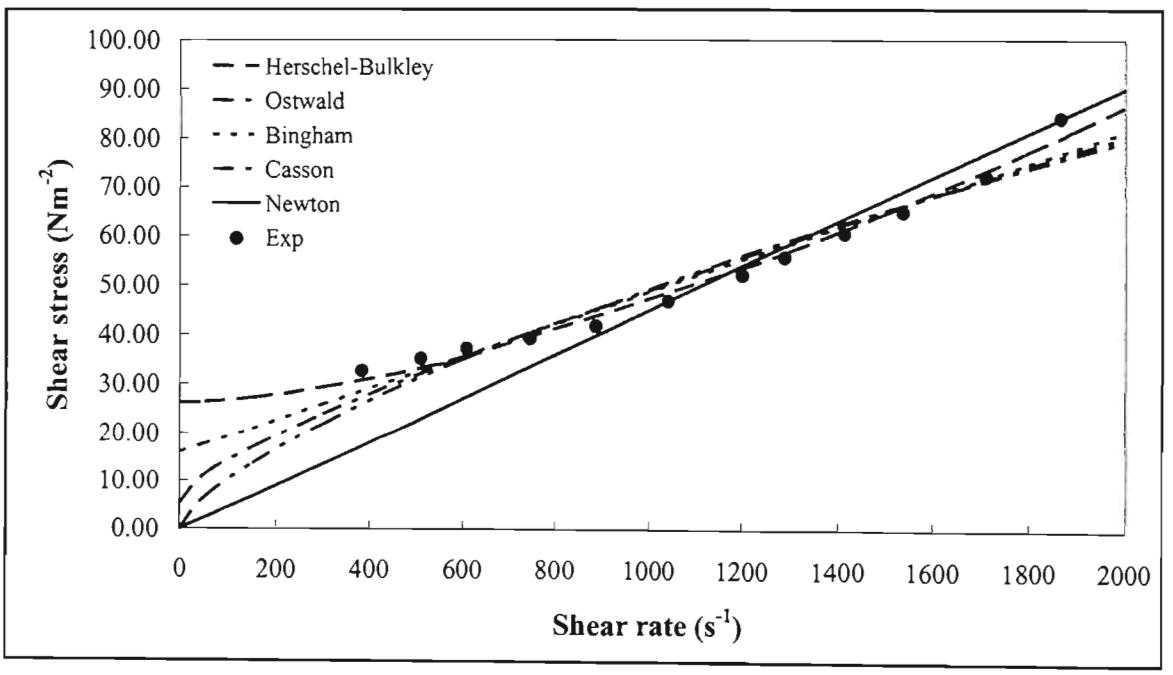

Figure A1.101 Regressed data for Mag #1 / Mag #2 for ratio 1:2 at specific gravity 2.9

A1.6.2.5 Regressed Ferrosilicon / Magnetite #2 Data Results

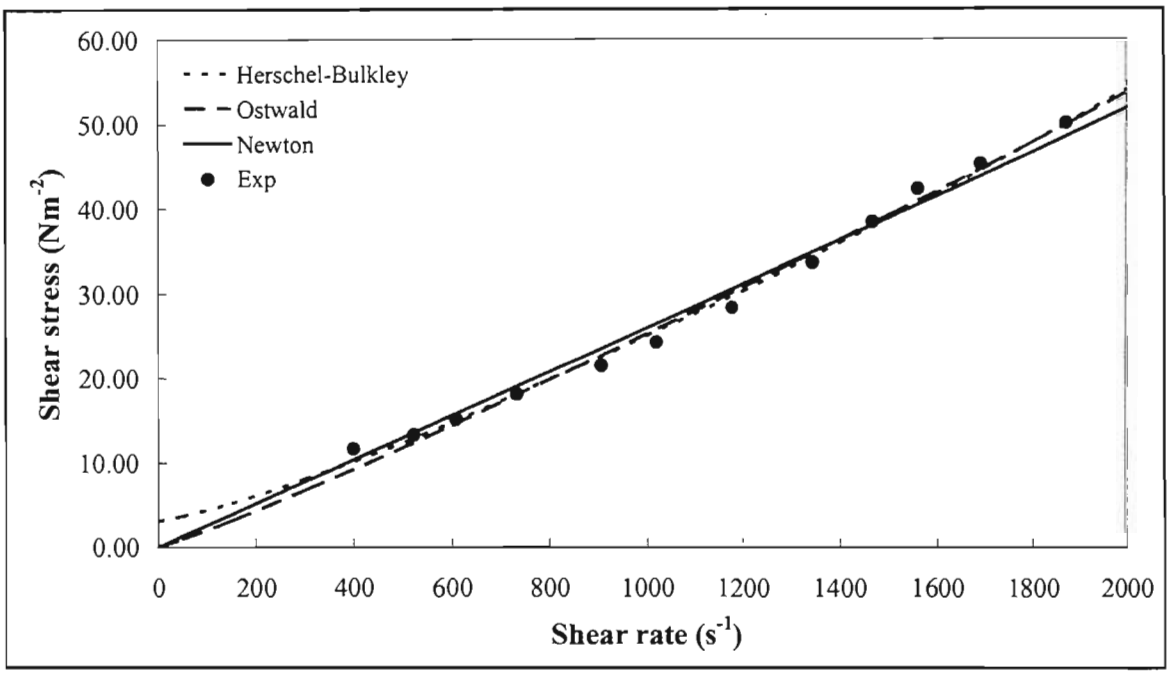

Figure A1.102 Regressed data for FeSi / Mag #2 for ratio 2:1 at specific gravity 3.0

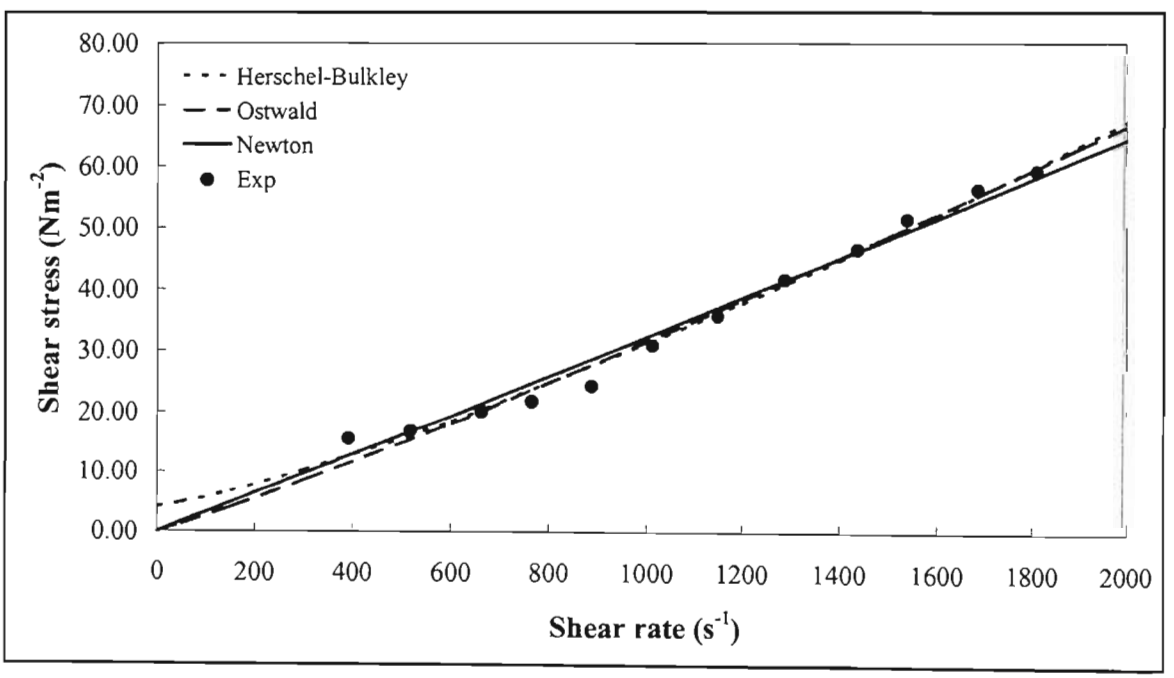

Figure A1.103 Regressed data for FeSi / Mag #2 for ratio 2:1 at specific gravity 3.1

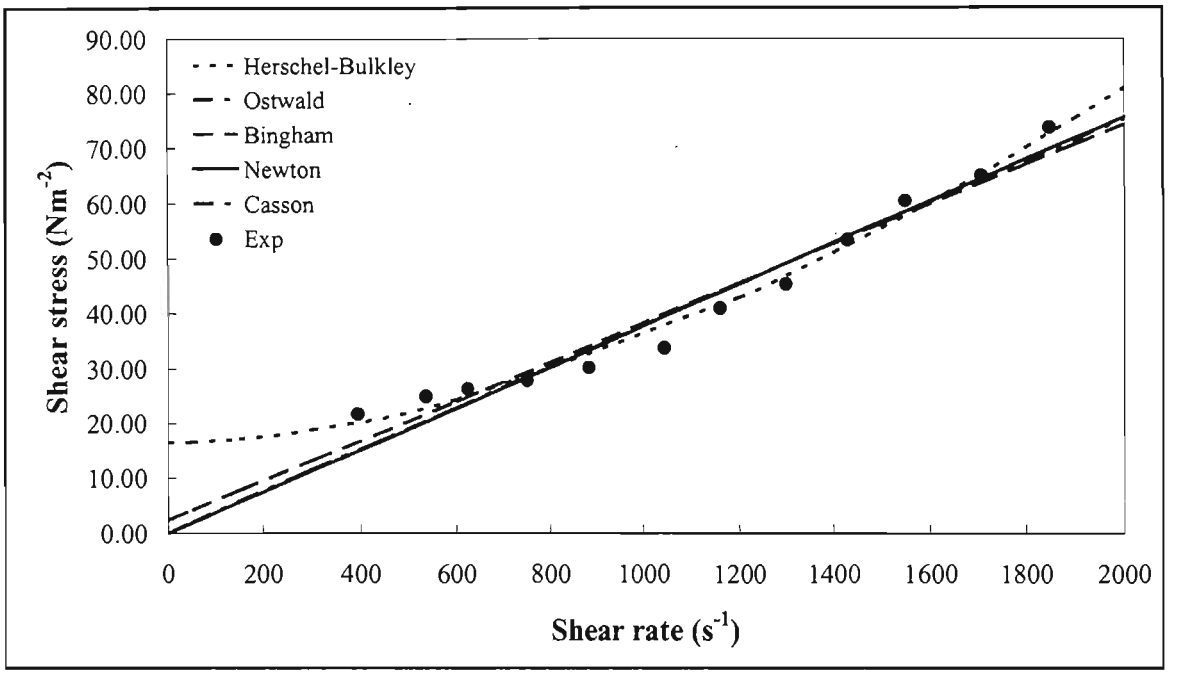

Figure A1.104 Regressed data for FeSi / Mag #2 for ratio 2:1 at specific gravity 3.2

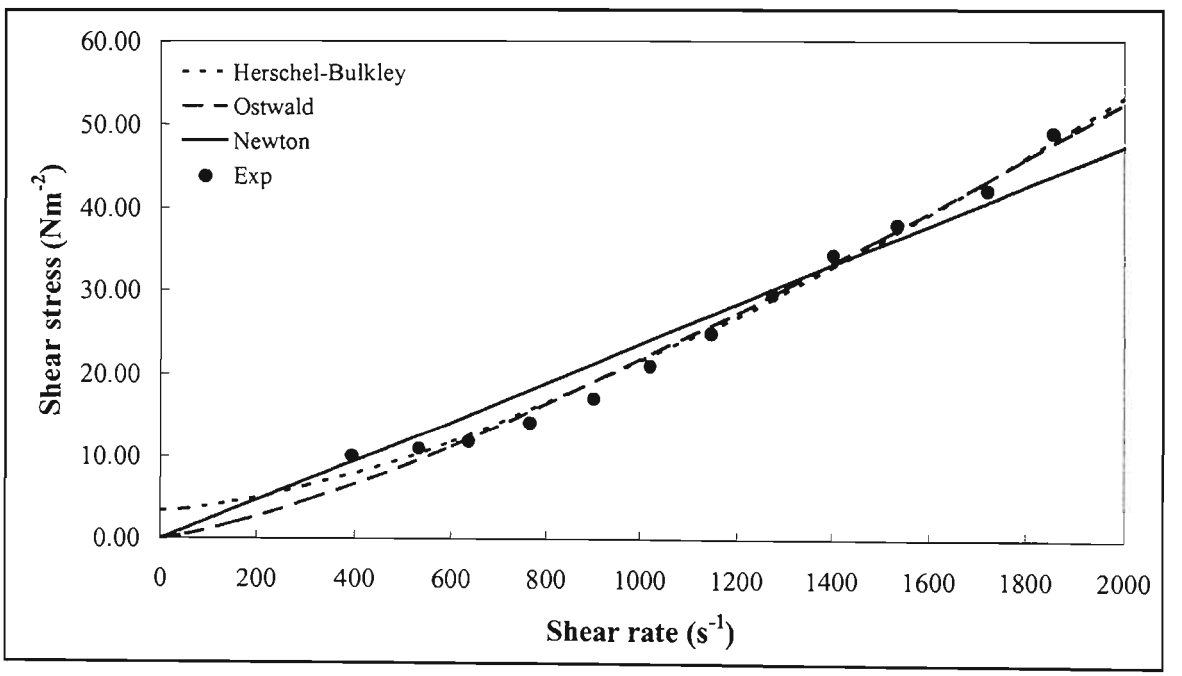

Figure A1.105 Regressed data for FeSi / Mag #2 for ratio 1:1 at specific gravity 3.0

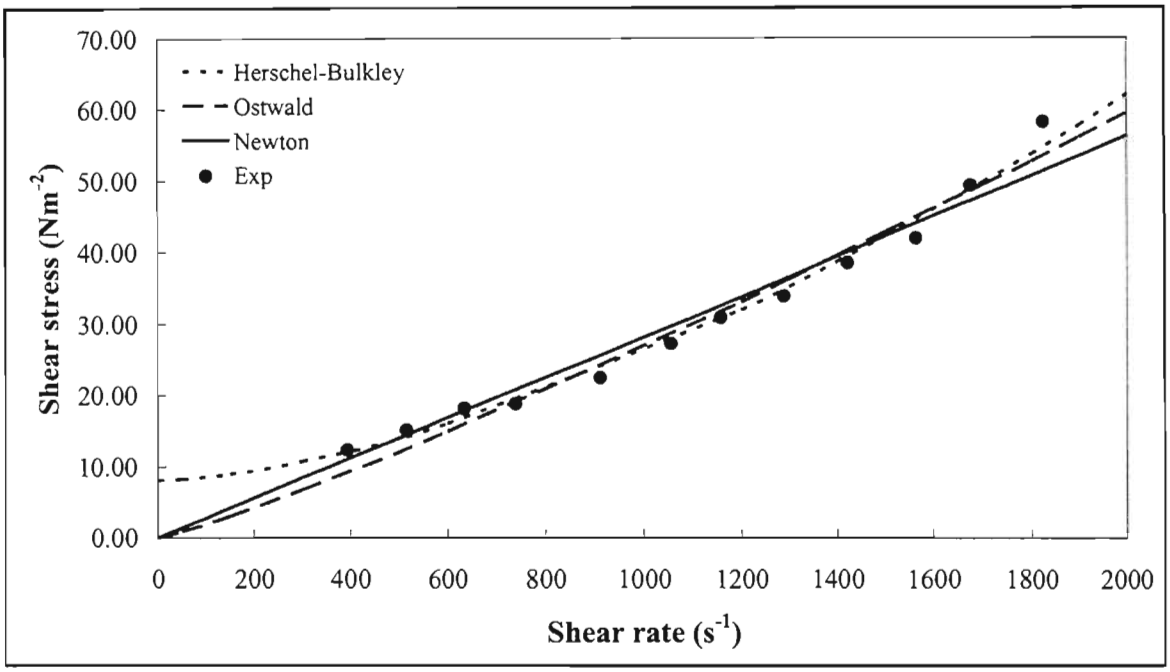

Figure A1.106 Regressed data for FeSi / Mag #2 for ratio 1:1 at specific gravity 3.1

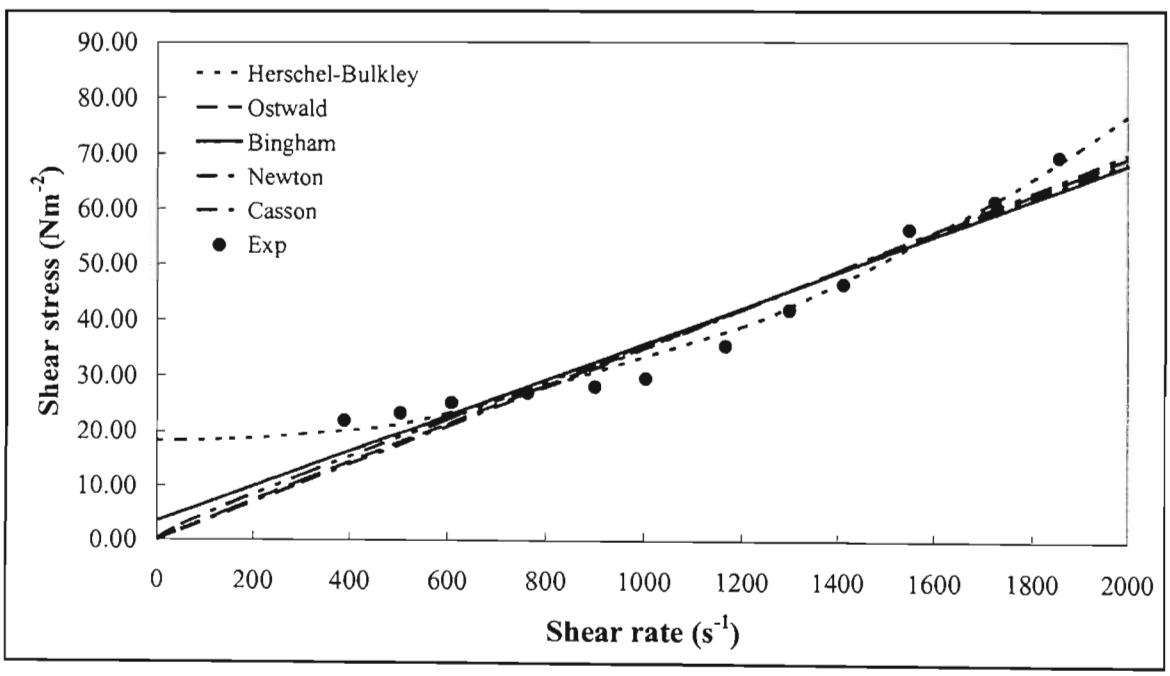

Figure A1.107 Regressed data for FeSi / Mag #2 for ratio 1:1 at specific gravity 3.2

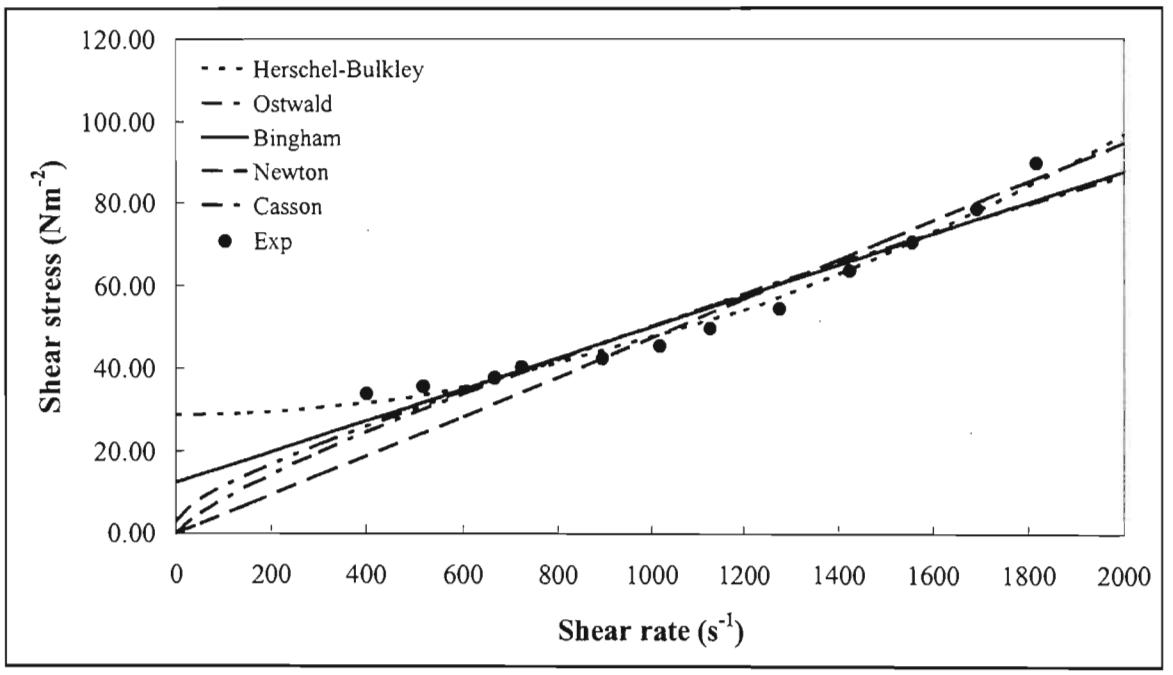

Figure A1.108 Regressed data for FeSi / Mag #2 for ratio 1:1 at specific gravity 3.3

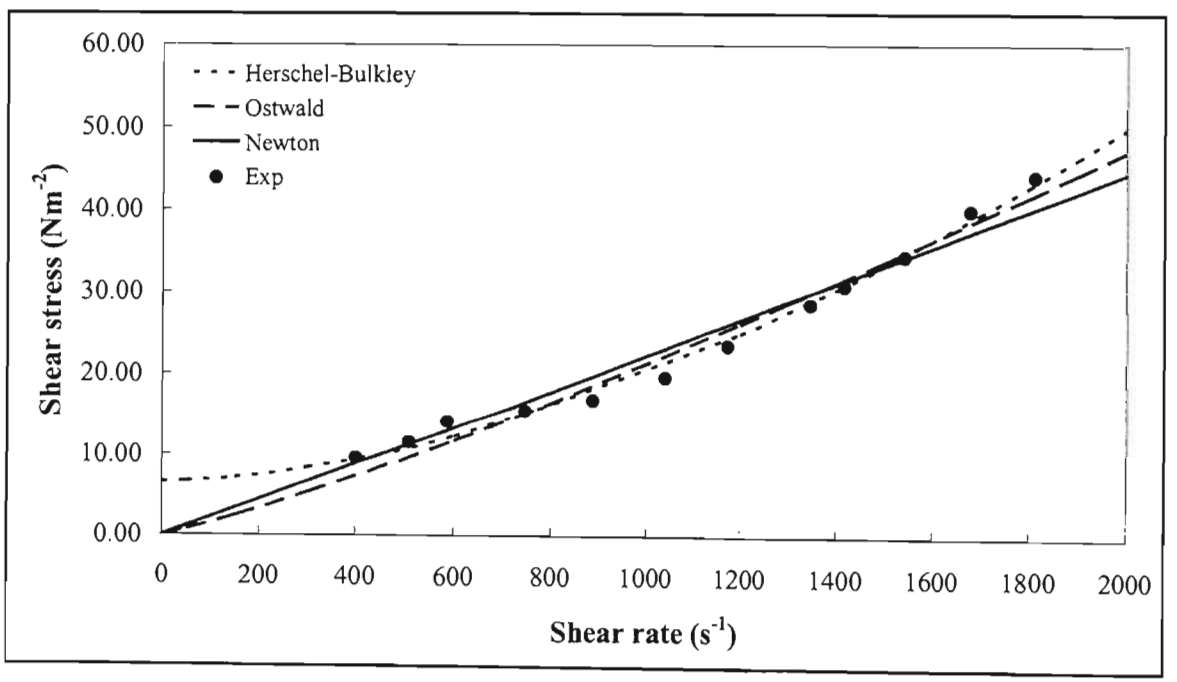

Figure A1.109 Regressed data for FeSi / Mag #2 for ratio 1:2 at specific gravity 3.0

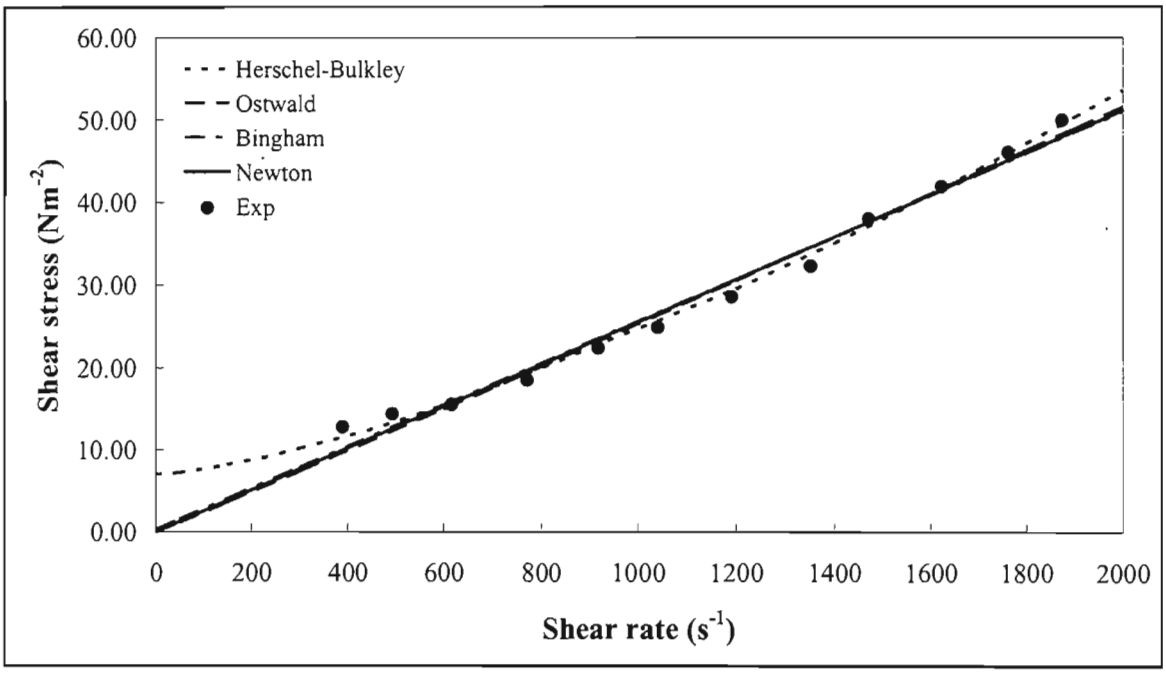

Figure A1.110 Regressed data for FeSi / Mag #2 for ratio 1:2 at specific gravity 3.1

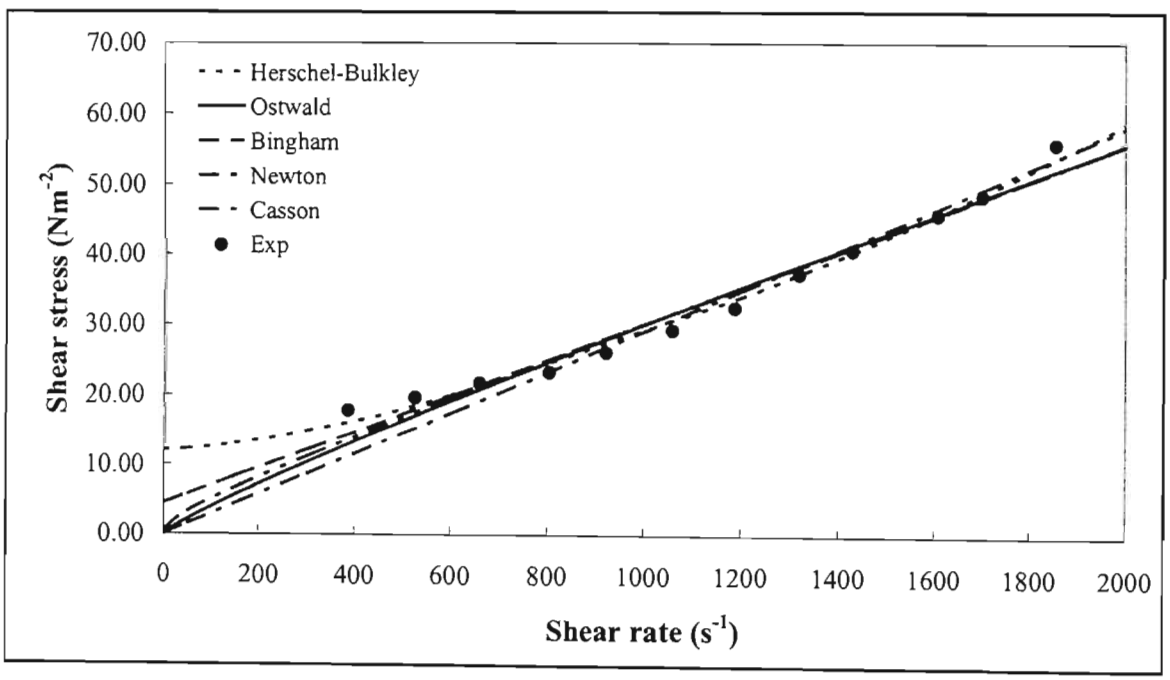

Figure A1.111 Regressed data for FeSi / Mag #2 for ratio 1:2 at specific gravity 3.2

Appendix 2

Experimental Procedures

A2.1 Density - Bottle Experimental Procedure

The density bottle technique was used to determine the density of the media particles used in these investigations. The method failed to get reproducible results for the clay-slime particles because of the tendency of these particles to absorb large amounts of water. The experimental procedure outlined here was taken from Wills (1997). The procedure is as follows:

(i). Measure the mass of the dry and empty density bottle. Label this mass as M_1.

(ii). Weigh at least 5 grams of the dry solid and add it into the density bottle.

(iii). Measure the mass of the density bottle + solids, and label this as M_2.

(iv). Slowly fill the density bottle containing the solids with distilled water. Ensure that there are no air bubbles. If there are, leave the bottle in a decanter for a couple of minutes.

(v). Once the bottle has been filled to the brim with water, and there are no visible air bubbles, measure the mass of the bottle and label this as M_3.

(vi). Empty the bottle and rinse it clean. Leave to dry, and then fill it with only distilled water. Measure the mass of the bottle and label this as M_4.

One the above procedure has been followed. And assuming that the density of the distilled water is 1000 kgm^{-3}, the density of the solid can be calculated from the following equation:

$$\rho_s = \frac{M_2 - M_1}{(M_4 - M_1) - (M_3 - M_1)} \qquad \text{(A2.1)}$$

where ρ_s is the density of the solid.

A2.2 Procedure for the Preparation and Determination of the Viscosity of the Heavy Medium Suspensions

The viscosity of the heavy medium suspensions prepared in these experiments was determined using the rheometers described in Chapter 5. The same experimental procedure was used for all the heavy media. The rheometers gave a digital read-out of the torque on the bob surface caused by the resistance of the suspensions. This was then used to calculate the viscosity of the suspensions using the methods developed in Chapter 3.

Initially the rheometers had to be calibrated with glycerine / water solutions. Mixtures of glycerine in water were prepared at mass fraction 0.80, 0.85, 0.90, and 0.95 w/w. These were then poured into the rheometers, and the shear stress and shear rate were determined from the torque and rotational speed, respectively. The calibration results are contained in Appendix A1.This section will give the experimental method and procedure for the preparation and determination of the suspension viscosity.

A2.2.1 Procedure for the Preparation and Rheometry measurement of the Heavy Medium Suspensions

The experimental procedure used was similar to that of Govier et al. (1957). The procedure is as follows:

(i). Measure 100 grams of distilled water in a round bottom flask.

(ii). Measure the amount of dry mineral solids needed to prepare a suspension of particular specific gravity and add solids to the round bottom containing water.

(iii). Shake mixture for a couple of minutes until a homogeneous suspension is obtained.

(iv). Empty the contents of the flask into the cup of the rheometer.

(v). Prior to pouring the contents of the flask into the rheometer cup, ensure that the bob is rotating at a speed of at least 200 rpm, and that the peristaltic pump is switched on to allow

immediate circulation of the pulp. This helps reduce the settling out of the solids from the suspension.

(vi). Start taking measurements at increasing speeds, recording the force at each speed. Tabulate results and calculate the shear stress and shear rate form the torque and rotational speeds respectively, using the developments outlined in Chapter 3.

(vii). For clay/slime and DP001 additions, measure the amount of each needed, and repeat steps (i) to (vi).

A2.3 DP001 Adsorption Procedure

This section details the experimental procedure for the adsorption of DP001 onto the surfaces of the media particles. The media particles tested were ferrosilicon and magnetite #1 particles. DP001 adsorption was determined by measuring the absorbance of the suspensions using a UV spectrometer.

A2.3.1 Determination of Operating Wavelength

Initially, the operating wavelength for the suspensions with DP001 had to be determined. The procedure is as follows:

(i). For yellow solutions start at 400 nm, for red solutions start at 485, and for blue solutions start at 620 nm.

(ii). Insert the blank (water) and zero the instrument using the 'set-blank' fine and coarse controls.

(iii). Insert the unknown and measure the absorbance.

(iv). Plot the result on a graph of absorbance against wavelength.

(v). Increase the wavelength; insert the blank and set zero. Insert the unknown and measure the absorbance.

(vi). Repeat this procedure so that a peak reading is established on the graph. The wavelength corresponding to the peak absorbance represents the operating wavelength which should be used.

The graph obtained for the DP001 solution operating wavelength is given below:

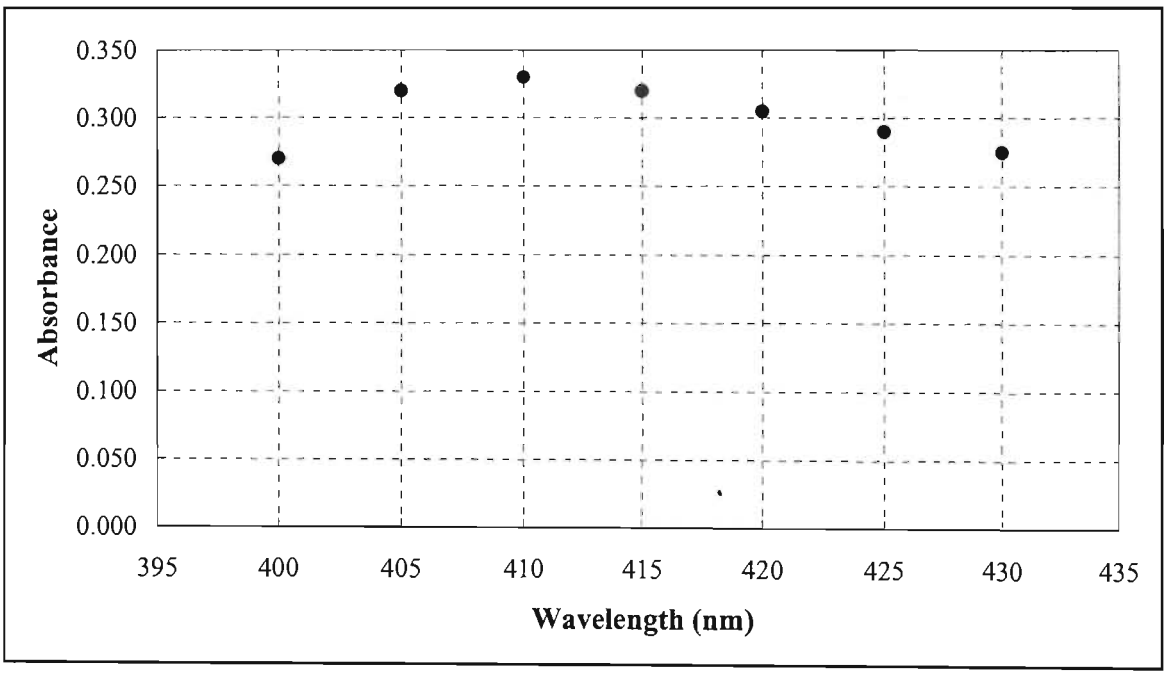

Figure A2.1 Graph showing the operating wavelength for DP001 solutions

A2.3.2 Procedure for Determining the Adsorption of DP001

Initially, a calibration graph of absorbance versus mass DP001 per 100 grams water had to be determined. Different amounts of DP001 were measured and added to 100 grams water, and their absorbance was measured on the UV spectrometer. From these results a calibration graph was plotted. Thereafter, the adsorption of DP001 on the ferrosilicon and magnetite #1 particles was measured. The procedure is as follows:

(i). Measure 100 g of water and amount DP001 needed to make up 1 gram DP001 / kg solids (FeSi or Mag #1).

(ii). Mix water and DP001 in a round bottom flask and shake until all the DP001 has dissolved.

(iii). Measure and record the absorbance of this solution using the UV spectrometer.

(iv). Measure the mass solids needed using a mass balance, and empty mass into the flask containing the water / DP001 solution.

(v). Shake the solution for at least 2 minutes, and then allow it to settle. Thereafter, filter the supernatant using a Buckner funnel and vacuum filter.

(vi). Remove the filtrate, and measure its absorbance using the UV spectrometer.

Form the absorbance before and after the solids were added to the solution, the mass of DP001 adsorbed can be determined from the calibration graph. The calibration graph for these measurements is shown below:

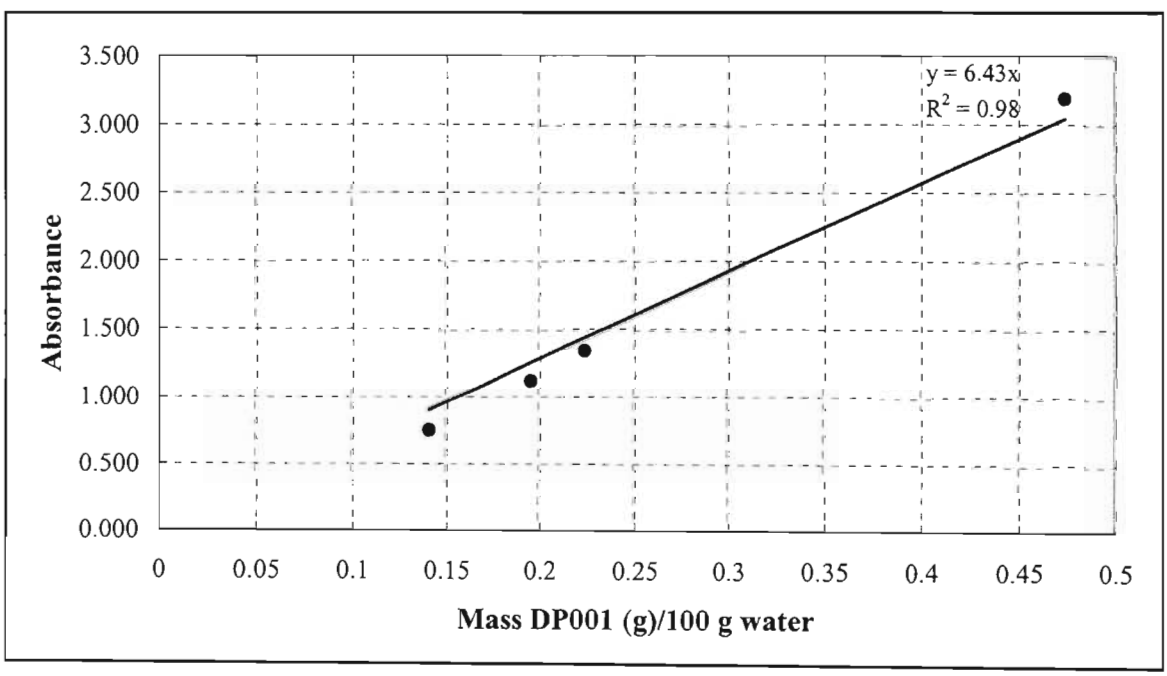

Figure A2.2 DP001 adsorption calibration graph

A2.4 Procedure for the Laboratory Heavy Liquids Tests

Laboratory tests were performed on coal samples with the following size ranges; -4mm + 1mm, -1mm + 500μm, and -500μm + 125μm. The objective of this exercise was to determine the economic separating density of the coal particles.

Liquids covering a range of densities in incremental steps are prepared, and the representative sample of the crushed ore is introduced into the liquid of highest density [Wills (1997)]. The floats product is removed and placed in the liquid of next lower density, whose float product is then transferred to the next lower density and so on. The sinks product is finally drained, washed, and dried, and then weighed, together with the final floats product to give the density distribution of the sample by weight [Wills (1997)]. Figure A2.3 is an illustration of the procedure.

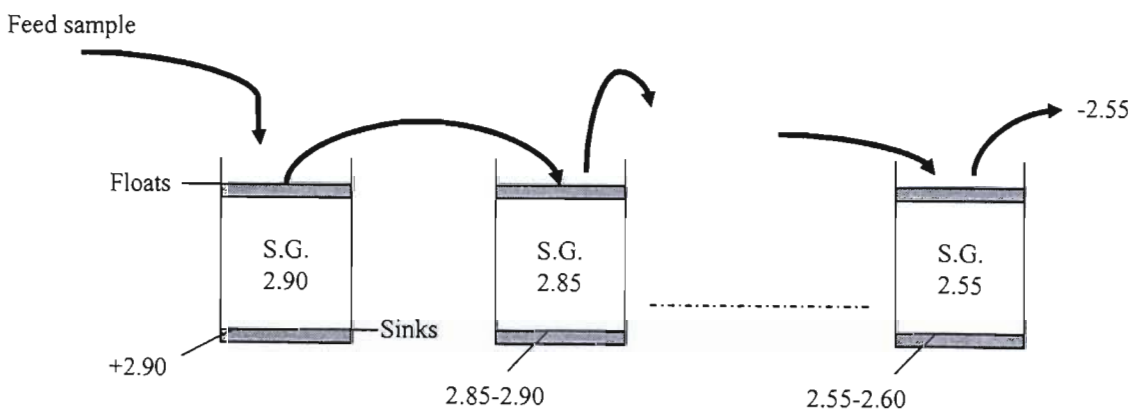

Figure A2.3 Heavy liquid testing [Wills (1997)].

The heavy liquid used in these experiments was tetrabromoethane (TBE), diluted with acetone. Because of the vapours released by TBE, the experiments had to be carried out in a fume cupboard. The safety data sheet for TBE is given in Appendix A4.

A2.4.1 Stepwise Experimental Procedure

(i). Measure the volumes TBE and acetone needed to prepare solutions with specific gravities ranging from 1.4 to 2.2, in units of 0.2.

(ii). Empty the measured volumes into a round bottom flask and shake well until a homogeneous liquid phase is achieved.

(iii). Pour the solutions in sample vials, and mark the vials according to the specific gravity of the solution it contains.

(iv). Measure at least 6 grams of a representative coal sample from the size range being tested, and add a small portion of it to the vial containing a solution with specific gravity 2.2 (highest density). The reason for adding a small portion at a time is to prevent particle entrainment.

(v). Stir the contents of the vial, allowing the contents to settle for about 3 minutes.

(vi). Using a spatula, scrape the float product into a container and rinse with acetone.

(vii). Allow the sample to dry and then add the sample to the vial with specific gravity 2.0.

(viii). Add another small portion of the remaining coal sample into the vial with specific gravity 2.2, and repeat steps (v) to (vii).

(ix). Repeat steps (vi) and (vii) for the vial with specific gravity 2.0. Adding the floats product to the vial with specific gravity 1.8.

(x). Continue repeating steps (v) to (ix) until the entire sample has been used, and until the lowest specific gravity (1.4) is reached.

(xi). Collect the final floats product from the lowest specific gravity and the sinks products from each sample vial. Rinse the products with acetone, allow them to dry.

(xii). Weigh each dried sample from each of the density size ranges.

(xiii). Place at least 1 gram of a representative sample in each density range in a crucible, and place in a furnace. Slowly raise the temperature to 800 °C, maintaining this temperature for at least 3 hours.

(xiv). The residue is cooled and then weighed. The ash content is the mass of ash expressed as a percentage of the initial sample weight taken.

The procedure outlined above is used for both the ash analysis, and sink-float analysis used to determine the amount of misplaced material for a particular separation. For sink-float analysis steps (xiii) and (xiv) are omitted.

A2.5 Procedure for the Dense Medium Cyclone Experiments

This section will detail the experimental procedure used in the cyclone tests. The media particles used for these experiments were magnetite #1 and magnetite #2. In both cases DP001 was added to the suspensions. The operating densities were 1.57, 1.70, and 1.83. The experimental cyclone loop was given in Chapter 5. The cyclone loop is, once again, presented below for the sake of clarity.

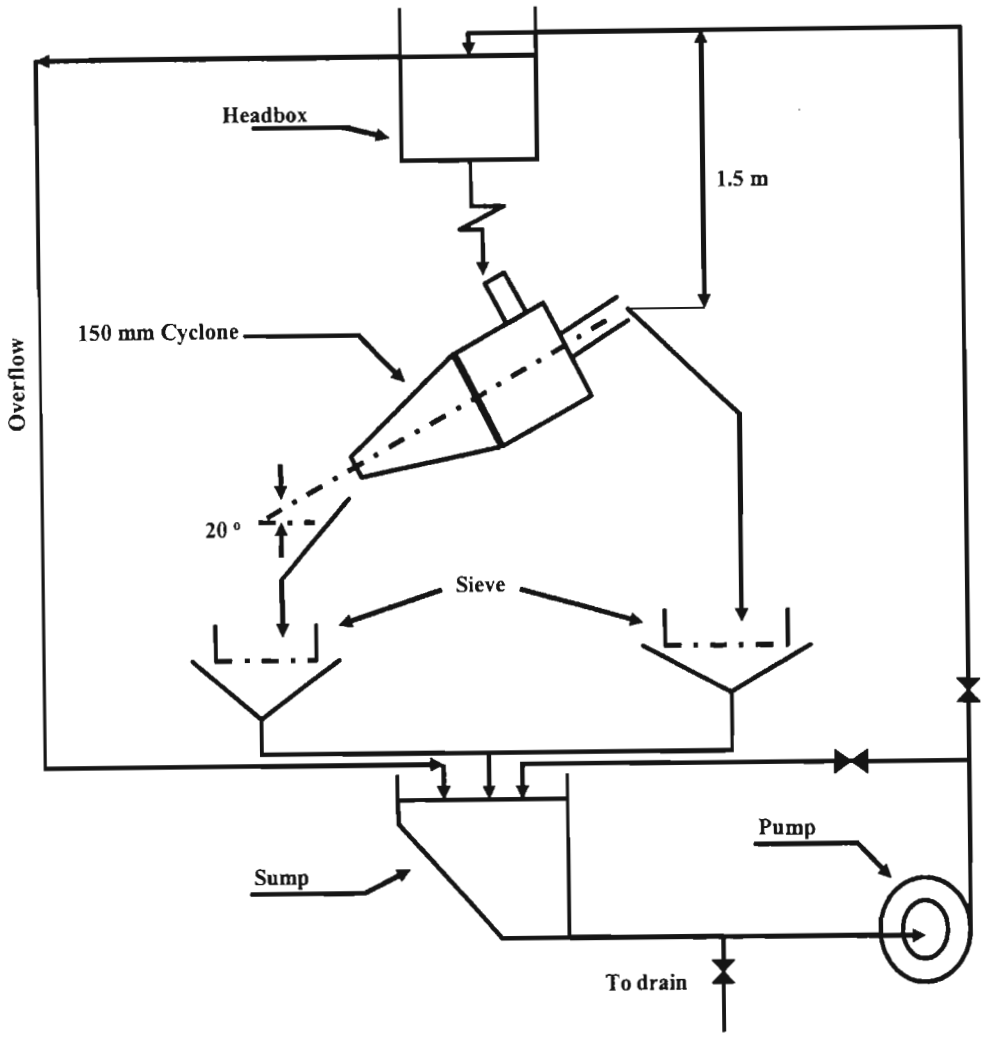

Figure A2.4 Experimental dense medium cyclone loop.

The procedure is as follows:

(i). Start by setting the cone elevation of the cyclone to 20 °.

(ii). Fill the sump with water up to the marker shown on the inside of the sump.

(iii). Start the pump to circulate the water through the system. Ensure that all valves are fully open, except for the drain valve.

(iv). Adjust vortex finder length until the desired type of flow from the spigot is obtained. There should be no short circuiting of feed material.

(v). Measure the mass of solids needed to prepare the required densities from the amount of water added, and slowly start adding the solids into the sump. The circulation of water through the system prior to the addition of solid particles ensures that there are pipe blockages.

(vi). Whilst adding the solids into the sump, monitor the density of the suspension entering the cyclone by opening the by-pass valve on the cyclone feed pipe (Figure A3). The density is determined by using the density can method described by Wills (1997). Using a measuring cylinder, measure the mass and volume of the slurry. And from this obtain the suspension density.

(vii). Once the solids have been added, and the required feed density achieved, measure the flowrate of the overflow and underflow by timing how long it takes to fill measuring cylinders held under these product streams. The contents of the cylinders are also used to calculate the density of the product streams.

(viii). Measure at least 120 grams from a particular coal sample range and add them into the Headbox.

(ix). After 3 minutes start collecting the samples by placing sieves of suitable aperture size under both the overflow and underflow. Three minutes is enough time to ensure that the coal samples circulate at least once through the loop without being broken up by the pump impellers.

(x). After the overflow and underflow products have been collected, rinse the products with water to remove any magnetite particles and allowed to dry.

(xi). For the DP001 experiments, first measure the amount of DP001 needed based on the amount of solid particles added. Add this into the Headbox, and wait at least 5 minutes before adding coal samples. This ensures that enough time was given for the DP001 to adsorb onto the media surfaces. Prior to DP001 addition, the density of the feed is measured and make up solid particles may need to be added.

(xii). Repeat steps (viii) to (x)

(xiii). Once the coal product samples are dry, analyse them using sink-float analysis to determine the amount of misplaced material.

Appendix 3

Equipment Diagrams and Photos

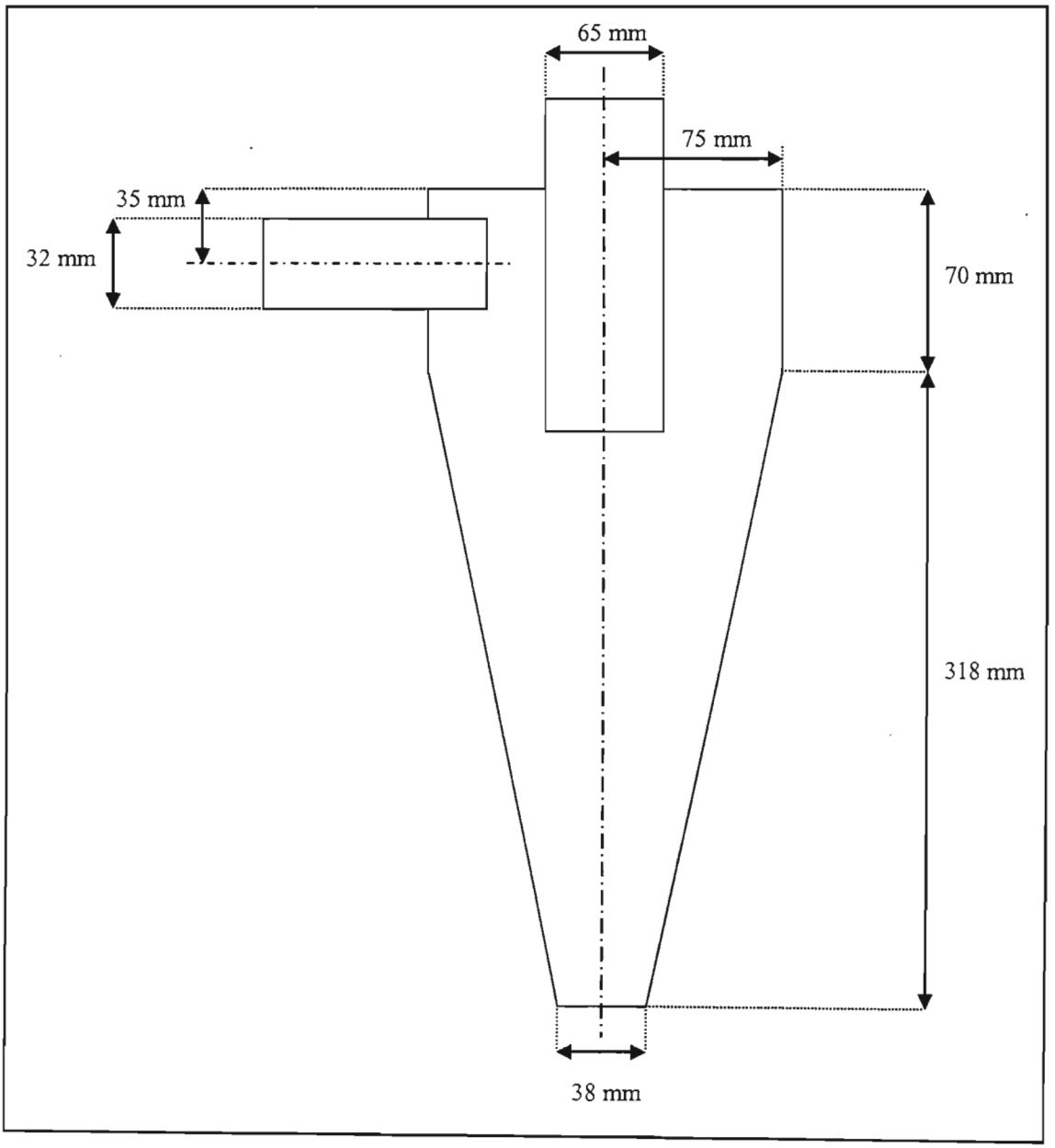

Figure A3.1 Diagram showing the dimensions of the cyclone used in the heavy medium separations

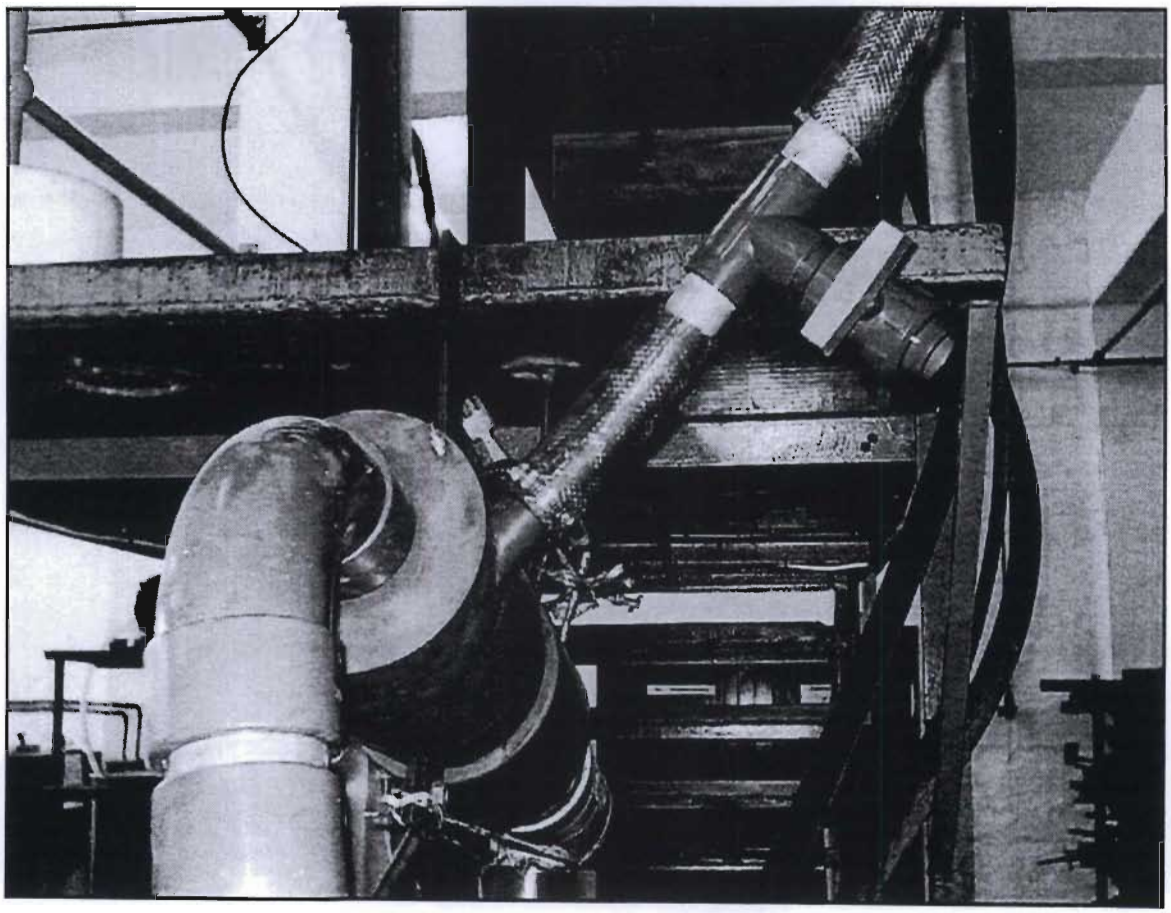

Figure A3.2 Picture showing the Feed density measurement valve

Figure A3.3 Picture showing the Malvern Metsizer 2000 [www.Malvern.co.uk (25/09/2004)]

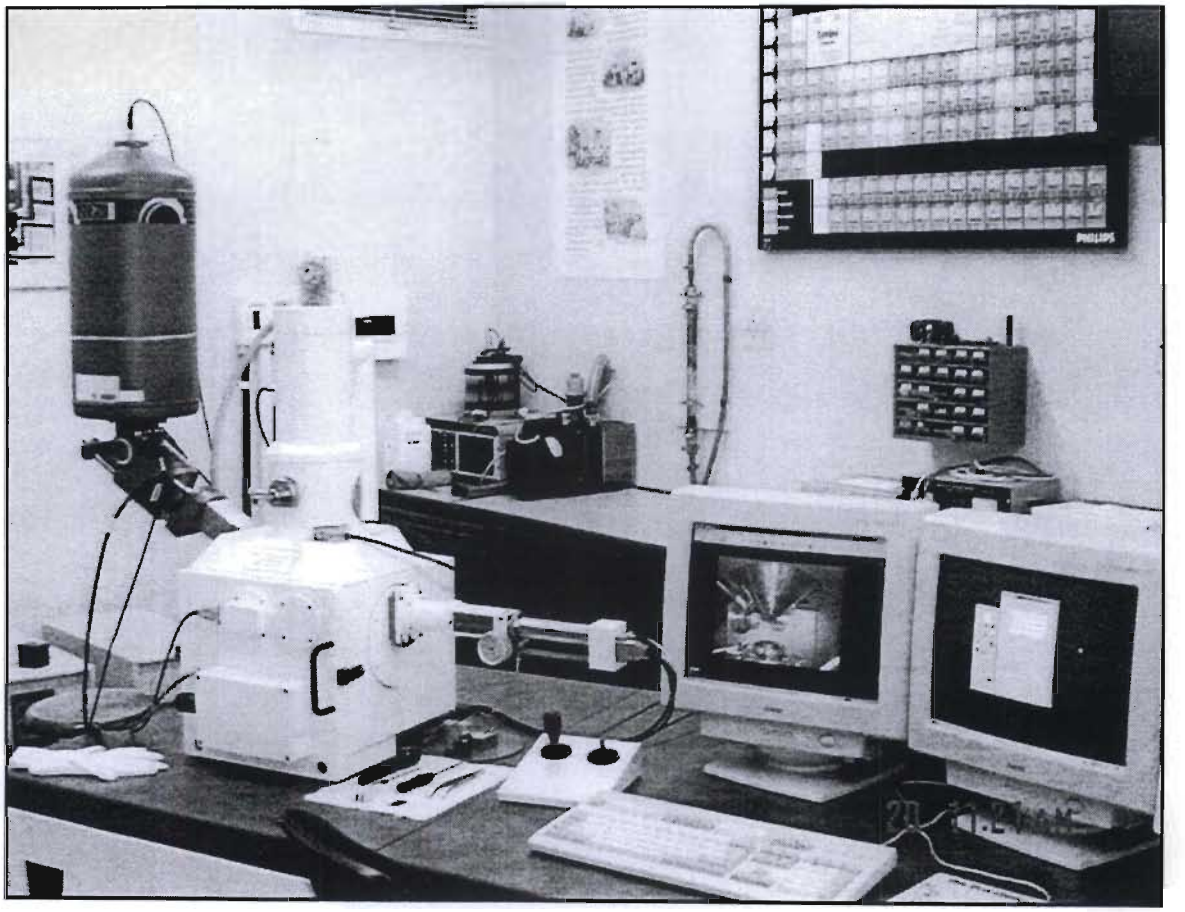

Figure A3.4 Picture of the LEO 1450–Standard Scanning Electron Microscope (SEM) Unit

Figure A3.5 Picture of the Hitachi S–520 Scanning Electron Microscope (SEM) Unit.

Appendix 4

Tetrabromoethane Safety Data Sheet

A4. Tetrabromoethane Safety Data Sheet

TYPES OF HAZARD/EXPOSURE	ACUTE HAZARDS/SYMPTOMS	PREVENTION	FIRST AID/FIRE FIGHTING
FIRE	Not combustible. Gives off irritating or toxic fumes (or gases) in a fire		In case of fire in the surroundings: all extinguishing agents allowed
EXPOSURE		Prevent Generation of Mists	
INHALATION	Abdominal pain. Cough. Headache. Sore throat.	Ventilation, local exhaust, or breathing protection	Fresh air, rest. Refer for medical attention
SKIN	Redness	Protective gloves. Protective clothing	Remove contaminated clothes. Rinse and then wash skin with water and soap. Refer for medical attention
EYES	Redness.	Face shield, or eye protection in combination with breathing protection	First rinse with plenty of water for several minutes (remove contact lenses if easily possible), then take to a doctor.
INGESTION	(further see Inhalation	Do not eat, drink, or smoke during work	Rinse mouth. Refer for medical attention
SPILLAGE DISPOSAL	Collect leaking and spilled liquid in sealable containers as far as possible. Absorb remaining liquid in dry sand or inert absorbent and remove to safe place (extra personal protection: self-contained breathing apparatus).		
STORAGE	Separated from strong oxidants, strong bases, food and feedstuffs. Cool. Well closed. Ventilation along the floor.		

Appendix 5

Journal Article Published from this Work

"The use of surface active chemicals in heavy medium viscosity reduction"

N.T. Mabuza., J. Pocock, and B.K. Loveday

Minerals Engineering **18** (2005) 25-31, Elsevier.

Available online at www. Sciencedirect.com

Available online at www.sciencedirect.com
SCIENCE DIRECT®
Minerals Engineering 18 (2005) 25–31
MINERALS ENGINEERING
This article is also available online at: www.elsevier.com/locate/mineng

The use of surface active chemicals in heavy medium viscosity reduction

N.T. Mabuza, J. Pocock *, B.K. Loveday

School of Chemical Engineering, Howard College Campus, University of KwaZulu-Natal, Durban 4041, Republic of South Africa

Received 26 April 2004; accepted 4 June 2004

Abstract

This paper discusses the use of polymeric surface active chemical agents for reducing the viscosity of dense medium suspensions. A laboratory-scale device was developed to measure shear stress at various shear rates, using a rotating bob and a circulating stream of heavy medium suspension. Ferrosilicon and magnetite suspensions were tested over a range of solid volume concentration and varying additions of clay, to simulate slimes build up. In most cases, a relatively modest addition of polymer reduced the viscosity of the medium by about 20% with up to 50% reduction achievable for some specific gravities and slimes levels.

Reduction of medium viscosity could allow separation of materials at a finer size than is currently economically feasible, increase the efficiency of separations at higher particle sizes, or allow for cheaper media through the use of mixed magnetite/ferrosilicon suspensions.

Keywords: Dense medium separation

1. Introduction

Dense medium suspensions are prepared by adding an aggregation of solid spheres to a liquid. The liquid can either be a Newtonian liquid or a non-Newtonian liquid. In most industrial processes the liquid used is a Newtonian fluid, usually water. Dense medium suspensions can further be classified as a heterogeneous material comprised of a dispersed phase and a continuous phase (Jinescu, 1974). The solid particles represent the disperse phase, while the liquid represents the continuous phase. It should also be mentioned that the solid particles themselves can also be a heterogeneous system comprised of solid particles of different nature and form. In some industrial processes solid particles of different form and nature have been used at different concentrations to facilitate the separation of certain mineral ores (Collins et al., 1974, 1983).

The dominating dense media particles used in making dense medium suspensions are magnetite and ferrosilicon particles. Magnetite is a naturally occurring iron oxide ore, while ferrosilicon is a manufactured alloy of iron and silicon. To reduce the corrodibility of ferrosilicon the silicon content should not be less than 15%, but it should not also be greater than 16% so as not to affect the magnetic capture of the particles in the dense medium circuit (Wills, 1997). Due to the synthetic nature of ferrosilicon the cost to the consumer is considerably higher (approximately 10 times within South Africa).

The two most important parameters for dense medium suspensions are their stability and viscosity. The stability of the suspensions is defined in terms of the rate of settling of the solid particles in the media. Suspensions with high settling rates are considered to be unstable, while those with low settling rates are considered as

* Corresponding author. Tel.: +27 31 2603377; fax: +27 31 2601118.
E-mail address: pocockj@ukzn.ac.za (J. Pocock).

0892-6875/$ - see front matter © 2004 Elsevier Ltd. All rights reserved.
doi:10.1016/j.mineng.2004.06.036

being stable. The viscosity of a suspension may be defined as its resistance to motion. The stability and the viscosity suspensions are interrelated, both dependant on the density, size and shape of the medium used and its volume concentration, and that this interrelation of stability and viscosity can be modified through the use of dispersing agents (Collins et al., 1974, 1983).

For a constant suspension specific gravity a higher density solid will reduce the viscosity and stability of the suspension by reducing the percentage volume of particles. A spherical medium reduces the viscosity and stability of the suspension by providing more slippage between adjacent solids in the suspension. A coarser medium reduces the viscosity and stability of the suspension by reducing the solid particle surface area, which in turn reduces the apparent solids volume concentration (Collins et al., 1974, 1983). Ferrosilicon media have a higher density ($\sim 6760\,kg\,m^{-3}$) than magnetite media ($\sim 4650\,kg\,m^{-3}$). Thus, magnetite media suspensions are primarily used for the separation of coal particles at densities up to $2500\,kg\,m^{-3}$, while ferrosilicon media suspensions are used for the separation of much heavier ores at densities as high as $3400\,kg\,m^{-3}$ for atomized ferrosilicon (Wills, 1997).

Despite the fact that ferrosilicon media are more costly compared to magnetite media, they are still used to maintain suspensions at high specific gravities because of the much higher viscosity and stability problems associated with magnetite suspensions at the same specific gravities. These much higher viscosities reduce the separation efficiency of fine ores and near specific gravity material. The reduction of magnetite suspension viscosities at these high specific gravities can be achieved through the use of coarser magnetite media compared to ferrosilicon media at the same specific gravities (Collins et al., 1974, 1983). The main problem associated with the use of a coarser medium is the increase in the settling rate of the medium. To alleviate this problem fine media or slimes would have to be used together with the coarse media to reduce the settling rates of the media. Alternatively, the viscosity can be reduced by using dispersants. There are a great variety of dispersants which may be used, such as (Aplan and Spedden, 1964): alkali phosphates; sodium silicate; ethylenediaminetetracetic acid; surface active agents, such as lignosulphonates and petroleum sulphonates. The main objective for this work is to investigate the use of surface active agents in the reduction of viscosity for dense medium suspensions. If surface active agents can be used to reduce the viscosities of magnetite suspensions at high specific gravities, without compromising the separation efficiency of dense medium separations, the use of the more expensive ferrosilicon media could be minimized.

The rheological behaviour of dense medium suspensions can be either Newtonian, Bingham plastic shear-thinning, or shear-thickening (Collins et al., 1974). Newtonian suspensions are those for which the viscosity of the suspension is independent of the shear rate. Bingham plastic suspensions are similar to Newtonian fluids but have a yield stress. The yield stress is a measure of the minimum shear stress needed before movement of the suspension occurs (Laskowski et al., 2001). For shear thinning suspensions the viscosity of the suspensions decreases with an increase in shear rate, while for shear thickening suspensions the viscosity increases with shear rate.

Although most suspensions show non-Newtonian behaviour, it is usually difficult to predict the type of non-Newtonian behaviour occurring in different systems (Lapsin et al., 1988). The type of non-Newtonian behaviour can vary within a single class of systems, especially when the concentration is varied. Some concentrated suspensions can show shear-thinning behaviour at low shear rates, and shear-thickening at higher shear rates. Collins et al. (1974) found that for ferrosilicon suspensions at low shear rates showed shear-thinning behaviour, and shear-thickening behaviour at higher shear rates. The above authors also found that by increasing the degree of contamination of the suspensions, or increasing the suspension specific gravity, the suspensions acquired a yield stress.

2. Experimental work and material

Samples of operating dense media were prepared from three different media types: 270D ferrosilicon media; magnetite media supplied by Martin and Robson, Middleburg, South Africa; and a slimes causing clay from a diamond processing operation (supplied by Debtech SA). Prior to laboratory experiments the samples were analyzed using a Malvern Sample analyzer from the department of geology at the University of KwaZulu-Natal to define their size ranges. Fig. 1 shows a graph of the size ranges of the media determined from the Malvern Sample Analyzer. From the graph the average size of the media ($D_{av}/\mu m$) can be determined; D_{av} ferrosilicon was $35.2\,\mu m$; D_{av} magnetite was $41.6\,\mu m$; and Dav clay was $25.3\,\mu m$. The densities of the media determined using the density-bottle method outlined by Wills (1997) were $6760\,kg\,m^{-3}$ for ferrosilicon and $4637\,kg\,m^{-3}$ for magnetite.

Viscosity tests were performed using a laboratory scale rotational viscometer designed in the School of Chemical Engineering, University of KwaZulu-Natal. The viscometer is a concentric cylinder device and was operated under Searle's principle. It was designed according to DIN 53019/ISO 3219 (Slatter et al., 2000), and is a shear rate controlled viscometer. The shear rate is manually controlled using a mounted motor and the torque at the bobbin surface measured using a load cell. Fig. 2 shows a cross section of the viscom-

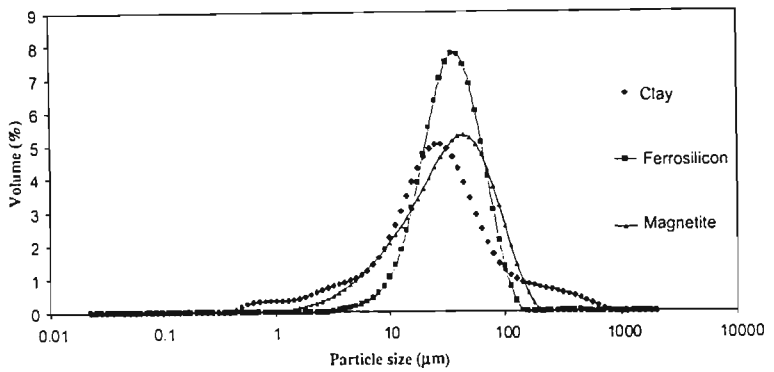

Fig. 1. Particle size ranges determined for the media and slimes.

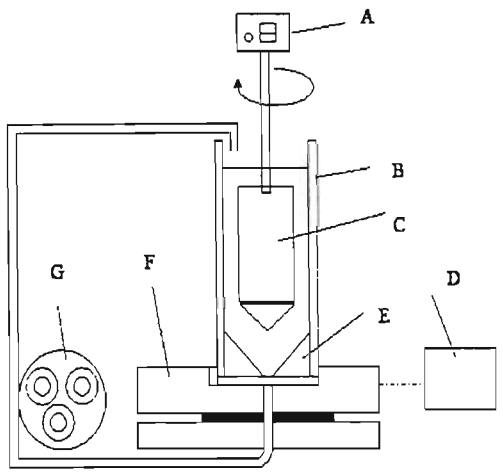

Fig. 2. Schematic diagram of a modified rotational Viscometer: A, variable speed motor; B, cup; C, bob; D, Load cell with digital readout; E, chamfer; F, turntable on Bearings; G, peristaltic pump.

eter. To overcome the settling nature of the dense media from the suspension, a chamfer was added at the bottom of the cup, and the suspension was kept in motion via a circulation stream by using a peristaltic pump. After each run the density of the recycle stream was measured to determine the extent of particles settling out of suspension.

The viscometer was calibrated using glycerol/water solutions. The viscosity of the glycerol/water solutions were first determined using a Brookfield viscometer. The shear stress and shear rate were calculated from the load cell torque output and bobbin rotational speed using the Eqs. 1 and 2, respectively (Slatter et al., 2000):

$$\tau_{rep} = \frac{M}{2\pi L R_b^2 c_L}, \quad (1)$$

$$\dot{\gamma}_{rep} = \frac{(1+\delta^2)}{(\delta^2-1)}\frac{2\pi}{60}n, \quad (2)$$

where τ_{rep}, representative torque; $\dot{\gamma}_{rep}$, representative shear rate; M, torque; L, bob length, R_b, bob radius; c_L, viscometer correction factor (obtained from calibration); δ, ratio of cup radius to bob radius; n, bob rotational speed (rpm).

The dispersant (surface active agent) used was an orange-brown calcium lignosulphonate powder commercially available under the code DP001 recovered from the paper and pulp industry as a by-product by Lignotech, South Africa. DP001 is a medium chain length anionic polymer with a high affinity for water, used mainly as a binder in the animal feed industry and as a dust suppressant.

3. Results and discussion

Initial investigations centred on the use of DP001 as a clay/slimes suppressant. It had been noted that ferrosilicon was not affected by addition of the dispersant on its own; however, it was effective as a dispersant for clays and slimes of a silicate nature. A number of rheograms were prepared using ferrosilicon suspensions with specific gravities between 2.9 and 3.5 with a constant shear rate ($240\,s^{-1}$) and increasing additions of clay (percentage given per kilogram of FeSi) to the suspension to simulate a build up of slimes in an HMS circuit. Fig. 3 shows a typical rheogram for an SG of 2.9.

As can be seen from this rheogram, the DP001 (in this case added at an addition of 1 g/kg FeSi) was effective in suppressing clay with reduction of the viscosity of up to 50% possible with slimes loadings of up to 18% clay added to the system. Investigations into the effect on the media itself have since focused upon the possibility of replacement of some ferrosilicon from the media solids with magnetite in conjunction with reduction of the viscosity of the magnetite contribution to the viscosity (due to its lower density). Initial results are detailed in the rest of this paper.

Fig. 4 shows the rheograms of uncontaminated ferrosilicon and magnetite media suspensions at a specific gravity of 2.2, along with suspensions at the same density with 2:1, 1:1 and 1:2 ratios of magnetite to

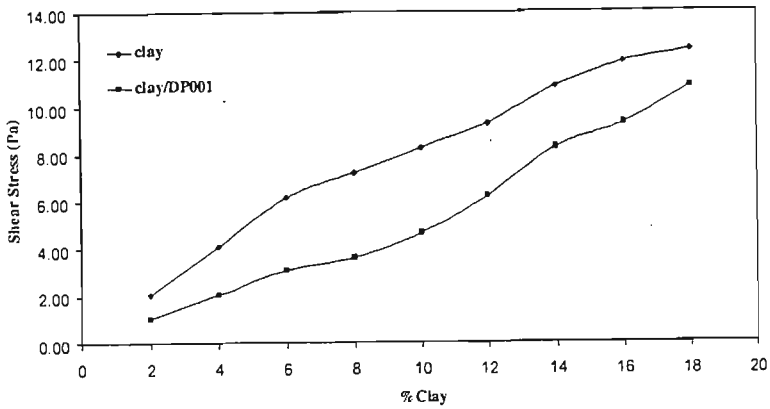

Fig. 3. Shear stress vs % clay for a ferrosilicon suspension (SG 2.9).

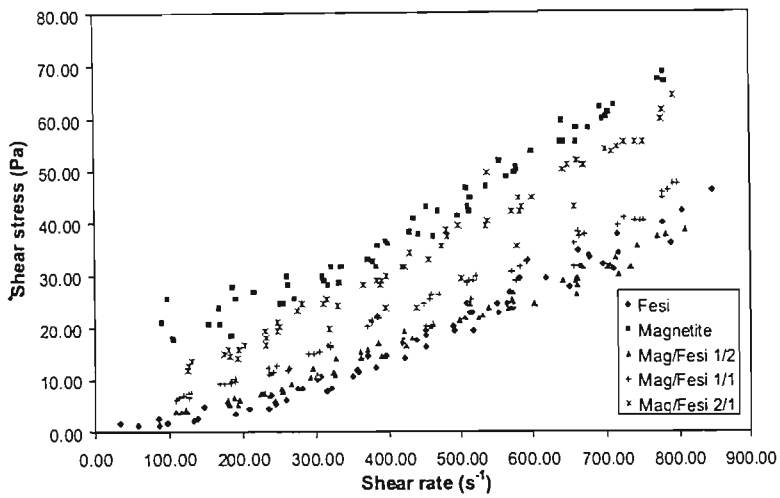

Fig. 4. Rheograms for uncontaminated suspensions at sp.gr.2.2 (without DP001).

ferrosilicon by mass at the same SG. The graph shows that pure uncontaminated ferrosilicon suspensions are pseudo-Newtonian, while pure magnetite is Bingham plastic. The non-Newtonian behaviour of magnetite suspensions at this specific gravity are attributed to their much higher solids volume concentration (33%). As the percentage magnetite is increased, the Bingham plastic nature of the different suspensions is accentuated, and the viscosity of the suspension increases. These observations are similar to those of Collins et al., 1974, 1983. They found that mixtures of FeSi and magnetite were essentially pseudo-plastic at magnetite concentrations $\leqslant$25%, but showed Bingham plastic conditions at magnetite concentrations $\geqslant$50%.

Fig. 5 shows the effect of DP001 on uncontaminated ferrosilicon suspensions at a specific gravity of 2.2. The results show that DP001 has a negligible effect, if any. DP001 additions as high as 5 g DP001 per kilogram of media have little effect on the viscosity of the suspensions. Aplan and Spedden (1964) report "that surface active agents have little effect on uncontaminated ferrosilicon suspensions, except for a minor amount of suspension of the finest particles, which is quite negligible in the case of ferrosilicon samples".

Figs. 6–8 are rheograms for mixtures of magnetite and ferrosilicon suspensions. The increase in yield stress as the amount of magnetite is increased is seen from the different graphs. The effect of DP001 appears to increase with the percentage magnetite media. Johnson et al. (2000) observed that mineral particles brought into contact with an aqueous environment often acquire substantial charge. This can be caused by ion adsorption, isomorphous ion substitution, differential ion dissolution and ionization of surface sites. These processes are of particular importance to oxide minerals. Since magnetite is an iron oxide, it should be more susceptible to DP001 than uncontaminated ferrosilicon media.

The figures above also show that the effectiveness of DP001 occurs at concentrations between 0.5 and 3 g DP001/kg solids (Fig. 9).

Fig. 10 shows the effect of DP001 on pure magnetite. A 0.5 g/kg solid DP001 shows a larger decrease in viscos-

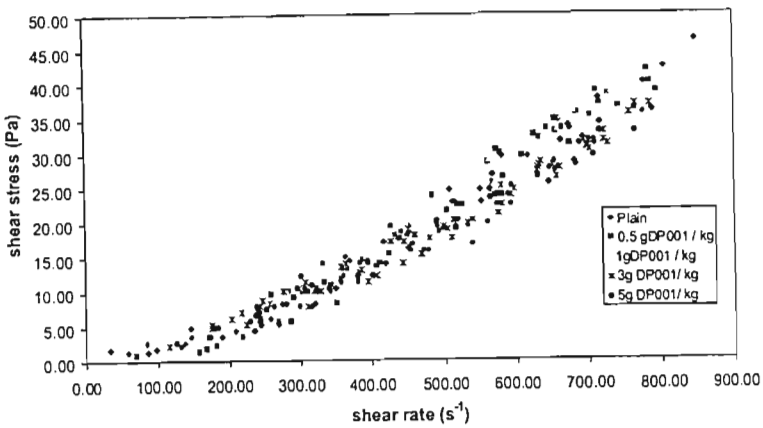

Fig. 5. Rheograms for pure uncontaminated ferrosilicon suspension at sp.gr. 2.2 (with DP001).

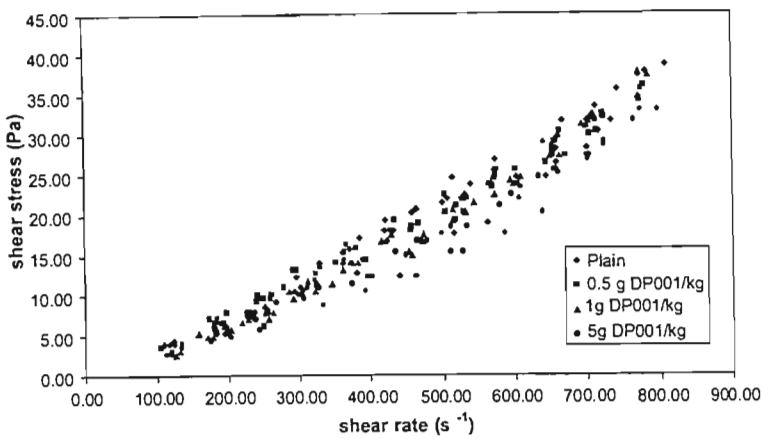

Fig. 6. Rheograms for Mag/FeSi 1/2 at sp.gr. 2.2.

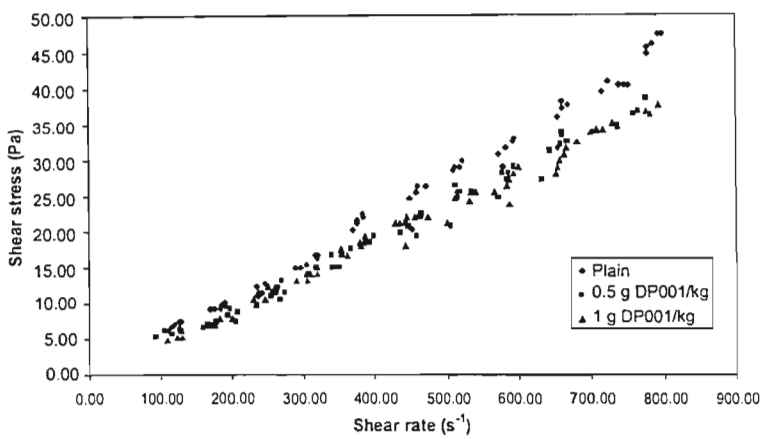

Fig. 7. Rheograms for Mag/FeSi 1/1 at sp.gr. 2.2.

ity than any of the other suspensions. Fig. 10 compares the viscosities of a pure ferrosilicon without DP001 to that of plain magnetite, and magnetite with 0.5g DP001/kg solid added. The graph shows that for magnetite suspensions with and without DP001, the behaviour appears to be shear-thinning. The reduction in viscosity in the presence of DP001 is seen on the graph. For shear rates $\leqslant 150\,s^{-1}$ the media start to become unstable. In this region the reported viscosities could be higher than the actual viscosities of the suspensions.

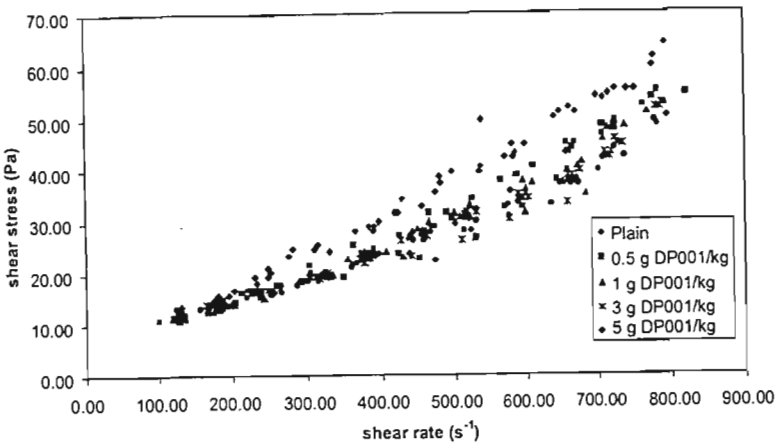

Fig. 8. Rheograms for Mag/FeSi 2/1 at sp.gr. 2.2.

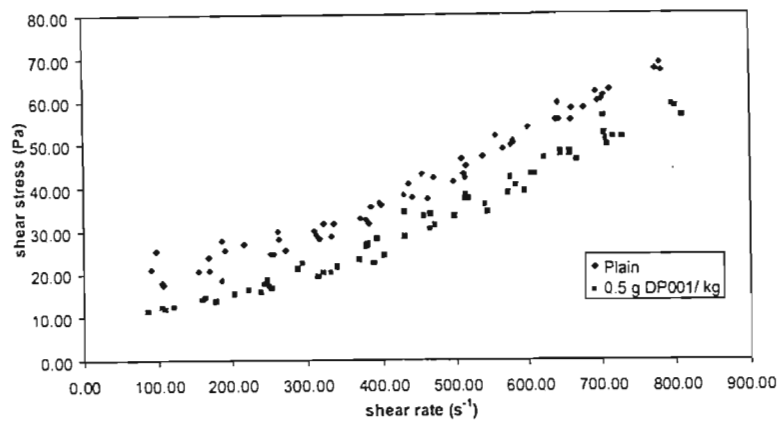

Fig. 9. Rheograms for magnetite at sp.gr. 2.2.

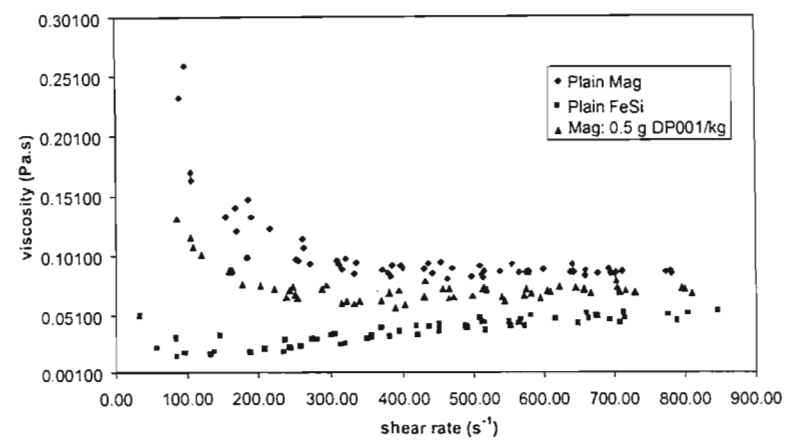

Fig. 10. Comparison of viscosities for ferrosilicon and magnetite suspensions sp.gr. 2.2.

4. Conclusions

Although most of the preliminary tests with DP001 were carried out at a relatively low specific gravity, the significance of the results cannot be altogether disregarded. The initial results illustrate that the presence of DP001 in dense medium suspensions, particularly for those containing magnetite, reduces the viscosity of the suspensions by a measurable amount at all shear rates tested, whilst the effect of slimes on increasing the viscosity of a ferrosilicon suspension can be reduced by up to 50% by a small addition of reagent. The addition of large amounts of DP001 appears to have little effect on the viscosities compared to additions at smaller concentrations with the optimum loading seemingly around 1 g/kg solids. The results show that the addition

of DP001 to mixed medium suspensions brings the viscosity down towards the range of ferrosilicon viscosities. This implies that the replacement of ferrosilicon is possible at low specific gravities and may be possible at higher specific gravities particularly where slimes build up can cause viscosity problems.

Acknowledgments

The authors would like to extend their sincere gratitude to Lignotech SA for the financing of this project. They would also like to thank the workshop staff at the Chemical Engineering and Geology Departments of the University of KwaZulu-Natal.

References

Aplan, F.F., Spedden, H.R., 1964. Viscosity Control in Heavy-Media suspensions, VII International Mineral Processing Congress: Vol. 1, AIM (American Institute of Mining), Presented 20–24 September 1964 AIM.

Collins, B., Napier-Munn, T.J., Sciarone, M., 1974. The production, properties and selection of ferrosilicon powders for heavy medium separation. JSAIMM (December), 103–115.

Collins, D.N., Turnbull, T., Wright, B.A., Ngan, W., 1983. Separation efficiency in dense medium cyclones. Transactions of the Institution of Mining and Metallurgy Section C, 39–51.

Jinescu, V.V., 1974. The rheology of suspensions. International Chemical Engineering 14, 397–420.

Johnson, S.B., Franks, G.V., Scales, P.J., Boger, D.V., Healy, T.W., 2000. Surface chemistry–rheology relationships in concentrated mineral suspensions. International Journal of Mineral Processing (Elsevier) 58, 267–304.

Lapsin, R., Ferrara, G., Ruscio, E., Schena, G.D., 1988. Rheological characterization of magnetite dense media. Coal Preparation 5, 167–183.

Laskowski, J.S., He, Y.B., Klein, B., 2001. Particle movement in non-Newtonian slurries: The effect of yield stress on dense medium separation. Chemical Engineering Science 56 (9).

Slatter, P., Knowlton, J., Masalova, I., Perret, D., 2000. Practical Rheology Course. Cape Technikon Rheology Centre, November 2000.

Wills, B.A., 1997. Mineral Processing Technology, sixth ed. Butterworth-Heinemann, Oxford.